

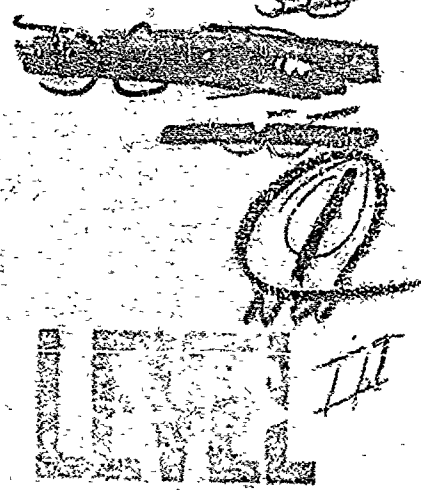
#130927  
(Continued)

~~Reminiscence~~

10th NAVY  
SYMPOSIUM on  
AEROBALLISTICS

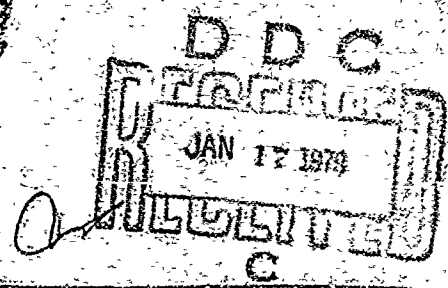
AD 63354

VOLUME 1



AD A0 63353

15-16-17 JULY



DDC FILE COPY

SPONSORED BY THE

NAVY AEROBALLISTICS ADVISORY COMMITTEE,

NAAC

HOSTED BY

NAVAL SURFACE WEAPONS CENTER  
DAHLGREN LABORATORY, DAHLGREN, VA.

HELD AT THE

SHERATON MOTOR INN  
FREDERICKSBURG, VA.

This document has been approved  
for public release and sale; its  
distribution is unlimited.

78 11 16 035

LEVEL

12

DDC  
RECEIVED  
JAN 17 1979  
C

6

PROCEEDINGS OF THE TENTH  
NAVY SYMPOSIUM ON AEROBALLISTICS (10th)

~~VOLUME 1~~

~~15-16-17 JULY 1975~~

HELD AT THE SHERATON MOTOR INN,  
FREDERICKSBURG, VIRGINIA

SPONSORED BY THE NAVY AEROBALLISTICS  
ADVISORY COMMITTEE NAAC

12

453 p.

11 17 Jul 75

This document has been approved  
for public release and sale; its  
distribution is unlimited.

nat.



**Best  
Available  
Copy**

## FOREWORD

These *Proceedings*, published in four volumes, comprise the 45 papers presented at the Tenth Navy Symposium on Aeroballistics held at the Sheraton Motor Inn, Fredericksburg, Virginia, 15, 16 and 17 July 1975.

This symposium was the tenth in a series begun in 1950 under the sponsorship of the then Bureau of Ordnance Committee on Aeroballistics, and currently conducted by the Naval Aeroballistics Advisory Committee as sponsoring committee for the Naval Air Systems Command and the Naval Ordnance Systems Command. The continuing purpose of the symposiums has been to disseminate the results of aeroballistics research and to bring the research findings of industry, the universities, and government laboratories to bear upon the Navy's aeroballistic research and development programs.

Over 160 research scientists representing 56 organizations attended this tenth symposium. Session I covered the subjects of missile stability and performance; Session II was concerned with missile stability and performance/launch dynamics; Session III dealt with heat transfer; Session IV covered inlets and diffusers/gas dynamics; and Session V presented aero-elasticity and structures.

The papers in these *Proceedings* have been reproduced in facsimile. They appear in the order of presentation except that all classified papers have been taken out of sequence and grouped together as Volume 4, a confidential volume. Volumes 1 through 3 are unclassified. This is Volume 1.

Requests for or comments on individual papers should be addressed to the respective authors.

THOMAS A. CLARE  
General Chairman  
Symposium Committee

ACCESSION for	
NTIS	Write Section <input checked="" type="checkbox"/>
DDC	Ref Section <input type="checkbox"/>
UNANNOUNCED	<input type="checkbox"/>
13 JAN 1976	
After on file	
DISCERNED FROM THE COPIES	
SPECIAL	
A	

## CONTENTS

	Page
Author Index . . . . .	xii
Greetings . . . . .	xiv
Welcome . . . . .	xv
Advisory Committee . . . . .	xviii
NACC Panels and Panel Chairman for 1975 . . . . .	xviii
Past NACC Panel Chairman . . . . .	xviii
U. S. Navy Symposium on Aeroballistics . . . . .	xvi-xvii
Paper Selection Committee and Acknowledgements . . . . .	xix
Attendees . . . . .	xx through xxxi

## Volume 1

1. Survey and Evaluation of Nonlinear Aeromechanics M. Michael Briggs <i>McDonnell Douglas Corporation</i> <i>Huntington Beach, California</i> . . . . .	1
2. Aerodynamic Roll Characteristics of Canard Missiles Richard E. Meeker <i>Naval Weapons Center</i> <i>China Lake, California</i> . . . . .	37
3. Roll Rate Stabilization of a Canard-Controlled Guided Missile Configuration at Subsonic and Supersonic Speed P. Daniels <i>Naval Surface Weapons Center, Dahlgren Laboratory,</i> <i>Dahlgren, Virginia</i> . . . . .	63
4. Supersonic Lifting-Surface Program for Cruciform Missiles With Applications to Induced Roll M. F. E. Dillenius, J. N. Nielsen, and M. J. Hemsch <i>Nielsen Engineering and Research, Inc.</i> <i>Mountain View, California</i> . . . . .	97
5. Prediction of Missile Aerodynamic Characteristics of Arbitrary Roll Orientation W. B. Brooks <i>Group Engineer</i> <i>McDonnell Douglas Astronautics Company</i> <i>Saint Louis, Missouri</i> . . . . .	160
6. Wing Planform Studies for a Span-Constrained Missile L. S. Jernell and W. C. Sawyer <i>NASA Langley Research Center</i> <i>Hampton, Virginia</i> . . . . .	197
7. An Experimental Study of the Effects of Missile Configuration Variables on Pitch Linearity William A. Corlett and Roger H. Fournier <i>NASA Langley Research Center</i> <i>Hampton, Virginia</i> . . . . .	198

CONTENTS (Continued)

Volume 1

	Page
9. Static and Dynamic Aerodynamics of Projectiles and Missiles Frankie G. Moore and Gil Y. Graff <i>Naval Surface Weapons Center</i> <i>Dahlgren Laboratory</i> <i>Dahlgren, Virginia</i> . . . . .	216
10. A Review and Status of Wrap-Around Fin Aerodynamics C. Wayne Dahlke <i>U. S. Army Missile Command</i> <i>Redstone Arsenal, Alabama</i> . . . . .	219
11. High Subsonic Aerodynamic Longitudinal Stability and Control Characteristics of Configurations Incorporating Wrap-Around Surfaces E. F. Lucero <i>Applied Physics Laboratory/The Johns Hopkins University</i> <i>Silver Spring, Maryland</i> . . . . .	325
12. Transonic Flight Dynamics of Long Shell W. H. Mermagen and V. Oskay <i>U. S. Army Ballistic Research Laboratories</i> <i>Aberdeen, Maryland</i> . . . . .	361

Volume 2

16. Store Separation State-of-the-Art Review A. R. Maddox J. R. Marshall <i>Naval Weapons Center</i> <i>China Lake, California</i> G. F. Cooper <i>Naval Missile Center</i> <i>Point Mugu, California</i> E. F. McCabe <i>Naval Research and Development Center</i> <i>Bethesda, Maryland</i> . . . . .	1
17. An Estimate of the Effect of Multiple Ejection Rack Flexibility on Six-Degree-of-Freedom Store Ejection Conditions Leroy Devan <i>Naval Surface Weapons Center</i> <i>Dahlgren Laboratory</i> <i>Dahlgren, Virginia</i> . . . . .	68
18. A Study of Variable Orifice Controlled Weapons Launching John Sun <i>Naval Surface Weapons Center</i> <i>Dahlgren Laboratory</i> <i>Dahlgren, Virginia</i> . . . . .	106
19. The Aerodynamic Environment of Rockets Launched From Helicopters B. Z. Jenkins <i>U. S. Army Missile Command</i> <i>Redstone Arsenal, Alabama</i> . . . . .	149

## CONTENTS (Continued)

## Volume 2

	Page
20. A Simple Method for Studying Some Aerodynamic Heating Problems Tse-Fou Zien <i>Naval Surface Weapons Center</i> <i>White Oak Laboratory</i> <i>Silver Spring, Maryland</i> . . . . .	174
21. Structural Studies of Rough-Wall Boundary Layers Robert J. Moffat <i>Stanford University</i> <i>Stanford, California</i> . . . . .	206
22. Heat Transfer From a Turbulent Boundary Layer on a Porous Hemisphere Robert H. Feldhuhn <i>Naval Surface Weapons Center</i> <i>White Oak Laboratory</i> <i>Silver Spring, Maryland</i> . . . . .	239
23. Performance Characteristics of Transpiration Nose Tips At High Angles of Attack J. L. Nardacci, N. C. Campbell, and D. Quan <i>McDonnell Douglas Astronautics Company</i> <i>Huntington Beach, California</i> . . . . .	273
24. Surface Temperature Measurements in Hypersonic Free Flight Daniel C. Reda, Robert A. Leverance and William G. Dorsey, Jr. <i>Naval Surface Weapons Center</i> <i>White Oak Laboratory</i> <i>Silver Spring, Maryland</i> . . . . .	344
25. The Augmentation of Stagnation Point Heat Transfer By Particle-Flow Interactions W. J. Grabowski <i>Science Applications, Inc.</i> <i>El Segundo, California</i> . . . . .	400
26. Heat Transfer to a Circumferential Gap On a Cone At Angle of Attack D. E. Nestler <i>General Electric Company</i> <i>Philadelphia, Pa.</i> . . . . .	401
27. Experimental Investigation of a Fin-Cone Interference Flow Field at MACH 5 Joseph D. Gillerlain, Jr. <i>Naval Surface Weapons Center</i> <i>White Oak Laboratory</i> <i>Silver Spring, Maryland</i> . . . . .	425
29. Aerodynamic Characteristics of a Missile Configuration Having a Forward Located Inlet M. Leroy Spearman and Clyde Hayes <i>NASA Langley Research Center</i> <i>Hampton, Virginia</i> . . . . .	467
Paper Withdrawn	

# 10th Navy Symposium on Aeroballistics

Vol. 1

## CONTENTS (Continued)

### Volume 2

	Page
30. Analysis and Design of Ejector Diffuser for Optimum Thrust Tsze C. Tai <i>Naval Ship Research and Development Center Bethesda, Maryland</i> .....	468
31. Evaluation of a Coaxial Gas Flow Chamber R. E. Lee <i>Naval Surface Weapons Center White Oak Laboratory Silver Spring, Maryland</i> .....	493
Paper Withdrawn	

### Volume 3

32. The Impact of Contemporary Fluid Mechanics Computational Techniques on Missile Design Technology Part I J. Xerikos <i>Chief, Aerodynamics Branch McDonnell Douglas Astronautics Company Huntington Beach, California</i> .....	1
Part II Clark H. Lewis <i>Virginia Polytechnic Institute and State University Blacksburg, Virginia</i> .....	26
33. Survey of Three-Dimensional Flow Fields in the Presence of Wings at $M = 2.48$ George S. Pick and R. M. Hartley <i>Naval Ship Research and Development Center Bethesda, Maryland</i> .....	97
34. Two-Dimensional Analysis of Base Drag Reduction Using External Burning R. Cavalleri <i>Atlantic Research Corporation Alexandria, Virginia</i> .....	148
35. Wind-Tunnel Study of Projectile Base Drag Reduction Through Combustion of Solid, Fuel-Rich Propellants F. P. Baltakis <i>Naval Surface Weapons Center White Oak Laboratory Silver Spring, Maryland J. R. Ward Ballistic Research Laboratories Aberdeen Proving Ground, Maryland</i> .....	175



## CONTENTS (Continued)

## Volume 3

	Page
36. A Three-Dimensional Flow Field Computer Program for Maneuvering and Ballistic Re-entry Vehicle C. L. Kyriss and T. B. Harris <i>General Electric Company</i> <i>Philadelphia, Pennsylvania</i> . . . . .	200
37. MACH 4.9 Turbulent Boundary-Layer Separation Induced by a Continuous Flow Compression Robert L. P. Voisinet <i>Naval Surface Weapons Center</i> <i>White Oak Laboratory</i> <i>Silver Spring, Maryland</i> . . . . .	240
38. Effects of Hypersonic Viscous Interaction on the Center of Pressure of Sharp and Blunt Cones as a Function of Angle of Attack A. G. Keel, Jr. and J. A. Darling <i>Naval Surface Weapons Center</i> <i>White Oak Laboratory</i> <i>Silver Spring, Maryland</i> . . . . .	279
39. A State-of-the-Art Review of Methods in Aeroelasticity and Structural Analyses for Guided Weapons G. Dailey <i>Applied Physics Laboratory/The Johns</i> <i>Hopkins University</i> <i>Silver Spring, Maryland</i> R. Oedy <i>Hughes Missile Division</i> <i>Canoga Park, California</i> W. J. Werback <i>Naval Weapons Center</i> <i>China Lake, California</i> . . . . .	294
40. Survey of Structural Materials Technology for Navy Tactical Missiles J. S. O'Connor and W. C. Caywood <i>Johns Hopkins University</i> <i>Applied Physics Laboratory</i> <i>Silver Spring, Maryland</i> . . . . .	315
41. Nonlinear Hypersonic Aero-Thermo-Elastic Effects on Missile Lifting Surfaces B. Almroth, J. A. Bailie, and F. R. Brogon <i>Lockheed Missiles and Space Company, Inc.</i> <i>Sunnyvale, California</i> . . . . .	337

# 10th Navy Symposium on Aeroballistics

Vol. 1

## CONTENTS (Continued)

### Volume 3

	Page
43. A Review of the Integral Theory of Impact Thomas B. McDonough <i>Aeronautical Research Associates of Princeton, Inc.</i> <i>Princeton, New Jersey</i> . . . . .	403
44. Thermostructural Analysis of IR Seeker Domes W. R. Compton C. F. Markarian B. M. Ryan <i>Aerothermodynamics Branch</i> <i>Naval Weapons Center</i> <i>China Lake, California</i> . . . . .	479
45. Effect of Multiple Impacts on Erosion Characteristics of Nose-Tip Materials N. W. Sheetz <i>Naval Surface Weapons Center</i> <i>White Oak Laboratory</i> <i>Silver Spring, Maryland</i> . . . . .	508

### Volume 4 (Classified Papers)

8. Aerodynamic Characteristics of a Missile Configuration in the Presence of an Exhaust Plume at Angles of Attack to 180° S. K. Carter <i>Naval Weapons Center</i> <i>China Lake, California</i> F. K. Shigeno M. M. Briggs <i>McDonnell Douglas Astronautics-West</i> <i>Huntington Beach, California</i> . . . . .	1
13. Spinning Tubular Projectile Ronald S. Brunsvold C. A. Kalivretenos <i>Naval Surface Weapons Center</i> <i>White Oak Laboratory</i> <i>Silver Spring, Maryland</i> . . . . .	52
14. Guided Projectile Aerodynamic Design Considerations H. Farley and F. Krens <i>Naval Surface Weapons Center</i> <i>Dahlgren Laboratory</i> <i>Dahlgren, Virginia</i> . . . . .	83
15. The Aeroballistic Development of the Flat-Trajectory Projectile G. C. A. Kalivretenos <i>Naval Surface Weapons Center</i> <i>White Oak Laboratory</i> <i>Silver Spring, Maryland</i> . . . . .	113

CONTENTS (Continued)

Volume 4  
(Classified Papers)

	Page
28. Survey of Airbreathing Missile Inlet Development J. L. Keirsey and R. L. Rumpf <i>Applied Physics Laboratory/The Johns Hopkins University Silver Spring, Maryland</i> . . . . .	159
42. Use of Rocket Sled Facilities in Missile Aeroelastic Investigations R. A. Deep and C. E. Brazzel <i>U. S. Army Missile Command Redstone Arsenal, Alabama</i> . . . . .	216

## Page

	Page		Page
Almroth, B., Paper No. 41, Vol. 3	337	Kyriss, C. L., Paper No. 36, Vol. 3	200
Baillie, J. A., Paper No. 41, Vol. 3	337	Lee, R. E., Paper No. 31, Vol. 2	493
Baltakis, F. P., Paper No. 35, Vol. 3	175	Leverance, R. A., Paper No. 24, Vol. 2	344
Brazzel, C. E., Paper No. 42, Vol. 4	216	Lewis, C. H., Paper No. 32, Vol. 3	26
Briggs, M. M., Paper No. 1, Vol. 1	1	Lucero, E. F., Paper No. 11, Vol. 1	325
Paper No. 8, Vol. 4	1		
Brogon, F. R., Paper No. 41, Vol. 3	337	Maddox, A. R., Paper No. 16, Vol. 2	1
Brooks, W. B., Paper No. 5, Vol. 1	160	Markarian, C. F., Paper No. 44, Vol. 3	479
Brunsvold, R. S., Paper No. 13, Vol. 4	52	Marshall, J. R., Paper No. 16, Vol. 2	1
		McCabe, E. F., Paper No. 16, Vol. 2	1
Campbell, N. C., Paper No. 23, Vol. 2	273	McDonough, T. B., Paper No. 43, Vol. 3	403
Carter, S. K., Paper No. 8, Vol. 4	1	Meeker, R. E., Paper No. 2, Vol. 1	37
Cavalleri, R., Paper No. 34, Vol. 3	148	Mermagen, W. H., Paper No. 12, Vol. 1	361
Caywood, W. C., Paper No. 40, Vol. 3	315	Moffat, R. J., Paper No. 21, Vol. 2	206
Compton, W. R., Paper No. 44, Vol. 3	479	Moore, F. G., Paper No. 9, Vol. 1	216
Cooper, G. F., Paper No. 16, Vol. 2	1		
Corlett, W. A., Paper No. 7, Vol. 1	198	Nardacci, J. L., Paper No. 23, Vol. 2	273
		Nestler, D. E., Paper No. 26, Vol. 2	401
Dahlke, C. W., Paper No. 10, Vol. 1	279	Nielsen, J. N., Paper No. 4, Vol. 1	97
Dailley, G., Paper No. 39, Vol. 3	294		
Daniels, P., Paper No. 3, Vol. 1	63	O'Connor, J. S., Paper No. 40, Vol. 3	315
Darling, J. A., Paper No. 38, Vol. 3	279	Oedy, R., Paper No. 39, Vol. 3	294
Deep, R. A., Paper No. 42, Vol. 4	216	Oskay, V., Paper No. 12, Vol. 1	361
Devan, L., Paper No. 17, Vol. 2	68		
Dillenius, M. F. E., Paper No. 4, Vol. 1	97	Pick, G. S., Paper No. 33, Vol. 3	97
Dorsey, W. G., Jr., Paper No. 24, Vol. 2	344		
		Quan, D., Paper No. 23, Vol. 2	273
Farley, H., Paper No. 14, Vol. 4	83		
Feldhuhn, R. H., Paper No. 22, Vol. 2	239	Reda, D. C., Paper No. 24, Vol. 2	344
Fournier, R. H., Paper No. 7, Vol. 1	198	Rumpf, R. L., Paper No. 28, Vol. 4	159
		Ryan, B. M., Paper No. 44, Vol. 3	479
Gillerlain, J. D., Jr., Paper No. 27, Vol. 2	425		
Grabowski, W. J., Paper No. 25, Vol. 2	400	Sawyer, W. C., Paper No. 6, Vol. 1	197
Graff, G. Y., Paper No. 9, Vol. 1	216	Sheetz, N. W., Paper No. 45, Vol. 3	508
		Shigeno, F. K., Paper No. 8, Vol. 4	1
Harris, T. B., Paper No. 36, Vol. 3	200	Spearman, M. L., Paper No. 29, Vol. 2	467
Hartley, R. M., Paper No. 33, Vol. 3	97	Sun, J., Paper No. 18, Vol. 2	106
Hayes, C., Paper No. 29, Vol. 2	467		
Hensch, M. J., Paper No. 4, Vol. 1	97	Tai, T. C., Paper No. 30, Vol. 2	468
Jenkins, B. Z., Paper No. 19, Vol. 2	149	Voisinot, R. L. P., Paper No. 37, Vol. 3	240
Jernell, L. S., Paper No. 6, Vol. 1	197		
		Ward, J. R., Paper No. 35, Vol. 3	175
Kalivretenos, C. A., Paper No. 13, Vol. 4	52	Werback, W. J., Paper No. 39, Vol. 3	294
Paper No. 15, Vol. 4	113		
Keel, A. G., Jr., Paper No. 38, Vol. 3	279	Xerikos, J., Paper No. 32, Vol. 3	1
Keirse, J. L., Paper No. 28, Vol. 4	159		
Krens, F., Paper No. 14, Vol. 4	83	Zien, Tse-Fou, Paper No. 20, Vol. 2	174

GREETINGS

The Navy Aeroballistics Advisory Committee (NAAC) provides valuable assistance to the Naval Air and Naval Sea Systems Commands. It is extremely active in promoting the exchange of technical information among Naval activities, Navy contractors, and other government agencies. It also provides effective guidance by recommending aeroballistics research investigations and identifying the new aeroballistic facilities necessary for future weapons development. We hope that this Symposium, as in the past, will provide for a stimulating exchange of information and will be of value to all participants. Best wishes for a successful Symposium.



*A. B. McCaulley*  
*Captain, USN*  
*Assistant Commander*  
*for Research & Technology*  
*Naval Air Systems Command*



*R. W. King*  
*Rear Admiral, USN*  
*Deputy Commander*  
*for Research & Technology*  
*Naval Sea Systems Command*

## 10th Navy Symposium on Aeroballistics

---

Vol. 1

### WELCOME

On behalf of the Dahlgren Laboratory of the Naval Surface Weapons Center, we are pleased to welcome you to the Tenth U. S. Navy Symposium on Aeroballistics.

The Navy Aeroballistics Advisory Committee, established jointly by the Naval Air Systems Command and the Naval Sea Systems Command, has prepared an excellent program covering diverse technical disciplines in the field of aeroballistics. It is noted that the Symposium brings together speakers and guests with special competence in aeroballistics from the Navy, Air Force, Army, other government agencies, universities, and from industry. It is our hope that we can provide a pleasant atmosphere for you during the Symposium.



C. J. Rorie  
*Captain, USN*  
*Commander*  
*Naval Surface Weapons Center*



U S. NAVY SYMPOSIUMS ON AEROBALLISTICS

**FIRST SYMPOSIUM – NOVEMBER 1950**

Hosted by ..... Defense Research Laboratory  
Held at ..... University of Texas  
Austin, Texas

**SECOND SYMPOSIUM – MAY 1952**

Hosted by ..... Naval Weapons Center  
Held at ..... Huntington Hotel  
Pasadena, California

**THIRD SYMPOSIUM – OCTOBER 1954**

Hosted by ..... Applied Physics Laboratory  
The Johns Hopkins University  
Held at ..... Applied Physics Laboratory  
The Johns Hopkins University  
Silver Spring (Howard County Location), Md.

**FOURTH SYMPOSIUM – NOVEMBER 1957**

Hosted by ..... Naval Weapons Laboratory  
Held at ..... Department of Commerce Auditorium  
Washington, D. C.

**FIFTH SYMPOSIUM – OCTOBER 1961**

Hosted by ..... Naval Ordnance Laboratory  
Held at ..... Naval Ordnance Laboratory  
White Oak, Md.

**SIXTH SYMPOSIUM – OCTOBER-NOVEMBER 1963**

Hosted by ..... Naval Ship Research and  
Development Center  
Held at ..... National War College  
Fort McNair, Washington D. C.

**SEVENTH SYMPOSIUM – JUNE 1966**

Hosted by ..... Naval Missile Center  
Held at ..... Naval Missile Center  
Point Mugu, Calif.

**EIGHTH SYMPOSIUM – MAY 1969**

Hosted by ..... Naval Weapons Center  
Held at ..... NWC Corona Laboratories  
Corona, Calif.

## **10th Navy Symposium on Aeroballistics**

---

### **Vol. 1**

#### **NINTH SYMPOSIUM - MAY 1972**

Hosted by ..... Applied Physics Laboratory  
The Johns Hopkins University  
Held at ..... Applied Physics Laboratory  
The Johns Hopkins University  
Silver Spring (Howard County Location), Md.

#### **TENTH SYMPOSIUM - JULY 1975**

Hosted by ..... Naval Surface Weapons Center  
Dahlgren Laboratory  
Dahlgren, Virginia  
Held at ..... Sheraton Fredericksburg Motor Inn  
Fredericksburg, Va.

## NAVAL AEROBALLISTICS ADVISORY COMMITTEE

## MEMBERS AND ALTERNATE MEMBERS FOR 1975

## Members

## Alternate

S. de los Santos, Chairman (NSRDC)	S. Gottlieb
L. Schindel (NAVSURFWPNCEN/WOL)	K. Enkenhaus
L. L. Cronvich (APL/JHU)	E. T. Marley
R. D. Cuddy (NAVSURFWPNCEN/DL)	F. G. Moore
J. W. Rom (NMC)	M. R. Marson
R. W. Van Aken (NWC)	R. E. Meeker
W. A. Langan (NADC)	V. C. Dailey

## ASSOCIATES

W. C. Volz, Executive Secretary (NAVAIRSYSCOM)  
 H. Andrews (NAVAIRSYSCOM)  
 L. Pasiuk (NAVSEASYSYSCOM)  
 C. Wheeler (NAVSEASYSYSCOM)

NAAC PANELS AND PANEL CHAIRMAN  
FOR 1975

Aeroelasticity and Structures	E. L. Jeter (NWC)
Air Inlets and Diffusers	R. L. Rumpf (APL/JHU)
Gas Dynamics	G. Pick (NSRDC)
Heat Transfer	W. C. Lyons (NSWC/WOL)
Missile Stability and Performance	T. A. Clare (NSWC/DL)
Launch Dynamics	G. Cooper (NMC)

## PAST NAAC CHAIRMEN

Feb 1949-Nov 1949	CDR H. M. Mott-Smith (BuOrd)
Dec 1949-Oct 1950	CDR L. G. Pooler (BuOrd)
Oct 1950-Feb 1953	CDR L. G. Pooler (NOL)
Mar 1953-Jul 1953	A. I. Moskovits (Acting) (BuOrd)
Sep 1953-Jul 1955	E. A. Bonney (APL/JHU)
Aug 1955-Aug 1957	H. H. Kurzweg (NOL)
Sep 1957-Jul 1959	W. R. Haseltine (NWC)
Aug 1959-Jul 1961	R. A. Niemann (NSWC/DL)
Jul 1961-Jan 1963	R. E. Wilson (NOL)
Jan 1963-Jan 1965	S. T. de los Santos (NSRDC)
Jan 1965-Jan 1967	R. H. Peterson (NMC)
Jan 1967-Jan 1969	W. A. Kemper (NSWC/DL)
Jan 1969-Jan 1971	L. L. Cronvich (APL/JHU)
Jan 1971-Jan 1973	W. R. Haseltine (NWC)
Jan 1973-Jan 1975	R. E. Wilson (NAVSURFWPNCEN/WOL)

## 10th Navy Symposium on Aeroballistics

Vol. 1

### PAPER SELECTION COMMITTEE

R. W. Van Aken, Chairman	NWC
T. C. Tai	NSRDC
R. Rumpf	APL/JHU
L. Schindel	NAVSURFWPNCEN/WOL
F. G. Moore	NAVSURFWPNCEN/DL
J. Rom	NMC
W. C. Volz	NAVAIRSYSCOM
L. Pasiuk	NAVSEASYSKOM

### ACKNOWLEDGEMENTS

Thanks to all who contributed to the Tenth Navy Symposium on Aeroballistics:

The host organization, the Dahlgren Laboratory of the Naval Surface Weapons Center.

Dr. T. A. Clary, Chairman of the Symposium; and Mrs. Mitzi Lumpkin and Miss Virginia Scott of NAVSURFWPNCEN/DL for their administrative and secretarial assistance.

Mr. E. T. Mable (APL), Mr. W. C. Volz (NAVAIRSYSCOM), Mr. L. Pasiuk (NAVSEASYSKOM) for their advice and assistance regarding arrangements and technical matters relating to the Symposium.

Mr. R. W. Van Aken, Chairman of the paper selection committee, and the committee members for their efforts in paper selection and session organization.

Mr. Amos Clary, Public Affairs Director at the Dahlgren Laboratory, Mr. C. Philbrick, Director of Security for the Symposium, and Mrs. Judy Kinnaman, Sheraton Fredericksburg Motor Inn, for their assistance in arrangements for the Symposium.

Session chairman, opening speakers and honored guests, for their contributions to the Symposium.

And, finally, the authors and presenters of the technical papers, without whom the Symposium would not be possible, for their excellent literary and oral presentation of technologies in the field of Aeroballistics.

## SYMPOSIUM ATTENDEE LIST

ANDERSON, C. W., JR.  
*Atlantic Research Corp.*  
*Guinesville, VA 22065*  
(703) 754-4111 - Ext. 279

ATHA, L. C.  
*Ballistic Missile Defenses*  
*Advanced Technology Center*  
*P. O. Box 1500*  
*Huntsville, AL 35807*  
(205) 895-3431

BAILIE, J. A.  
*Lockheed Missiles & Space Co.*  
*D81-12, B154*  
*Box 504*  
*Sunnyvale, CA 94088*  
(408) 742-9226

BARNARD, H. R.  
*Texas Instruments*  
*P. O. Box 6015*  
*M/S 96*  
*Dallas, TX 75222*  
(214) 238-3582

BAUER, R. L.  
*Raytheon Co.*  
*Missile Systems Division*  
*Hartwell Road*  
*Bedford, MA 01730*  
(617) 274-7100 - Ext. 2849

BECKER, M.  
*Naval Surface Weapons Center*  
*Dahlgren Laboratory*  
*Code DK-21*  
*Dahlgren, VA 22448*  
(703) 663-8107

BELL, R. W.  
*Naval Postgraduate School*  
*Dept. of Aeronautics*  
*Monterey, CA 93940*

BEUKY, R. C.  
*Naval Surface Weapons Center*  
*Dahlgren Laboratory*  
*Code DK-70*  
*Dahlgren, VA 22448*  
(703) 663-8835

BENSIMON, M.  
*NASA-Goddard Space Flight Center*  
*Code 742*  
*Greenbelt, MD 20771*  
(301) 982-4865

BERGSTEN, B.  
*Wright-Patterson AFB, OH 45433*  
(513) 225-2449

BOLICK, R. G.  
*Naval Surface Weapons Center*  
*Dahlgren Laboratory*  
*Code DG-40*  
*Dahlgren, VA 22448*  
(703) 663-7646

BOURGEOIS, B. M.  
*Naval Surface Weapons Center*  
*Dahlgren Laboratory*  
*Code DN-10*  
*Dahlgren, VA 22448*  
(703) 663-8565

BRAZZEL, C. E.  
*AMSMI-RDK*  
*Bldg. 5400*  
*Redstone Arsenal, ALA 35809*  
(205) 876-7276

BRIGGS, M. M.  
*McDonnell Douglas Astronautics Co.*  
*Dept. A3-203, M/S 11-2*  
*5301 Bolsa Ave.*  
*Huntington Beach, CA 92647*  
(714) 896-3352

**10th Navy Symposium on Aeroballistics**

---

**Vol. 1**

**SYMPOSIUM ATTENDEE LIST**

**BROOKS, W. B.**

*McDonnell Douglas Astronautics Co.  
P. O. Box 516  
Dept E241, Bldg. 10614, M/S 39  
St. Louis, MO 63166  
(314) 232-7479*

**BROWNE, P. E.**

*LTV Aerospace Corp.  
Vought Systems Division  
Unit 2-53364  
P. O. Box 5907  
Dallas, TX 75222  
(214) 266-3237*

**BRUCE, C. F.**

*MIT-Lincoln Laboratory  
Rm. D-382  
P. O. Box 73  
Lexington, MA 02173  
(617) 862-5500 - Ext. 7872*

**BRUNSVOLD, R. S.**

*Naval Surface Weapons Center  
White Oak Laboratory  
Silver Springs, MD 20910  
(202) 394-2080*

**BURNS, G. P.**

*Naval Surface Weapons Center  
Dahlgren Laboratory  
Code DK-22  
Dahlgren, VA 22448  
(703) 663-8368*

**CARTER, S. K.**

*Naval Weapons Center  
Code 4063  
China Lake, CA 93555  
(714) 939-2627*

**CAVALLERI, R.**

*Atlantic Research Corp.  
5390 Cherokee Avenue  
Alexandria, VA 22314  
(703) 354-3400 - Ext. 288*

**CAYWOOD, W. C.**

*Johns Hopkins University  
Applied Physics Laboratory  
8621 Georgia Avenue  
Silver Spring, MD 20910  
(202) 953-7100 - Ext. 7408*

**CHALK, J. B.**

*Naval Intelligence Support Center  
4301 Suitland Road  
Washington, D. C. 20390*

**CHAPMAN, G. T.**

*NASA - Ames Research Center  
Moffet Field, CA 94035*

**CLARE, T. A.**

*Naval Surface Weapons Center  
Dahlgren Laboratory  
Code DK-26  
Dahlgren, VA 22448  
(703) 663-8829*

**COOPER, G. F.**

*Pacific Missile Test Center  
Code 1241  
Poin. Mugu, CA 93042  
(805) 982-8941*

**CORLETT, W. A.**

*NASA-Langley Research Center  
Mail Stop 406  
Hampton, VA 23665  
(804) 827-3181*

**CRESCI, R. J.**

*Polytechnic Institute of N. Y.  
Route 110  
Farmingdale, NY 11735  
(516) 694-5500*

**CRONVICH, L. L.**

*Johns Hopkins University  
Applied Physics Laboratory  
8621 Georgia Avenue  
Silver Spring, MD 20910  
(202) 953-7100 - Ext. 7475*



SYMPOSIUM ATTENDEE LIST

**CURRY, W. H.**

*Sandia Laboratories  
Division 5625  
Albuquerque, NM 87115  
(505) 264-8500*

**DAHLKE, C. W.**

*U. S. Army Missile Command  
AMSMI-RDK  
Redstone Arsenal, AL 35809  
(205) 876-7753*

**DAILEY, V. C.**

*Naval Air Development Center  
Warminster, PA 18974  
(215) 672-9000 - Ext. 2316*

**DANIEL, D. C.**

*AFATL/DLDD  
Eglin AFB, FL 32542*

**DANIELS, P.**

*Naval Surface Weapons Center  
Dahlgren Laboratory  
Code DK-21  
Dahlgren, VA 22448  
(703) 663-8107*

**DE LOS SANTOS, S.**

*Naval Ship Research & Development Center  
Carderock Laboratory  
Aviation & Surface Effects Dept (1606)  
Bethesda, MD 20084  
(202) 227-1463*

**DENYSYK, B.**

*Naval Surface Weapons Center  
Dahlgren Laboratory  
Code DK-55  
Dahlgren, VA 22448  
(703) 663-8615*

**DEVAN, L.**

*Naval Surface Weapons Center  
Dahlgren Laboratory  
Code DK-21  
Dahlgren, VA 22448  
(703) 663-8107*

**DILLENUS, M. F.**

*Nielsen Engineering & Research, Inc.  
510 Clyde Avenue  
Mountain View, CA 94043  
(415) 968-9457*

**DRAGOWITZ, C. J.**

*Grumman Aerospace Corp.  
Dept. 393, Plant 35  
Bethpage, NY 11714  
(516) 575-3671*

**DUNBAR, L.**

*Science Applications, Inc.  
101 Continental Bldg.  
Suite 310  
El Segundo, CA 90245  
(213) 640-0480*

**DUP. DONALDSON, C.**

*Aeronautical Research Association  
of Princeton, Inc.  
50 Washington Rd.  
P. O. Box 2229  
Princeton, NJ 08540  
(609) 452-2950*

**EAVES, R. H., JR.**

*ARO, Inc.  
VKF-Tunnel F Bldg.  
Arnold Air Force Station, TN 37389  
(615) 455-2611 - Ext. 650*

**ENKENHUS, K.**

*Naval Surface Weapons Center  
White Oak Laboratory  
Flight Measurement Div.  
Bldg. 430-109  
Silver Spring, MD 20910  
(202) 394-1939*

**FARLEY, H. C.**

*Naval Surface Weapons Center  
Dahlgren Laboratory  
Code DG-44  
Dahlgren, VA 22448  
(703) 663-7481*

SYMPOSIUM ATTENDEE LIST

FELDHUHN, R. H.  
Naval Surface Weapons Center  
White Oak Laboratory  
Aerodynamics & Structural Branch  
WA-21  
Silver Spring, MD 20910  
(202) 394-1675, 2890

FIDLER, J. E.  
Martin Marietta Aerospace  
Orlando Division  
P. O. Box 5837, MP-88  
Orlando, FL 32805  
(305) 352-2204

FISHER, P. D.  
Atlantic Research Corp.  
P. O. Box 38  
Gainesville, VA 22065  
(703) 754-4111 - Ext. 258

FORTUNATO, E.  
Naval Surface Weapons Center  
White Oak Laboratory  
Code 312  
Silver Spring, MD 20910  
(202) 394 2070

FRIERSON, J. L.  
Naval Surface Weapons Center  
Dahlgren Laboratory  
Code DG-44  
Dahlgren, VA 22448  
(703) 663-7481

GARNER, J. P.  
Naval Surface Weapons Center  
Dahlgren Laboratory  
Code DK-21  
Dahlgren, VA 22448  
(703) 663-8107

GILLERLAIN, J. D.  
Naval Surface Weapons Center  
White Oak Laboratory  
Silver Spring, MD 20910  
(202) 394-2086

GIRAGOSIAN, P. A.  
Wright-Patterson AFB, OH 45433

GNAGY, J. R.  
Pacific Missile Test Center  
Code 1241  
Point Mugu, CA 93042  
(805) 982-8941

GORECLAD, A. J.  
Naval Surface Weapons Center  
White Oak Laboratory  
Silver Spring, MD 20910  
(202) 394-1651

GOTTLIEB, S. M.  
Naval Ship Research & Development Center  
Bethesda, MD 20084

GRACEY, C.  
Naval Surface Weapons Center  
Dahlgren Laboratory  
Code DK-21  
Dahlgren, VA 22448  
(703) 663-8107

GRAFF, G. Y.  
Naval Surface Weapons Center  
Dahlgren Laboratory  
Code DG-44  
Dahlgren, VA 22448  
(703) 663-7481

GUIOU, CAPT M.  
Arnold Air Force Station  
AEDC/DYR  
Arnold AFS, TN 37389  
(615) 455-2611 - Ext. 7834

GURKIN, L. W., III  
NASA - Wallops Island Flight Cntr.  
Wallops Island, VA 23337  
(804) 3411 - Ext. 2566, 2200

## SYMPOSIUM ATTENDEE LIST

## HALDEMAN, C. W.

Massachusetts Inst. of Technology  
560 Memorial Drive  
Cambridge, MA 02139  
(617) 253-2602

## HALL, R. B.

Naval Weapons Center  
Code 4576  
China Lake, CA 93555  
(714) 939-7395

## HARRIS, T. B.

General Electric Company  
Valley Forge Space Techn. Center  
Rm. U-3217  
King of Prussia, PA 19406  
(215) 962-1340

## HARTLEY, R. M.

Naval Ship Research & Development Center  
Code 166  
Bethesda, MD 20084

## HASTINGS, S. M.

Naval Surface Weapons Center  
White Oak Laboratory  
Silver Spring, MD 20910  
(202) 394-1669

## HAYES, C.

NASA - Langley Research Center  
Mail Stop 406  
Hampton, VA 23665  
(804) 827-3181

## HERRON, R. D.

ARO, Inc.  
PWT-4T  
Arnold Air Force Station, TN 37389  
(615) 455-2611 - Ext. 7150, 7433

## HESSMAN, F. W.

Rockwell International  
Missile Systems Division  
4300 East Fifth Avenue  
Columbus, OH 43216  
(614) 239-2667

## HOLESKI, D. E.

Pacific Missile Test Range  
Code 1232  
Point Mugu, CA 93042  
(805) 982-8403

## HUANG, S. L.

Naval Air Development Center  
Code 3033  
Warminster, PA 18974  
(215) 672-9000 - Ext. 2041

## HUMPHREYS, D. E.

Naval Coastal Systems Laboratory  
Code 710.2  
Panama City, FL 32401  
(904) 234-4213

## INGALLS, P.

Pacific Missile Test Center  
Point Mugu, CA 93042  
(805) 982-8941

## INGRAM, C. W.

Systems Research Lab., Inc.  
28000 Indian Ripple Rd.  
Dayton, OH 45440  
(513) 426-8961

## JENKINS, B. Z.

U. S. Army Missile Command  
AMSMI-RKD  
Redstone Arsenal, AL 35809  
(205) 876-7278

**10th Navy Symposium on Aeroballistics**

**Vol. 1**

**SYMPOSIUM ATTENDEE LIST**

**JOHNSON, G. G.**

*LTV Aerospace Corp.  
Unit 2-53363  
P. O. Box 5907  
Dallas, TX 75222  
(214) 266-7494*

**KALIVRETENOS, C. A.**

*Naval Surface Weapons Center  
White Oak Laboratory  
Silver Spring, MD 20910  
(202) 394-4267*

**KATZ, W. M.**

*Naval Surface Weapons Center  
Dahlgren Laboratory  
DK-21  
Dahlgren, VA 22448  
(703) 663-8107*

**KAUFMAN, L. G., III**

*Grumman Aerospace Corp.  
Research Dept. - Plant 35  
Bethpage, NY 11714  
(516) 575-2323*

**KEARNS, J. P.**

*Johns Hopkins University  
Applied Physics Laboratory  
8621 Georgia Avenue  
Silver Spring, MD 20910  
(202) 953-7100 - Ext. 646*

**KEMPER, W. A.**

*P. O. Box 129  
Dillon, Colorado 80435*

**KING, RADM R. W.**

*Naval Sea Systems Command  
SEA 03  
Washington, D. C. 20362  
(202) 692-8696*

**KRENS, F. J.**

*Naval Surface Weapons Center  
Dahlgren Laboratory  
Code DG-40  
Dahlgren, VA 22448  
(703) 663-7646*

**KUSTER, F. A.**

*Advanced Missile Project Office  
Naval Air Development Center  
Code 30P4  
Warminster, PA 18974  
(215) 674-9000 - Ext. 2574*

**KUTSCHINSKI, C. R.**

*Hughes Aircraft Co.  
8433 Fallbrook Avenue  
Bldg. 265/X35  
Canoga Park, CA 91304  
(213) 883-2400 - Ext. 3618*

**KYRISS, C. L.**

*General Electric Co.  
Room U-3217, VFSTC  
P. O. Box 8555  
Philadelphia, PA 19101  
(215) 962-5725*

**LA GRANGE, D. E.**

*Naval Ammunition Depot  
Code 5041  
Crane, IN 47522  
(812) 854-1603*

**LANDO, D. W.**

*Naval Surface Weapons Center  
Dahlgren Laboratory  
Code DK-55  
Dahlgren, VA 22448  
(703) 663-8359*

**LARSEN, K. A.**

*Pacific Missile Test Center  
Code 1241  
Point Mugu, CA 93042  
(805) 982-8941*

## SYMPOSIUM ATTENDEE LIST

LEE, K. W.

Naval Air Development Center  
AVTD-3014  
Warminster, PA 18974  
(215) 672-9000 - Ext. 2344 or 2166

LEWIS, C. H.

Virginia Polytechnic Inst. &  
State University  
214 Randolph Hall  
Blacksburg, VA 24061  
(703) 951-6126 - Ext. 6742

LINDORM, C. A.

Naval Surface Weapons Center  
Dahlgren Laboratory  
Code DN-30  
Dahlgren, VA 22448  
(703) 663-8731

LUCERO, E. F.

Johns Hopkins University  
Applied Physics Laboratory  
11100 Johns Hopkins Road  
Laurel, MD 20810  
(301) 953-7100 - Ext. 7450

LYNCH, J. P., III

Naval Surface Weapons Center  
Dahlgren Laboratory  
Code DG-50  
Dahlgren, VA 22448

MADDOX, A. R.

Naval Weapons Center  
Code 40604  
China Lake, CA 93555  
(714) 939-2935

MARKARIAN, C. F.

Naval Weapons Center  
Aerothermodynamics Branch  
Code 4061  
China Lake, CA 93555  
(714) 939-2824

MARLEY, E. T.

Johns Hopkins University  
Applied Physics Laboratory  
11100 Johns Hopkins Road  
Laurel, MD 20810  
(301) 953-7100 - Ext. 7477

MAYER, W. E.

Boeing Aerospace Corp.  
Seattle, WA 98124  
(206) 655-3479

MATTHEWS, M. L.

Boeing Aerospace Corp.  
P. O. Box 3999  
Seattle, WA 98124  
(206) 773-1525

MCCABE, E. F., JR.

Naval Ship Research & Development Center  
Code 166  
Bethesda, MD 20084  
(202) 227-1670

MARSHALL, J. R.

Naval Weapons Center  
Code 4063  
China Lake, CA 93555  
(714) 939-2820

MCCAULLEY, CAPT H. B./USN

Assistant Commander for Research  
and Technology  
AIR-03  
Naval Air Systems Command  
Washington, D. C. 20361  
(202) 692-7439

MASON, L. A.

Naval Surface Weapons Center  
Dahlgren Laboratory  
Code DK-21  
Dahlgren, VA 22448  
(703) 663-8107

SYMPOSIUM ATTENDEE LIST

MASSEY, J. M.

*Naval Surface Weapons Center  
Dahlgren Laboratory  
Code DK-63  
Dahlgren, VA 22448  
(703) 663-8468*

MORRISSETTE, R. C.

*Naval Surface Weapons Center  
Dahlgren Laboratory  
Code DG-30  
Dahlgren, VA 22448  
(703) 663-8411*

MEEKER, R. E.

*Naval Weapons Center  
Code 4063  
China Lake, CA 93555  
(714) 939-2820*

MOORE, F. G.

*Naval Surface Weapons Center  
Dahlgren Laboratory  
Code DG-40  
Dahlgren, VA 22448  
(703) 663-7481*

MATTHEWS, M. L.

*Boeing Aerospace Corp.  
P. O. Box 3999  
Seattle, WA 98124  
(206) 773-1525*

MURPHY, C. H.

*Aberdeen Proving Ground  
Exterior Ballistics Laboratory  
R. H. Kent Bldg. (120)  
Aberdeen Proving Ground, MD 21005  
(301) 278-3109*

MILTON, J. E.

*University of Florida  
Graduate School  
P. O. Box 1918  
Eglin AFB, FL 32542  
( ) 882-5614*

NARDACCI, J. L.

*McDonnell Douglas Astronautics Co.  
5301 Bolsa Avenue  
Huntington Beach, CA 92647  
(714) 896-5223*

MOFFAT, R. J.

*Leland Stanford Junior University  
Dept. of Public Safety  
711 Serra Street  
Stanford, CA 94305*

NESTLER, D. E.

*General Electric Company  
P. O. Box 8555  
Philadelphia, PA 19101  
(215) 962-6090*

MOGAVERO, M. A.

*Computer Science Center  
221-C Preston Court  
Baltimore, MD 21228  
(301) 788-5832*

NEWQUIST, J. C.

*Naval Surface Weapons Center  
Dahlgren Laboratory  
Code DG-50  
Dahlgren, VA 22448  
(703) 663-8586*

MONTAG, W. H.

*NASA-Goddard Space Flight Center  
Code 742  
Greenbelt, MD 20771  
(301) 982-4865*

NIELSEN, J. N.

*Nielsen Engineering and  
Research, Inc.  
510 Clyde Avenue  
Mountain View, CA 94043  
(415) 968-9457*



## SYMPOSIUM ATTENDEE LIST

**OBERKAMPF, W. L.**

*University of Texas at Austin  
Austin, TX 78712  
(512) 471-4585*

**OHLMEYER, E. J.**

*Naval Surface Weapons Center  
Dahlgren Laboratory  
Code DG-40  
Dahlgren, VA 22448  
(703) 663-7481*

**OSBOURNE, B. P., JR.**

*Defense Research & Engineering  
Rm. 3D1089  
The Pentagon  
Washington, D. C. 20301  
(202) OX-5-0552*

**OSKAY, V.**

*Director, U. S. Army Ballistic  
Research Laboratories  
Attn: AMXBR-EB  
Aberdeen Proving Grounds, MD 21005  
(301) 278-3405*

**O'CONNER, J. S.**

*Johns Hopkins University  
Applied Physics Laboratory  
Johns Hopkins Road  
Laurel, MD 20810  
(301) 953-7100 - Ext. 7416*

**ON, T. J.**

*Naval Surface Weapons Center  
Dahlgren Laboratory  
Code DK-21  
Dahlgren, VA 22448  
(703) 663-8107*

**PARRY, E. M.**

*Naval Surface Weapons Center  
Dahlgren Laboratory  
Code DG-30  
Dahlgren, VA 22448  
(703) 663-8411*

**PASIERB, J. J.**

*Johns Hopkins University  
Applied Physics Laboratory  
8621 Georgia Avenue  
Silver Spring, MD 20910  
(301) 953-7100 - Ext. 3260*

**PASIUK, L.**

*Naval Sea Systems Command  
SEA-03513  
Washington, D. C. 20362  
(202) 692-1151*

**PEPITONE, T. R.**

*Naval Surface Weapons Center  
Dahlgren Laboratory  
Code DK-21  
Dahlgren, VA 22448*

**PERPER, D. N.**

*Hughes Aircraft Co.  
Missile Division  
Bldg. 268/W83  
Canoga Park, CA 91304  
(213) 883-2400 - Ext. 1294*

**PICK, G. S.**

*Naval Ship Research & Developm. Cntr.  
Code 1660  
Bethesda, MD 20084  
(202) 227-1670*

**PLATZER, M. F.**

*Naval Postgraduate School  
Dept. of Aeronautics  
Monterey, CA 93940  
(408) 646-2944*

**RAUSCH, J. R.**

*General Dynamics Corporation  
5001 Kearny Villa Road  
P. O. Box 80847  
San Diego, CA 92138*

SYMPOSIUM ATTENDEE LIST

REDING, J. P.

*Lockheed Missiles & Space Co.  
Dept. 81-11, Bldg. 154  
P. O. Box 504  
Sunnyvale, CA 94088  
(408) 742-1944*

ROM, J. W.

*Pacific Missile Test Center  
Code 0101  
Point Mugu, CA 93042  
(804) 982-7831 - Ext. 7833*

RUMPF, R. L.

*Johns Hopkins University  
Applied Physics Laboratory  
8621 Georgia Avenue  
Silver Spring, MD 20910  
(202) 953-7100 - Ext. 7440*

SANDERS, D. K.

*Naval Ammunition Depot  
Code 5041  
Crane, IN 47522  
(812) 854-1603*

SCHINDEL, L. H.

*Naval Surface Weapons Center  
White Oak Laboratory  
Silver Spring, MD 20910  
(202) 394-1245*

SCHMIDT, L. V.

*Naval Air Systems Command  
Code AIR-3200  
Washington, D. C. 20361  
(202) 692-7417*

SHEA, G. C.

*Naval Surface Weapons Center  
Dahlgren Laboratory  
Code DN-30  
Dahlgren, VA 22448  
(703) 663-8731*

SHEETZ, N.

*Naval Surface Weapons Center  
White Oak Laboratory  
Code 323  
Silver Spring, MD 20910  
(202) 394-2323*

SINGLETON, R. E.

*U. S. Army Research Office  
Box 12211  
Research Triangle Park, N. C. 27709  
(919) 549-0641*

SLYKER, R. W.

*Pacific Missile Test Center  
PMTIC 2144  
Point Mugu, CA 93042  
(805) 982-8063*

SMITH, R. E.

*Naval Weapons Center  
Code 4063  
China Lake, CA 93555  
(714) 939-2477*

SMITH, R. H.

*NASA OAST Headquarters  
600 Independence Avenue  
Washington, D. C. 20546  
(202) 755-2383*

SOKOL, C. R.

*Naval Surface Weapons Center  
Dahlgren Laboratory  
Code DG-40  
Dahlgren, VA 22448  
(703) 663-7481*

SOLIS, R. E.

*Naval Surface Weapons Center  
Dahlgren Laboratory  
Code DK-21  
Dahlgren, VA 22448  
(703) 663-8107*

## SYMPOSIUM ATTENDEE LIST

STEVENS, F. L.

Naval Surface Weapons Center  
Dahlgren Laboratory  
Code DK-21  
Dahlgren, VA 22448  
(703) 663-8107

STOEHR, G.

Naval Surface Weapons Center  
Dahlgren Laboratory  
Code DK-55  
Dahlgren, VA 22448  
(703) 663-8359

SUN, J.

Naval Surface Weapons Center  
Dahlgren Laboratory  
Code DK-21  
Dahlgren, VA 22448  
(703) 663-8107

SWANSON, R. C.

Naval Surface Weapons Center  
Dahlgren Laboratory  
Code DG-10  
Dahlgren, VA 22448  
(703) 663-7561

TAI, T. C.

Naval Ship Research & Developm. Center  
Code 1606  
Bethesda, MD 20084  
(202) 227-1462

TALBOT, J. F.

Naval Ship Research & Developm. Center  
Bethesda, MD 20084  
(202) 227-1670

TISSERAND, L. E.

Johns Hopkins University  
Applied Physics Laboratory  
11100 Johns Hopkins Road  
Laurel, MD 20810  
(301) 953-7100 - Ext. 7452, 7477

VAN AKEN, R. W.

Naval Weapons Center  
Code 406  
China Lake, CA 93555  
(714) 939-3374

VAN TUYL, A. H.

Naval Surface Weapons Center  
White Oak Laboratory  
Code 331  
Silver Spring, MD 20910  
(202) 394-2265

VAS, I. E.

Gas Dynamics Laboratory  
Forrestal Campus  
Princeton University  
Princeton, NJ 08540  
(609) 452-5135

VOISINET, R. L. P.

Naval Surface Weapons Center  
White Oak Laboratory  
Silver Spring, MD 20910  
(202) 394-2061

VOLZ, W. C.

Naval Air Systems Command  
AIR-320C  
Washington, D. C. 20361  
(202) 692-7417

WERBACK, W. J.

Naval Weapons Center  
Code 4062  
China Lake, CA 93555  
(714) 939-3348

WILSON, G. G.

Sandia Laboratories  
Division 5625  
Albuquerque, NM 87115  
(505) 264-3939

**10th Navy Symposium on Aeroballistics**

---

**Vol. 1**

**SYMPOSIUM ATTENDEE LIST**

**WING, L. D.**

*NASA-Goddard Space Flight Center  
Code 742  
Greenbelt, MD 20771  
(301) 982-4865*

**ZIEN, T. F.**

*Naval Surface Weapons Center  
White Oak Laboratory  
Bldg. 402, Rm. 204  
Silver Spring, MD 20910  
(202) 394-2082*

**XERIKOS, J.**

*McDonnell Douglas Astronautics, Co.  
Space Systems Center  
5301 Bolsa Avenue  
Huntington Beach, CA 92647  
(714) 896-3563*

PAPER NO. 1

SURVEY AND EVALUATION OF NONLINEAR  
AEROMECHANICS

M. MICHAEL BRIGGS

MCDONNELL DOUGLAS CORPORATION  
HUNTINGTON BEACH, CA.

SUMMARY

McDonnell Douglas Astronautics Company-West is currently conducting a survey and evaluation of nonlinear aeromechanics, under contract to NSWC-Dahlgren. This effort involves assembling the state of knowledge concerning linear and nonlinear aeromechanics in conjunction with study and assessment of the information base to identify key aeromechanics phenomena as they relate to the several configuration classes, establish the adequacy and utility of the assembled information base in application to Navy tactical weapons development, and to formulate recommendations describing active steps required to make the state of knowledge meet current and projected Navy requirements.

Since this contracted effort is a direct result of a very strong recommendation by the 1973 NAAC Stability and Performance Panel, a key element of our information acquisition approach involved capitalizing upon the cooperative spirit of the NAAC Stability and Performance Panel recommendation in terms of providing leverage and incentive for NAAC members to provide their contributions to the state of knowledge; as of this writing, 50% of the Navy members and 40% of the industry members of the NAAC stability and performance panel have responded. Fortunately, the Navy respondents were largely key labs involved in weapons development and testing; by contrast, many key aerospace firms have not participated. This paper summarizes the work accomplished to date toward performing the subject contracted effort, especially as regards information acquisition, cataloging and classification.

It appears at this point in the survey that the state of knowledge concerning linear and nonlinear aeromechanics is largely contained in approximately 1600 information elements that can be referenced, excepting the estimating 100 to 200 elements held as sacred and proprietary by certain aerospace concerns. The information base consists of classified and unclassified US Government-sponsored work, some classified work performed by NATO countries and allies available through DDC and national and international information published in the open literature. Roughly 25 percent of the information base treats derivation, evolution, and application of analytic methods, whereas the remaining (approximately) 75 percent is devoted to experimental information.

## INTRODUCTION

During the 1973 meeting of the Navy Aeroballistics Advisory Committee (NAAC), the stability and performance panel formulated a recommendation that the Navy fund the panel to assemble and assess the state of knowledge relating to nonlinear aeromechanic in the incidence range from 0 to 180 deg. for Mach numbers consistent with the flight of tactical weapons.

The following quotation, extracted from the text of the NAAC Stability and Performance Panel recommendation, provides insight into the background, justification, and rationale for conducting this proposed effort.

"Linear-angle-of-attack aerodynamics have been addressed over the past several decades resulting in a fairly organized approach to either calculating or experimentally measuring the required loads.

"The long-term trend in missile design, however, is toward ever-increasing performance and maneuverability. This has and will result in either high angle of incidence flight where nonlinear aerodynamics are omnipresent or low to moderate angles of incidence where nonlinear characteristics have also been observed. This creates considerable uncertainties in load estimates, guidance and control requirements, etc. The state of the art has caused considerable diversity of approach to the solution of problems associated with specific weapon system requirements. This has resulted in a somewhat



confused state of affairs regarding what is known and unknown concerning both data availability and analytical methodology.

"An assemblage and evaluation of the overall technology base by a working group is therefore required such that a reasonably intelligent course of action may be planned and pursued to meet the present and future needs of the Navy."

A modified version of this stability and performance panel recommendation was further adopted by the NAAC as its first-listed recommendation to the respective commanders of NAVAIR and NAVORD. As a result of the forcefulness of the Stability and Performance Panel recommendation and the diligence of its chairman, the recommendation was fulfilled by means of a competitive solicitation and subsequent award of a contract to McDonnell Douglas Astronautics Company-West (MDAC-W). The contract is jointly sponsored by NAVAIR and NAVORD through NSWC-Dahlgren.

Although the task of assembling and assessing the state of knowledge concerning nonlinear aeromechanics is an ambitious one, such an undertaking is not unprecedented. For example, consider the 1938 work, Modern Developments in Fluid Dynamics, prepared by the Fluid Motion Panel of the Aeronautical Research Committee (United Kingdom)

"to present and summarize methods of experiment and development of theory in certain branches of hydrodynamics of special interest to aeronautical science." A more recent parallel to the current work is found in the Handbook of Supersonic Aerodynamics, a massive undertaking

## 10th Navy Symposium on Aeroballistics

### Vol. 1

of the Aerodynamics Handbook Staff of the Johns Hopkins University Applied Physics Laboratory under Navy sponsorship, the production of which ran from 1950 to 1964. Other similar works worthy of note include Hoerner's "Fluid Dynamic Drag" and the "USAF Stability and Control DATCOM."

### INFORMATION ACQUISITION

Information concerning nonlinear aeromechanics was solicited and acquired from internal McDonnell Douglas Corporation (MDC) corporate-wide sources (mainly MDAC-West, MDAC-East, McDonnell Aircraft, and Douglas Aircraft, and the library services divisions of these companies in the corporate family); also from MDC consultant, the Navy laboratories represented on NAAC panels, industry members of the NAAC Stability and Performance panel, other Government agencies (Department of Defense, Air Force, Army, and NASA), industry members of the aerospace community not represented on NAAC panels, aeromechanics faculty members of colleges and universities, and the published literature.

Information was solicited from non-McDonnell Douglas sources by:

- A. Identifying and listing Government agency offices, industrial concerns, institutions, and periodicals that may provide relevant information.
- B. Identifying key personnel at the listed Government agency offices, industrial concerns, and institutions that are potential contacts for information (e. g. , NAAC panel members, AIAA members, published authors, MDC academic consultants, applicable Government agency and industry people, etc.).

- C. Conducting telephone interviews with identified key personnel, followed by letters, to describe our effort, request support in facilitating technical interchange, and offer respondents documented acknowledgment in and copies of our final reports (subject to Navy approval).
- D. Preparing and forwarding standardized aeromechanics information summary forms (one version each for experimental data/methods and analytic techniques) for completion of cooperating information sources.
- E. Meeting directly, when feasible, with survey respondents to facilitate the effective transfer of information in the form of documents, computer output, and other forms of data that require explanation and discussion.

Navy laboratories were requested to lend their on-base support to assist MDAC-W in its information-gathering task by providing aerodynamic data for existing Navy tactical missiles, rockets, bombs, and projectiles, and by performing literature searches in laboratory libraries.

An extensive literature search for relevant aeromechanics information was conducted through the MDC library system, which has divisions in each of the four prime companies of the Corporate family; the focal point for this effort was the MDAC-W library at Huntington Beach, California. Automated literature searches were conducted (via programmed key work associations) through all reference matter contained in the MDC library chain and the DOD and NASA reference systems.

## 10th Navy Symposium on Aeroballistics

### Vol. 1

Information available in periodicals not involved in automated searches (current and historical) was located and acquired through inspection of yearly subject indices and direct review of all relevant periodical articles published in the first half of 1975.

Figure 1 summarizes the current status of information acquisition activities as of 1 July 1975. At this point, only about 60 percent of the organizations contacted have responded.

Figure 2 lists the organizations and individuals contacted, and their responses to our requests for information in terms of documents, reference, and synopses supplied as of 1 July 1975. As may be noted from the figure, Martin/Orlando, General Dynamics/Pomona, Nielsen Engineering and Research (NEAR), Lockheed, and MDAC are the only aerospace concerns that have contributed significantly to this effort.

Based upon the data of Figure 2, it appears that the state of knowledge concerning linear and nonlinear aeromechanics, as relates to tactical weapons, is contained in approximately 1600 information elements or documents. The actual number of documents, reference citations, and independent synopses indicated in Figure 2 total 2102; the 1600 figure was derived assuming a duplication factor of approximately 20 percent.

### CATALOGING, CATEGORIZING, AND EVALUATION OF INFORMATION ELEMENTS

As information is acquired, it is cataloged, annotated, and summarized using formats similar to those illustrated in Figures 3 and 4 (using one format for experimental and another for analytical information), and classified in one or more of the following configuration classes:

## **SUMMARY OF INFORMATION ACQUISITION PROGRESS**

### **TO 1 JULY 1975**

12041A

1. MORE THAN 40 PERSONAL CONTACTS MADE AT 30 ORGANIZATIONS
  - ALL PROMISED SUPPORT IN ASSEMBLING STATE OF KNOWLEDGE
2. FORMAL, DETAILED REQUESTS FOR ASSISTANCE AND SYNOPSIS FORMS FORWARDED TO ALL CONTACTS
3. EIGHTEEN RESPONSES RECEIVED
  - FOUR CONSIDERED INADEQUATE
  - FOURTEEN CONSIDERED ADEQUATE
4. APPROXIMATELY 650 INFORMATION ELEMENTS (DOCUMENTS, PAPERS, ETC.) ACQUIRED TO DATE
5. 190 EXPERIMENTAL INFORMATION SOURCES EVALUATED AND SYNOPSIS
6. 50 ANALYTIC INFORMATION ELEMENTS EVALUATED AND SYNOPSIS
7. AUTOMATED "KEY WORD" LITERATURE SEARCHES COMPLETED THROUGH MDC SYSTEM, DDC, NSWC-WHITE OAK, NASA, NSRDC, AND NWC; ALL RELEVANT DOCUMENTS NOW ON ORDER

FIGURE 1

# SUMMARY OF CONTACTS AND RESPONSES

AS OF 1 JULY 1975

12042

Vol. 1

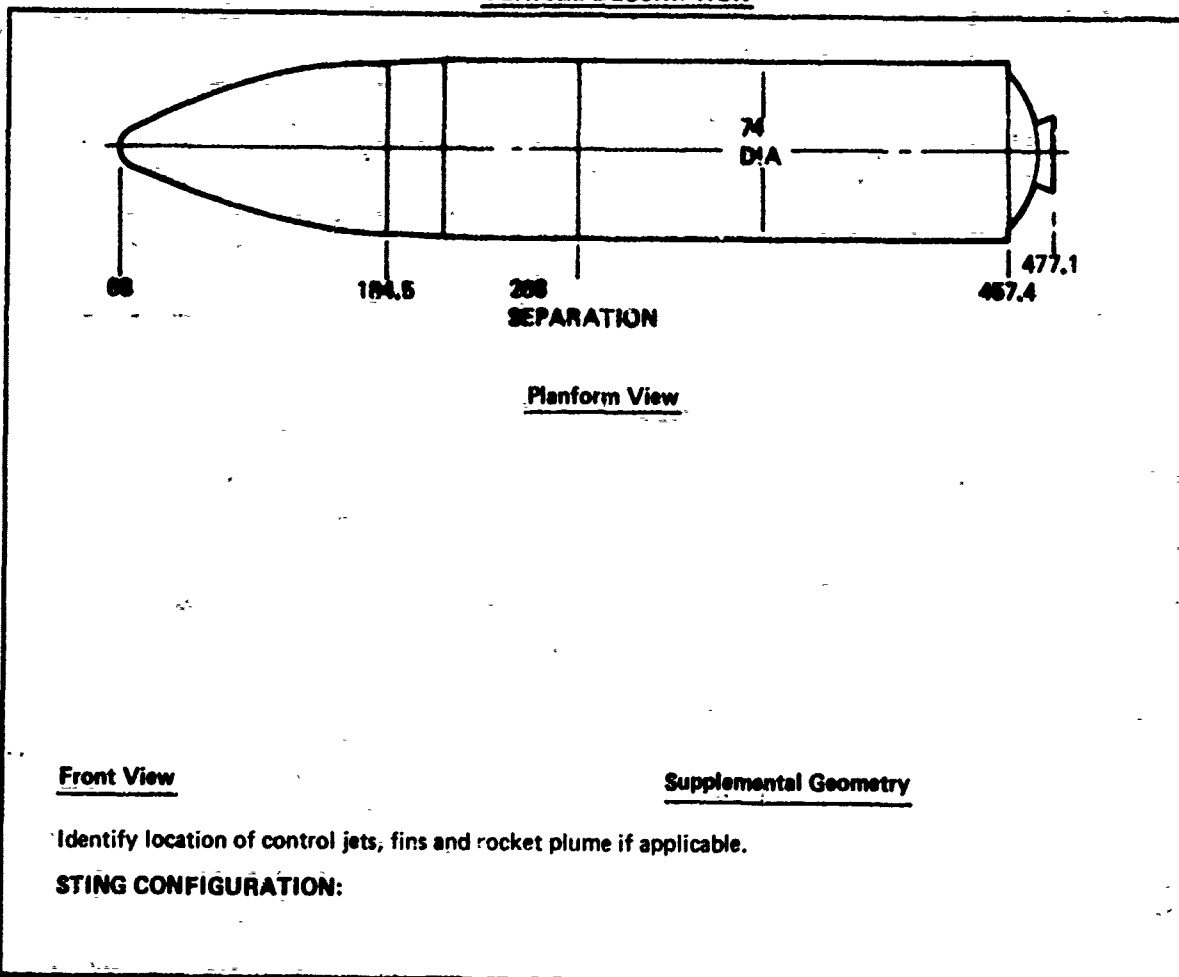
10th Navy Symposium on Aeroballistics

NAVY AGENCIES		CONTACT	DOCU- MENTS SUPPLIED	REFER- ENCES SUPPLIED	SYNOPSIS SUPPLIED	INDUSTRY - NAAC MEMBERS		DOCU- MENTS SUPPLIED	REFER- ENCES SUPPLIED	SYNOPSIS SUPPLIED
ORGANIZATION						ORGANIZATION	CONTACT			
NSWC-DANBORN		H. B. FARLEY, JR.	10		21	NEAR	J. INELSEN	8	218	
NSWC-WHITE OAK		S. M. HARTINGS	98	180+		HUGHES	J. B. HARRISBERGER			
		A. B. WARDLAW				MARTIN-G	J. FIDLER	3	~217/24	7
NSWC-CHINA LAKE		S. K. CARTER		196	7	ROCKWELL-C	F. NEWMAN			
		W. H. CLARK				GB-POMONA	F. C. THOMAS			
APL		L. E. TIDEBRAND		16		SANDERS	B. M. MEINER		14	12
NAVORD		W. B. GREENLEES				RAYTHEON	J. SMITH			
NAVVAR		T. F. MARTIN				HONEYWELL	D. P. FORSMO	2		
NSWC		R. M. HARTLEY				MDAC-W	S. SOPCZAK	~150		
		G. PICK	2	220		MDAC-E	M. M. DRIGGS			
NAAC		F. KUSTER					J. BLEDDOE			
NAVY PG SCHOOL		DR. L. V. SCHWINDT			2	OTHER INDUSTRY				
NSWC		N. L. POWER				CALSPAN	C. E. ROGERS			
		K. A. LARSEN				LOCKHEED/ LINCOLN	J. P. ANDER		12	7
						BOEING	A. M. LEVY			
						BOEING	DR. P. E. ROBERT	1		
						BOEING	R. P. SCHLESINGER			
						AIR FORCE				
						AFBFL	R. C. NELSON			
						AFATL	F. HOWARD	4	31	
						NAASA/AMES	DR. G. B. FIDLEY	2		
						ARO/AEDC	MAJOR H. M. ALBOM	1		
							MICHAEL HIGH			
LITERATURE SEARCHES										
DDC										329
NAASA										181
NSWC								141		

FIGURE 2

FIGURE 3(a)

Vol. 1

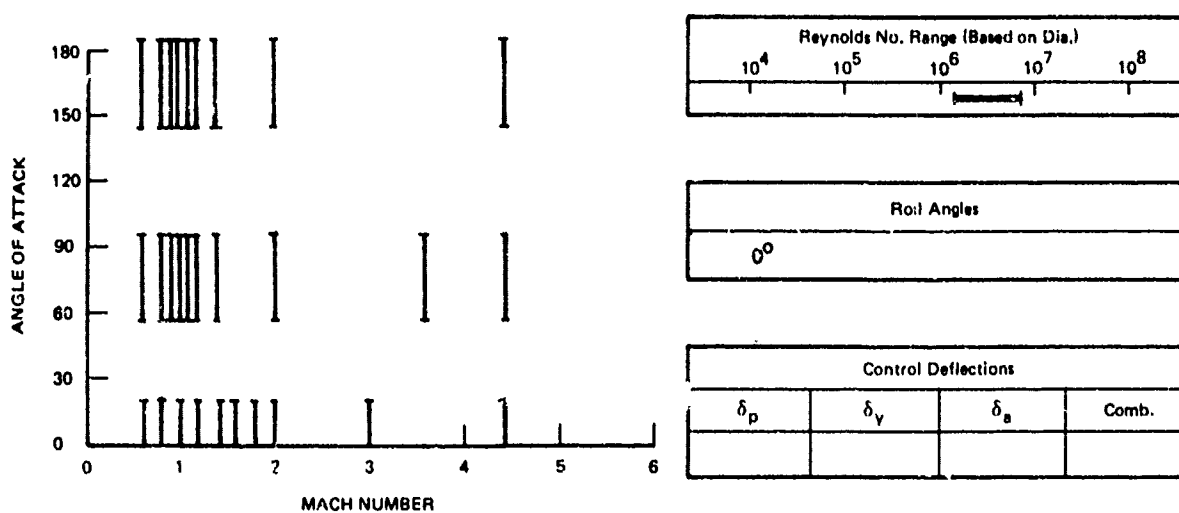
**EXPERIMENTAL AEROMECHANICS INFORMATION****INFORMATION SOURCE:** Lockheed Missiles and Space Co.**CONTACT:** N. J. French  
(408) 742-5847**VEHICLE DESIGNATION:** Poseidon C3**ABSTRACT:** Static stability test to obtain range safety data at Mach 0.6 to 4.4 and  $\alpha = 0^\circ$  to  $180^\circ$ . Tested were: 1st and 2nd stages; nose fairing alone; and 1st and 2nd stage motors alone. Also obtained was effect of simulated exhaust jet at  $\alpha = 145^\circ$ **VEHICLE DESCRIPTION****REFERENCE DOCUMENTS:** J. R. Phillips, "Results of the Transonic/Supersonic Static Stability Test of Several Poseidon C3X Configurations for Range Safety Requirements (E-75)", LMSC/D051049, TM 55-21-165, June 1962

M. V. Navone, "Presentation and Discussion of Results of Transonic and Supersonic Wind Tunnel Test AX-1 on Several C3 Poseidon Configurations", LMSC/806903, TM 55-21-106, August 1967

**TEST FACILITY DESIGNATION AND LOCATION:** Lockheed 4 x 4 Foot Supersonic Wind Tunnel, Rye Canyon, Calif.

FIGURE 3(b)  
TEST CONDITIONS

M237



AERODYNAMIC DATA

PRIMARY DATA COORDINATE SYSTEM:

Circle Appropriate  
Coefficient or  
Descriptor

Forebody and Base Axial Force Coefficients	$C_{AF}$ , $C_{AB}$ , $C_{PB}$
Normal Force and Pitching Moment Coefficients	$C_N$ , $C_m$
Side Force, Yawing Moment and Rolling Moment Coefficients	$C_Y$ , $C_n$ , $C_l$
Surface Pressure Coefficients other than Base	nose, body, afterbody
Panel Loads and Centers of Pressure	$C_{Np}$ , $C_{Hm}$ , $C_{Ap}$ , $C_{Bm}$
Dynamic Stability Derivatives	$C_{Nq}$ , $C_{mq}$ , $C_{\ell p}$
Control Effectiveness, Forces and Moments Due to Fin Motion	$\Delta C_N/\delta_p$ , $\Delta C_m/\delta_p$ , $\Delta C_Y/\delta_y$ $\Delta C_n/\delta_p$ , $\Delta C_l/\delta_a$ , $\Delta C_A/\delta$
Control Cross-Coupling	$dC_N/d\delta_a$ , $dC_l/d\delta_y$
Main Rocket Plume Simulation	Solid body, <u>cold gas</u> , hot gas
Control Jet Simulation	roll, pitch, yaw
Static Stability Derivatives	$C_{N\alpha}$ , $C_{m\alpha}$ , $C_{Y\beta}$ , $C_{n\beta}$
Others:	



**ANALYTIC AEROMECHANICS INFORMATION****INFORMATION SOURCE:** RAE Technical Report No. 66070, 1966**AUTHOR:** J. H. B. Smith**METHOD DESIGNATION:** Improved Calculations of Leading-Edge Separation from Slender Delta Wings

**DESCRIPTION OF ANALYTIC TECHNIQUE:** In Reference 1, the pressure and normal-velocity (stream-surface) conditions are enforced at only three points on the vortex sheet because of computational complexity. In the age of high-speed computers, computational complexity is less of a hindrance, and a more complete enforcement of the boundary conditions on the vortex sheet is thus carried out here. The rolled-up part of the vortex sheet is represented by a concentrated vortex, connected to the free end of the (rest of the) vortex sheet by a cut (i.e., a vortex sheet with infinitesimal strength). The position and strength of the concentrated vortex are three unknowns of the problem. The vortex sheet is broken into  $n$  finite segments, of unequal arc length, from the wing leading edge to the free end. At each end point of the segments, the distance to the concentrated vortex and the strength constitute two unknowns. The  $(2n + 3)$  unknowns of the problem are theoretically determined by  $(2n + 3)$  equations representing the no-force condition applied to the concentrated vortex plus the cut, the Kutta condition applied at the wing leading-edge and the pressure and normal velocity conditions applied at an intermediate point of each of the segments. The polar coordinates (with the concentrated vortex as the origin) of the intermediate points are the arithmetic means of those of the end points. The vortex sheet is discretized by using a first-order difference scheme for differentiation and the trapezium rule for integration along the sheet. The  $(2n + 3)$  nonlinear algebraic equations are solved by iterations in three loops. In the first loop, the  $n$  pressure conditions and the Kutta condition are used to iterate the strengths of the concentrated vortex and the vortex-segment end points. The second loop uses the no-force condition to iterate the position of the concentrated vortex. Finally, the distances between the vortex-segment end points and the concentrated vortex are iterated by using the  $n$  normal-velocity conditions. At each step of the second loop, the first loop is repeated and, at each step of third, the first two are repeated. The results of Reference 1 are used as the initial guesses for  $4\alpha/A = 0.91$ . The initial guesses for other values of  $4\alpha/A$  are obtained by linear extrapolation from existing solutions. The normal force is calculated both by integrating the surface pressure and by using contour integration in the cross-flow plane at the trailing edge. Close agreement between the two values serves as a final check on the self-consistency and accuracy of the calculations.

Note that the vortex model of Reference 2 is reached when the extent of the vortex sheet vanishes

**LIST BASIC ASSUMPTIONS:**

- (1) Small disturbances,  $\alpha \ll 1$ .
- (2) Slender delta wings,  $A \ll 1$ .
- (3) A pair of concentrated vortices and vortex sheets.

**DESCRIBE LIMITATIONS:**

(See Assumptions)

**DESCRIBE NUMERICAL METHOD:**

(See Analytic Technique)

**FIGURE 4(a)**

## CIRCLE APPROPRIATE CONFIGURATIONS

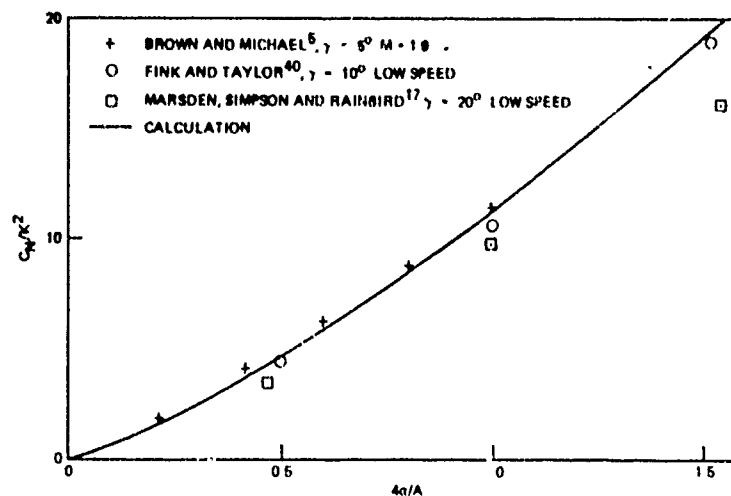
Applicable Geometries for Reasonable Precision	Body of Revolution	Non-Circular Body	W/Tail	W/Wing	Canard Control	Wing Control	Tail Control
Mach Number Range for $\pm 10\%$ Precision	Subsonic to Low Supersonic						
Angle-of-Attack Range for $\pm 10\%$ Precision	Depends Upon Aspect Ratio						
Automated? (State Language/System)	Yes						
Analytical Semi-Empirical or Empirical	Analytical						

**DEFINITIONS:** Analytical -- Based entirely on theoretical principles  
 Semiempirical -- Based on theoretical principles but using experimental data to start solutions, improve precision and/or extend applicability  
 Empirical -- Blind curve-fit or other representation of experimental data

## REFERENCES:

1. Mangler, K. W. and J. H. B. Smith, A Theory of the Flow Past a Slender Delta Wing with Leading-Edge Separation, Proceedings of the Royal Society, A-251, pg. 200-217, 1959.
2. Brown, C. E. and W. H. Michael, Jr., On Slender Delta Wings with Leading-Edge Separation, NACA TN3430, 1955

## SHOW REPRESENTATIVE COMPARISONS WITH EXPERIMENTAL DATA:



**PRECISION COMMENTS:** The Tolerances used for the convergence criteria, the extent and number of segments used for the vortex sheet all affect the accuracy and economy of the calculations. Optimum values can be obtained by trials and have been discussed in the report for  $4\alpha/A = 0.91$ . The improvements over the results of References 1 and 2 are mainly in the details of the flow field, such as the surface pressure distribution and the position of the concentrated vortex. So far as the normal-force prediction is concerned, the result is very closely matched by the first-order asymptotic result of Reference 2, and is also close to the result of Reference 1.

FIGURE 4(b)

- A. Bodies of revolution without fins (projectiles, flare stabilization, reaction-controlled bodies, etc.).
- B. Bodies of revolution with stabilizing or control tailfins - fixed or movable (bombs, rockets, missiles).
- C. Bodies of noncircular cross-section, with or without wings/fins (special-purpose missiles).
- D. Wing-or-canard control configurations with or without tailfins and/or wings.
- E. Wing-body-tail control configurations.
- F. Missile configurations whose aeromechanics are affected by internal flow (e. g. , air inlets for airbreathing propulsion, spinning tabular projectile, etc.).

Subclassification is accomplished within configuration classes with respect to the functional topics of categories delineated below:

- A. Pitch-plane static stability.
- B. Lateral-directional (yaw, or out-of-plane) static stability, including the effects of configurational unsymmetries, bank angle, asymmetric shedding of vortices, and magnus effects
- C. Dynamic stability and damping (pitch, yaw, and roll) at arbitrary incidence.
- D. Control coupling (effects of control surface deflection upon static stability in plane or about axis of deflection) and cross-coupling (static stability cross-talk from a control function in one plane or about a given axis to forces and moments in another plane or about another axis where

no control effect was intended or desired), including consideration of gyroscopic coupling effects.

- E. Roll aerodynamics, stability, and control.
- F. Interaction between aerodynamics and missile guidance and control system performance, loop stability, and design criteria, especially identification and characterization of important aerodynamic parameters and induced motion associated with the several autopilot, control, and guidance schemes.

As information is cataloged and classified, reference documentation is filed in systematic order for ease in retrieval during and after the contracted effort.

Evaluation of individual elements of the information base is conducted in two phases: (1) as the analyst reviews a given information element, the work is characterized by the filling out of the synopsis forms (Figures 3 and 4) and a comprehensive IBM Data Card Load Sheet, and (2) a review of the information content, competence, utility, and applicability is made from information contained on the completed synopsis forms.

#### AEROMECHANICS PHENOMENA IDENTIFICATION

Available experimental and analytic information found relevant to the configuration classes during information acquisition, cataloging, and classification is being studied to identify the most important aeromechanical phenomena as they relate to the stability, control, and performance of each of the several configuration classes. The prime focus is on cause-effect relationships wherein the general flowfield characteristics of each configuration class will be described, and the

variational aspects of configuration geometry as they relate to missile/flowfield interactions will be discussed. Figure 5 lists the format currently being applied to each configuration class.

#### EVALUATION OF THE COMPLETE AEROMECHANICS INFORMATION BASE

The adequacy (completeness) and utility (usefulness and applicability) of the assembled information base (representative of the state of knowledge) will be evaluated in view of current and projected Navy tactical weapon systems requirements.

Navy near-and long-term requirements for aeromechanics information in the form of experimental data and methods, and analytic predictive techniques, will be established by the sequential approach outlined in Figure 6.

Evaluation of the complete experimental information base will be accomplished by automated sorting and display of reference identification numbers by configuration class, functional topic (dependent variables), and the geometric and environmental independent variables. To facilitate experimental information base evaluation, the 80 information bits available from a single data card are allocated to fully characterize relevant reference matter, as illustrated in Figure 7. Sorting logic is currently being formulated to generate an executive code that will allow sorting by selected specific dependent variables and selected ranges of the independent variables.

With respect to the analytical literature, work has been carried out simultaneously insofar as the cataloging and the evaluation tasks are concerned. A preliminary categorization of the aeromechanics method-

# IDENTIFICATION OF IMPORTANT AEROMECHANICAL PHENOMENA

## 1. GENERAL FLOW-FIELD CHARACTERISTICS

- 1.1 LOW INCIDENCE (0 TO  $\sim 10^\circ$  OR  $180^\circ$  TO  $170^\circ$  W/O PLUME)
- 1.2 MEDIUM INCIDENCE ( $\sim 10^\circ$  TO  $\sim 25^\circ$  OR  $170^\circ$  TO  $155^\circ$  W/O PLUME)
- 1.3 HIGH INCIDENCE ( $\sim 25^\circ$  TO  $70^\circ$  OR  $155^\circ$  TO  $110^\circ$  W/O PLUME)
- 1.4 EXTREME INCIDENCE ( $\sim 70^\circ$  TO  $110^\circ$  W/O PLUME, AND  $70^\circ$  TO  $180^\circ$  WITH PLUME)

## 2. VARIATIONAL ASPECTS OF CONFIGURATION GEOMETRY

## 3. STABILIZATION AND CONTROL METHODS AND CONTROL LOOP CHARACTERISTICS

## 4. GENERAL GUIDELINES FOR THE TACTICAL WEAPONS DESIGNER IN TERMS OF CONFIGURATION SELECTION AND AIRFRAME/CONTROL SYSTEM DESIGN, SIMULATION, AND EVALUATION

FIGURE 5

12123

## **DETERMINATION OF NAVY AEROMECHANICS INFORMATION REQUIREMENTS**

- MDAC-W WILL FORMULATE DESCRIPTIONS OF CURRENT TACTICAL THREATS AND MISSIONS, AND POSTULATE PHYSICAL AND AEROMECHANICAL CHARACTERISTICS OF THE WEAPONS, CONSISTENT WITH EACH APPLICATION
- CURRENT NAVY INFORMATION REQUIREMENTS WILL BE DERIVED FROM THE VARIOUS POSTULATED WEAPON AEROMECHANICAL CHARACTERISTICS
- A SUMMARY OF THESE REQUIREMENTS AND THEIR DERIVATION WILL BE PROVIDED TO KEY PERSONS FROM NAVY LABORATORIES AND ORGANIZATIONS FOR THEIR REVIEW AND COMMENT
- MDAC-W WILL POSTULATE FUTURE THREATS AND MISSIONS, AND FURTHER POSTULATE CORRESPONDING WEAPON CHARACTERISTICS AND ASSOCIATED AEROMECHANICAL INFORMATION REQUIREMENTS

FIGURE 6

12043

## INPUT CARD LOAD SHEET DESCRIPTION

20

LOCATION	DESCRIPTION	LOGIC	LOCATION	DESCRIPTION	LOGIC
1-4	REFERENCE SEQUENCE NO.		34	CONTROL DEFLECTIONS TESTED	0 NONE
5-9	AUTHOR				1 $\delta p$
14	PRINCIPAL CONFIGURATION				2 $\delta y$
15	SECONDARY CONFIGURATION				3 $\delta a$
16	SECONDARY CONFIGURATION				4 $\delta p - \delta y$
					5 $\delta p - \delta a$
					6 $\delta y - \delta a$
					7 $\delta p - \delta y - \delta a$
					8 COMB
					0 0
TEST MACH NO.			35	BODY L/D PRIMARY	0 0 $\rightarrow$ 2
17	M = 0 $\rightarrow$ 0.6		36	BODY L/D SECONDARY	1 0 $\rightarrow$ 4
18	M = 0.6 $\rightarrow$ 0.8		37	BODY L/D SECONDARY	2 2 $\rightarrow$ 8
19	M = 0.8 $\rightarrow$ 1.0				3 4 $\rightarrow$ 10
20	M = 1.0 $\rightarrow$ 1.2				4 8 $\rightarrow$ 12
21	M = 1.2 $\rightarrow$ 1.4				5 10 $\rightarrow$ 16
22	M = 1.4 $\rightarrow$ 2.0				6 12 $\rightarrow$ 20
23	M = 2.0 $\rightarrow$ 4.0				7 16 $\rightarrow$ 30
24	M = 4.0 $\rightarrow$ 8.0				8 20 $\rightarrow$ 100
25	M = 8.0 $\rightarrow$ 10.0				9 30 $\rightarrow$ 100
			38	NOSE L/D PRIMARY	SAME AS ABOVE
			39	NOSE L/D SECONDARY	
			40	NOSE L/D SECONDARY	
			41	NOSE GEOMETRY PRIMARY	
			42	NOSE GEOMETRY SECONDARY	
			43	NOSE GEOMETRY SECONDARY	
26	MINIMUM ALPHA - FROM ABOVE ALPHA RANGE				0 CONE-BLUNTNESS
27-29	MINIMUM REYNOLDS NUMBER (BASED ON DIA)				1 CONE-BLUNTNESS
30-32	MAXIMUM REYNOLDS NUMBER (BASED ON DIA)				2 CONE-BLUNTNESS
33	NUMBER OF ROLL ANGLES TESTED (1 THROUGH 9)				3 OGIVE-BLUNTNESS
					4 OGIVE-BLUNTNESS
					5 OGIVE-BLUNTNESS
					6 CONE OR OGIVE BLUNTNESS
					7 HEMISPHERE
					8 POWER-LAW
					9 OTHERS
					0 - 0.2
					0.2 - 0.4
					0.4 - 0.6
					0 - 0.2
					0.2 - 0.4
					0.4 - 0.6
					0.6 - 1.0

FIGURE 7



## INPUT CARD LOAD SHEET DESCRIPTION (CONT)

LOCATION	DESCRIPTION	LOGIC	LOCATION	DESCRIPTION	LOGIC
44	NO. OF WING PANELS		61	(TAIL OR CANARD AR)	0
45	WING PLANFORM PRINCIPAL	0	62	PRINCIPAL	1
46	WING PLANFORM SECONDARY	1	63	SECONDARY	2
47	WING PLANFORM SECONDARY	2		SECONDARY	3
		3			4
		4			5
		5			6
48	WING s/r PRINCIPAL	NONE	64	AXIAL, DRAG OR BASE DRAG COEF	0
49	WING s/r SECONDARY	0.2	65	NORMAL FORCE/PITCHING MOMENT COEF	1
50	WING s/r SECONDARY	0.5			2
		1.0			3
		2.0			4
		3.0			5
		4.0			6
		6.0			7
		10.0			8
		100.0			9
51	WING AR PRINCIPAL	NONE	66	PANEL LOADS OR HINGE MOMENTS	0
52	WING AR SECONDARY	0	68	STATIC STABILITY DERIVATIVES	1
53	WING AR SECONDARY	0.1	70	DYNAMIC STABILITY DERIVATIVES	2
		1.2			3
		0.4			4
		0.6			5
		1.0			6
		2.0			7
		4.0			8
		10.0			9
54	NO. OF TAIL OR CANARD PANELS		71	PRESSURE COEF	0
55	PRINCIPAL	0	72	WING PLUME SIMULATION:	1
56	(TAIL OR CANARD PLANFORM) PRINCIPAL	1			2
57	SECONDARY	2			3
	SECONDARY	3			4
		4			5
		5			6
58	PRINCIPAL	NONE	73	CONTROL JETS	0
59	SECONDARY	0.2			1
	SECONDARY	0.5			2
		1.0			3
		2.0			4
		3.0			5
		4.0			6
		6.0			7
		10.0			8
		100.0			9
60			74	OTHERS	0
					1
					2
					3
					4
					5
					6
					7
					8
					9
			75-76	TUNNEL LOCATION AND DESIGNATION CODE (1-99)	
			77-80	UNASSIGNED	

## FIGURE 7

ology applicable to general wing-body-tail configurations was made after the first several months of study, as shown in Figure 8. No significant change in format has been found necessary based on work accomplished to date. The evaluation process has so far concentrated on nonlinear methods; among these methods, the leading-edge-suction-analogy method is limited to sharp-edged delta wings and the finite-element lifting-surface-theory methods are still in their infancy (e. g. , two papers were presented in AIAA 13th Aerospace Sciences Meeting, 1975) as tools for predicting nonlinear forces and moment. Furthermore, the latter methods may require excessive computing-machine time for frequent engineering use.

Some preliminary impressions regarding the two principal categories of methods of nonlinear aeromechanics can now be given. The inviscid-vortex-modeling methods are based on the solution of the linearized potential equation and are thus restricted theoretically from being applied at very high angles of attack. The nonlinear effect comes from the boundary conditions imposed on the shed vortex sheets as indicated in Figure 9. Usually the methods also invoke the slender-body approximation; hence the accuracy of results depends on a combination of the configurational slenderness and the angle of attack. Although published results often show adequate agreement with experimental data at angles of attack up to 25 degrees or even higher, it must be borne in mind that the error committed by neglecting the nonlinear terms in the differential equation becomes more significant at increasingly higher angles of attack.

09773

## **AEROMECHANICS METHODOLOGY**

### **SUITABLE FOR WING-BODY-TAIL CONFIGURATIONS**

1. LINEAR METHODS
  - a. FINITE-ELEMENT LIFTING-SURFACE-THEORY METHODS (ANALYTICAL)
  - b. SUPERPOSITION-OF-COMPONENT-CONTRIBUTIONS METHODS (SEMIEMPIRICAL) - INCLUDING INTERFERENCE EFFECTS
2. NONLINEAR METHODS
  - a. INVISCID-VORTEX-MODELING METHODS (SLENDER-BODY-THEORY)
    - i. SHEDDING FROM SHARP LEADING OR SIDE EDGES OF WINGS (ANALYTICAL)
    - ii. SHEDDING FROM SMOOTH-CONTOURED BODIES (SEMIEMPIRICAL)
      - SYMMETRIC SHEDDING
      - ALTERNATE SHEDDING
  - b. VISCOUS-CROSS-FLOW METHODS (EMPIRICAL)
  - c. LEADING-EDGE-SUCTION-ANALOGY METHOD (EMPIRICAL)
  - d. FINITE-ELEMENT LIFTING-SURFACE THEORY METHODS (ANALYTICAL)

FIGURE 8

12124

# THE INVISCID-VORTEX-MODELING METHODS

SMALL-DISTURBANCE ASSUMPTION,  $\alpha \ll 1$

$$(1 - M_\infty^2) \phi_{XX} + \phi_{YY} + \phi_{ZZ} = 0$$

SLENDER-BODY ASSUMPTION,  $d/l \ll 1$  OR  $A \ll 1$

$$\phi_{YY} + \phi_{ZZ} = 0$$

BOUNDARY CONDITIONS

ON THE BODY: ZERO NORMAL VELOCITY

ON THE VORTEX SHEET: A STREAM SURFACE

ZERO PRESSURE DIFFERENCE

FIGURE 9

When applied to configurations which experience vortex shedding at sharp edges or corners, the inviscid-vortex-modeling methods are purely analytical and the variations dwell largely on the modeling of the shed vortex sheets, as indicated in Figure 10. Although secondary and even tertiary sheddings have been observed, the methods in existence all deal with only the primary shed vortices. The simplest model is pair of concentrated vortices (viewed in the cross-sectional plane) connected to the shedding points by vortex sheets of infinitesimal strength.

The exact solution of this formulation, which requires numerical iterations to solve the nonlinear equations, usually yields a normal-force prediction which does not agree very well with experimental data. A vastly neglected fact is the virtue of an approximate, asymptotic solution. For many cases, the asymptotic solution is so simple as to be obtainable in closed form. At least for delta wings, the asymptotic solution has been shown to yield a normal-force prediction exactly the same as that yielded by the numerical solution of a much more elaborate vortex-sheet model. Understandably, subsequent efforts at modeling try to improve the prediction accuracy by distributing the vorticity over the entire vortex sheet; however, compared with asymptotic solution of the simplest model, the improvements brought about by these elaborate models at the expense of considerable calculational complexity is in the detailed description of the flow field but not in the normal-force prediction. It is felt that the asymptotic-solution-of-the-simplest-model approach should be exploited more, especially in the attack of more complicated problems such as various wing-body combinations, banked wings and cruciform wings.

12125

## CONFIGURATIONS WITH SHARP EDGES INVISCID MODELING

SIMPLEST MODEL ~ A PAIR OF CONCENTRATED VORTICES CONNECTED TO THE SHEDDING POINTS BY VORTEX SHEETS OF INFINITESIMAL STRENGTH

- NO-FORCE CONDITION
- KUTTA CONDITION

ASYMPTOTIC SOLUTION ~ THE VORTICES ARE CLOSE TO THE SHEDDING POINTS

- $\alpha < 1$ ,  $A < 1$ , AND  $\alpha/A < 1$
- SIMPLE, CLOSED FORM
- GOOD ACCURACY FOR NORMAL-FORCE PREDICTION

MORE ELABORATE MODEL ~ DISTRIBUTE THE VORTICITY

- CALCULATIONAL COMPLEXITY
- IMPROVEMENT IN FLOW-FIELD DETAILS

FIGURE 10

When the inviscid-vortex-modeling methods are applied to configurations with smooth-contoured cross sections, one element of empirical information, namely the shedding position, must be provided (Figure 11). Experience has proven, unfortunately, that the results of the computations are fairly sensitive to the shedding position. Two kinds of empiricism have been employed: one is to determine the shedding position by experimental visualization, the results of which seem to depend somewhat on the visualization technique; the other is to vary the shedding position as a parameter in the calculation until the resultant normal-force prediction matches the experimental data. So far the available shedding position experimental data have not been sufficiently well organized to indicate whether data are sufficient to cover all configurations and flow conditions of interest. The demonstrated success of isolated cases does not guarantee success in other cases. One may attempt to predict the shedding position by solving the problem of the separation of three-dimensional boundary layers, the complexity of which necessitates application of grossly simplifying assumptions and tarnishes the attractiveness of this approach. When alternate shedding occurs, additional empirical properties are needed in the inviscid modeling; some are more reliably obtainable than others. Currently most prediction methods for alternate shedding are built on the experimental work of Thomson and Morrison, who invoked the Karman vortex-street theory to relate the vortex strength and the vortex spacing, even though the real situation is far from Karman's model of two infinite rows of vortices of equal strength. Furthermore, the side-force prediction is often forced to agree with experimental measurements by introduction of additional arbitrariness such as accounting for only the first two or three vortices closest to the body.

## CONFIGURATIONS WITH SMOOTH CROSS SECTIONS

### SYMMETRIC SHEDDING ~ SHEDDING POSITION?

- EXPERIMENTAL VISUALIZATION
- MATCHING WITH EXPERIMENTAL NORMAL-FORCE MEASUREMENT
- SOLVING THE SEPARATION OF THREE-DIMENSIONAL BOUNDARY LAYERS

### ALTERNATE SHEDDING

- SHEDDING POSITIONS?
- VORTEX STRENGTHS?
- VORTEX SPACINGS?

### THOMSON AND MORRISON (1971)

#### KARMAN VORTEX-STREET THEORY

$$U_V/U = (1/2) (\Gamma/Ud) (d/l) \tan h (\pi h/l)$$

- INCOMPRESSIBLE
- TWO INFINITE ROWS OF VORTICES OF EQUAL STRENGTH

FIGURE 11



The viscous-cross-flow method, as originally formulated by Allen, is also meant for moderate angles of attack, not only because of the linearity of the potential-flow term but also because of the additive nature of the viscous correction (see Figure 12). In Allen's version, the cross-flow drag coefficient is assumed to be a constant, that of a two-dimensional cylinder in the cross flow. For a preliminary prediction method, its predictions should be viewed as satisfactory, in terms of the normal force. Subsequent efforts have aimed principally at improving center-of-pressure predictions. Kelly's resort to an unsteady analogy improves predictions for low-fineness-ratios bodies but degrades predictions for high-fineness-ratio bodies. The approach formulated by Perkins and Jorgensen makes Kelly's method purely empirical. They deduced the cross-flow contribution from the experimentally measured normal-force distribution and arrived at a correlated cross-flow drag distribution curve for ogive-nosed bodies. In this approach, the viscous term may actually contain inviscid effects left over by the linear inviscid term at higher angles of attack. Consequently the method may be applied at angles of attack higher than anticipated by Allen. In fact, design engineers often use the method up to 90 degrees of angle of attack. The distribution curve is unfortunately dependent on the configuration, especially the nose geometry; thus one curve finely tuned for one body may not be confidently used for other bodies. Another unresolved problem is how to handle the situation when the axial flow is transitional or turbulent. In contemporary applications, a recorrelated distribution of cross-flow drag is expressed as a function of dimensionless time,  $(X/d) \tan \alpha'$ , returning to the original cross-flow analogy.

## CROSS-FLOW METHODS

ALLEN (1949)

$$f = q \left[ 2(dS/dX) \alpha + 2 \eta C_{dC} r \alpha^2 \right], C_{dC} = \text{CONSTANT}$$

KELLY (1954) ~ UNSTEADY ANALOGY

$$C_{dC} = A \frac{X}{r} \tan \alpha + B \frac{X^3}{r^3} \tan^3 \alpha + C \frac{X^5}{r^5} \tan^5 \alpha$$

PERKINS AND JORGENSEN (1954)

$$C_{dC}/C'_{dC} = f(X/lm)$$

GOLDMAN AND BRIGGS (1973)

$$C_{dC}/C'_{dC} = f(x/d \tan \alpha')$$

FIGURE 12

Finally, it should be pointed out that existing literature on the methods discussed here show applications mostly to individual missile components, such as wings and bodies. Much development work obviously lies ahead for realistic missile configurations.

#### REMAINING EFFORT TO BE ACCOMPLISHED

The information acquisition task has proven to be much more time-consuming than originally anticipated, mainly due to a distinct lack of spontaneous response to our requests for information and support. In general, it may be said that it is relatively easy for an individual to verbally accept a responsibility to support an ambitious and needed effort such as this survey and evaluation, but it is entirely a different matter for him to deliver a meaningful response that requires his setting aside his own, funded duties to fulfill a request that will bring no direct remuneration. As a result of information acquisition problems, the scheduled periods for Tasks 1 and 2 have been stretched, thus crowding the remaining tasks into a few months, as illustrated in Figure 13.

Planned near-term activities, that will be completed in time for the NAAC panel meetings in October, are listed in Figure 14.

The state of knowledge concerning nonlinear aeromechanics, as represented by the information accumulated and derived in Tasks 1 and 2 of Figure 13, will be summarized in the Final Report—Volume I. The assembled experimental methods and data base, and analytic methodology will be completely discussed in terms of specific individual information sources and characterization of the content of such sources. Information summaries of each referenced source will contain a crisp verbal sum-

12122

# REVISED SCHEDULE SURVEY AND EVALUATION OF NONLINEAR AEROMECHANICS

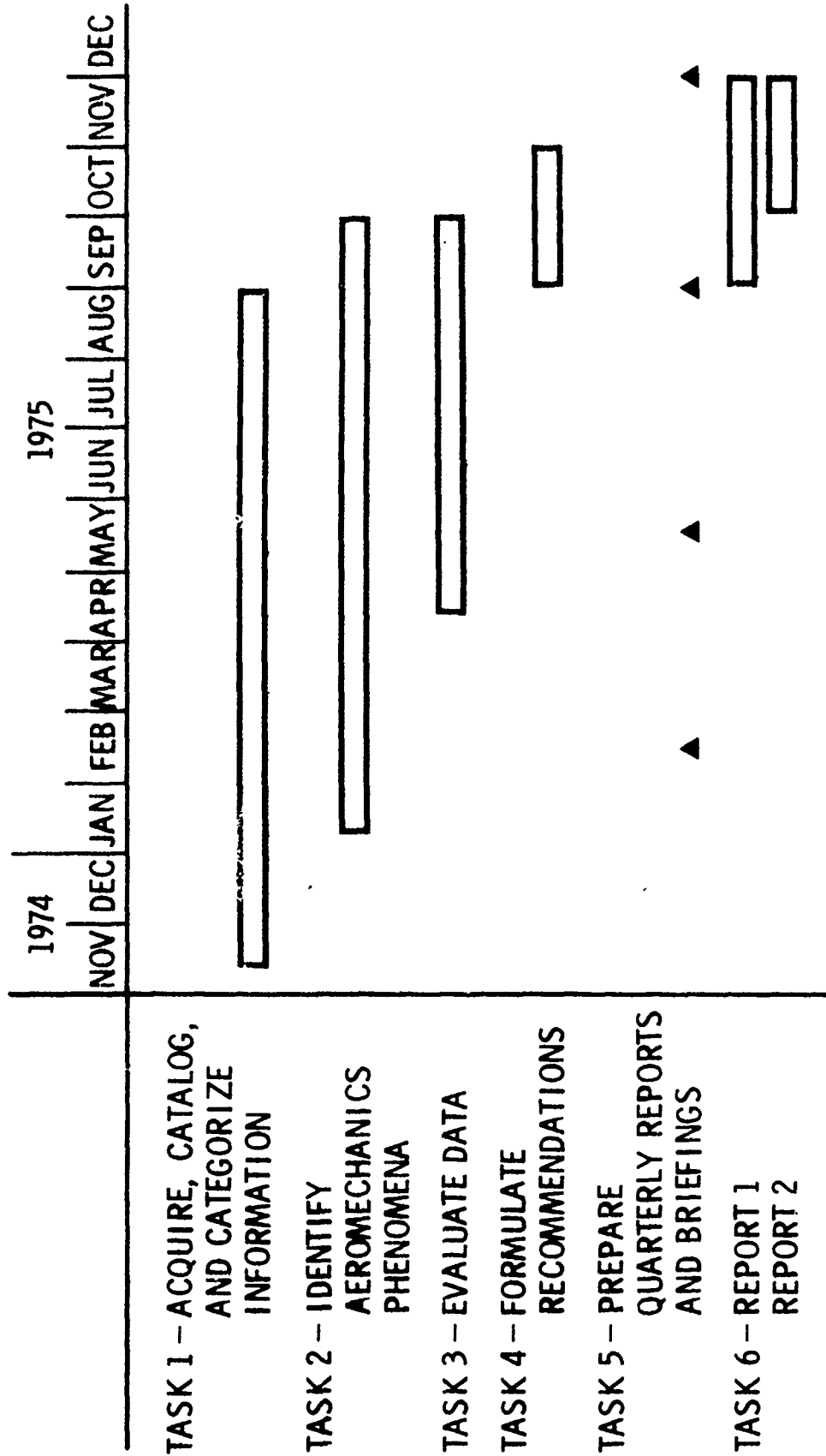


FIGURE 13

12121

## PLANNED NEAR - TERM ACTIVITIES

- EVOLUTION OF SORTING LOGIC AND CODE TO ALLOW AUTOMATIC DATA BASE CHARACTERIZATION
- ACCELERATED APPLICATION OF REVISED INFORMATION ACQUISITION APPROACH
- ORDERING OF DOCUMENTS IDENTIFIED IN NASA AND DDL LITERATURE SEARCHES
- ACCELERATED EVALUATION/SYNOPSIZING OF INFORMATION ELEMENTS
- IN-DEPTH STUDY AND IDENTIFICATION OF IMPORTANT AEROMECHANICAL PHENOMENA

FIGURE 14

**Vol. 1**

mary, configuration sketches where relevant, important geometric and aeromechanics parameters, and examples of results.

Subsequent to evaluating the adequacy and utility of the assembled aeromechanics information base in terms of Navy requirements, deficiencies in the information base will be identified and characterized. Alternative active steps required to make the technology base meet Navy requirements will be postulated for further evaluation in terms of cost effectiveness; the most cost-effective active steps will then be identified, and recommendations will be formulated that encompass the desired spectrum and sequence of activities. The recommendations will be presented in Volume II of the final report.

The MDAC-W assessment of the state of knowledge concerning nonlinear aeromechanics will be documented in a report that comprehensively encompasses all of the work accomplished under Tasks 3 and 4 of Figure 13 (evaluation of state of knowledge and formulation of recommendations). This report will identify and discuss the inadequacies and deficiencies existing in the nonlinear aeromechanics technology base, and recommendations for remedial action will be made. Although this report will necessarily summarize (in brief) the Volume I work wherein the information/technology base was assembled and documented, the contents of the Volume I report may be heavily referenced. It is thus felt that the two physically separate report volumes, coupled as a unified work, will provide the user maximum usefulness.

**TENTATIVE CONCLUSIONS**

Based upon our comprehensive review of several hundred experimental information sources, and the reading of the abstracts and synopses of

more than a thousand others, it is concluded that if the complete experimental information base were made generally available, the need for wind tunnel testing would be obviated insofar as preliminary design and advanced development of axisymmetric or cruciform weapons is concerned; this is especially true as regards bodies of revolution with or without tailfins. The amount of near-duplication in the information base is significant, underscoring the lack of real, useful communication between aeromechanics practitioners, and an apparent general reluctance to pursue the historical information base due to time limitations or lack of an effective approach. In recent years, high-incidence wind tunnel testing has been pursued in the context of evolving new weapons systems and for purely heuristic purposes, to the extent that high-incidence technology has been heralded as an area of severe need, almost as an end in itself. The historical information base shows that numerous high-incidence wind tunnel tests have been conducted, over the past 25 years, and that contemporary aeromechanics problems are in most respects similar to those treated and studied by aeromechanics specialists in the 1950s.

Insofar as analytic methods are concerned, most of the emphasis has been upon development and extension of the applicability of over-simplified methods, wherein underlying simplifying assumptions are too readily violated in application of a certain method; instead of reducing the extent of simplifying assumptions and reformulating the problem, most analysts try to extend analytic methods into regions where they are not well-posed by adding empiricisms or by arbitrary selection of otherwise unspecified boundary conditions. Finally, the emphasis upon numerical methods

associated with iterative solution using automatic computing machines has led analysts away from pursuing more complete analytic specification of their methods to thus allow formulation and solution of more complex, detailed flow-field problems that would otherwise defeat or render impractical the more numerically-solved methods.



PAPER NO. 2

AERODYNAMIC ROLL CHARACTERISTICS  
OF CANARD MISSILES

Richard E. Meeker

Naval Weapons Center  
China Lake, California

## INTRODUCTION

The canard controlled airframe has several features which make it attractive for use in guided missiles. The fact that the seeker, guidance computer, servo system, warhead and propulsion system can be located in sequence from front to rear naturally tends to minimize the number of joints and the number of electrical or hydraulic lines which must pass through the warhead and the propulsive unit. The canard is also a powerful control capable of trimming a missile to large angles of attack and producing high levels of maneuverability. As an example, these features are very attractive for incorporation into a family of modular weapons.

However, there are a few difficulties. The canard airframe tends to possess highly non-linear aerodynamic characteristics, including large induced rolling moments, which are complex functions of the control deflections, angle of attack, roll attitude and Mach number. These characteristics have greatly complicated the complete six-degree-of-freedom simulations of missile motions. Also, the use of the canards for roll control by differential deflections has been shown, in a few tests, to be impractical due to large variation of the roll control power, even control reversals, with angle of attack and Mach number.

The objective of the work described in this paper is to develop a better understanding of the induced roll characteristics of the canard missile airframe and thus perhaps stimulate fresh thinking about ways to alleviate problems related to roll control.

PROGRAM OVERVIEW

In order to meet the objectives of the program, three separate but related efforts have been pursued as follows:

- A. Development of an engineering method of predicting the induced rolling moments.
- B. Investigation of a method for more simply modeling the aerodynamic characteristics for simulation purposes.
- C. Experimental investigation of promising concepts for alleviating the effects of large induced roll moments and producing roll control.

The first two items are discussed in this paper. Due to financial limitations only one concept for alleviating induced roll moments could be investigated - the use of slots in the canards and/or tails. That will be the subject of a paper to be presented by Mr. Pete Daniels of Naval Surface Weapons Center, Dahlgren Laboratories.

ENGINEERING PREDICTION

The development of a method for predicting the induced roll characteristics of canard controlled missiles was contracted to Nielsen Engineering and Research, Inc. (NEAR) of Mountain View, California. The method was to be of engineering application in nature and to cover subsonic and supersonic speeds, arbitrary roll attitudes, angles of attack up to 20 degrees and pitch and yaw control deflections up to 20 degrees in any combination.

It is impossible to do justice to the work of NEAR in a short space. The reader is urged to consult the references at the end of the paper for a detailed description of the prediction method and its development. The following is a very brief review of the work and some of the results obtained to date.

The first step was to assess the (at that time) state-of-the-art. To this end, NEAR calculated the induced roll moments for the Navy AIM-9L Sidewinder missile, shown in Fig. 1. Consideration was given to panel-panel interference effects and primarily, to canard vortex-tail interference effects. The results of one such calculation are shown in Fig. 2. As can be seen, the results show a reasonable reproduction of the trends with angle of attack, for the orientation shown, but the calculated magnitudes are about 50 percent of the wind tunnel data. As a result of these calculations, it was determined that difficulties existed primarily in the following areas:

- A. Panel-panel interference effects, small for the AIM-9L, might still be important for other canard configurations.

- B. The method used to obtain a relation between the canard span loading and shed vorticity needed experimental verification.
- C. The effect of vortices shed from the body, particularly aft of the canards, was entirely neglected, but was considered important.
- D. Interactions between free vortices and between bound or free vortices and lifting surfaces needed further development.

In order that these effects might be better assessed, the next step was a wind tunnel test. The model, shown in Fig. 3, was supplied by the Army Missile Command at Redstone Arsenal and the tests were performed by NASA Ames Laboratory. Tests were performed to both Army and Navy requirements. The Navy portion of the test encompassed Mach numbers of 0.8, 1.3 and 1.75, at angles of attack from 0 to 24 degrees, roll angles of 0, 10, 20, 30 and 45 degrees and canard deflections of 0 and 15 degrees. Three component force and moment data were obtained for each canard and tail panel as well as six-component data for the total model. Vapor screen and schlieren photographs were obtained at selected test conditions. NEAR has analyzed the needed portions of the force data and the vapor screen data. Again, the reader is referred to the references for more details of the test. A report of the test will also be published by NASA in the future.

Based on the analyses of the test data NEAR then completed the method for predicting the rolling moments. The method incorporates

the use of non-linear wing alone normal force information for the canard and tail panels. The method accounts for the effects of nose vortices, canard vortices and afterbody vortices. Vortex trajectories are computed to the tail and the effects on the tail are computed. Control cross coupling and panel-panel interference effects are included.

As of this time, the method has been checked against data to a very limited extent. The result of one comparison is shown in Fig. 4. As may be seen the results show fair agreement. The results of about four other check cases compared so far show both better and worse agreements. Checking and assessment of the method will continue next year.

## SIMPLIFIED MODELING OF AERODYNAMICS

One of the stumbling blocks to accurate six-degree-of-freedom simulations is the large increase in the amount and complexity of the aerodynamic information which must be input to the computer to describe the effects of varying roll attitude. The objective of this part of the program was to investigate the utility of a proposed simplified way of representing the pitch and yaw canard control deflections and their effects on the aerodynamics of a canard controlled missile.

This notation will be referred to as the phase angle axes system or PAAS. The basic idea and the notation used is illustrated in Fig. 5. Note that  $\alpha_T$  and  $\phi_M$  represent the standard aeroballistic quantities of total angle of attack and aerodynamic roll angle. In the same fashion  $\delta_M$  and  $\phi_S$  describe a total control deflection and a roll orientation of that total control deflection. Note also that, in a wind tunnel test  $\alpha_T$  and  $\delta_M$  would remain fixed in space relative to the tunnel axes, i.e.,  $\phi_S$  would remain fixed while  $\phi_M$  is varied. Thus, the pitch and yaw control deflections  $\delta_p$  and  $\delta_y$ , would vary as the model is rolled. As will be shown subsequently, this definition of the control deflections makes the aerodynamic coefficients nearly independent of the missile roll attitude, at least for the two configurations checked so far.

The first test of the concept was performed by conducting a wind tunnel test with a model designed so that the quantities  $\delta_M$  and  $\phi_S$  could be directly set into the model and held constant while  $\alpha_T$  and  $\phi_M$  were varied. The tests were conducted in the AEDC tunnel 1T under the sponsorship of the Air Force Armament Laboratory at Eglin Air Force Base. The configuration tested is shown in Fig. 6. Typical results

are shown in Figures 7 through 11. Coefficients of normal force, side force, pitching moment, yawing moment and rolling moment are shown. These results show that the coefficients are nearly independent of aerodynamic roll attitude,  $\phi_M$ , for fixed values of  $\delta_M$  and  $\phi_S$  over the range of angle of attack tested.

A second check of the concept was made by converting the Sidewinder AIM-9L wind tunnel data to the PAAS. The missile configuration is shown in Fig. 1. Typical results are shown in Figures 12 through 17. Figures 12, 14 and 16 each show coefficients of pitching moment, yaw moment and roll moment for conventional fixed canard deflections for various roll orientations. Figures 13, 15 and 17 show similar data converted to the PAAS. As before, the PAAS curves show much less dependence on the roll angle.

The ultimate utility of this concept depends of course upon how broad its application may be, and from this point on, that will depend largely on how many other people will investigate the idea. At NWC, it is planned to incorporate the PAAS formulated aerodynamic data for Sidewinder into a digital simulation currently in use.



## REFERENCES

1. Nielsen Engineering & Research, Inc. A Study of Induced Rolling Moments for Cruciform-Winged Missiles, by J. N. Nielsen, S. B. Spangler, and M. J. Hemsch. Mountain View, Calif. NEAR, December 1973. (NEAR TR 61).
2. \_\_\_\_\_. Test Report for Canard Missile Tests in Ames 6- by 6-Foot Supersonic Wind Tunnel, by M. J. Hemsch and J. N. Nielsen. Mountain View, Calif., NEAR, August 1974. (NEAR TR-72).
3. \_\_\_\_\_. Reduced Vapor Screen Data from Canard Missile Tests in Ames 6- by 6-Foot Supersonic Wind Tunnel, by M. J. Hemsch. Mountain View, Calif., NEAR, February 1975. (NEAR TR 81).
4. \_\_\_\_\_. The Induced Rolling Moments of Cruciform Wing-Body Combinations as Influenced by Panel-Panel Interference, by J. N. Nielsen, M. J. Hemsch, and M. F. E. Dillenius. Mountain View, Calif., NEAR, November 1974. (NEAR TR-75).
5. \_\_\_\_\_. Further Studies of the Induced Rolling Moments of Canard-Cruciform Missiles as Influenced by Canard and Body Vortices, by J. N. Nielsen, M. J. Hemsch, and M. F. E. Dillenius. Mountain View, Calif., NEAR, January 1975. (NEAR TR 79).
6. \_\_\_\_\_. Method for Calculating Induced Rolling Moments for Cruciform Canard Missiles at Angle of Attack up to  $20^\circ$ . M. J. Hemsch, J. N. Nielsen, and M. F. E. Dillenius. Mountain View, Calif., NEAR. (NEAR TR 85). Also published as NWC TP 5761.
7. R. A. Paulk - ARO, Inc., "Canard Control Study of the Induced Roll Model at Mach Numbers 0.7, 1.15, and 1.4" - Final Report for Period 10 July - 12 September 1973 - February 1974. AEDC-TR-74-e - AFATL-TR-74-2.
8. Naval Weapons Center. AIM-9L Wind Tunnel Test Report, by E. M. Piper and A. E. Brown. China Lake, Calif., NWC, October 1972. (NWC TN 4063-233).

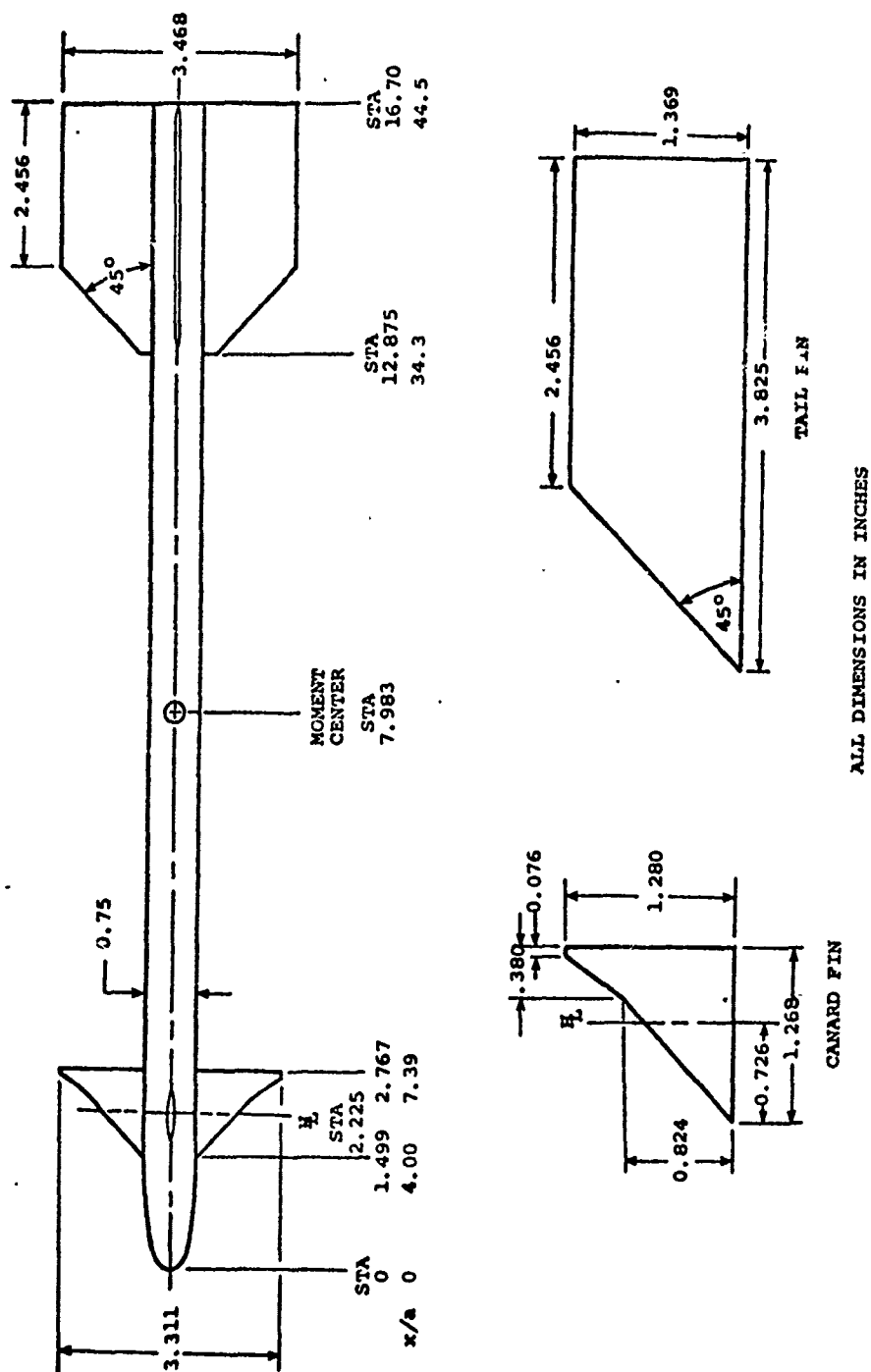
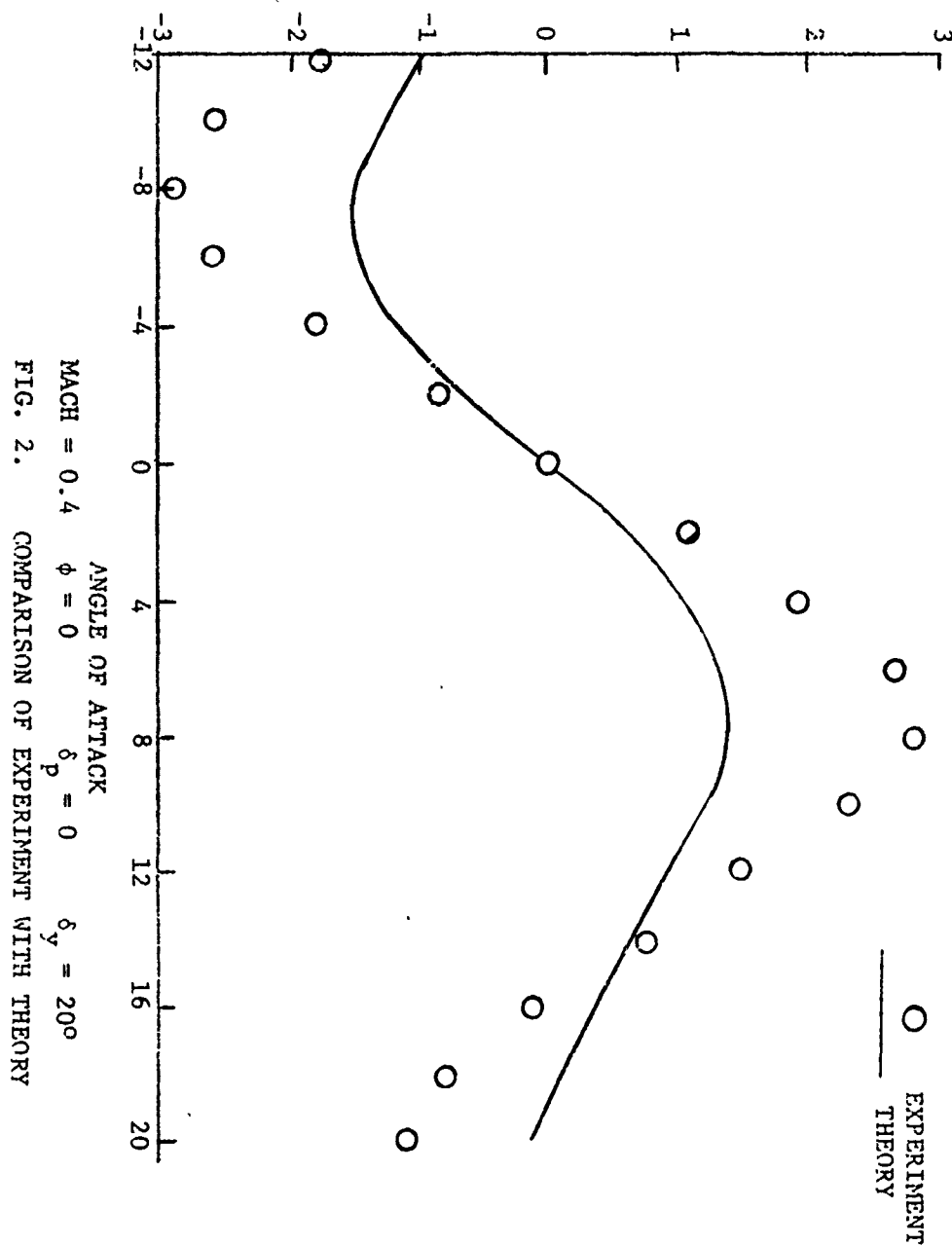


FIG. 1. AIM-9L SIDEWINDER WIND TUNNEL MODEL

## ROLL MOMENT COEFFICIENT



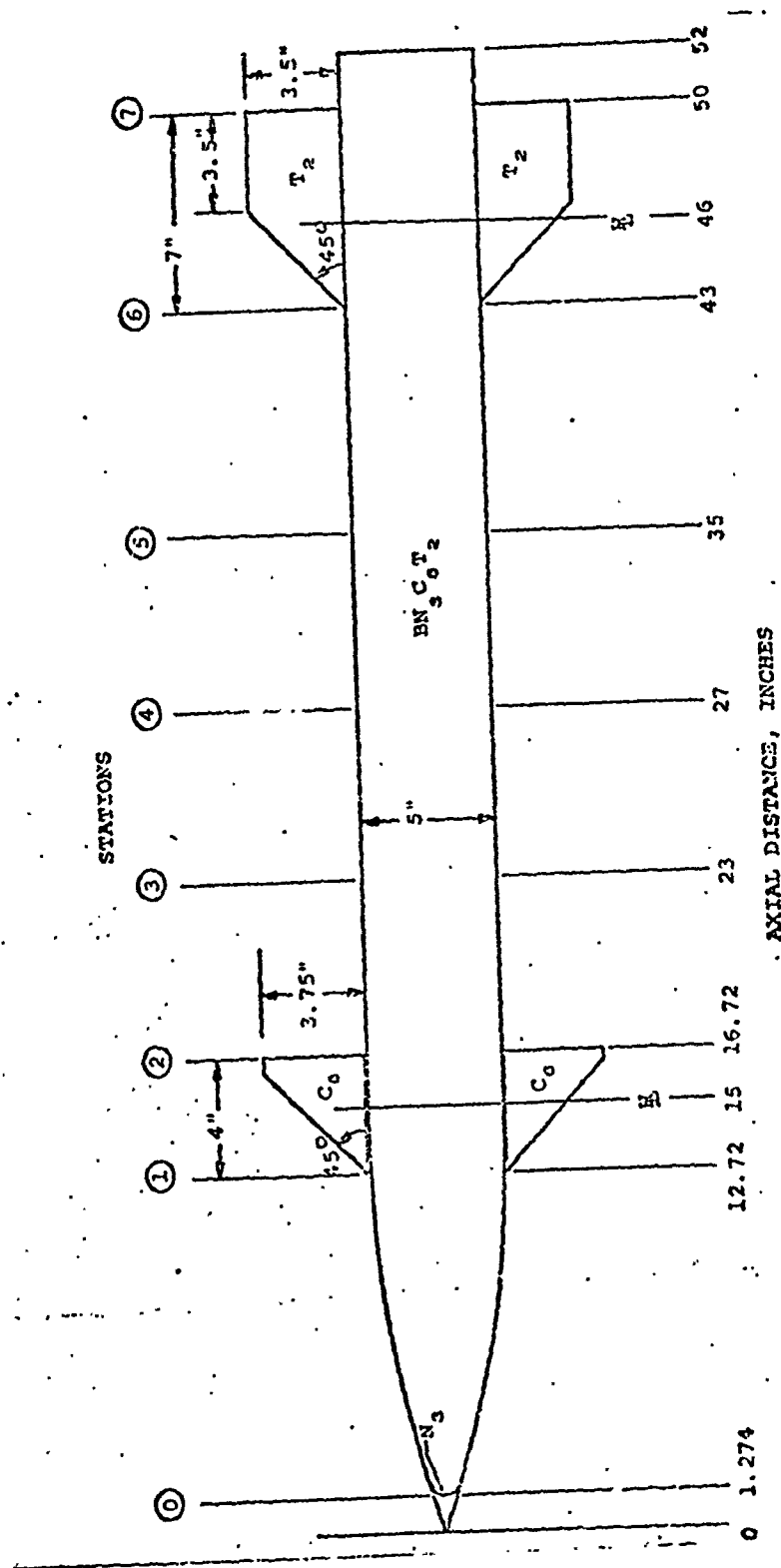
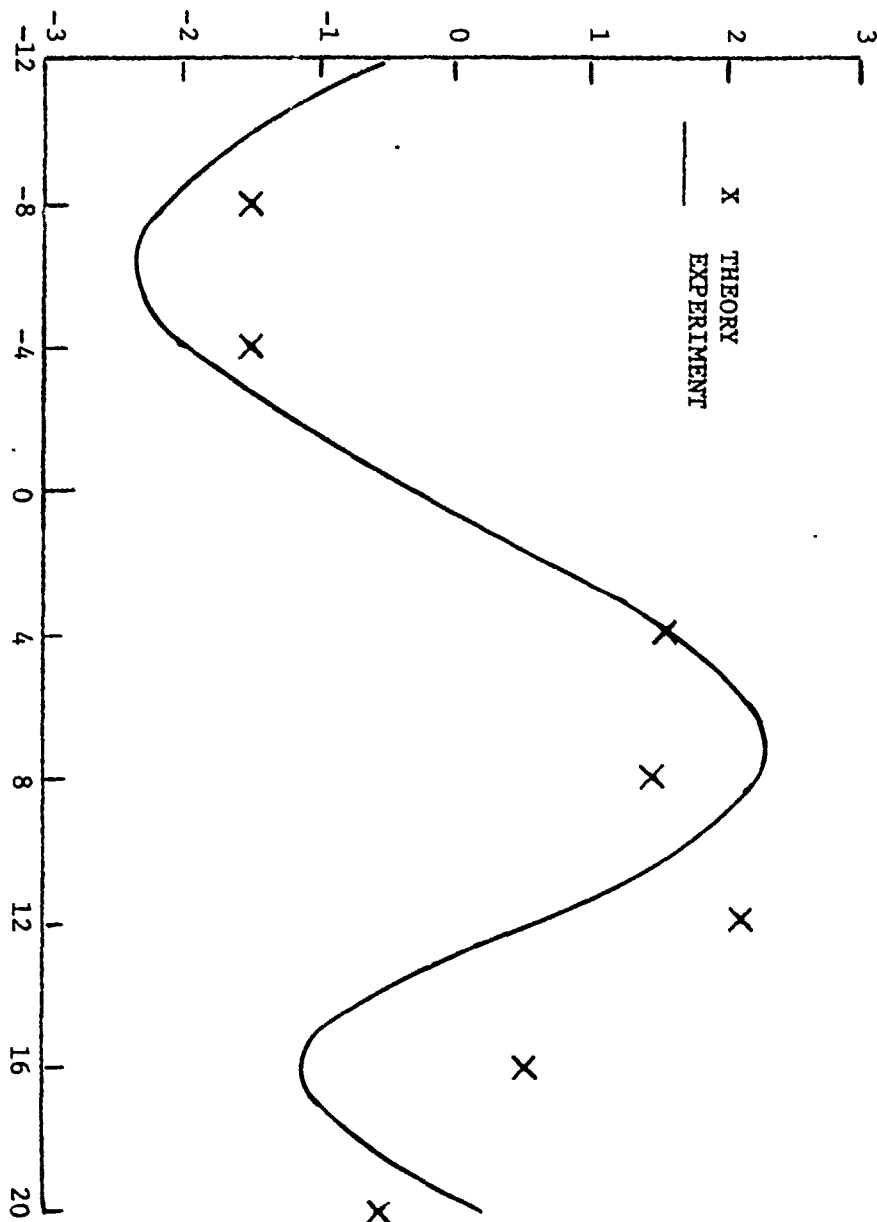


FIG. 3. AMES WIND TUNNEL TEST MODEL

## ROLL MOMENT COEFFICIENT



ANGLE OF ATTACK  
Mach = 1.75  $\phi = 0$   $\delta_p = 0$   $\delta_y = 20$   
FIG. 4. COMPARISON OF EXPERIMENT AND THEORY

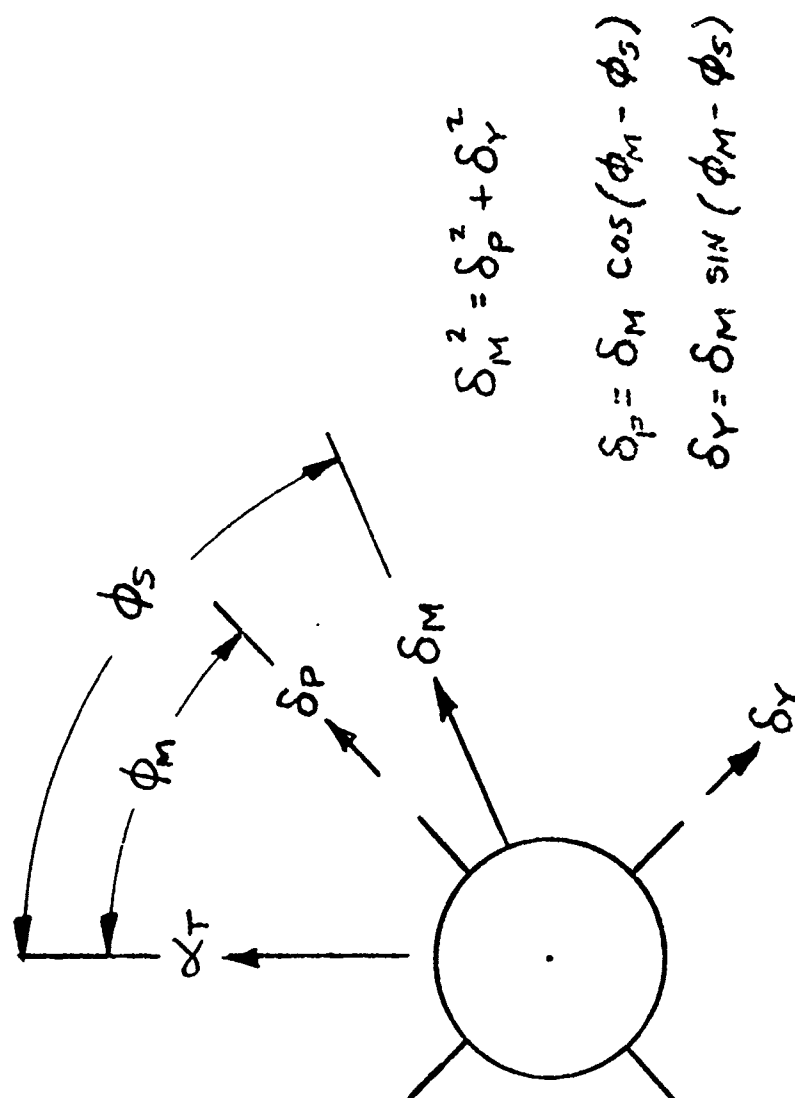
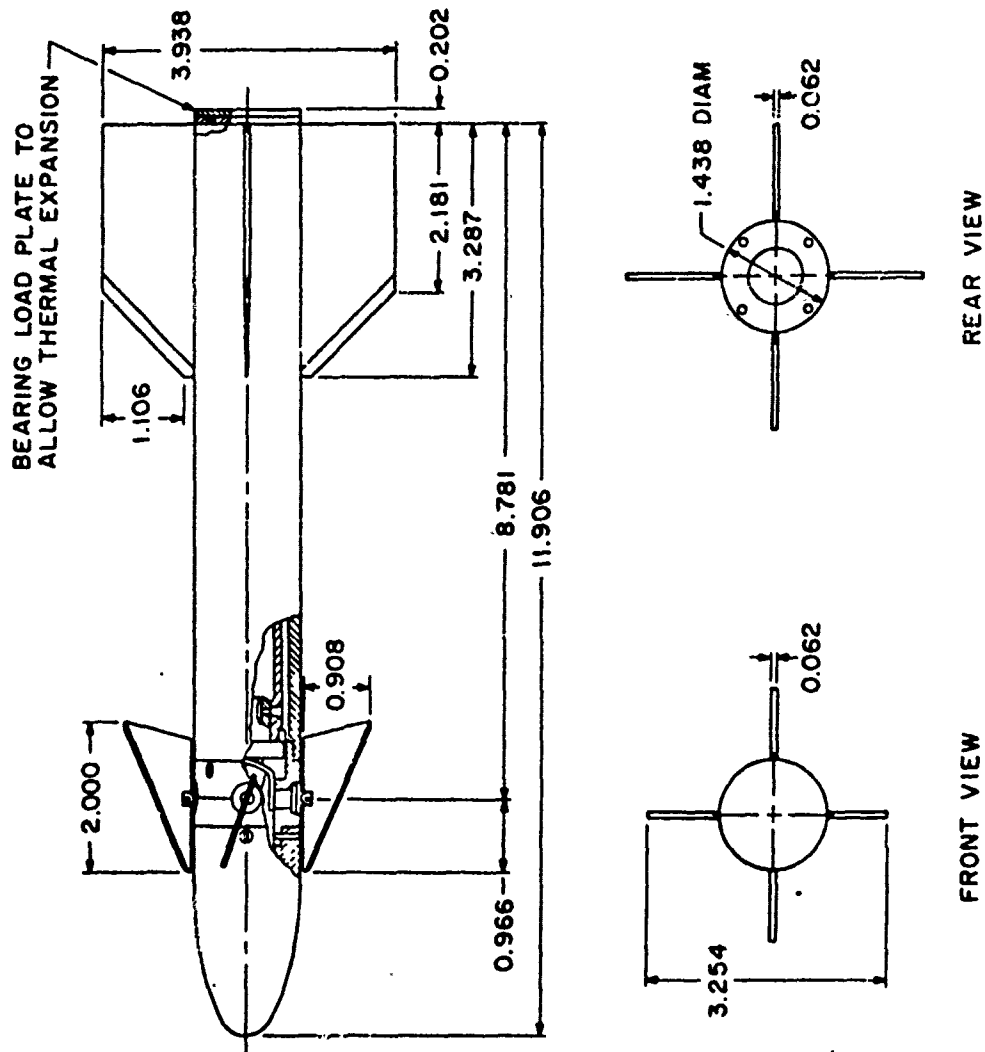


FIG. 5. PHASE ANGLE AXIS SYSTEM



SYMBOL	M	•S	•M	•M	
□	.7	90	0	10	225
○	.7	90	30	10	211
△	.7	90	60	10	217
◊	.7	90	90	10	222

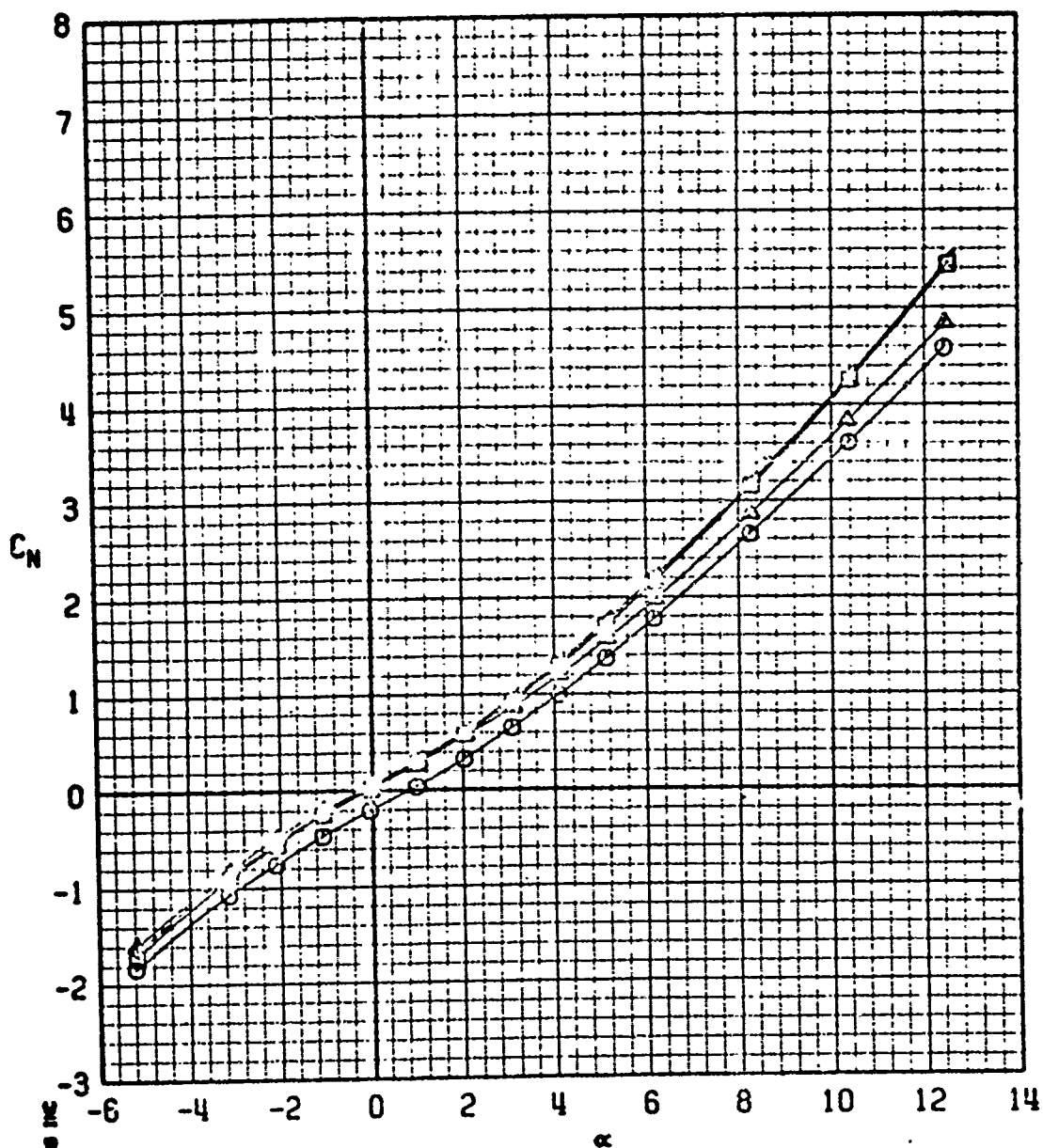


FIG. 7



SYMBOL	M	$\phi$ S	$\phi$ M	$\phi$ H	
□	.7	90	0	10	225
○	.7	90	30	10	211
△	.7	90	60	10	217
◊	.7	90	90	10	222

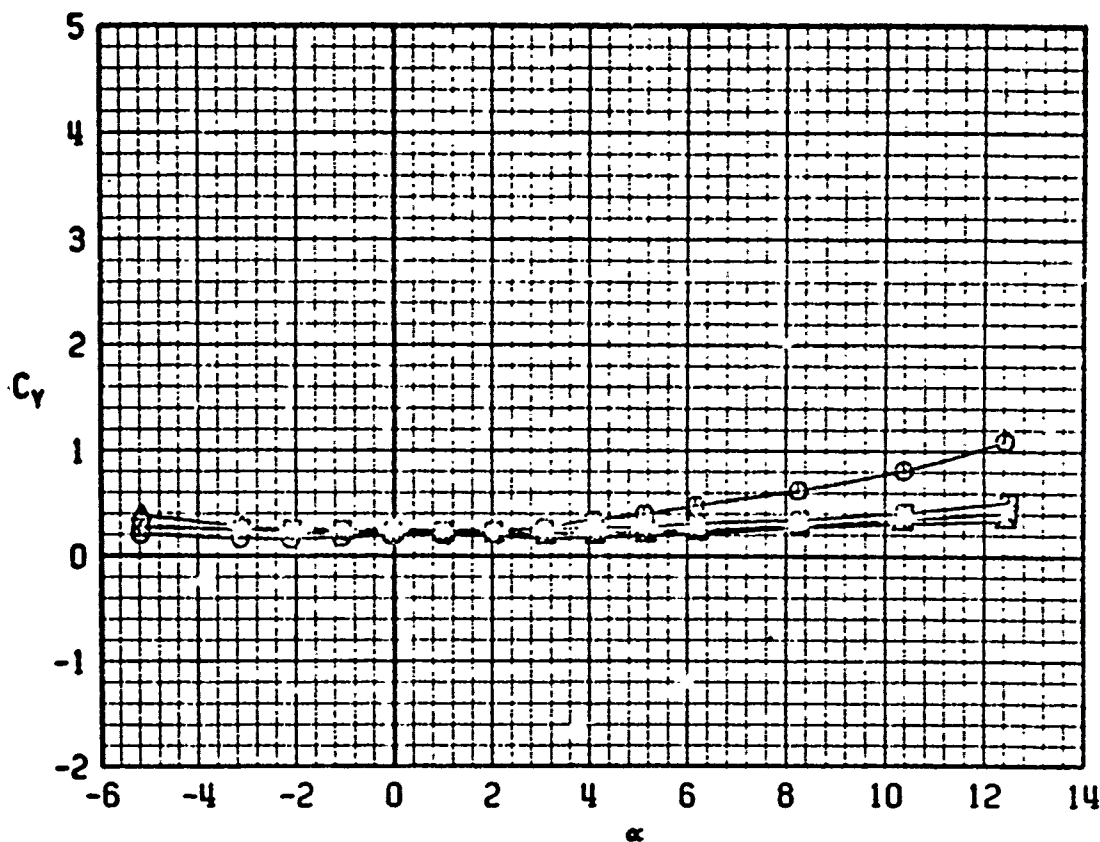


FIG. 8

SYMBOL	M	$\phi S$	$\phi M$	$\phi H$	
□	.7	90	0	10	225
○	.7	90	30	10	211
△	.7	90	60	10	217
4	.7	90	90	10	222

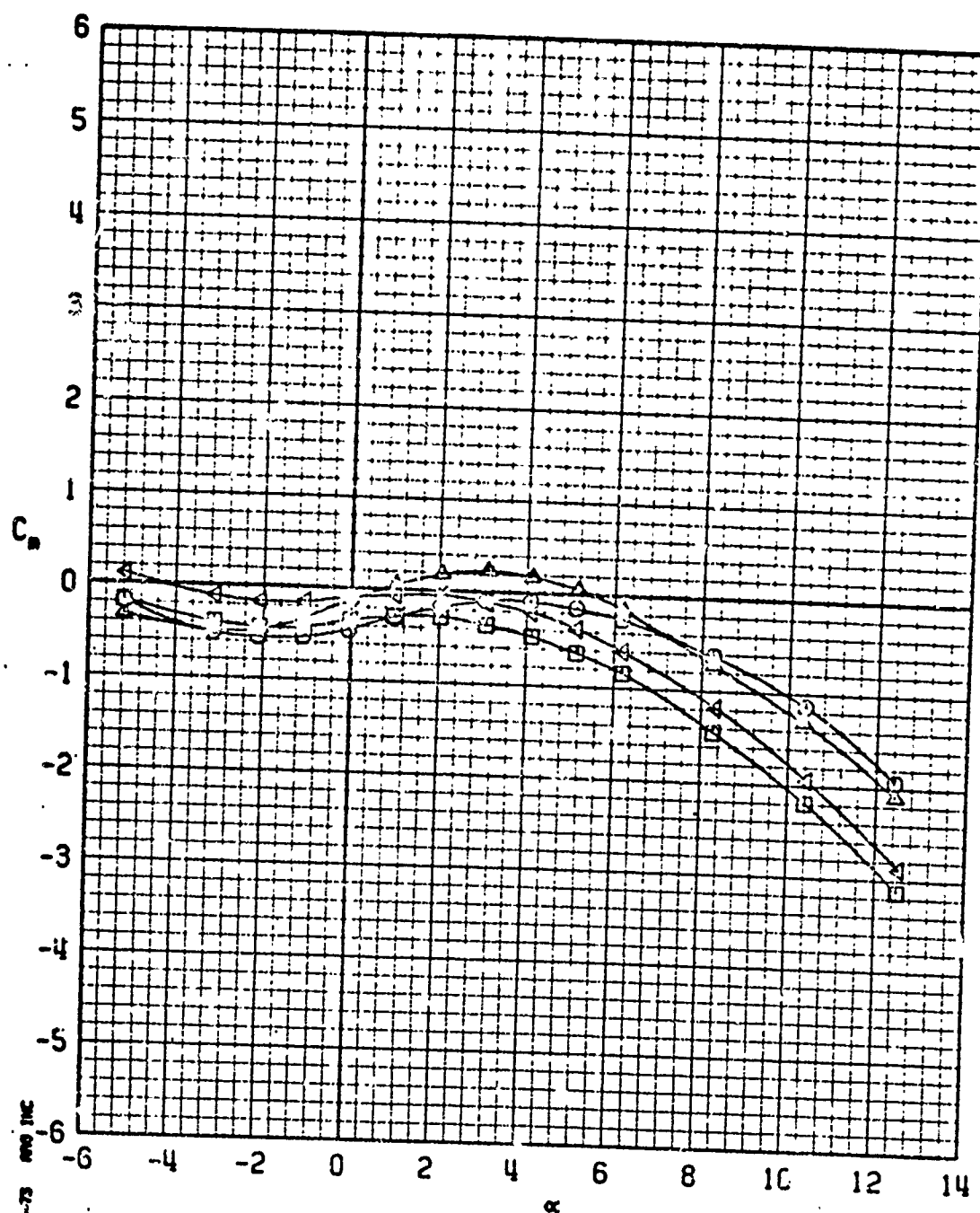


FIG. 9

SYMBOL	M	$\phi$ S	$\phi$ M	$\phi$ M	
$\square$	.7	90	0	10	225
$\circ$	.7	90	30	10	211
$\triangle$	.7	90	60	10	217
$\nabla$	.7	90	90	10	222

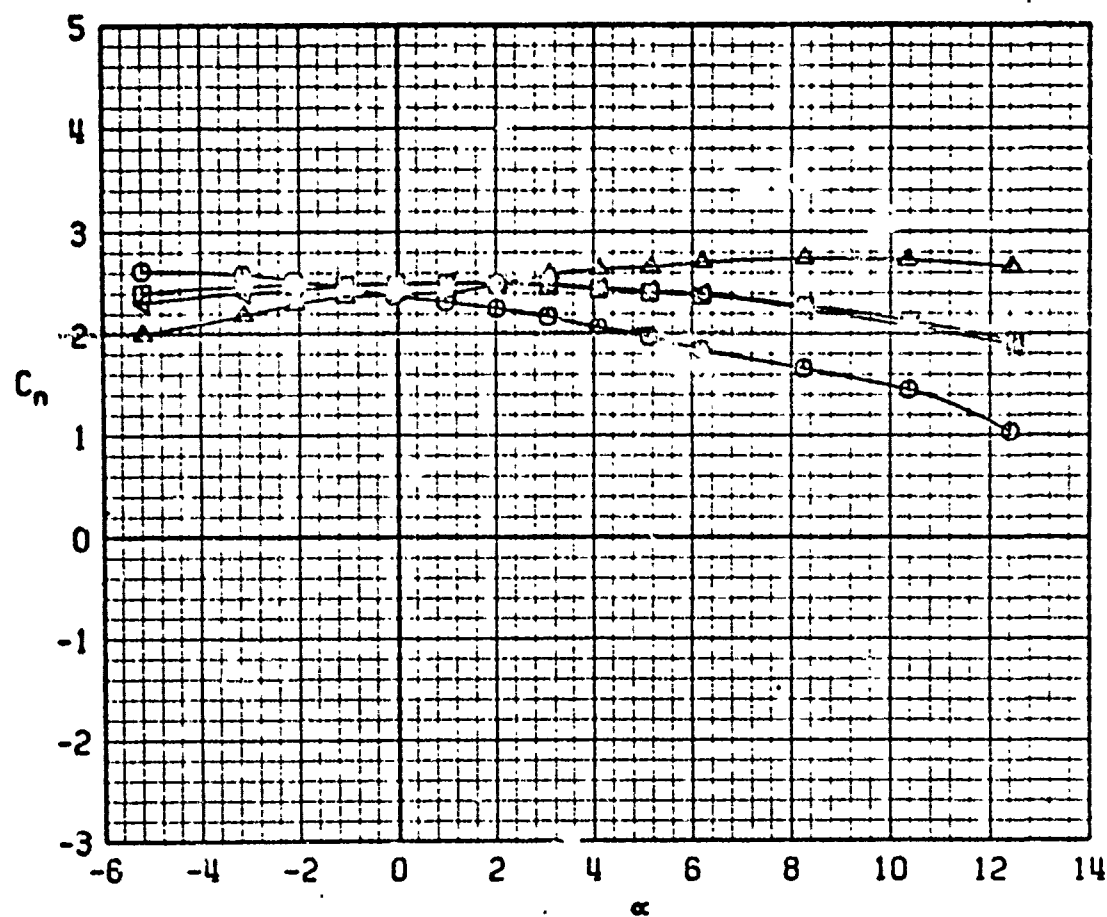


FIG. 10

SYMBOL	M	$\delta S$	$\delta M$	$\delta K$	
$\square$	.7	90	0	10	225
$\circ$	.7	90	30	10	211
$\triangle$	.7	90	60	10	217
$\diamond$	.7	90	90	10	222

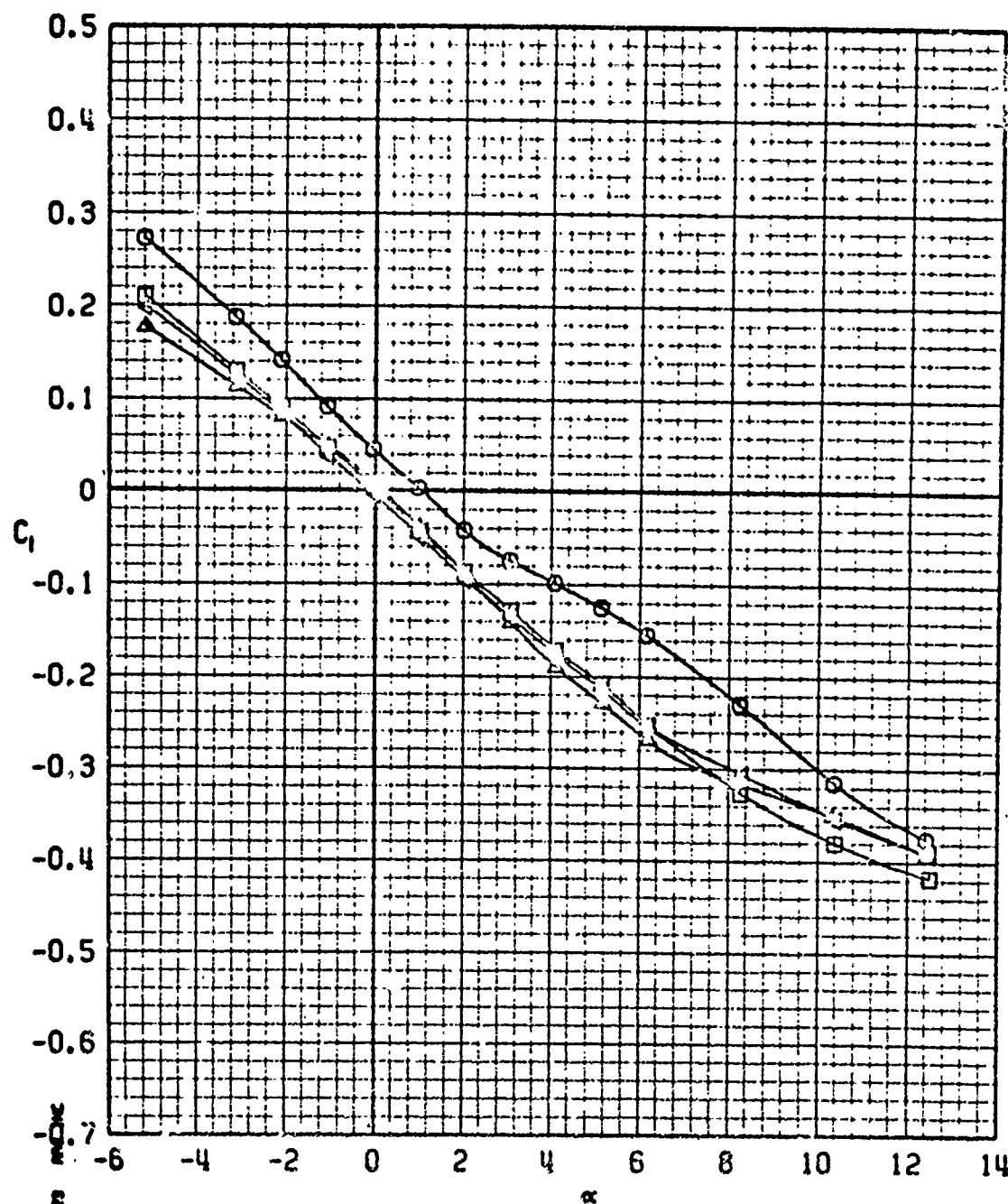
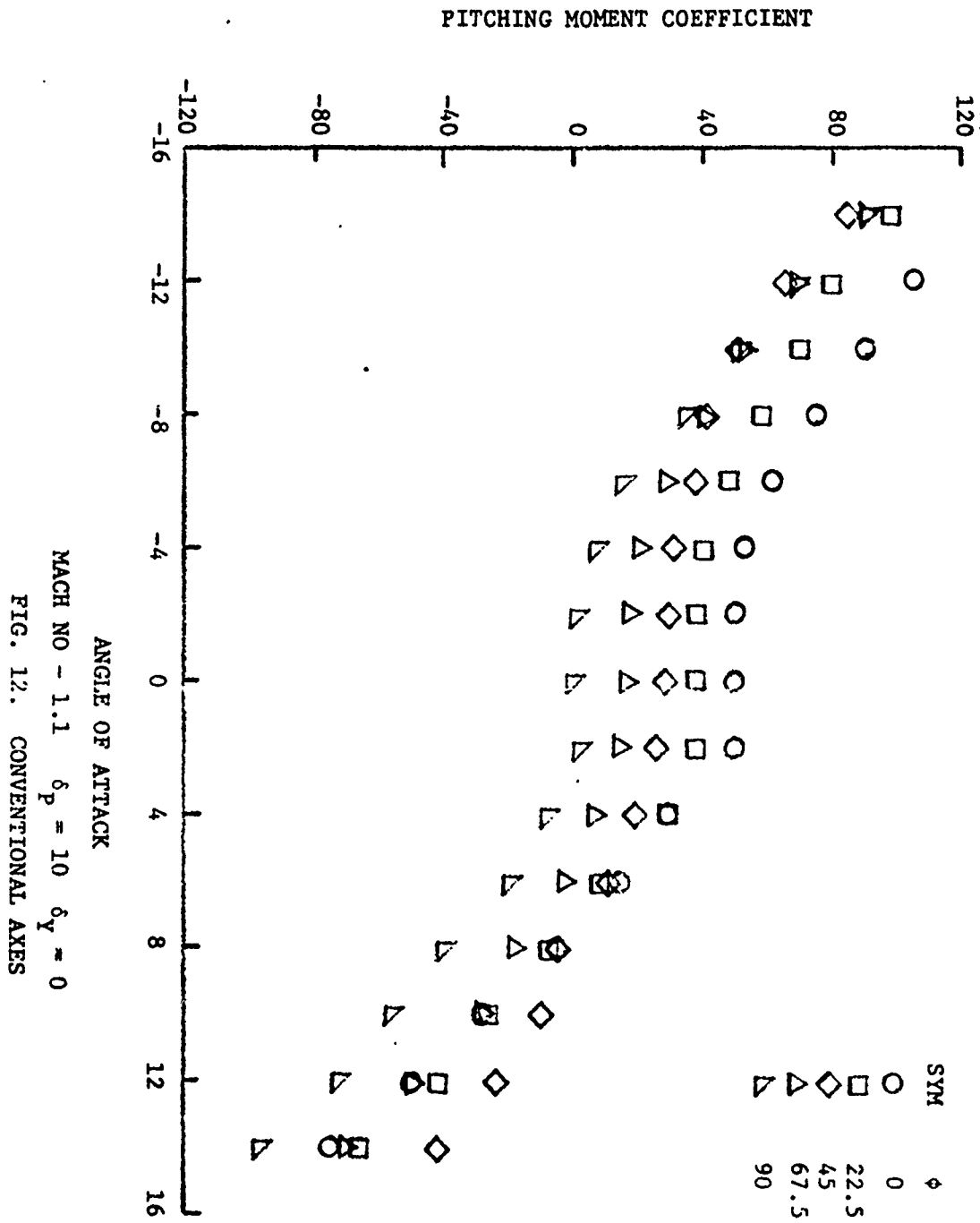
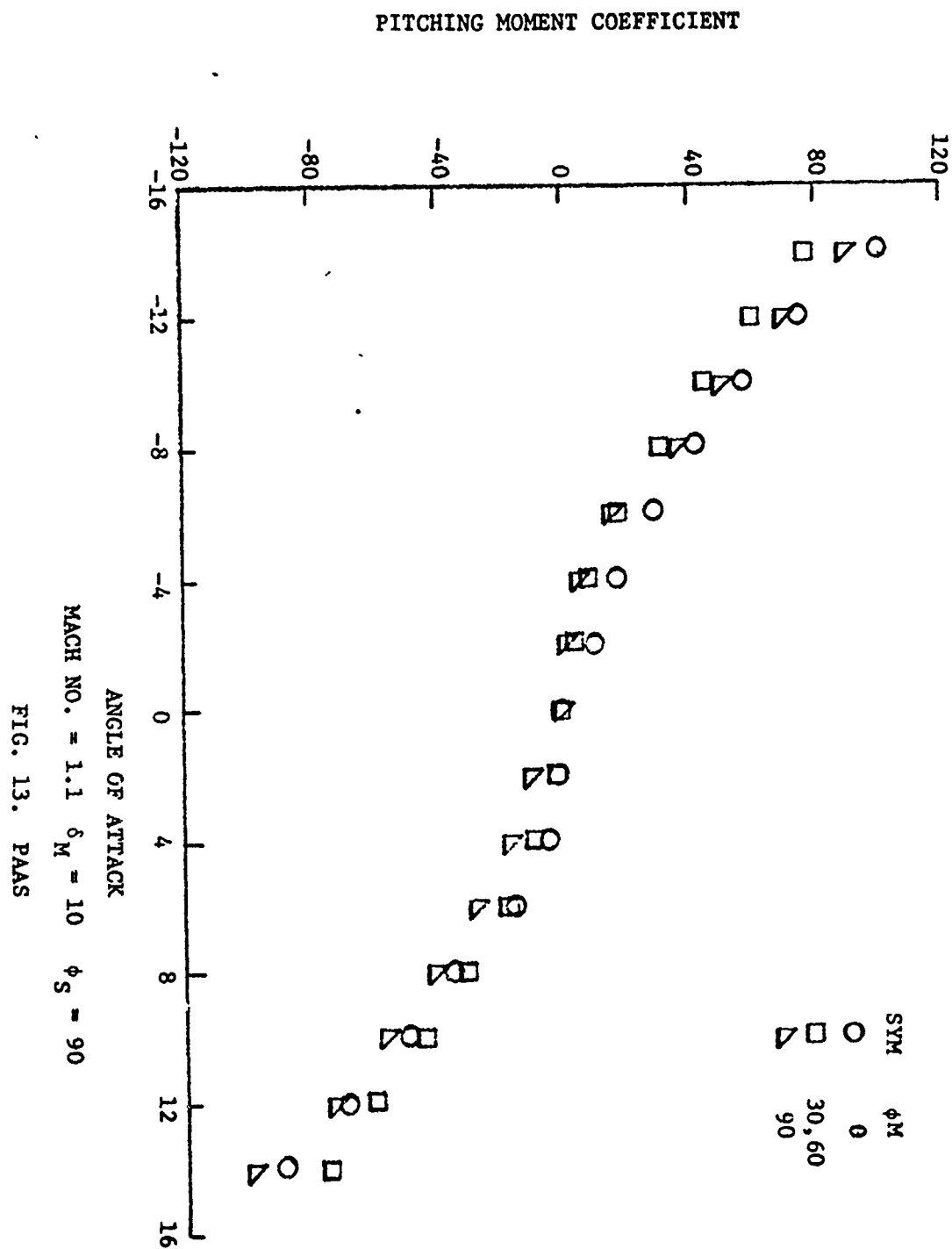
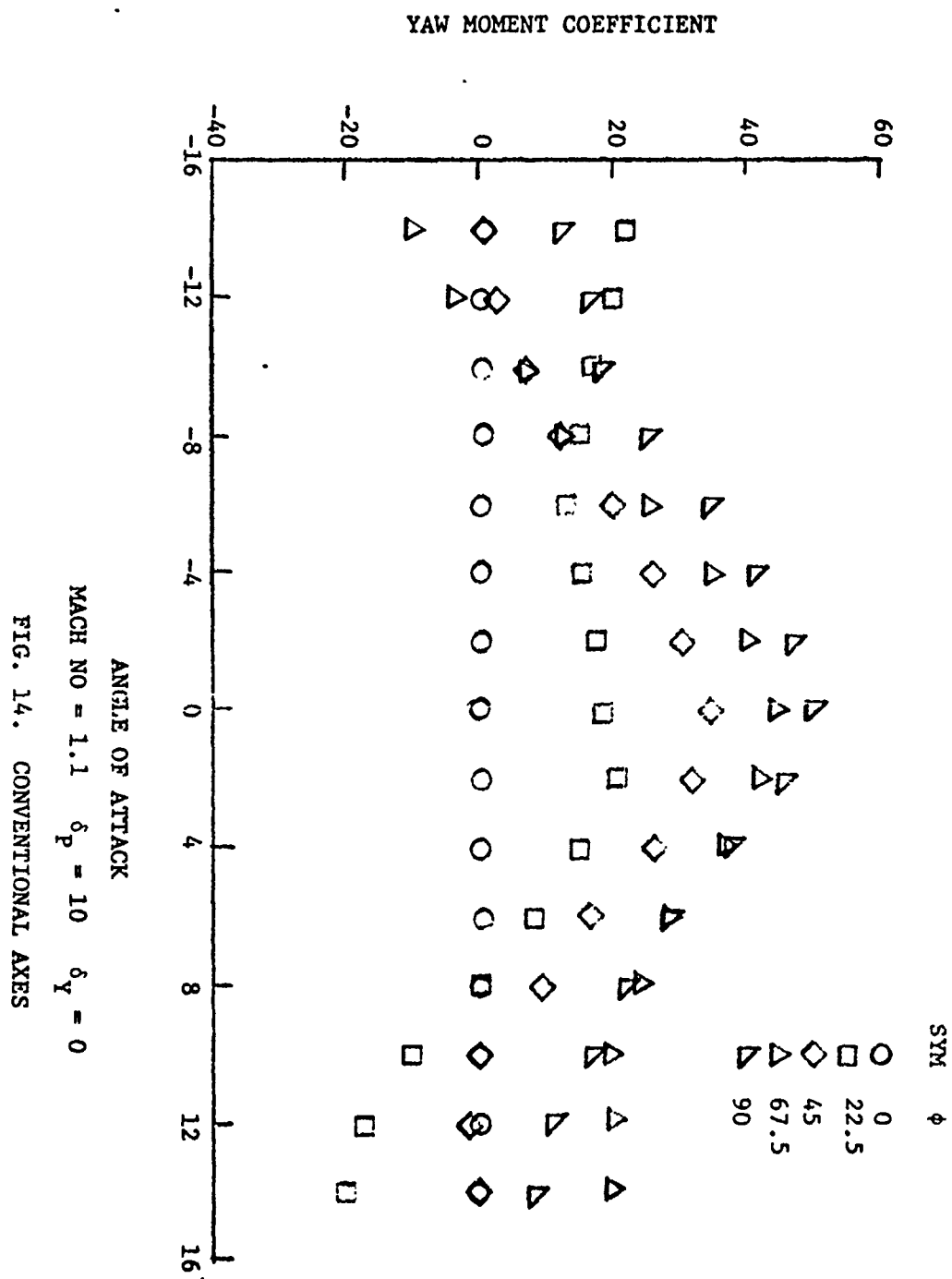
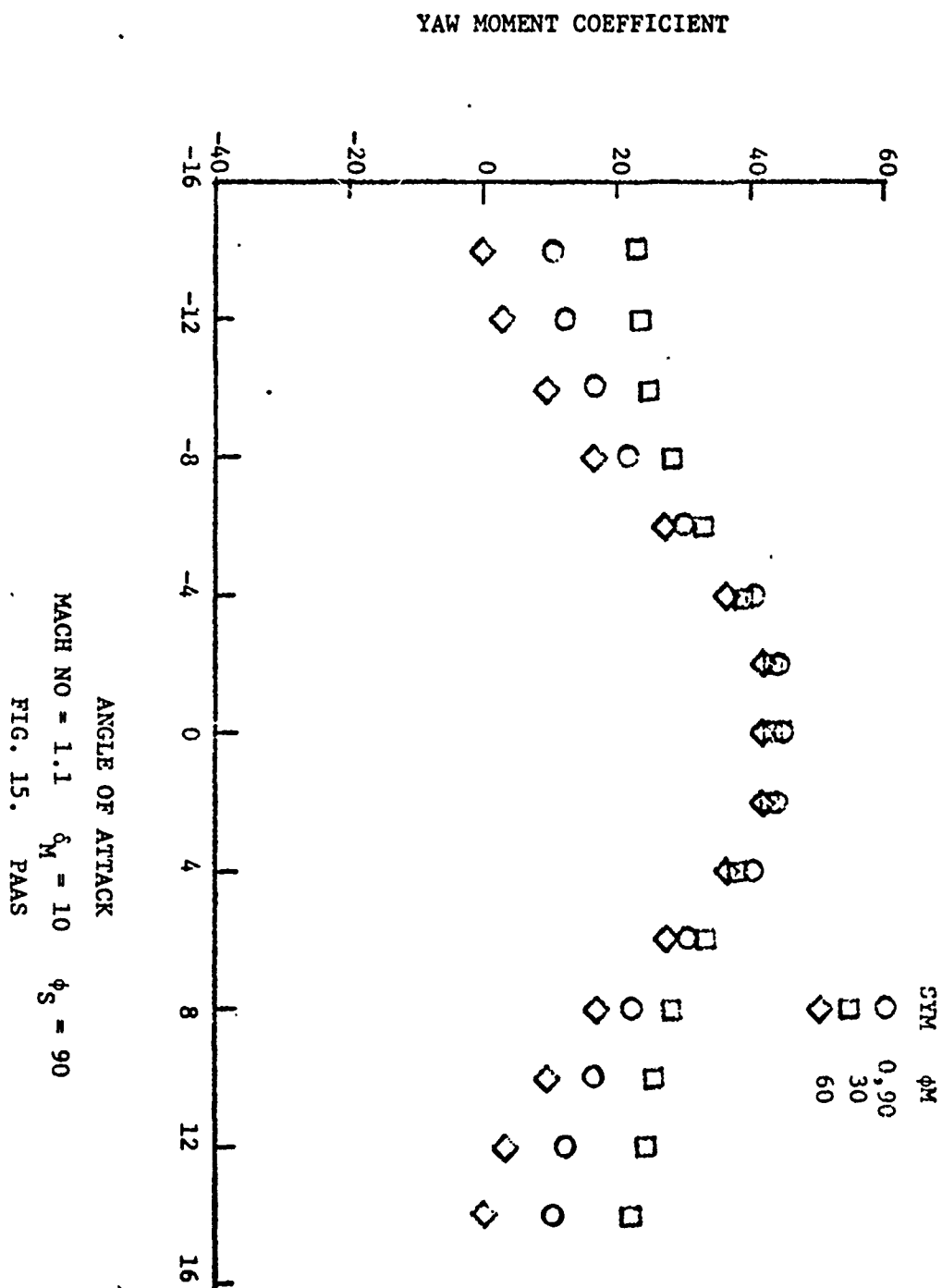


FIG. 11

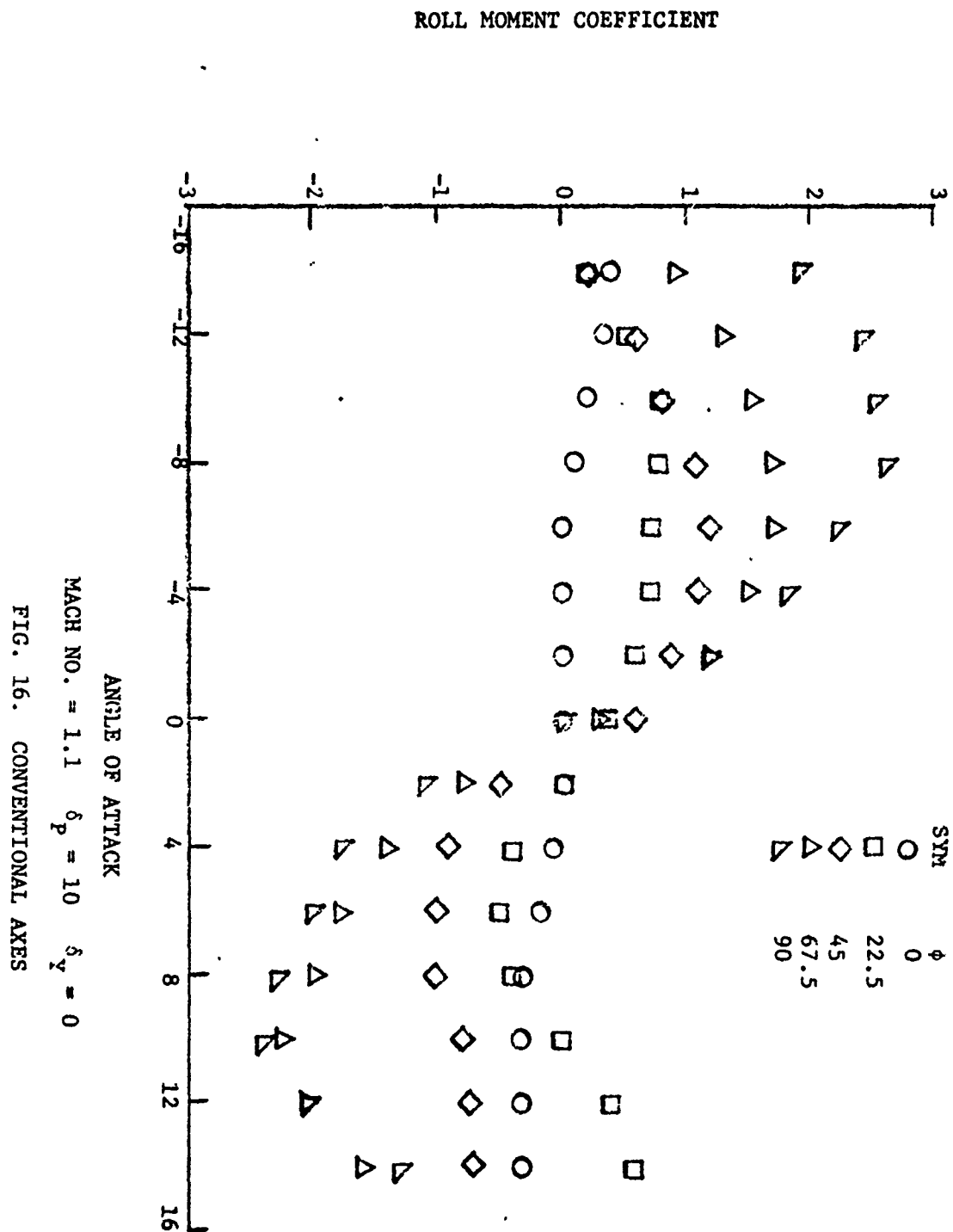












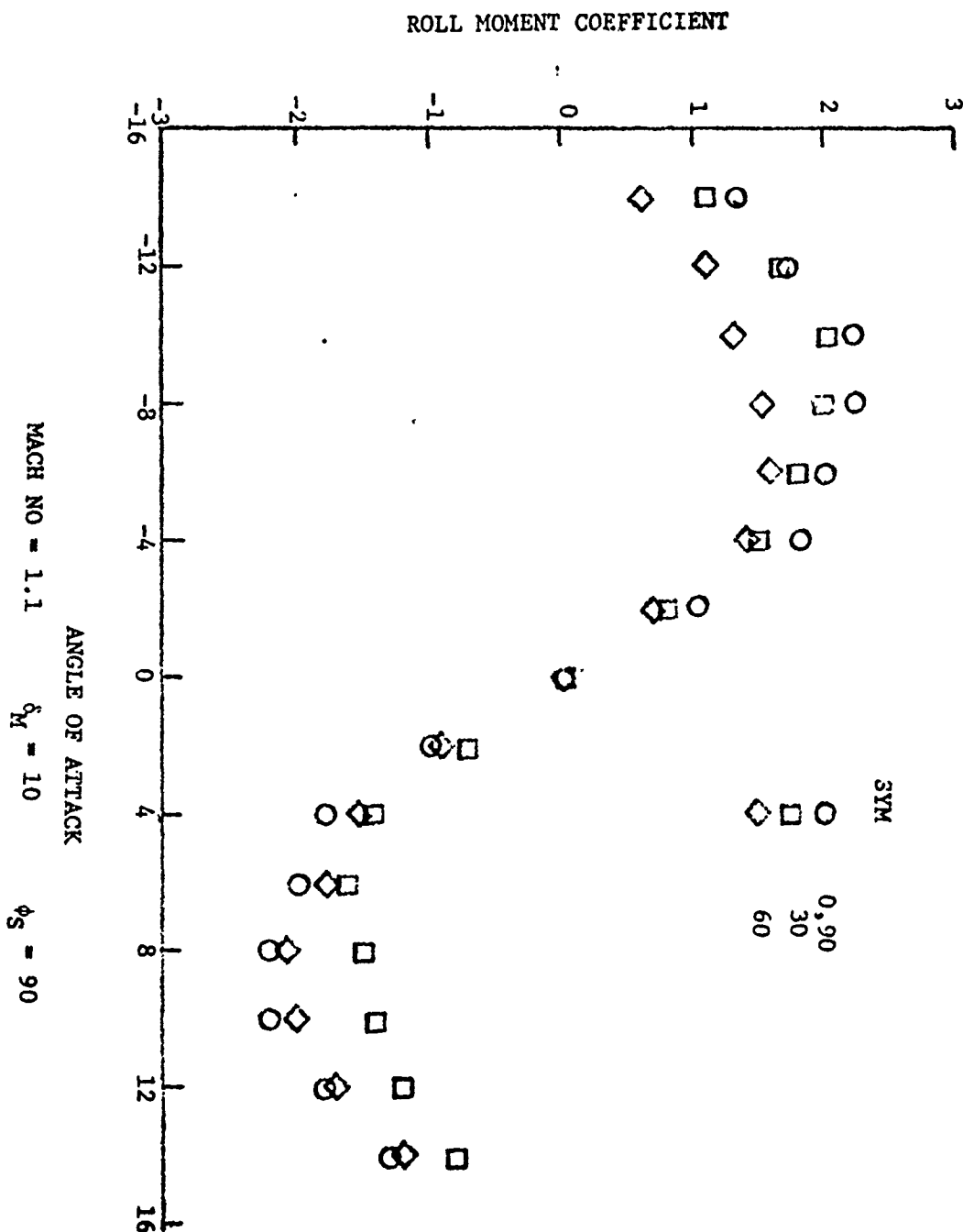


FIG. 17 - PAAS

PAPER NO. 3

ROLL RATE STABILIZATION OF A CANARD CONTROLLED  
GUIDED MISSILE CONFIGURATION AT SUBSONIC AND  
SUPERSONIC SPEED

by

P. Daniels  
Naval Surface Weapons Center  
Dahlgren Laboratory  
Dahlgren, Virginia

Acknowledgement;

Acknowledgement is due Mr. R. E. Meeker of the Naval Weapons Center, who suggested the study and conceived and designed the basic test configuration.

NOMENCLATURE

$\delta_e$	Canard pitch angle
$\delta_R$	Canard yaw angle
$\Phi$	Model roll angle
$\beta$	Angle of yaw
$V$	Free stream tunnel velocity
$p$	Spin rate
$d$	Model fin span, 4 in. (unless otherwise specified)
$c$	Canard slot area
$C$	Canard area
$t$	Tail slot area
$T$	Tail area
$F_r$	Canard rudder force
$F_e$	Canard elevator force

## I. INTRODUCTION

Guided missile systems can be designed without active methods of roll stabilization, if the induced rolling velocity due to maneuvering is sufficiently low. However, if the missile experiences large angles of incidence, it may also develop prohibitively large roll rates. The canard controlled guided missile is of particular interest at this time because of the simplicity of the accompanying guidance system. Minimization of rolling velocity during maneuver is also desirable.

Fin slots<sup>(1,2)</sup> have been shown to be an effective method for alleviating the undesirable roll characteristics of unguided cruciform finned missiles and it was suggested that they might be used to improve the roll characteristics of guided missiles with canard controls. Consequently, subsonic and supersonic wind tunnel tests were conducted at Edgewood Arsenal and the Naval Surface Weapons Center in order to explore this possibility. This paper presents the results of that study.

## 11. WIND TUNNELS AND TEST SPECIMEN

The test specimen, a sting mounted, free rolling missile with cruciform canards and tail fins was supplied by Naval Weapons Center/China Lake. The model was designed such that the canards could have either a fixed deflection with roll angle or could commute, e.g.  $\delta_R = [\delta_R]_{\Phi=0} \cos \Phi$ ,  $\delta_e = [\delta_e]_{\Phi=0} \sin \Phi$ . The commutation feature is designed to simulate active guidance in that the canards provide a nearly constant control force with missile roll angle in any desired plane. The commutation feature is provided through a mechanical linkage with the model sting support. A sketch of the model giving pertinent dimensions is shown in Figure 1. A photograph of the model is shown in Figure 2.

The subsonic free rolling test was conducted in the 28 in. by 40 in. low-speed wind tunnel at Edgewood Arsenal.<sup>(3)</sup> This wind tunnel has continuous flow and is of the induction type. Maximum tunnel speed is about 150 miles per hour.

The supersonic wind tunnel tests were conducted in the Supersonic Tunnel No. 1 at the Naval Surface Weapons Center/White Oak.<sup>(4)</sup> This wind tunnel is of the intermittent, blow down type and has a trisonic capability.

### III. SUBSONIC FREE ROLLING TEST RESULTS

The induced roll characteristics of the missile configuration with commutating canards was first investigated for a sequence of yaw angles with the yaw control force in the plane of yaw. The model was installed in the tunnel such that;

$$[\delta_R]_{\Phi = 0} = -20 \text{ deg.}, [\delta_e]_{\Phi = 0} = 0.$$

(At  $\Phi = 0$  the canard elevators are yawed left resulting in a negative canard force that is in the direction of positive yaw. The canard elevators are undeflected at  $\Phi = 0$ .) The resulting steady-state rolling motion is shown in Figure 3.

Low roll rates exist for the angle-of-attack region ( $-30^\circ \leq \alpha \leq 30^\circ$ ) and are probably due to aerodynamic asymmetry. At high angles-of-attack the missile can roll in either direction and the roll rate can increase considerably. The bars indicate stable roll trim points, e.g., when the motion is stopped it will remain stopped.

The induced roll characteristics of the missile configuration with commutating canards producing a pitch control force ( $F_e$  is negative) normal to the plane of yaw ( $[\delta_R]_{\Phi = 0} = 0$ ,  $[\delta_e]_{\Phi = 0} = -20 \text{ deg.}$ ) is presented in Figure 4. Fairly large roll rates now exist throughout the angle-of-attack range. The roll rate in the region  $-30^\circ \leq \alpha \leq 30^\circ$  can be

interpreted as being produced by asymmetric lift on the canards due to sideslip. (No explanation of the roll reversal,  $-30^\circ < \alpha < 30^\circ$ , is suggested.) The data at high angles of attack in Figures 3 and 4 indicates an instability in spin similar to "roll speed-up" and is probably due to vortex shedding from the tail fins and canards.

In an effort to understand the roll producing interaction between canard and tail fins, tests were conducted with the tail removed. The roll history for the tailless missile is presented in Figure 5. A comparison of Figures 5 and 4 indicates that the roll torque produced by the tail can reinforce or reduce the roll torque due to the canards depending upon the angle of yaw.

Figure 6 shows the effect of a large canard slot ( $c/C = 0.42$ ) on the rolling motion of the test specimen with tail removed. The canard control force is still normal to the angle of yaw and no rolling motion is observed between  $-60^\circ \leq \alpha \leq 60^\circ$ . However, one might suspect that the canard is ineffective due to the large slot size. In an effort to crudely assess the canard effectiveness, a slotted tail was installed. Figure 13 shows that the model with extremely large canard slots still has a significantly large roll rate. This effect suggests that the canard with large slot ( $c/C = 0.42$ ) is still effective since it produces significant downwash and consequently must produce lift.

Figure 14 shows the effect of systematically reducing the slot size for the missile with the tail removed. Thus, when  $c/C$  is as small as 0.23



the roll rate can be fairly well controlled. It was expected that further optimization of the canard slot size and location was possible.

At this point it was obvious that the body could be roll rate stabilized provided that a tail configuration could be found which would minimize the interaction between the tail and the canards.

Slotting the tail fins eliminated the instability of spin at high angles of attack. However when used in combination with slotted canards, roll rates at low angles of attack were not sufficiently reduced. Consequently, other tail configurations were tested.

Varying the number of tail fins, interdigitating tail and canards, increasing the distance between tail fins and canards, and free spinning the tail fins all had a negligible effect on the steady state roll rates. However, two tail configurations were tested that showed considerable promise. Figures 9 and 10 show the steady state roll rates for the guided missile configuration with canard slots ( $c/C = 0.23$ ) and ring or flared tail. Roll rates are well stabilized up to high angles of attack.

The combination of slotted canard and axisymmetric tail is unique, as shown in Figure 11, since the combination of solid canards and axisymmetric tail produces significant roll rates.

Figure 12 shows photographs of both configurations that were successfully roll stabilized at a velocity of 60 miles per hour. The thickened aft section of the model was the result of the free spinning tail

modification and was not changed for the remainder of the study. The tail span was consequently increased to 4.75 inches.

Further testing showed that a modified slot with a 20% slot size ( $c/C = 0.20$ ) did not degradate the roll stability at a tunnel velocity of 60 miles per hour. The new configurations were then tested at the maximum tunnel speed of 150 miles per hour. The results of these tests are shown in Figures 13 and 14. Slight velocity effects are noted. Some very low roll rates were recorded that may have been hidden by the bearing friction at the lower velocity. It should be noted that originally the test could not be run at high velocity because the large model roll rates caused the canards to shed from the model.

## SUPERSONIC TESTS

Free rolling wind tunnel tests were conducted at NSWC/WO in order to study roll rate stabilization of the guided missile configurations at high subsonic and supersonic speed. The angle-of-attack range was limited to  $\pm 40$  degrees due to the test section size limitation. Data was obtained at Mach numbers of 0.8, 2.03 and 3.02. It should also be noted that dynamic pressure could not be held constant over the Mach number range. This would have helped to minimize the effect of variation in bearing friction.

A comparison of the steady state roll rates of the basic configuration at Mach numbers of 0.08, 0.8, 2.0, and 3.0 are presented in Figures 15 and 16 for the cases where the canard control force was in the plane of yaw and perpendicular to the plane of yaw.

Roll rates are small for angles of yaw up to  $\pm 35$  degrees for all Mach numbers tested when the canard control force is in the plane of yaw. The reduced frequency ( $Pd/2V$ ) at the higher Mach numbers (.80, 2.03, 3.02) are generally less than for the very low Mach number (.080) when the canard control force is perpendicular to the plane of yaw.

During the subsonic tests at Edgewood Arsenal, roll rate stabilization was accomplished by removing the cruciform tail and stabilizing the forbody with canard slots. The axisymmetric tail (flare or ring) provided stability without destabilization of the roll rate. Data obtained at NSWC/WO indicated that the configuration with optimum slot and ring was less

effective at a Mach number of 0.80. At supersonic speeds this configuration was totally ineffective.

Roll rate stabilization at higher Mach numbers was attempted by removing the ring tail and increasing the slot size. Significant roll rates were observed even for large slot sizes (Figure 17). Figure 18 further illustrates that although slots still reduce the roll rate at supersonic speeds the dramatic roll rate stabilization obtained at low subsonic speed is no longer present.

Based on these data it appeared that the axisymmetric tail and slotted canards would not be beneficial roll rate stabilizers at high speed.

Paradoxically, the cruciform tail that had a destabilizing effect at subsonic speed was found to have a stabilizing effect at supersonic speed. Figure 19 compares the basic configuration with solid canards to the tail off configuration with solid canards. Reduction in roll rate is probably due to the roll lock-in moment<sup>(1)</sup> induced by the cruciform tail. A further reduction in roll rate of the cruciform tail configuration is obtained by canard slots (Figure 20).

It was felt that the possible loss in effectiveness of the canard slots to roll rate stabilize the vehicle at supersonic speeds might be due to blockage of the airflow through the canard slots. Consequently, the nose of the configuration was blunted to reduce the Mach number in the region of the canards. In addition to reducing the local Mach number, the shorter nose also provided less shielding of the leeward canard in yaw. A reduction in roll rate was noted at the lower angles and this result is presented in Figure 21. A photograph of the blunt nose model is presented in Figure 22.

## IV. CONCLUSIONS

The following conclusions were made based on the results of this study:

1. Rolling velocity of the model is extremely dependent upon angle of incidence and the direction of the canard control torque.
2. At low angles of attack, roll rates are higher when the canard control force is perpendicular to the plane of yaw. This roll phenomenon is produced by the canards.
3. At high angles of attack and subsonic speed, roll rates are fairly independent of the canard deflection and are probably due to vortex shedding from the fins.
4. At subsonic speed canard slots are ineffective in controlling roll rate if cruciform tail fins are present because of interference effects. Canard slots are effective roll stabilizers if used in the presence of a ring tail or flare tail.
5. At supersonic speeds roll rates were significantly reduced by combining cruciform fins with slotted canards. Nose blunting further reduced the observed rates.

## V. COMMENT

Six component force tests are presently being conducted to determine the effectiveness of slotted canards and no data is available at this time. However, data taken previously indicates that small slots (of the order of 25% fin area) inserted in missile fins do not appreciably degrade lift or restoring moment. (1,6)

REFERENCES

1. Daniels, P. and Clare, T. A., "Aerodynamic Characteristics of the Slotted Fin," Journal of Aircraft, Vol. 9, No. 8, August 1972, pp. 603-605.
2. Daniels, P., "A Comparison of the Stability Characteristics of Standard Fin and Slotted Fin MARK 81 Low Drag Bombs," NWL Technical Report TR-2722 of April 1973, Naval Weapons Laboratory, Dahlgren, Virginia.
3. Flatau, A., "Facilities and Capabilities of Aerodynamics Group, Research Laboratories," EASP 100-79 of June 1970, Edgewood Arsenal, Edgewood, Maryland.
4. "Aeroballistic Research Facilities," NOLR 1233, Naval Ordnance Laboratory, White Oak, Silver Spring, Maryland.
5. Daniels, P., "Effect of Fin Slots and Fin Tabs on the Dynamic Stability Characteristics of the Navy Low Drag Bomb," Journal of Spacecraft and Rockets, Vol. 7, Sept. 1970, pp. 1151-1152.
6. Daniels, P., "Minimization of Lock-In Roll Moment on Missiles Via Slots," NSWC/DL Technical Report TR-3250 of January 1975. Naval Surface Weapons Center, Dahlgren, Virginia.

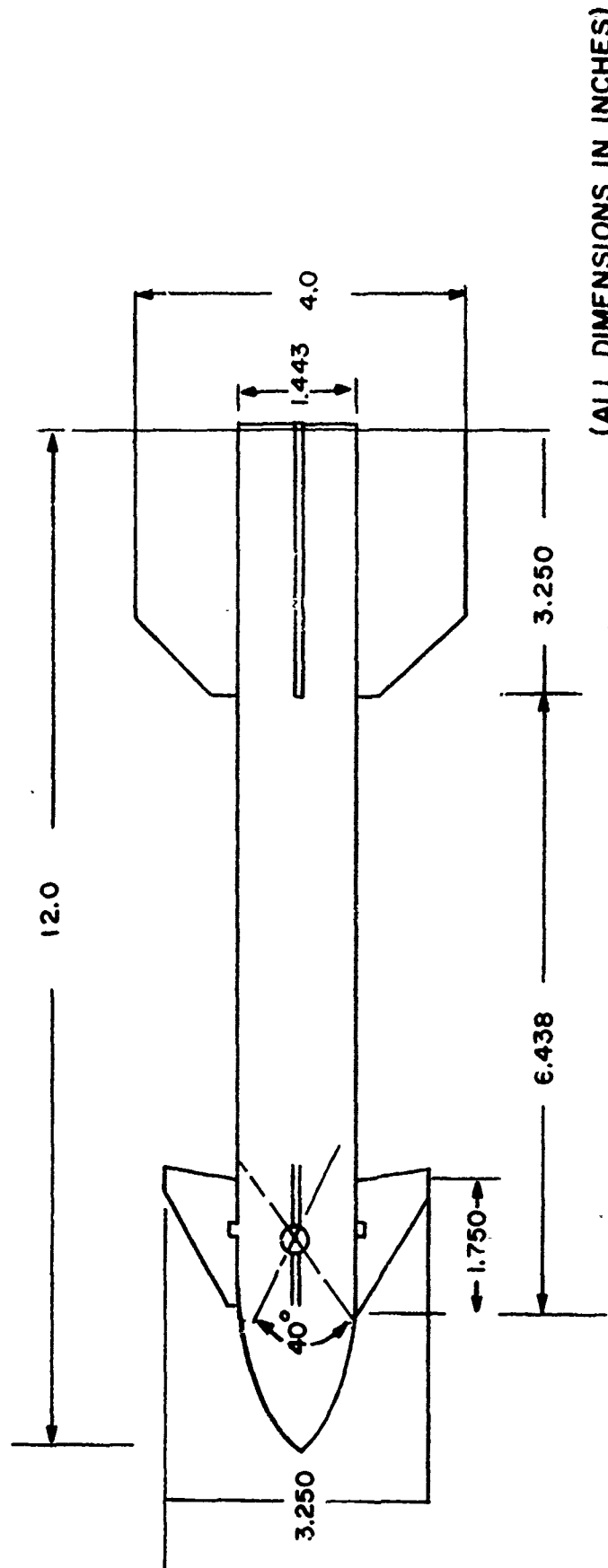
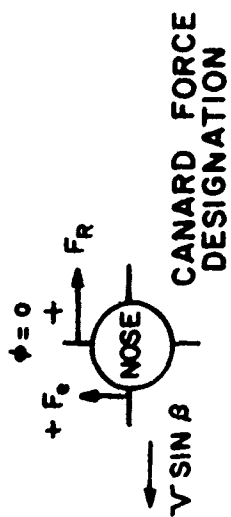


FIGURE 1 SKETCH OF FREE ROLLING MODEL WITH COMMUTATING CANARDS.

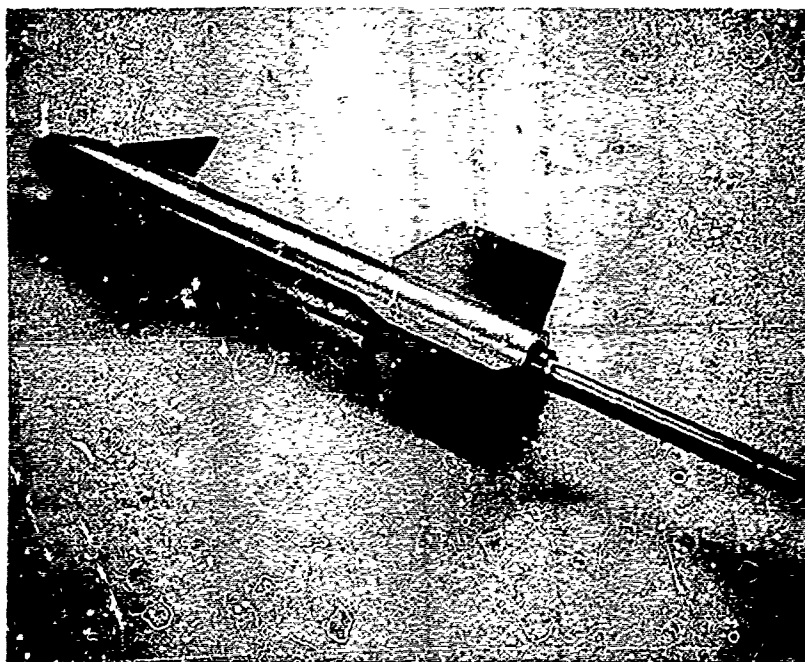


FIGURE 2 FREE ROLLING MODEL WITH  
COMMUTATING CANARDS



$$V = 60 \text{ MPH}$$

$$[\delta_0]_{\phi=0} = 0 \text{ DEG.}$$

$$[\delta_R]_{\phi=0} = -20 \text{ DEG.}$$

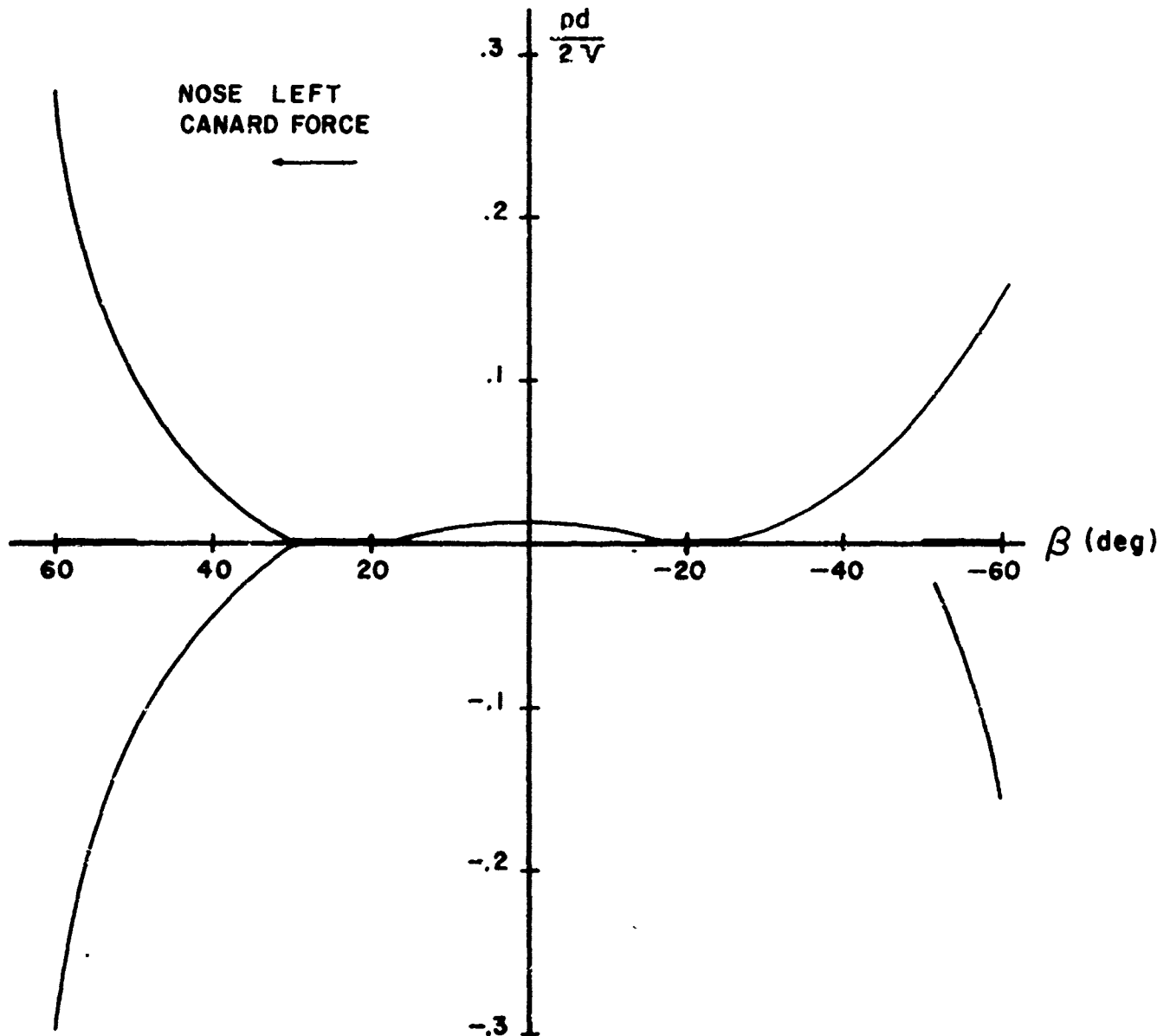


FIGURE 3. STEADY STATE ROLL RATE VERSUS ANGLE OF YAW FOR MODEL WITH COMMUTATING CANARDS PRODUCING NOSE LEFT CONTROL FORCE ( $C/C=0$ ,  $1/T=0$ )

$$\begin{aligned} V &= 60 \text{ MPH} \\ [\delta_e]_{\phi=0} &= -20 \text{ DEG.} \\ [\delta_R]_{\phi=0} &= 0 \text{ DEG.} \end{aligned}$$

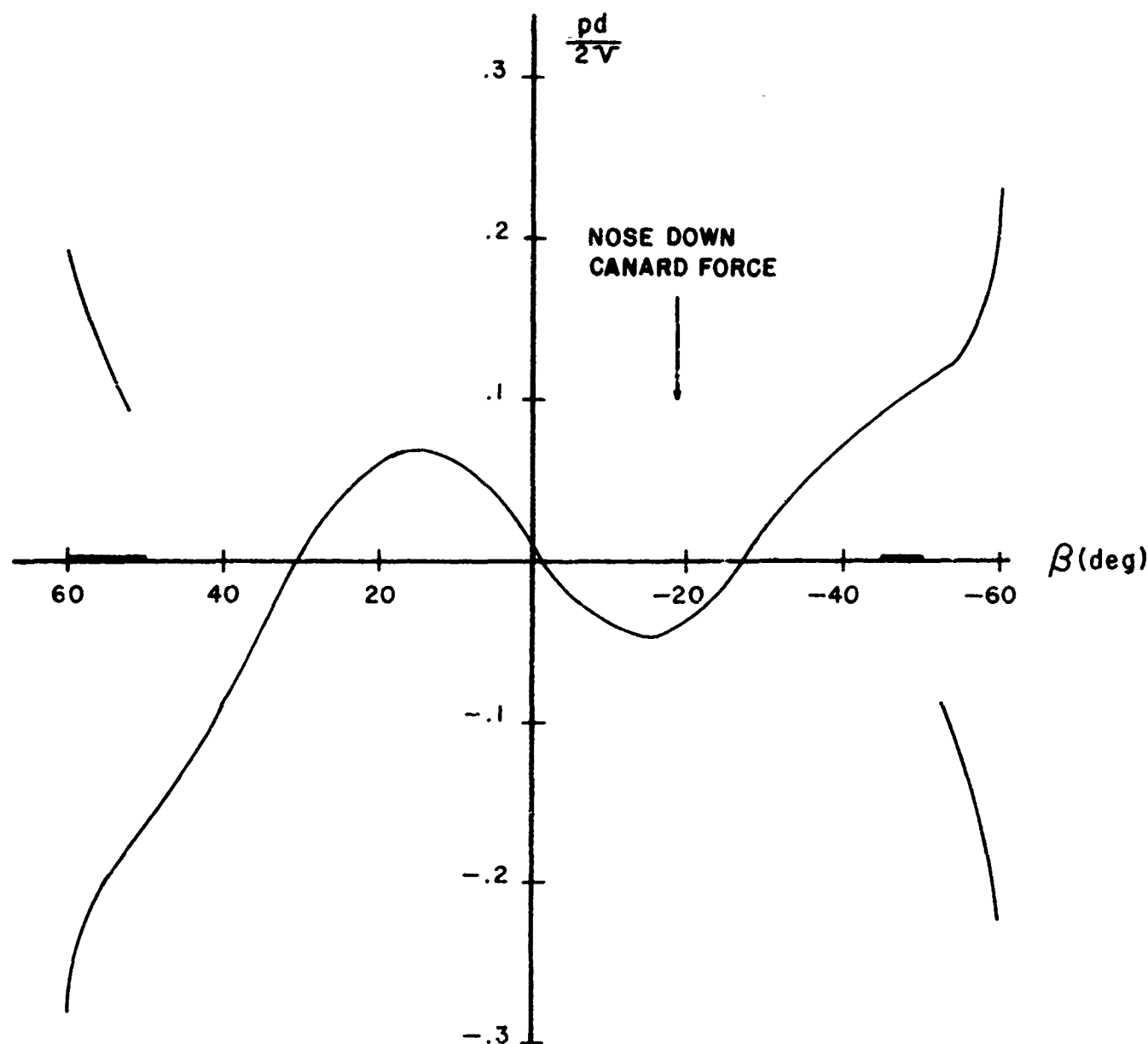


FIGURE 4. STEADY STATE ROLL RATE VERSUS ANGLE OF YAW FOR MODEL WITH COMMUTATING CANARDS PRODUCING NOSE DOWN CONTROL FORCE ( $c/c=0$ ,  $t/T=0$ )

$$V = 60 \text{ MPH}$$

$$[\delta_e]_{\phi=0} = -20 \text{ DEG.}$$

$$[\delta_R]_{\phi=0} = 0 \text{ DEG.}$$

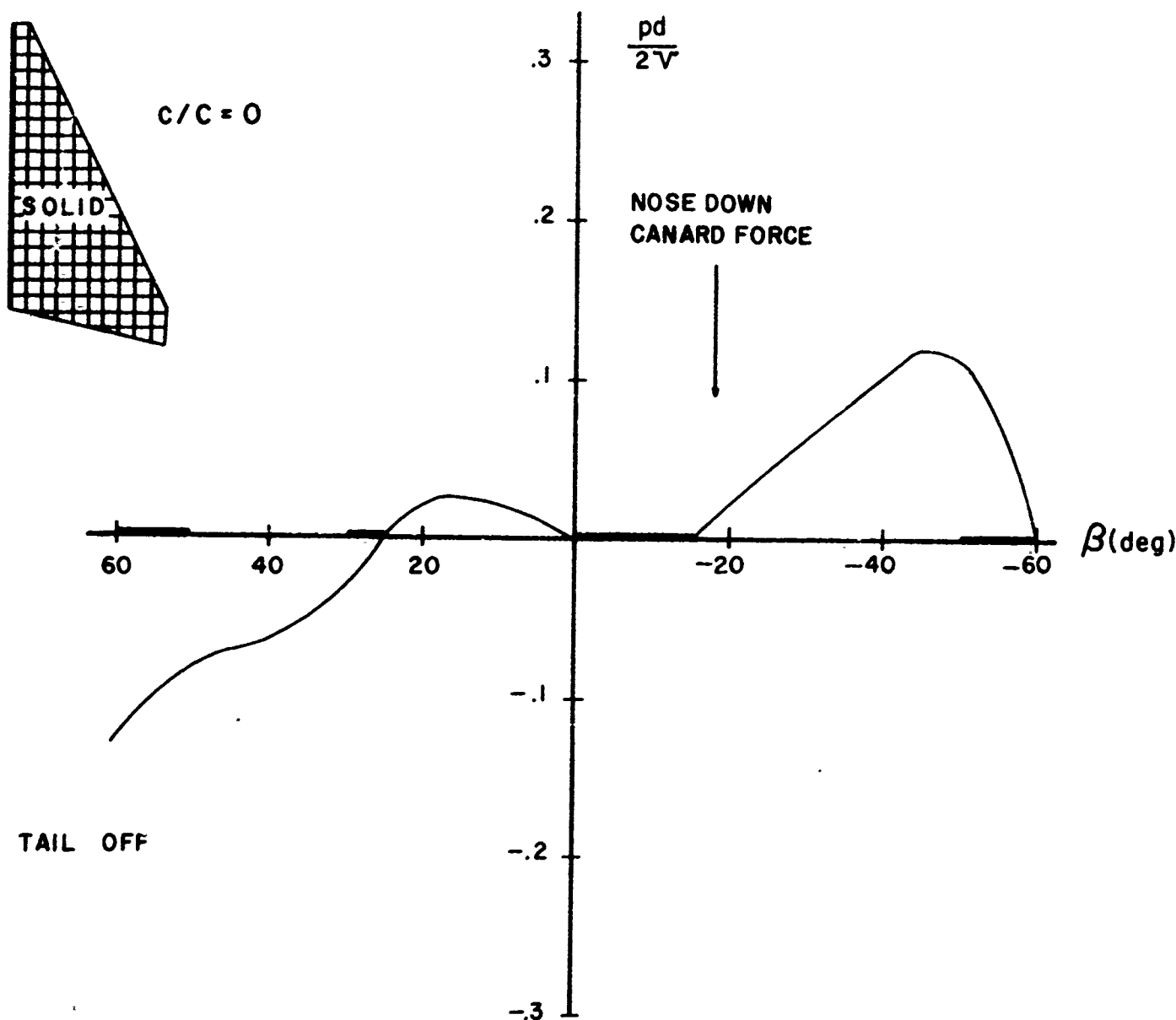


FIGURE 5. STEADY STATE ROLL RATE VERSUS ANGLE OF YAW FOR MODEL WITH COMMUTATING CANARDS PRODUCING NOSE DOWN CONTROL FORCE ( $c/c = 0$ , TAIL OFF)

$$V = 60 \text{ MPH}$$

$$[\delta_e]_{\phi=0} = -20 \text{ DEG}$$

$$[\delta_R]_{\phi=0} = 0 \text{ DEG.}$$

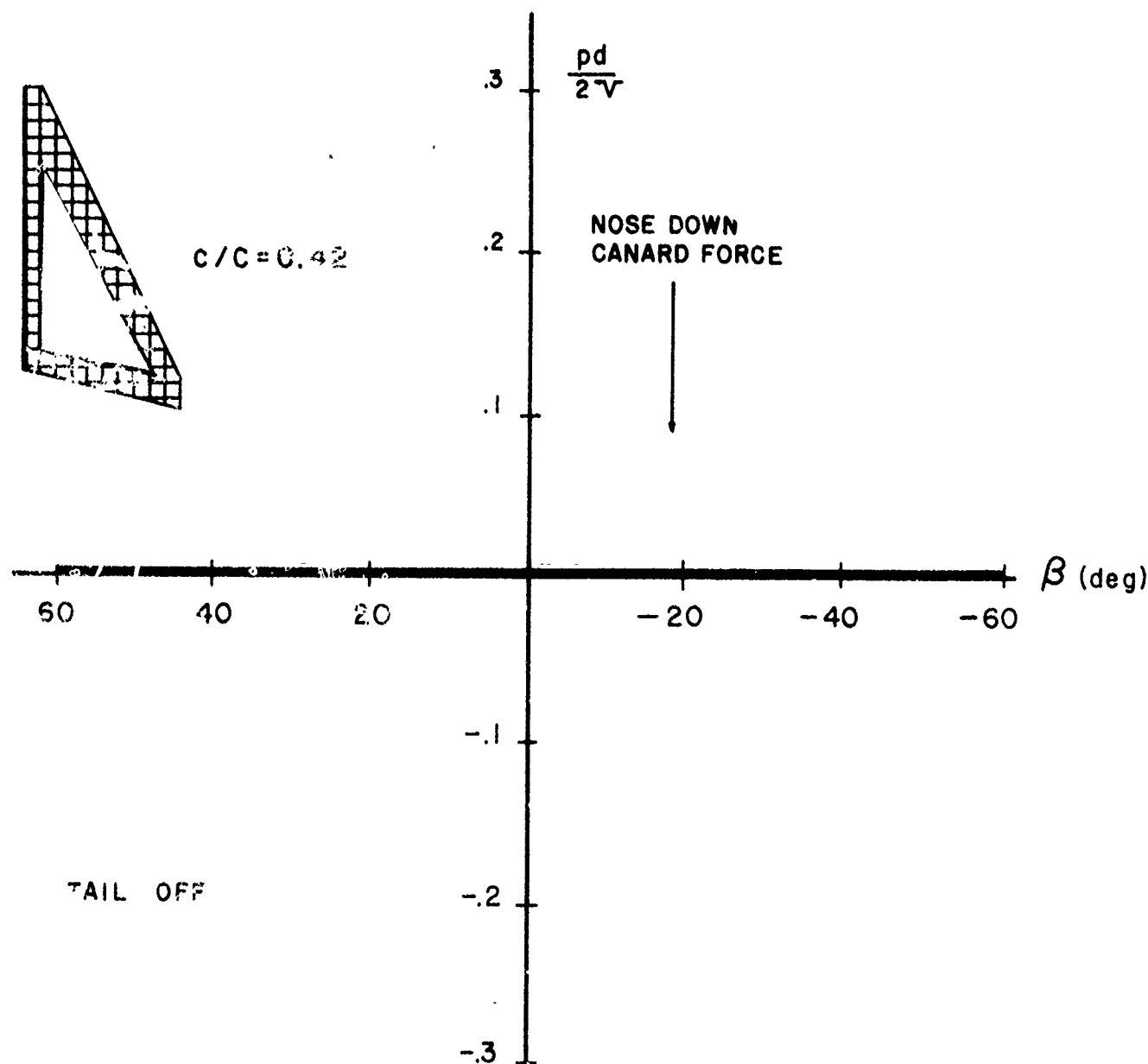


FIGURE 6. STEADY STATE ROLL RATE VERSUS ANGLE OF YAW FOR MODEL WITH COMMUTATING CANARDS PRODUCING NOSE DOWN CONTROL FORCE ( $c/C = 0.42$ , TAIL OFF)

$V = 60$  MPH Vol. 1

$$[\delta_o]_{\phi=0} = -20 \text{ DEG.}$$

$$[\delta_R]_{\phi=0} = 0 \text{ DEG.}$$

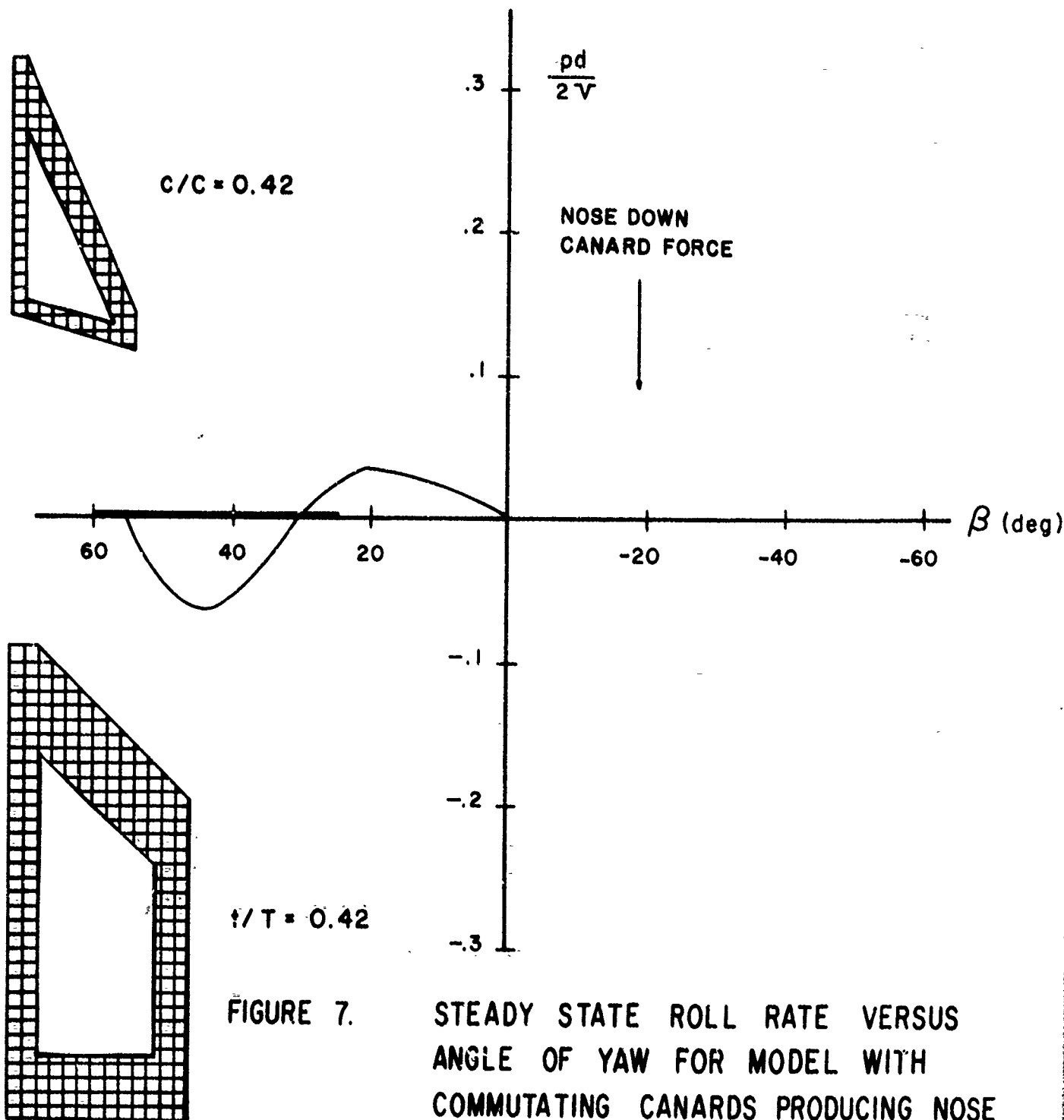


FIGURE 7.

STEADY STATE ROLL RATE VERSUS  
ANGLE OF YAW FOR MODEL WITH  
COMMUTATING CANARDS PRODUCING NOSE  
DOWN CONTROL FORCE ( $c/C = t/T = 0.42$ )

$V = 60 \text{ MPH}$ 

$$[\delta_e]_{\phi=0} = -20 \text{ DEG.}$$

$$[\delta_R]_{\phi=0} = 0 \text{ DEG.}$$

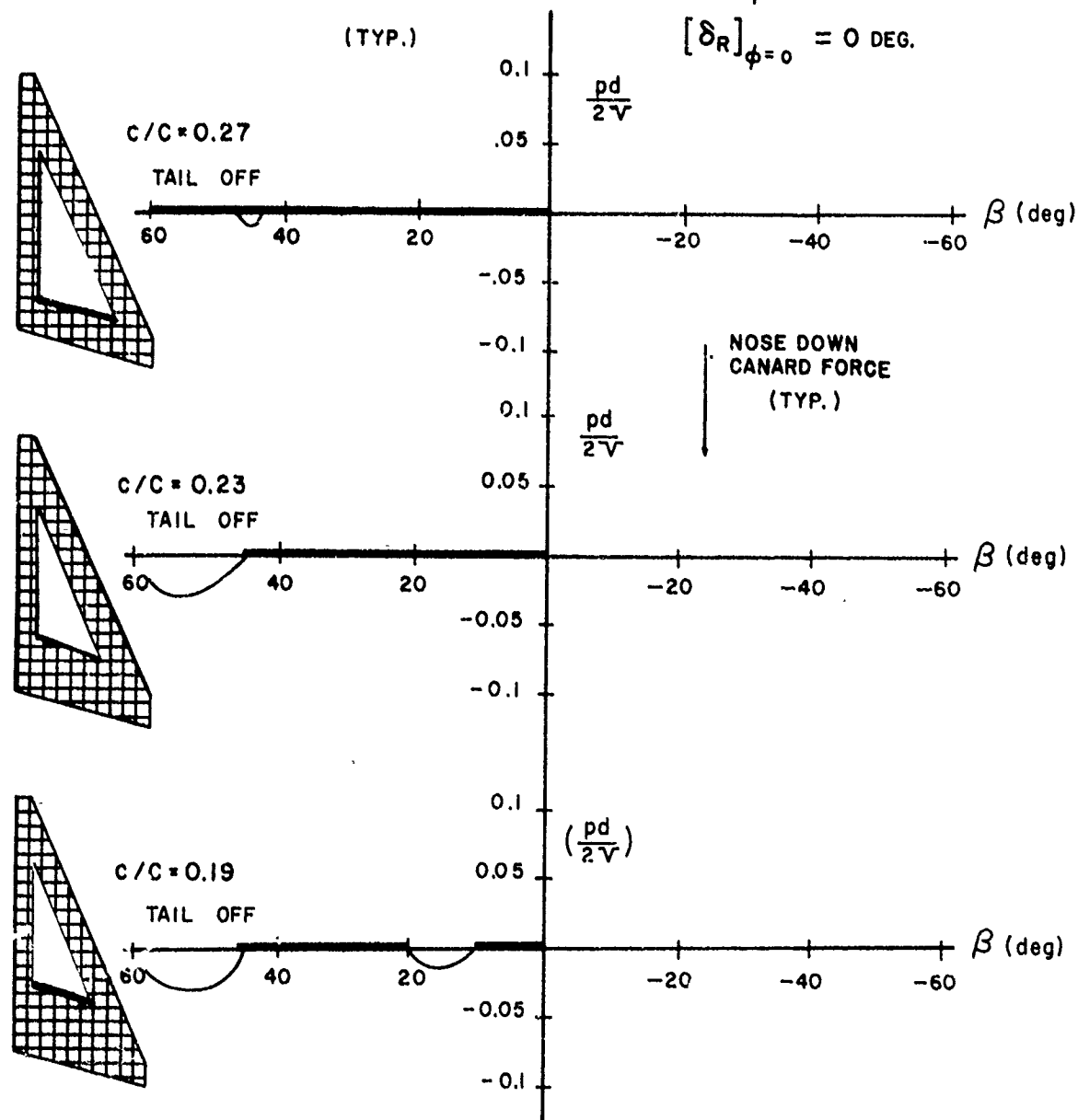


FIGURE 8. STEADY STATE ROLL RATE VERSUS ANGLE OF YAW FOR MODEL WITH COMMUTATING CANARDS PRODUCING NOSE DOWN CONTROL FORCE (TAIL REMOVED, VARIABLE CANARD SLOT)

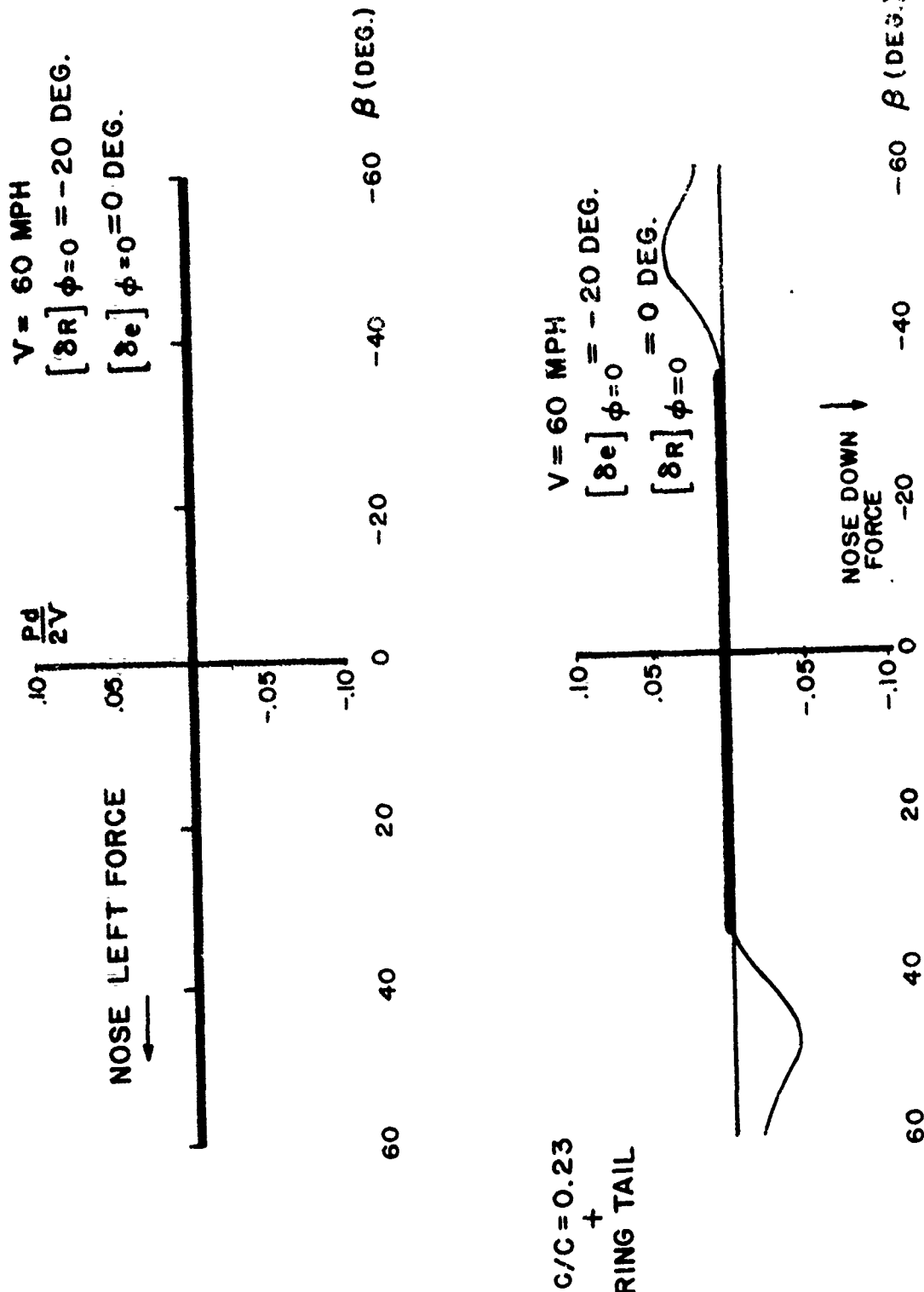


FIGURE 9. STEADY STATE ROLL RATE VERSUS ANGLE OF ATTACK FOR MODEL WITH COMMUTATING CANARDS PRODUCING NOSE LEFT CONTROL FORCE AND NOSE DOWN CONTROL FORCE (C/C = 0.23, RING TAIL)

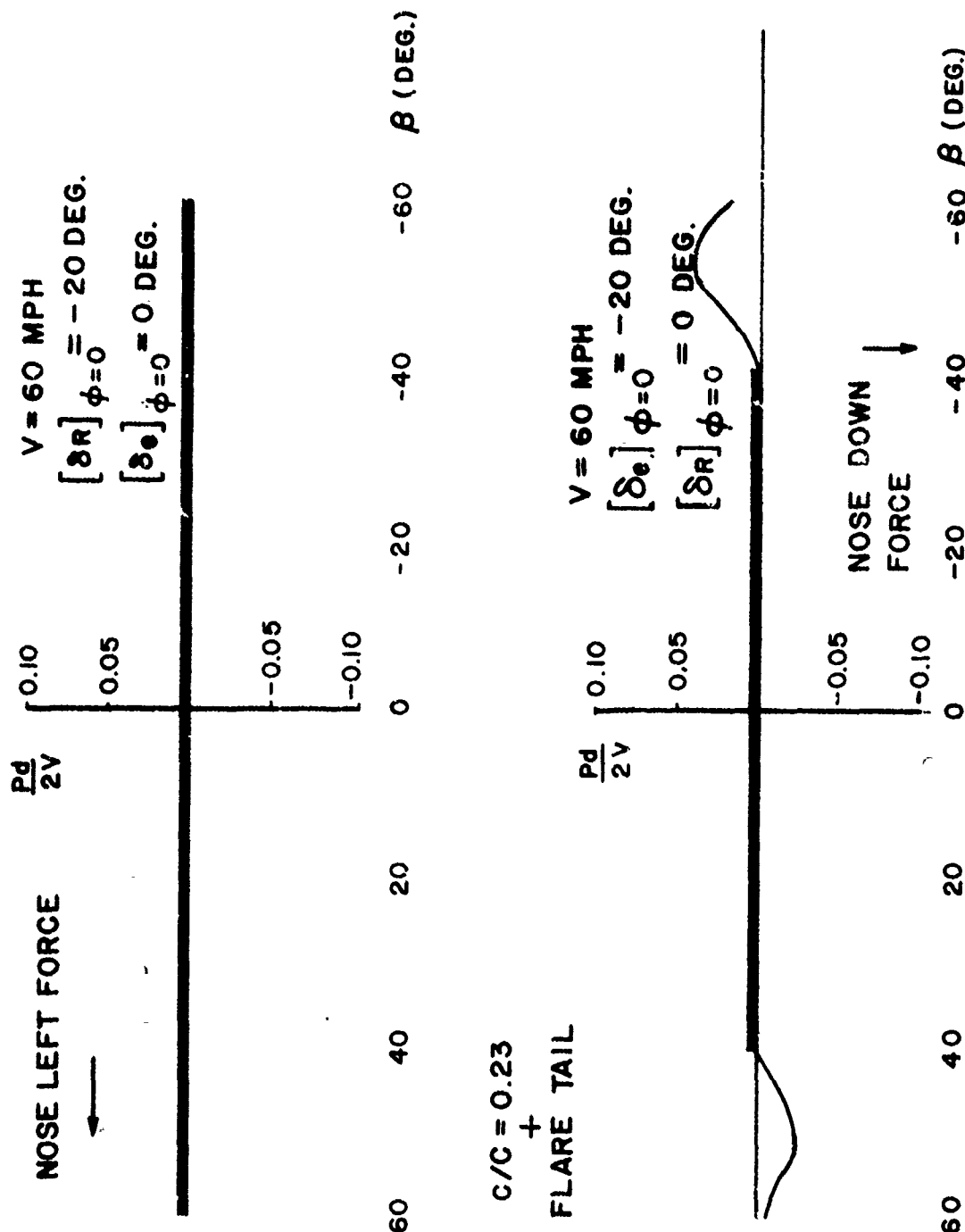


FIGURE 10. STEADY STATE ROLL RATE VERSUS ANGLE OF ATTACK FOR MODEL WITH COMMUTATING CANARDS PRODUCING NOSE LEFT CONTROL FORCE AND NOSE DOWN CONTROL FORCE (  $C/C = 0.23$ , FLARE TAIL )



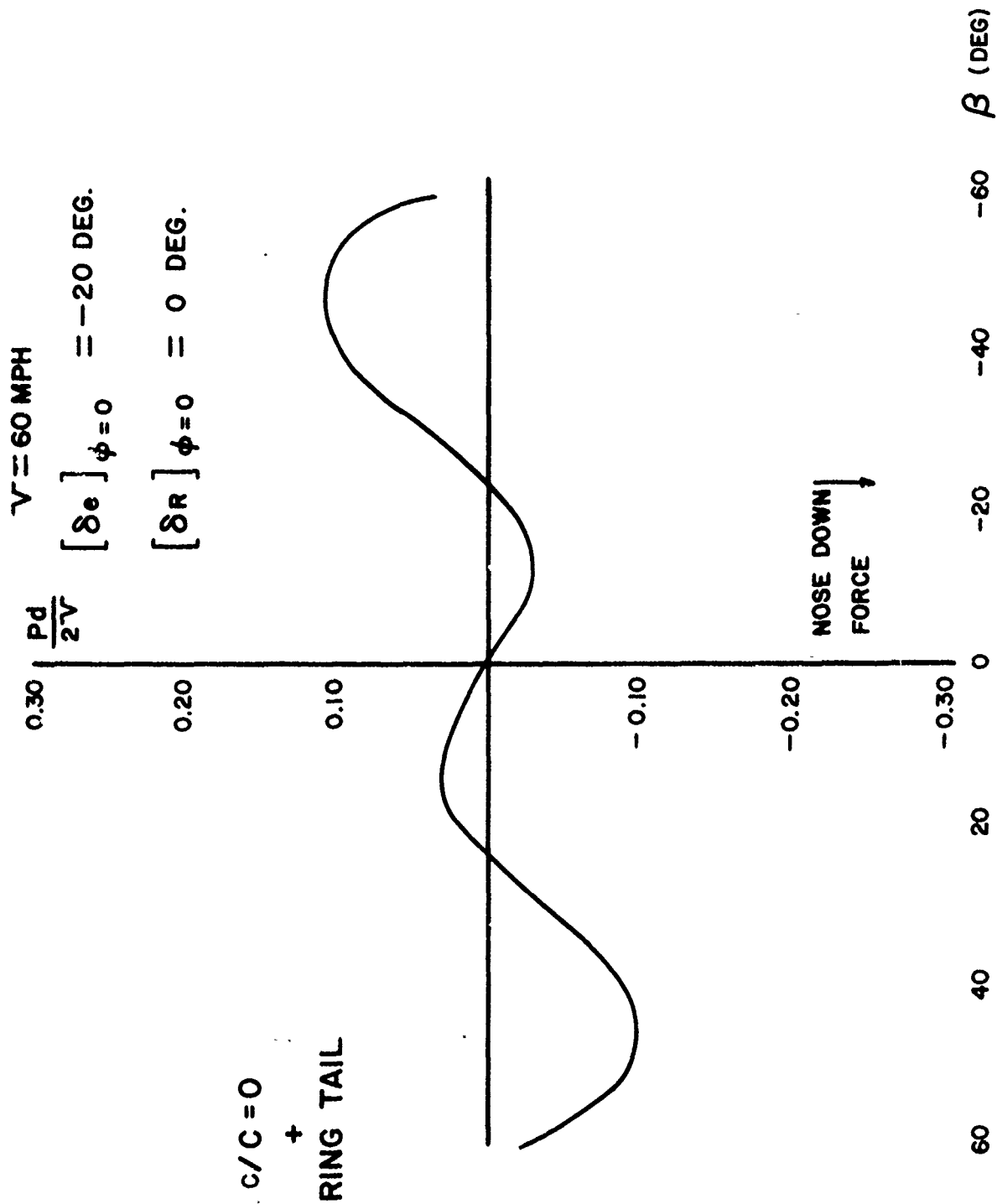


FIGURE 11. STEADY STATE ROLL RATE VERSUS ANGLE OF ATTACK FOR MODEL WITH COMMUTATING CANARDS PRODUCING NOSE DOWN CONTROL FORCE (SOLID CANARDS, RING TAIL)

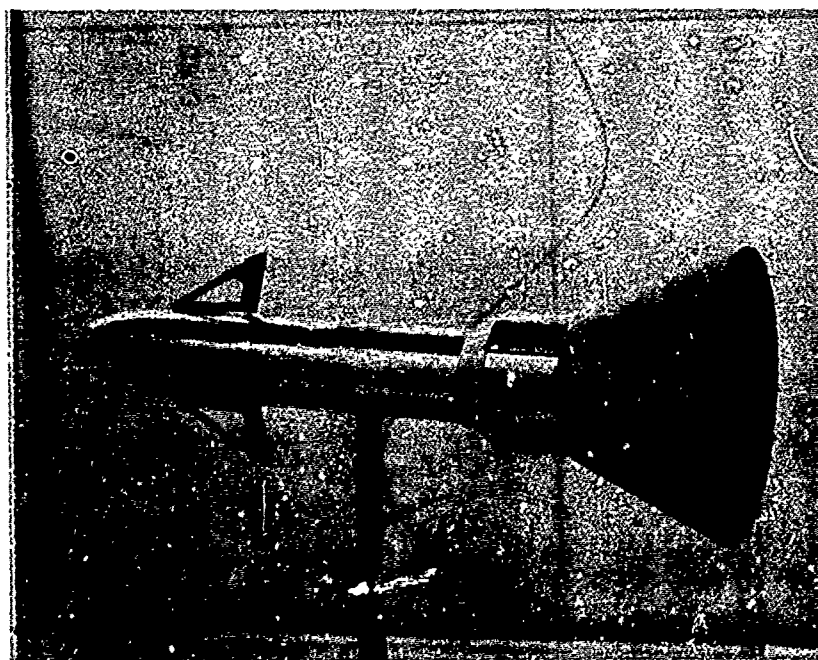
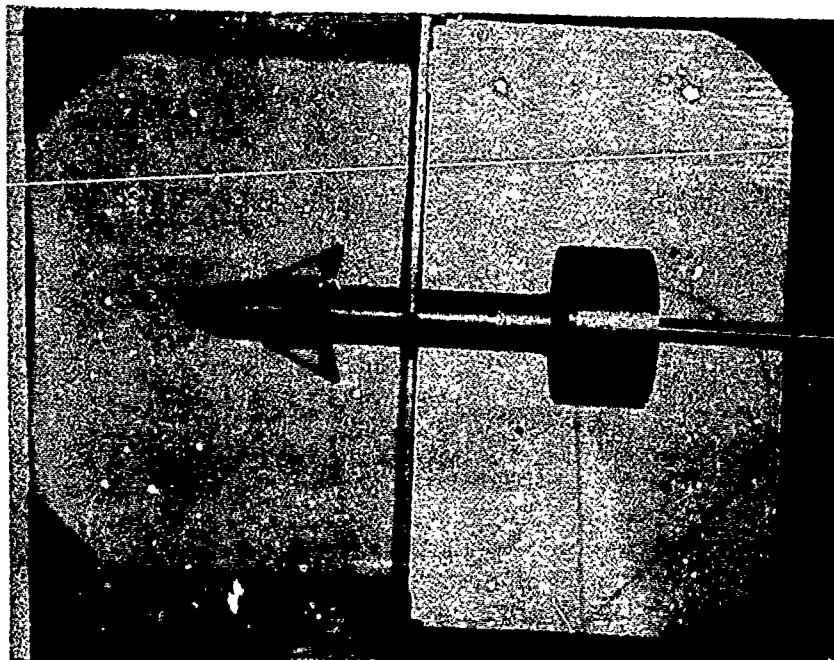


FIGURE 12. ROLL RATE STABILIZED  
GUIDED MISSILE CONFIGURATIONS

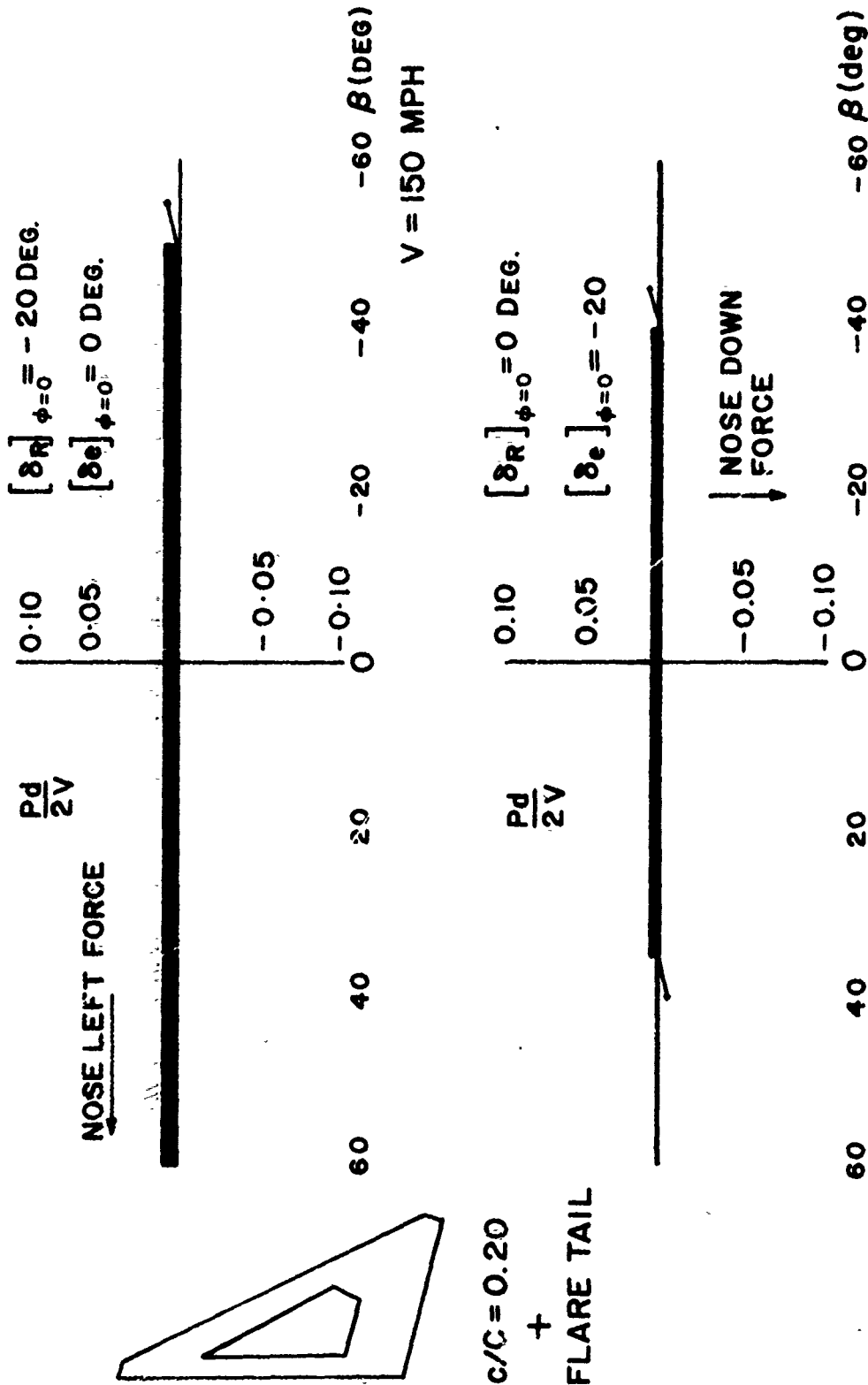


FIGURE 13. Steady State Roll Rate Versus Angle of Attack for Model with Commutating Canards Producing Nose Left and Nose Down Control Force ( $c/C=0.20$  + Flare Tail)

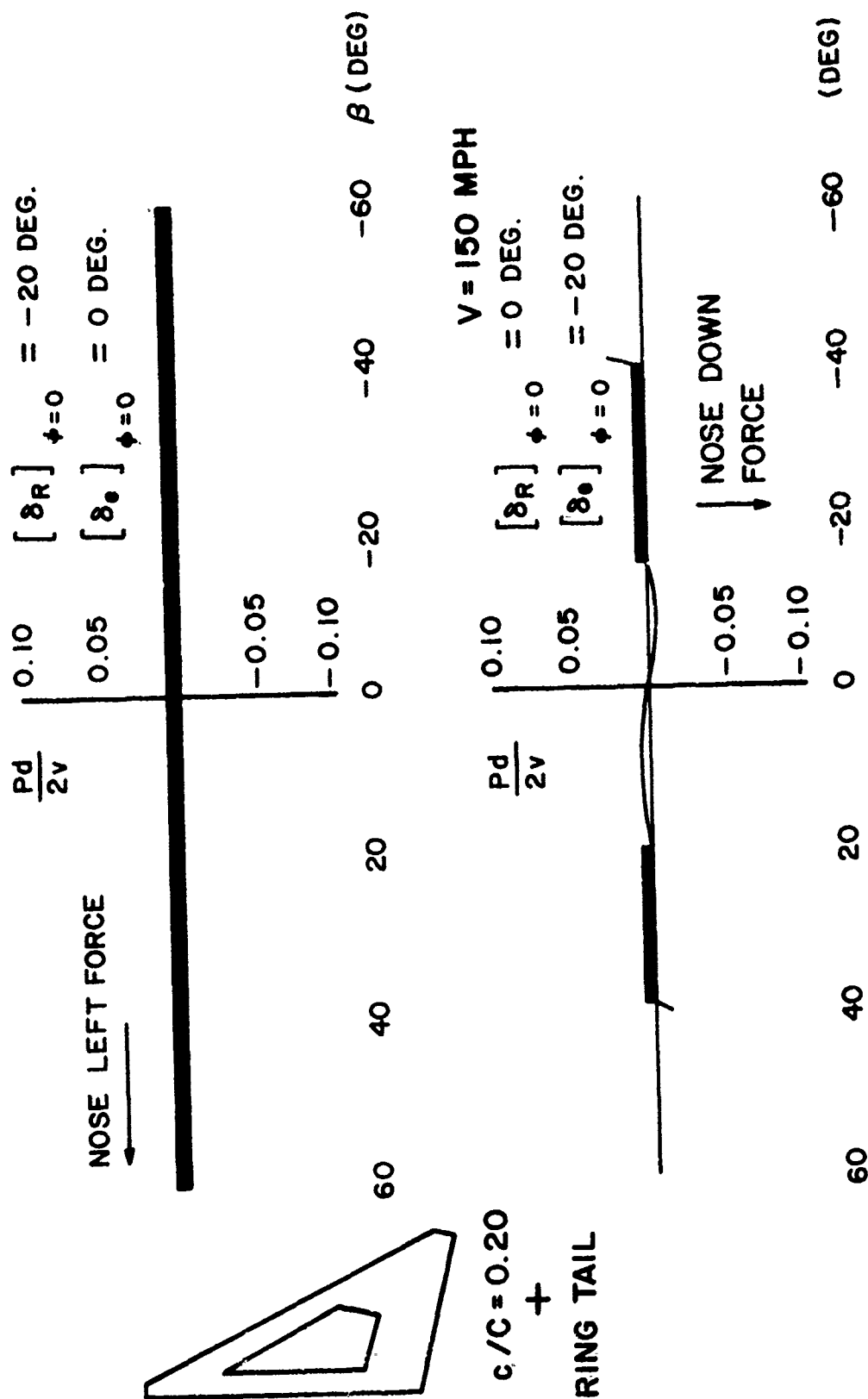


FIGURE 14. Steady State Roll Rate Versus Angle of Attack for Model with Commutating Canards Producing Nose Left and Nose Down Control Force ( $c/C = 0.20 + \text{Ring Tail}$ )

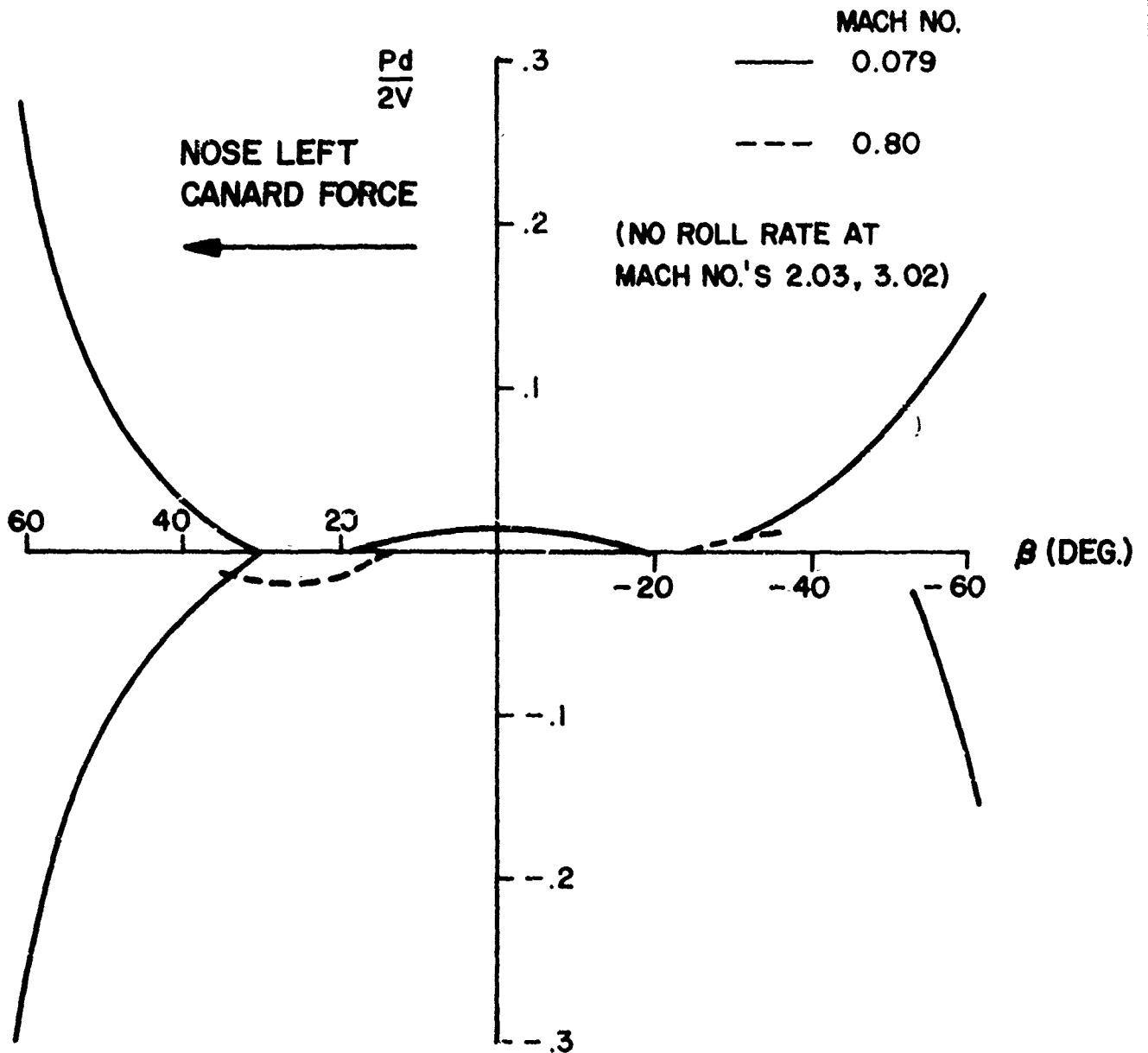


FIGURE 15. Comparison of Steady State Roll Rates Versus Mach Number for Basic Configuration with Commutation Canards Producing Nose Left Control Force.

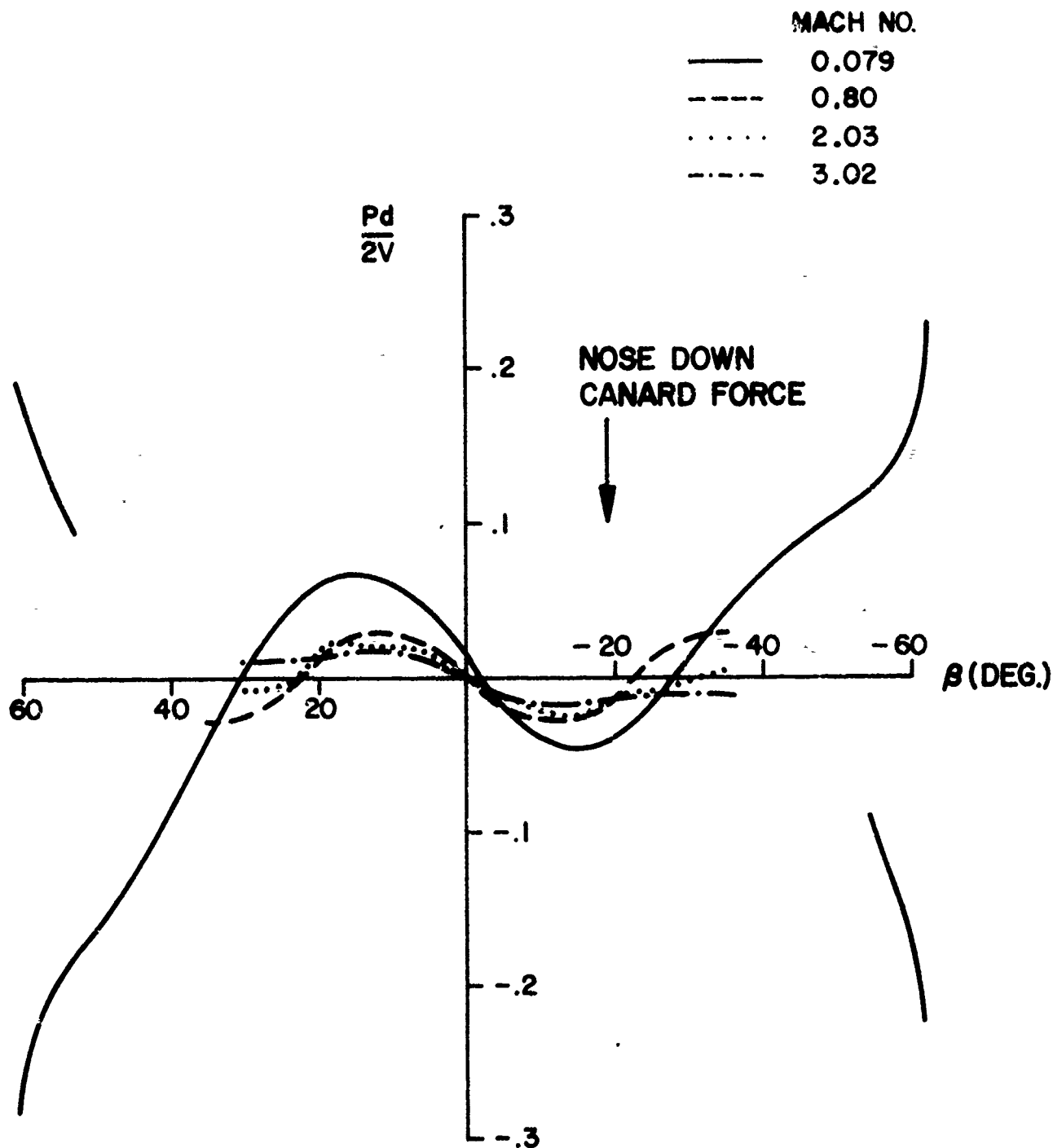


FIGURE 16. Comparison of Steady State Roll Rates Versus Mach Number for Basic Configuration with Commutation Canards Producing Nose Down Control Force

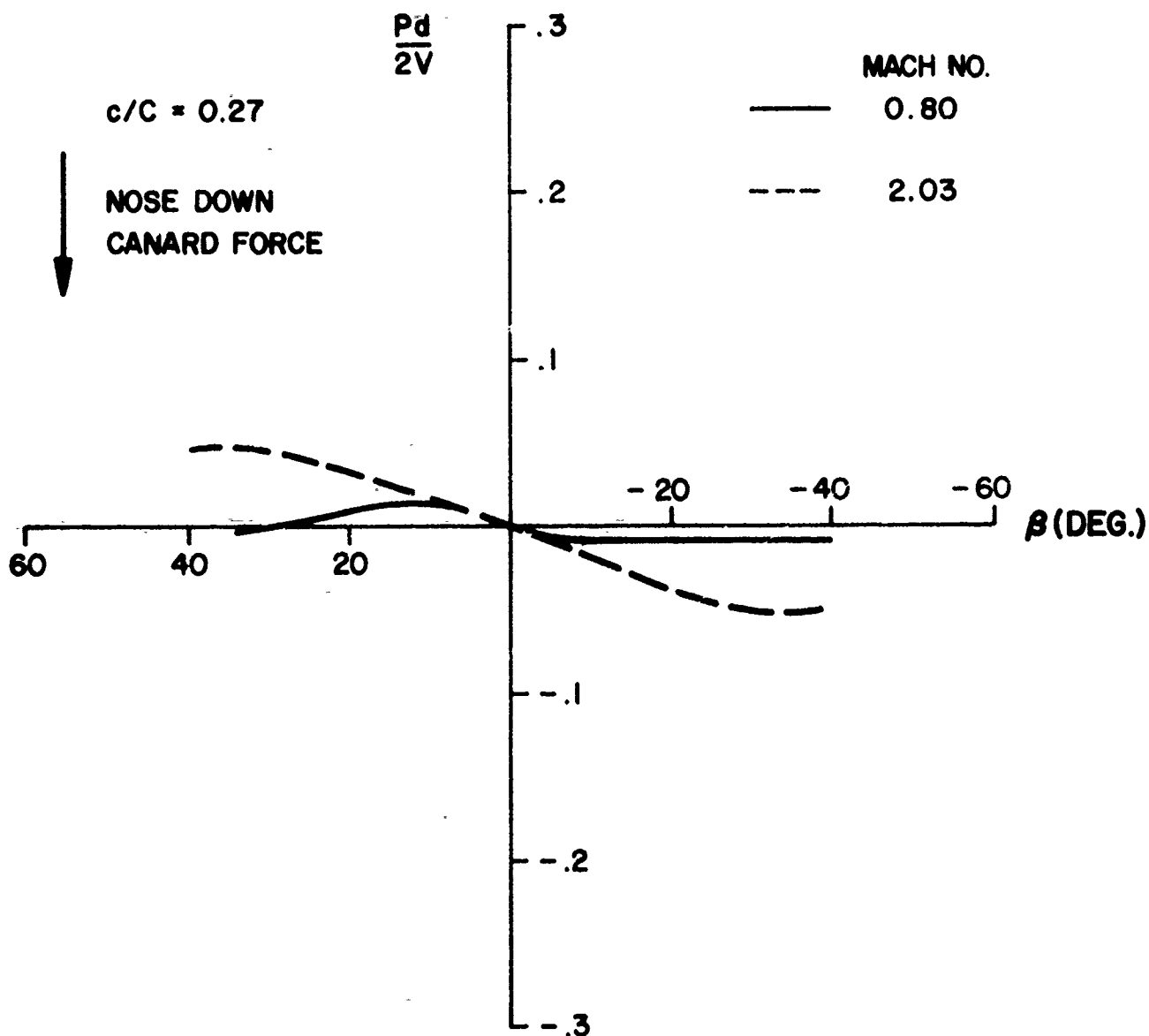


FIGURE 17. Effect of Mach Number on Steady State Roll Rate Versus Angle of Yaw for Model with Commutating Canards Producing Nose Down Control Force (Tail Removed,  $c/C = 0.27$ )

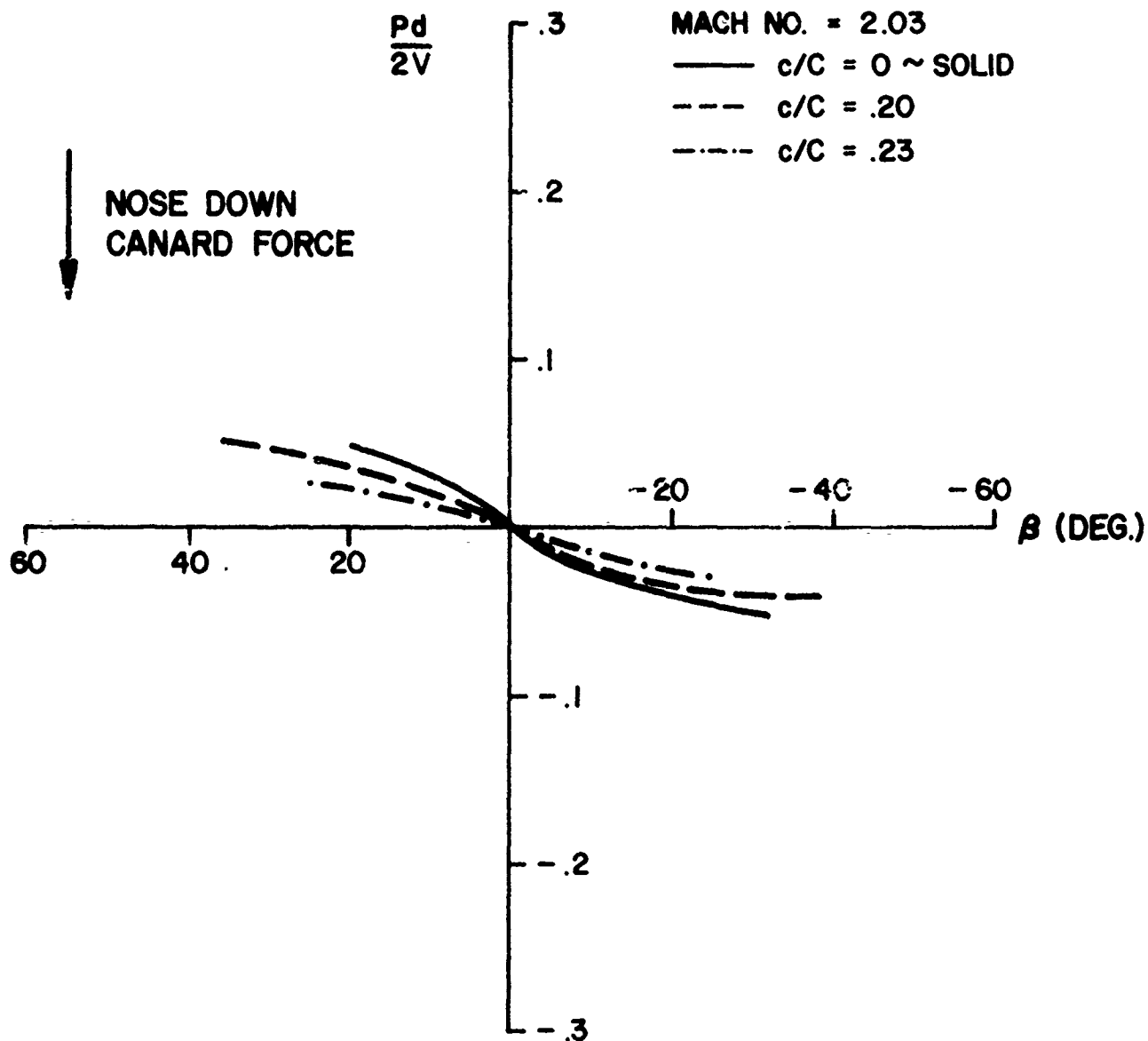


FIGURE 18. Effects of Slot Size at Supersonic Speed on the Steady State Roll Rate Versus Angle of Yaw for Model with Commutating Canards Producing Nose Down Control Force ( $c/C = 0, .2, .23$ , and Tail Off)



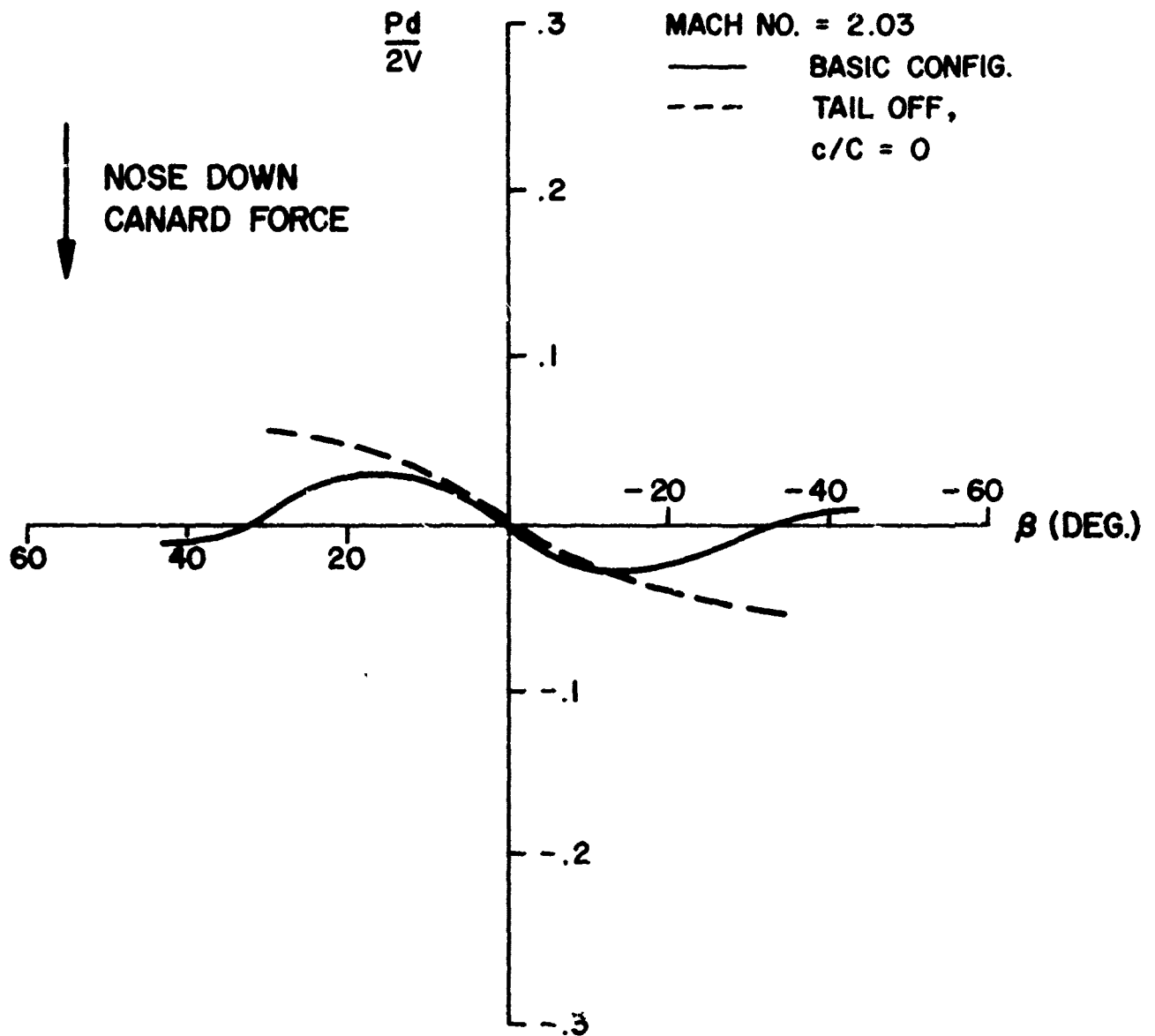


FIGURE 19. Comparison of Steady State Roll Rate Versus Angle of Yaw for Basic Configuration with Solid Commutating Canards Producing Nose Down Control Force (Tail On and Tail Off)

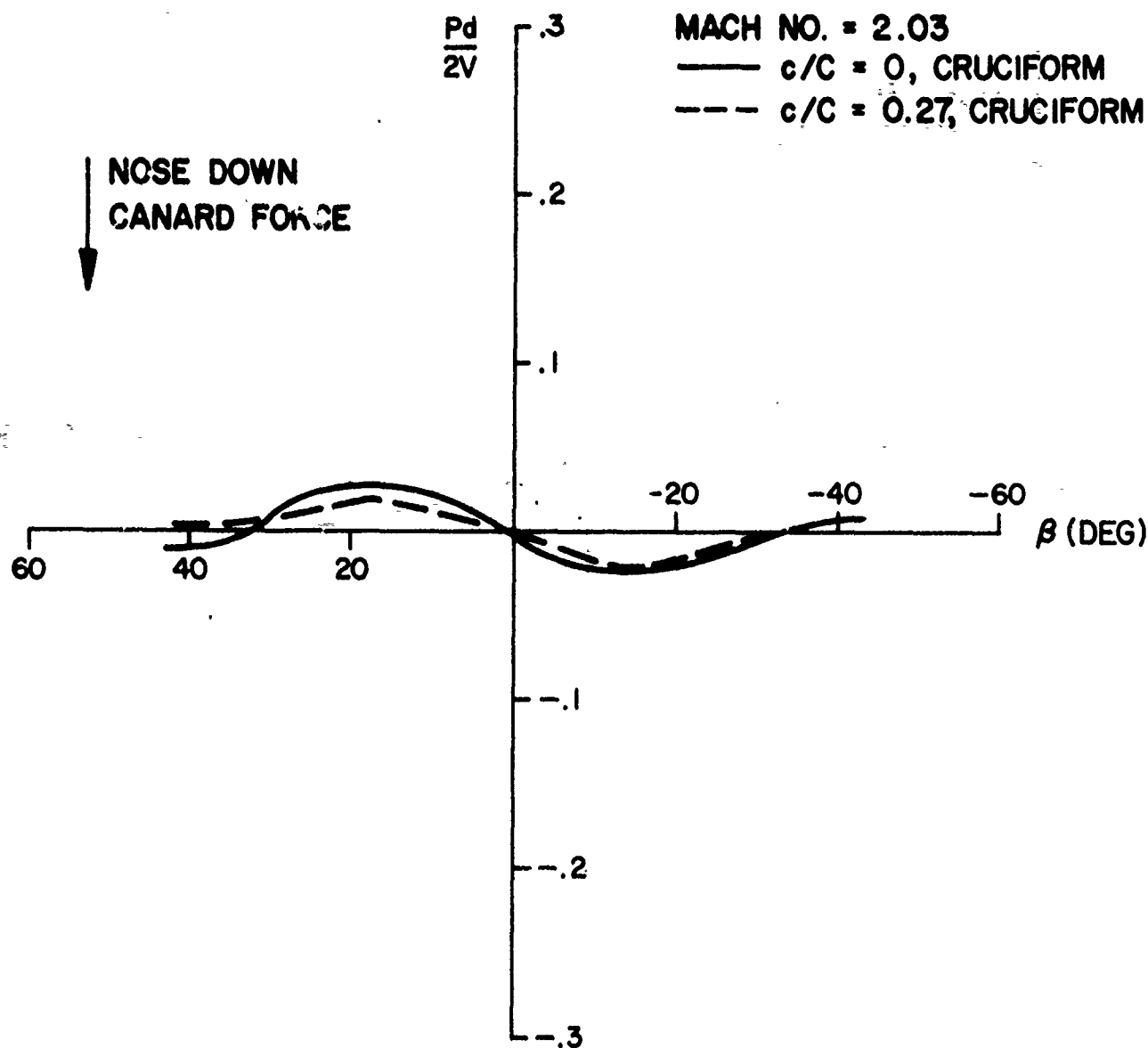


FIGURE 20. Comparison of Steady State Roll Rate Versus Angle of Yaw for Basic Configuration With and Without Slotted Commutating Canards Producing Nose Down Control Force

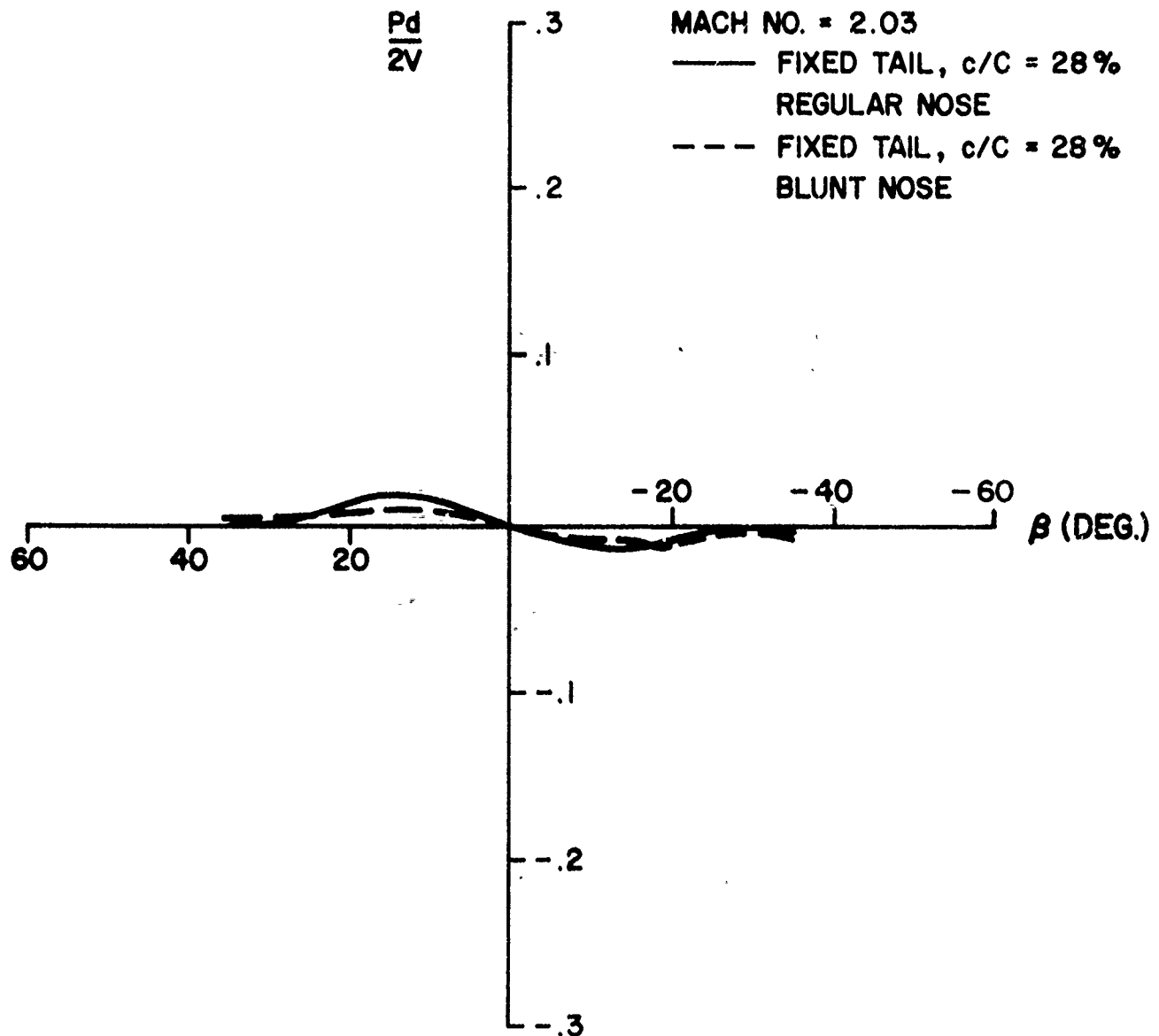


FIGURE 21. Effect of Nose Bluntness on Steady State Roll Rate Versus Angle of Yaw for Model with Commutating Canards Producing Nose Down Control Force ( $c/C = .28$ , Cruciform Tail, Blunt Nose)

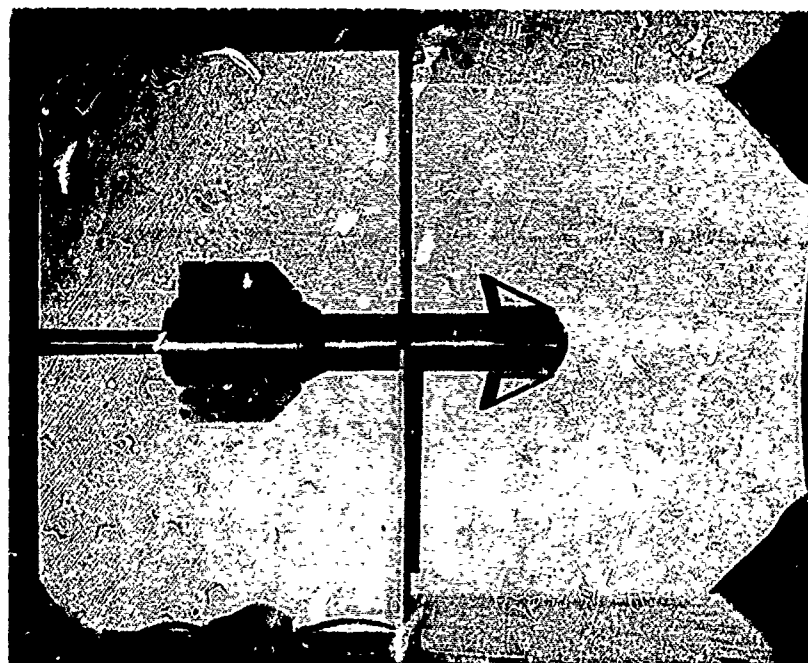


FIGURE 22. Minimum Roll Rate Configuration at Supersonic Speed

PAPER NO. 4

SUPERSONIC LIFTING-SURFACE PROGRAM  
FOR CRUCIFORM MISSILES WITH  
APPLICATIONS TO INDUCED ROLL

by

Marnix F. E. Dillenius, Jack N. Nielsen  
and Michael J. Hensch

NIELSEN ENGINEERING & RESEARCH, INC.  
510 Clyde Avenue  
Mountain View, CA 94043

THIS PAGE IS BEST QUALITY PRACTICABLE  
FROM COPY FURNISHED TO DDG

## ABSTRACT

A computer program has been written for supersonic cruciform wing-body combinations under combined pitch and yaw. The program is based on supersonic potential flow theory and involves line sources and doublets to model the body and uses constant  $u$ -velocity panels to represent the wing and to account for wing-body interference. The wing surfaces or fins can be of general planform and may be deflected. Loading pressures are determined from the flow field by means of the Bernoulli pressure equation so that significant nonlinear effects such as induced roll can be calculated. The computer program is designed to study high angle-of-attack characteristics such as calculating the effect of body nose vortices on canard fin loading. It can also determine the suction-force distributions along the leading edges and side edges of the fins. These quantities are useful in setting up the separation vortex pattern by the Polhamus analogy. It also provides a means for determining the loading on the tail section due to trailing vortices from the body nose, canard fins and missile afterbody. The program has been used to develop and check engineering methods designed specifically to calculate rolling moments. Comparisons between predicted and experimental results for wings alone and for a cruciform wing-body combination for several Mach numbers indicate good agreement.

## LIST OF SYMBOLS

AR	aspect ratio
B	$\sqrt{M^2 - 1}$
$\frac{b}{2}$	semispan of a wing surface or fin, length measured from root chord to tip; figure 1
c	length of panel chord passing through centroid of constant u-velocity panel
CNC, CN	normal-force coefficient acting on a canard fin, $N/qS_{ref}$ , see sketch in section 3.5 for sign convention
CRMC, CRM	rolling-moment coefficient of canard fin measured about body axis, see sketch in section 3.5 for sign convention
$C_p$	pressure coefficient, $(p - p_\infty)/q$
$C_N$	normal-force coefficient, $N/qS_{ref}$
$C_L$	lift coefficient, $L/qS_{ref}$
$C_l$	rolling moment, $M_R/qS_{ref}l_{ref}$ , positive clockwise when viewed from rear
$F_x$	force acting in the plane of the wing surface in the positive $x_w$ direction
$F_y$	force acting in the plane of the wing in the positive $y_w$ direction
L	lift force
$l_{ref}$	specified reference length
M	free-stream Mach number
$M_R$	rolling-moment measured about body axis
N	force normal to fin planform
p	local static pressure

Vol. 1

$p_{\infty}$	free-stream static pressure
$q$	dynamic pressure based on free-stream conditions
$s$	width of constant $u$ -velocity panel
$S_{ref}$	specified reference area
$V$	resultant flow velocity
$V_N$	perturbation velocity normal to body interference panel
$V_{\infty}$	free-stream velocity vector
$u, v, w$	perturbation velocities nondimensionalized with $V_{\infty}$ in the $x, y, z$ directions and associated with the semi-infinite triangle, figure 2, except in section 2.5 where $u, v, w$ are in wing-body coordinate system $x_B, y_B, z_B$
$\bar{u}, \bar{v}, \bar{w}$	perturbation velocities nondimensionalized with $V_{\infty}$ in the wind axis system, $\bar{u}$ along free-stream direction, $\bar{v}$ positive to the right and $\bar{w}$ positive upwards
$u_w, v_w, w_w$	perturbation velocities, nondimensionalized with $V_{\infty}$ in the $x_w, y_w, z_w$ directions associated with the wing surfaces, figure 1
$x, y, z$	coordinate system associated with semi-infinite triangle, figure 2. Origin is at apex, $x$ axis coincident with side edge in downstream direction, $y$ axis positive to the right when looking upstream, and $z$ axis positive in upwards direction. Triangle lies in $x, y$ plane.
$x_B, y_B, z_B$	body rectangular coordinate system with origin at body nose, figure 4; $x_B$ axis positive downstream along centerline; $y_B$ and $z_B$ axes aligned with fins such that $y_B$ positive to right when looking upstream and $z_B$ positive upwards for zero roll angle



$x_W, y_W, z_W$	wing coordinate system with origin located at leading edge of wing root chord, figure 1. If wing is attached to body, the origin is moved to the body centerline, $x_W$ axis back in streamwise direction, $y_W$ positive to the right when looking forward, and $z_W$ positive in upwards direction. Horizontal wing lies in $x_W, y_W$ plane
$\alpha$	angle of pitch, degrees
$\beta$	angle of sideslip, degrees
$\gamma$	ratio of specific heats, $\gamma = 1.4$ for air
$\alpha_c$	angle between body centerline and free-stream direction, "included angle", degrees
$\delta$	fin deflection angle, degrees
$\phi$	roll angle, positive in clockwise direction when looking upstream
$\Lambda$	leading- or trailing-edge sweep angles, degrees sweep angle of bound leg of horseshoe vortex
$\Gamma$	circulation strength of one horseshoe vortex

## SUBSCRIPTS

B	body
cen.	centroid
i	induced
N	normal
LE, $l_e$	wing leading edge
TE, $t_e$	wing trailing edge
RM	rolling moment
w	wing

Vol. 1      SUPERSONIC LIFTING-SURFACE PROGRAM  
             FOR CRUCIFORM MISSILES WITH  
             APPLICATIONS TO INDUCED ROLL

by

Marnix F. E. Dillenius, Jack N. Nielsen,  
and Michael J. Hensch  
Nielsen Engineering & Research, Inc.  
Mountain View, California

1. INTRODUCTION

In recent years, there has been renewed interest in missile aerodynamics particularly in the areas of high angle-of-attack characteristics and other nonlinear behavior such as induced roll. Many missile configurations of interest employ cruciform wing-body configurations in either the canard section or tail section or both. Better methods for calculation of the aerodynamics of such configurations are needed.

Until recently, methods for calculating missile aerodynamics have been dominated by slender-body theory. The need for a rational and accurate prediction method applicable to configurations with general fin shapes has long been unfilled. Although airplane lifting-surface computer programs have been developed by several investigators (refs. 1, 2, and 3), nonplanar programs applicable to cruciform missiles have not been available until now. To be useful, such programs must be able to compute the surface loadings and flow fields generated by modern high performance cruciform missiles. Essentially, this means that the programs must handle the following conditions:

- (a) Combined angle of attack and sideslip with unequal fin deflection. This capability allows the user to determine

loadings for actual control situations.

(b) Leading and Side-Edge Vortex Separation. At high angles of attack ( $\alpha > 10^\circ$ ), most fin planforms shed either leading or side-edge separation vortices. Recently, Polhamus developed an analogy which helps in estimating the strength of these vortices (ref. 4). Since his method requires the determination of the leading- and side-edge suction forces, the program should have this capability.

(c) Nose-Canard Fin Interference. At moderate angles of attack, separated flow can be generated by the missile nose. This flow can strongly influence the loading on the canard fins. Hence, the computer program must be able to determine the effects of the vortices on the fin loadings.

(d) Vortex-Tail Interference. An important source of interference is that caused by the canard trailing vortices and body-separation vortices as they influence the tail. The usual method of tracking these vortices requires the approximations of slenderness and incompressibility. To remove these restrictions requires the use of the wave equation. Hence, the program should be able to track the interfering vortices from the regions where they originate to the tail using the wave equation.

A computer program possessing all of the above capabilities will obviously be very useful in developing and checking simpler engineering methods for high angle-of-attack missile aerodynamics.

Under the consistent sponsorship of the Office of Naval Research,\* Nielsen Engineering & Research, Inc. has been actively involved in a continuing effort to develop a computer program to calculate the aerodynamic characteristics of cruciform missiles at combined pitch and yaw conditions. The work was initiated under the direction of Mr. David Siegel. The initial effort is documented in reference 5.

It is the purpose of this paper to describe the analysis contained in the computer program in general terms and to present comparisons with experimental data for wings alone and for a cruciform wing-body combination.

An augmented version of the program was used to generate data required by the engineering methods in missile aerodynamics developed for the Naval Weapons Center published in reference 6. This reference also contains the most recent computer program description as an appendix. Detailed accounts of the basic theoretical method are given in reference 5.

## 2. ANALYTICAL PROCEDURE

The methods summarized below for determining the aerodynamic characteristics of a cruciform wing-body configuration in supersonic flow are based on potential flow theory. First, the representation of the wing surfaces or fins in terms of constant  $u$ -velocity panels is described. After a short discussion of the body flow model, which is a superposition

---

\*ONR Contract N00014-74-C-0050, Task NR 215-226, Commander P. R. Hite, Scientific Officer.

of fundamental solutions, it will be shown how the cruciform wing and body potentials are combined, taking full account of mutual interference. Then a description is given of the nonlinear pressure relationship used in the calculation of the individual fin loadings.

## 2.1 Finite Element Method for Wings Alone

The planform of each wing surface or fin is divided into many trapezoidal area elements each with a uniform but unknown axial velocity over its area. These area elements are called constant  $u$ -velocity panels. The computer program lays out these panels on the planar wing surfaces or fins taking account of the following geometric parameters.

Leading-edge shape: Straight line which may be swept. For wing-body combinations the program allows for breaks in sweep.

Trailing-edge shape: Straight line which may be swept. For wing-body combinations the program allows for breaks in sweep.

Taper: Uniform, unless there are breaks in sweep.

Mean camber surface: Planar.

Tips: Straight.

Dihedral: None.

Thickness: Zero.

The following discussion applies to the case of zero sideslip. Special care must be taken with planar wings in sideslip as will be discussed in section 3.3.

## Vol. 1

Figure 1 shows the planform of one wing surface or fin. The side edges of the constant  $u$ -velocity panel\* are always taken parallel to the free-stream vector, and the leading and trailing edges of the panel are usually swept. These edges are called subsonic or supersonic depending on whether or not the component of the free-stream velocity perpendicular to the edge is subsonic or supersonic. Each constant  $u$ -velocity panel contains a control point at the 95-percent chord which passes through the panel centroid. The flow tangency condition applied at these points gives rise to a set of simultaneous equations if the solution for a constant  $u$ -velocity panel is known.

The solution for the constant  $u$ -velocity panel, such as the crosshatched one shown in figure 1, is obtained through a superposition scheme of the solutions for four semi-infinite triangular shapes with their apexes at each of the corners. The solution to the wave equation for a semi-infinite triangle subject to a jump condition in axial (or  $u$ ) velocity is derived in reference 1 by Woodward. The procedure is summarized and its solution characteristics are discussed in reference 5. The layout of the semi-infinite triangle with a subsonic leading edge and its relationship to the free-stream Mach cone are shown in figure 2. Induced upwash  $w$  is always singular on the side edge and on the leading edge if it is subsonic. The perturbation velocity components,  $u, v, w$ , become zero on the Mach cone. The

\*We will refer to the individual wings or tails as fins and use the word "panel" to apply to the constant  $u$ -velocity panels exclusively.

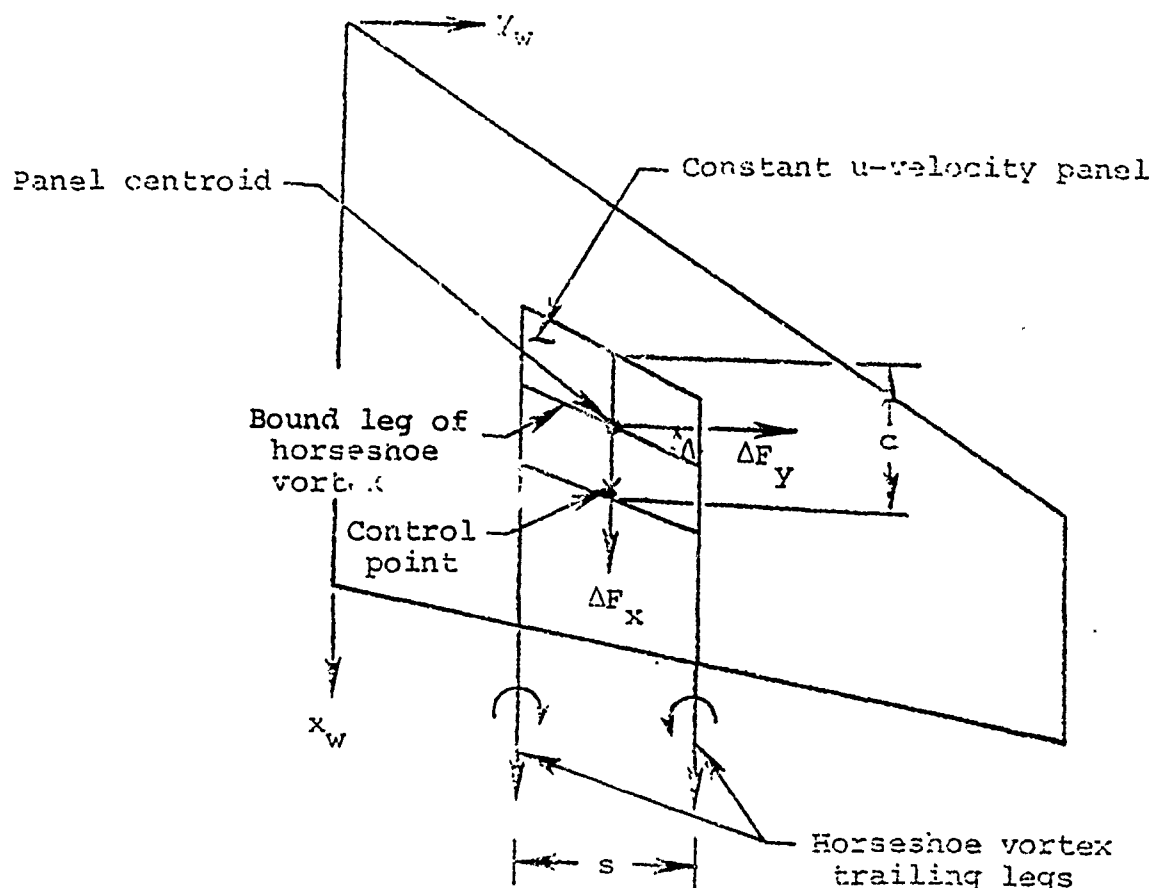
superposition scheme for two cases is shown in figure 3. These panels may have sweptback, sweptforward, or mixed leading and trailing edges.

With the induced velocity expressions for the panels known, it is possible to formulate the influence of a constant  $u$ -velocity panel of unknown strength at any control point accounting for the region of influence inherent in supersonic flight. By using the flow tangency condition and by considering interactions among all panels making up the cruciform or planar wing, there results a set of simultaneous equations from which the unknown panel strengths can be determined. The flow tangency condition states that there is no flow through the fin surfaces at each control point.

## 2.2 Leading Edge and Side Edge Suction Forces

If the strengths of the constant  $u$ -velocity panels on the fin are assumed to be known, it is possible to replace these singularities by another type of singularity in a scheme to evaluate the suction forces. Specifically, the panel strengths can be converted into equivalent horseshoe vortices lying in the trapezoidal panels. The bound portions of each horseshoe passes through the panel centroid while the trailing legs extend in the streamwise direction as shown in the following sketch.

THIS PAGE IS BEST QUALITY PRACTICABLE  
FROM COPY FURNISHED TO DDC



The aerodynamic forces acting on the filaments of the horseshoe vortices can be calculated by applying the Kutta-Joukowski theorem. For example, the in-plane force acting normal to the bound leg shown in the sketch is proportional to the product of the net upwash at the panel centroid times the vortex strength. The net upwash is the sum of the free-stream component  $V_\infty \sin \alpha$  and the sum of the perturbation upwash velocities induced by the constant  $u$ -velocity panels. The axial and side force components,  $\Delta F_x$  and  $\Delta F_y$ , are then calculated for each panel and summed over all the panels.



covering the wing surface or fin to give in-plane forces  $F_x$  and  $F_y$ . For further details, refer to reference 5.

It should be noted that the in-plane forces,  $F_x$  and  $F_y$ , must appear at the edges of the fin since the fin surface cannot sustain in-plane forces in lifting-surface theory. The trailing edge has no singularities by virtue of the Kutta trailing-edge condition, if subsonic, and in no event if supersonic. Thus,  $F_x$  and  $F_y$  appear either as leading-edge or side-edge suction forces. In the case of no side edge and a straight trailing edge as for a delta wing, the vector sum of  $F_x$  and  $F_y$  must be normal to the leading edge. The distribution of leading-edge and side-edge suction forces can thus be completely determined by the computer program.

At high angles of attack, the Polhamus vortex-lift concept advanced in reference 4 states that the additional lift due to flow separation along the leading and side edges can be obtained from the suction along the edges. Furthermore, if the suction distribution is known along the leading edge, then the spanwise location of the leading-edge separation vortex can also be calculated. For fins with supersonic leading edges, the leading-edge suction will be zero, and there is no vortex lift.

### 2.3 Flow Model for Body Alone

The potential flow method used to represent the axisymmetric body in supersonic flow makes use of a distribution of line sources (cone solutions) and line doublets on the body centerline to account for volume and angle of incidence.

## Vol. 1

effects, respectively. The strengths of these singularities are determined from the flow tangency condition applied at control points on the body surface. The computer program makes use of the fact that this problem can be split into an axial and crossflow part which can be treated separately. It also takes advantage of the fact that the strengths of the body singularities can be determined in a step-by-step method which is characteristic of solutions to the wave equation. Successive steps do not influence those portions of the upstream flow which have already been solved. Theoretical details are given in reference 5.

The computer program described here is patterned after the body modeling program associated with reference 3. It has been arranged to handle the following body-nose configurations.

- a. Parabolic nose
- b. Sears-Haack nose
- c. Tangent ogive nose
- d. Ellipsoidal nose
- e. Conical nose

The first and fourth categories result in blunt noses. The body flow modeling scheme effectively modifies the nose into a point. In all cases, the nose is followed by a cylindrical part of the body.

#### 2.4 Flow Model for Cruciform or Planar Wing-Body Combination in Supersonic Flow

The methods of modeling the wing alone and body alone have been given. The method for accounting for mutual interference between a wing and body must now be addressed.

The following method is used. A cylindrical shell of constant velocity panels is constructed to cover the length along the body measured from the leading edge of fin root chord as far downstream as the body loading is desired. A typical layout to account for interference is shown in figure 4 for one cruciform fin and one quarter of the body. This layout is sufficient for determining fin loads for fins with supersonic trailing edges. For fins with subsonic edges, the body shell must be extended rearward.

The layout shown in figure 4 is also used for combined pitch and yaw. In this case the wave equation in body axes rather than wind axes is valid within the framework of supersonic linear theory. However, it is necessary to use the proper nonlinear pressure-velocity relationship in determining forces and moments. In this fashion the side edges of the control panels are always parallel to the axis or the Mach cone and the singularities along the side edges do not cross the control points at any angle of attack and sideslip. The same panel layout can thus be used for all angles of attack and sideslip.

Once the body interference panels are laid out, the interference account proceeds as follows. The three-dimensional source and doublet singularities used to model the body alone, as described above, induce perturbation velocities  $v_1, w_1$  at the control points distributed over the wing surfaces or fins. These velocities are then included in the wing flow tangency boundary conditions. The flow tangency condition applied to the body interference panels

## Vol. 1

states that the sum of the perturbation velocities induced by all constant u-velocity panels normal to the body surface must be zero. Effects of both the constant u-velocity panels laid out on the fins and the body-interference shell are included.

By considering all components of the velocity normal to each control point and setting the sum equal to zero for each point produces a well-conditioned set of simultaneous equations for calculating all panel strengths.

## 2.5 Pressure Equations

During the most recent development stages of the cruciform missile program, a number of relationships between velocity field and pressure field were investigated. In the computer programs of reference 1 through 3, which are concerned with planar wing-body configurations, the constant u-velocity panels are called constant pressure panels. This means that in the referenced programs, the pressure is related to the axial perturbation velocity  $u$  through the ordinary linear relationship

$$C_P = - \frac{2u}{V_\infty} \quad (1)$$

This expression is categorized as a first-order result and is usually employed in the case of a wing alone. It was found, however, that this specification was not accurate enough in the application to a cruciform wing-body combination either pitched and yawed or with deflected panels (such as yaw control). For these cases, certain significant phenomena

could only be determined if nonlinear pressure relationships were used. (It is known that certain square terms in the pressure relationships are significant within the framework of slender body theory.) Important effects such as induced roll due to panel-panel interference are second order and can only be treated using second-order terms. Thus, the flow field is solved as a linear problem and the pressure field is determined by a nonlinear formula. The various pressure equations investigated are listed below. Further details can be found in references 7 and 8.

In addition to the simple linear relationship given by equation (1), there is the extended linear version which is an attempt to keep the simple formulation and yet to account for the axis of  $u$  not being in the free-stream direction. The result is given by

$$C_P = - \frac{2\bar{u}}{V_\infty} \quad (2)$$

where

$$\bar{u} = u \cos \alpha_c - v \sin \alpha_c \sin \phi + w \sin \alpha_c \cos \phi$$

Note that  $u, v, w$  are in the coordinate system fixed in the wing-body as shown in figure 4.

The Bernoulli equation for compressible isentropic flow can be written

$$C_P = \frac{p - p_\infty}{\rho_\infty} = \frac{2}{\gamma M_\infty^2} \left\{ \left[ 1 + \frac{\gamma - 1}{2} M_\infty^2 \left( 1 - \frac{V^2}{V_\infty^2} \right) \right]^{\gamma/(\gamma-1)} - 1 \right\} \quad (3)$$

where  $V$  is the magnitude of the resultant flow velocity.

In terms of perturbation velocities  $u, v, w$

$$\frac{v^2}{V_\infty^2} = 1 + \frac{2u}{V_\infty} \cos \alpha_c - \frac{2v}{V_\infty} \sin \alpha_c \cos \phi + \frac{2w}{V_\infty} \sin \alpha_c \cos \phi + \frac{(u^2 + v^2 + w^2)}{V_\infty^2} \quad (4)$$

By expanding Bernoulli's equation in powers of the perturbation velocity components, the second-order pressure equation is expressed in terms of the velocity components  $\bar{u}, \bar{v}, \bar{w}$  associated with the free-stream direction as

$$C_P = -\frac{2\bar{u}}{V_\infty} - \frac{(\bar{v}^2 + \bar{w}^2)}{V_\infty^2} + \frac{(M^2 - 1)\bar{u}^2}{V_\infty^2} \quad (5)$$

where  $\bar{u}$  is specified in equation (2) and

$$\left. \begin{aligned} \bar{v} &= v \cos \phi + w \sin \phi \\ \bar{w} &= -u \sin \alpha_c - v \cos \alpha_c \sin \phi + w \cos \alpha_c \cos \phi \end{aligned} \right\} \quad (6)$$

In slender-body theory, the last term of equation (5) is not significant and the result is

$$C_P = -\frac{2\bar{u}}{V_\infty} - \frac{(\bar{v}^2 + \bar{w}^2)}{V_\infty^2} \quad (7)$$

where  $\bar{u}, \bar{v}, \bar{w}$  are given by equations (2) and (6).

The various equations and resulting load results were compared with one another and experiment for cruciform wing-body combinations. As a result, the Bernoulli equation, equation (3), was retained on the basis of best overall

correlation with experimental data for individual fin loadings, some of which will subsequently be shown.

The pressure loading acting on a constant  $u$ -velocity panel is calculated by taking the difference between the pressure coefficients acting on the top and bottom of the panel near its control point. The normal-force and rolling-moment coefficients are then determined directly from the pressure distributions and panel areas.

### 3. COMPARISONS BETWEEN PROGRAM PREDICTIONS, OTHER THEORIES, AND EXPERIMENT

A series of comparisons between program predictions and experimental data will now be presented. They are designed to illustrate certain aerodynamic phenomena. Comparisons are first shown for delta wings of three different aspect ratios for which experimental data are available. Both unyawed and yawed cases are discussed. A yawed planar and a cruciform wing are also compared in terms of rolling moment as a function of the number of constant  $u$ -velocity panels used. Comparisons of individual fin loadings are then given for a cruciform canard-body model. A separate section is concerned with certain important aspects of induced roll. Finally, an example is given illustrating the effects of a specified external vortex on the fin loadings.

#### 3.1 Delta Wing with Subsonic Leading Edge

Figure 5 shows comparison between calculated and experimental lift data from reference 9 for a triangular wing with aspect ratio 1. The Mach number is 1.96 and the

wing has subsonic leading edges. For low angles of attack, the theory closely matches the experiment. As  $\alpha$  is increased, the theory underestimates the lift. The increased lift is known to be associated with leading-edge separation and the associated shed vorticity. Polhamus, reference 4, in his study of this phenomena has termed the increased lift associated with the separation "vortex lift." He has advanced the "vortex-lift analogy" as a means for estimating the increased lift. To apply this analogy requires a knowledge of the leading-edge suction force theoretically developed by the wing. The present program has been designed to supply this information. Carrying out the calculation yields the curve in figure 5 labeled "Present Method + Polhamus Vortex Lift." This result is closer to the experimental data for the higher angles of attack than the theory neglecting vortex lift. Until the present program was developed, it was not possible to calculate vortex lift for fins mounted on bodies, for fins at combined pitch and yaw, or for fins subject to vortex influence. For fins with side edges, suction forces also develop which can produce vortex lift as described in reference 10 by Lamar.

The dashed line labeled "conical flow theory" in figure 5 represents the analytical theory for a triangular wing with a subsonic leading edge as described in reference 7. The present theory and conical flow theory agree very closely and should ideally coincide. Conical flow theory does not account for vortex lift.



### 3.2 Delta Wing with Supersonic Leading Edge

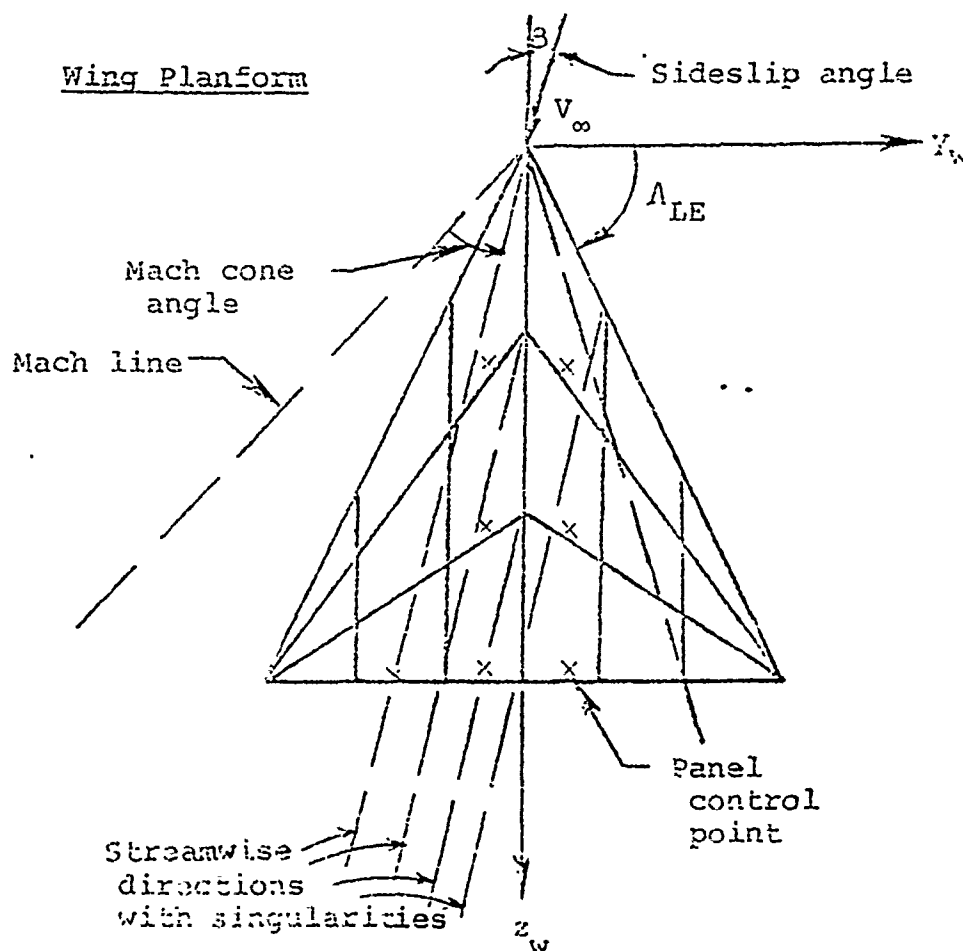
Supersonic leading edges develop no leading-edge suction, and the present theory can be applied to delta wings with such edges without the complicating factor of vortex lift. Comparison of the predicted normal-force curve with experimental data from reference 11 for an aspect ratio 3.652 triangular wing is shown in figure 6. For the specified Mach number of 1.968, this wing has supersonic leading edges. The present method is based on five panels along the chord and ten along the semispan for a total of 50 panels per half wing. Agreement with experiment is very good. The result from conical flow theory, reference 7, is also shown. The computer program predicts a residual amount of leading edge suction which is very small. If a larger number of panels is used on this wing, the residual approaches zero.

For unyawed wings, the present results indicate that the use of 50 panels per fin with about four or five panels in the chordwise direction will produce quite accurate gross results. (Probably more panels are required for accurate side-edge suction forces on wings with stream-wise tips) Further details on the wing-alone comparisons can be found in reference 5.

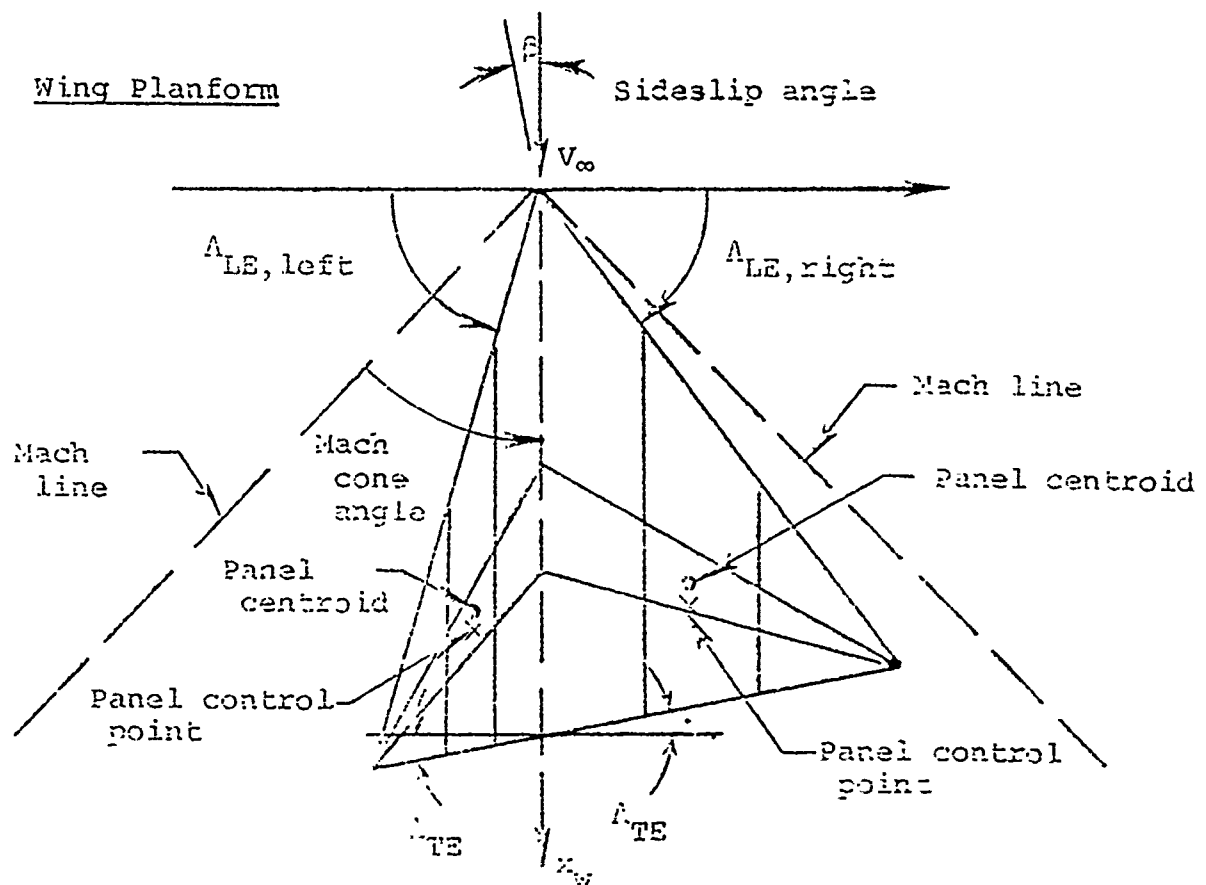
### 3.3 Delta Wing in Pitch and Sideslip

In treating a delta wing in sideslip, the first thought was to maintain a symmetric panel layout with the side edges parallel to the wing root chord, and with the control points fixed at the 95-percent location on the centroid chord since

in this way the panel layout and control-point locations would not depend on the angle of sideslip  $\beta$ . A constant u-velocity panel with side edges which are not streamwise has a singularity along the streamwise directions from all its corners as shown in the sketch below. Such a singularity can fall on top of control points behind the panel for certain sideslip angles and produce infinite influence coefficients. Under these conditions, the matrix solution for the panel strengths may still proceed by adjusting the influence coefficients but the results show erratic variations in panel



strengths over the wing planform. Furthermore, as the number of panels is increased, the wing loading results will not converge. Consequently, the asymmetric elemental panel layout was adopted as shown in the following sketch. On account of



the rotation of the wing coordinate system such that the  $x_w$  axis is aligned with the free stream, it is noted that the sweeps of the wing leading edges now differ for each edge and depend on angle of sideslip. The trailing-edge sweeps are now nonzero. Depending on the Mach number and the vertex angle of the wing, there can be subsonic, supersonic,

or mixed wing leading and trailing edges. Rolling moment, unlike wing lift, is sensitive to angle of sideslip; it, therefore, presents a critical test of the theory for sideslip.

In order to test the computer program, it was applied to a delta wing of  $AR = 2.3$  in sideslip for a range of supersonic Mach numbers. The quantity calculated is the rolling-moment coefficient  $C_l$  per unit angle of attack in radians and is given by

$$\frac{C_l}{\alpha} = \frac{\text{Rolling moment about wing centerline}}{S_{\text{ref}}^2 \ell_{\text{ref}} q \alpha} \quad (8)$$

where

$S_{\text{ref}}$  = reference area, wing planform area

$\ell_{\text{ref}}$  = reference length, wing span

$q$  = dynamic pressure

$\alpha$  = angle of attack, radians

In figure 7, results obtained from present theory, conical flow theory (ref. 12), and data (refs. 13 and 14) for the rolling-moment coefficient at  $\alpha = 10^\circ$  and  $\beta = 5^\circ$  are shown as a function of Mach number for a delta wing of aspect ratio 2.3. For low Mach numbers, both leading edges of the delta wing are subsonic. For sideslip angle of  $5^\circ$ , the forward leading edge becomes sonic at  $M = 1.8$ , and the "mixed" leading-edge condition exists from here up to about

$M = 2.4$ . At  $M = 2.4$  and above, both edges are supersonic. The change in sign of  $C_p$  at  $M = 2.3$  is noteworthy. Also, it should be noted in Figure 7 that the conical flow theory shows cusps at  $M = 1.8$  and  $2.4$ .

Calculations were made with three different numbers of control panels. The linear pressure expression, equation (1), was used. At  $M = 1.4$  with 190 control panels there is close agreement with conical flow theory. At  $M = 1.8$ , where a cusp in Jones' theory occurs, the predictions of the present method are definitely low. For supersonic edges, both theories agree well even for fewer panels. It is of interest that the wind-tunnel data do not exhibit the sharp cusp at  $M = 1.3$ , and are in better agreement with the results of the present method than those of conical flow theory.

For yawed wings, a minimum of five elemental panels in the chordwise direction should be used if accurate rolling-moment results are desired.

### 3.4 Pitched and Yawed Cruciform Wing in Supersonic Flow

In the next example the computer program is applied to a cruciform wing at combined pitch and sideslip. At this condition, both the horizontal and vertical wing leading edges have unequal sweeps and the trailing-edge sweeps are nonzero. Depending on the vertex angle of the horizontal and vertical wings and the Mach number, the leading edges can be subsonic, supersonic, sonic, or mixed. Further details on the panel layout can be found in reference 5.

## Vol. 1

Some theoretical comparisons between the predicted rolling moments of the  $AR = 2.3$  delta wing previously shown and a cruciform wing made of two such wings are shown in figure 8 versus the number of panels. The planar results for  $M = 1.4$  are from figure 7. Also shown is the conical flow theory of reference 12. It is seen that the effect of adding a vertical wing is to reduce the rolling moment to a low value. A minimum of 100 panels should be used in order to obtain a converged result. For both planar and cruciform wings, the chordwise number of panels has a dominant effect on rolling moment. A minimum of five chordwise panels should be used as already mentioned above in connection with the yawed delta wing.

## 3.5 Cruciform Canard-Body Combination in Supersonic Flow

The cruciform wing-body computer program was applied to the cruciform canard-body combination shown in figure 9. This configuration is part of a missile wind-tunnel model\* recently tested by NEAR in the Ames 6- by 6-Foot Supersonic Wind Tunnel under contract to the Naval Weapons Center, China Lake, CA, NWC Contract No. N00123-74-C-0829, reference 15.

Normal force and rolling moment for each individual cruciform fin were measured. Data were taken over a range of angles of attack for several Mach numbers. Normal-force and rolling-moment coefficients are specified as follows.

$$C_N = \frac{\text{Normal Force}}{S_{\text{ref}} q}$$

\* NEAR Inc. is indebted to Mr. Ray Deep of MICOM for the use of the missile model.

$$C_{RM} = \frac{\text{Rolling Moment about Body Axis}}{S_{ref} l_{ref} q}$$

$S_{ref} = 19.62 \text{ in}^2 = \text{reference area, body cross-sectional area}$

$l_{ref} = 5.0 \text{ ins.} = \text{reference length, body diameter}$

$q = \text{dynamic pressure}$

The positive directions of the individual fin normal forces and rolling moments are shown in the following sketch looking upstream (the last letter C denotes canard).

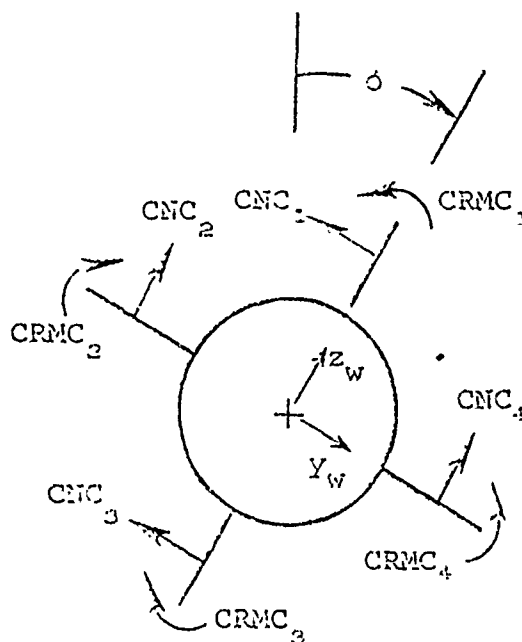


Figure 10 shows a comparison between predicted and measured fin normal-force and rolling-moment coefficients versus angle of attack. The vertical panels are deflected  $15^\circ$  and roll angle is zero. The results shown are for

## Vol. 1

$M = 1.3$  corresponding to subsonic fin leading edges. As the angle of incidence is increased, the normal force  $CNC1$  acting on the upper fin  $C_1$  decreases while the normal force  $CNC3$  on the lower fin  $C_3$  increases. The flow velocity above the horizontal fins  $C_2$  and  $C_4$  increases with angle of attack resulting in a higher Mach number in the region of fin  $C_1$ . This has the effect of lowering the loading on fin  $C_1$ . Conversely, the flow velocity below fins  $C_2$  and  $C_4$  decreases with angle of attack and the Mach number around fin  $C_3$  is reduced thereby increasing its loading. In figures 10(b) and 10(d), the effect of nose vortices on fins  $C_2$  and  $C_4$  for  $\alpha_c$  larger than  $16^\circ$  is to lower the rate of increase in measured fin loading.

The predictions in figure 10 were calculated with a distribution of 192 constant u-velocity panels. Each cruciform canard fin was divided into 4 panels in the chordwise and 9 panels in the spanwise direction for 36 panels. The body interference shell contained 43 constant u-velocity panels, 4 lengthwise by 12 on the body circumference in accordance with the layout shown in figure 4 for one fin and one quarter of the body. The ogive-cylinder body was modeled by 22 sources to account for volume and 22 doublets to account for incidence. In general, the theory indicates the trends described above. The variations with angle of attack of the calculated loadings of fins  $C_1$  and  $C_3$ , based on the Bernoulli pressure equation, agree well with the measured trends. It is worth noting that if the linear



pressure expression were used, there would be no changes in loading with angle of attack. This is an example of non-linear effects that can be predicted by linear potential theory (i.e., the use of constant u-velocity panels) in conjunction with nonlinear pressures as given by the Bernoulli expression.

In figure 11, a comparison is shown for the same configuration of figure 10 at  $M = 1.75$  corresponding to supersonic fin leading edges. In this instance, the normal-force and rolling-moment coefficients are generally lower than for the subsonic leading edge case discussed above. This behavior is also predicted by the computer program with the same panel layout and body model specification which were used for figure 10. The proper trends are indicated as the angle of attack is increased.

The behavior of the individual fin loadings at  $20^\circ$  roll is shown in figure 12. The panel deflection angles are zero and the Mach number is 1.3 corresponding to subsonic fin leading edges. The loadings on all the fins increase with included angle,  $\alpha_c$ , and this behavior is matched by the predictions which were based on the same paneling layout and body modeling scheme used to generate the results of figure 10. The effects of body-nose vortices can be noticed in the measured loadings of fins  $C_1$  and  $C_2$ .

### 3.6 Induced Rolling Moment

The differences in normal-force and rolling-moment coefficients between fins  $C_1$  and  $C_2$  are shown in figure 13 and the

## Vol. 1

differences between  $C_2$  and  $C_4$  are shown in figure 14. The case considered is the same as in figure 11; the vertical panels are deflected  $15^\circ$  at zero roll and the Mach number,  $M$ , is 1.75. The difference in rolling moment between fins  $C_1$  and  $C_3$  will be called direct roll and the difference in rolling moment between fins  $C_2$  and  $C_4$  will be called reverse roll.

The reverse roll is seen to be about one sixth of the direct roll. The predictions follow the data well for fins  $C_1$  and  $C_3$  and appear to indicate the proper trends for fins  $C_2$  and  $C_4$ . A special nonlinear phenomenon will now be described. It is possible to plot the paths of a disturbance originating at the leading edge of a fin root chord around the body surface. The method is based on the fact that a disturbance makes a constant angle, the Mach angle, with all generators of the cylindrical body as it moves around the body.

The paths are shown in planform in figure 15 for several Mach numbers. Note that for  $M = 1.75$ , linear theory dictates that small deflection angles of the vertical fins will not influence the horizontal fins. In other words, there should be no pressure exerted by the deflected vertical fins on the horizontal fins and the reverse roll should be zero. However, the measurements show a small reverse rolling moment possibly as a result of viscous effects, fin or flow misalignment or changes in the region of influence such as those shown in figure 15. On the high pressure side of the vertical fin the Mach number will be lower than the free stream value of 1.75. As a result, the region of influence of the vertical

fin on the horizontal fin can change as shown in figure 15. However, the fin deflection tends to counteract this change.

The computer program should predict zero reverse roll at all angles of attack since it assumes that the region of influence corresponds to the  $M = 1.75$  line shown in figure 15 and that it does not change with angle of attack. The fact that the computer program does not predict zero reverse rolling moment is due to numerical inaccuracy. The finite size body-interference panels allow some "leakage" from one fin to another. Increasing the number of body-interference panels from 48 to 96 reduces the error about 30 percent and does not influence the direct roll. These results are shown by the flagged symbols in figures (13) and (14).

### 3.7 Normal Forces and Moments on the Fins Induced by External Vortex; Comparison with Reverse-Flow Theory

A comparison between the effects of a vortex predicted by the cruciform missile computer program and reverse-flow theory is now given. The latter method is described in reference 16. It is a slender-body method which has been corrected for slenderness. Good comparison between the two methods means that the faster reverse-flow method can be used in engineering prediction schemes. Consider an infinite vortex parallel to the body centerline of the configuration of figure 9. For purposes of calculation the following nondimensionalized vortex strength and crossflow plane vortex coordinates in the body-coordinate system shown in figure 4 have been prescribed.

$$\frac{\Gamma}{2\pi V_{\infty} a} = 0.16$$

$$\frac{Y_v}{a} = 0.18$$

$$\frac{Z_v}{a} = 1.26$$

a = body radius, 2.5 inches.

The vortex is positive counterclockwise, when viewing upstream.

Incremental values of the normal-force coefficient,  $(\Delta CN)_v$ ,

and of the rolling-moment coefficient,  $(\Delta CRM)_v$ , have been

calculated by applying the computer program with the vortex

absent and with the vortex present, and taking differences.

The flow conditions are given by  $\alpha_c = 20^\circ$ ,  $\beta = 20^\circ$ ,  $\delta's = 0$

and  $M = 1.75$ . Calculated results obtained by considering

vortex-induced velocities parallel and normal to the fins

did not differ significantly from those results calculated

using only the vortex normal induced velocities in Bernoulli's

equation. The parallel velocity components induced by the

vortex can generally be neglected in determining vortex-

induced fin loads. Details of these calculations are given

in reference 8.

Figure 16 lists the increments in fin normal-force and rolling-moment coefficient caused by the above vortex.

Results obtained from reverse-flow theory are also listed.

The reverse-flow method does not predict the individual

fin normal forces and moments. The computer program pre-

diction can only be compared with reverse-flow theory in

terms of total normal force, total side force and total

rolling moment developed by all canard fins. The agree-

ment between the computer program results using the

Bernoulli equation and reverse-flow theory is good.

Note that if individual fin forces, rolling moment or loading distributions are desired, the present cruciform missile program must be used.

#### 4. CONCLUDING REMARKS

A computer program has been written for supersonic cruciform wing-body combinations under combined pitch and yaw. The method makes use of supersonic three-dimensional sources and doublets to model the body alone and uses constant u-velocity panels to model the wing. The effect of the wing on the body is also modeled using constant u-velocity panels. The computer program has a number of noteworthy features. First, it treats cruciform wing-body combinations with wings of general planform, accounting for sideslip (roll) and fin deflection. Second, it determines the distribution in the plane of the fin of the suction forces on the leading edge or side edge of the fin. Third, it determines loading pressures from the flow field by means of the nonlinear Bernoulli pressure equation so that significant nonlinear effects such as induced roll can be determined.

Comparisons are shown between the results calculated by the computer program and experimental data for wings alone and for a cruciform wing-body combination for several Mach numbers. In general, the agreement between prediction and experimental data is good. A typical run requires about 65 CPU seconds on a CDC 6600 computer.

The computer program has the capability of accounting for high angle-of-attack characteristics such as vortex lift

due to fin leading-edge separation since it determines the leading-edge suction-force distributions used in the Polhamus vortex-lift analogy. It also provides a means for determining the forces and moments on canard or tail sections due to trailing vortices from the body nose, canard fins, or the missile afterbody.

Work is now underway to include the capability of determining the vortex paths from the trailing edges of the canard fins to the leading edges of the tail fins using the wave equation rather than the usual slender-body method which neglects compressibility. The results of this study should yield more accurate methods of determining vortex trajectories, a question of prime concern in high angle-of-attack missile aerodynamics.

The computer program has been used in the development of an engineering method for determining induced rolling moments of canard-cruciform missiles. In this instance, it was used to evaluate panel-panel interference factors and to determine the accuracy of the reverse-flow method employed in calculating vortex-induced rolling moments.

This computer program can be naturally extended to handle wrap-around fins. More accurate body flow modeling schemes can be incorporated to increase the range of application. It is possible to extend the program to calculate pitch and roll damping.

## References

1. Woodward, F. A. and Larson, J. W.: A Method of Optimizing Camber Surfaces for Wing-Body Combinations at Supersonic Speeds. Part I - Theory and Application. Doc. D6-10741, Pt. I, The Boeing Co., 1965.
2. Woodward, F. A., Tinoco, E. N., and Larson, J. W.: Analysis and Design of Supersonic Wing-Body Combinations, Including Flow Properties in the Near Field. Part I - Theory and Application. NASA CR-73106, Aug. 1967.
3. Carmichael, R. L. and Woodward, F. A.: An Integrated Approach to the Analysis and Design of Wings and Wing-Body Combinations in Supersonic Flow. NASA TN D-3685, Oct. 1966.
4. Polhamus, E. C.: Prediction of Vortex-Lift Characteristics Based on a Leading-Edge Suction Analogy. AIAA Paper No. 69-1133, Oct. 1969.
5. Dillenius, M. F. E. and Nielsen, J. N.: Supersonic Lifting-Surface Computer Program for Cruciform Wing-Body Combinations in Combined Pitch and Sideslip. Office of Naval Research Tech. Rept. No. 1, Dec. 1974 (also NEAR TR 74).
6. Hemsch, M. J., Nielsen, J. N., and Dillenius, M. F. E.: Method for Calculating Induced Rolling Moments for Canard-Cruciform Missiles for Angles of Attack Up to  $20^\circ$ . Naval Weapons Center, NEAR TR 85, March 1975.
7. Nielsen, J. N.: Missile Aerodynamics. New York, N.Y., McGraw-Hill Book Co., 1960.
8. Nielsen, J. N., Hemsch, M. J., and Dillenius, M. F. E.: Further Studies of the Induced Rolling Moments of Canard-Cruciform Missiles as Influenced by Canard and Body Vortices, NEAR TR 79, Jan. 1975.
9. Hill, W. A., Jr.: Experimental Lift of Low-Aspect-Ratio Triangular Wings at Large Angles of Attack and Supersonic Speeds. NACA RM A57I17, Nov. 1957.
10. Lamar, J. E.: Prediction of Vortex Flow Characteristics of Wings at Subsonic and Supersonic Speeds. AIAA Paper No. 75-249, Jan. 20-22, 1975.
11. Lampert, S. L.: Aerodynamic Force Characteristics of Delta Wings at Supersonic Speeds. Jet Propulsion Lab. Rept. No. 45-32, Sept. 1954.

Vol. 1

12. Jones, A. L., Spreiter, J. R., and Alksne, A.: The Rolling Moment Due to Sideslip of Triangular, Trapezoidal, and Related Planforms in Supersonic Flow. NACA TN 1700, Oct. 1948.
13. Lipowski, K.: Die Schieberollmomente von Fünf Tragflügeln mit verschiedenen Umrissformen bei Überschallgeschwindigkeit. Zeitschrift für Flugwissenschaften, 13, Heft 12, p. 453, 1965.
14. Mantle, P. J.: On the Rolling Motion of Low-Aspect-Ratio Delta Wings. Jour. Aero. Sci., vol. 28, 1961, p. 427.
15. Hemsch, M. J. and Nielsen, J. N.: Test Report for Canard Missile Tests in the Ames 6- by 6-Foot Supersonic Wind Tunnel. NEAR TR 72, Aug. 1974.
16. Spangler, S. B.: A study of Induced Rolling Moments for Cruciform-Winged Missiles. Task II - Body Vortex-Tail Interference. NEAR TR 58, Oct. 1973.

THIS PAGE IS BEST QUALITY PRACTICABLE  
FROM COPY FURNISHED TO DDC



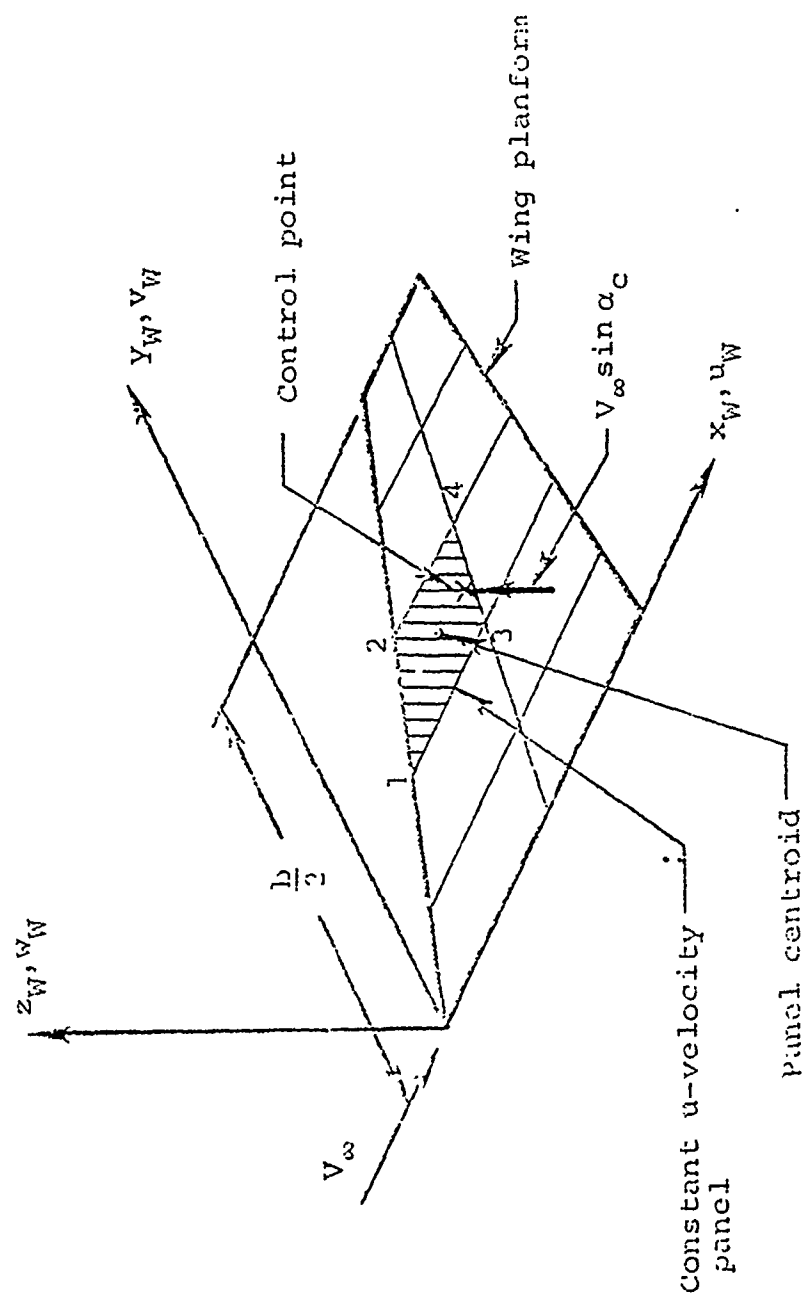


Figure 1.- Layout of constant u-velocity panels and control points on a wing planform.

THIS PAGE IS BEST QUALITY PRACTICABLE  
FROM COPY FURNISHED TO DDC

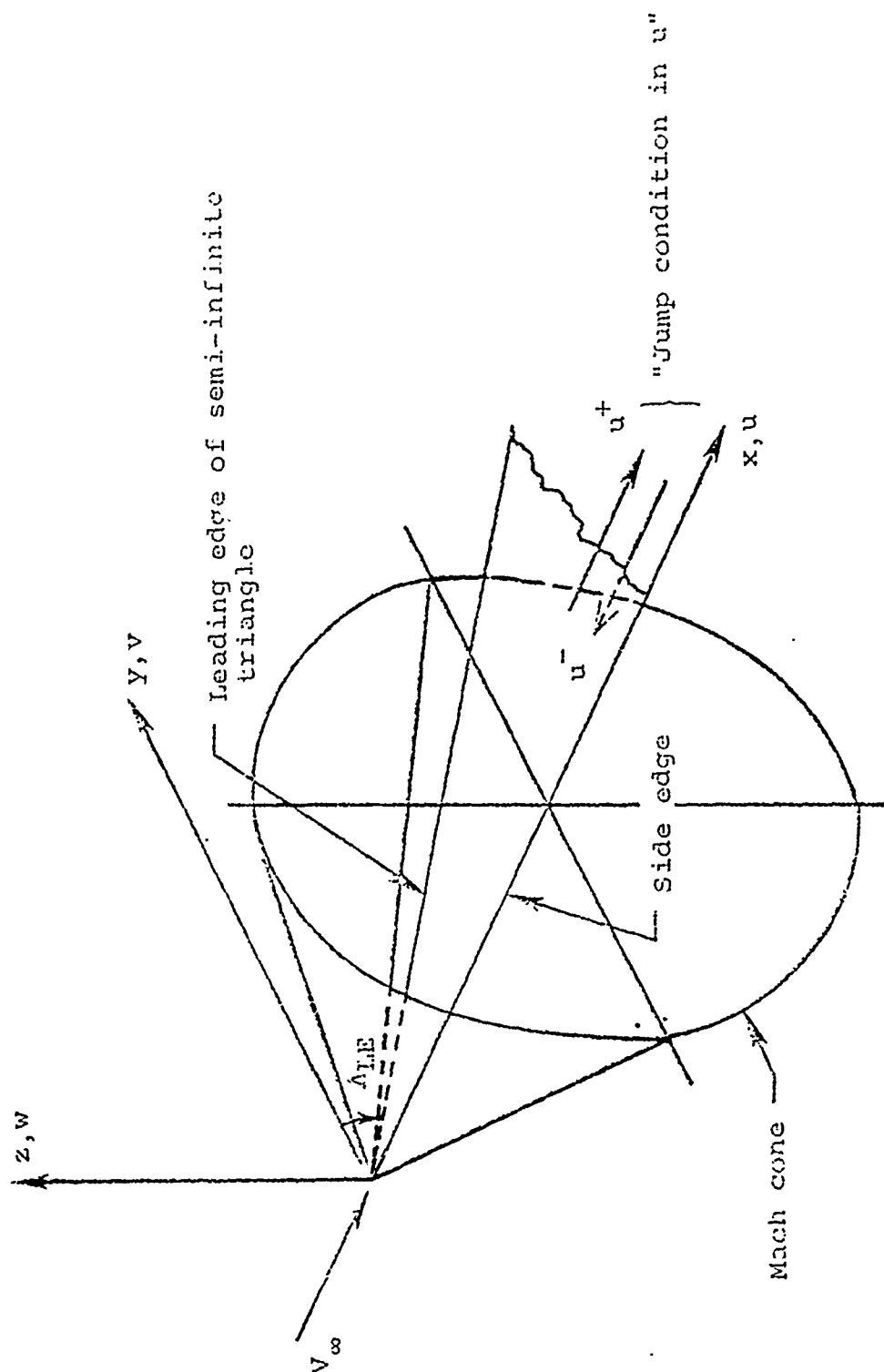
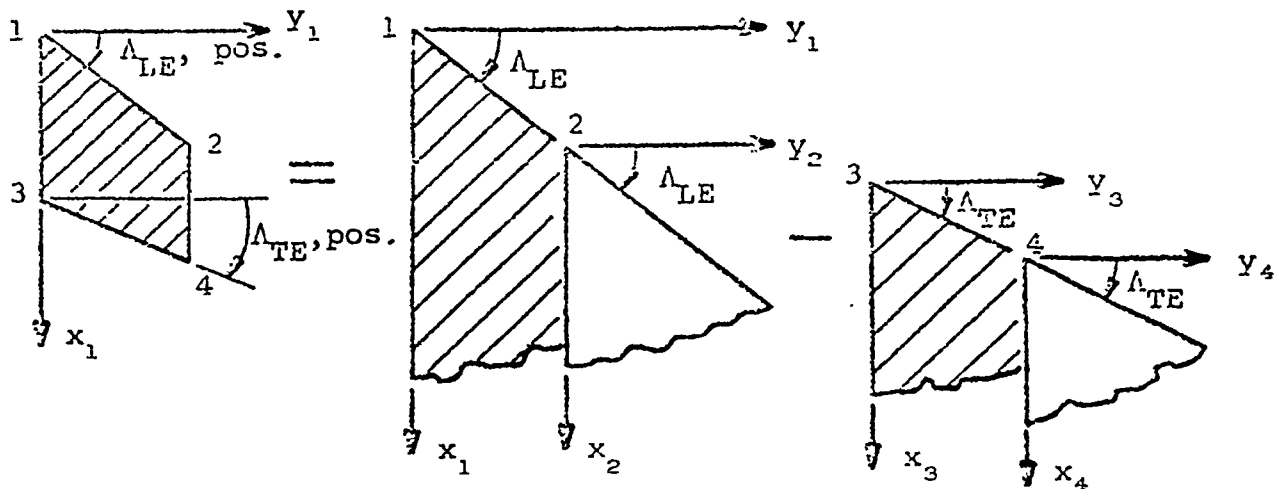


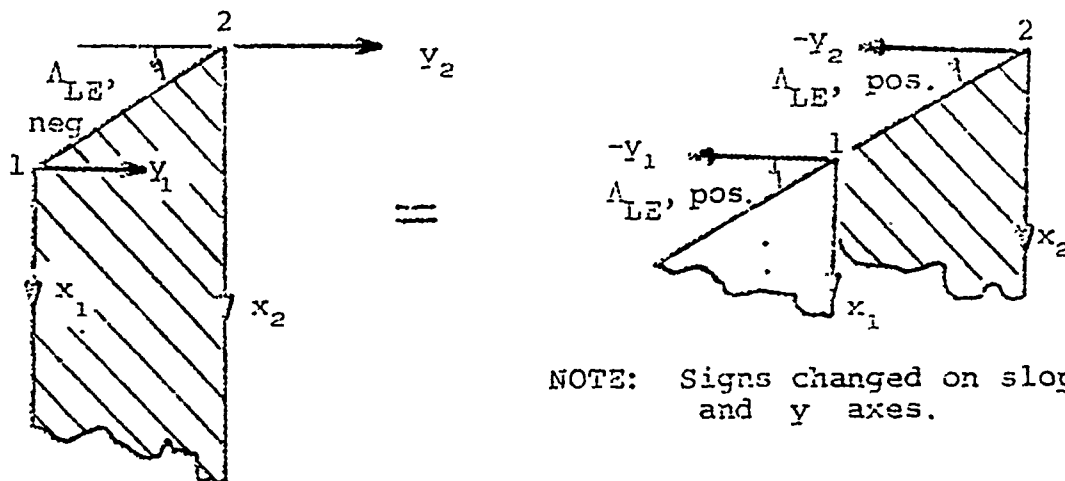
Figure 2.- Layout of semi-infinite triangular shape.

THIS PAGE IS BEST QUALITY PRACTICABLE  
FROM COPY FURNISHED TO DDC



Trapezoidal Panel = (Triangle 1 - Triangle 2) - (Triangle 3 - Triangle 4)

(a) Panel with sweptback leading and trailing edges.



NOTE: Signs changed on slope and y axes.

Strip with sweptforward leading edge

(Triangle 2 - Triangle 1)

(b) Panel with sweptforward leading edge.

Figure 3.- Superposition schemes.

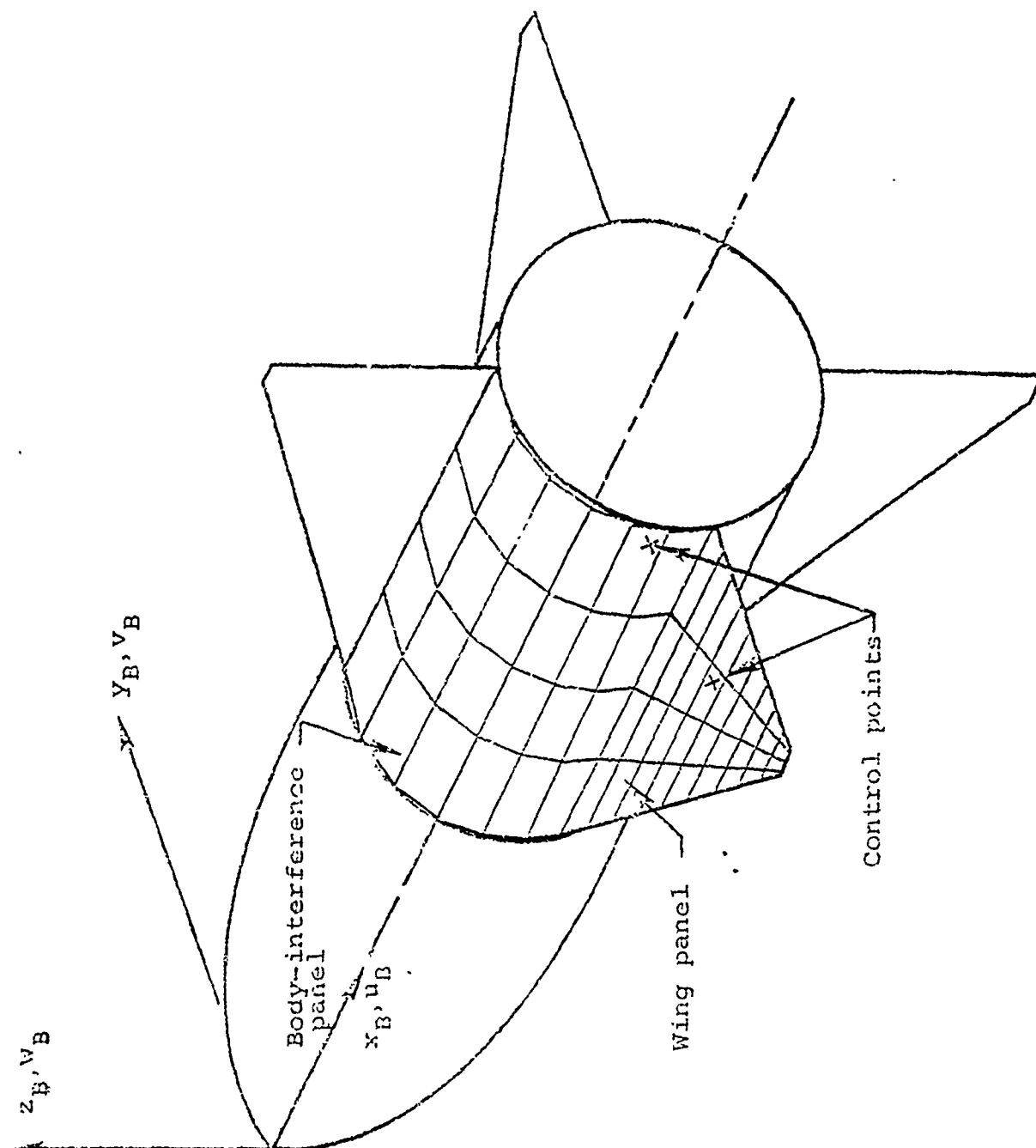


Figure 4.- Panel layout on cruciform wing-body combination.

THIS PAGE IS BEST QUALITY PRACTICABLE  
FROM COPY FURNISHED TO DDC

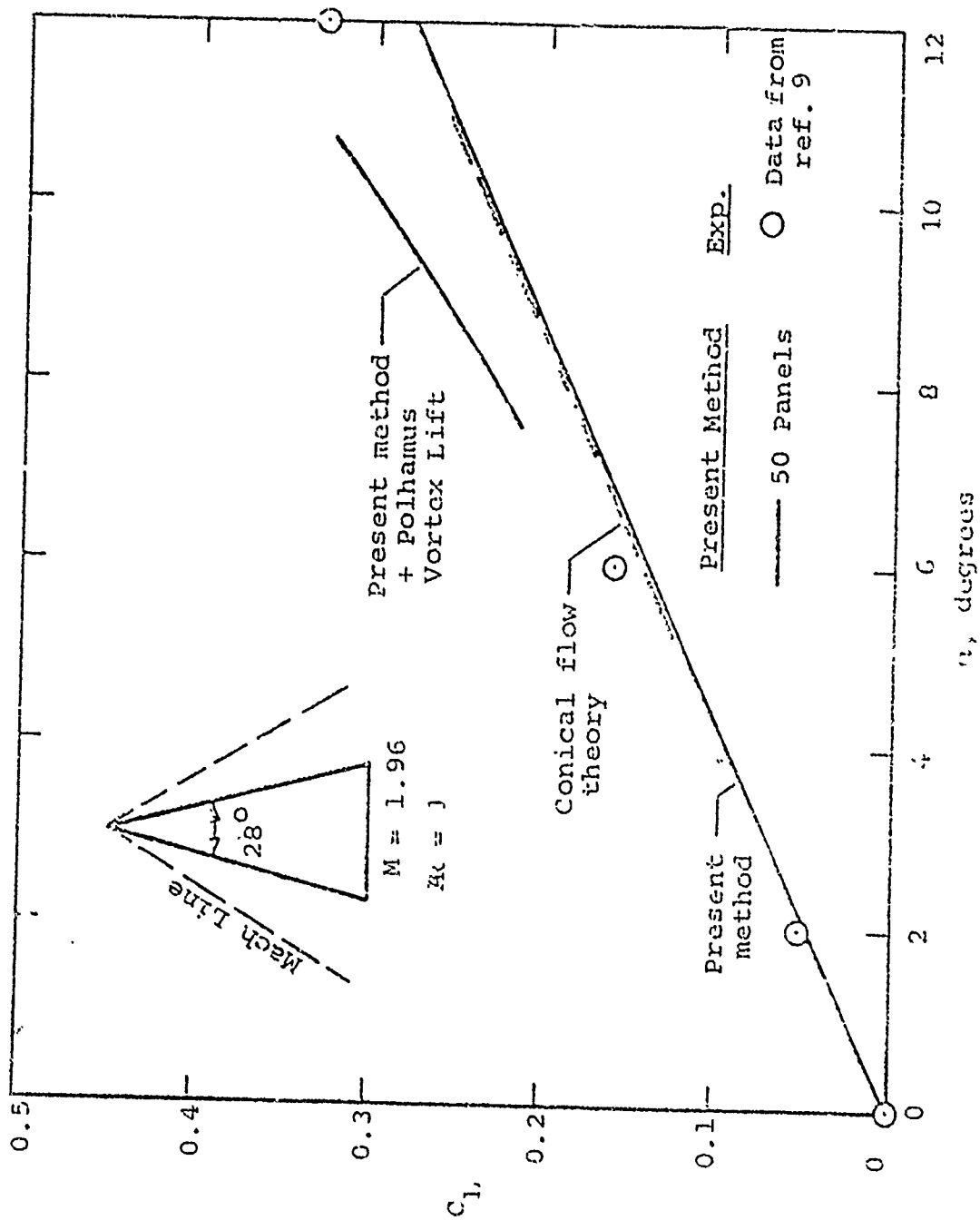


Figure 5.- Comparison between theoretical lift results and data for a triangular wing with subsonic edges.

THIS PAGE IS BEST QUALITY PRACTICABLE  
FROM COPY FURNISHED TO DDG

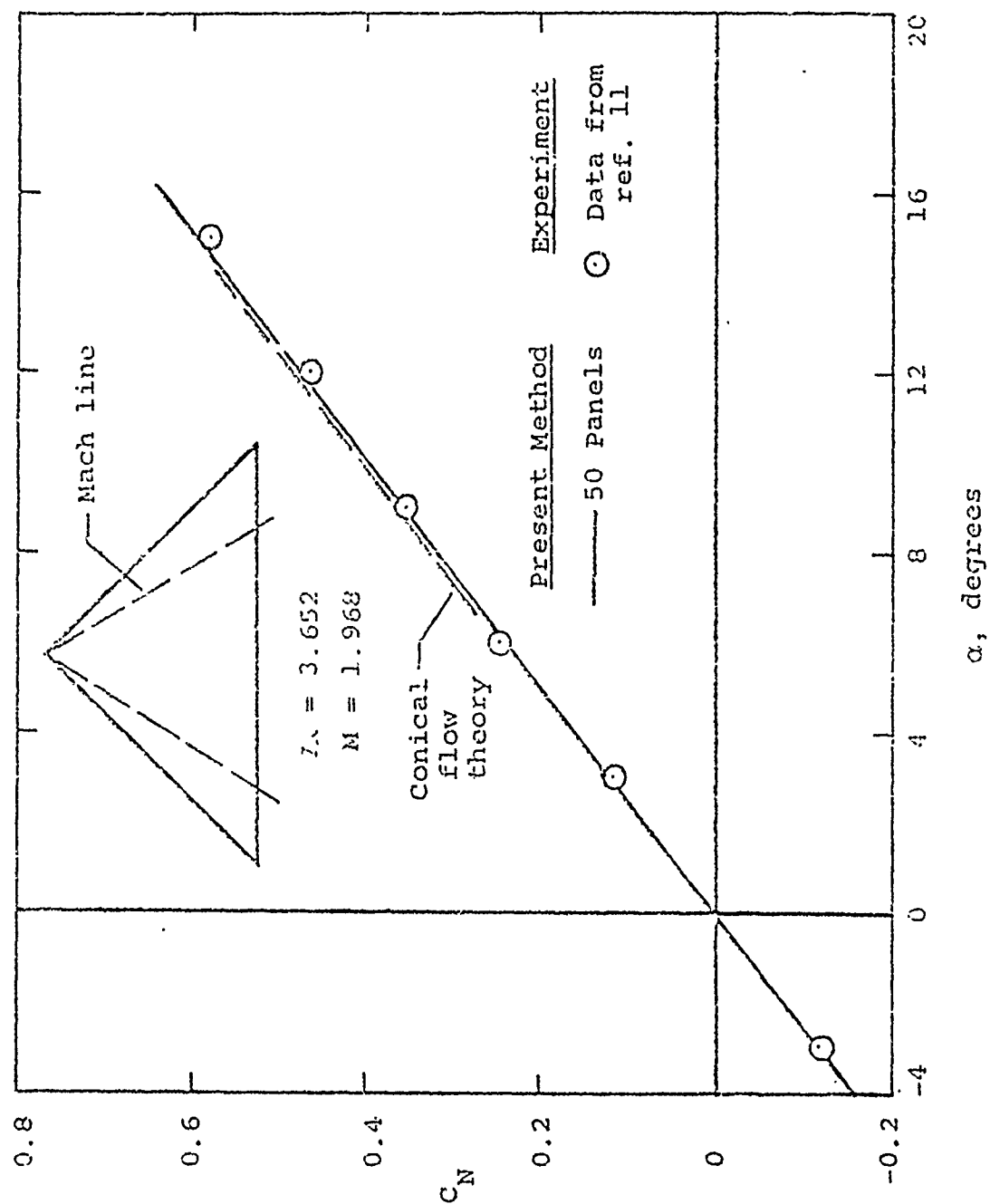


Figure 6.- Comparison between theoretical normal-force results and data for a triangular wing with supersonic edges.

THIS PAGE IS BEST QUALITY PRACTICABLE  
FROM COPY FURNISHED TO DDC

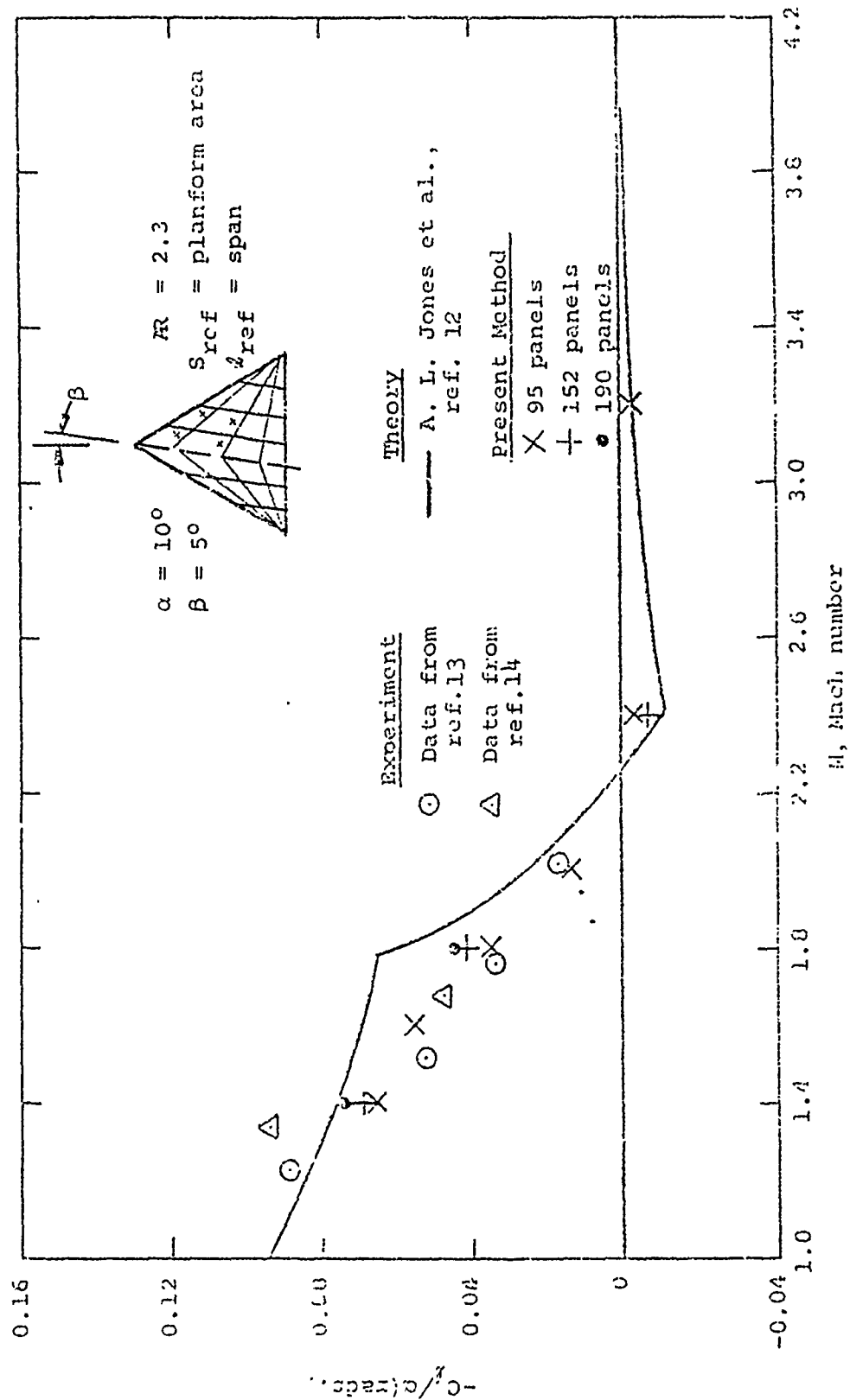


Figure 7.- Comparison between theories and experiment for rolling moment due to sideslip for  $AR = 2.3$  delta wing.

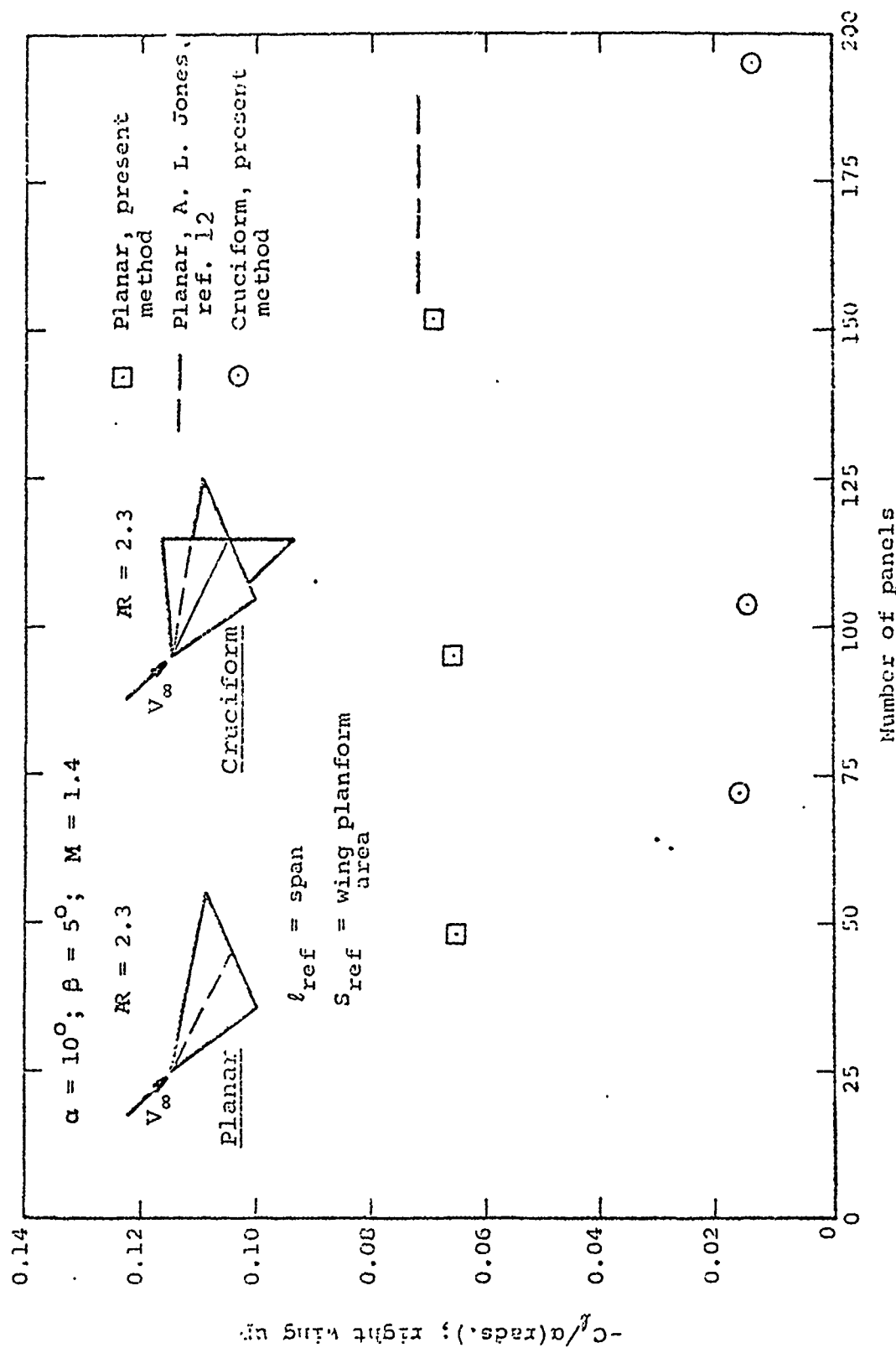


Figure 8.- Theoretical rolling moment due to sideslip for planar and cruciform wing versus number of panels used.



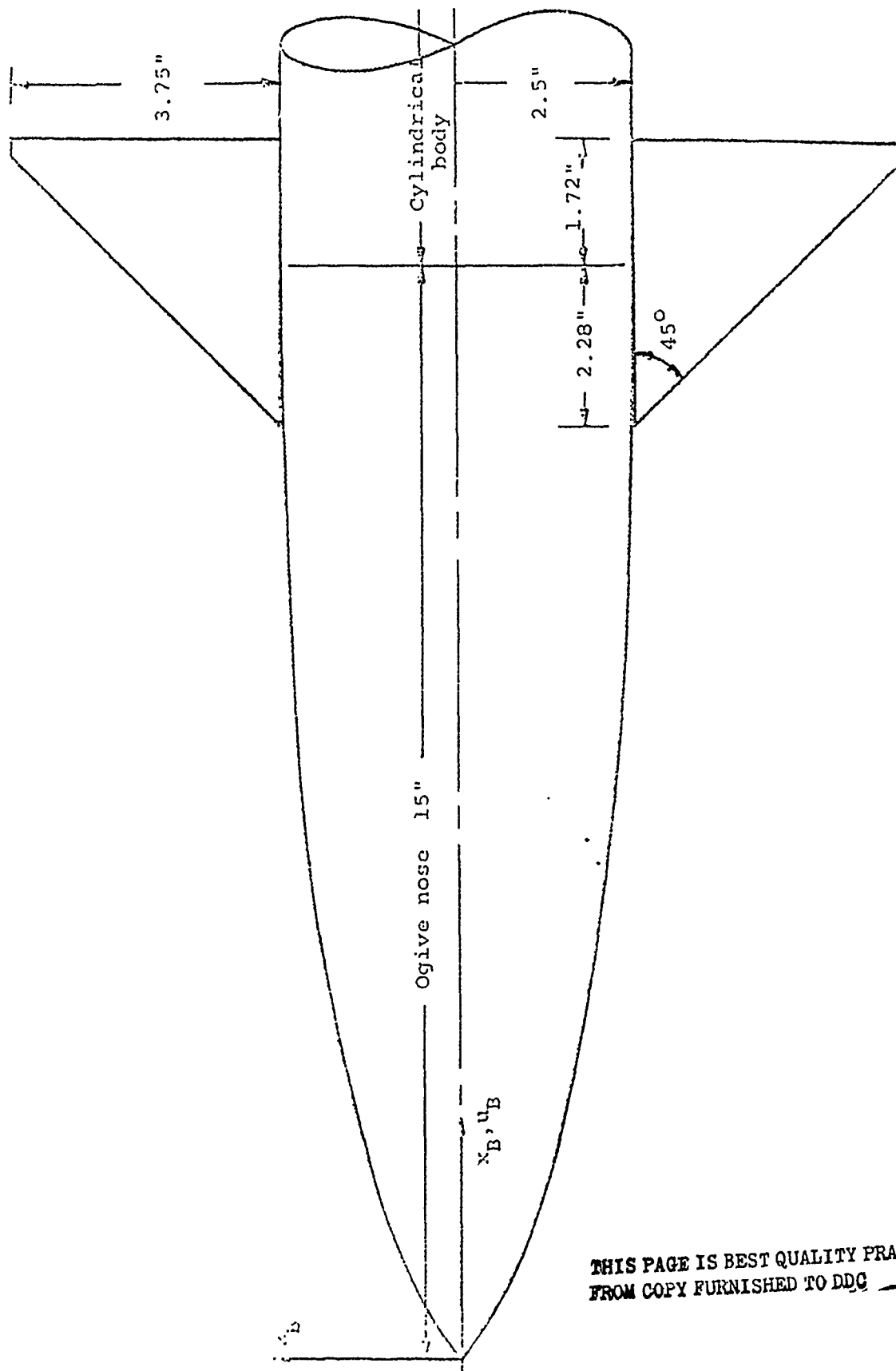


Figure 9.- Cruciform canard-body combination of reference 15.

THIS PAGE IS BEST QUALITY PRACTICABLE  
FROM COPY FURNISHED TO DDG

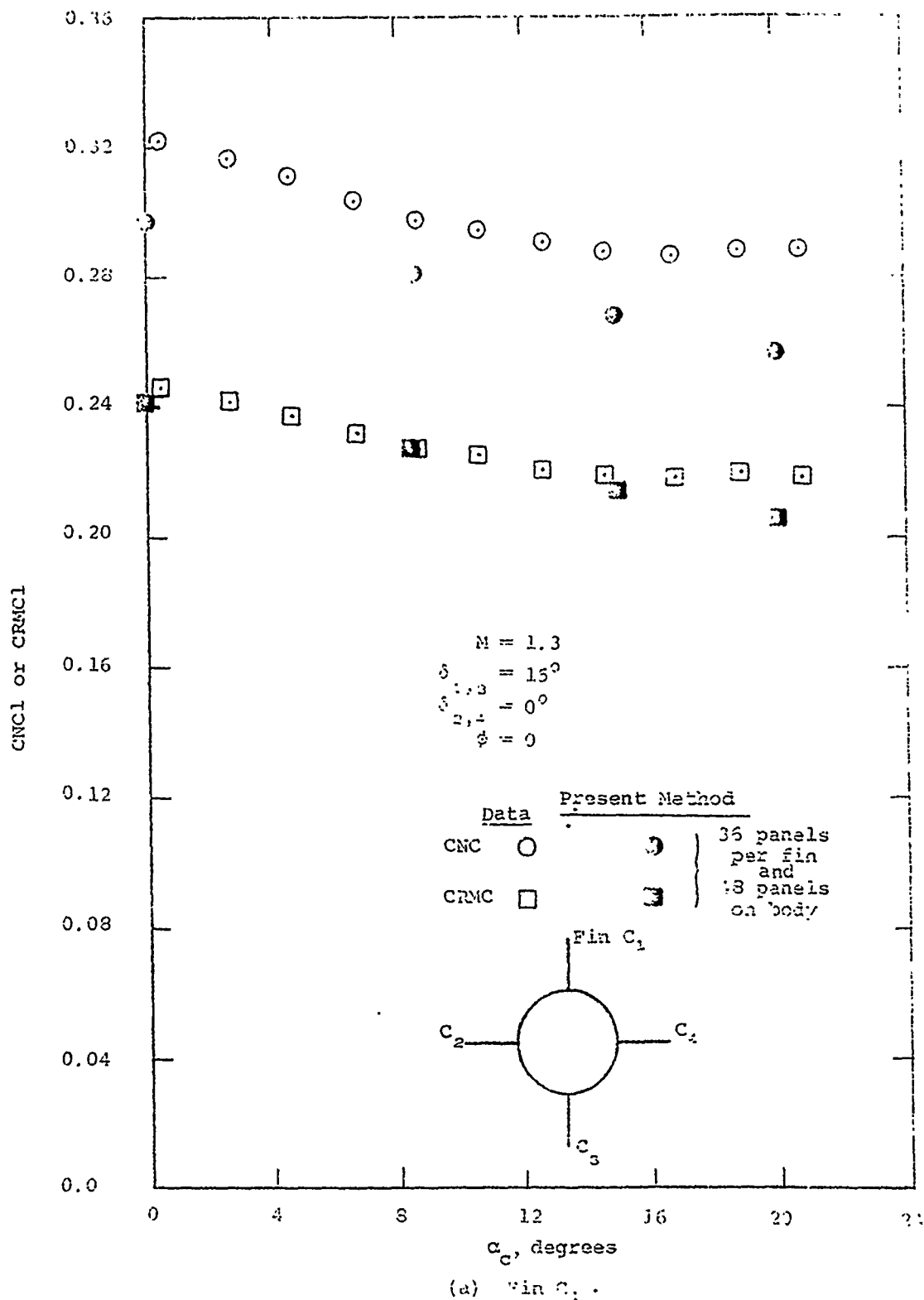


Figure 10.- Normal force and rolling moment of canard fins with  $15^\circ$  deflection of yaw control fins, subsonic leading edge.

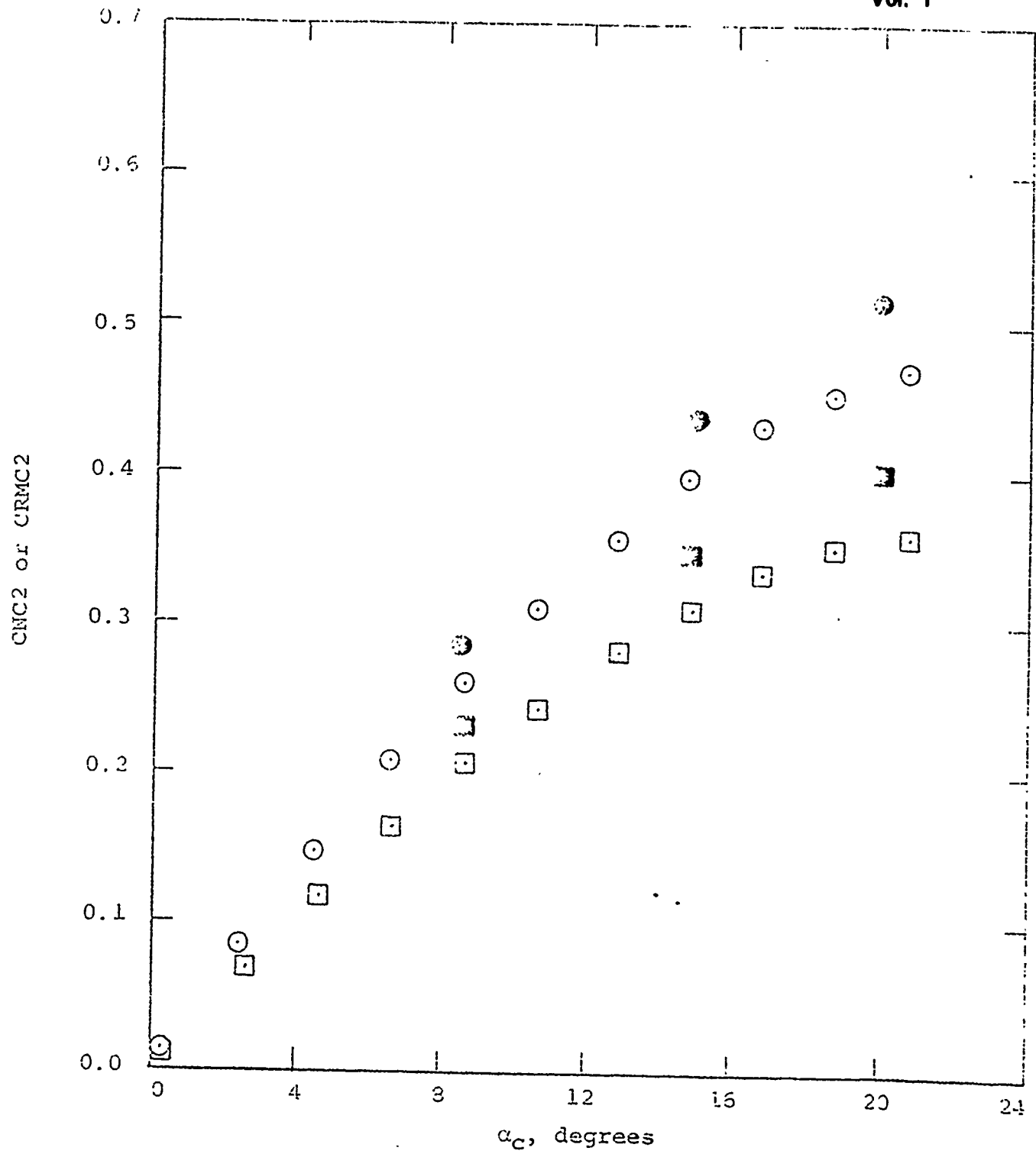
(b) Fin  $C_2$ .

Figure 10- Continued.

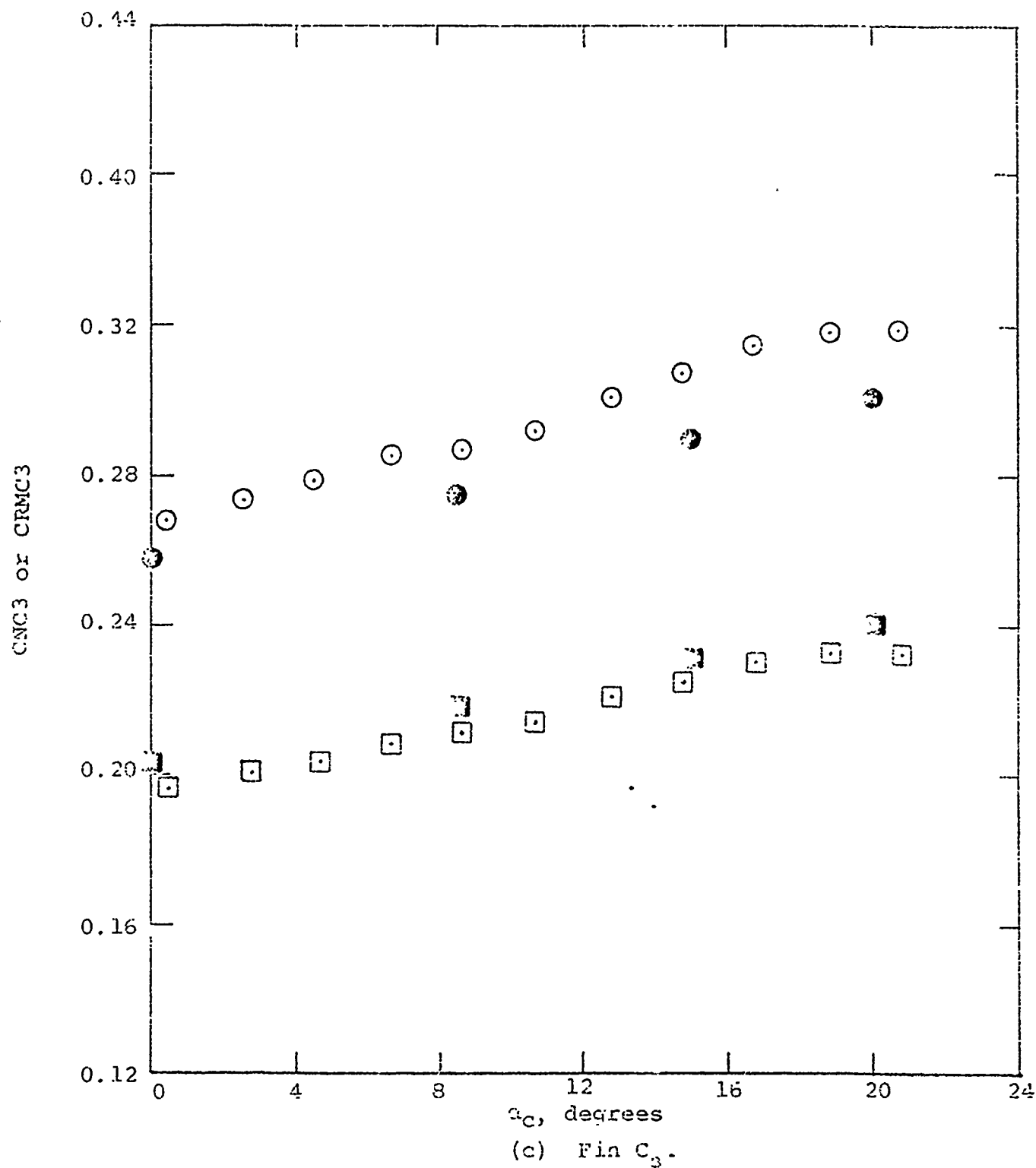


Figure 10.- Continued.

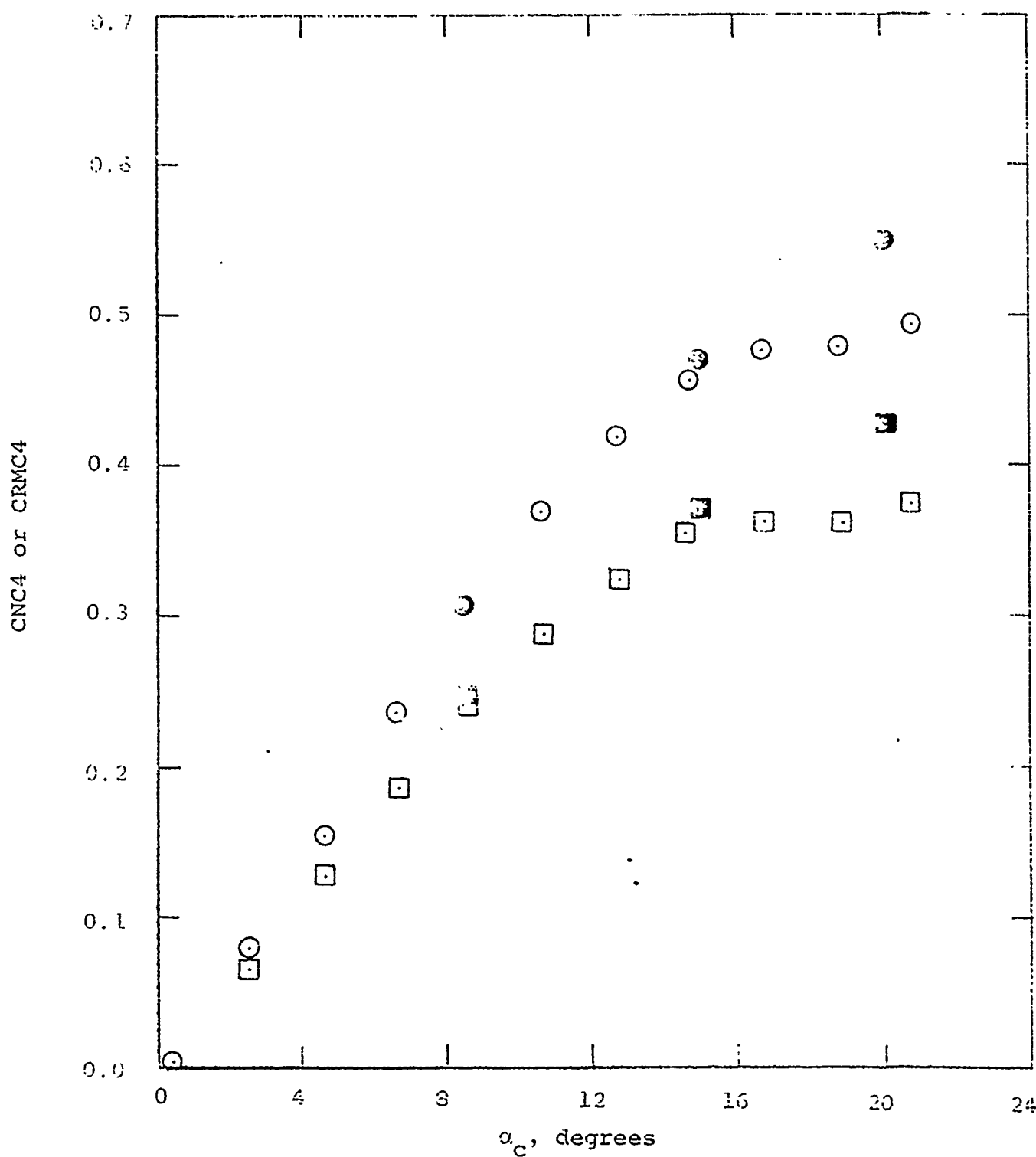
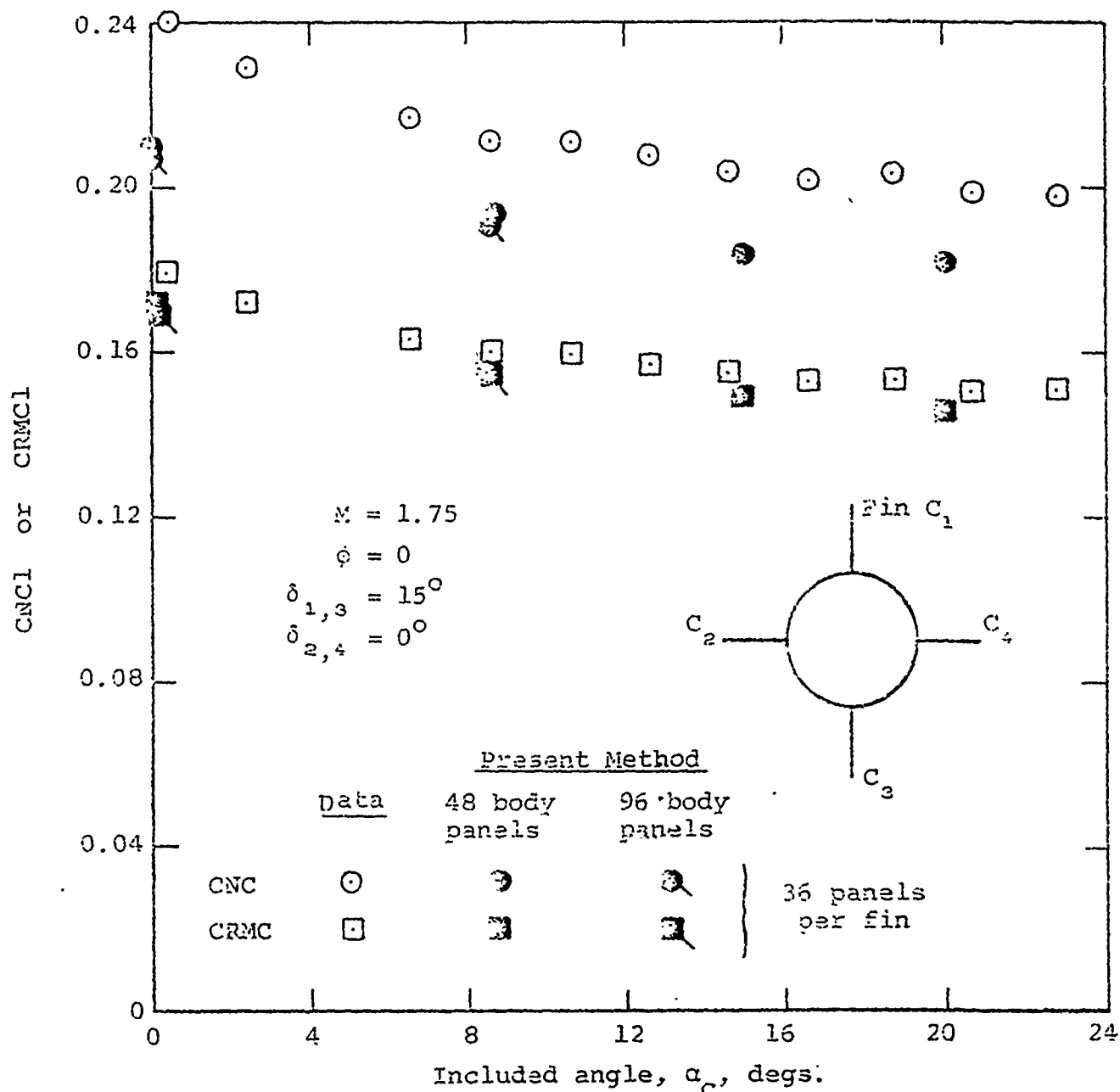
(d) Fin  $C_{L_2}$ .

Figure 10. - Concluded.



(a) Canard  $C_1$

Figure 11.- Normal force and rolling moment of canard fins with  $15^\circ$  deflection of yaw control fins, supersonic leading edge.

THIS PAGE IS BEST QUALITY PRACTICABLE  
 FROM COPY FURNISHED TO DDC

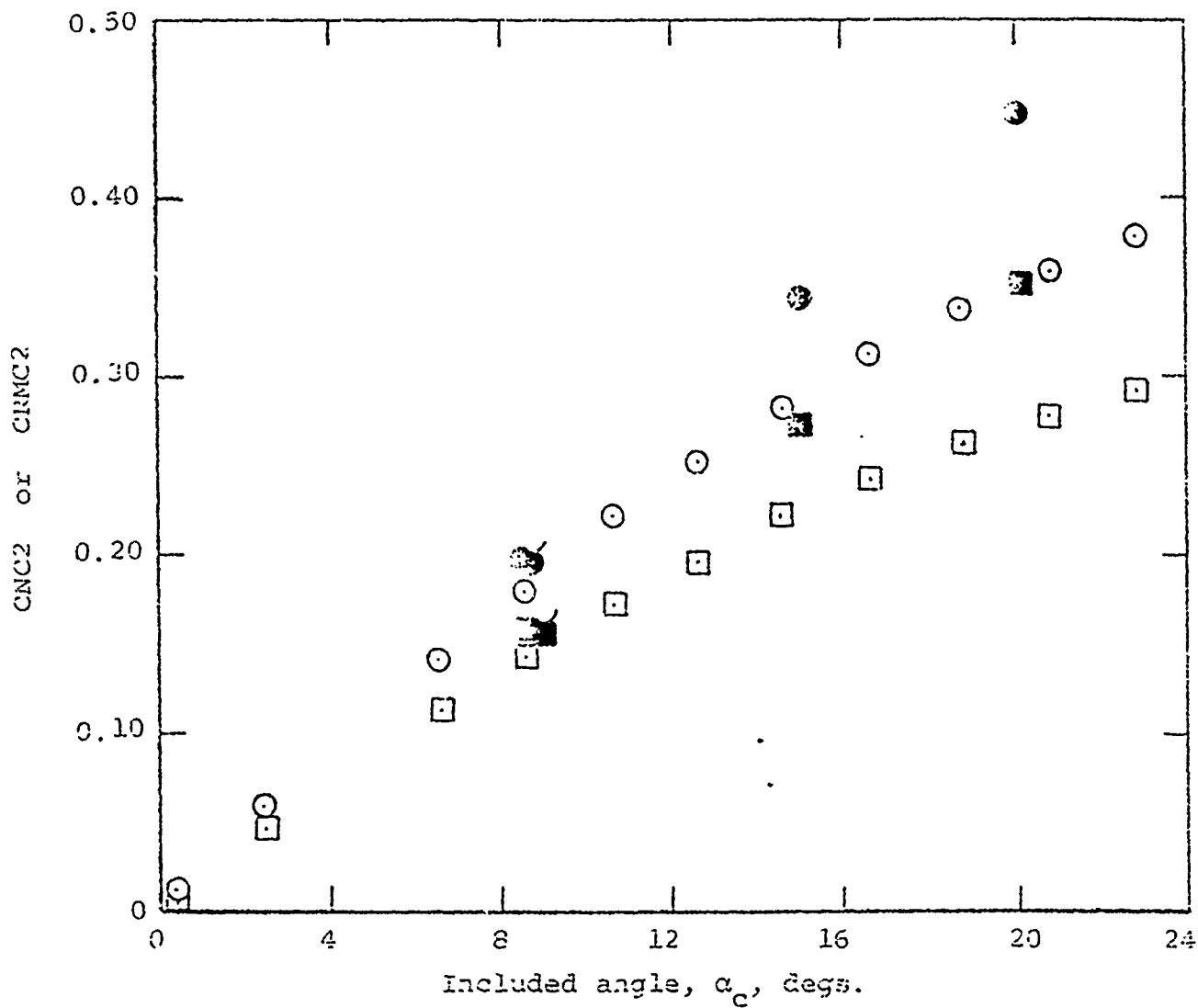
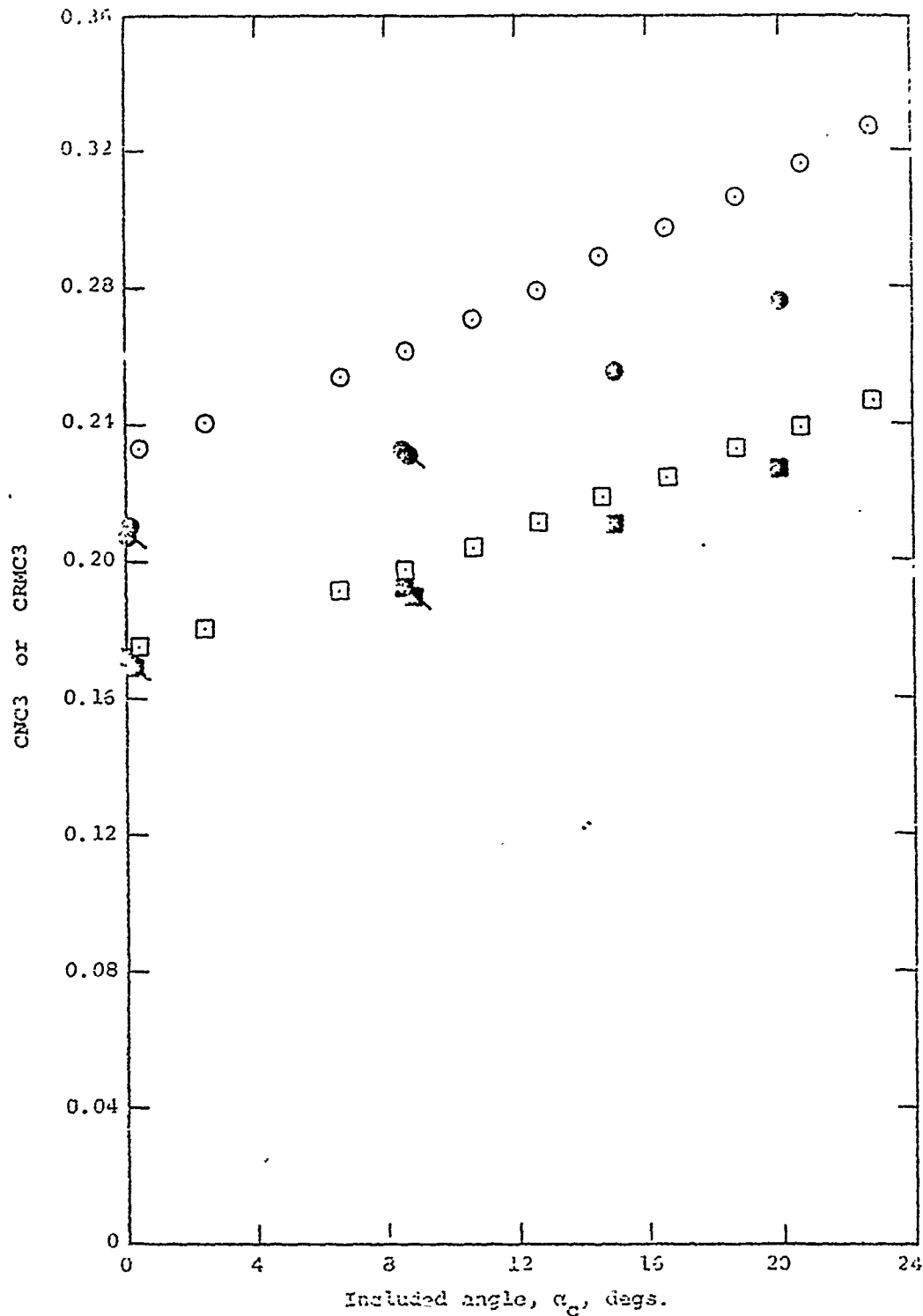
(b) Fin  $C_2$ .

Figure 11- Continued.

THIS PAGE IS BEST QUALITY PRACTICABLE  
FROM COPY FURNISHED TO DDC



(c) fin  $C_3$ .

Figure 11.- Continued



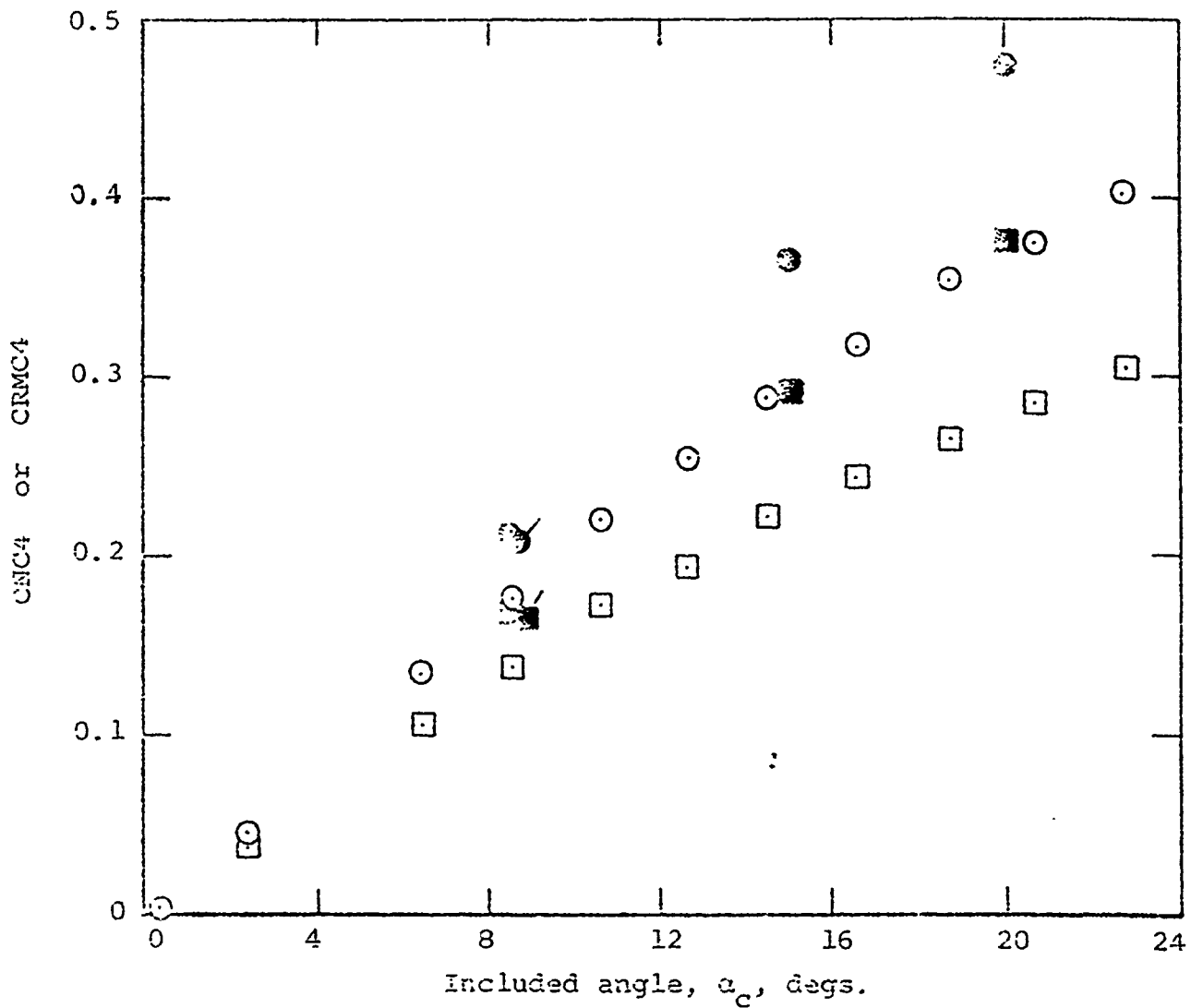
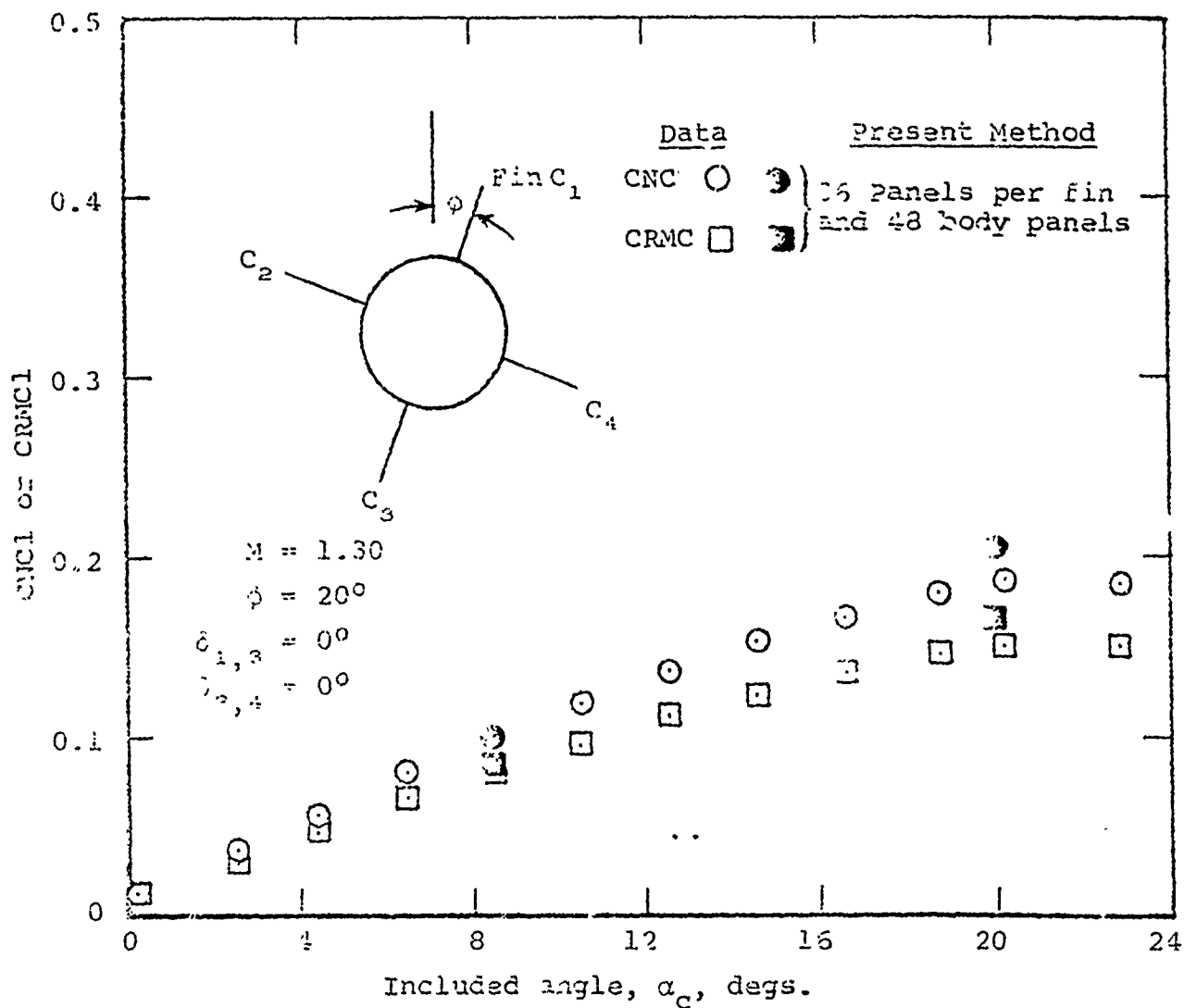
(d) Fin  $C_4$ .

Figure 11.- Concluded.

THIS PAGE IS BEST QUALITY PRACTICABLE  
FROM COPY FURNISHED TO DDG



(a) Fin  $C_1$ .

Figure 12.- Normal force and rolling moment of canard fins due to roll, subsonic leading edge.

THIS PAGE IS BEST QUALITY PRACTICABLE  
 FROM COPY FURNISHED TO DDC

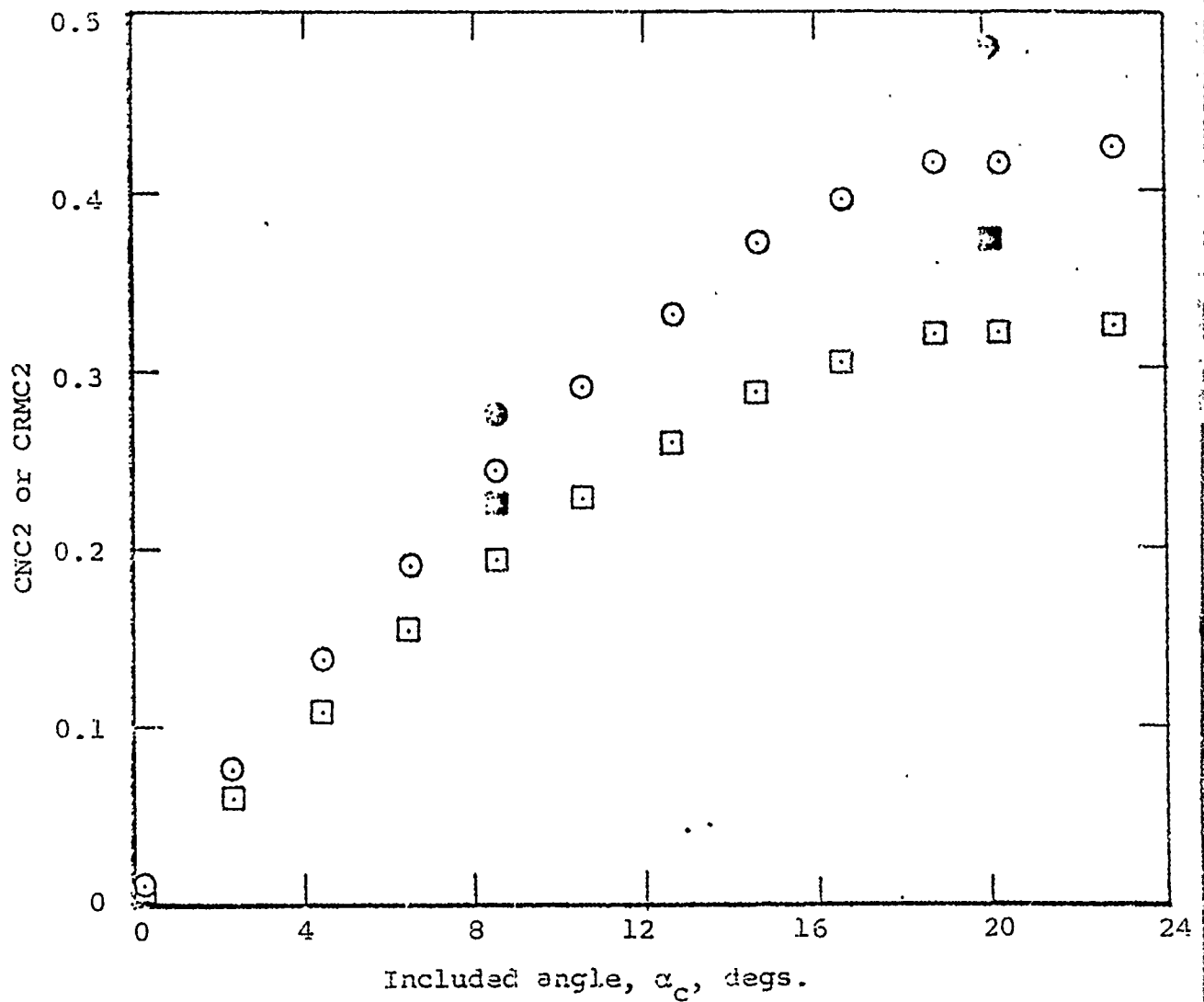
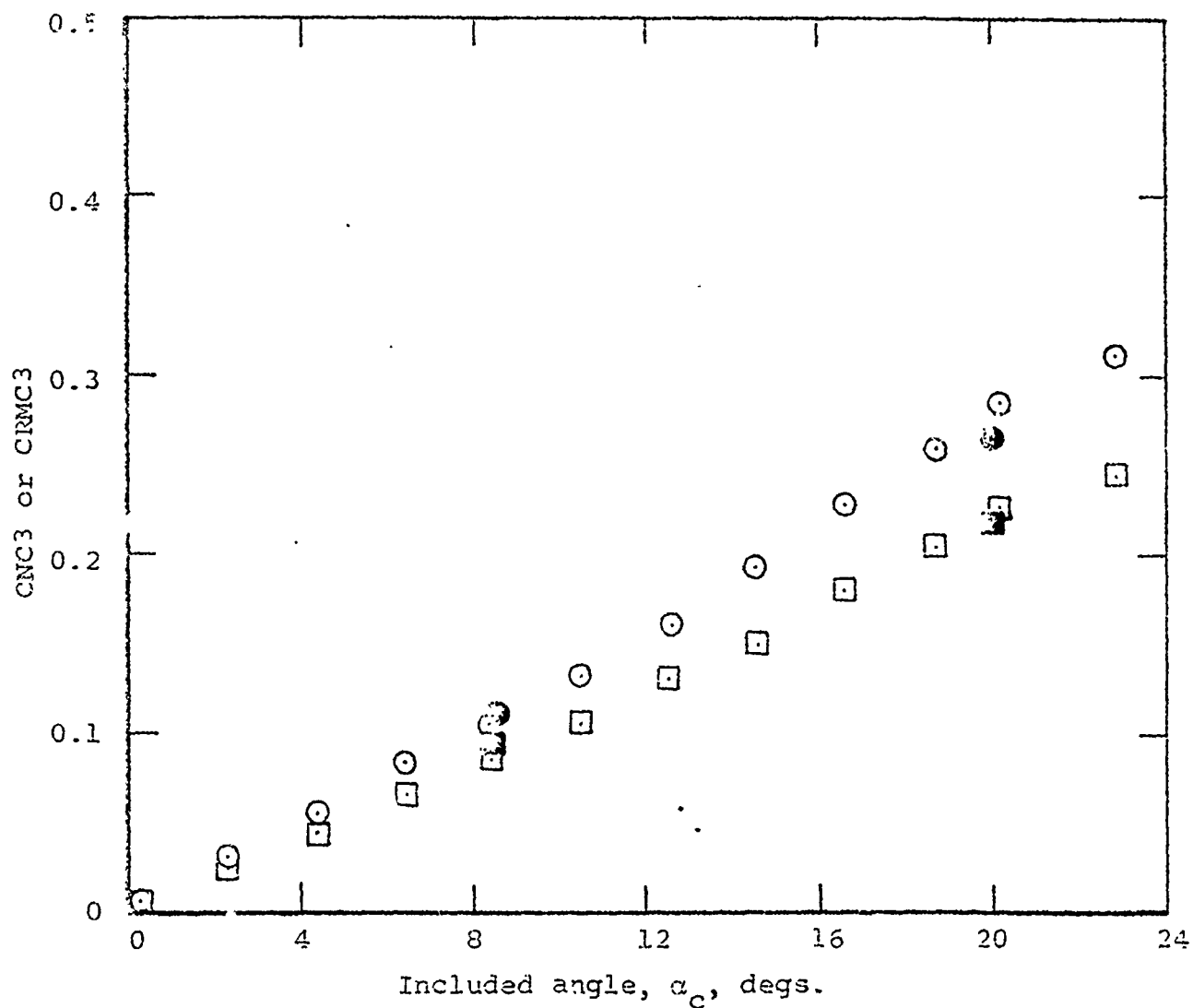
(b) Fin  $C_2$ .

Figure 12.-- Continued.

THIS PAGE IS BEST QUALITY PRACTICABLE  
FROM COPY FURNISHED TO DDC



(c) Fin  $C_3$ .

Figure 12.- Continued.

THIS PAGE IS BEST QUALITY PRACTICABLE  
FROM COPY FURNISHED TO DDC

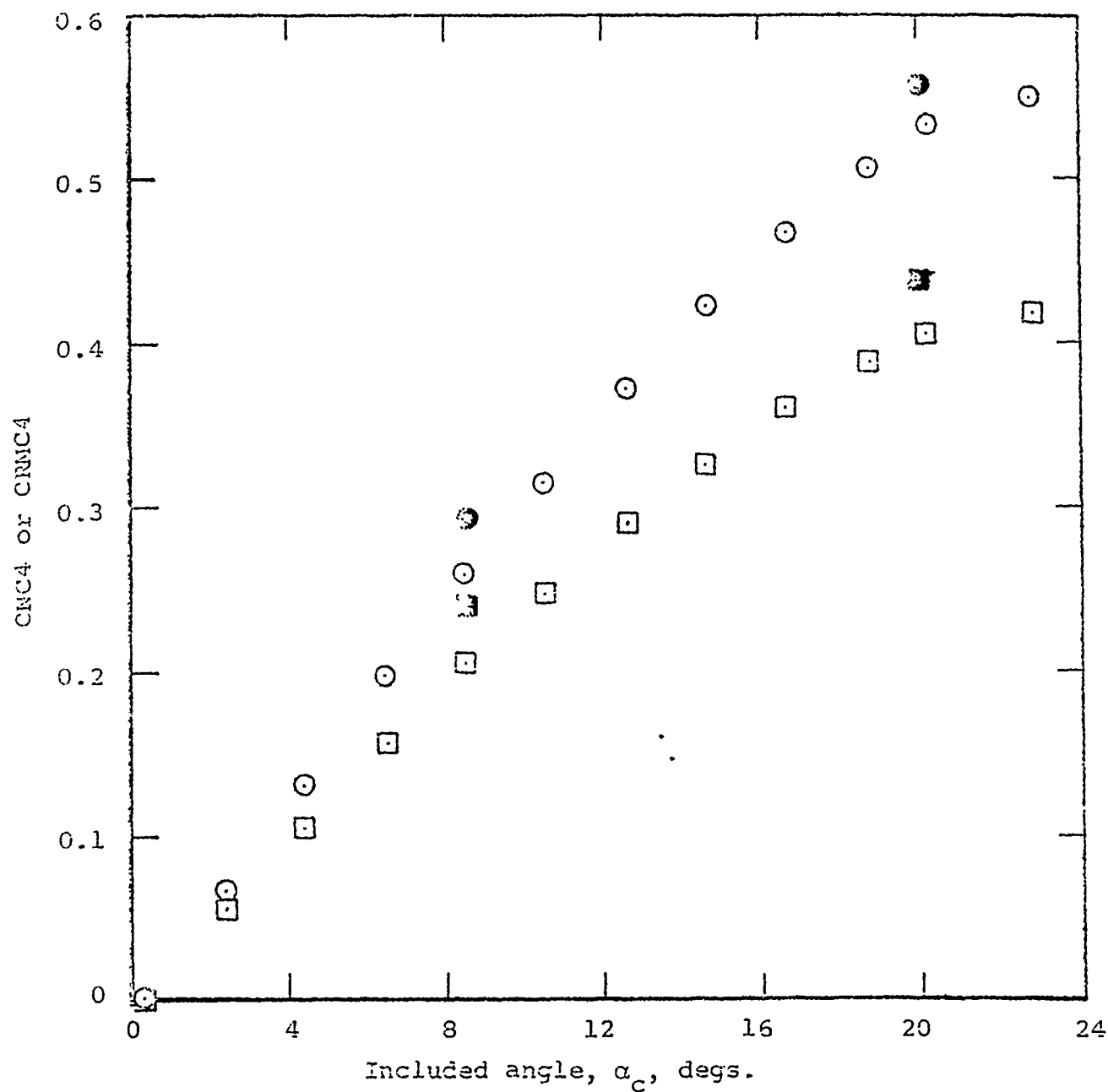
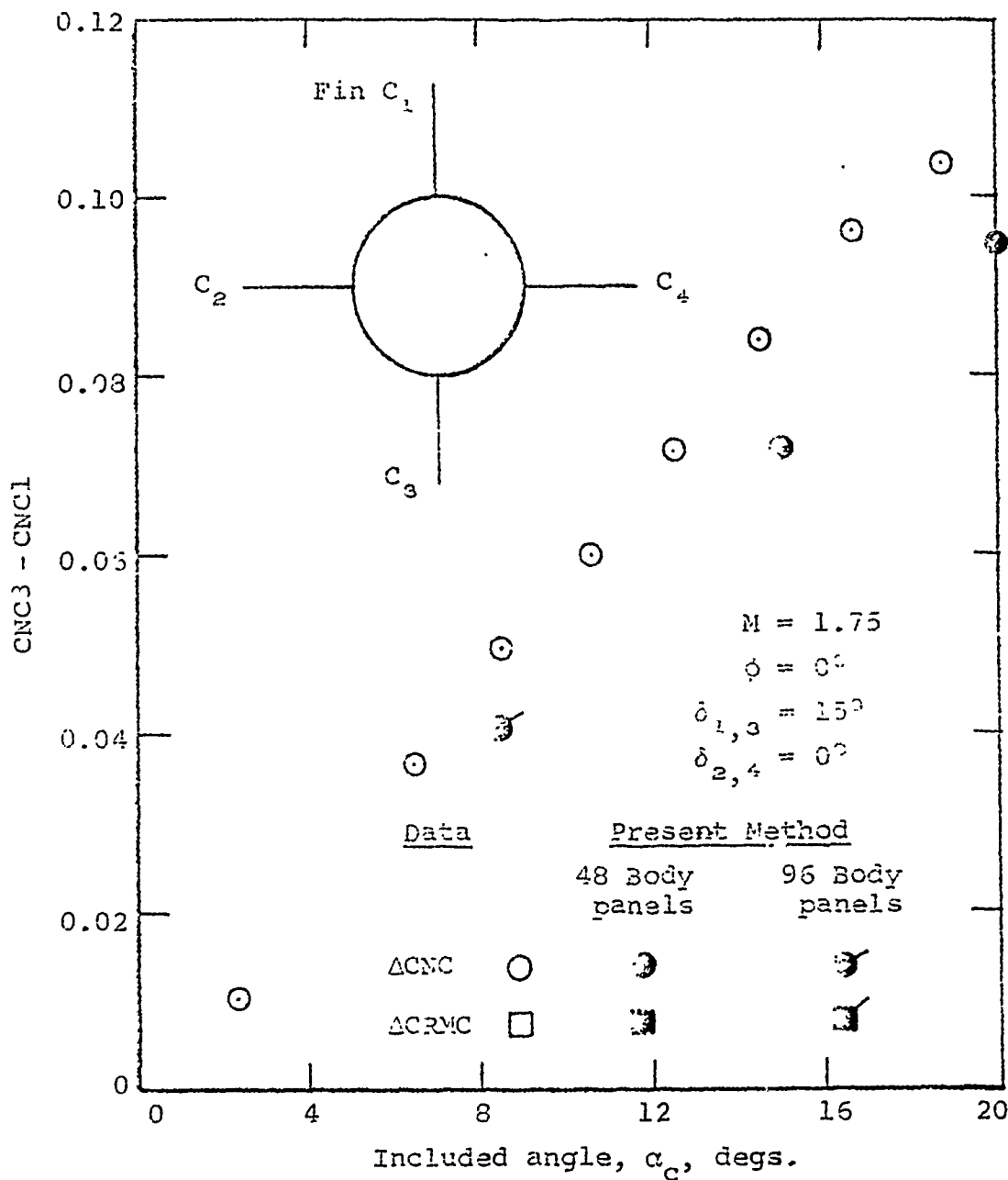
(3) Fin  $C_4$ .

Figure 12.- Concluded.

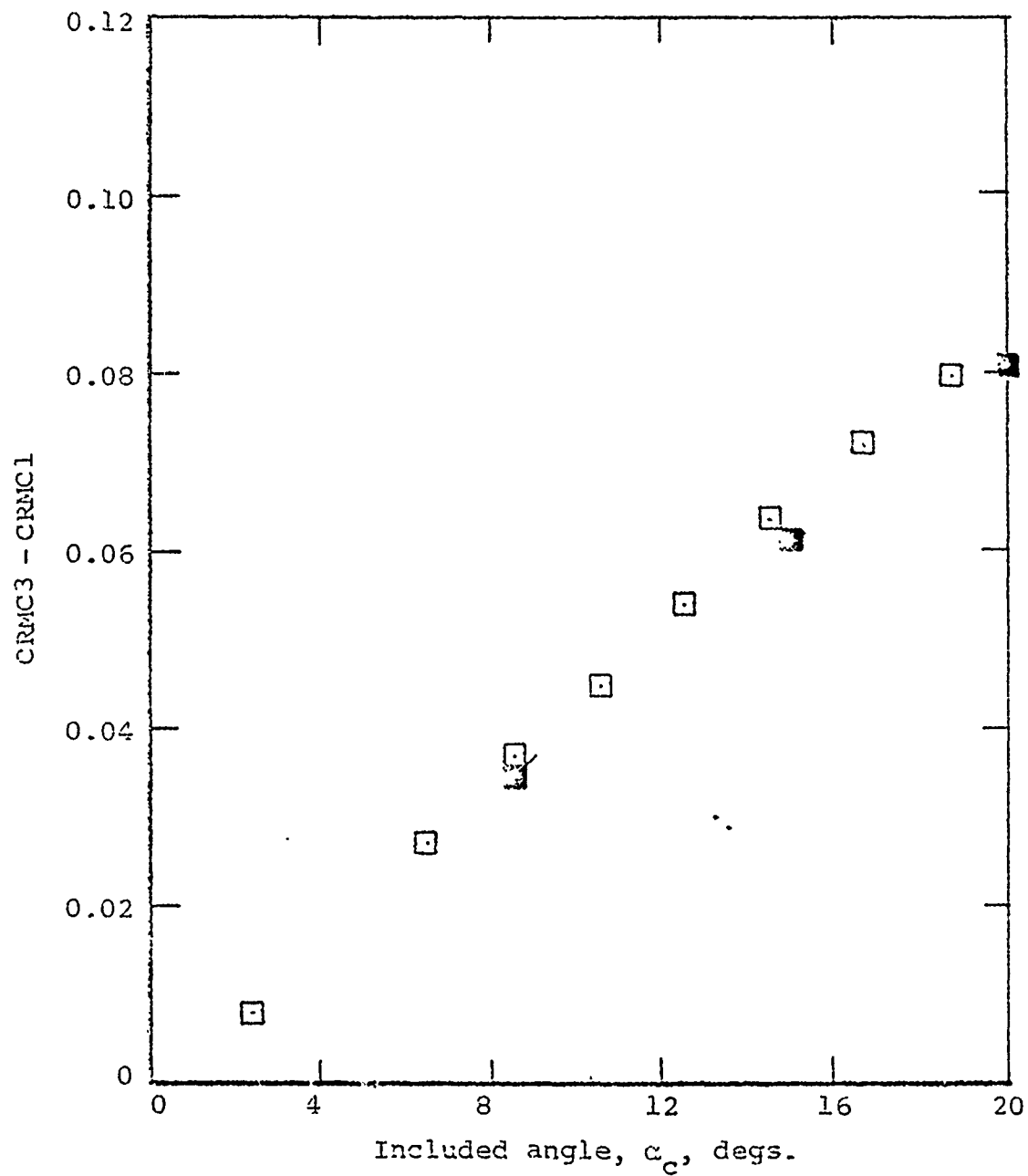
THIS PAGE IS BEST QUALITY PRACTICABLE  
FROM COPY FURNISHED TO ADC



(a) Normal Force.

Figure 13.- Effect of included angle on direct roll of vertical fins due to yaw control.

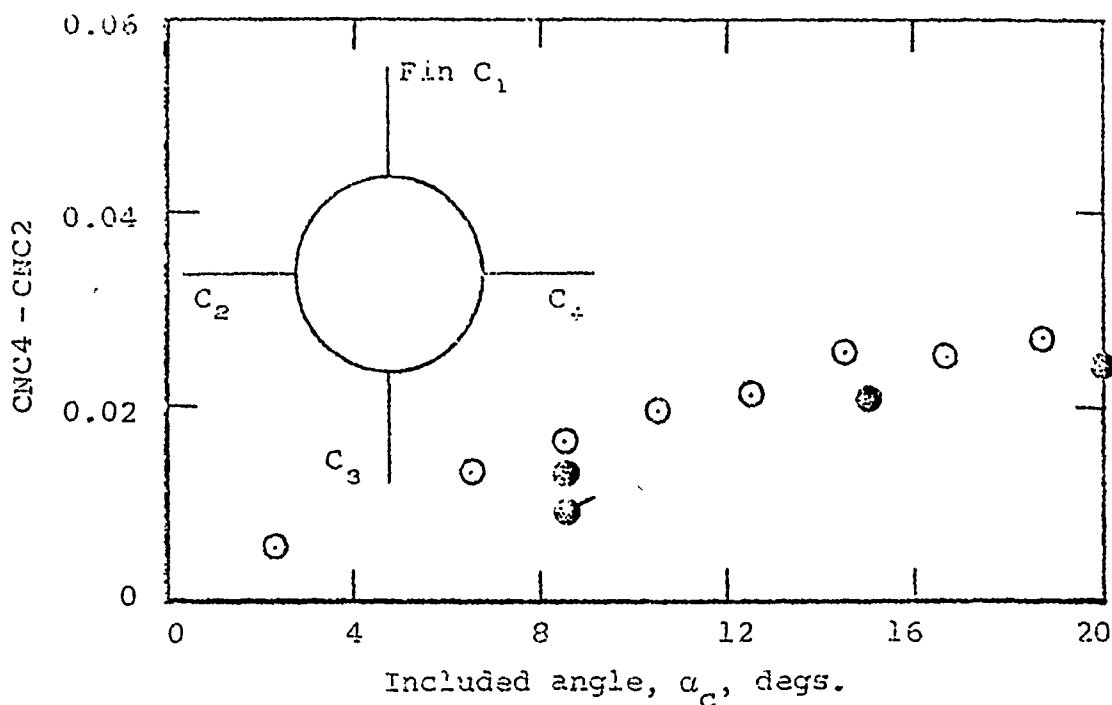
THIS PAGE IS BEST QUALITY PRACTICABLE  
 FROM COPY FURNISHED TO DDC



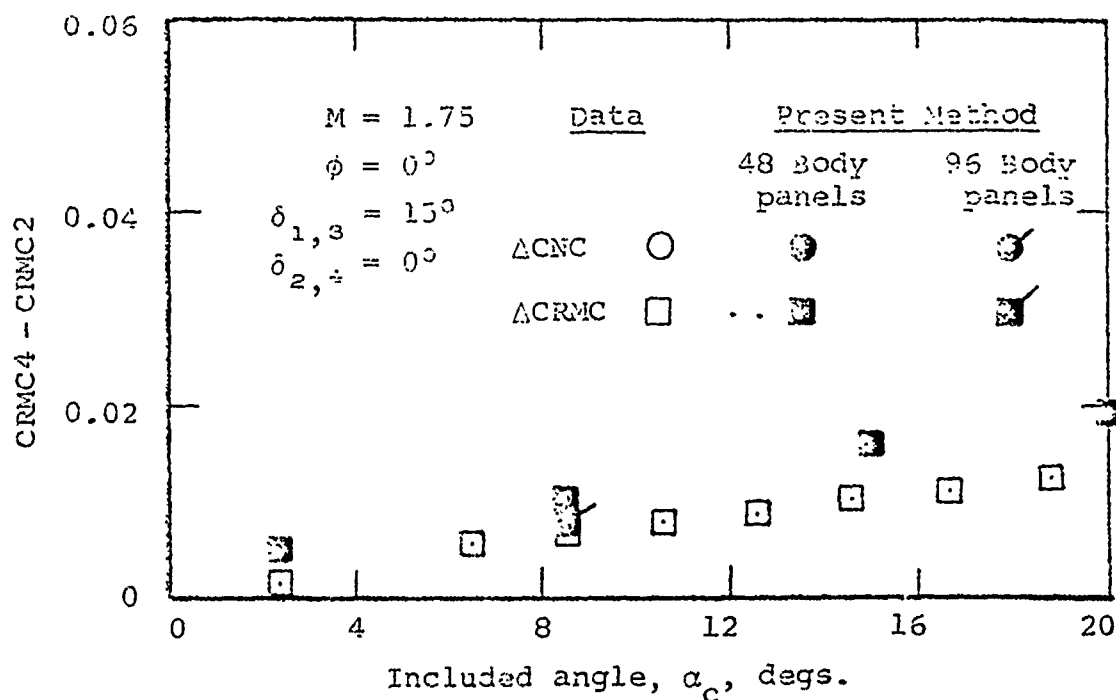
(b) Rolling moment.

Figure 13.- Concluded.

THIS PAGE IS BEST QUALITY PRACTICABLE  
FROM COPY FURNISHED TO DDC



(a) Normal force.



(b) Rolling moment.

Figure 14.- Effect of included angle on reverse roll of horizontal fins due to yaw control.



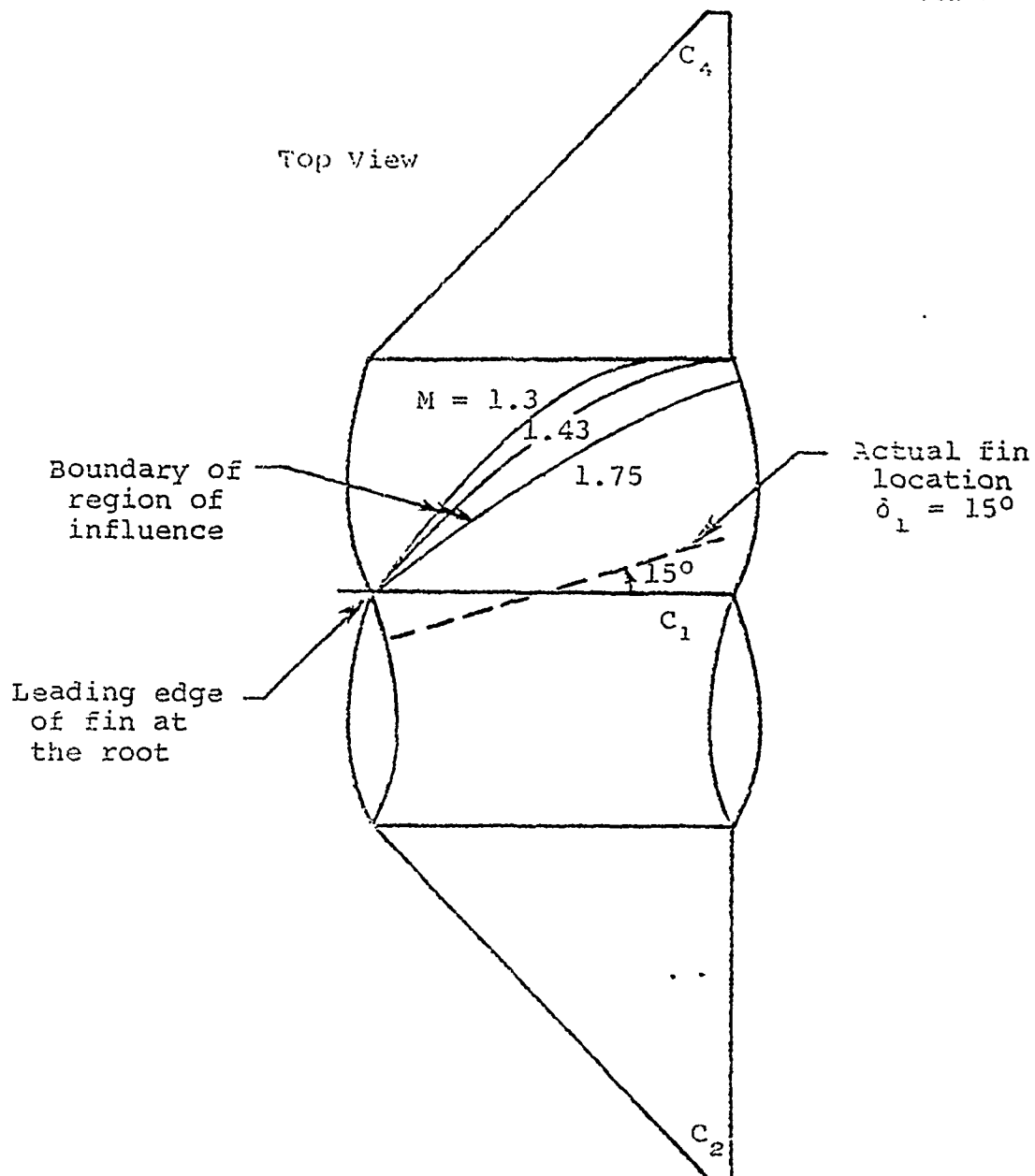


Figure 15.- Paths around body of disturbance originating at leading edge of fin root chord for various Mach numbers.

THIS PAGE IS BEST QUALITY PRACTICABLE  
FROM COPY FURNISHED TO DDC

THIS PAGE IS BEST QUALITY PRACTICABLE  
FROM COPY FURNISHED TO DDG

Quantity	Reverse- Flow Theory	Present Method
$(\Delta CRM1)_v$		-0.04763
$(\Delta CRM2)_v$		0.00048
$(\Delta CRM3)_v$		0.01083
$(\Delta CRM4)_v$		-0.00364
$(\Delta C_{l_C})_v$	0.05855	0.06253

$$(\Delta C_{l_C})_v = CRM2 + CRM3 - CRM1 - CRM4$$

(b) Rolling-moment coefficient increments\*  
due to vortex,  $(\Delta CRM)_v$ .

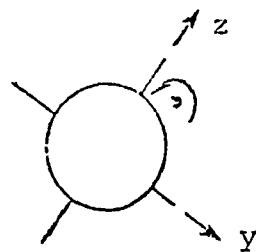
Figure 16.- Concluded.

\*Normal vortex induced velocity only.

$$M = 1.75$$

$$\alpha_c = 20^\circ$$

$$\phi = 20^\circ$$



$$\frac{\Gamma}{2\pi V_\infty a} = 0.160 \quad \frac{y_v}{a} = 0.180$$

$$\frac{z_v}{a} = 1.257$$

Quantity	Reverse-Flow Theory	Present Method
$(\Delta CN1)_v$		-0.08453
$(\Delta CN2)_v$		0.00081
$(\Delta CN3)_v$		0.01376
$(\Delta CN4)_v$		-0.00526
$(\Delta CN1)_v + (\Delta CN3)_v$	-0.0791	-0.0707
$(\Delta CN2)_v + (\Delta CN4)_v$	-0.0060	-0.00445

(a) Normal-force coefficient increments\*  
due to vortex,  $(\Delta CN)_v$ .

Figure 16.- Comparison of lifting-surface theory  
and reverse-flow theory for calculating  
induced vortex effects on canard fins.

\*Normal vortex induced velocity only.

PAPER NO. 5

PREDICTION OF MISSILE AERODYNAMIC  
CHARACTERISTICS OF ARBITRARY  
ROLL ORIENTATION

Presented by: Dr. William B. Brooks

MCDONNELL DOUGLAS ASTRONAUTICS COMPANY  
ST. LOUIS, MISSOURI

ABSTRACT

The need for engineering predictions of missile characteristics at the advanced design stage has lead to the development of several methods and computer codes such as those reported in Reference 1, 2 and 3. The most readily available codes, such as those mentioned above, are restricted to vehicles in the zero roll (no side slip) position. Unfortunately most current missiles, are flown in the nominal "X" orientation. Furthermore, the most prevalent guidance schemes use a fixed vertical axis. Consequently, the aerodynamic roll attitude of the vehicle can vary significantly from the nominal position.

This difference between predictive capability and advanced design requirements has lead McDonnell Douglas Astronautics Company to undertake a continuing development of a conversational computer code to predict missile aerodynamic characteristics for arbitrary roll orientation. This code, based primarily on the methods of Reference 3, has been supported not only by analytical effort, Harpoon and Cruise Missile wind tunnel tests, but also by a parametric test in the McDonnell Douglas Advanced Design Wind Tunnel. As described in this paper the current version is formulated to allow:

- o Arbitrary body area distribution
- o Four sets of tandem aerodynamic surfaces
- o Up to 6 aerodynamic panels at arbitrary orientations per set of surfaces
- o Aerodynamic control by any one set of surfaces
- o Individual aerodynamic panels may have camber and incidence.

Do to lack of experimental data, verification of the entire formulation is not complete at this time;

however, many options have been examined and the expected program accuracies are discussed. The particular configurations for which experimental comparisons have been made are:

- o Cruciform configurations with one, two and three sets of tandem aerodynamic surfaces
- o Planar wings with "X" and "+" tail configurations.

Stability and control comparisons are presented for several configurations.

NOMENCLATURE

$A$  = aspect ratio

$A_{ik} = \int \rho \phi_i n_k dc$

$A_w = (2s)^2/S_r$

$a$  = local body radius

$b$  = wing span

$b_e$  = exposed wing span

$\bar{b}_k = \int \rho \bar{x}_l n_k dc$

$b_{ik} = - \int \rho x_l n_k dc$

$C = - \int \rho \bar{x}_l \epsilon_{lke} z_k n_e dc$

$C_L$  = lift coefficient

$C_{L_w}$  = lift coefficient producing wake

$K$  = rolling moment

$k$  = downwash correction factor

$l_r$  = reference length

$M$  = Mach number

$n_k$  = outward unit normal to the body surface

$r_e$  = distance from the origin to a point on the surface

$\bar{r}_k$  = vector from the origin to the intersection of the body cross section and the  $x_l$  axis

$S$  = reference area

$s$  = semi-span of the wake

$Y_{arm}$  = span wise distance to the center of pressure measured along the span from the x-axis =  $b/2 [1 + 2\lambda] / [3 (1 + \lambda)]$

$$z = x_2 + i x_3$$

$$\alpha = \text{angle of attack}$$

$$\alpha_{ik} = - \int \rho \phi_i \epsilon_{kem} r_e n_m dc$$

$$\beta = \sqrt{1 - M^2}$$

$$\beta_{ik} = - \int \rho x_i \epsilon_{kem} r_e n_m dc$$

$$\epsilon_k = r_k - \bar{r}_k$$

$$\Lambda_{C/2} = \text{sweep of the mid chord}$$

$$\lambda = \text{wing taper ratio}$$

$$\lambda_k = \text{angular fluid impulse}$$

$$\epsilon_k = \text{linear fluid impulse}$$

$$\rho = \text{fluid density}$$

$$\phi = \text{local velocity potential}$$



INTRODUCTION

The accepted pattern for the computation of missile aerodynamics was established in the paper of Pitts, Nielsen and Kaattari, Reference 1. Most of the current approaches, References 2 and 3 (and the approach of this paper) follow the same analytical approach. This approach follows slender-body theory in assuming that the flow in each crossflow lamina can be considered primarily as a two dimensional flow problem. Axial flow influence are considered primarily as empirical corrections to the basic cross-flow solutions.

This basic assumption of near independence of the individual cross-flow lamina permits the various missile parts (body, wings, tails, booster surfaces) to be considered independently. The values of the aerodynamic contributions of these elements are then estimated from the existing store of aerodynamic data and methods available in the open literature. The overall characteristics can then be obtained by summing the individual components using empirical correction factors to account for mutual interference.

For nonlifting elements, the assumption of independence of crossflow lamina is quite satisfactory; however, for lifting surfaces, the wake and/or trailing vortices are in fact fluid extensions to the generating surface which pass through and consequently influence all subsequent crossflow lamina. Only by including the appropriate wake and/or vortex cross sections can one of the subsequent lamina be considered independent of the other lamina. Unfortunately the computation of the axial development of the wake/trailing vortex cross sections, for even the simplest of lifting surface geometries, is too complex for efficient inclusion in the current advanced design computer codes. Consequently empirical correlations and approximations to the wake geometry are still required.

One difficulty in applying the methods of Reference 1 directly to most missile configurations is the relatively limited amount of aerodynamic data available for anything other than planar lifting surface configurations. In this paper an attempt is made to use existing data to predict the aerodynamic characteristics and the downwash contributions of arbitrary multi-fin geometries. Particular emphasis is placed on tandem sets of cruciform fins at arbitrary aerodynamic roll orientation.

SLENDER BODY FORMULATION

In slender-body theory, the fluid motions are assumed to be primarily constrained to motion within the crossflow lamina. With the coordinate system shown in Figure 1,

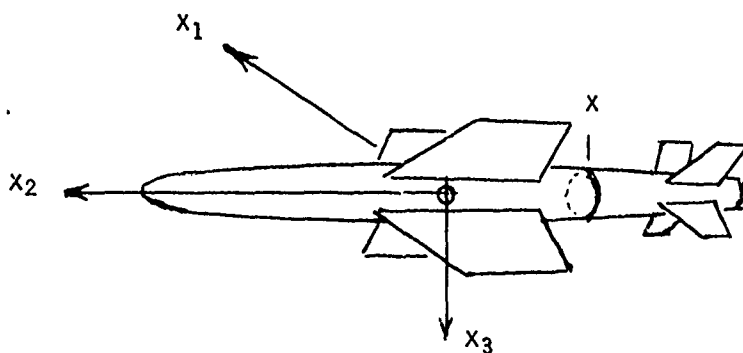


Figure 1 - Coordinate System

the fluid impulses generated by the aerodynamic force forward of station  $x$  are

$$\xi_k = \int_x^\infty \oint \rho \phi n_k dc dx \quad 1$$

$$\lambda_k = - \int_x^\infty \oint \rho \phi \epsilon_{kem} r_e n_m dc dx \quad 2$$

For incompressible flow both the potential and the boundary conditions are linear functions of the missile linear and angular velocities. Thus, with complete generality, the velocity potential can be expressed as:

$$\phi = \phi_i u_i + X_i \omega_i \quad 3$$

Where  $\phi_i$  and  $X_i$  are independent of the vehicle linear and angular velocities.

Inserting this form into equations 2 and 3 allows the fluid impulses to be written as:

$$\xi_k = \int_x^\infty A_{ik} dx u_i + \int_x^\infty b_{ik} dx \omega_i \quad 4$$

$$\lambda_k = \int_x^\infty \alpha_{ik} dx u_i + \int_x^\infty \beta_{ik} dx \omega_i \quad 5$$

with virtual mass coefficients determined from the integrals

$$A_{ik} = - \oint \rho \phi_i n_k dc$$

$$b_{ik} = - \oint \rho X_i n_k dc$$

$$\alpha_{ik} = - \oint \rho \phi_i \epsilon_{kem} r_e n_m dc$$

$$\beta_{ik} = - \oint \rho X_i \epsilon_{kem} r_e n_m dc$$

Within the slender-body theory the impulses acting on a lamina can be related to the partial derivatives of the fluid kinetic energy within the lamina. Specifically, if the kinetic energy within a lamina is denoted  $T$ , then

$$\begin{aligned} A_{ik} &= \frac{\partial^2 T}{\partial U_i \partial U_k} \\ b_{ik} &= \frac{\partial^2 T}{\partial U_k \partial \omega_i} \\ \alpha_{ik} &= \frac{\partial^2 T}{\partial U_i \partial \omega_k} \\ \beta_{ik} &= \frac{\partial^2 T}{\partial \omega_i \partial \omega_k} \end{aligned} \quad 6$$

Thus the symmetry relations

$$A_{ik} = A_{ki}$$

$$b_{ik} = a_{ki}$$

$$\beta_{ik} = \beta_{ki}$$

7

significantly reduce the number of independent elements to be determined.

The linear form of the velocity potential shown in equation 3 is quite general. If specific use of the slender-body theory is made the number of independent potentials can be reduced from 6 to 4. Since the fluid motion is assumed to be confined primarily to lamina parallel to the  $x_2 - x_3$  plane, the velocity potential can be written as:

$$\phi = \phi_i [U_i + \epsilon_{ijk} \omega_j \bar{r}_k] + \bar{X}_1 \omega_1$$

8

NOTE: This form differs from that used either by Nielson, Reference 1 or Bryson, Reference 4, in that a potential proportional to  $U_1$  is included in the formulation.

With this notation,

$$X_j = \phi_i \epsilon_{ijk} \bar{r}_k + \bar{X}_1 \delta_{j1}$$

9

the matrix symmetry relation can be used with equation 9 to write the  $b_{ik}$  and  $\beta_{ik}$  matrices as:

$$b_{ik} = \epsilon_{jie} \bar{r}_e A_{jk} + \bar{b}_k \delta_{i1}$$

$$\beta_{ik} = \epsilon_{kem} \epsilon_{ipj} \bar{r}_e \bar{r}_p A_{jm} + [\delta_{i1} \epsilon_{kem} + \delta_{k1} \epsilon_{iem}] \bar{r}_e \bar{b}_m + C \delta_{i1} \delta_{k1}$$

10

The modified virtual mass coefficients are given by the integrals

$$\bar{b}_k = - \oint \rho \bar{x}_1 n_k dc$$

$$C = - \oint \rho \bar{x}_1 \epsilon_{1ke} \zeta_k n_e dc$$

11

Thus in slender-body theory only the 6 independent elements of the  $A_{ij}$  matrix, the three elements of the  $\bar{b}_k$  vector and the scalar  $C$  need be determined to completely specify the fluid impulses.

The forces and moments on the missile, forward of station  $x$  are equal to the negative of the time rate of change of the fluid impulses as shown in equations 4 and 5. In a body centered coordinate system these forces and moments can be written in the form:

$$\begin{aligned} F_k &= - \int_x^\infty A_{ik} dx \dot{U}_i - \int_x^\infty b_{ik} dx \dot{\omega}_i \\ &\quad - U_1 [A_{ik} U_i + b_{ik} \omega_i] \end{aligned} \quad 12$$

$$- \epsilon_{kem} \left[ \int_x^\infty A_{im} dx U_i + \int_x^\infty b_{im} dx \omega_i \right] \omega_e$$

$$\begin{aligned} M_k &= - \int_x^\infty \alpha_{ik} dx \dot{U}_i - \int_x^\infty \beta_{ik} dx \dot{\omega}_i \\ &\quad - U_1 [\alpha_{ik} U_i + \beta_{ik} \omega_i] \\ &\quad - \epsilon_{kem} \omega_e \left[ \int_x^\infty \alpha_{im} dx U_i + \int_x^\infty \beta_{im} dx \omega_i \right] \\ &\quad - \epsilon_{kem} U_e \left[ \int_x^\infty A_{im} dx U_i + \int_x^\infty b_{im} dx \omega_i \right] \end{aligned} \quad 13$$

The static aerodynamic force and moments are proportional to the partial derivatives

$$\frac{\partial^2 F_k}{\partial U_1 \partial U_j} \quad \text{and} \quad \frac{\partial^2 M_k}{\partial U_1 \partial X_j}.$$

From equations 12 and 13 these derivatives are

found to be:

$$\frac{\partial^2 F_k}{\partial U_1 \partial U_j} = -A_{jk} - A_{ik} \epsilon_{j1} \quad 14$$

$$\frac{\partial^2 M_k}{\partial U_1 \partial U_j} = -\alpha_{jk} - \alpha_{ik} \epsilon_{j1} - \epsilon_{klm} \int_x^\infty A_{jm} dx - \epsilon_{kjm} \int_x^\infty A_{lm} dx \quad 15$$

With the normal aerodynamic nomenclature the static forces and moments on the missile forward of station  $x$  can be written as:

$$\begin{aligned} (F_1)_{\text{STATIC}} &= -\rho U_1 S [C_{A_0} U_1 + C_{A_\beta} U_2 + C_{A_\alpha} U_3] \\ (F_2)_{\text{STATIC}} &= \rho U_1 S [C_{Y_0} U_1 + C_{Y_\beta} U_2 + C_{Y_\alpha} U_3] \\ (F_3)_{\text{STATIC}} &= -\rho U_1 S [C_{N_0} U_1 + C_{N_\beta} U_2 + C_{N_\alpha} U_3] \end{aligned} \quad 16$$

$$\begin{aligned} (M_1)_{\text{STATIC}} &= \rho U_1 S l_r [C_{l_0} U_1 + C_{l_\beta} U_2 + C_{l_\alpha} U_3] \\ (M_2)_{\text{STATIC}} &= \rho U_1 S l_r [C_{m_0} U_1 + C_{m_\beta} U_2 + C_{m_\alpha} U_3] \\ (M_3)_{\text{STATIC}} &= \rho U_1 S l_r [C_{n_0} U_1 + C_{n_\beta} U_2 + C_{n_\alpha} U_3] \end{aligned} \quad 17$$

The desired aerodynamic coefficients can thus be obtained by equating the corresponding terms of equations 16 and 17 with those of 14 and 15.

CROSS FLOW COEFFICIENTS

The general method followed is that the wings and fins are relatively small appendages on a dominate axis-symmetric body with the  $X_1$  axis of symmetry.

In this case, the basic solutions are the expected:

$$\phi_2 = R_e (-a^2/z)$$

$$\phi_3 = R_e (-i a^2/z)$$

$$\bar{X}_1 = 0$$

The wings and tail surface effects are added to the basic body solution at their aerodynamic centers in the form of concentrated aerodynamic forces and moments. These forces and moments are currently estimated from empirical and semi-empirical wing relationships. Since these relations are primarily for planar lifting surfaces, however, they must be modified for the missile fin geometry before incorporation into the estimate of overall missile characteristics. These modifications are discussed in the following sections.

Multi-Panel Interference

The computation of virtual mass and aerodynamic coefficients for slender bodies with multiple fins has been discussed extensively by several authors. Miles, Reference 6, has computed the effect of multiple fins on an axisymmetric body. For most configurations; however, it is anticipated that wing-body interference will dominate over the wing-wing interference. The neglect of wing-wing interference would permit the aerodynamic characteristics of the various wing configurations to be estimated from available planar data.



Within linear theory the lift on a wing is proportional to the angle of attack measured in a plane normal to the span of the wing. The resulting lift vector would also be in the same plane normal to the wing span. This geometry is shown in Figure 2.

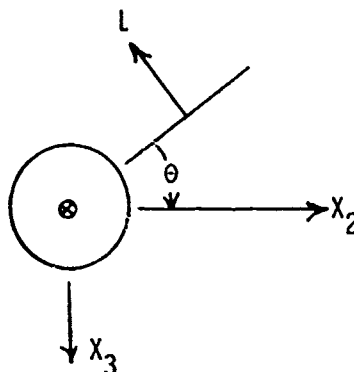


Figure 2 - Roll Orientation

Thus the angle of attack in the plane of the wing is, for small angles of attack:

$$\alpha_e = \alpha \cos \theta \quad 18$$

The panel lift force is:

$$L_p = q S [C_{L_\alpha} \alpha \cos \theta + C_{L_0}] \quad 19$$

Resolving this force into components gives a lift of:

$$L = q S [C_{L_\alpha} \alpha \cos^2 \theta + C_{L_0} \cos \theta] \quad 20$$

and a side force of:

$$Y = q S [C_{L_\alpha} \alpha \sin \theta \cos \theta + C_{L_0} \sin \theta] \quad 21$$

If it is assumed that the  $C_{L_\alpha}$  in equation 19 is equal to 1/2 the 2 panel value given by Miles, Reference 6, then the lift and side force of multiple panel configurations can be estimated by the formula:

$$L = \sum_i q S [(C_{L_\alpha})_i \alpha \cos^2 \theta_i + (C_{L_0})_i \cos \theta_i] \quad 22$$

$$Y = \sum_i q S [(C_{L_\alpha})_i \alpha \cos \theta_i \sin \theta_i + (C_{L_0})_i \sin \theta_i] \quad 23$$

The results of this estimation are compared with the exact formulation of Miles, Reference 6, for multi-panel configurations in Figure 3. As would be expected, for a relatively few panels, say 6 or less, and for the range of radius to semi-span ratios expected in missile configurations, say 0.4 or greater, the neglect of panel-panel interference results in an error of 10% or less in the predicted force.

#### Aspect Ratio Effects

Pitts, Nielson, and Kaattari, Reference 1, have extended the results of slender-body theory to wings of larger aspect ratio by replacing the term containing the panel lift slope in the above formulation by:

$$(C_{L_\alpha})_p \{ [K_{WB} + K_{BW}] \alpha \cos^2 \theta + [k_{WB} + k_{BW}] \delta \cos \theta \} \quad 24$$

In this approximation

$(C_{L_\alpha})_p$  is determined for the panel from Lowry-Polhamus theory for a 2 panel wing, and

$K_{WB}$ ,  $K_{BW}$ ,  $k_{WB}$ ,  $k_{BW}$  are determined from slender-body theory again for 2 panel wing configurations.

The interference factors  $K_{WB}$ ,  $K_{BW}$ ,  $k_{WB}$  and  $k_{BW}$  are taken from Reference 1 and are shown in Figure 4.

COMPARISON BETWEEN THEORETICAL AND PREDICTED LIFT FOR MULTI-FIN  
COEFFICIENTS

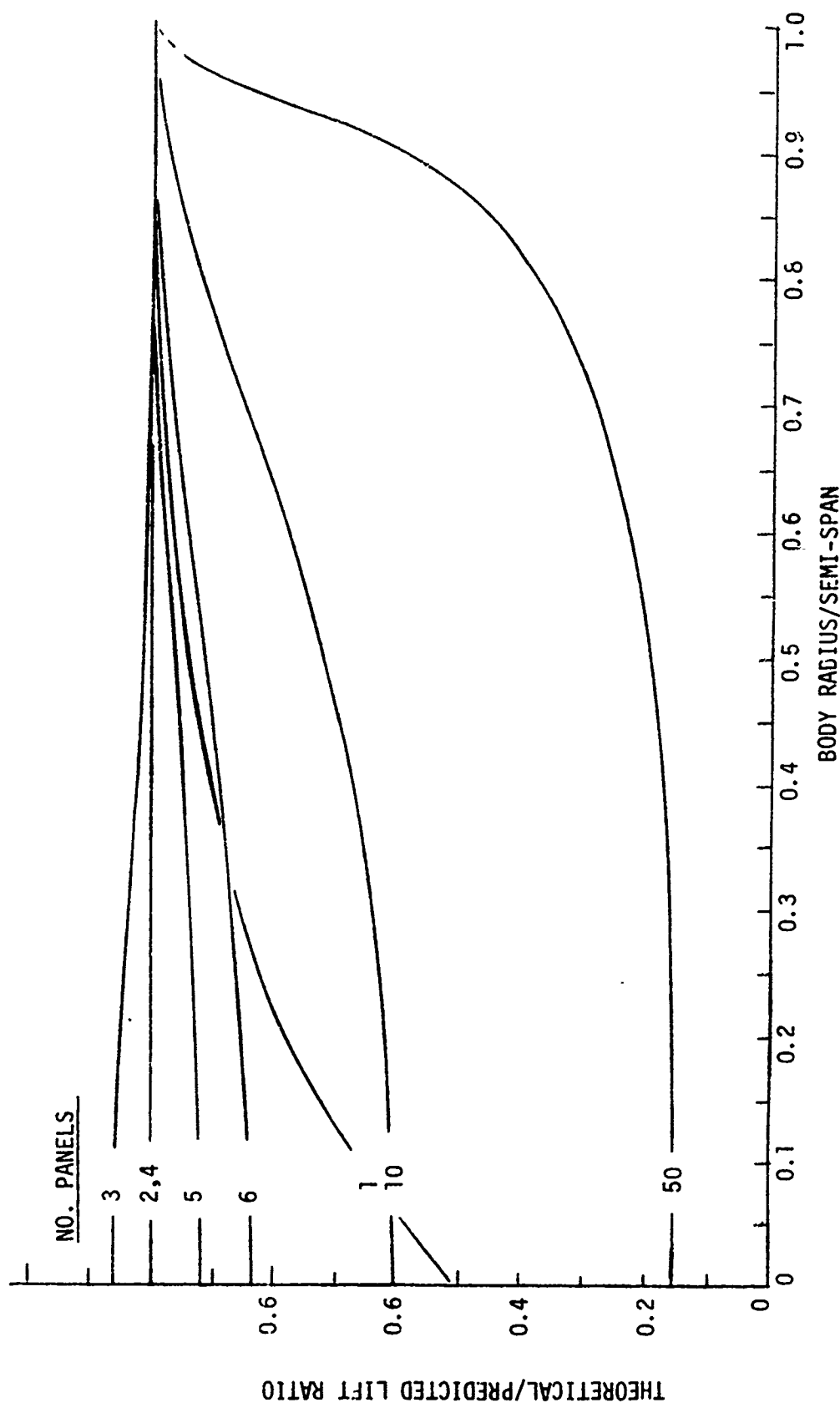


FIGURE 3

WING-BODY INTERFERENCE FACTORS

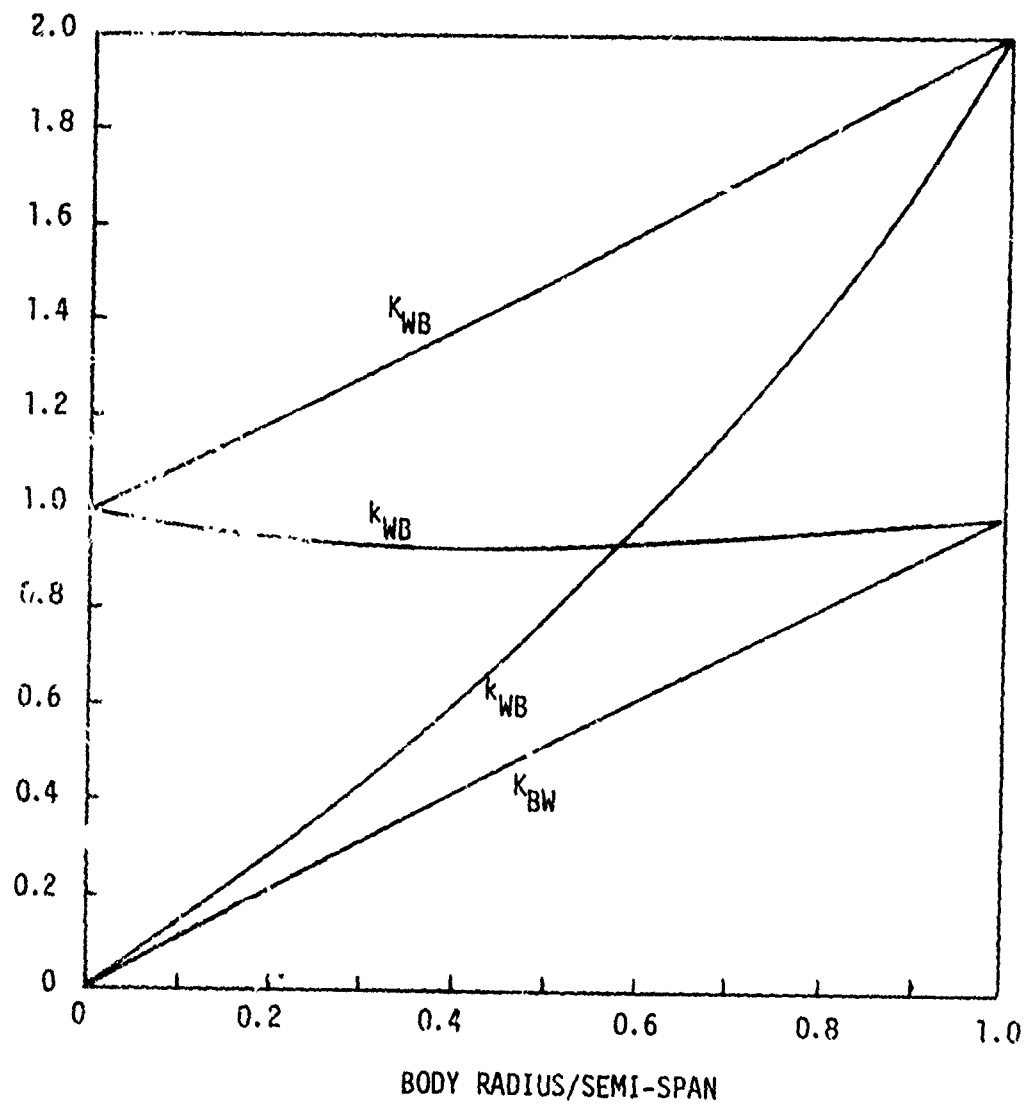


FIGURE 4

### Rolling Moment

To compute the rolling moment of a multi-panel configuration it is necessary to estimate the center of pressure of the single panel body configuration. Since, for symmetric configurations, the rolling moment is zero, the results of either Miles, Reference 6, or Bryson, Reference 5, are not directly applicable to the problem. Within the extension of slender-body theory discussed in the previous sections; however, the rolling moment may be determined by using semi-empirical wing center of pressure data. The particular value used was taken from Reference 7. If it is assumed that the "body carry over forces" do not contribute to the rolling moment then

$$K = q S \sum_i (C_{L_{\alpha}})_i [K_{WB} \alpha \cos \phi + k_{WB} \delta] Y_{arm} \quad 25$$

### Axial Force Contribution

While slender-body theory normally does not lead to axial force computations, axial force may be obtained by extensions to the basic theory. In the extensions careful distinction must be made between lift and normal force.

In slender-body theory a wing is assumed to produce a force normal to its surface, and consequently, inclined aft relative to the wind velocity. Conversely in high aspect ratio wing theory, a wing is assumed to produce the force essentially normal to the relative wind vector and hence inclined forward relative to the wing reference chord. While this relative rotation of the force vector between the two theories is of only small consequences with respect to the normal and/or lift forces (indeed the distinction is overlooked entirely in the Lowry-Polhamus formulation), it can be of dominate importance in the computation of axial and/or drag forces. Consequently an empirical correction to the slender-body theory previously discussed is required if axial forces are to be predicted.

The methods used to estimate the rotation of the lift force have been taken almost directly from Reference 3. This method can be summarized briefly into the following steps:

1. The wing body forces are divided into body carry-over components and wing panel components.
2. The body carry-over components are assumed to be normal to the body centerline and hence do not contribute to the axial forces.
3. The wing panel forces predicted by the Lowry-Polhamus equation are assumed to be normal to the relative wind velocity and are then resolved into wing normal and axial components.
4. The axial component, which in general results in a negative axial force is assumed to be produced by leading edge suction. Reference 3 contains an empirical correction for the leading edge suction based on wing geometry and Mach number. This correction is shown in Figure 5.

This approach to the axial force contribution from the leading edge suction is not entirely compatible with the results of References 8 and 9. The method does however lead to the correct limiting solutions in most cases. In particular low aspect wings with high leading edge sweep have essentially no leading edge suction while high aspect ratio wings with low leading edge sweep have almost full leading edge suction.

#### Tandem Surface Interference

Within slender-body theory it is normally assumed that the wing wake follows behind the wing (and in its plane) well into the Trefftz plane. Consequently any trailing surface in the plane of the wing, as shown in Figure 6, would only be effective to the extent that its span extended beyond the wake of the leading wing.

LEADING EDGE SUCTION CORRELATION

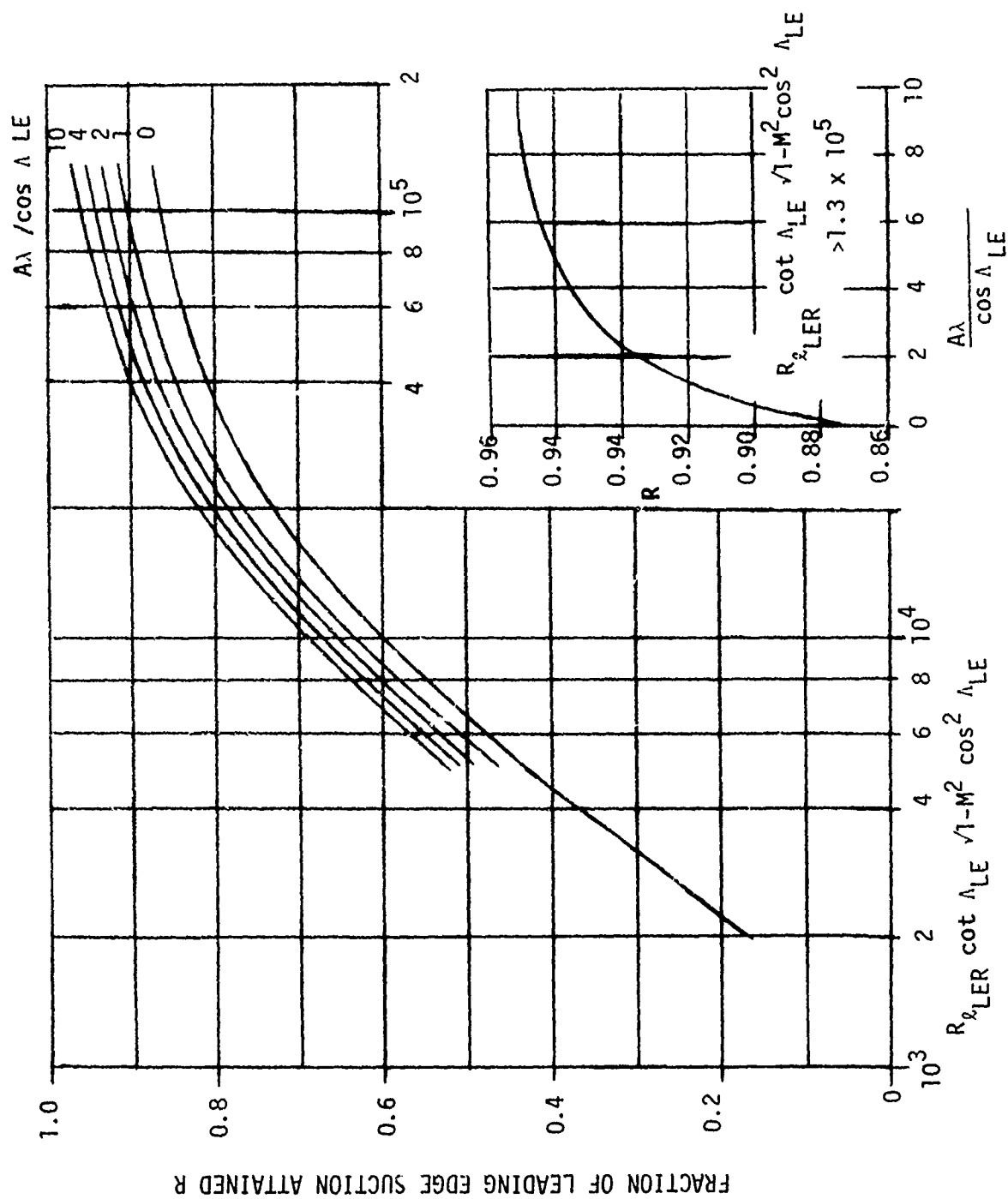


FIGURE 5

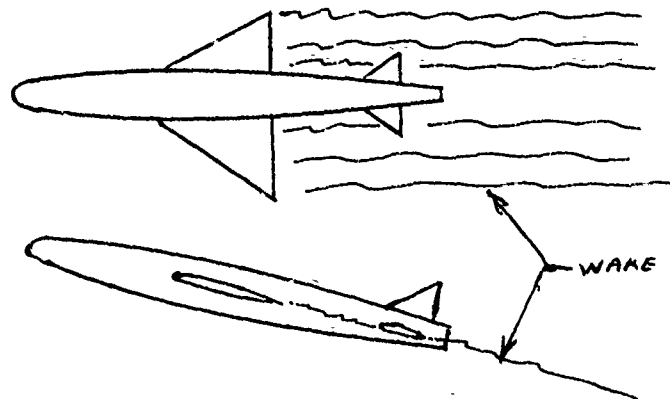


Figure 6

## Slender Body Wake Geometry

In practice, however, it is discovered that the tail, through seriously affected, is rarely blanketed completely even if the tail span is smaller than the wing span. Because of the moment arms involved, even a small tail contribution can lead to significant moment contributions. Pitts, Nielson and Kaattari, in Reference 1, have taken an alternate approach. They have assumed that the wake from the leading surface has rolled up completely into two trailing vortices which are aligned with the relative wind vectors as shown in Figure 7.

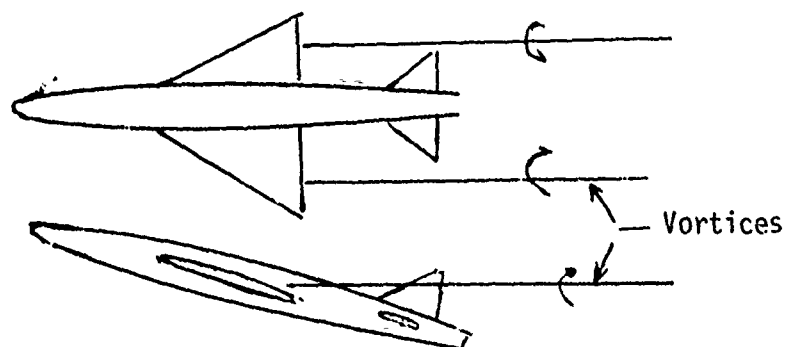


Figure 7

## ROLLED UP WAKE GEOMETRY



The velocity field generated in the vicinity of the tail is computed and then used to estimate average downwash effects on the trailing surfaces.

Because all the vorticity shed by the leading surface is concentrated into two vortices, the average downwash produced by a given amount of vorticity is significantly less than that which would be produced by a plane wake. Thus the method of Reference 1 leads to significantly smaller downwash contributions than the normal slender-body results. Indeed this method will probably seriously underestimate the downwash effects for cases where the wake has not rolled up completely.

Kaden, Reference 10, has estimated the distance necessary to produce a fully rolled up wake. In terms of semi-spans, Kaden's estimate is:

$$n = 0.48 A/C_L$$

For all aspect ratios

$$C_L \leq \pi/2 A \alpha$$

Hence

$$n \geq 0.306 1/\alpha$$

26

From this estimate it is apparent that for low angle of attack stability and control computations, the wake can not be expected to have achieved a completely rolled up configuration unless the trailing surface is many semi-spans behind the leading surface.

At the higher angles of attack; however, significant wake roll up may in fact be present. Consequently, neither method can be expected to give good moment computations over the entire angle of attack range without significant modifications. Because initial interest centered around low angle of attack stability and control computations, it was decided to attempt to empirically modify the planar wake model. Two modifications

were made. These were to modify slender-body theory for the effect of wing aspect ratio and to trail the wake back in the free stream direction.

A Trefftz plane analysis of a planar wake with elliptical vorticity distribution can be used to estimate the complex velocity field. The results of this analysis is:

$$(U_2 - i U_3)/U_1 = \frac{2 C_{LW}}{\pi A_W} \left[ \sqrt{\frac{z}{s^2 - z^2}} + i \right] \quad 27$$

As an engineering approximation the  $C_{LW}$  required is estimated by the Lowry-Polhamus equation using slender-body carry over factors. The resulting approximation is

$$C_{LW} = \frac{\pi^2 b_e^2/S [(K_{WB} + K_{BW}) \alpha \cos \theta + (k_{WB} + k_{BW}) \delta]}{2 + \sqrt{4 + \frac{b_e^4}{(S)^2} (\beta^2 + \tan^2 \Lambda_{C/2})}} \quad 28$$

If the body is assumed to form an effective end plate, then the equation can be used to compute the normal component of downwash produced by the wake of a forward lifting panel at the planform center of pressure of a trailing surface. For multiple wake surfaces, the individual downwash contributions are added directly. Because of the assumption that the body effectively end plates a panel, a wake is assumed to produce a downwash only on panels that lie within  $\pm 90^\circ$  of the wake plane.

The predictions for tail surfaces which are not parallel to the wake surfaces can be compared to the results of Miles, Reference 6, multi-fin analysis.

By Miles analysis the total lift generated by the wing wake configuration is given by the equation:

$$(C_L)_{WT} = 4 \alpha \left\{ (s/a)^2 \left[ \frac{1 + (r/a)^{2N}}{2} \right]^{2N} - 1 \right\} ; N = 3, 4, \dots \quad 29$$

If half the panels are assumed to be wings and the other half are assumed to be interdigitated tail surfaces then the lift by either wing or tail surfaces are given by the equation:

$$(C_L)_{W,T} = 4 \alpha \left\{ (s/a)^2 \left[ \frac{1 + (a/s)^N}{2} \right]^{4N} - 1 \right\} ; N = 3, 4, \dots \quad 30$$

The loss in lift because of wing-tail interference is then

$$\Delta C_L = \{ (C_L)_{WT} - [(C_L)_W + (C_L)_T] \} \alpha$$

The effective downwash produced by the total wing wake system on the tail system is

$$\epsilon = \Delta C_L / (C_L)_T \quad 31$$

Since the downwash produced should be proportional to the lift developed by the wing system, it should be possible to write:

$$\epsilon = k(N, a/s) \frac{C_{LW}}{2} (a/s)^2 \quad 32$$

The values of the downwash correction factor,  $k$ , computed from Miles analysis are compared with the results of the plane wake model in Figure 8.

The downwash comparison is similar to, though generally not as good, as that observed in the panel interference comparisons previously discussed. For wing geometries of 6 panels or less (but greater than 3) the downwash factor,  $k$ , is within 20% of the theoretical value for radius to semi-span ratios of 0.5 or greater. For smaller radius to semi-span ratios, it is apparent that both the assumption concerning the body end plate effects, and the assumption concerning the direct summation of the individual panel contributions are increasingly invalid.

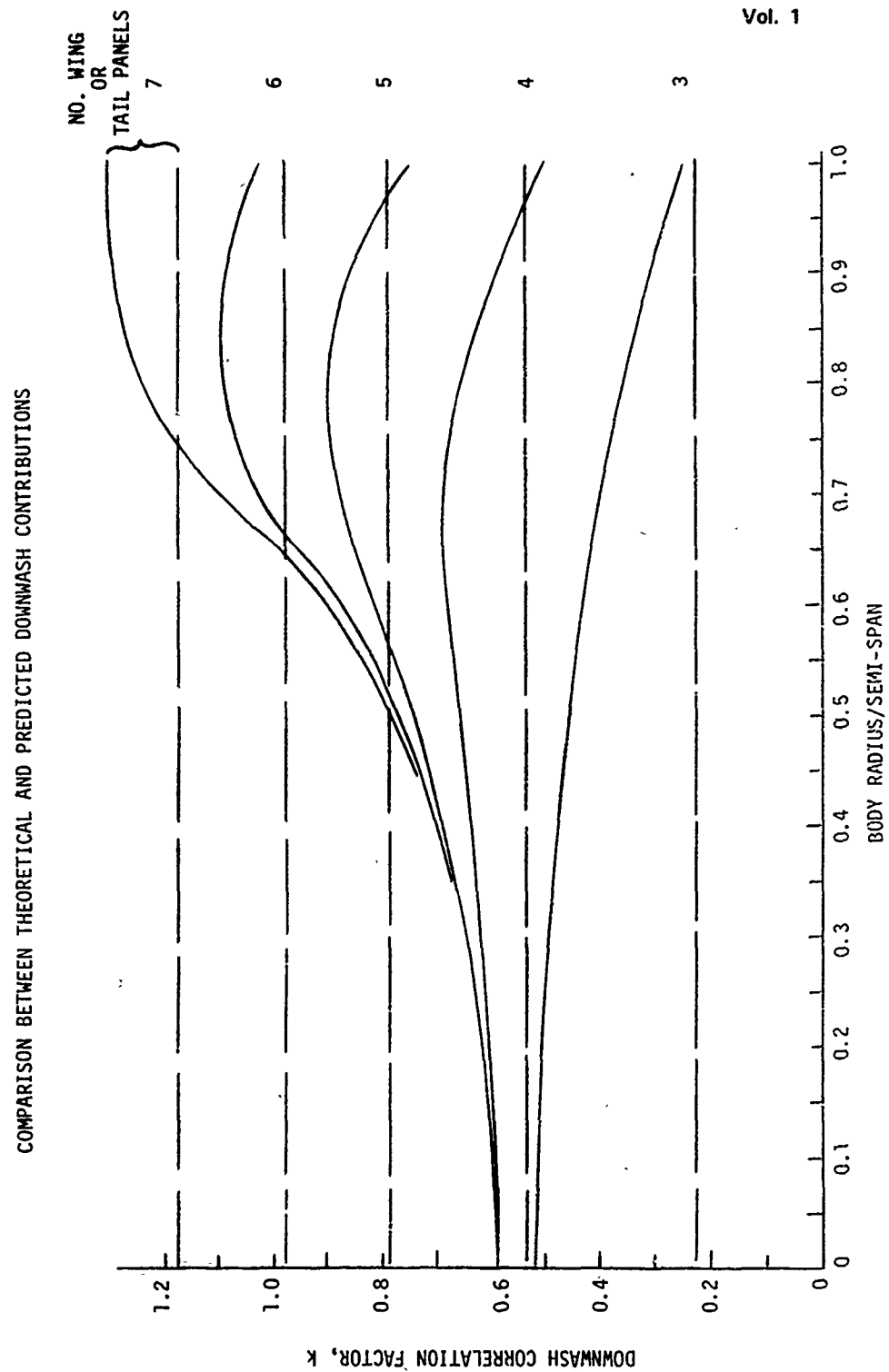


FIGURE 8

Fortunately the most interesting case of four wing and four tail surfaces (this case would also include a planar wing with cruciform tail) is within 20% of the theoretical value for all radius to semi-span ratios.

#### EXPERIMENTAL COMPARISONS

The results of the semi-empirical computations just discussed have been compared with the results of wind tunnel tests for several missile systems. These configurations which include examples of both inline and interdigitated wing and tail surfaces can be used to evaluate several of the assumptions in the computations.

#### Computation Accuracy

The most extensive wind tunnel data available was for the Harpoon missile. This data has been used to evaluate the accuracy of the proposed computations as a function of vehicle roll orientation. Figure 9 shows the Harpoon missile in the air launch configuration.

Figure 10 and 11 show the normal force comparison for predicted and experimental data for the air launch Harpoon configuration in both the "x" and "+" configurations. While the current computations do not reproduce the nonlinear character of the normal force versus angle of attack curves, (as would be expected) the agreement below 12 degrees is quite acceptable for either roll configurations. The corresponding comparisons for the stability and control plots are shown in Figures 12 and 13. While the agreement on the "x" position is not quite as good as that in the "+" configuration, the overall agreement is acceptable. In particular the experimental differences in control power between the two configurations is also reflected in the predicted values. Most of the errors shown are attributed to the downwash computation.

AIR LAUNCH HARPOON CONFIGURATION

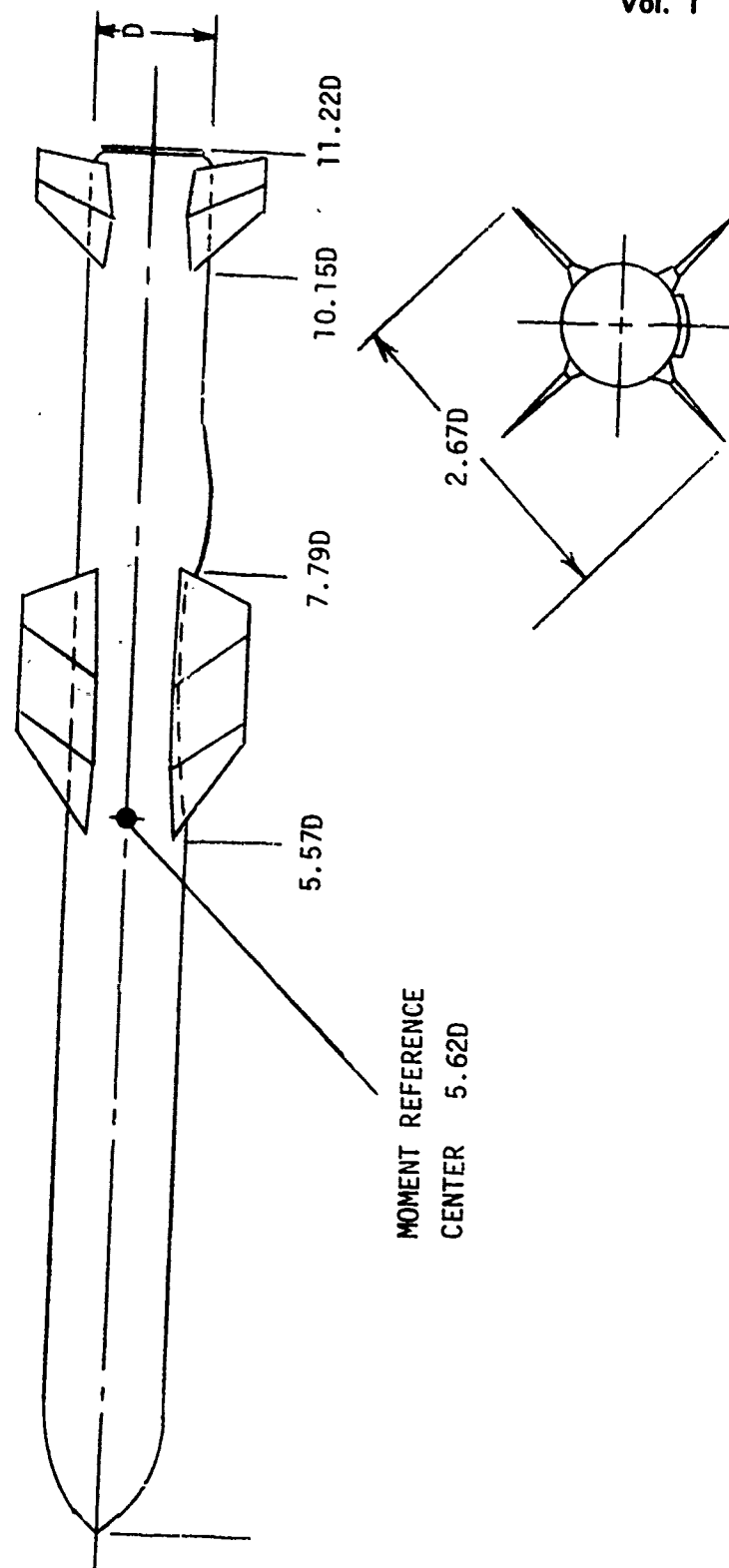


FIGURE 9

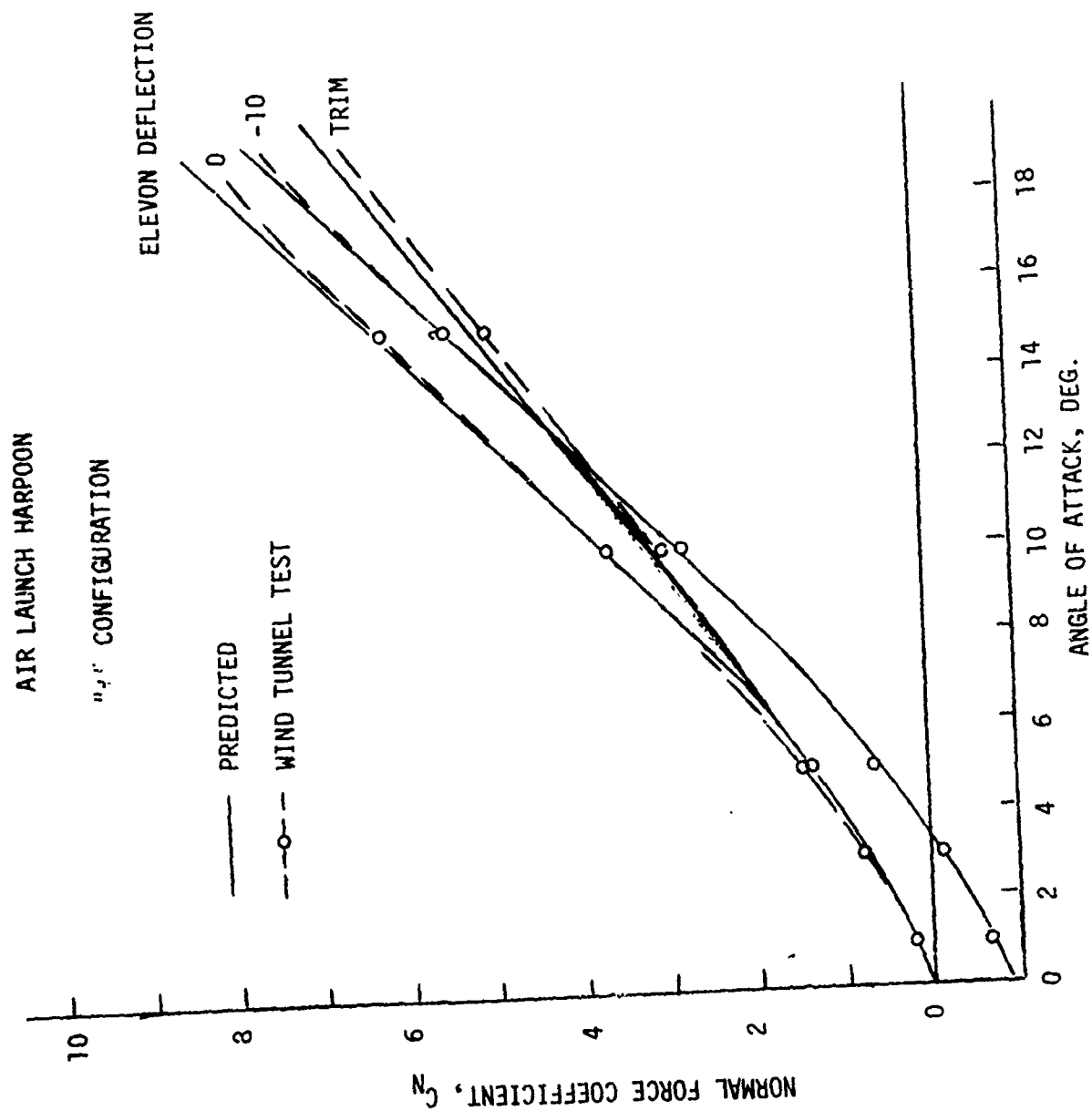


FIGURE 10

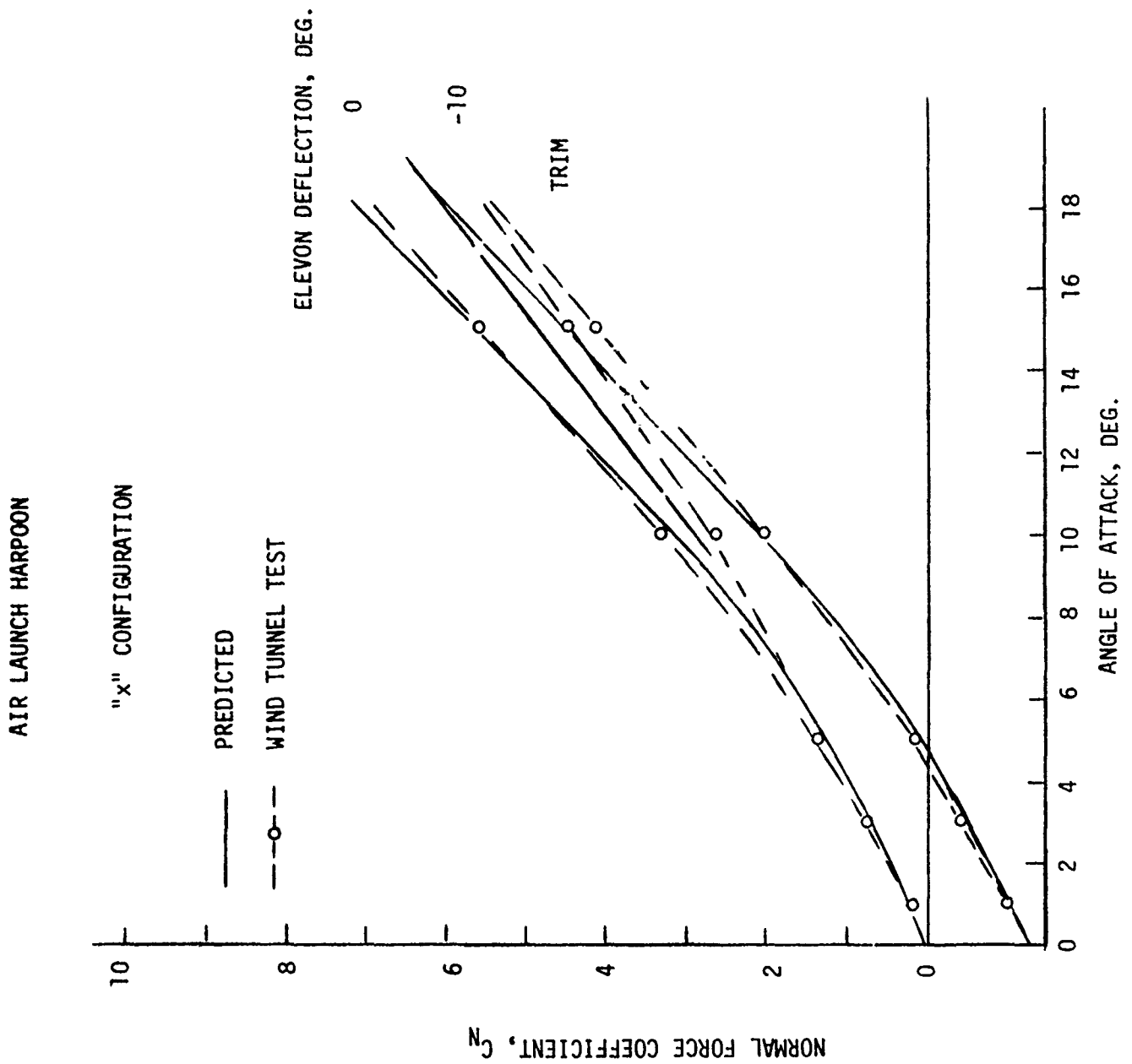


FIGURE 11



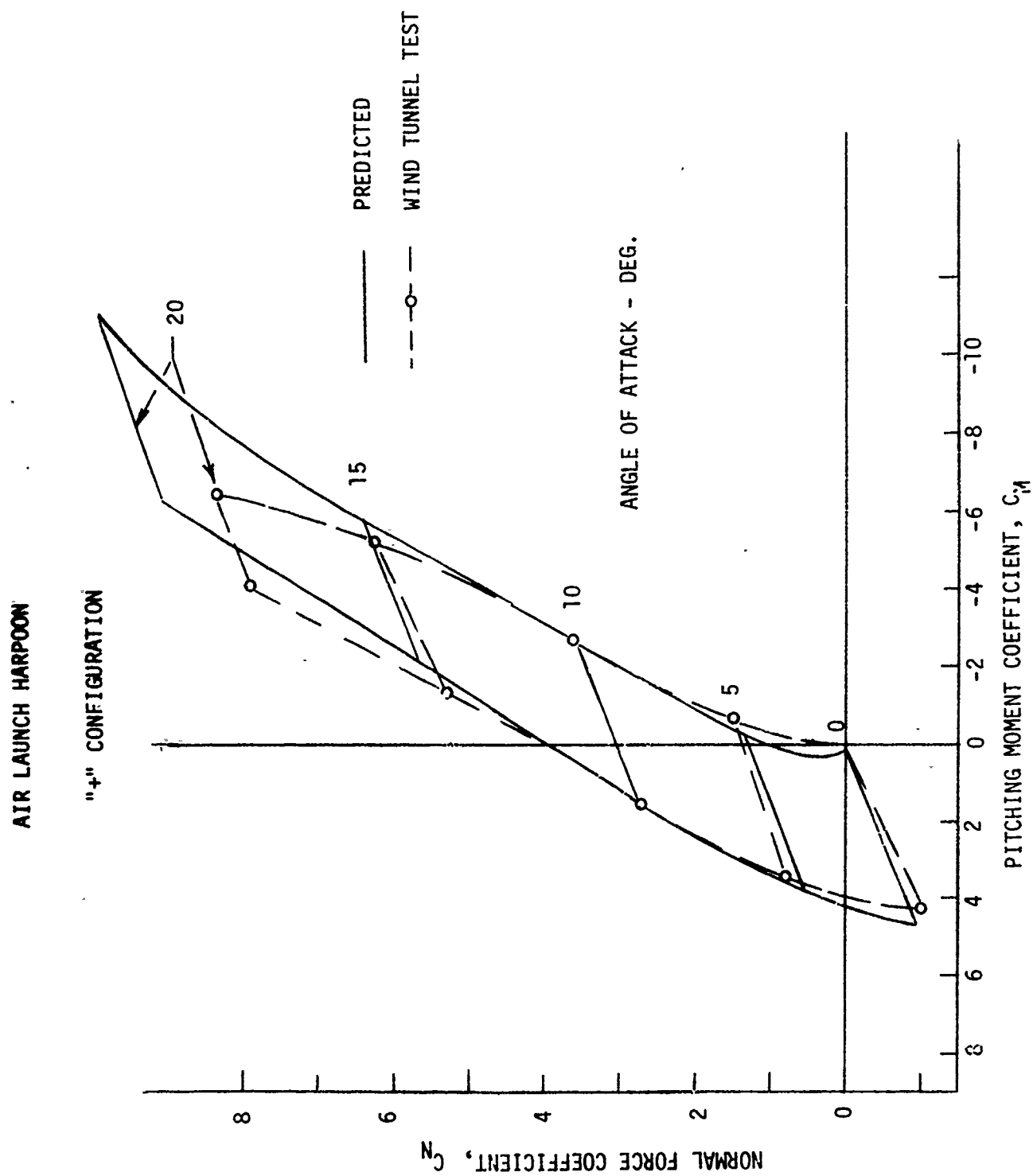


FIGURE 12

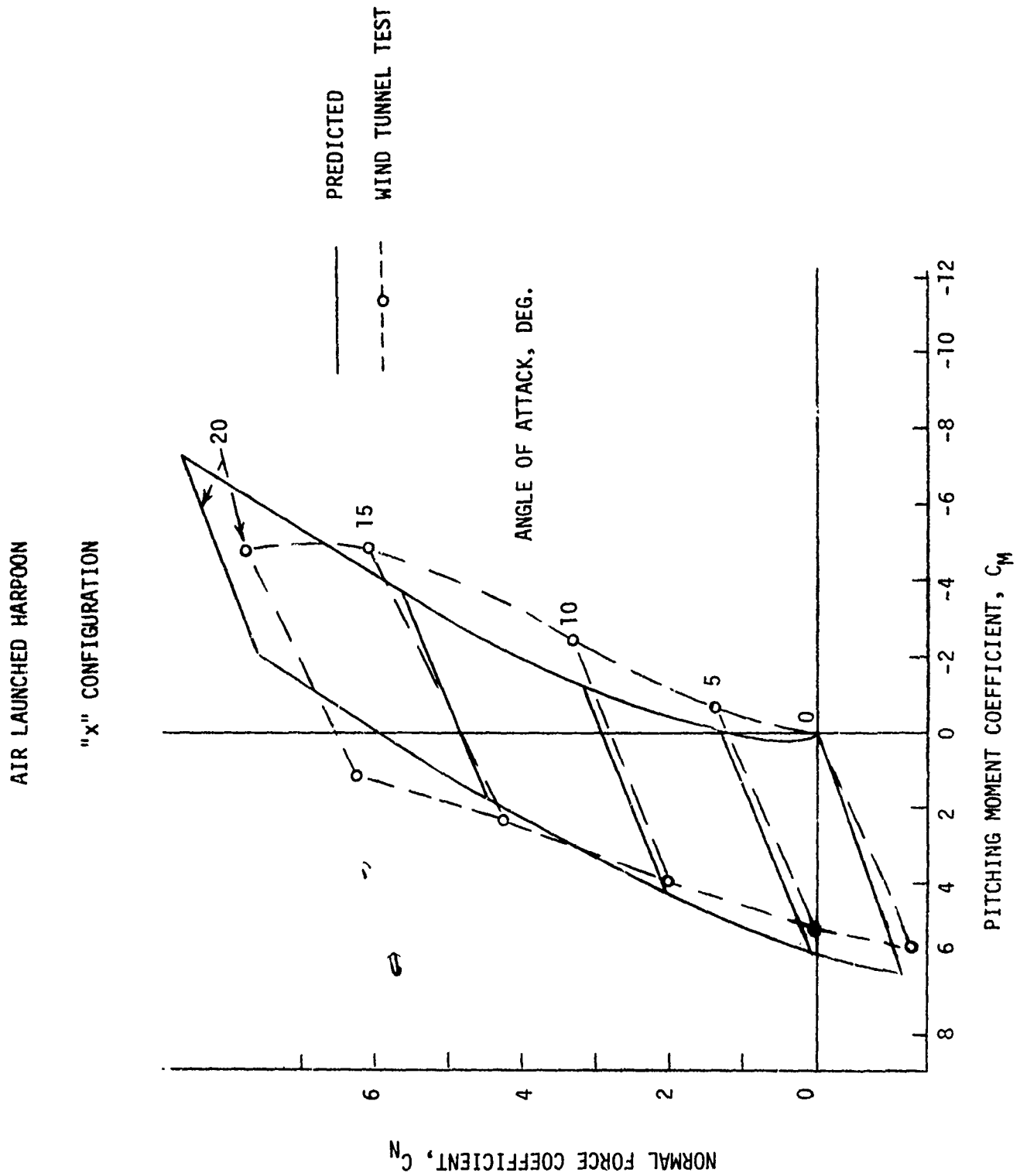


FIGURE 13

The Harpoon missile has the wing positioned some 2.1 semi-spans ahead of the aerodynamic center of the tail surfaces. Consequently the neglect of any wake roll up leads to an overestimate of the effective downwash. This is particularly evident in the "x" configuration. In the "+" configuration this overestimate of the downwash effect is over compensated by the error introduced by the neglect of any wake deflection from the free stream direction. This neglect of the wake deflection underestimates the distance between the plane of the wake and the tail surfaces. This error is particularly evident for the "x" configuration.

#### Downwash Computation Accuracy

In the Cruise Missile study both "+" and "x" tail configurations were tested behind a planar wing of fairly high aspect ratio. Figure 14 shows the pitching moment data for the two tail configurations. As expected from Miles work (Reference 6), the body-tail data below tail stall (about 11 degrees) is virtually independent of roll orientation. At low angles of attack, however, the downwash contributions from the wing on the "x" tail surface is measurable less than those on the "+" tail. Wing stall for the model occurred at 8°. The differences of deflection characteristics of the wake after stall was felt to be responsible for the increased stability of the "+" tail characteristics at higher angles of attack. The tail increment of the moment was determined from wind tunnel data component breakdown. This increment was modified by the predicted downwash contributions from the wing and was added to the body plus wing data to predict the total configuration pitching moment. The predicted values are compared with the measured values in Figure 14. The two are in reasonable agreement at low angles of attack.

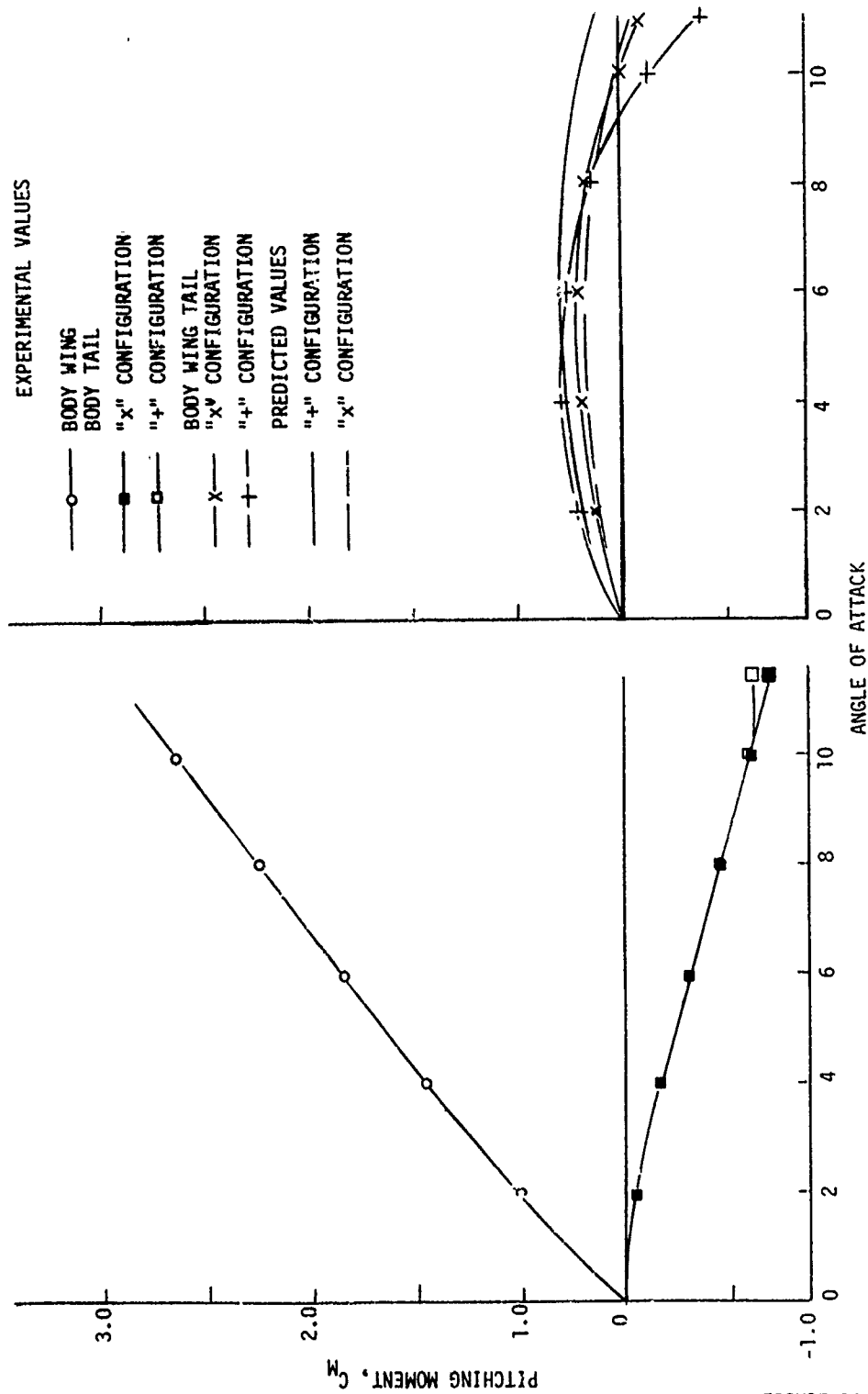
COMPARISON OF DOWNWASH EFFECTS OF PLANAR WING ON "+" AND "X"  
CONFIGURATION TAILS

FIGURE 14

Multiple Tandem Surface

The Harpoon ship launch boost configuration has 3 tandem lifting surfaces. This configuration, shown in Figure 15, can be used to evaluate the direct summation of contributions of upstream surfaces. The stability plots for both the air launch and ship launch configurations are shown in Figure 16. In both cases, the neglect of the roll up of the wing wake leads to an overestimate of the wing downwash. The change in characteristics produced by the booster fins, however, agrees very well with the difference in measured values.

HARPOON SHIP LAUNCH CONFIGURATION

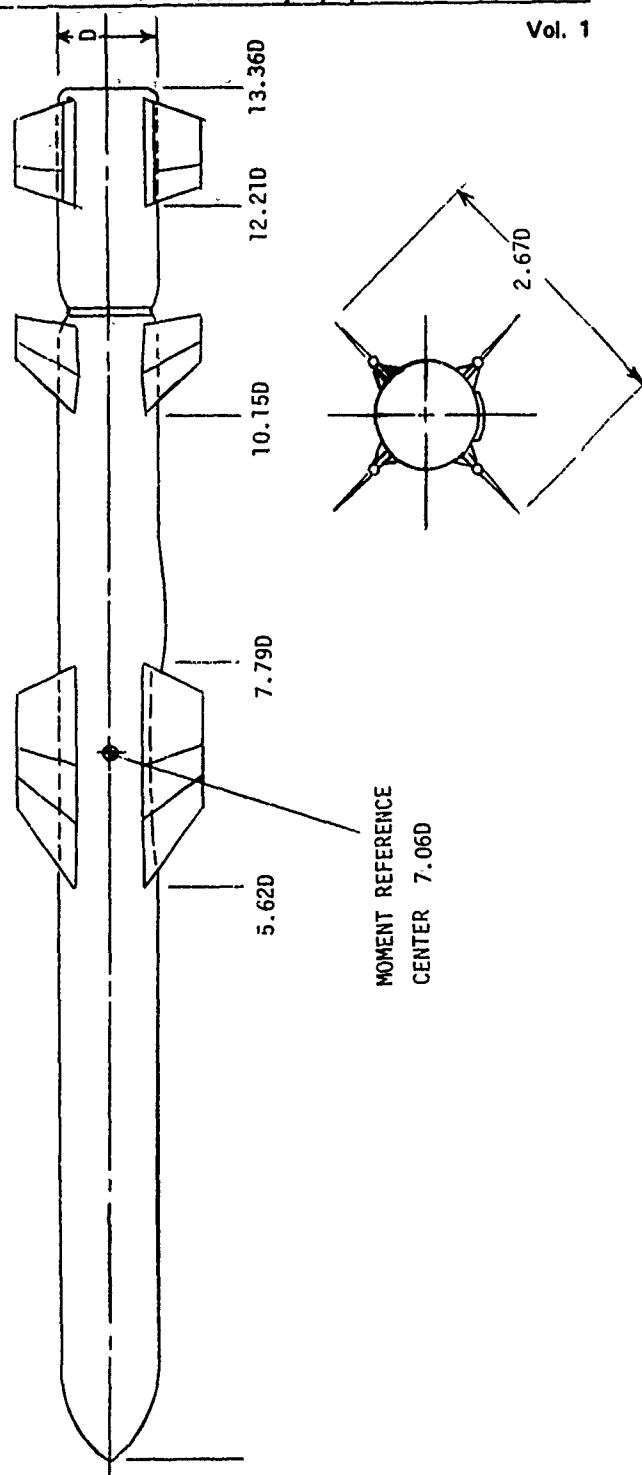
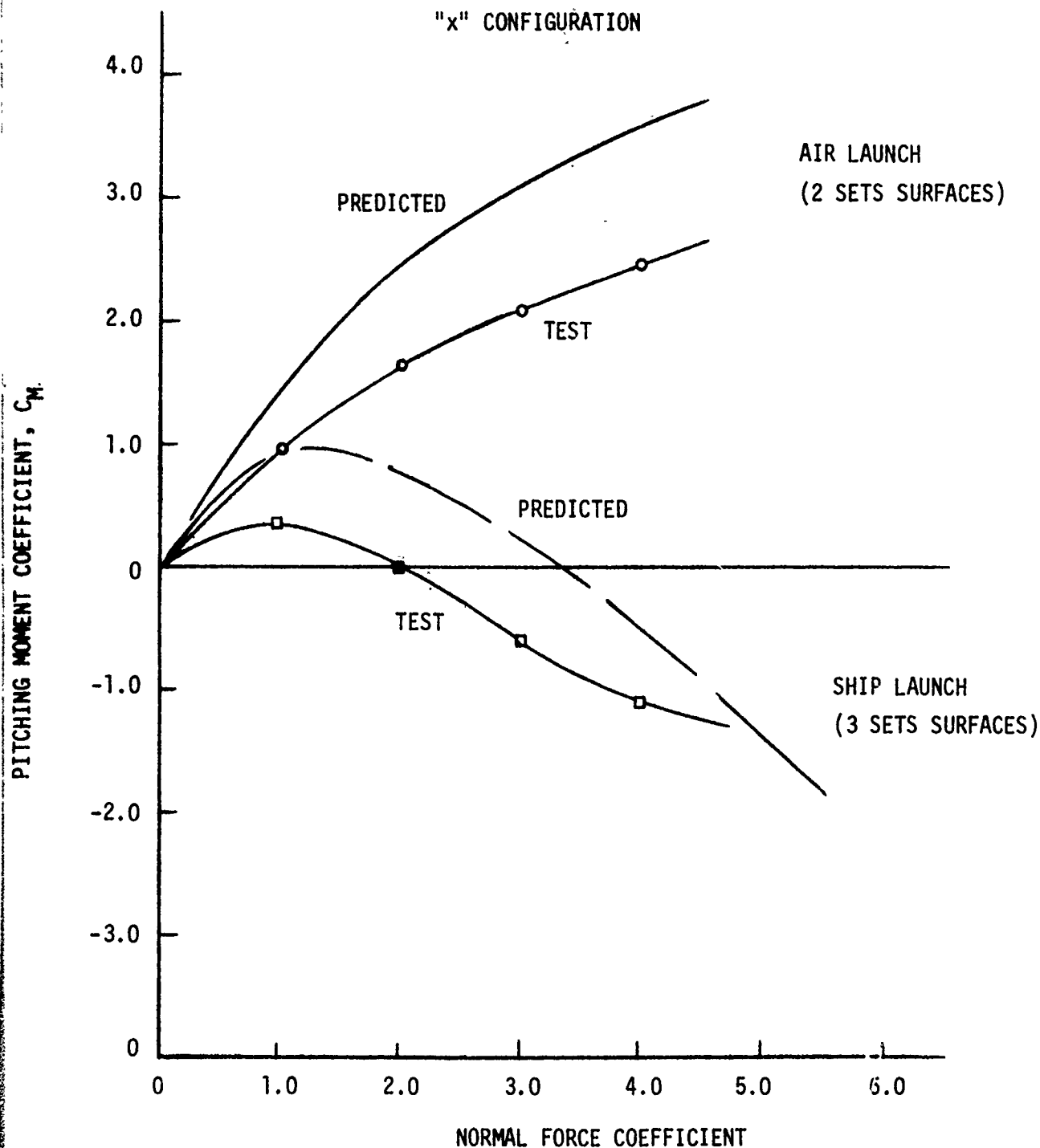


FIGURE 15

EFFECT OF MULTIPLE TANDEM  
SURFACES ON THE  
HARPOON CONFIGURATION

MOMENT REFERENCE CENTER = 7.06D

"X" CONFIGURATION



CONCLUSIONS

In the preceding discussion a means for using existing planar wing data to predict the aerodynamic characteristics and the downwash contributions of arbitrary multi-fin geometries has been proposed. Comparisons of the aerodynamic characteristics predicted by this method have been made with the theoretical work of Miles, Reference 6, and experimental values.

Since the method assumes that each fin is independent of other fins at the same axial location, favorable agreement with theory is generally confined to geometries with no more than 6 fins at each axial location. For multi-fin geometries favorable agreement is generally confined to body radius to semi-span ratios of 0.5 or greater. The neglect of wake roll up and deflection from the free stream direction does produce some errors in the downwash effects for configurations with the fins several semi-spans from the wing surface. This trend becomes increasingly noticeable at higher angles of attack, particularly for "x" configurations.

In general, the agreement shown has been considered to be satisfactory; however, the comparisons do suggest several areas requiring improvement. Particular development efforts are now being made to improve the downwash estimates for the lower body radius to semi-span ratios by relaxing the assumption of body end plate effects and allowing for some wake-wake interference.



## 10th Navy Symposium on Aeroballistics

---

### Vol. 1

#### REFERENCES:

1. Pitts, W.C., Nielsen, J. N. and Kaattari, G.E., "Lift and Center of Pressure of Wing-Body-Tail Combinations at Subsonic, Transonic and Supersonic Speeds," NACA Report 1307, 1957.
2. Howard, M. L. and Brooks, E.N., "Missile Aerodynamic Predictions to 180°", Journal of Spacecraft and Rockets, May 1971, pp 488-493.
3. Mehlich, G. J., Murray, S.C. and Washburn, S. S., "A Fortran Program for Computing Aerodynamic Static Stability Characteristics Using USAF Datcom Methods", AFFDL-TR-73-23, Vol. 1 and 2.
4. Bryson, A.E., Jr., "Evaluation of the Inertia Coefficient of the Cross Section of a Slender Body", Journal of the Aeronautical Sciences, Vol. 21, No.6, June 1954.
5. Ashley, Holt and Landahl, Martin, Aerodynamics of Wings and Bodies, Addison-Wesley Publishing Co, Inc., 1965.
6. Miles, J.W., "On Interference Quotes of Tunnel Bodies", Journal of the Aeronautical Sciences, Vol 18, No.4, April 1952 :
7. Etkin, Bernard, Dynamics of Flight, John Wiley & Sons, Inc., 1959.
8. Gardner, D., AND Weir, J., "The Drag Due to Lift of Plane Wings at Subsonic Speeds", RAS Journal, Vol. 70, May 1966.
9. Anon, Royal Aeronautical Society, Engineering Services Data (Aeronautical Series). Vol. 2, Item 66032, 1966.
10. Kaden, H., Reported in Vol II p. 325, Aerodynamic Theory, Durand Editor, Dover Publications, Inc. 963.

PAPER NO. 6

WING PLATFORM STUDIES

FOR A

SPAN-CONSTRAINED MISSILE

L. S. JERNELL

W. C. SAWYER

PAPER WITHDRAWN

AN EXPERIMENTAL STUDY OF THE EFFECT OF MISSILE  
CONFIGURATION VARIABLES ON PITCH LINEARITY  
(U)

(Paper UNCLASSIFIED)

by

William A. Corlett and Roger H. Fournier

NASA Langley Research Center  
Hampton, Virginia

INTRODUCTION

The design of recent U.S. missile systems, in many cases, has not relied heavily on aerodynamic technology to optimize performance. NASA is currently developing a technology base for improving aerodynamic efficiency within realistic system constraints. This technology base will allow the aerodynamics of missile concepts to be considered earlier in the preliminary design, help to eliminate system concepts that would result in unsatisfactory aerodynamic designs and allow greater emphasis to be placed on design concepts having a good balance between aerodynamic and nonaerodynamic disciplines.

In order to meet the threat of the 1980/1990 time period, ground-to-air and air-to-air missiles must have a high degree of maneuverability and will be required to operate through a wide range of Mach numbers and altitudes. There are a number of static stability problems encountered under these conditions. Examples include nonlinear variations of pitching moment, induced rolling moments and panel-panel interference for multipanel wing and tail arrangements.

## 10th Navy Symposium on Aeroballistics

### Vol. 1

An aerodynamic requirement for a highly maneuverable missile should be a low stability with linear pitching-moment characteristics throughout a high lift range. Currently nonlinear aerodynamic effects at high lift conditions are unpredictable by analytical methods such as those of References 1 and 2. The technology to evaluate these effects must be obtained through analysis of experimental data. Experimental studies of several cruciform missile configurations are presented in Reference 3 through Reference 10.

A recent experimental study has been conducted to provide the effects of wing location, control location, afterbody geometry and body fineness ratio on pitch linearity for a class of maneuverable missiles. The experimental results were obtained in the Langley Unitary Plan wind tunnel through a Mach number range from 1.5 to 4.6 with variations in angle of attack from minus 5 degrees to 25 degrees and model roll angles of 0 degree and 45 degrees. The present paper presents some of the pertinent results of an analysis of these data.

### SYMBOLS

The coefficients of forces and moments are referred to the stability-axis system. The moment reference was varied with wing location in order to maintain a constant static margin of about 3 percent body length. (See Figure 1.) All coefficients are based on the maximum cross-sectional area and the diameter of the body.

- A      maximum cross sectional area of body
- $C_m$       pitching-moment coefficient,  $\frac{\text{Pitching moment}}{qAd}$
- $C_L$       lift coefficient,  $\frac{\text{Lift}}{qA}$

d	maximum diameter of body
M	Mach number
q	free-stream dynamic pressure
$\phi$	model roll angle ( $0^\circ$ , wings in the horizontal and vertical planes)

Dimensional details of the model are presented in Figure 1. Configurations tested included: A common body having a length to diameter ratio of 10 with cruciform delta wings which could be located in three longitudinal positions; afterbody additions consisting of cylinders of one and two diameters in length and moderate boattail and flare angles; and aft control surfaces installed on the longer cylindrical afterbody at two longitudinal locations. The analysis of the pitching moment data is presented for conditions of 3 percent static margin at  $C_L = 0$ ,  $M = 2.3$ , and  $\phi = 0^\circ$  except when noted.

The effects of longitudinal wing position on pitch-linearity is quite large as shown in Figure 2. The results show that the configuration with the wing in the most aft location has a severe pitch-up tendency. Moving the wing forward one body diameter provides much improvement and moving the wing forward two body diameters yields a near linear pitching-moment curve.

The variation of lift coefficient with angle of attack (not shown) indicate that moving the wing forward also provides for small increase in lift. Although moving the wing forward reduces the lift provided by the forebody, this loss is more than compensated by the increase in wing carry-over lift to the afterbody. Also, long forebodies inherently have a large center of pressure movement with increase in angle of attack, and at high angles of attack, vortices generated by the body nose pass close

to the wing panels and modify their aerodynamic characteristics. These obviously have a dramatic effect on pitching moment linearity. Moving the wing forward in this series of configurations balances the effects of each component in a manner to provide a more linear variation of pitching moment with lift.

The effect of wing carry-over lift was investigated by adding cylindrical afterbodies of one and two body diameters in length to the basic wing-aft configuration. The results shown in figure 3 indicate (as previously mentioned) that carry-over lift increases at high angle of attack resulting in an increased stabilizing moment. This significantly improves pitching-moment linearity; however, the long forebody continues to contribute to pitch-up nonlinearities.

The effects of moderate boattail angles were investigated and the results are presented in figure 4. Base diameters of the two boattailed configurations are the same and the lengths are one and two body diameters, respectively. The boattail provides less lift and therefore reduces the afterbody contribution to stability and pitching moment linearity for these configurations.

In continuing the study of afterbody geometry, the effect of flares is shown in Figure 5. The base diameter is the same for both flared afterbodies and the length of the flared positions of the afterbodies are one and two body diameters, respectively. The pitch characteristics of the flares are generally favorable; however, the increase in drag tends to offset the favorable contributions to stability and linearity.

The location of the primary lifting surface has a predominate effect on the pitch characteristics, but the effects of the wing flow field on the tail surface can adversely effect the pitching moments. Figure 6 shows the effect of wing and tail location on pitching moment linearity. This configurations series utilizes the length to diameter ratio 12 configuration with cruciform control surfaces added to the cylindrical afterbody. Both the tails and the wings were tested in for and aft positions. The configuration with the most severe pitch-up tendency is the configuration with the wing aft and the close coupled tail surface. Moving the tail aft with the wing in the aft position has a favorable effect on stability and pitch linearity. However, the configuration with the near linear pitching moment curve is the one with the wings forward and the tails forward. Moving the tails aft provides an increase in stability at relatively low lift coefficients which gives the configuration a pitch-down tendency.

The effect of Mach number on the wing forward-tail forward configuration is shown in Figure 7. This configuration which has near linear pitch characteristics to lift coefficients in excess of 10 at Mach number 2.3 exhibits a pitch-down tendency at Mach number 4.63. The moment reference was not varied with Mach number, thus the reduction in stability level with increase in Mach number is apparent. This figure typically shows the sensitivity of pitch linearity with Mach number.

The effect of model roll orientation on pitch characteristics must also be considered. Figures 8 and 9 show the effect of roll angle for the wing forward tail forward configuration at Mach numbers 2.3 and 4.63,

respectively. At Mach 2.3, the  $\phi = 45^\circ$  configuration has a slight pitch up and a lower stability level than the  $\phi = 0^\circ$  configuration. At Mach 4.63, there is a slight reduction in stability but the pitch-down tendency is reduced.

In summary, this study illustrates the significant impact that configuration variables have on missile aerodynamics. Specifically for a class of configurations with large highly-swept wings, the pitch-linearity effects at high angle of attack are shown to be strongly influenced by a balance of destabilizing forebody effects on the wings and stabilizing carry-over lift of the afterbody. Tail position, Mach number (in the supersonic speed range), and roll angle appeared to have less effect on pitch linearity than wing position.



## REFERENCES

1. Jackson, Charlie M., Jr.; Sawyer, Wallace C.; and Smith, Rudeen S.: Estimation of Zero-Lift Drag of Missile Configurations in Supersonic Flow With Turbulent Boundary Layer, NASA TM X-1890 1969
2. Jackson, Charlie, M., Jr.; and Sawyer, C.: A Method For Calculating the Aerodynamic Loading on Wing-Body Configurations at Small Angles of Attack in Supersonic Flow. NASA TN D-6441 1971 .
3. Corlett, William A.: Aerodynamic Characteristics at Mach 2.50 to 4.63 of a Cruciform Missile Model With Delta Wings and Trapezoidal-Tail Controls Including Effects of Wing Locations. NASA TM C-2364, 1971 .
4. Corlett, William A.: Aerodynamic Characteristics of a Cruciform-Wing Missile Model With a Systematic Variation of Canard and Tail Locations at Mach 1.60 to 4.63 . NASA TM X-1834 , 1969 .
5. Spearman, M. Leroy; and Trescot, Charles D., Jr.: Effects of Wing Planform on the Static Aerodynamics of a Cruciform Wing-Body Missile for Mach Numbers Up to 4.63 . NASA TM X-1839 , 1969
6. Hayes, Clyde; and Fournier, Roger H.: Effect of Fin-Flare Combinations on the Aerodynamic Characteristics of a Body at

10th Navy Symposium on Aeroballistics

Vol. 1

Mach Numbers 1.51 and 2.20 . NASA TN D-2626, 1965

7. Spearman, M. Leroy; and Fournier, Roger H.: Aerodynamic Characteristics of a Maneuverable Missile With Cruciform Delta Wings and Aft Tail Controls at Mach Numbers From 1.50 to 4.63 . NASA TM X-1863, 1969 .
8. Corlett, William A.: Aerodynamic Characteristics at Mach Numbers From 0.40 to 2.86 of a Maneuverable Missile With Cruciform Trapezoidal Wings and Aft Tail Controls. NASA TM X-2681, 1972 .
9. Corlett, William A.: Aerodynamic Characteristics at Mach Numbers From 1.60 to 2.86 of a Current Missile Configuration With Modified Wing and Tail Components. NASA TM X-2455, 1972
10. Corlett, William A.: Aerodynamic Characteristics at Mach 0.60 to 4.63 of Two Cruciform Missile Models, One Having Trapezoidal Wings With Canard Controls and The Other Having Delta Wings With Tail Controls. NASA TM X-2780

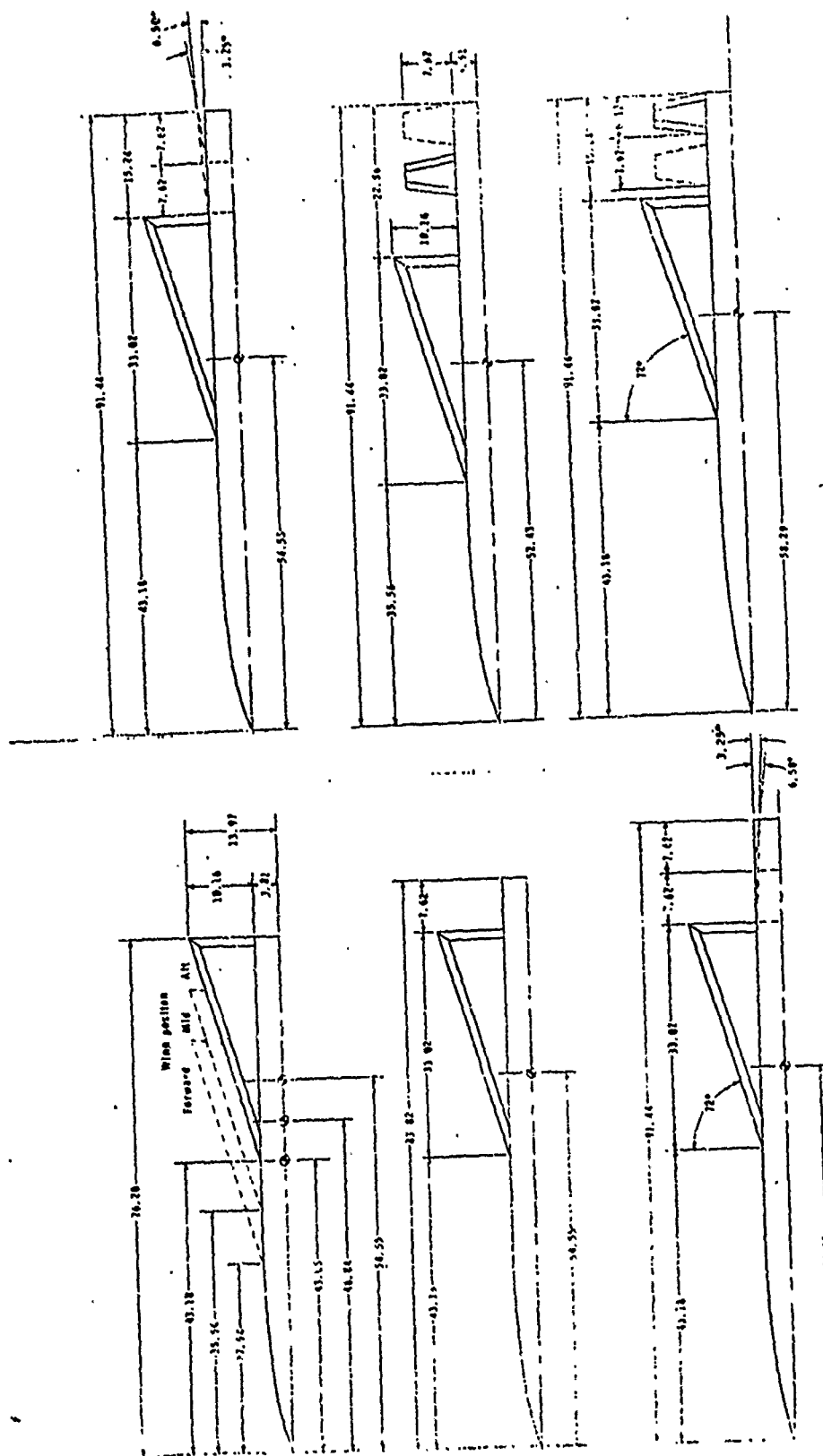


Figure 1.- Model details.

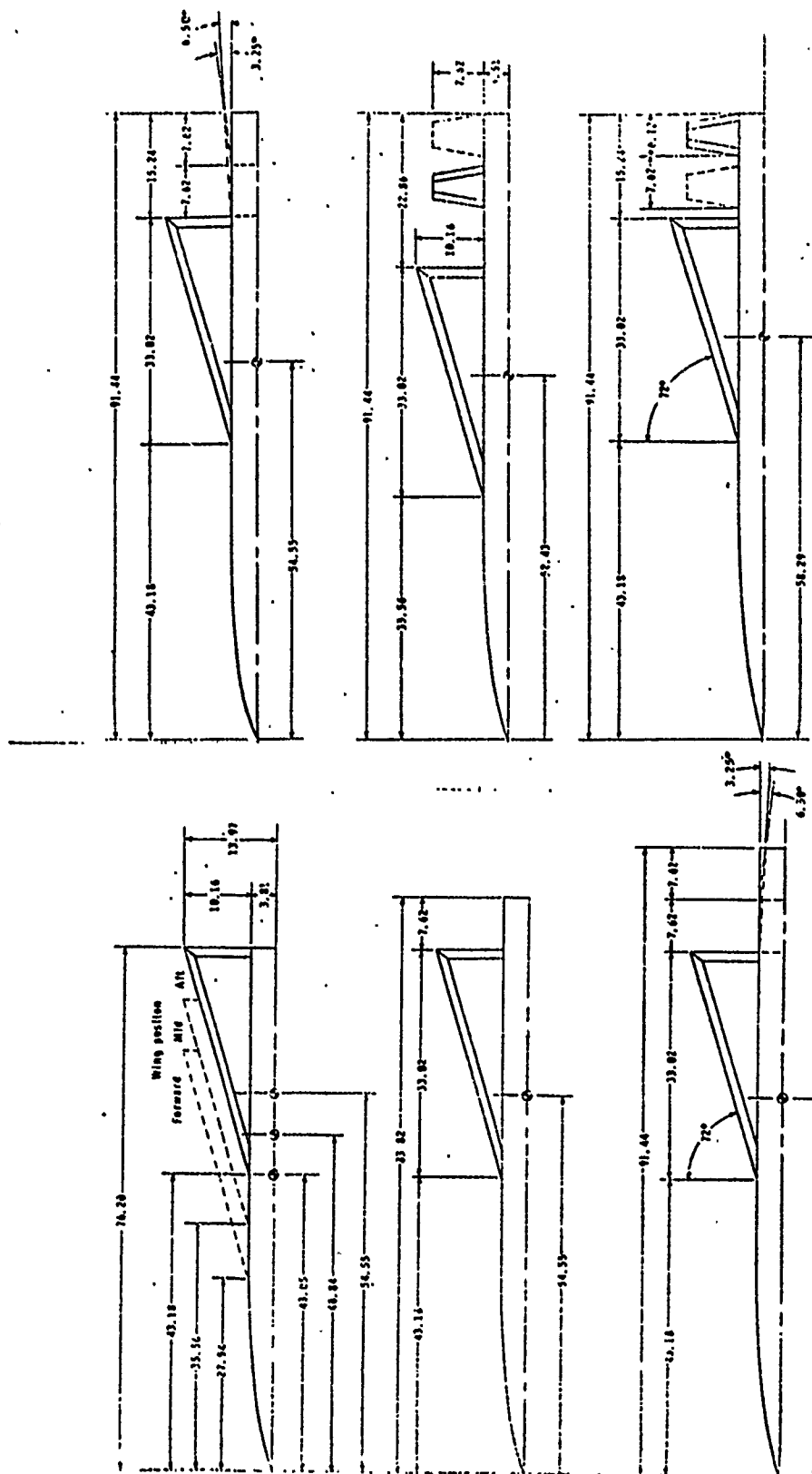


Figure 1.- Model details.

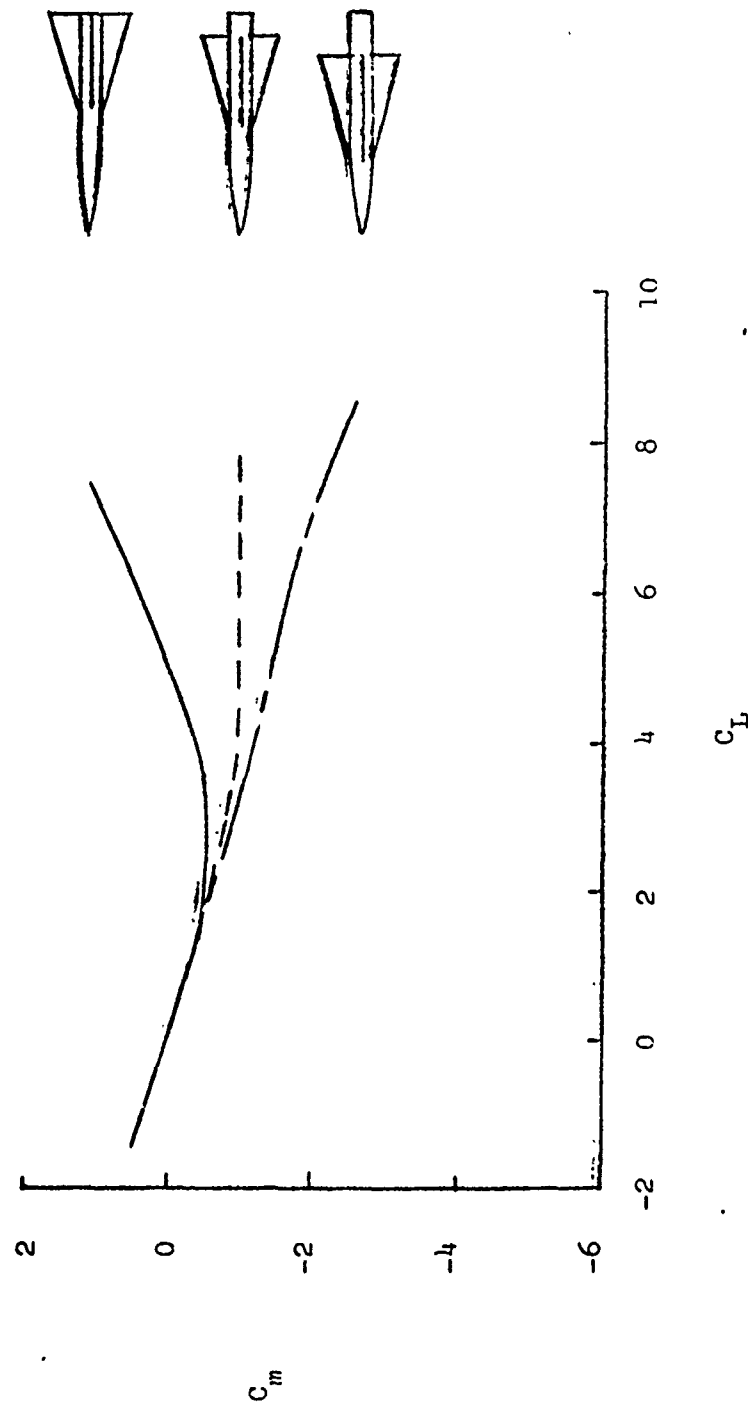
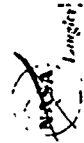


Figure 2.- Effect of wing position,  $M = 2.30$ ,  $\phi = 0^\circ$

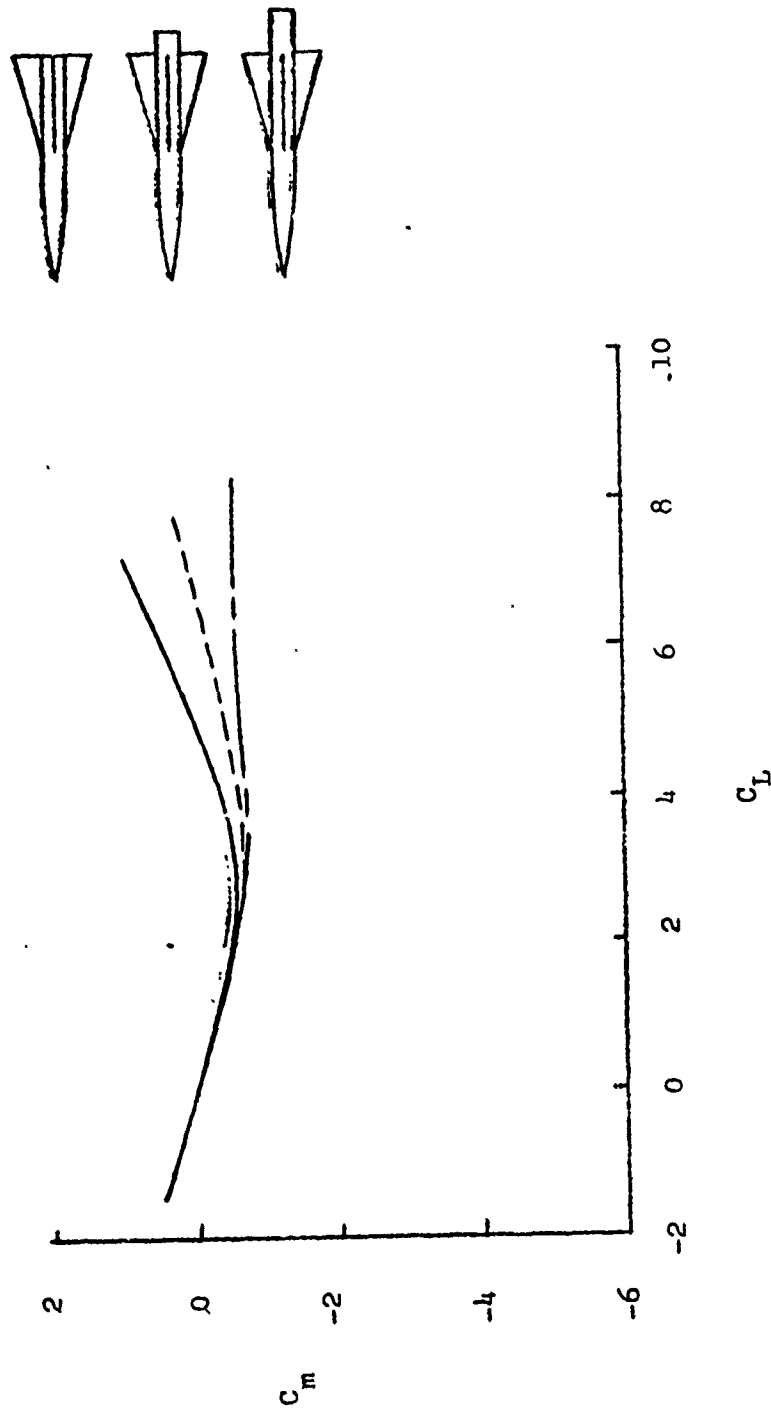


Figure 3.- Effect of cylindrical afterbody length,  $M = 2.30$ ,  $\phi = 0^\circ$ .

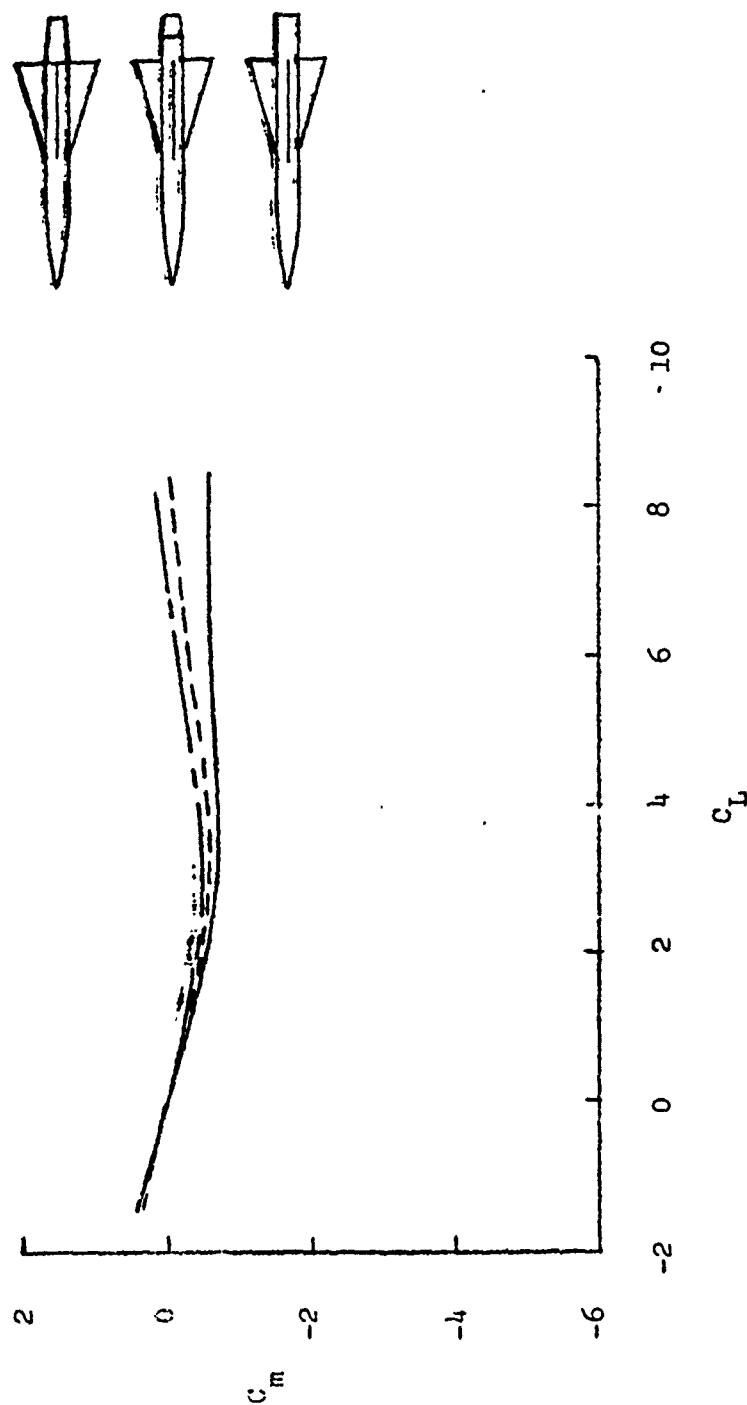


Figure 4.- Effect of afterbody boattail angle,  $M = 2.30$ ,  $\phi = 0^\circ$ .

*(Handwritten signature)*

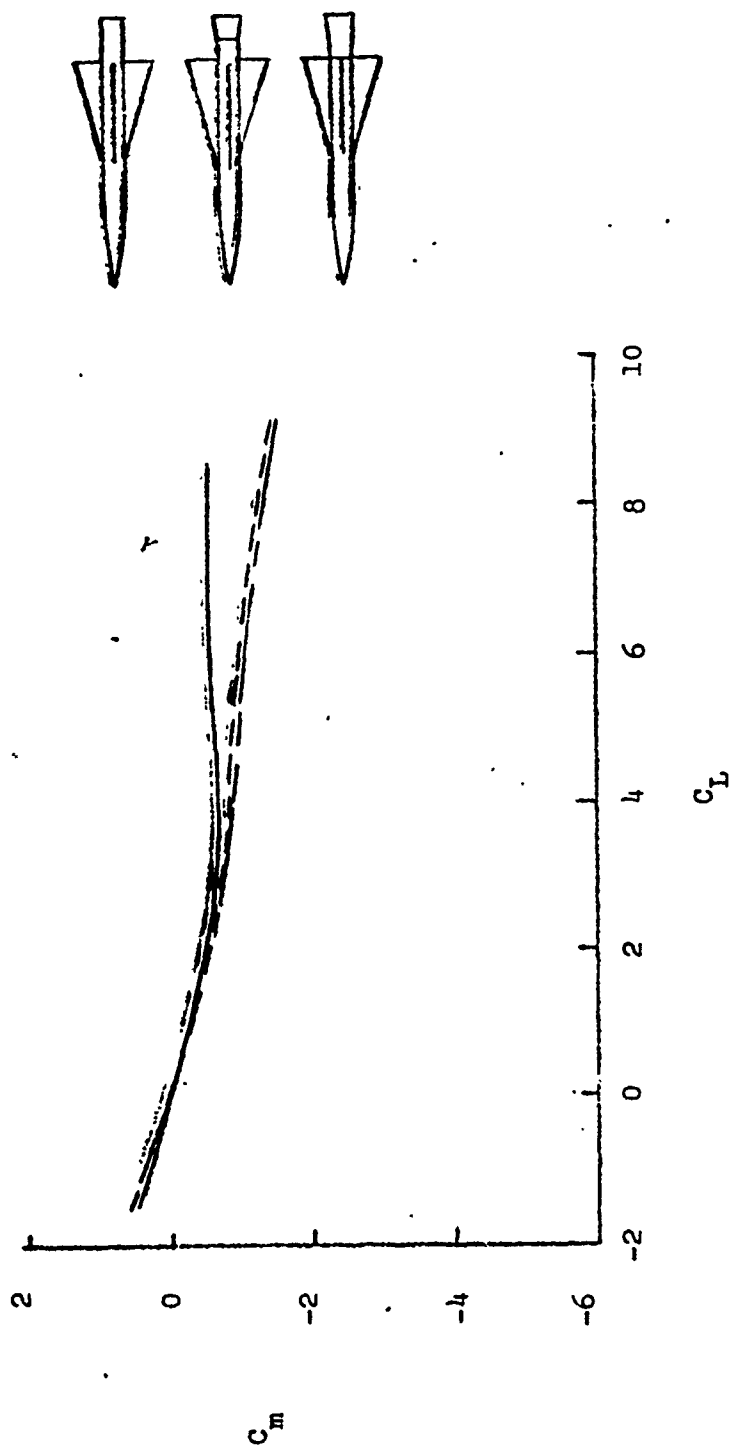


Figure 5:- Effect of afterbody flare angle,  $M = 2.30$ ,  $\theta = 0^\circ$ .



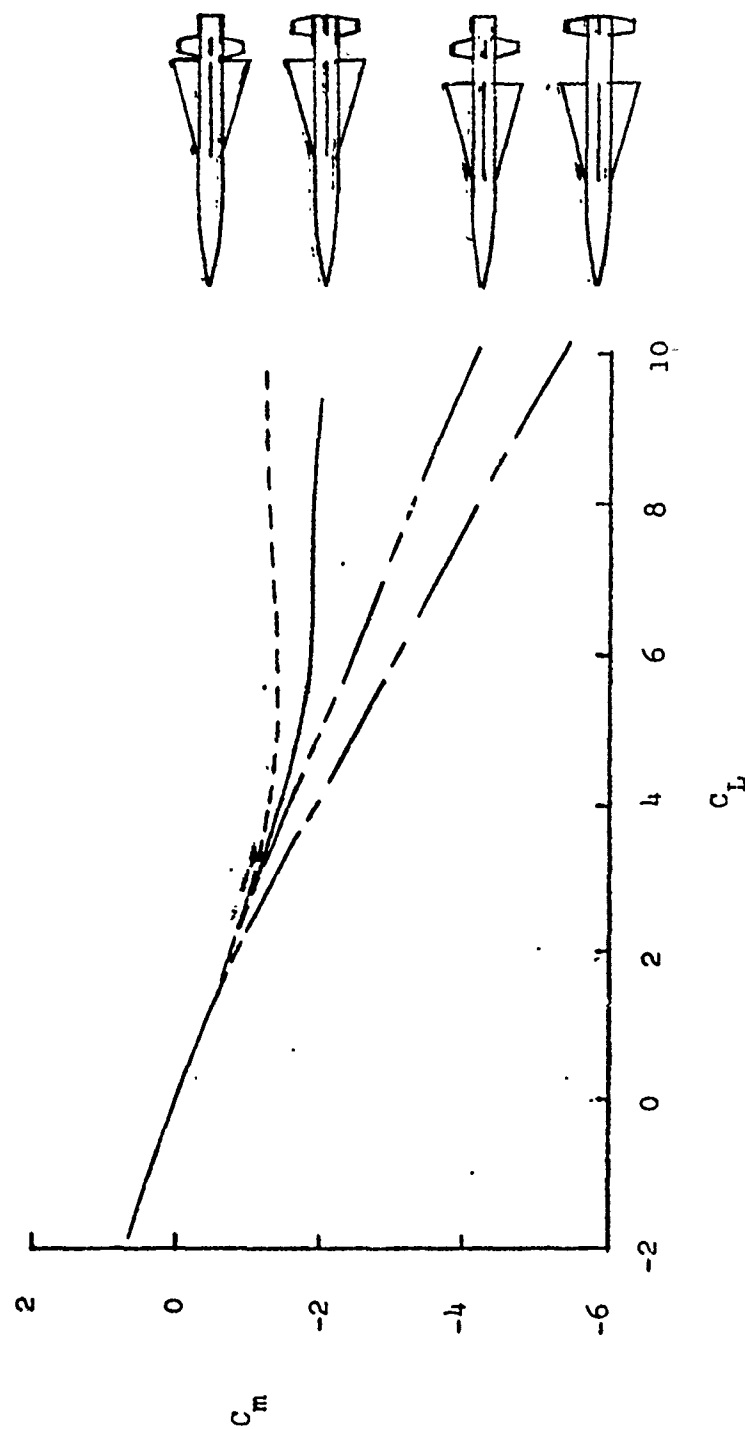


Figure 6.- Effect of wing and tail location,  $M = 2.30$ ,  $\phi = 0^\circ$ .

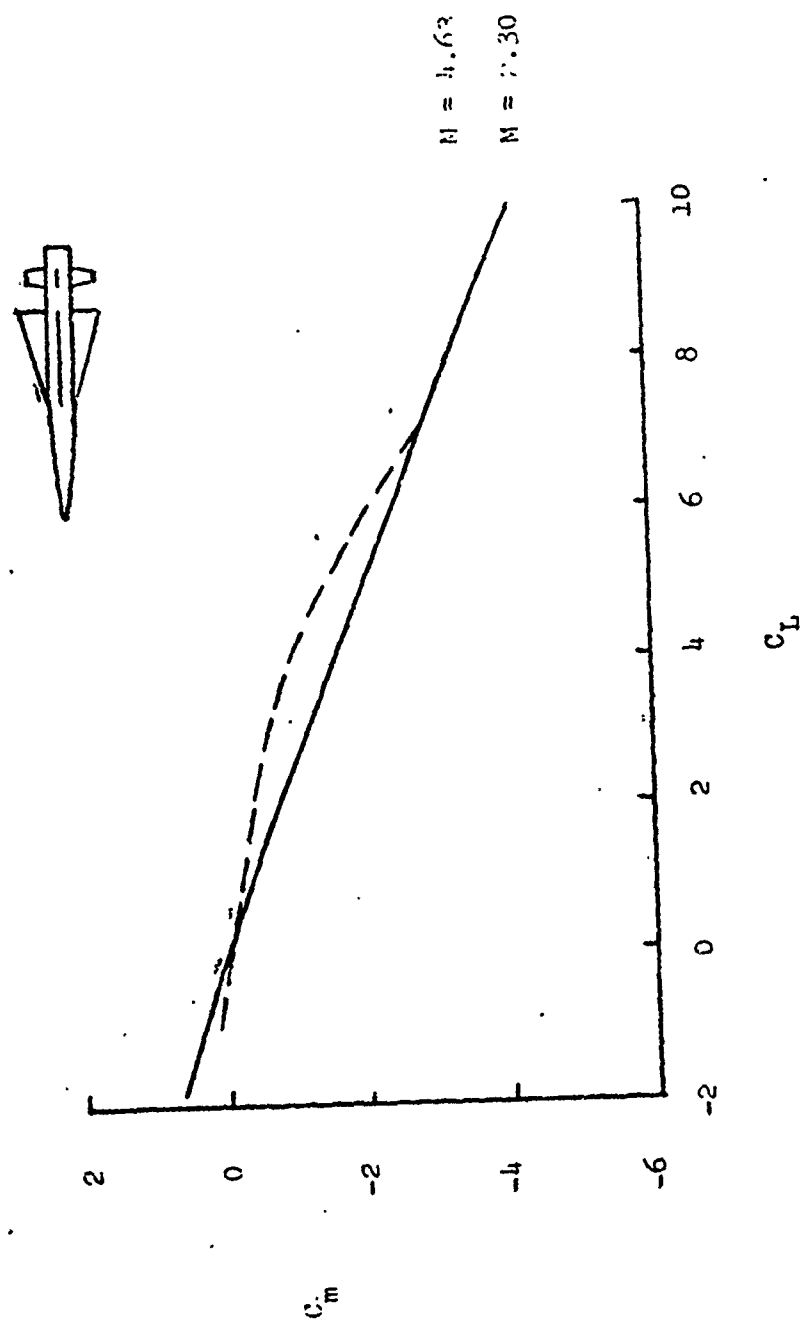
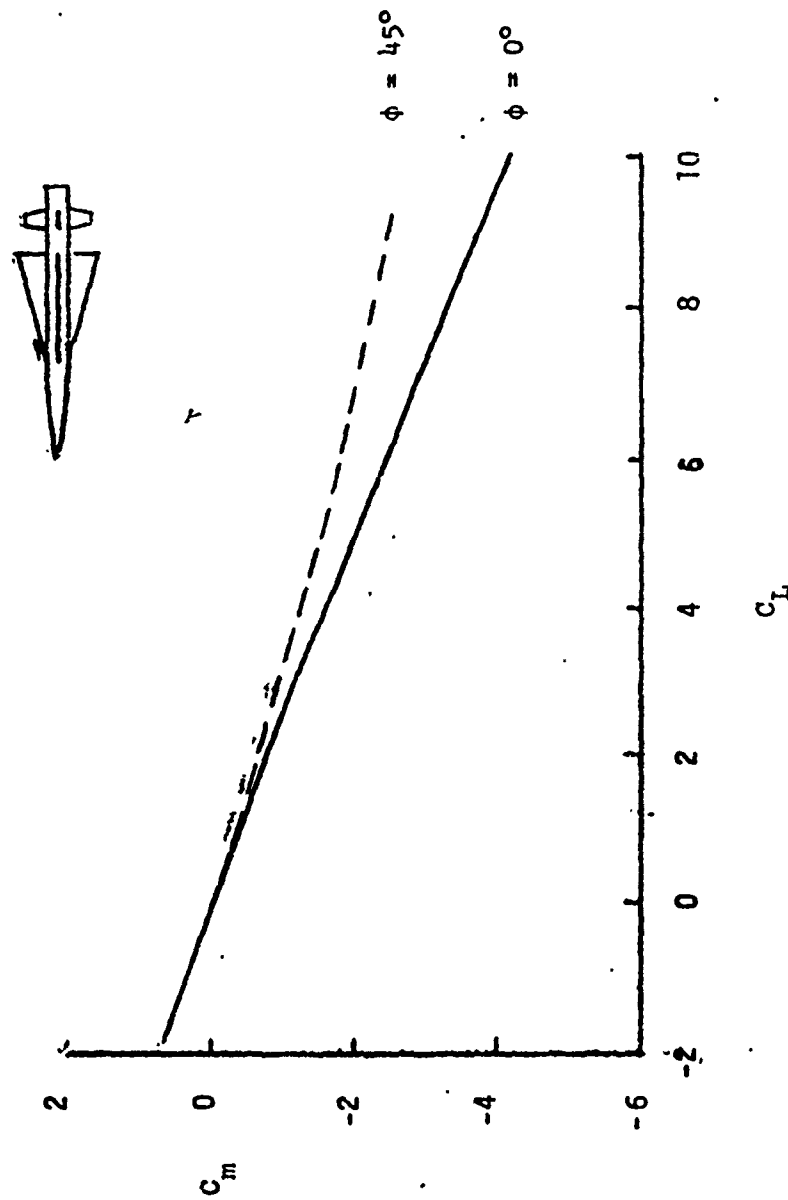


Figure 7.- Effect of Mach number,  $\phi = 0^\circ$ .

Figure 8.- Effect of model roll angle,  $M = 2.30$ .

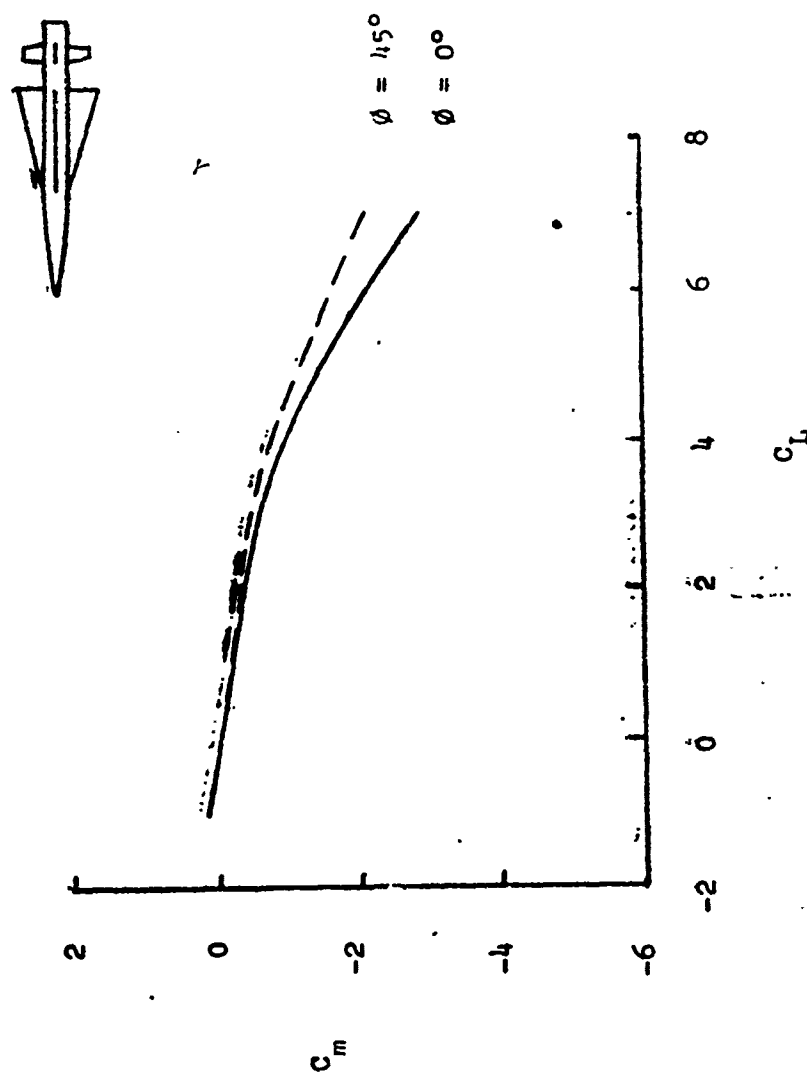


Figure 9.- Effect of model roll angle,  $M = 4.63$ .

STATIC AND DYNAMIC AERODYNAMICS OF  
PROJECTILES AND MISSILES\*

by

Frankie G. Moore†

Gil Y. Graff††

## ABSTRACT

Several theoretical and empirical procedures are combined to form a useful design tool for computing static and dynamic aerodynamics on missiles, projectiles, and rockets. The Mach number and angle-of-attack range over which the method is applicable are  $0 \leq M_{\infty} \leq 3$  and  $0 \leq \alpha \leq 15^\circ$ , respectively. Body and wing geometries can be quite general in that pointed or blunt nose bodies and sharp or blunt leading edge wings can be assumed. Computed results for several configurations compare well with experimental and other analytical results. The computer program is cost effective as it costs about five dollars per Mach number to compute the lift, drag, pitching moment, magnus moment and roll damping moment of a typical wing-body shape on the CDC 6700 computer. The pitch damping moment will be added to the calculation procedure in FY 76 so a reasonably accurate dynamic stability analysis can be made for most configurations without wind tunnel tests.

## I. INTRODUCTION

Quite often the aerodynamicist, when he works with or near a design group, is faced with the task of estimating such important design parameters as range, static margin, maneuverability, dynamic stability, time to half amplitude, etc., for a given configuration. Once the design engineer obtains the data he is seeking, the next

\*Research sponsored by Naval Sea Systems Command under SEATASK 35A-501/090-1/UR02-302-001. In addition, partial support for magnus wind tunnel testing was provided by Eglin Air Force Base (Mr. Ken Cobb and Mr. Sears) and AEDC.

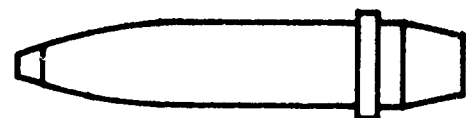
†Research Aerospace Engineer in Guided Projectile Division.

††Aerospace Engineer in Guided Projectile Division.

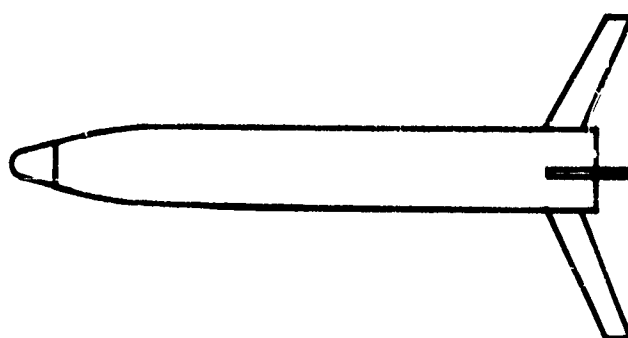
question the aerodynamicist must answer is "how can I improve the configuration so its aerodynamic properties are better"? Ultimately, an iteration cycle will probably be made in which several different configurations will be considered before the two or three most optimum candidates are chosen for further study. The important point to be made here is that for each of the above configurations, static aerodynamics (lift, drag, and pitching moment), and dynamic aerodynamics (roll damping, pitch damping, and magnus moment) must be estimated before questions concerning such things as range, maneuverability and flying qualities can be addressed.

To obtain the above set of aerodynamic coefficients, the engineer can go one of three directions: he can conduct wind tunnel tests which will be costly and time consuming and probably produce results which are more accurate than warranted for preliminary and intermediate design, he can perform hand calculations using handbook techniques<sup>(1)</sup> and applicable experimental data but not have a good accuracy estimate of the results, or he can develop a computer program based on analytical techniques which is efficient and produces accuracies on the order of  $\pm 10\%$  for most configurations. The latter alternative, although being more costly and time consuming initially, is the best approach for long term use and is the procedure which will be addressed in this paper.

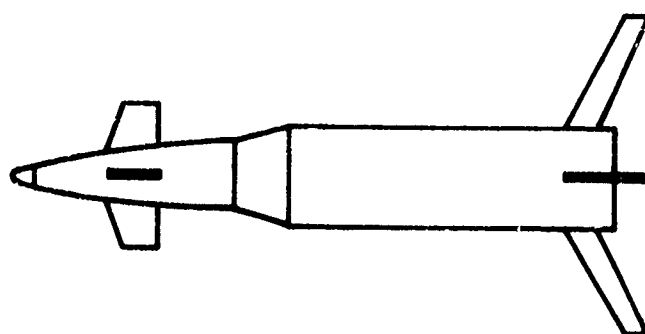
To be of practical use to the Navy, the theory must compute aerodynamics for the Mach number and angle of attack range of most projectiles and missiles, that is,  $0 \leq M_{\infty} \leq 3$  and  $0 \leq \alpha \leq 15^\circ$ , respectively. Also, quite general body and wing geometries must be considered. This arises from the fact that projectile noses may be pointed, truncated, or spherically blunt. Another contributing factor to the complex geometries is the high setback forces at launch which means the wings and canards must be quite thick to survive the initial high "g" loads. Moreover, there may be two cgives on the nose (in the case of a fuze or blunt seeker) and a boattail present for drag reduction purposes. Figure 1 illustrates the general type of projectile geometries that are encountered. By designing a computer program to handle such complex geometries means that most missile configurations can also be considered.



a. SPIN STABILIZED PROJECTILE



b. UNGUIDED FIN-STABILIZED PROJECTILE



c. GUIDED FIN-STABILIZED PROJECTILE

FIGURE 1. BASIC CONFIGURATIONS (ILLUSTRATION ONLY)

Several works existed previously which could fulfill portions of the present goal of a general aerodynamic prediction program, but none of which was satisfactory in its entirety. The most notable of these is that due to Woodward.<sup>(2)</sup> Woodward uses perturbation theory to compute the pressure distribution on wing-body combinations in subsonic and supersonic flow. However, the bodies must be pointed and the wing leading edge sharp. Also, he does not calculate the base and skin-friction drag or the nonlinear angle of attack effects. Moreover, no consideration is given to transonic flow or to the computation of the dynamic derivatives.

Another method available for calculating aerodynamics on wing-body configurations is that of Saffell, et al.<sup>(3)</sup> This procedure computes static aerodynamics on low aspect ratio missile configurations. Its applicability to general aspect ratio configurations is thus questionable, particularly at small  $\alpha$ . Furthermore, drag was calculated by handbook techniques<sup>(1)</sup> and is also quite inaccurate at small  $\alpha$ . Again, no attention was given to the dynamic derivatives.

The other method of practical use in projectile work is the all empirical GE "Spinner" program.<sup>(4)</sup> This program computes all six aerodynamic coefficients so a dynamic stability analysis can be conducted on a spin-stabilized projectile without going to the wind tunnel. Its shortcomings are its lack of attention to guided weapons and limited use in body alone design due to its empirical nature. That is, effects of nose bluntness, ogive shape, boattail shape, or other discontinuities in slope cannot be estimated in detail. On the other hand, it does give total force predictions which are reasonably accurate on spin stabilized rounds which are similar in shape to the empirical data base.

To summarize the above state-of-the-art in aerodynamic prediction, it is fair to say there are several analytical or empirical methods available to compute a particular force or moment in a given Mach number regime. However, these methods have not been combined together to form a useful design tool, allowing one to not only estimate aerodynamics accurately, but to conduct static and dynamic stability analysis or trajectory simulations on a given configuration over the Mach number range zero to three and angle of attack range zero to twenty degrees. It is the purpose of the present work to provide such a tool.



## II. ANALYSIS

### A. Static Aerodynamics

The static aerodynamics have been computed previously and the reader is referred to References 5 through 9 for the details of that portion of the present work. Only a synopsis of that work will be included here for continuity purposes.

#### 1. Body Alone Aerodynamics

A summary of the various methods for computing body alone aerodynamics appears in Figure 2. All the methods are standard in the literature (References 10 through 15) with the exception of the empirical schemes derived for transonic lift and wave drag and the combined Newtonian-perturbation theory for calculating nose wave drag in supersonic flow. The combined Newtonian-perturbation theory was developed so reasonable results for static aerodynamics could be obtained at low supersonic Mach numbers for blunt nosed configurations. Comparisons with experimental data indicate this method accurately predicts pressure coefficients and total force coefficients down to supersonic Mach numbers of 1.2.

#### 2. Wing and Interference Aerodynamics

The methods used to compute the wing alone and interference aerodynamics are listed in Figure 3. Again the methods are standard in the literature (References 16 through 22) except for the empirical techniques used for wing-body interference, trailing edge separation drag, and body base pressure drag caused by tailfins and except for the theoretical computation of wing wave drag in supersonic flow. For the details of these techniques, the reader is again referred to either References 7 or 9.

### B. Roll Damping Moment

The body alone roll damping moment is estimated using the same procedure as the "Spinner" program.<sup>(4)</sup> That is, if one knows  $C_{q_p}$  as a function of Mach number for a given configuration, then

COMPONENT \ MACH NUMBER REGION	SUBSONIC	TRANSONIC	SUPERSONIC
NOSE WAVE DRAG	—	Wu and AOYOMA PLUS EMPIRICAL	2 <sup>nd</sup> ORDER VAN DYKE PLUS MODIFIED NEWTONIAN
BOATTAIL WAVE DRAG	—	Wu and AOYOMA	2 <sup>nd</sup> ORDER VAN DYKE
SKIN FRICTION DRAG	VAN DRIEST II		
BASE DRAG	EMPIRICAL		
INVISCID LIFT and PITCHING MOMENT	EMPIRICAL	Wu and AOYOMA PLUS EMPIRICAL	TSIEN 1 <sup>st</sup> ORDER CROSSFLOW
VISCOUS LIFT and PITCHING MOMENT	ALLEN and PERKINS CROSSFLOW		

FIGURE 2 METHODS USED TO COMPUTE BODY ALONE AERODYNAMICS

COMPONENT \ MACH NUMBER REGION	SUBSONIC	TRANSONIC	SUPERSONIC
INVISCID LIFT AND PITCHING MOMENT	LIFTING SURFACE THEORY	EMPIRICAL	LINEAR THEORY
WING-BODY INTERFERENCE	SLENDER BODY THEORY AND EMPIRICAL		LINEAR THEORY, SLENDER BODY THEORY & EMPIRICAL
WING-TAIL INTERFERENCE	LINE VORTEX THEORY		
WAVE DRAG	—	EMPIRICAL	LINEAR THEORY + MODIFIED NEWTONIAN
SKIN FRICTION DRAG	VAN DRIEST		
TRAILING EDGE SEPARATION DRAG	EMPIRICAL		
BODY BASE PRESSURE DRAG CAUSED BY TAIL FINS	EMPIRICAL		

**FIGURE 3 METHODS USED TO COMPUTE STATIC WING ALONE AND INTERFERENCE AERODYNAMICS**

$$C_{\ell_P} = (C_{\ell_P})_1 \frac{\ell}{\ell_1}$$

where the subscript represents known data. This estimate should prove reasonable so long as the data available is for a configuration of similar dimensions to the configuration for which data is required.

For a wing-body configuration, the wing completely dominates the roll damping moment so it is of primary concern to have a good estimate of the wing alone roll damping.

For supersonic and subsonic flow calculations, the wing is assumed to be thin so that small perturbation theory can be employed for flow-field calculations. In addition, the wing is assumed to have zero chamber with aeroelastic effects being small. In transonic flow, empirical methods are used for roll damping calculations. Body interference and wing interference effects are then estimated using slender body theory.

The individual methods used for calculating the wing roll damping moment coefficient derivatives in subsonic, supersonic, and transonic flow, along with the interference effects, are discussed below.

1. Subsonic Flow ( $M_\infty < M_{crit}$ )

The small perturbation equation for three-dimensional steady flow is:<sup>(16)</sup>

$$\beta^2 \phi_{x_0 x_0} - \phi_{y_0 y_0} - \phi_{z_0 z_0} = 0 \quad (1)$$

where the subscripts  $x_0$ ,  $y_0$ ,  $z_0$  indicate partial differentiation and where the velocity potential,  $\phi$ , is related to the perturbation velocities by

$$\phi_{x_0} = u, \quad \phi_{y_0} = v, \quad \phi_{z_0} = w. \quad (2)$$

The boundary conditions are that the flow is undisturbed at an infinite distance from the surface, is tangential to the surface, and is continuous at the wing trailing edge. Mathematically, these boundary conditions can be treated in respective order by:

$$u = v = w = 0 \quad \text{as} \quad \sqrt{x_c^2 + y_c^2 + z_c^2} \rightarrow \infty \quad (3a)$$

$$\vec{V}_m \cdot \nabla F = 0 \quad (3b)$$

$$\begin{aligned} u_u[(x_0)_{TE}, y_0, z_0] &= u_l[(x_0)_{TE}, y_0, z_0] \\ v_u[(x_0)_{TE}, y_0, z_0] &= v_l[(x_0)_{TE}, y_0, z_0] \\ w_u[(x_0)_{TE}, y_0, z_0] &= w_l[(x_0)_{TE}, y_0, z_0] \end{aligned} \quad (3c)$$

The boundary condition (3c) is simply a definition of the Kutta condition which requires the velocity at the trailing edge to be continuous from the upper to lower surfaces. If the equation of the surface is defined as  $z_0 = F(x_0, y_0)$ , then (3b) implies

$$\frac{w(x_0, y_0)}{V_\infty} = \phi_{z_0} = \frac{\partial F(x_0, y_0)}{\partial x_0} = \alpha(x_0, y_0) \quad (4)$$

The angle of attack,  $\alpha(x_0, y_0)$  can be expressed as

$$\alpha(x_0, y_0) = \alpha_0 + py_0/V_\infty + q(x_0 - x_{ref})/V_\infty \quad (5)$$

where  $\alpha_0$  is the angle of attack of the wing planform,  $py/V_\infty$  is the induced angle of attack due to a steady roll rate,  $p$ , and  $q(x - x_{ref})/V_\infty$  is the induced angle of attack due to a constant pitch rate,  $q_0$ .

Equation (1) is a linear partial differential equation so that superposition of solutions is valid. Therefore, for roll damping calculations, one can set  $\alpha_0 = q = 0$  in Equation (5) so the boundary condition of interest is

$$\phi_{z_0} = py_0/V_\infty \quad (6)$$

Equation (1) can be simplified somewhat by using Gothert's extension to the Prandtl Glauert transformation. This transformation is equivalent to

$$\left. \begin{aligned} x &= x_0/\beta \\ y &= y_0 \\ z &= z_0 \\ \phi(x, y, z) &= \phi(x_0, y_0, z_0) \end{aligned} \right\} \quad (7)$$

where  $\beta = \sqrt{1 - M_\infty^2}$ . Equation (1) then simplifies to

$$\phi_{xx} + \phi_{yy} + \phi_{zz} = 0 \quad (8)$$

Thus, the compressible flow on a wing of given geometry can be solved for by affinely relating the wing to another wing with the properties of Equation (7), and solving for the flow field on the new wing at  $M_\infty = 0$ . Once this is done, the pressure coefficient at any point on the wing is:<sup>(16)</sup>

$$C_p(x_0, y_0, z_0) = -2\phi_x/\beta \quad (9)$$

The solution to Equation (8) can be shown to be:<sup>(17)</sup>

$$\phi(x, y, z) = -\frac{1}{8\pi} \iint_S \frac{\Delta C_p(x_1, y_1)}{(y - y_1)^2 + z^2} z \left[ 1 + \frac{x - x_1}{\sqrt{(x - x_1)^2 + (y - y_1)^2 + z^2}} \right] dx_1 dy_1 \quad (10)$$

where  $\Delta C_p = C_{p_l} - C_{p_u}$ . It is required to determine the pressure loading  $\Delta C_p$  over the entire surface. Following Chadwick,<sup>(17)</sup> Equation (10) is first differentiated with respect to  $z$  and the limit as  $z \rightarrow 0$  taken. The result is then equated to the boundary condition, Equation (6), to obtain:

$$\frac{py}{V_\infty} = \frac{1}{8\pi} \oint \frac{\Delta C_p(x_1, y_1)}{(y - y_1)^2} \left[ 1 + \frac{x - x_1}{\sqrt{(x - x_1)^2 + (y - y_1)^2}} \right] dx_1 dy_1 \quad (11)$$

The cross on the  $y_1$  indicates a singularity at  $y = y_1$ , in which case Manglers principal-value technique<sup>(16)</sup> can be applied. The details of the solution of the integral Equation (10) for  $\Delta C_p(x, y)$  will not be repeated here as they are given in detail in many references (see for example, Reference 17). Worthy of note, however, is the fact that Equation (11) is an integral equation for which the wing loading

$\Delta C_p$  is to be found as a linear function of the induced angle of attack,  $py/V_\infty$ .

Once the span loading  $\Delta C_p(x,y)$ , due to roll, is known over the entire wing, the local rolling moment coefficient at a given spanwise airfoil section,  $y$ , is

$$c_l = \frac{y}{c\ell_{ref}} \int_{x_{LE}}^{x_{TE}} (\Delta C_p)_P dx \quad (12)$$

where the subscript P indicates the loading due to a roll velocity  $p$ . The total rolling moment on the entire wing is then

$$C_l = \frac{2}{S_{ref}} \int_0^{b/2} c_{l_P} dy \quad (13)$$

Assuming the rolling moment is a linear function of roll rate, the roll damping moment coefficient derivative is

$$C_{l_P} = \frac{C_l}{p \ell_{ref}/V_\infty} \quad (14)$$

## 2. Supersonic Flow ( $M_\infty \geq 1.2$ )

For supersonic flow past thin wings, Equation (1) is still applicable along with the associated boundary condition (3b). Since the flow is supersonic, disturbances in the flow-field are not felt upstream of the point of disturbance. Thus, the boundary condition (3a) can be modified to,



$$u(0^-, y, z) = v(0^-, y, z) = w(0^-, y, z) = 0 \quad (15)$$

where it is assumed the disturbance occurs at  $x = 0$ . It will be assumed the wing trailing edge is supersonic (Mach number normal to wing trailing edge is greater than one) so that the Kutta condition need not be applied. The solution to Equation (1) is:<sup>(18)</sup>

$$\phi(x_0, y_0) = -\frac{1}{\pi} \iint_{S_1} \frac{\alpha(x_0, y_0)}{\sqrt{(x_0 - x_1)^2 - \beta^2(y_0 - y_1)^2}} dx_1 dy_1 \quad (16)$$

where  $S_1$  is the wing planform. The lifting pressure coefficient, due to a constant roll rate  $p$ , is then related to the velocity potential  $\phi$  through the relation

$$(\Delta C_p)_p = -\frac{4\phi_{x_0}}{V_\infty} \quad (17)$$

The limits of integration of Equation (16) are dependent on whether the leading edge is subsonic or supersonic. Each of these cases will be considered separately below.

#### a. Supersonic Leading Edge

By supersonic leading edge, one means the Mach number normal to the leading edge is greater than one. Referring to Figure 4, this implies the Mach line emanating from the root chord, OA, lies behind the wing leading edge. If the Mach line intersects the wing tip, as shown in Figure 4, there are five distinct disturbance regions present and hence, five different perturbation solutions. If the

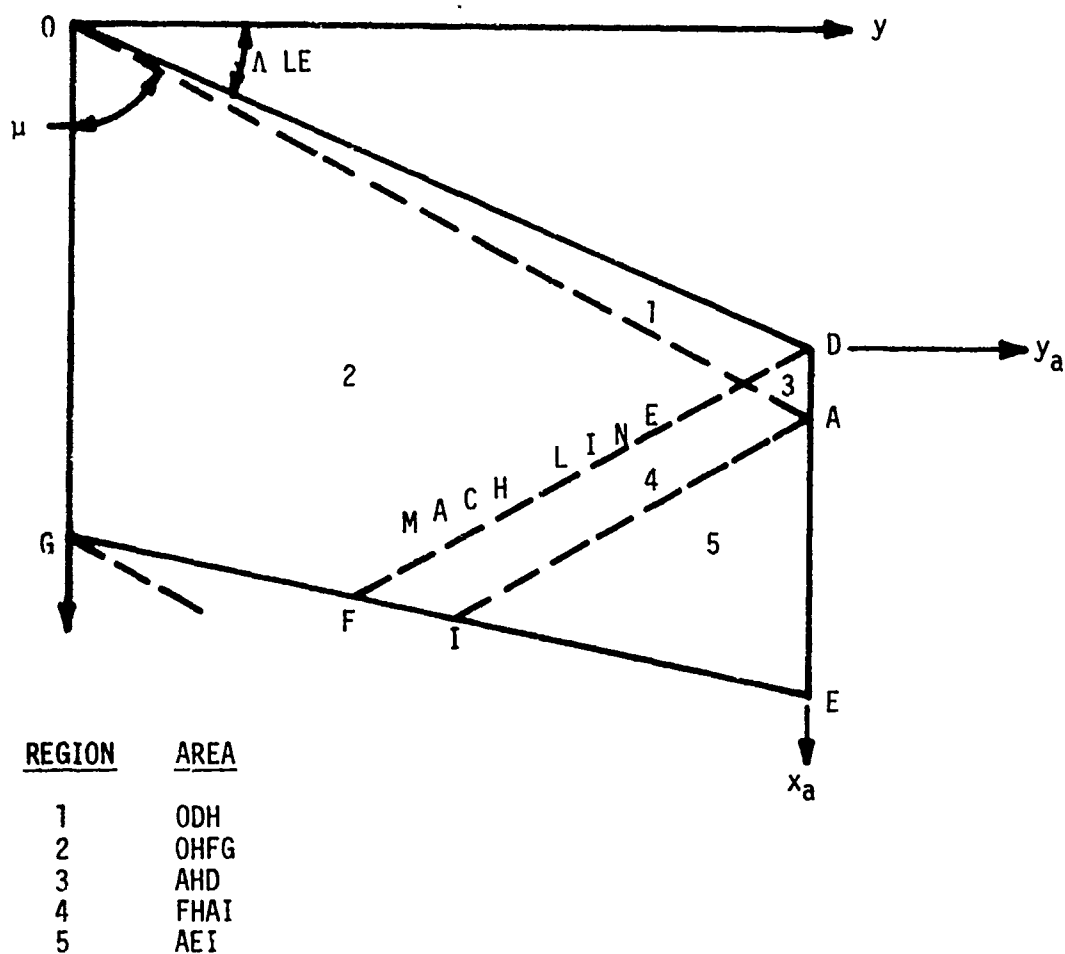


FIGURE 4  
FLAT PLATE WING PLANFORM WITH SUPERSONIC  
LEADING AND TRAILING EDGES; MACH LINE  
INTERSECTS WING TIP

Mach line intersects the wing trailing edge, the disturbance created by the Mach line OA impinging on the wing tip is eliminated so that only four perturbation solutions are needed.

The generalized formulas for the lifting pressure distributions on a wing in steady roll are derived in Reference 21. For convenience, the final equations are repeated here. For region 1, the flow is two-dimensional and the resulting lifting pressure is

$$(\Delta C_p)_p = [(\Delta C_p)_p]_1 = \frac{4pm^2 x_0 (m^2 \sigma - 1)}{\beta^2 V_\infty (m^2 - 1)^{3/2}} \quad (18)$$

In region 2, the total lifting pressure is:

$$(\Delta C_p)_p = [(\Delta C_p)_p]_2 = \frac{4pm^2 x_0}{\pi \beta^2 V_\infty (m^2 - 1)^{3/2}} \left\{ (1 + m^2 \sigma) \cos^{-1} \left[ \frac{1 + m^2 \sigma}{m(1 + \sigma)} \right] \right. \\ \left. - (1 - m^2 \sigma) \cos^{-1} \left[ \frac{1 - m^2 \sigma}{m(1 - \sigma)} \right] \right\} \quad (19)$$

The induced pressure caused by the tip Mach line DF is:

$$[(\Delta C_p)_p]_3 = \frac{4pm}{\pi V_\infty \beta (m^2 - 1)^{3/2}} \left\{ \left[ \frac{mx_a}{\beta} - m^2 y_a - \frac{b}{2}(m^2 - 1) \right] \cos^{-1} \left[ \frac{\frac{mx_1}{\beta} + y_a(2m + 1)}{y_a - \frac{mx_a}{\beta}} \right] \right. \\ \left. - 2m \sqrt{-\frac{my_a}{\beta} (x_a + \beta y_a)(m + 1)} \right\} \quad (20)$$

The total lifting pressure in region 3 is then:

$$(\Delta C_p)_p = [(\Delta C_p)_p]_1 + [(\Delta C_p)_p]_3 \quad (21)$$

The lifting pressure in region 4 is a combination of that in Regions 2 and 3. Thus, in Region 4:

$$(\Delta C_p)_p = [(\Delta C_p)_p]_2 + [(\Delta C_p)_p]_3 \quad (22)$$

Again, if the Mach line OA intersects the wing trailing edge, Equations 18 through 22 allow one to determine the complete lifting pressure distribution over the wing surface. If the Mach line OA intersects the wing tip, another perturbation is induced in the flow field. The total pressure differential in region 5 is then:

$$(\Delta C_p)_p = \frac{4\pi m}{\pi\beta V_\infty (m^2 - 1)^{3/2}} \left\{ \left[ \frac{mx_a}{\beta} + m^2 y_a + \frac{b}{2}(m+1) \right] \cos^{-1} \left( \frac{mx_a/\beta - y_a(1-2m) + b}{mx_a/\beta + y_a + b} \right) - 2m \sqrt{-y_a(m-1)(mx_a/\beta + my_a + b)} \right\} \quad (23)$$

#### b. Subsonic Leading Edge

If the Mach number normal to the leading edge is less than one (and the trailing edge Mach number is greater than one), there are only two flow regions to consider. However, the solution is complicated somewhat by the leading edge singularity where the velocity goes like  $1/x$ .<sup>(22)</sup> Referring to Figure 5, the pressure differential of upper and lower surfaces in Region 1 is:<sup>(22)</sup>

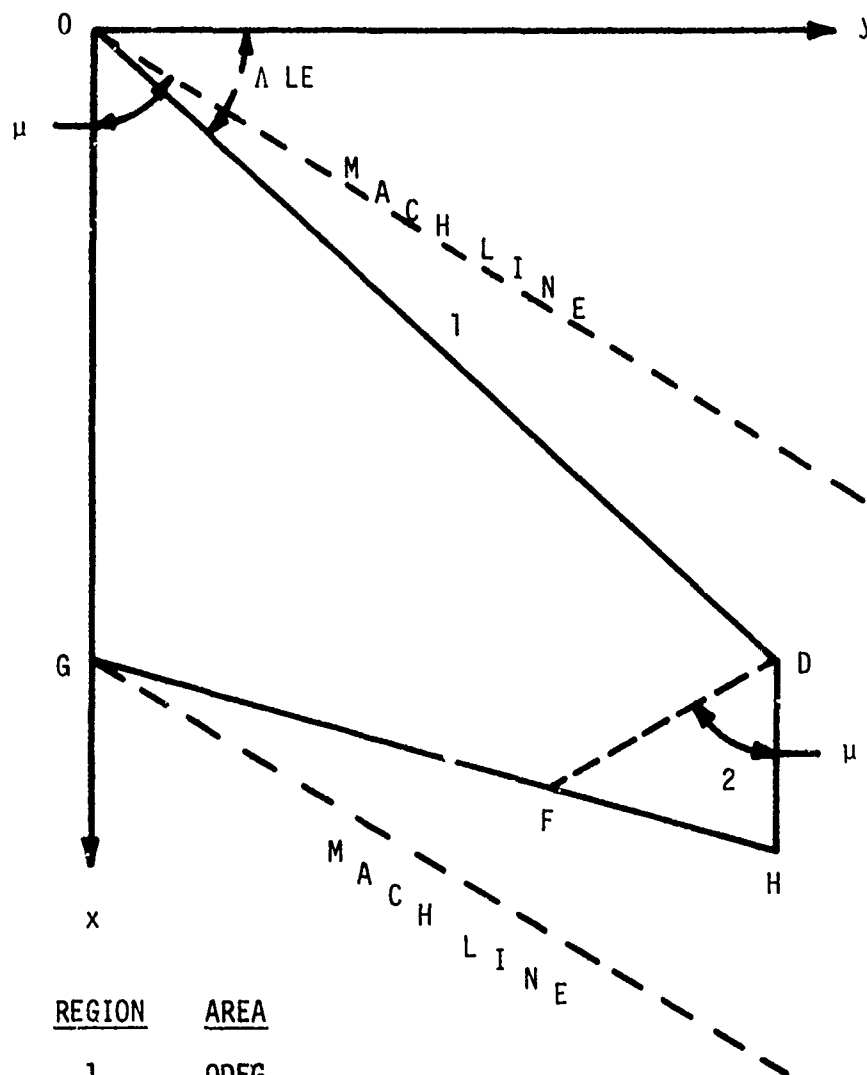


FIGURE 5

FLAT PLATE WING PLANFORM WITH SUBSONIC  
LEADING EDGE AND SUPERSONIC TRAILING EDGE

$$(\Delta C_p)_p = \frac{2l(m)pm^2 x_0 \sigma}{\beta^2 V_\infty \sqrt{1 - \sigma^2}} \quad (24)$$

where

$$I(m) = \frac{2(1 - m^2)}{(2 - m^2)E(m) - m^2 F(m)}$$

$$E(m) = \int_0^{\pi/2} \sqrt{1 - k^2 \sin^2 \theta} d\theta$$

$$F(m) = \int_0^{\pi/2} \frac{d\theta}{\sqrt{1 - k^2 \sin^2 \theta}}$$

$$k = \sqrt{1 - m^2}$$

Values of the complete elliptic integrals of the first and second kind ( $F(m)$  and  $E(m)$ , respectively) have been tabulated and appear in standard mathematical handbooks.

Region 2, which is affected by the wing tip Mach cone, has a lifting pressure differential given by:

$$(\Delta C_p)_p = \frac{-8pm}{\pi\beta V_\infty} \sqrt{b/2 - y} \left[ \frac{3mx_0/\beta + y(1 - 2m) - b/2(1 + m)}{3(1+m)\sqrt{(1+m)(mx_0/\beta + y_0)}} \right] \quad (25)$$

For a flow with a subsonic leading edge and supersonic trailing edge, Equations (24) and (25) determine the complete pressure distribution due to a steady roll,  $p$ .

The local roll moment, total rolling moment, and roll damping moment for both the subsonic and supersonic leading edge cases can then be determined by Equations (12), (13) and (14), respectively.

### 3. Transonic Flow ( $M_{fb} \leq M_\infty < 1.2$ )

There are currently no simple, accurate analytical methods available for calculating transonic roll damping. With the increased emphasis on transonic aerodynamics in the last few years, it is envisioned a simple theoretical method will become available within a reasonable time frame. Until that time, one must resort to the full Navier Stokes equations of motion or empirical techniques. Since the former approach is beyond the scope of this work, the empirical approach will be followed.

Without a theoretical model to calculate transonic roll damping, it has been current practice by some engineers<sup>(23)</sup> to estimate roll damping in direct proportion to the lift. That is

$$(C_{\ell_p})_M = (C_{\ell_p})_{M=M_{fb}} \frac{(C_{N_\alpha})_M}{(C_{N_\alpha})_{M=M_{fb}}} \quad (26)$$

This means that if the roll damping is known at say  $M_\infty = 0.85$  and  $C_{N_\alpha}$  is known throughout the transonic speed regime, then the roll damping can be estimated according to Equation (26). This is the procedure used in the present analysis for calculating roll damping.

One of the main problems inherent in calculating transonic aerodynamics is a need to account for thickness, and in some cases, aeroelastic effects. An empirical technique proposed by Edmondson<sup>(24)</sup> to correct for thickness and aeroelastic effects on rectangular wings is

$$C_{\ell_p} = (C_{\ell_p})_{theory} (1 - t/c)^{2R/3} \quad (27)$$

where  $t/c$  is the overall thickness to chord ratio of the wing planform. However, the present values of  $(C_{L_p})_{\text{theory}}$  in transonic flow are calculated based on the lift curve slope which has already accounted for thickness. In addition, intuitively, one would expect a Mach number effect to be present in Equation (27), since thickness is most important in transonic flow. For these two reasons, Equation (27) was not applied in the present analysis.

#### 4. Interference Effects

There are two types of interference effects which need to be examined in the process of predicting roll damping. These are the body-fin and fin-fin interference effects. The first arises due to the presence of the body and the latter as a result of fin shed vortices.

Using slender body theory, the effect of the body has been calculated by Adams and Dugan<sup>(25)</sup> for both planar and cruciform wing-body combinations. The results of their calculations are presented in Figure 6 as a function of the parameter

$$\xi = r_b / (r_b + b/2)$$

It is seen that there is little difference between the planar and cruciform wing configuration and furthermore, that the body has little effect on the roll damping for values of  $\xi$  up to 0.4. Although these results are analytical, they have been verified qualitatively by the experimental results presented in Reference 26.

The effect of the number of fins on roll damping has also been determined using slender body theory.<sup>(27)</sup> The results are presented in Figure 7 as a function of the number of fins,  $n$ , where the basis for comparison is  $C_{L_p}$  of a planar wing configuration. It is seen that the addition of fins to a missile adds to the damping in roll at a decreasing rate, as expected.



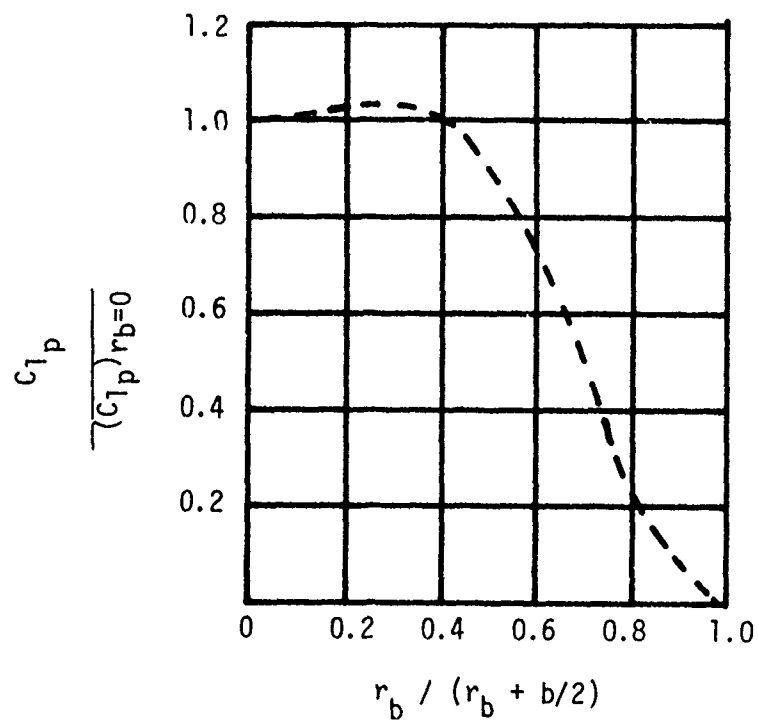


FIGURE 6

Effect of body radius on damping in roll for fixed span.

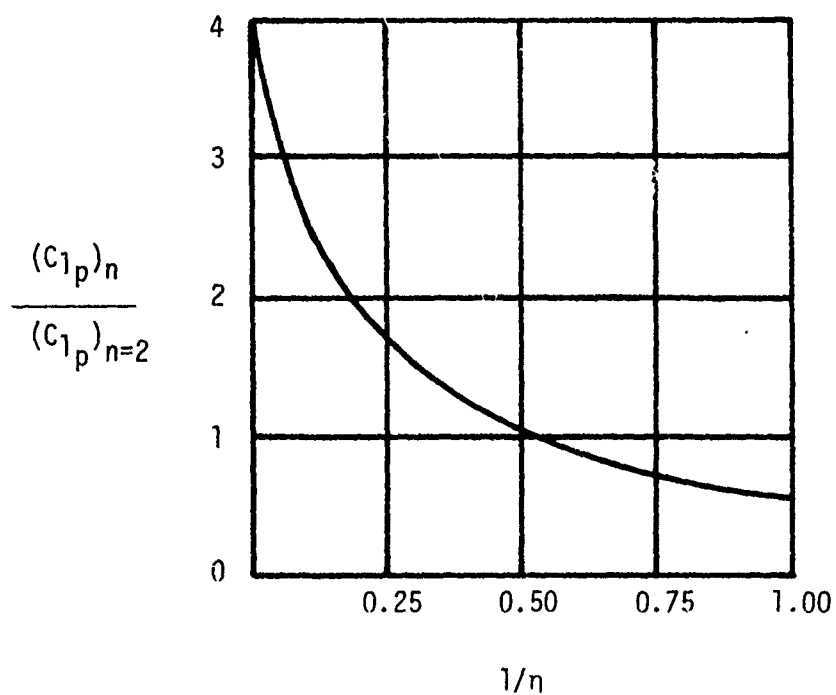


FIGURE 7

EFFECT OF NUMBER OF FINS ON DAMPING IN ROLL

### C. Magnus Force and Moments

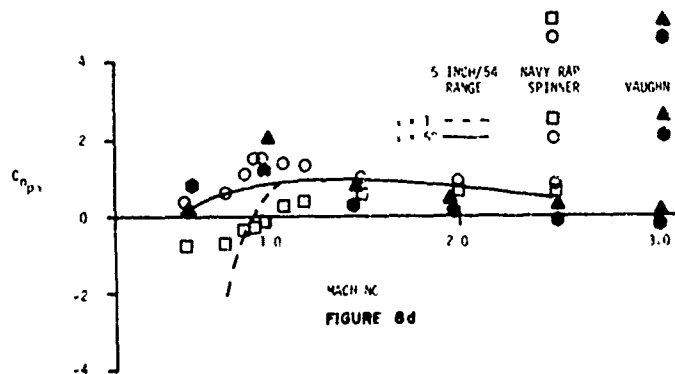
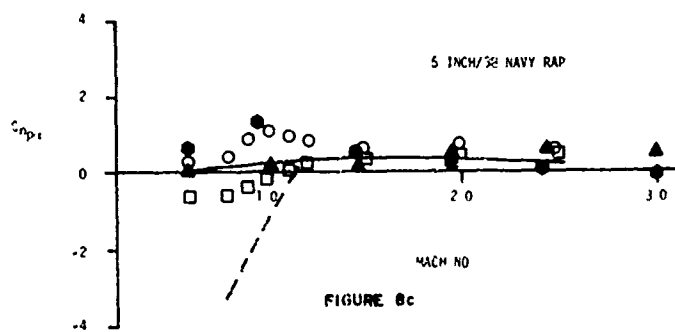
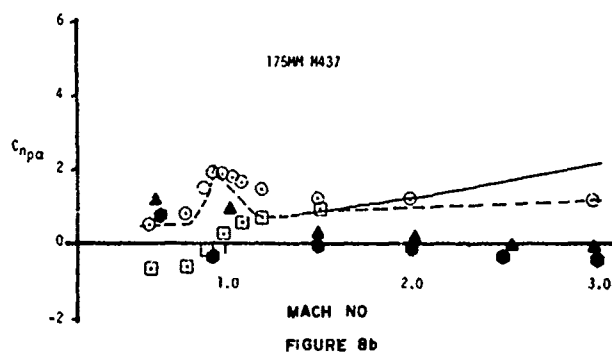
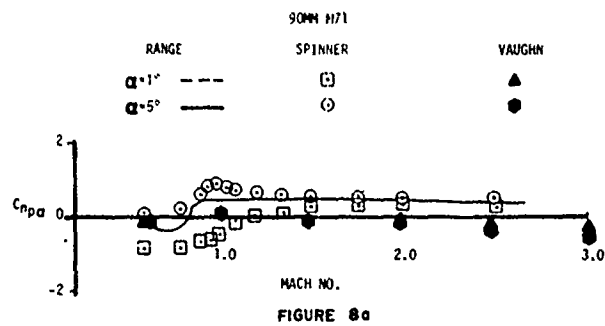
There have been several analytical attempts at predicting Magnus (References 28 through 31) characteristics as a function of the main variables of interest; that is, Mach number, Reynolds number, body shape and various properties of the boundary layer. All of these methods have given some success for given conditions but as of yet, there is still no accurate analytical method by which one can calculate Magnus as a function of Mach number and body shape for typical projectile ordnance. The latest of the theoretical attempts to predict Magnus is due to Vaughn.<sup>(31)</sup> To evaluate the capability of Vaughn's method, several projectile configurations were considered in which his method was compared with experimental data and an all-empirical prediction model "SPINNER".<sup>(4)</sup> Figures 8a, 8b, 8c and 8d present the results of these calculations. As seen in the figures, the empirical model is better for predicting Magnus than the theoretical model of Vaughn. It thus appears that there is still much analytical work to be done before Magnus forces and moments on projectile and missile ordnance can be predicted.

For the near term, it appears more promising to revise the empirical methodology for estimating Magnus than to develop a new theoretical approach to the problem. Along these lines, the "SPINNER" predicts Magnus to be a linear function of body length without regard to boattail shape or nose shape. It has been shown by theory and experiments that nose shape has a second-order effect on Magnus in comparison to body length. However, the Naval Surface Weapons Center, Dahlgren Laboratory, through wind tunnel tests on low drag shapes at AEDC, has found that boattail shape has a first-order effect on Magnus.<sup>(32)</sup> This result was later confirmed by Platou<sup>(33)</sup> with tests on similar shapes. In order that boattail effects might not be confused with the effects of other projectile parameters, a wind tunnel program was initiated in which only the boattail shape was varied. From these results, it was hoped to correlate Magnus as a function of boattail shape and total projectile length.

# 10th Navy Symposium on Aeroballistics

Vol. 1

## MAGNUS MOMENT COEFFICIENT DERIVATIVE FOR FOUR PROJECTILES



### Test Program

Wind tunnel tests were conducted at AEDC in which the boattail shape was systematically varied in length, boattail angle and base diameter (Figure 9). The projectile nose was typical of recently designed ordnance.<sup>(32)</sup> Overall projectile length remained a constant 5.2 calibers in keeping with Naval gun mount constraints and previous observations (Reference 34) of the dependence of the Magnus forces and moments on length. Magnus force and moment coefficients were measured over a range of angle of attack from  $-2^\circ$  to  $8^\circ$ , of non-dimensional spin ( $pd/2V_\infty$ ) variation from 0.3 to 0, and variation in Mach number from 2.5 to 0.5. In order to avoid variations in Magnus due to changes in Reynolds number, a free-stream Reynolds number of 4.0 million per foot was selected for all the Magnus tests to insure fully developed turbulent flow on the boattail section.

#### D. Pitch Damping Moment

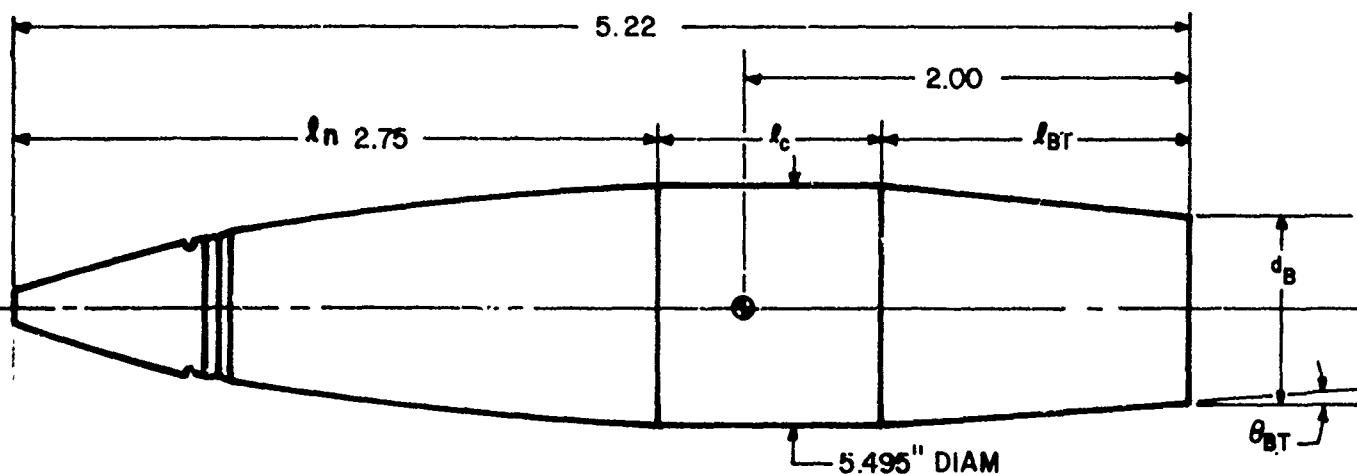
The pitch damping moment will be generated in FY 76 to complete the matrix of aerodynamic coefficients. It is envisioned that supersonic thin wing theory, lifting surface theory, and empirical techniques will be used for the calculation procedures.

Figure 10 summarizes the methods used for the calculation of the dynamic aerodynamics. At present, the prediction program is available in terms of the static aerodynamics only.<sup>(8)</sup> By the end of FY 76, the total prediction program along with a design handbook, should be available.

### III. RESULTS AND DISCUSSION

#### A. Static Aerodynamics

Three cases are presented to show comparison of the present static aerodynamics methodology with experimental data. These cases consist of a spin stabilized projectile (body alone configuration), an unguided missile (body-tail configuration), and a guided projectile (canard-body-tail configuration). These cases are sufficiently different and complex to test all the individual theoretical and empirical procedures of Figures 2 and 3, and to indicate typical results to be expected from the prediction of static forces and moments.

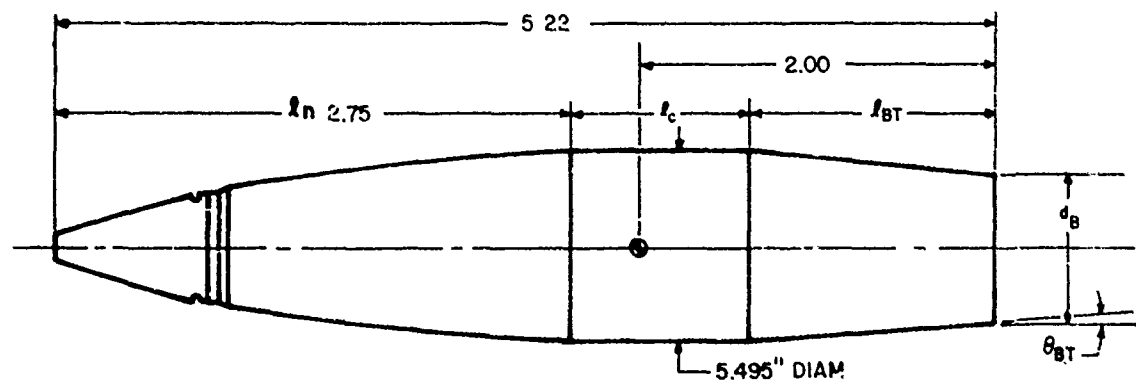


ALL DIMENSIONS IN CALIBERS

CONFIGURATION	CALIBERS	DEG	CALIBERS	CALIBERS
0	0	0	1.0000	2.400
1	1.00	2.5	0.9126	1.400
2	1.00	3.0	0.8240	1.400
3	1.00	7.5	0.7306	1.400
4	0.50	5.0	0.9124	1.900
5	1.35	5.0	0.7637	1.110
6	1.70	5.0	0.7024	0.730
7	0.45	18.4	0.7000	2.000
8	0.05	18.0	0.7000	1.000
9	1.25	6.9	0.7000	1.205

## VARIATIONS IN BOATTAIL SHAPE USED IN MAGNUS WINDTUNNEL STUDY

FIGURE 9



ALL DIMENSIONS IN CALIBERS

CONFIGURATION	CALIBERS	DEG	CALIBERS	CALIBERS
0	0	0	1.0000	2.460
1	1.00	2.5	0.9126	1.400
2	1.00	3.0	0.8240	1.400
3	1.00	7.5	0.7306	1.400
4	0.50	5.0	0.9124	1.959
5	1.35	5.0	0.7637	1.110
6	1.70	5.0	0.7624	0.759
7	0.45	13.4	0.7000	2.009
8	0.85	10.0	0.7000	1.609
9	1.25	6.9	0.7000	1.205

### VARIATIONS IN BOATTAIL SHAPE USED IN MAGNUS WINDTUNNEL STUDY

FIGURE 9

COMPONENT	MACH NUMBER		SUBSONIC	TRANSONIC	SUPERSONIC
	REGION				
BODY ALONE ROLL DAMPING MOMENT			EMPIRICAL		
WING AND INTERFERENCE ROLL DAMPING			LIFTING SURFACE THEORY	EMPIRICAL	LINEAR THEORY
BODY ALONE MAGNUS MOMENT			EMPIRICAL		
WING AND INTERFERENCE MAGNUS MOMENT			ASSUMED ZERO		
BODY ALONE PITCH DAMPING MOMENT			EMPIRICAL		
WING AND INTERFERENCE PITCH DAMPING MOMENT			TO BE DETERMINED FOR FY 76		

FIGURE 10 METHODS USED TO COMPUTE DYNAMIC DERIVATIVE



Figure 11 gives the static aerodynamic coefficients for the improved 5"/54 projectile. The improved round has a 2.75 caliber nose and a 1.0 caliber boattail with a discarding rotating band. Excellent agreement with experimental data is obtained for the drag coefficient throughout the entire Mach number range. Fair agreement is obtained for normal force coefficient and hence pitching moment and center of pressure. The comparison for the lifting properties is Mach number dependent: in the low supersonic region the theory is consistently about ten percent low on normal force whereas at high supersonic speeds it compares very well with experiment. The reason is the failure of the inviscid theory to predict afterbody lift correctly at low supersonic Mach numbers. At subsonic and transonic Mach numbers, the theory does about as well as could be expected considering the amount of empirical methodology in that region.

The second case is a ten caliber missile with clipped delta tailfins. The experimental data are taken from Reference 35, which gives the static aerodynamics for  $0.8 \leq M_\infty \leq 1.3$ . Figure 12 compares theoretical drag coefficient, normal force coefficient derivative, and center of pressure with the experiment as a function of Mach number and for  $\alpha = 1^\circ$ . Recall from Figure 3 that for  $M_\infty \geq 1.2$ , the lift and drag (except for base drag) was calculated numerically whereas for  $0.8 < M_\infty < 1.2$ , the theory consists of mostly empirical procedures. For  $M_\infty \leq 0.8$ , the wing lift is calculated analytically but most other force components are computed empirically. With the exception of the normal force coefficient slope at  $M_\infty = 0.8$  and  $0.85$ , the theory is well within ten percent of experiment. The maximum error in center of pressure for this configuration is five percent of the length or half a caliber.

The final example chosen is a complex canard-body-tail configuration. The body nose is sixty percent blunt with two ogive segments and a 0.7 caliber boattail. The canard has an aspect ratio of two with a sweepback angle of  $15^\circ$ . Its shape consists of a sharp wedge leading edge with a constant thickness section following. The trailing edge is truncated parallel to the leading edge. The tail has an aspect

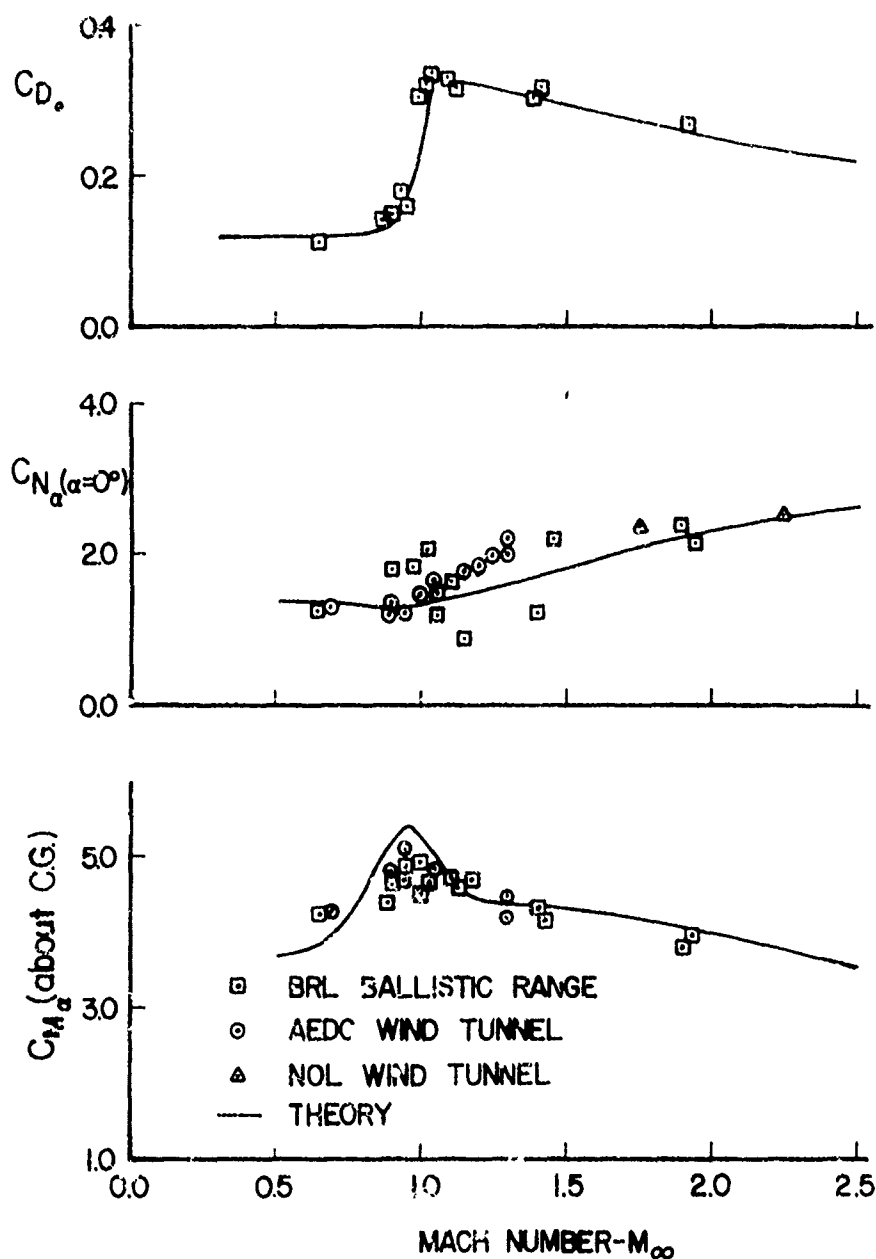


FIGURE 11 COMPARISON OF THEORY AND TEST DATA FOR IMPROVED 5"/54 PROJECTILE.

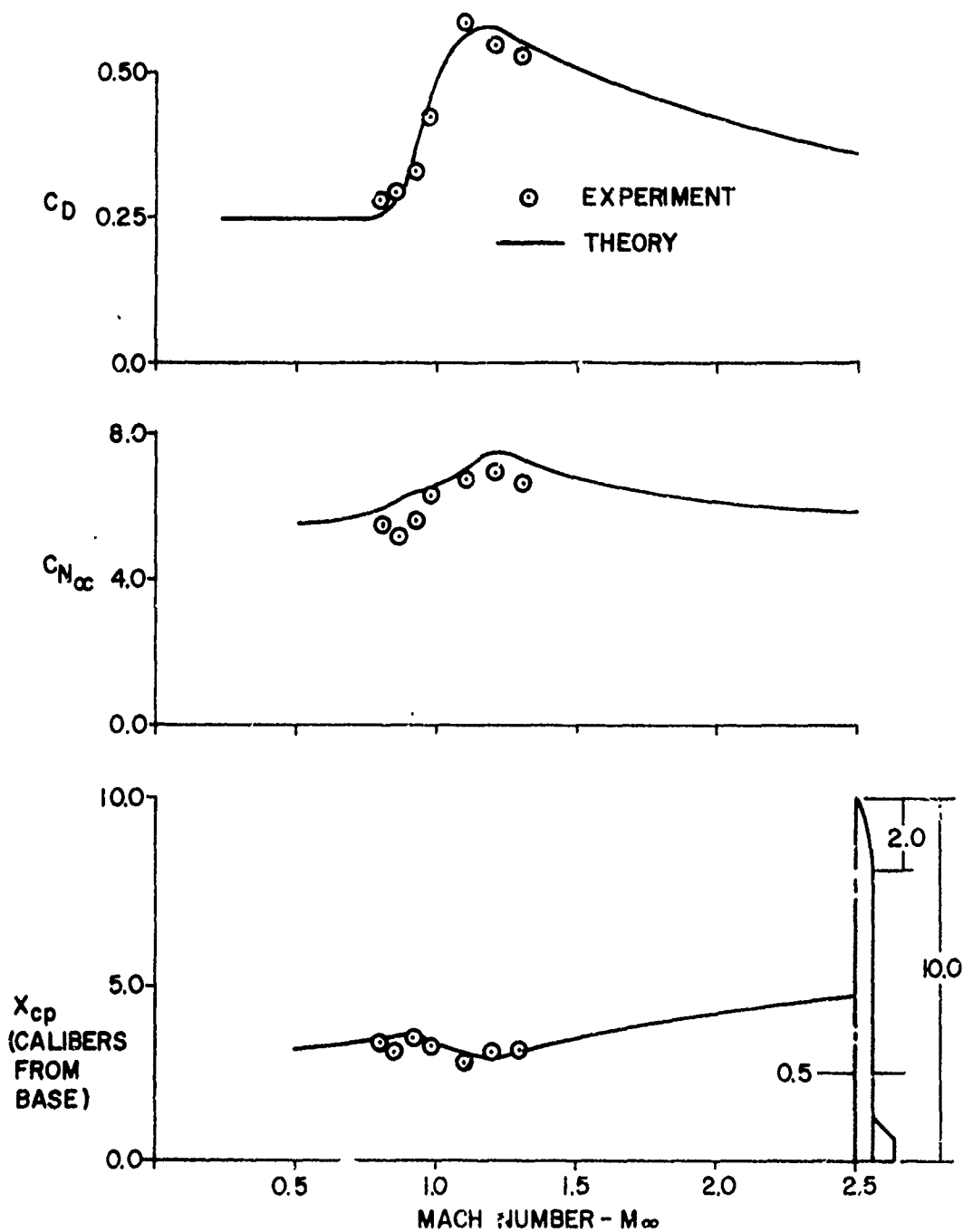


FIGURE 12 STATIC AERODYNAMICS OF A MISSILE CONFIGURATION;  
 $R=1.0$ ,  $\mathcal{L}_1=53.1^\circ$ ,  $\lambda=0.5$ ,  $\alpha=1^\circ$

ratio of four with cylindrical leading and trailing edges and where  $\Lambda_1 = 30^\circ$ ,  $\Lambda_2 = 22.5^\circ$ ,  $\Lambda_3 = 37^\circ$ , and  $\Lambda_4 = 30^\circ$ . The tail thickness to chord ratio also varies along the span. The detailed canard and wing geometry listed above is not needed in calculating lift, but it must be known for drag computations. The results of the calculations for this configuration are shown in Figure 13. Figure 13A gives the normal force and center of pressure for  $M_\infty = 1.6$  and at various angles of attack. Four curves are shown in the figure: canard-body-tail with canards deflected up by ten degrees, canard-body-tail with no canard deflection, body-tail, and finally, body alone. Several points are worthy of note in this figure. First of all the body alone solution agrees very well with the unpublished experimental data up to  $\alpha = 16^\circ$ . Above  $\alpha = 16^\circ$ , the theory is low which is probably due to not taking into account Reynold's number effect in the body crossflow drag coefficient. The next point is that for this configuration, the tail lift is about ten percent too high and the canard lift about 15% too low so that the total lift agrees almost perfectly with the experimental data up to the point where stall begins to occur ( $\alpha \geq 14^\circ$ ). This in turn causes the center of pressure to be more rearward than the experimental data suggest by about up to 0.75 calibers. It is suspected that the theory being high for the high aspect ratio tail and low for the moderate aspect ratio canard is due to the flowfield interaction effects from the complex configuration and will not, in general, be true for other cases. However, it does indicate that the theory can be used quite effectively in design, even for quite complex wing-body-tail geometries. The final point to be emphasized from Figure 13A is the fact that no attempt has been made to predict stall characteristics. As seen in the figure, for this configuration, stall occurs around  $\alpha = 15^\circ$  at  $M_\infty = 1.6$ . However, if the wing thickness or freestream Mach number is changed, the stalling angle of attack will also change.

The drag characteristics for this same missile are shown in Figure 13B. The drag is shown as a function of Mach number and again the total force is broken

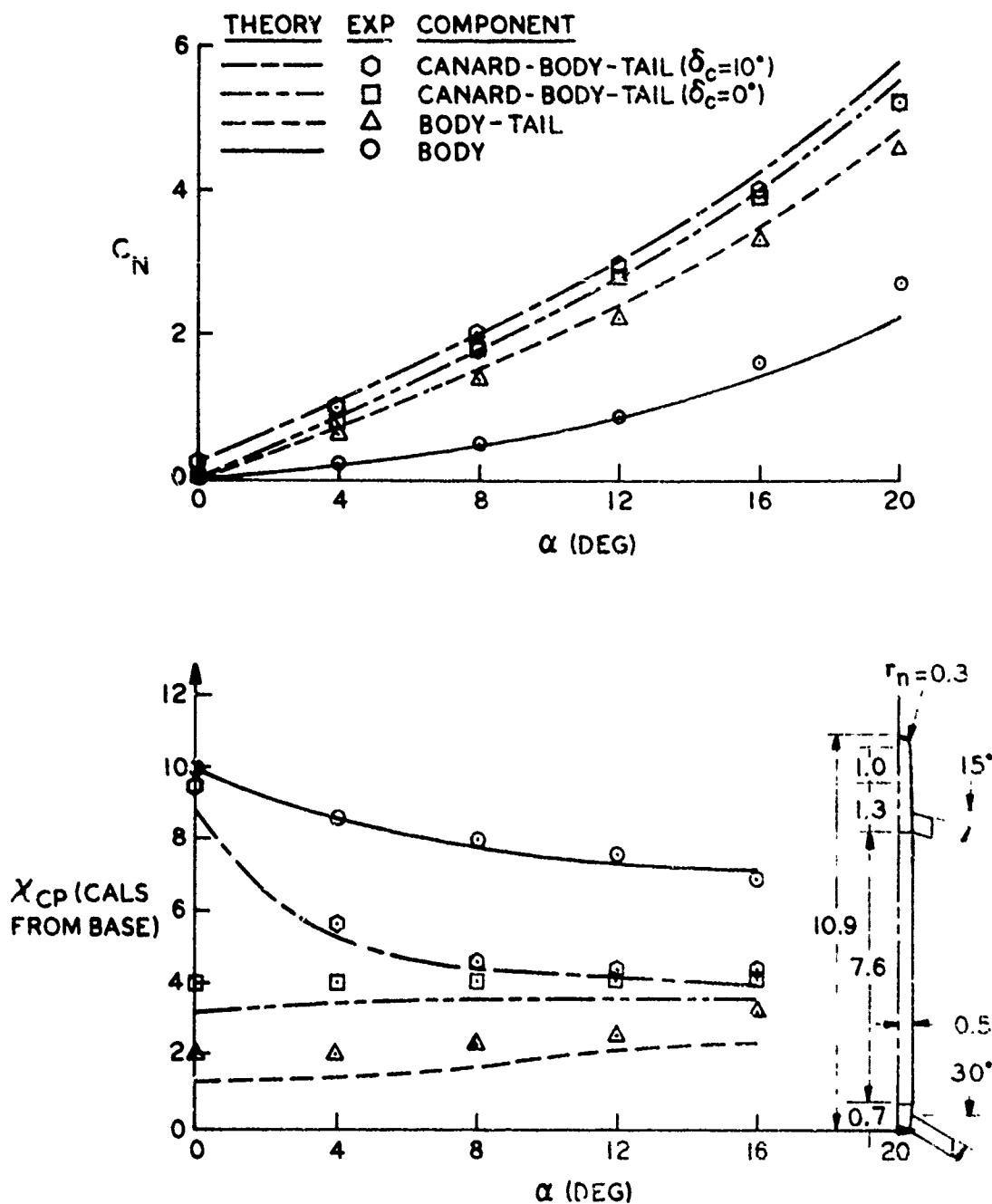


FIGURE 13A. NORMAL FORCES AND CENTER OF PRESSURE OF A MISSILE CONFIGURATION;  $R_t=4$ ,  $R_c=2$ ,  $M_\infty=1.6$

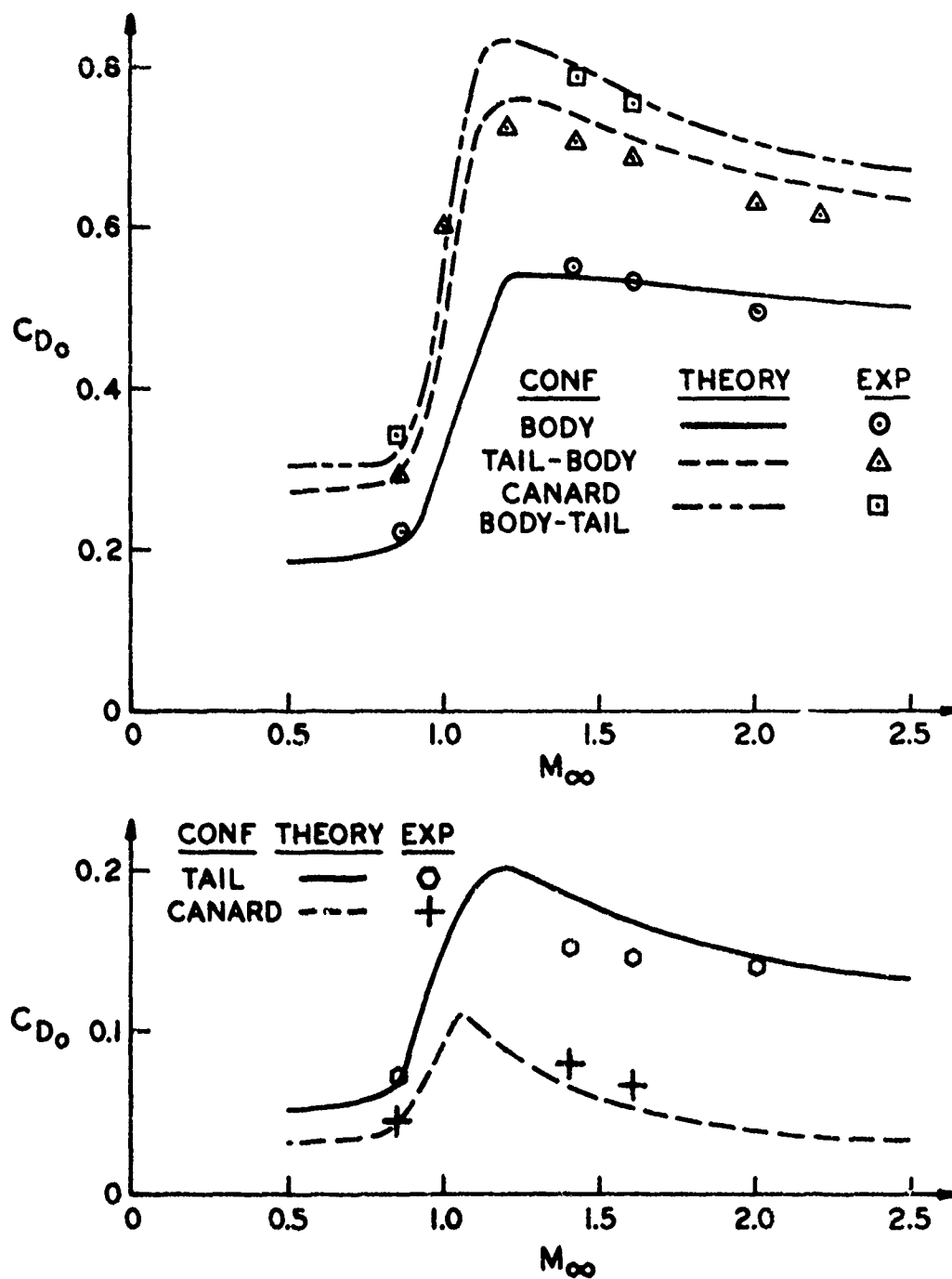


FIGURE 13B. DRAG OF A MISSILE CONFIGURATION AND ITS COMPONENTS

down into its components: body alone, body tail, and canard-body-tail. The body alone drag is acceptable in supersonic and subsonic flow but is unacceptable in transonic flow where the empirical nature of the theory does not account for nose bluntness correctly. The wing alone drag shown at the bottom figure, includes the increase in base drag due to tails. This causes the tail drag to be high because the theory predicts this base drag increase to be significantly higher than the experimental data suggest. However, the body-tail drag is still within the  $\pm 10\%$  category. Finally, the canard drag shown at the bottom figure, is added to the body-tail drag and the overprediction of tail drag is compensated somewhat by the under prediction of canard drag.

#### B. Roll Damping Moment

##### 1. Comparison With Exact Linear Theory

The present method of computing roll damping moment in supersonic flow is to compute the pressure coefficients and integrate these numerically over the entire wing planform. This is as opposed to computing  $C_{\ell_p}$  for simple planform geometries using very lengthy closed formed solutions. The advantage to the former approach is that if one is interested in pressure coefficients and local wing loadings, in addition to roll damping coefficients, it is easier to numerically integrate the known pressure coefficients than to program the lengthy equations for  $C_{\ell_p}$  and  $C_{m_q} + C_{m_{\dot{\alpha}}}$ .

In subsonic flow, closed formed solutions are not possible so no comparisons with exact theories can be made. However, the methodology used is basically that of References 17 and 36, with minor modifications, and extensive checkout has been performed in those references.

Empirical methods are used for the damping moment calculations in transonic flow so that comparison with experiment will have to suffice for check-out of the approach.

Three cases are considered as test cases to compare the numerical solutions with closed form analytical solutions such as presented in References 21 and 22. These include a wing with subsonic leading and supersonic trailing edges

and a wing with supersonic leading and trailing edges with the Mach line intersecting the tip and then the trailing edge. Each of these cases is sufficiently different so as to check the present numerical results with the closed form analytical solutions. These cases are presented in Figures 14, 15, and 16. The results are shown as local wing loading,  $cc'_{nP}$ , as a function of the position along the wing semispan. The local wing loading is defined by:

$$cc'_{nP} = \int_{x_{LE}}^{x_{TE}} \frac{(\Delta C_p)_p}{p \ell_{ref}/V_\infty} dx \quad (28)$$

As expected, the numerical results duplicate the analytical solutions in all cases.

## 2. Comparison With Experiment

Much work has been done in measuring roll damping, both with rocket powered techniques in the early fifties and in the last few years with the wind tunnel. Comparison of these experimental results with the 3-D thin wing theory in supersonic flow and lifting surface theory in subsonic flow has, in general, shown reasonable agreement. The theory typically overestimates the actual experimental results, particularly in the transonic and low supersonic speed regimes.

Two examples in which roll damping have been calculated are shown in Figures 17 and 18. Figure 17 is a comparison of theory and experiment for the delta wing configuration of Reference 37. As seen in the figure, the present methodology gives reasonable agreement for wing t/c values of 0.04.



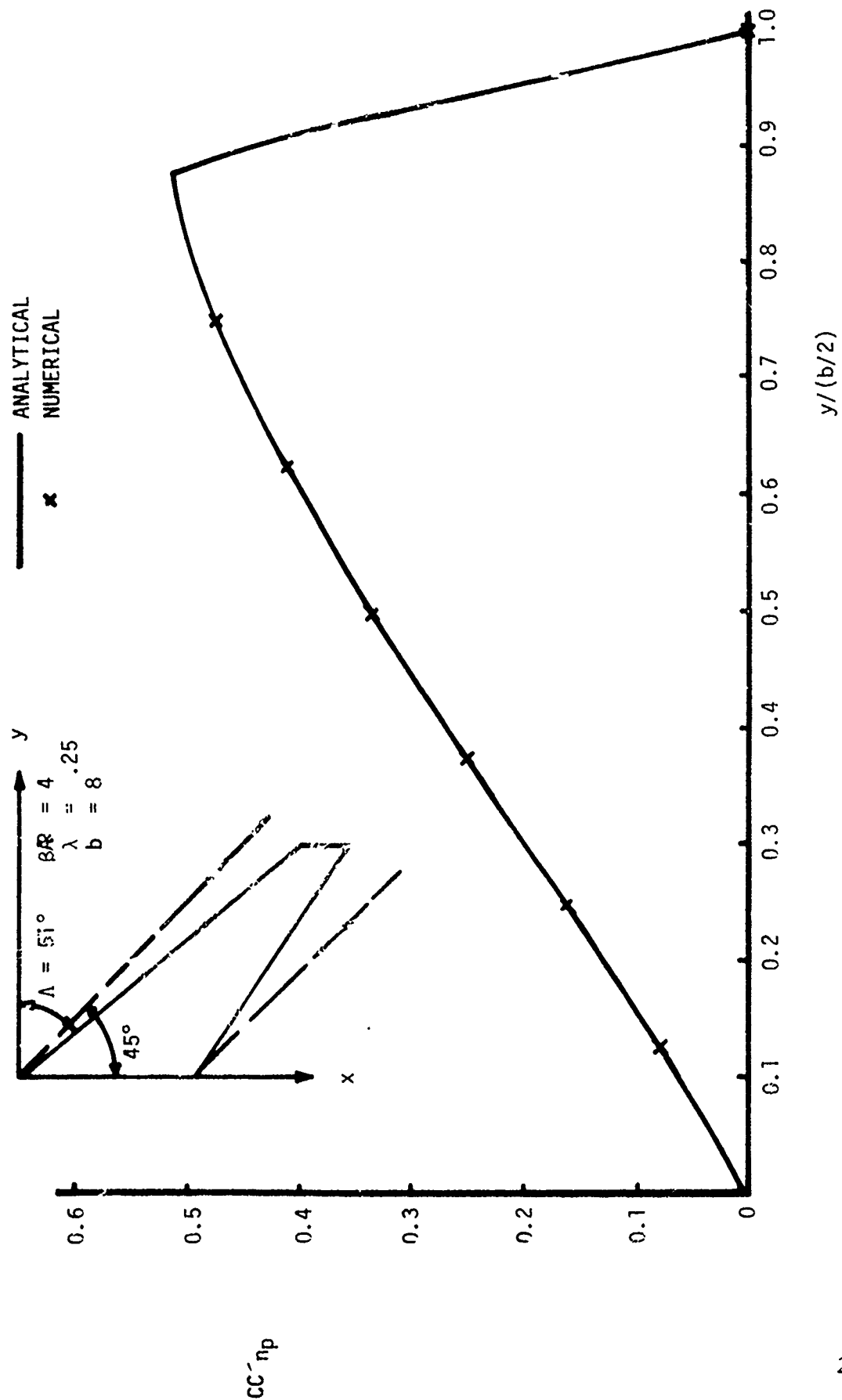


FIGURE 14 WING WITH SUBSONIC LEADING AND SUPERSONIC TRAILING EDGE

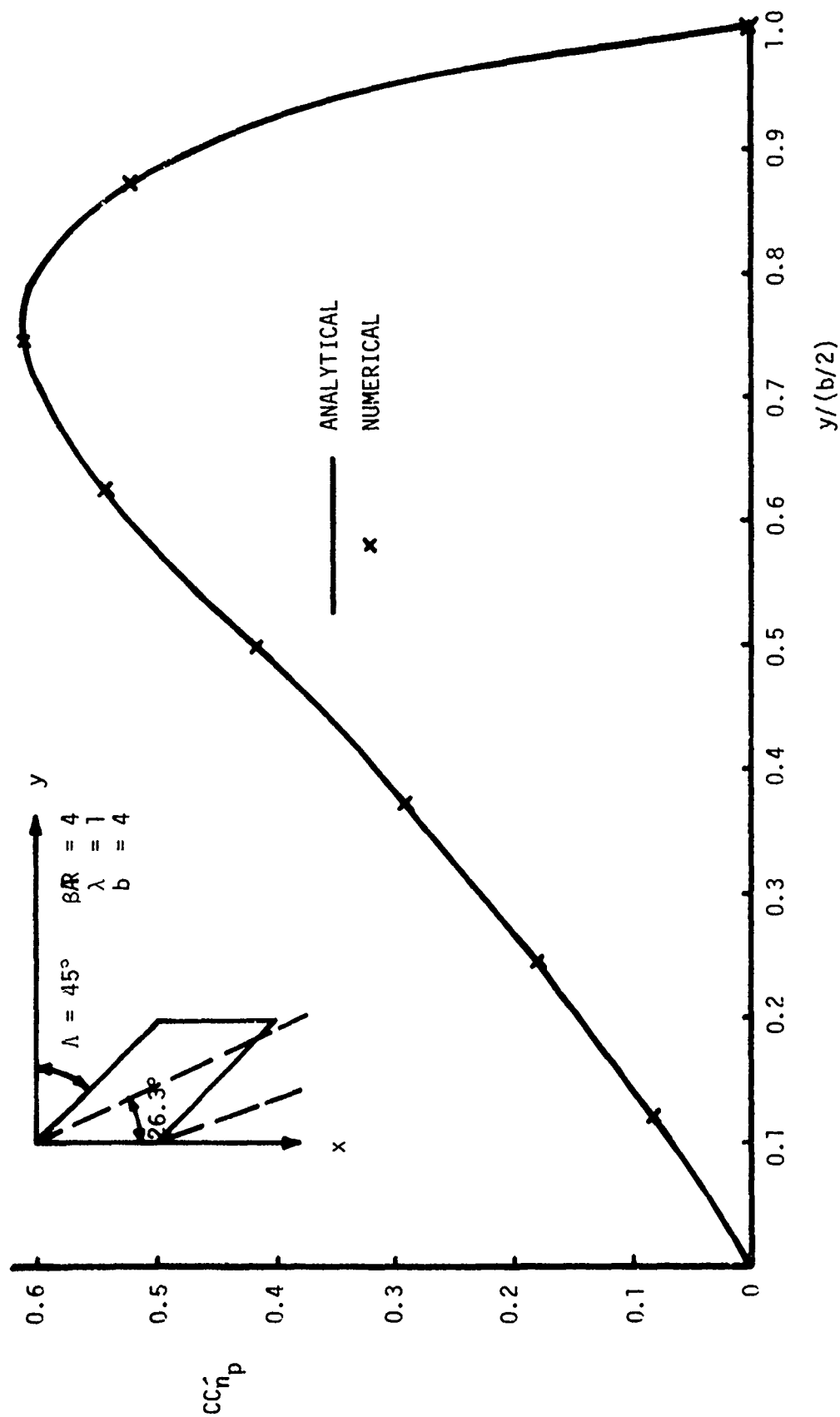


FIGURE 15 WING WITH SUPERSONIC LEADING AND TRAILING EDGE; MACH LINE INTERSECTS TRAILING EDGE

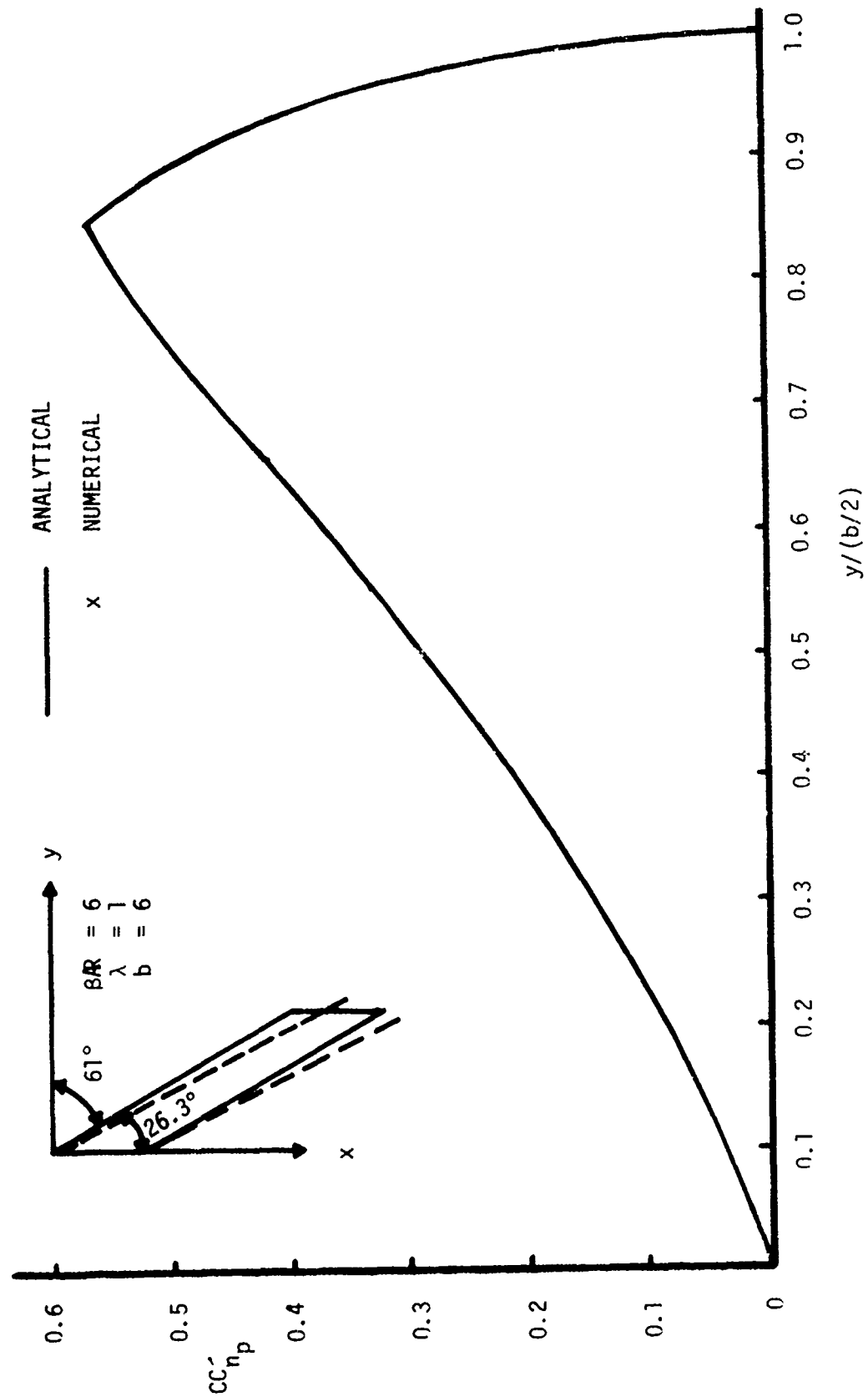


FIGURE 16 WING WITH SUPERSONIC LEADING AND TRAILING EDGE; MACH LINE INTERSECTS TIP

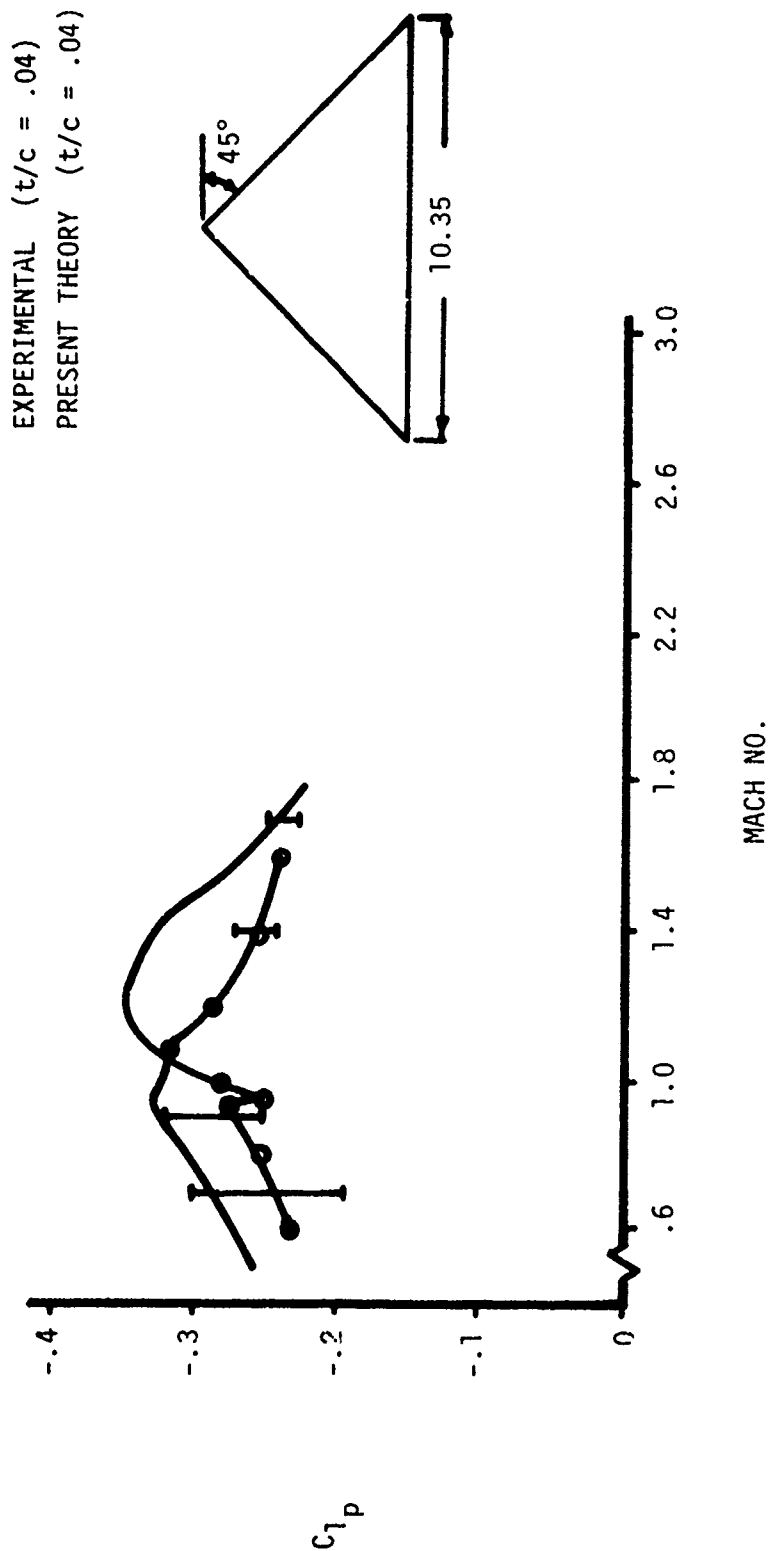


FIGURE 17 COMPARISON OF THEORY AND EXPERIMENT FOR DELTA WING

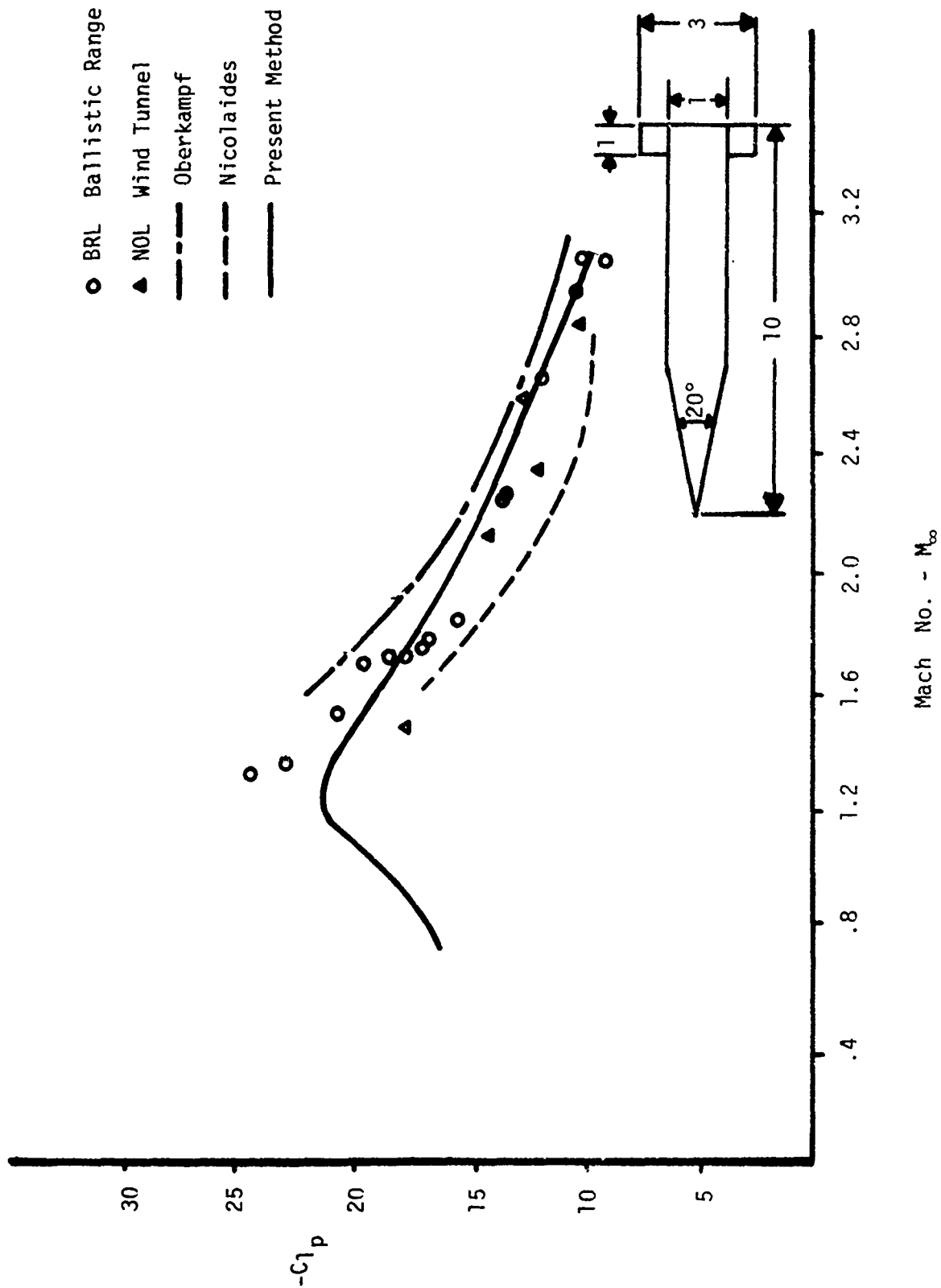


FIGURE 18 ROLL DAMPING COEFFICIENT DERIVATIVE FOR ARMY - NAVY FINNER

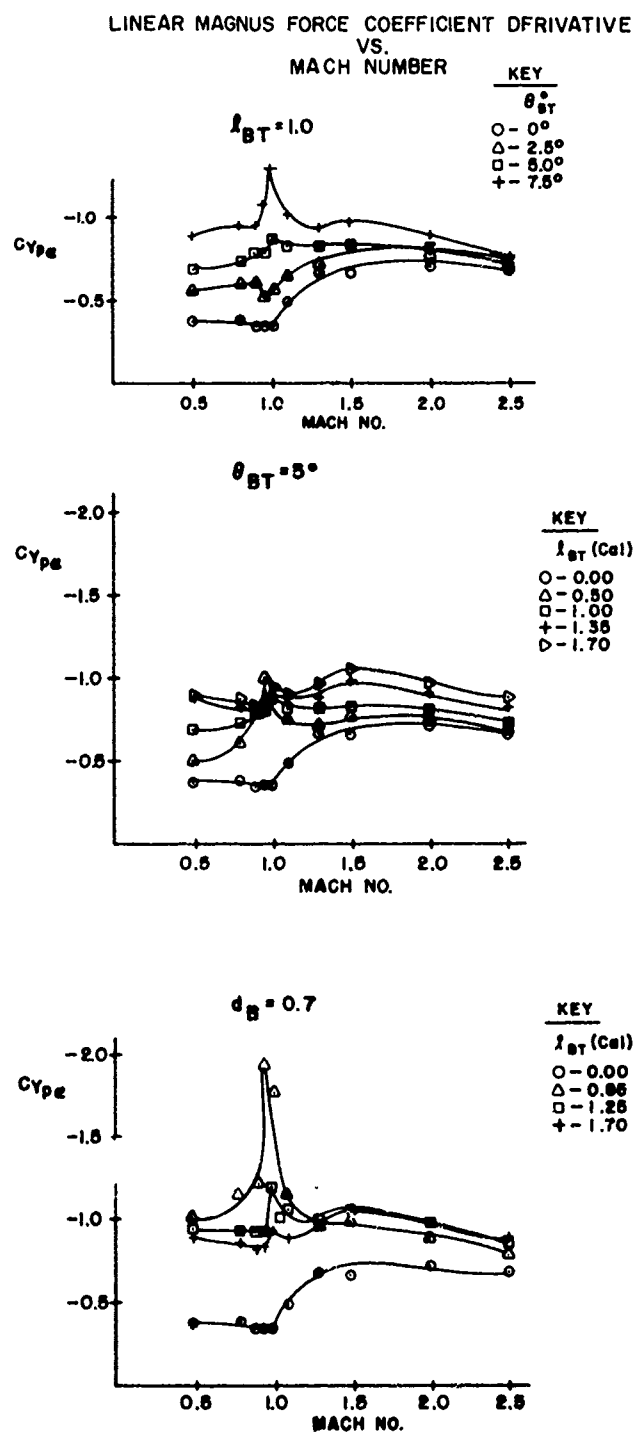


FIGURE 19

# LINEAR MAGNUS MOMENT COEFFICIENT DERIVATIVE VS MACH NUMBER

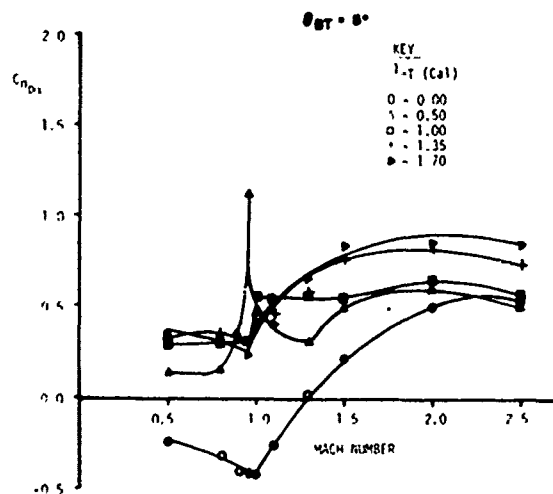
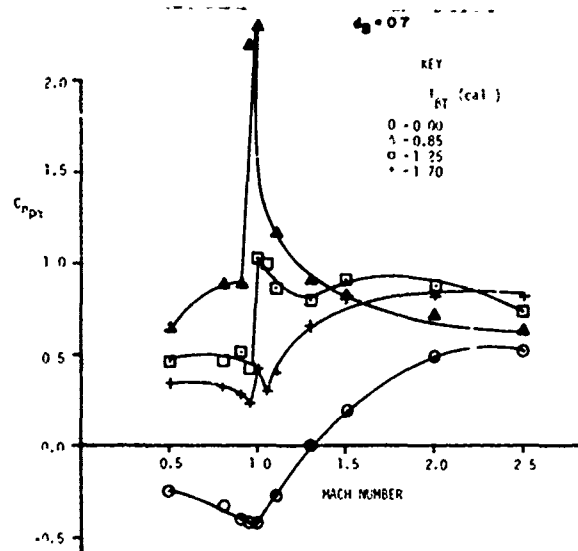
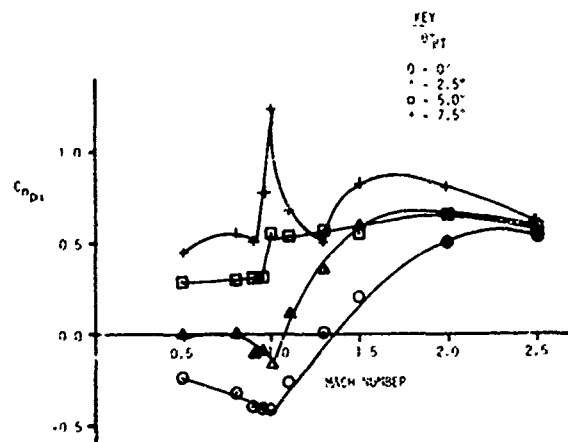
 $\alpha_{BT} = 1.0$ 


FIGURE 20

# VARIATION OF $C_{np\alpha}$ WITH BOATTAIL GEOMETRY

$d_B = 0.7 \text{ Cal}$

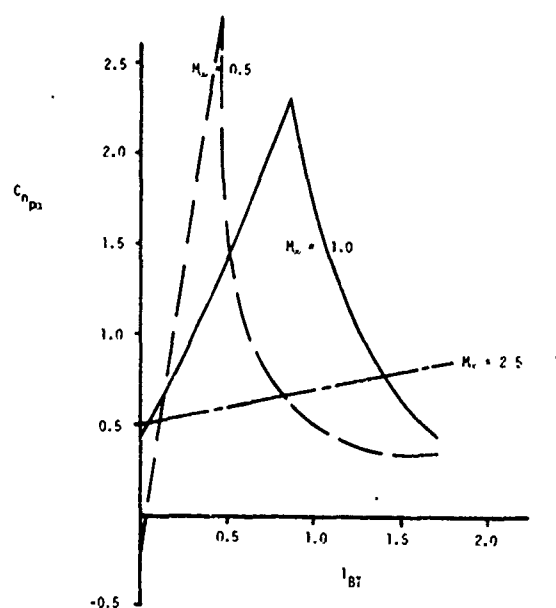


FIGURE 21a

$l_{BT} = 5'$

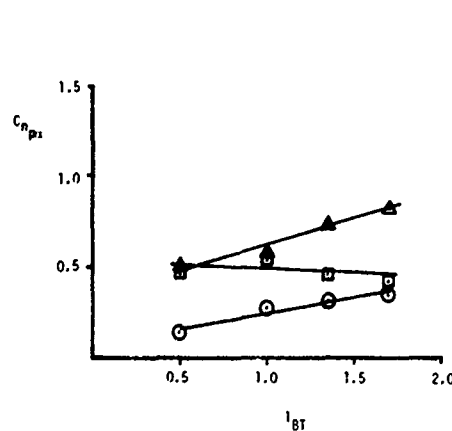


FIGURE 21b

$l_{BT} = 1.0 \text{ Cal.}$

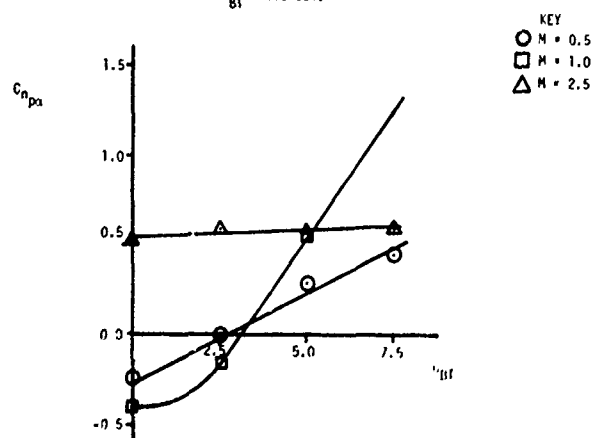


FIGURE 21c



A second comparison of experiment and the present methodology is shown in Figure 18. This case is for the cruciform wing-body Army-Navy finner so the interference theory procedures can also be employed. Considerable experimental data exists for this case at supersonic speeds. In addition, the quasi-two-dimensional approaches of Nicolaides<sup>(38)</sup> and Oberkampf<sup>(39)</sup> are shown for comparison. The theoretical approaches are all within the experimental accuracy, lending support to the linearized supersonic flow theory. There were no data available for this case in subsonic flow to compare the present theory with theoretical estimates of roll damping.

In general, theoretical estimates of roll damping compared with experimental data is similar to Figure 17. That is, the roll damping is overestimated by linear theory. The reasons are several.<sup>(40),(41)</sup> First of all, aeroelastic effects can contribute as much as 25-30% loss in roll damping. Thickness effects can contribute at least that much again in the transonic speed regime. The other reason sometimes given, mutual interference between wings and between wing-body, seems to be of lesser importance in the present work due to accounting for these through slender body theory. The thickness effects are also accounted for empirically in transonic flow but not in subsonic and supersonic flow. It thus appears that if an accurate estimate of roll damping ( $\pm 10\%$ ) throughout the Mach number range is desired, thickness and aeroelastic effects must be accounted for. On the other hand, neglecting these variables gives accuracies within 25% for most cases.

### C. Magnus

#### 1. Wind Tunnel Results

Results of the wind tunnel testing program are shown in Figures 19 and 20. These figures reveal a strong Magnus dependence on boattail length and angle. Furthermore, it is shown in Figures 21a and 21b that the effects of boattail length and angle are interrelated. Figure 21a reveals an apparent sharp peak of  $C_{n p_\alpha}$  at a boattail length of 0.85 calibers ( $\theta_{BT} \approx 10^\circ$ ). However, in comparison with

Figure 21b and 21c, it is seen that the previously shown peaking phenomena is due mainly to nonlinearities associated with large boattail angles ( $\theta_{BT} > 10^\circ$ ). In Figures 21a, 21b, and 21c, it is also shown that the transonic dependence of the Magnus force and moments on the boattail parameters is itself a strong function of Mach number. Supersonic results, on the other hand, indicate consistent increases in  $C_{y_{p_\alpha}}$  and  $C_{n_{p_\alpha}}$  with boattail angle and boattail length; and weak dependence on Mach number.

## 2. Magnus Prediction Methodology

From Figures 21a and 21b it can be seen that the functionalization of the Magnus coefficient derivatives would be difficult in terms of the simple boattail variables  $\theta_{BT}$ ,  $l_{BT}$  and  $d_B$ .

Another geometrical parameter was developed from the Magnus theory of Vaughn and Reis.<sup>(31)</sup> This variable is based on the boattail geometry and is given by:

$$\eta = \left[ \frac{\int_{-l_{BT}}^l r^2 dx}{r_{ref}^2 l_{BT}} \right]^{1/2} \quad (29)$$

which for conical boattails integrates to:

$$\eta = .5774 \left[ 1 + \left( \frac{r_b}{r_{ref}} \right) + \left( \frac{r_b}{r_{ref}} \right)^2 \right]^{1/2} \quad (30)$$

Plots of the Magnus coefficient derivatives versus  $\eta$  are shown for various Mach numbers in Figures 22a, b, c, and d and Figures 23a, b, c, and d. The linearity of the Mangler correlation is quite evident (with the exception of the moment derivatives near  $M = 1.0$ ). The very linear variation of  $C_{y_{p_\alpha}}$  and  $C_{n_{p_\alpha}}$  with  $\eta$  suggests an empirical correlation of magnus force and moment with the Howarth-Mangler variable. This can be expressed in the form:

VARIATION OF  $C_{yp\alpha}$  WITH THE  
HOWARTH-MANGLER VARIABLE

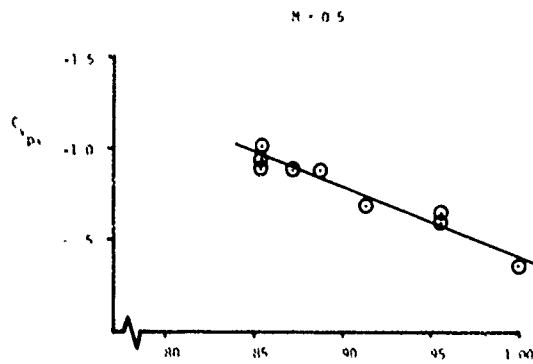


FIGURE 22a

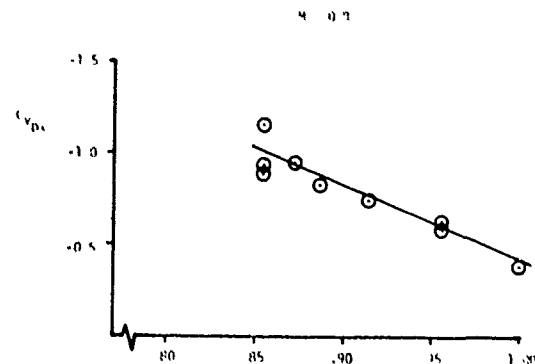


FIGURE 22b

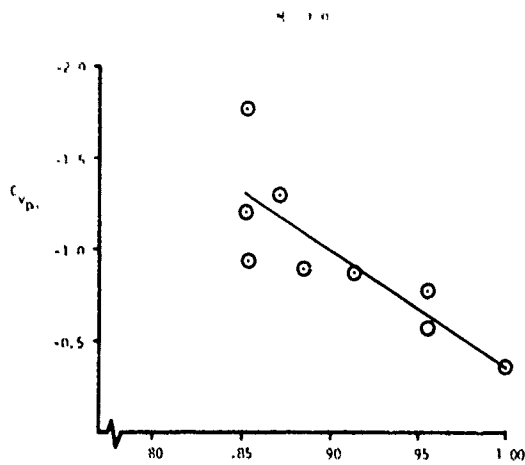


FIGURE 22c

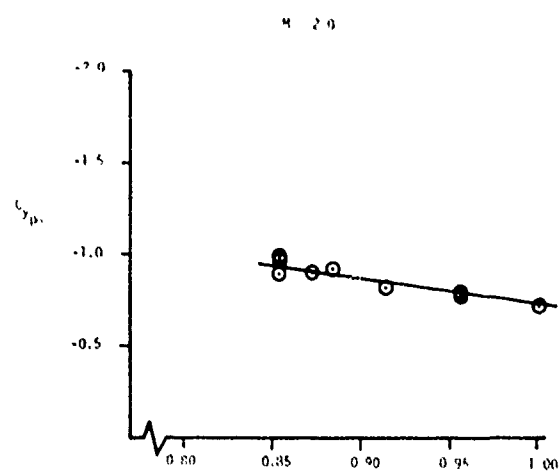


FIGURE 22d

VARIATION OF  $C_{np\alpha}$  WITH THE  
HOWARTH-MANGLER VARIABLE

$M = 0.5$

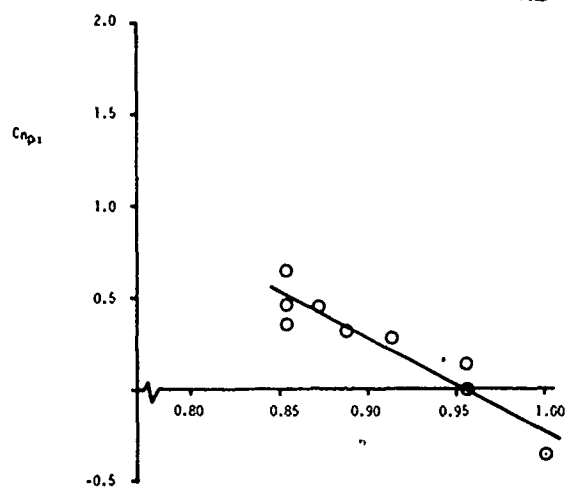


FIGURE 23a

$M = 0.8$

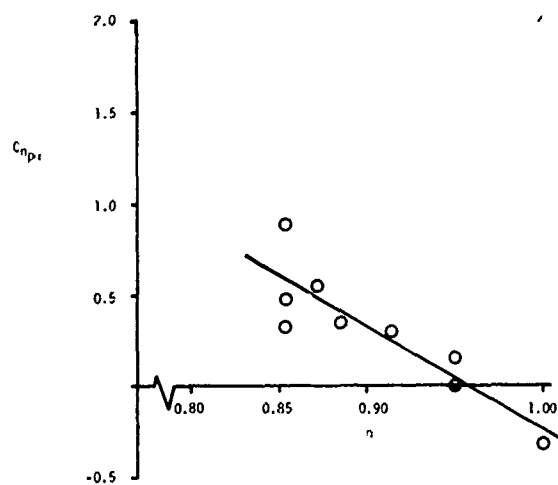


FIGURE 23b

$M = 1.0$

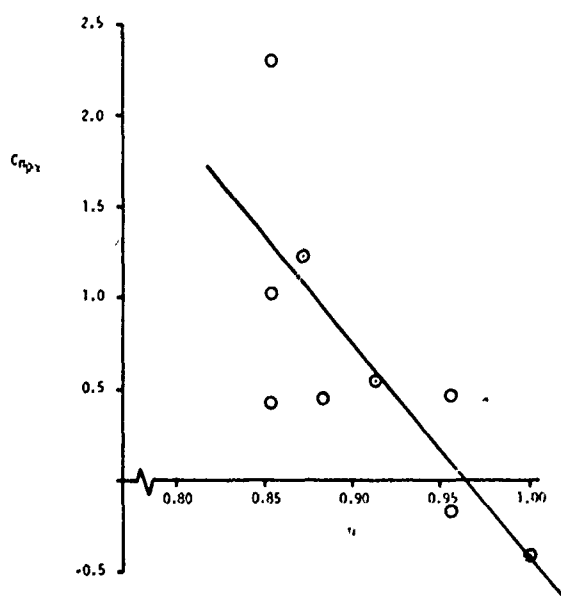


FIGURE 23c

$M = 2.0$

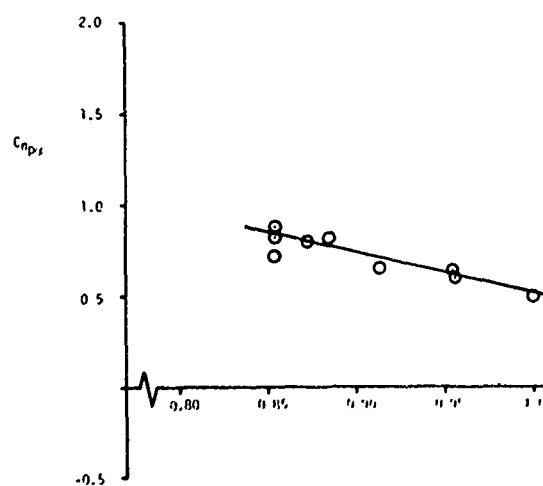


FIGURE 23d

$$C_{y p_{\alpha}} = a + b\eta \quad (31)$$

$$C_{n p_{\alpha}} = c + d\eta \quad (32)$$

where a, b, c, and d are based on least square fits of  $C_{y p_{\alpha}}$  and  $C_{n p_{\alpha}}$  with  $\eta$ . Values of a, b, c, and d and the standard deviation of each fit have been calculated and are given in Table 1.

TABLE 1

Mach No.	0.5	0.8	0.9	1.0	1.5	2.0	2.5
a	-4.411	-4.410	-4.268	-6.766	-3.125	-2.362	-1.889
b	4.134	4.001	3.820	6.409	2.446	1.658	1.228
$\sigma(C_{y p_{\alpha}})$	.036	.074	.118	.221	.032	.030	.036
c	4.475	5.412	5.479	10.710	4.107	2.650	2.020
d	-4.650	-5.644	-5.721	-11.108	-4.066	-2.133	-1.526
$\sigma(C_{n p_{\alpha}})$	.089	.152	.197	.501	.064	.050	.069

The current empirical method is employed as follows: (1) for a given boattail geometry, the value of  $\eta$  would be calculated (2) values of  $C_{y_{p_\alpha}}$  and  $C_{n_{p_\alpha}}$  would be calculated using Equations (31) and (32) in conjunction with Table 1 resulting in  $C_{y_{p_\alpha}}$  and  $C_{n_{p_\alpha}}$  for a configuration 5.2 calibers in length (3)  $C_{y_{p_\alpha}}$  and  $C_{n_{p_\alpha}}$  for projectiles of different length are calculated according to Equations (33) and (34)

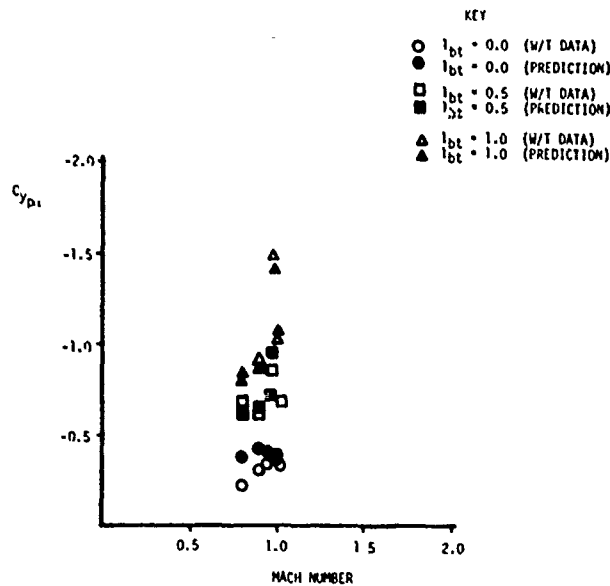
$$C_{y_{p_\alpha}}(\ell) = \frac{\ell}{5.2} \cdot C_{y_{p_\alpha}}(\ell = 5.2) \quad (33)$$

$$C_{n_{p_\alpha}}(\ell) = \frac{\ell}{5.2} \cdot C_{n_{p_\alpha}}(\ell = 5.2) \quad (34)$$

### 3. Comparison of Magnus Predictions on Other Shells

Comparison between wind tunnel derived  $C_{y_{p_\alpha}}$  data and predictions based on the Mangler correlation (Figures 24a, b, c and d) reveals general agreement within experimental error. The sharpness of the Magnus force and moment spike for some configurations ( $\eta \sim .9$ ) indicates the possibility of missing the spike in wind tunnel tests if data is taken at too few Mach numbers between 0.9 and 1.05. Excellent correlation between the Mangler parameter and the peak Magnus force and moment coefficient derivatives from the wind tunnel data of the Army-Navy spinner boattail variation study<sup>(33)</sup> is shown in Figures 25a and 25b. Data in this study were taken at the transonic Mach numbers: 0.9, 0.94, 0.98 and 1.02. The slopes and intercepts of the Mangler lines (based on the data of Reference 33) were then included in the set of lines upon which Magnus predictions were made for other projectiles. Peak predictions based on these lines are represented by crosses in Figures 24, 26, and 27.

# COMPARISON BETWEEN MAGNUS MODELS AND WIND TUNNEL DATA



COMPARISON BETWEEN  $C_{yp1}$  PREDICTION AND WIND TUNNEL DATA  
OF THE 5 CAL A-N SPINNER (Ref 11)

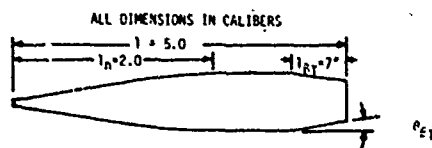
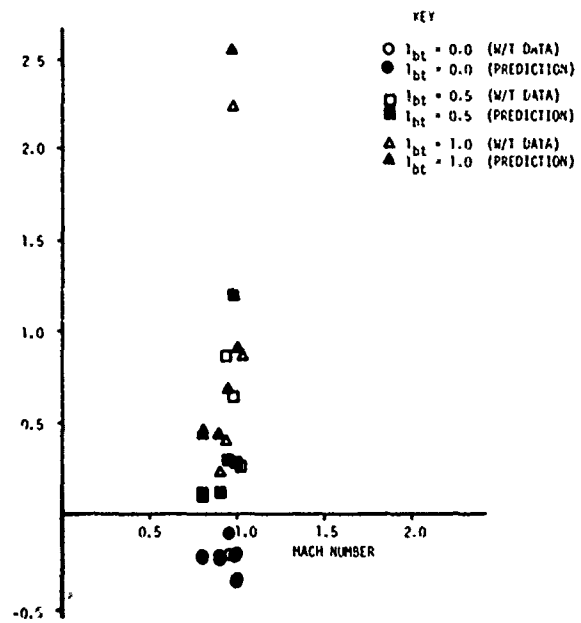
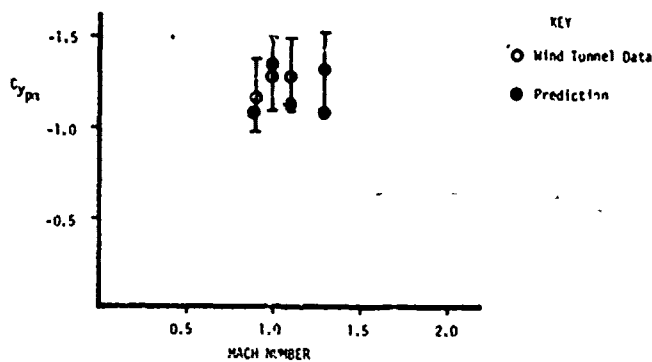
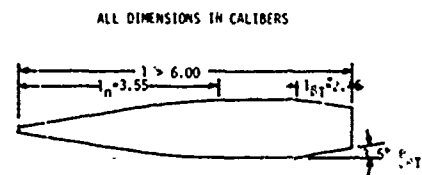
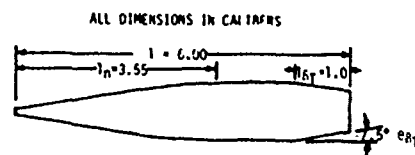


FIGURE 24a



COMPARISON BETWEEN  $C_{np1}$  PREDICTION AND WIND TUNNEL DATA  
OF THE 5 CAL A-N SPINNER (Reference 33)

FIGURE 24b

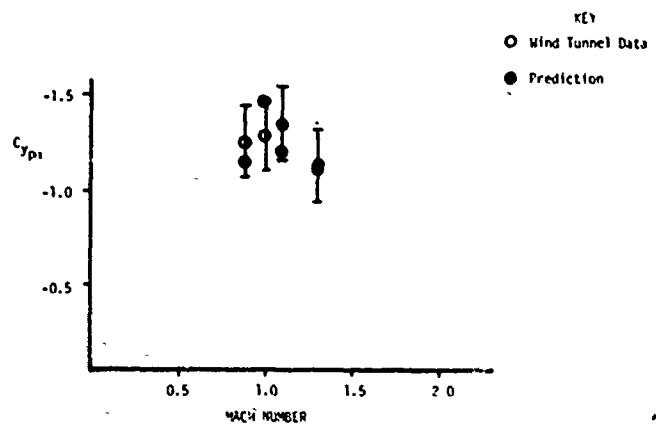


COMPARISON BETWEEN NML-TR-2586 AND PREDICTIONS FOR

$$C_{yp1} \bar{p} = .1$$

CONFIGURATION 2

FIGURE 24c



COMPARISON BETWEEN NML-TR-2586 AND PREDICTIONS FOR

$$C_{yp1} \bar{p} = .1$$

CONFIGURATION 3

FIGURE 24d

MANGLER CORRELATION OF 5" A-N SPINNER  
PEAK TRANSONIC MAGNUS WIND TUNNEL DATA  
(Ref 33)

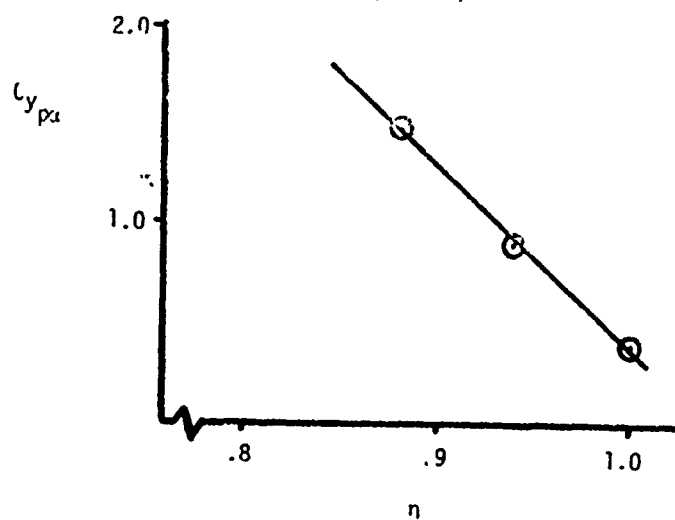


FIGURE 25a

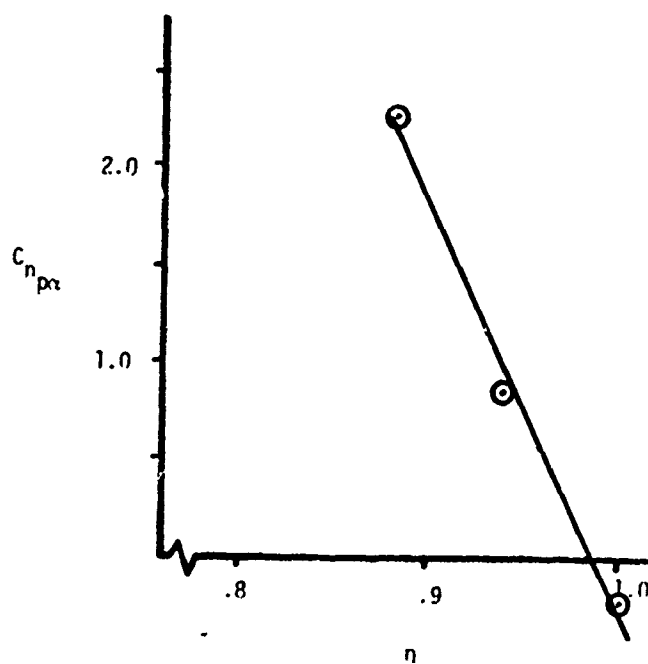


FIGURE 25b



Comparison between wind tunnel data, spark range data (Figures 26 and 27) and prediction demonstrates agreement within experimental error and scatter. However, several spark range tests (Figures 27a and 27b) reveal negative Magnus moments, larger than any observed in wind tunnel testing. Two factors regarding the spark range tests quoted should be noted. All spark range data gathered in this report predate Chapman-Kirk data reduction and the data in References 44, 45 and 46 are given without likely error margins. Also, most of the spark range models considered herein have rotating bands as opposed to the wind tunnel models.

Therefore, based on the comparisons made to date of the current empirical technique for predicting Magnus with experiment and other procedures, it is concluded that the current method works at least as well if not better than other methods. However, additional comparisons need to be made before any conclusive statement can be made concerning accuracy.

#### IV. CONCLUSIONS AND RECOMMENDATIONS

1. A general method has been developed consisting of several theoretical and empirical procedures to calculate lift, drag, pitching moment, magnus moment, and roll damping moment on wing-body-tail configurations from Mach number zero to three and angles of attack up to stall. The pitch damping moment will be added to the calculation procedure in FY 76.
2. Comparison of the overall methodology with experiment for several configurations indicates that accuracies of  $\pm 10\%$  can be obtained for static force coefficients of most configurations. Roll damping moments are within 25% of experimental data for most cases. This is at a cost of less than \$10 per Mach number for the entire set of aerodynamic coefficients.
3. A new empirical method for predicting magnus forces and moments as a function of body length and boattail shape is developed. It relies on the linearity of the Magnus force with body length and with the Howarth-Mangler variable.

# COMPARISON BETWEEN MAGNUS MODELS AND WIND TUNNEL DATA

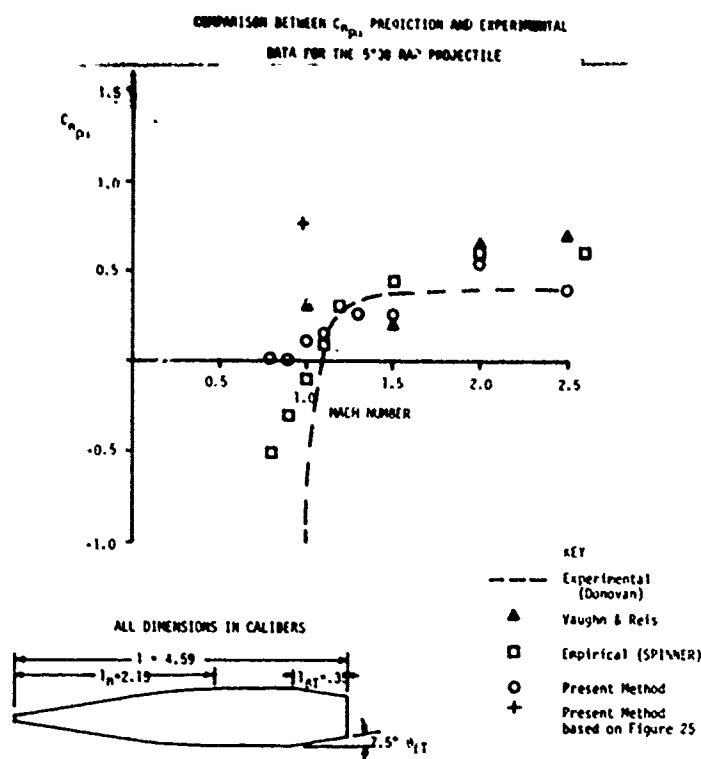


FIGURE 26a

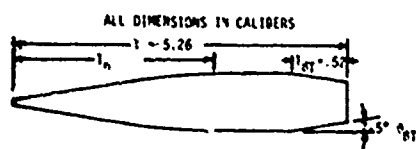
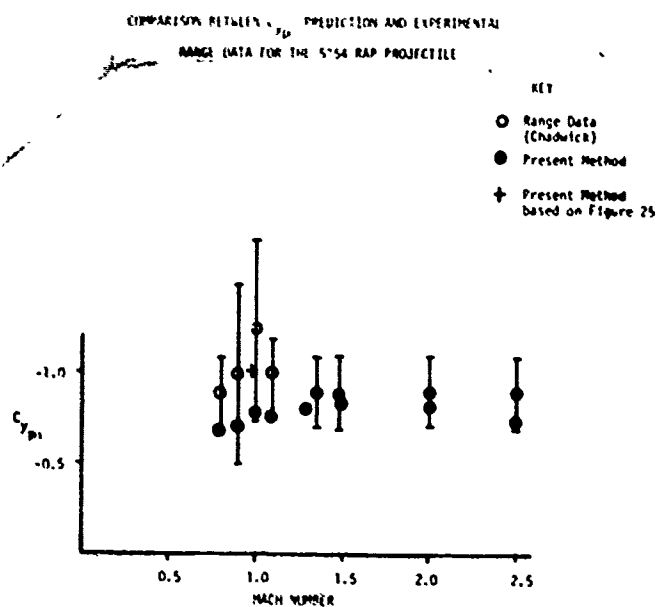


FIGURE 26b

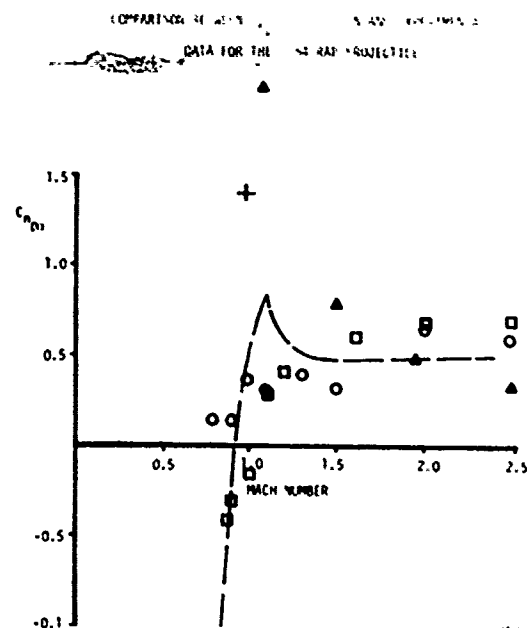


FIGURE 26c

# COMPARISON BETWEEN MAGNUS MODELS AND EXPERIMENTAL RANGE DATA

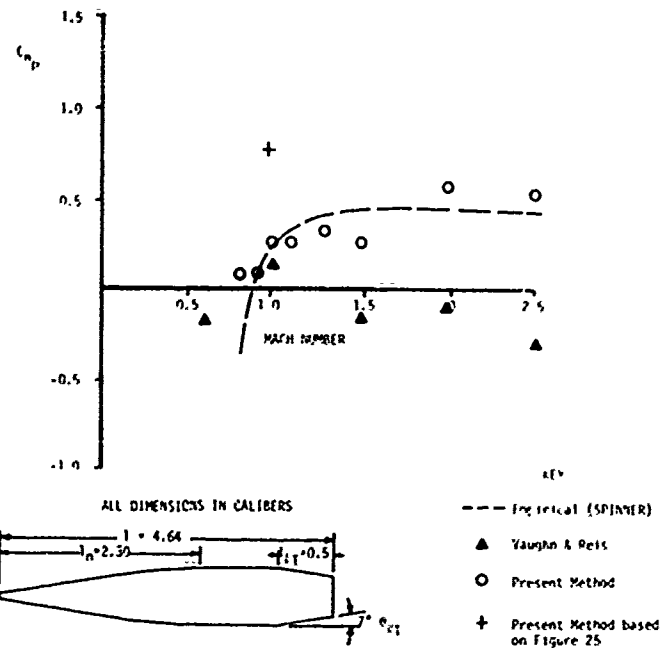


FIGURE 27a

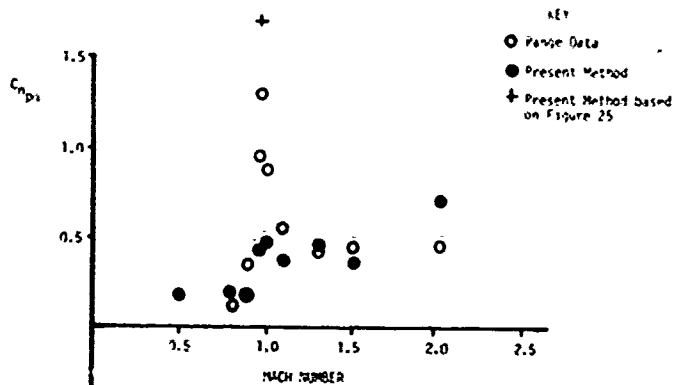


FIGURE 27b

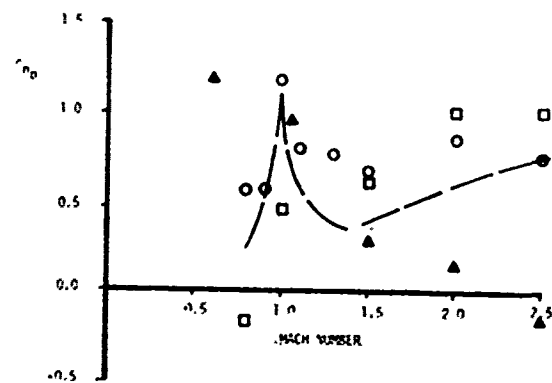


FIGURE 27c

Comparisons with experimental data and other techniques show this method to work at least as well as any available for spin-stabilized projectiles.

4. If roll damping is desired within  $\pm 10\%$  for most configurations, thickness and aeroelastic effects should be accounted for.

5. It is recommended the magnus correlations with the Howarth-Mangler variable be extended to higher angles of attack and also that the effect of fins on Magnus force and moments be examined.

6. The prediction methodology in transonic flow is almost entirely empirical due to the current state-of-the-art in simple (but yet accurate) analytical methods for use in flow computations. It is thus recommended that work be continued in this Mach number regime with reasonable emphasis on simple techniques.

#### V. REFERENCES

1. Douglas Aircraft Co., Inc. **USAF Stability and Control DATCOM**, Revisions by Wright-Patterson Air Force Base, July 1963, 2 Vols.
2. Woodward, F. A., *Analysis and Design of Wing-Body Combinations at Subsonic and Supersonic Speeds*, Journal of Aircraft, Vol. 5, No. 6, 1968, pp. 528-534.
3. Saffert, B. F., Jr., Howard, M. L., Brooks, E. N., Jr., *A Method for Predicting the Static Aerodynamic Characteristics of Typical Missile Configurations for Angles-of-Attack to 180 Degrees*, NSRDC Report 3645, 1971.
4. Whyte, R. H., *Spinner - A Computer Program for Predicting the Aerodynamic Coefficients of Spin Stabilized Projectiles*, General Electric Class 2 Reports, 1969.
5. Moore, F. G., *Aerodynamic Drag and Lift of General Body Shapes at Subsonic, Transonic, and Supersonic Mach Numbers*, AGARD Conference preprint No. 124 on Aerodynamic Drag, Paper No. 2, 1973.
6. Moore, F. G., *Body Alone Aerodynamics of Guided and Unguided Projectiles at Subsonic, Transonic, and Supersonic Mach Numbers*, NWL TR-2796, 1972.
7. Moore, F. G., *Aerodynamics of Guided and Unguided Weapons: Part I - Theory and Application*, NWL TR-3018, December 1973.

8. Moore, F. G., McKerley, C. W., *Aerodynamics of Guided and Unguided Weapons; Part II - Computer Program and Usage*, NWL TR-3036, 1974.
9. Moore, F. G., *Static Aerodynamics of Missile Configurations for Mach Number Zero to Three*, AIAA Paper No. 74-538.
10. Van Dyke, M. D., *First and Second-Order Theory of Supersonic Flow Past Bodies of Revolution*, JAS, Vol. 18, No. 3, March 1951, pp. 161-179.
11. Tsien, H. S., *Supersonic Flow Over an Inclined Body of Revolution*, JAS, Vol. 5, No. 12, October 1938, pp. 480-483.
12. Wu, J. M., Aoyoma, K., *Transonic Flow-Field Calculation Around Ogive Cylinders by Nonlinear-Linear Stretching Method*, U. S. Army Missile Command Technical Report No. RD-TR-70-12, April 1970. Also AIAA 8<sup>th</sup> Aerospace Sciences Meeting, AIAA Paper 70-189, January 1970.
13. Van Driest, E. R., *Turbulent Boundary Layer in Compressible Fluids*, JAS, Vol. 18, No. 3, pp. 145-160, 216.
14. Allen, J. H., Perkins, E. W., *Characteristics of Flow Over Inclined Bodies of Revolution*, NACA RM A 50L07, 1965.
15. Love, E. S., *Base Pressure at Supersonic Speeds on Two-Dimensional Airfoils and on Bodies of Revolution With and Without Turbulent Boundary Layers*, NACA TN-3819, 1957.
16. Ashley, H., Landahl, M., *Aerodynamics of Wings and Bodies*, Addison-Wesley Publishing Company, Reading, Massachusetts.
17. Chadwick, W. R., *The Application of Non-Planar Lifting Surface Theory to the Calculation of External Store Loads*, Complete 1972.
18. Jones, R. T., Cohen, Doris, *High Speed Wing Theory*, Princeton Aeronautical Paperbacks, Number 6, 1960.
19. Chapman, D. R., Wimbrow, W. R., Kester, R. H., *Experimental Investigation of Base Pressure on Blunt-Trailing-Edge Wings at Supersonic Velocities*, NACA Rep. 1109, 1952 (supersedes NACA TN-2611).

20. Pitts, W. C., Nielsen, J. N., Kaattari, G. E., *Lift and Center of Pressure of Wing-Body-Tail Combinations at Subsonic, Transonic, and Supersonic Speeds*, NACA TR 1307, 1957.
21. Martin, J. C. and Jeffreys, I., *Span Load Distribution Resulting From Angle-of-Attack, Rolling, and Pitching for Tapered Sweptback Wings With Streamwise Tips*, NACA TN 2643, 1952.
22. Malvestuto, F. S., Jr., Margolis, K., Ribner, H., *Theoretical Lift and Damping in Roll at Supersonic Speeds of Thin Sweptback Tapered Wings With Streamwise Tips, Subsonic Leading Edges, and Supersonic Trailing Edges*, NACA TR 970, 1950.
23. Lockwood, V. E., *Effects of Sweep on the Damping-in-Roll Characteristics of Three Sweptback Wings Having an Aspect Ratio of 4 at Transonic Speeds*, NACA RM L50J19, December 1950.
24. Edmondson, J. L., *Damping in Roll of Rectangular Wings of Several Aspect Ratios and NACA 65A Series Airfoil Sections of Several Thickness Ratios at Transonic and Supersonic Speeds as Determined With Rocket-Powered Models*, NACA RM L50E26, 1950.
25. Adams, G. J., Dugan, D. W., *Theoretical Damping in Roll and Rolling Moment Due to Differential Wing Incidence for Slender Cruciform Wings and Wing-Body Combinations*, NACA TR 1088, 1952.
26. Douglas Aircraft Co., Inc., **USAF Stability and Control DATCOM**, revisions by Wright Patterson Air Force Base, July 1963, 2 vols.
27. Nielsen, J. N., **Missile Aerodynamics**, the McGraw-Hill Book Company, Inc., New York, 1960.
28. Kelly, H. R., Thacker, R. G., *The Effect of High Spin on the Magnus Force on a Cylinder at Small Angles of Attack*, NAVORD Report 5036, February 1956.
29. Martin, J. C., *On Magnus Effects Caused by the Boundary Layer Displacement Thickness on Bodies of Revolution at Small Angles of Attack*, Ballistic Research Laboratories Report No. 870, June 1955.
30. Sedney, R., *Laminar Boundary Layer on a Spinning Cone at Small Angles of Attack*, Ballistic Research Laboratories Report No. 991, September 1956.

31. Vaughn, H. R., Reis, G. E., *A Magnus Theory for Bodies of Revolution*, SC-RR-720537, January 1973.
32. Sokol, C. R., *Dynamic Stability of Three Low Drag Projectiles*, Naval Weapons Laboratory Report No. TR-3027, August 1973.
33. Platou, A. S., Nielsen, G. I., *The Effect of Conical Boattails on the Magnus Characteristics of Projectiles at Subsonic and Transonic Speeds*, BRL R1720, 1974.
34. Holmes, J. E., Regan, F. J., Falusi, M. E., *Supersonic Wind-Tunnel Magnus Measurements of the 7-, 8-, 9-, and 10-caliber Army-Navy Spinner Projectile*, Naval Ordnance Laboratory TR 68-172, 1968.
35. Craft, J. C. and Skorupski, J., *Static Aerodynamic Stability Characteristics of Munitions Designs at Transonic Mach Numbers*, U. S. Army Missile Command, Redstone Arsenal, Alabama, 1973.
36. Purvis, J. W., *Lifting Surface Theory Calculations of Aerodynamic Wing-Tail Load Distributions During Subsonic Maneuvers*, NWL-2787, 1972.
37. Bland, W. M., Jr., Sandahl, C. A., *A Technique Utilizing Rocket-Propelled Test Vehicles for the Measurement of the Damping in Roll of Sting-Mounted Models and Some Initial Results for Delta and Unswept Tapered Wings*, NACA TN 3314, 1955.
38. Bolz, R. E., Nicolaides, J. D., *A Method of Determining Some Aerodynamic Coefficients from Supersonic Free-Flight Tests of a Rolling Missile*, Journal of the Aeronautical Sciences, Vol. 17, No. 10, October 1950, pp. 639-621.
39. Oberkampf, W. L., *Theoretical Prediction of Roll Moments on Finned Bodies in Supersonic Flow*, AIAA Paper No. 74-111.
40. Sanders, E. C., Jr., Edmondson, J. L., *Damping in Roll of Rocket-Powered Test Vehicles Having Swept, Tapered Wings of Low Aspect Ratio*, NACA RM L51G06, October 1951.
41. Edmondson, J. L., Sanders, E. C., Jr., *A Free-Flight Technique for Measuring Damping in Roll by Use of Rocket-Powered Models and Some Initial Results for Rectangular Wings*, NACA RM L9101, 1949.
42. Chadwick, W. R., Sylvester, J. F., *Dynamic Stability of the 5-Inch/54 Rocket Assisted Projectile (The Influence of a Nonlinear Magnus Moment)*, NWL TR-2059, October 1966.

43. Ohlmeyer, E. J., Pepitone, T. R., *Transonic Magnus Characteristics of Two Low Drag Projectile Configurations*, NWL TR-2586, November 1971.
44. Whyte, R. H., *Effects on Boattail Angle on Aerodynamic Characteristics of 175mm M437 Projectile at Supersonic Mach Numbers*, PATM 1646, September 1965.
45. Donovan, W. F., *Free-Flight Range Tests of the 5-Inch/38 Rocket Assisted Projectile (Inert)*, BRL MR 2071, November 1970.
46. Boyer, E. D., *Aerodynamic Properties of the 90mm M-71 Shell*, BRL MR 1475, April 1963.
47. Krial, K. S., McAllister, L. C., *Aerodynamic Properties of a Family of Shells of Similar Shape - 105mm XM 380E5, XM 380E6, T388 and 155mm T387*, BRL MR 2023, February 1970.



## VI. NOMENCLATURE

$AR$	Aspect ratio.
$b$	Wing span (does not include body radius).
$c$	Chord length at any point along span.
$C_{D0}$	Zero lift drag coefficient.
$C_{\ell}$	Rolling Moment Coefficient of wing planform.
$c_{\ell}$	Local rolling moment of a given airfoil section.
$C_{\ell p}$	Roll damping moment coefficient $[C_{\ell}/(p\ell_{ref}/2V_{\infty})]$ .
$C_M$	Pitching moment coefficient measured about nose tip (positive nose up).
$C'_{M\alpha}$	Pitching moment coefficient derivative $(dC_M/d\alpha)$ .
$C_{m\dot{q}} + C_{m\alpha}$	Total damping in pitch derivative.
$C_N$	Normal force coefficient.
$C_{N\alpha}$	Normal force coefficient derivative $(dC_N/d\alpha)$ .
$C'_n$	Local loading of an airfoil section at a spanwise station $y$ due to rolling velocity $p$ .
$C'_{np}$	$\frac{dC'_n}{d(P\ell_{ref}/2V_{\infty})}$
$C_{np\alpha}$	Magnus moment coefficient derivative.
$C_{yp\alpha}$	Magnus force coefficient derivative.
$C_p$	Pressure coefficient.
$(\Delta C_p)$	Difference in pressure coefficients of upper and lower surfaces of wing planform.
$(\Delta C_p)_p$	Difference in pressure coefficients of upper and lower surfaces of wing planform due to a rolling velocity, $p$ .

$d$	Body diameter.
$\ell_{ref}$	Reference length (body diameter for wing-body configuration).
$\ell_{BT}$	Boattail length.
$M$	Mach number.
$m$	$\beta \cot \Lambda_1$ .
$n$	Number of tailfins.
$p$	Roll velocity.
$q$	Pitch velocity.
$r_b$	Body Radius.
$r_n$	Body nose radius.
$u, v, w$	Perturbation velocities in $x_0, y_0, z_0$ directions, respectively.
$V$	Total velocity.
$x, y, z$	Transformed coordinates.
$x_0, y_0, z_0$	Rectangular coordinate system with $x$ at nose tip, $y$ out right wing, and $z$ positive up. If configuration consists of wing only, $x$ begins at wing root chord.
$x_a, y_a$	Coordinates of wing tip.
$\alpha$	Angle of attack.
$\beta$	$\sqrt{M^2 - 1}$ .
$\delta$	Canard deflection (degrees).
$\eta$	Howarth-Mangler variable.
$\theta_{BT}$	Boattail angle.
$\Lambda_i$	Sweepback angle of a wing generator ( $i = 1, 2, 3, 4$ ) with $i = 1$ , the wing leading edge, and $i = 4$ the wing trailing edge.

$\lambda$  Taper ratio.

$\sigma$   $\tan \Lambda_1 (y/x)$ .

PAPER NO. 10

A REVIEW AND STATUS OF WRAP-AROUND FIN AERODYNAMICS

by

C. Wayne Dahlke  
US Army Missile Command  
Redstone Arsenal, Alabama

ABSTRACT

Results of investigations into many of the geometric and flow parameters influencing the aerodynamics of wrap-around fins are presented in this paper. Particular emphasis is placed on defining static and dynamic roll characteristics between Mach numbers of 0.3 to 3.0. Among the geometric parameters highlighted are fin span, aspect ratio, leading edge sweep, leading edge shape, fin opening angle, and afterbody geometry. Comparisons of static stability, dynamic stability, and drag are made between the flat and the wrap-around fin. Problems associated with measurement of wrap-around fin rolling moments are also discussed. An overview of the wrap-around fin roll moment characteristics are presented as an aid for making estimates and establishing testing techniques.

## 1. INTRODUCTION

During the last (9th) Navy Symposium on Aeroballistics a paper<sup>1</sup> was presented on wrap-around fins (WAF) with particular emphasis on data from WAF panel pressure tests. This paper presented a discussion of the general need the military services have for more knowledge of the unique behavior of the aerodynamics for WAF. It also noted that this interest was stated by members of the Technical Cooperation Program (TTCP) Panel 0-7, and through encouragement by this panel the various organizations represented were to take part of the task for studies of the WAF. As part of this study, the US Army Missile Command (MICOM) and the Air Force Armament Laboratory (AFAL) took the task of obtaining static force measurements for the agreed upon standard configuration WAF. The Army has been interested in missile designs that have tube-launched applications. It was found that the need was much broader than the TTCP configuration. The TTCP standard configuration was used as the basic configuration from which many fin geometric variations were made. The immediate needs were considered, and while it would be useful to have an analytical model to describe the flow phenomena defining the unique WAF aerodynamic forces, it would be more beneficial to define the characteristics through more of a brute force parametric investigation. It was hoped that this study would provide sufficient data, along with the Navy pressure data and data from the other agencies involved, to begin development of an analytical model. However, the tests used for this study were designed primarily to uncover

characteristics and provide trends that can be used in missile design where the analytical models are not available.

This paper contains a condensed summary of the findings from wind tunnel tests conducted, with important characteristics and trends highlighted. The data are presented with comparison of several of the parameters in an attempt to illustrate those parameters that have the largest effect upon the WAF rolling moment coefficient. Problems associated with measurement of WAF roll moment coefficients using conventional techniques are mentioned. The overall objective of this WAF effort has been to provide the weapon designer with adequate information to make confident aerodynamic estimates for preliminary design studies. Based upon present data, the intermediate objective is to provide the missile designer with aerodynamic guidelines for estimating WAF effects and the direction for improving experimental approaches.

## 2. MODELS AND EXPERIMENTAL TEST

MICOM and AFAL undertook the study of fins and afterbody geometric effects on the static rolling moment characteristics of WAF, as agreed to in the initial planning of the cooperative program. Fin geometry was varied around the standard WAF shown in the Arnold Engineering Development Center's (AEDC) 4-T wind tunnel in Figure 1. The models consisted of a 2-caliber secant ogive nose with an 8-caliber cylindrical afterbody with 3 afterbody shapes and fin configurations. The basic body configuration had a straight cylindrical afterbody, (4 inches in diameter) and two alternate afterbody shapes stepped

Vol. 1

down to a diameter of 3.6 inches over a length of 7 and 4 inches, respectively, from the base (Figure 2).

The exposed semispan  $b/2$  for the WAF was chosen to be approximately the chord length for the arc that encloses a quadrant of tubular body cross section or  $0.707D$  (Figure 3 and Table 1). These variations (Table 1) included two larger aspect ratios (same span as standard WAF with shorter chords of 2.0 and 4.0 inches), two smaller thickness ratios, four different leading edge shapes, seven leading edge sweep angles, one tip alteration, two shorter span fins, one fin body gap, and several fins tested on a step down body configuration (Figure 2). Also, for the standard WAF, and investigation of fin opening/closing angle was conducted for seven opening positions ranging from fully closed to  $10^\circ$  beyond the standard fully opened case. Static aerodynamic measurements, including total airframe and individual fin force and moment characteristics, were conducted in three wind tunnel facilities. The majority of transonic tests were carried out in the AEDC 4-foot transonic wind tunnel, while the majority of supersonic tests were conducted in the NASA Langley 4-foot unitary plan wind tunnel. Limited transonic and supersonic tests were conducted in the McDonnell Douglas Aerophysics 4-foot trisonic wind tunnel. In addition, limited roll damping characteristics were conducted in the AEDC 4-foot transonic facility and both subsonic and supersonic free flight tests were conducted in the Jet Propulsion Laboratory (JPL) 20-inch supersonic wind tunnel for the standard WAF configuration and its equivalent planar fin (Figure 4). Test variables for the

static aerodynamic tests are listed in Table 2 for the varying geometry tests. In addition to these MICOM/AFAL sponsored tests to specifically study the WAF effects, several projects have considered use of the WAF, some are listed by Holmes<sup>1</sup> and others are briefly mentioned in this paper. A more complete description of the models and testing conducted by MICOM is contained in other reports.<sup>2-5</sup>

### 3. TESTING TECHNIQUES AND ACCURACY

There are questions concerning the accuracy and repeatability of the rolling moment coefficient data. The magnitude of the self-induced rolling moment coefficients of the WAF are small in relation to the size of the coefficients of fins with large cants. The only ready means of obtaining force data in a wind tunnel is with a strain gage balance. The balance must be sized to meet special requirements, but it must be capable of handling the forces and moments of the complete model in the test facility to be used. To obtain sensible rolling moment coefficients induced by WAF, wind tunnel dynamic pressure and fin sizes must be made large within practicable limits. Both cause larger aerodynamic loads on the model which results in requirements of larger strain gage balances. To date, strain gage balances and associated instrumentation are not ideal for measurement of these small rolling moments; however, from the available balances one can be chosen that is optimum for given requirements. A composite plot of rolling moment data precision is shown in Figure 5. At transonic speeds, the rolling moment gage was large because of the requirements dictated by normal force and pitching moment loads. As a result the



data precision, as quoted by AEDC<sup>2,3</sup> are larger than desirable; however, as shown later, the repeatability from duplicate points during the same test and from separate entries show that the data are reproducible well within these precision limits. An attempt was made to measure the cant of each fin during the transonic test<sup>2,3</sup>. These measurements of 76 fin installations had a mean cant of  $0.011^\circ$  with a standard deviation of  $0.142^\circ$ , with a quoted measurement accuracy of  $\pm 0.1^\circ$ . If all four fins for one configuration have a  $0.1^\circ$  cant, the rolling moment coefficient would be 0.004 to 0.010 which is within the quoted (Figure 5) data precision for the subsonic/transonic test. Because of the uncertainty of the cant measurements and the small magnitude of fin cant-induced rolling moment relative to the data precision, corrections to rolling moment coefficient caused by fin cant are not presented.

Several comparisons were made from the numerous duplications and other geometric similarities. Figure 6 shows a comparison of the 1.0-caliber chord WAF configuration tested on the straight body with four main balances and in three different facilities. A separate test<sup>5</sup> was conducted explicitly to check the rolling moment obtained in an earlier test<sup>2</sup> at transonic speeds. This test was conducted with a balance that had a 100-in./lb roll moment gage. The normal force and pitching moment gages were also low capacity and angle of attack was restricted to less than  $2^\circ$ . The main purpose of this test was to observe the self-induced WAF rolling moment coefficient at zero angle of attack, and compare these to previously obtained coefficients with

the less sensitive balance. Comparisons of this repeat test are shown in Figure 6 by the square symbol.

Another method used to validate the rolling moment data was to compute rolling moment coefficient from the four fin panel balances. These are shown by the flagged symbols on Figure 7 along with the main balance data for the TTCP standard WAF. Fin cant can produce roll moments equally as large as any WAF-induced roll moment observed during all tests. Included on Figure 6 is the roll moment coefficient for a typical tactical hardware fin tolerance of  $\pm 0.1^\circ$ . The overall value of this analysis is to indicate the difficulty in obtaining the precise magnitudes that a WAF may exhibit with flight hardware; however, the trends shown and those in the following sections are realistic. To obtain the accuracy of the magnitudes desired will require extreme care in model fabrication and sophisticated measurement techniques tailored for precise roll moment measurement.

#### 4. COMPARISON OF WAF TO FLAT FIN STABILITY AND DRAG

The major concern of the effects of WAF has been the self-induced rolling moment; however, a comparison of static stability parameters was made for a flat fin and standard WAF. The flat fin had the same total exposed span and projected area as the WAF. These two fins were tested through the Mach number range of 0.3 to 3.0 on a body of revolution. The normal force coefficient slope at zero angle of attack and the center of pressure are shown in Figure 8 for the flat fin and WAF. Any difference in total configuration static stability coefficients appears to be within the uncertainty of measurement accuracy.

Vol. 1

Included on the center of pressure data are points from the JPL free flight bi-planar results at Mach 0.86, 2.0, and 3.03. Similar results were obtained from a comparison of data for the flat fin and WAF tested on a splitter plate at transonic speeds and from body mounted fin panel data.

Drag coefficient comparisons between the flat and WAF configurations are shown on Figure 9. The upper portion shows the drag force coefficient for body alone, the WAF and body, and the flat fin (of equal projected area to the WAF) and body. The lower portion shows the same data with the body alone (drag subtracted out). The WAF is approximately 10% higher which corresponds to the additional frontal area that the WAF has because of the curvature. The other geometric parameters (leading edge sweep, thickness, leading edge shape, and aspect ratio) shown their influence on drag to be as expected for flat fins with the same geometric changes.

#### 5. ROLLING MOMENT COEFFICIENT

The main objective for this study was to investigate the effects on WAF rolling moment due to the various geometric and flow parameters. The variation of rolling moment is considered for three flow parameters: Mach number, Reynolds number, and angle of attack for several geometric variations. Featherstone<sup>6</sup> et al.<sup>7</sup> have shown the WAF to have self-induced normal forces at zero angle of attack. The most significant effect with Mach number appears to be at transonic speeds where, in general, a change in sign occurs for rolling moment. In initial studies, Featherstone has suggested the self-induced force is

directed toward the center of curvature at subsonic speeds and away from the center of curvature at supersonic speeds with the crossover occurring close to  $Mach = 1$ . This was demonstrated for those fin configurations on smooth body with a  $C_R/D = 1.75$  with the exception of the fin with maximum thickness  $t/C = 0.045$ . This trend exists for fins with rectangular and trapezoidal planforms, for leading edge profile modification, and for modifications to the root chord (gap fin) and the tip chord.

The various parameters are arranged into two groups: those of most importance as determined from analysis of existing data, and those that show lesser effect over the range and within the constraints of data available. It is difficult to isolate and illustrate many specific parametric effects without pointing out the influence of another parameter. There is also the case of the influence of Reynolds numbers which, at this time, is not clearly shown to be an important parameter with the exception of the otherwise unexplained difference between the crossover point shown by the JPL free flight data and the results from static test. Grit was used as boundary layer trips on the body of JPL models, but grit was not used on fin leading edges which Mr. Jaffe (JPL) and this author agree may have been a mistake. The effect of three parameters are shown on Figure 10 for the standard TTCP WAF. The Reynolds numbers vary from 7 to  $40 \times 10^6$  based on body length for the static test and for the JPL models was  $2.5 \times 10^6$ . As can be seen, the effect of  $R_N$  on smooth and step down body, except for JPL, show differences well within data accuracy. Illustrated on this

Vol. 1

same curve is the variation of rolling moment with Mach number and the difference of trends with a smooth body and a step-down body which may more realistically simulate flight hardware hinge recesses. More information will be presented for the Mach number and body with step down later in this paper.

Other parameters which appear to have lesser influence on the WAF rolling moment are leading edge sweep and fin thickness (Figure 11). The surprising result from the leading edge sweep data is the level of magnitude, and the trend with Mach number appears very much the same as the rectangular fin with the same root chord length. The effect of modifying the leading edge shape is shown in Figure 12. There is a large change in roll moment, as expected, with the unsymmetrical leading edge. This may be related to regimes of subsonic and supersonic leading edge due to detached and attached shocks over the curved fin, which is neither an axisymmetric body of revolution or a two-dimensional surface. The symmetrical leading edge variation with included angles of  $20.0^\circ$ ,  $45.0^\circ$ , and blunt shown an effect, but is incomplete at this time. Navy WAF pressure data<sup>1</sup> have shown the leading edge pressure difference between the convex and concave side to be larger than any other chordwise location except  $M = 1.3$  data which show the largest difference to occur at approximately 31% chord from leading edge. Unfortunately neither the  $20^\circ$  or blunt leading angles have been tested supersonically. However, as presented by Featherstone<sup>6</sup>, this leading edge pressure effect may be an inlet phenomena due primarily to fin curvature and not influence

significantly by leading edge shape of fin thickness. Figure 13 presents the rolling moment coefficient for three rectangular planform WAF's with different chord length, therefore, having different aspect ratios. The primary influence seems to be the fin body juncture geometry and/or boundary layer, which in this case is fin root chord length rather than aspect ratio. Aspect ratio was also varied by sweeping the leading edge. The leading edge for the  $C_R/D = 1.75$  was swept up to  $60^\circ$ , and for  $C_T/C_R = 0.0$ , a delta planform. From these variations it is shown<sup>2</sup> that data with like chord length tend to look similar and that the effect seen in Figure 13 is a subsonic fin-body juncture (chord) length effect.

One of the most significant changes in WAF rolling moment coefficient occurs with variation of angle of attack. The roll producing force increases with angle of attack at all Mach numbers and missile roll orientation and is directed toward the fin away from the fin center of curvature. Figure 14 presents the WAF compared to the flat fin at supersonic Mach numbers from the Langley and McDonnell tests. This trend was shown to be essentially unchanged with missile roll attitude with fins of equal exposed span and to a lesser extent at subsonic Mach numbers<sup>3,4</sup>. Navy Zuni data have also demonstrated this phenomena and it has been shown by Stevens<sup>8</sup> that this driving moment may be a useful design tool for avoiding roll-yaw resonance problems during missile flight.

The span for all but two WAF's tested had nearly equal exposed semispans of 0.66 body diameters. These two had shorter spans of

0.54 and 0.35, respectively. The zero angle of attack rolling moments are shown at supersonic Mach numbers (Figure 15). Significant reductions in induced rolling moments occur at Mach numbers above two for WAF's with spans less than a quarter circle. This suggests the possibility of tailoring the induced rolling moment variation with Mach number by varying the fin radius of curvature. This design procedure is only allowed when adequate space exists around the rocket nozzle to the fin curvature to depart from the body surface. The variation with angle of attack and missile roll attitude are shown in Figures 16 and 17 for the three spans. There are two significant effects that should be pointed out. There appears to be much less variation with angle of attack induced with shorter span WAF (Figure 16); however, at the supersonic Mach numbers, roll moment will be dominated by body vortex and span (Figure 17). The interaction is not necessarily unique to the WAF but is related to the relative position of the body vortex core at angle of attack, fin span, and missile roll attitude, where the fin arrangement is not symmetrical at angle of attack (e.g.,  $\phi = 22.5^\circ$ ).

The step-down body effect is probably the most significant trend that must be considered in WAF designs requiring a hinge recess and/or body step-down geometry. The standard WAF is shown on the smooth and step-down body in Figure 10. All symmetrical leading edge fins on the smooth body show only one crossover point for Mach numbers less than 3.0, but the step-down body demonstrated an additional crossover at low supersonic Mach numbers and is opposite to the Featherstone

postulation that the force at supersonic Mach numbers is directed away from the WAF center of curvature. Two additional fins that show this are shown in Figure 18. These fins have a 1-caliber root chord, one is rectangular and the other has a  $20.6^\circ$  swept leading edge. The Navy Zuni missile has a fin recess that resembles the MICOM step-down body. The available Zuni aero-roll moment coefficients from the Naval Ship Research and Development Center (NSRDC) and Ames Research Center are shown compared to the standard WAF on the step-down body (Figure 19). The sign on the Zuni data has been reversed because of the  $180^\circ$  fin curvature difference. The flow mechanism that causes this trend may be the key toward development of supersonic analytical methods.

#### 6. SIDE FORCES AND MOMENTS

It has been suggested<sup>7</sup> that in addition to induced rolling moments, the WAF causes side force and moment variations with pitch angle of attack. A typical comparison between flat and WAF at supersonic Mach numbers is shown as a function of angle of attack in Figure 20. Nothing was observed during this series of testing that substantiates the generation of cross derivatives of significant magnitude over the angle of attack range  $\pm 6^\circ$  contributable to cruciform WAF at subsonic and transonic Mach numbers. Small variations with angle of attack may be seen at supersonic Mach numbers as shown in Figure 20. Zuni data at Mach 3.0 are shown to have a similar trend to the MICOM data at Mach 2.86. The step-down body does not show any significant differences in side force or moment with angle of attack variation.



The same mechanism that causes large roll moment changes with short span fins at roll orientation and angle of attack also induces large yawing moments (Figure 21). This trend is not considered to be unique to the WAF and may be, as expected, a function of roll orientation especially at angles of attack at supersonic Mach numbers that cause body vortex cores to rise to fin tip and for fin arrangement such as three fins. Missile roll rate will tend to average out this phenomena and usually will not present a problem in flight. Outside of this effect, cruciform WAF's do not appear to have significant cross derivatives except possibly at Mach numbers above 2.5.

#### 7. OPENING ANGLE

The standard WAF was tested on the smooth body for seven opening/closing angles defined as fully open when a line passes the body center, the fin pivot point, and tip chord. The fin is fully closed and conforms to the body surface at  $\theta = 135^\circ$ . The test matrix is shown in Table 3. Most transonic data were obtained at AEDC, and all supersonic data were obtained at McDonnell Douglas Aerophysics Laboratory. Figure 22 presents the model with three opening angles of 0, 45, and  $90^\circ$ . Fin lift effectiveness (Figure 23) is shown for three Mach numbers over the range of closing angles tested. Lift effectiveness is defined as the ratio of the fin normal force at a given closing angle  $\theta$  to the fin normal force at the fully open case  $\theta = 0.0$ . The fin center of pressure appears to be essentially invariant with closing angle and is a function only of Mach number as for the fully open case. A geometric fit of  $\cos^{2/3} \theta$  is shown in

comparison to the fin lift effectiveness. Figure 24 shows the zero angle of attack rolling moment variation with closing angle for Mach 0.8 to 3.0. No large influence was noted for small variations and, at any given angle, appear to follow the roll moment variation with Mach number as the fully open case does.

#### 8. WAF ROLL DYNAMICS

Tests were conducted where roll damping was measured for several fin configurations. Included in this was a comparison between a flat fin and the standard WAF. These data are in a MICOM report<sup>9</sup>. The model was spun up in the wind tunnel by an internal hydraulic motor. At a prescribed roll rate, the motor clutch was released and the model was allowed to free spin until the steady state roll rate was reached. Roll damping for one of the WAF's and one flat are shown to vary little (Figure 25). Theoretical calculations of  $C_{\ell\rho}$  by modified slender body theory are shown to be good except at transonic speeds.

A three phase investigation was conducted by JPL. Several small scale models were flown in the JPL 20-inch wind tunnel. Some were flown solely for obtaining rolling moment and roll damping coefficients, others were flown for a bi-planar dynamic investigation. A sting-mounted free spinning test was conducted initially to observe the roll direction of models with WAF as a function of Mach number. Data for the standard WAF and equivalent flat fin from the AEDC spinning test, theoretical estimate, and the JPL free-flight data for the flat and WAF are shown on Figure 26. The JPL data points have too much scatter for a thorough analysis. Even though some had initial

Vol. 1

roll rates with and against the fin fold direction, the scatter prohibits definition of roll damping for spin in any given direction.

Future flight testings are being studied for the Ballistic Research Laboratory ballistic range.

9. CONCLUSIONS

The general characteristics of a number of WAF's on a body of revolution at Mach numbers 0.3 to 3.00 have been presented. The effects of geometric and flow parameters are summarized in the following statements:

a) The static stability derivatives at  $\alpha = 0$  of missiles with WAF's are essentially the same as with equivalent planar fins and may be estimated by using the flat fin techniques.

b) Drag of the WAF is larger than the flat fin with the same projected planform area. This increase is approximately a factor of 1.1, for the fins tested, which corresponds to the increase in frontal area of the WAF over the flat fin.

c) The WAF does induce roll moment to the missile at zero angle of attack and zero fin cant. This self-induced roll moment can change direction as a function of Mach number shown, from static data, to crossover near Mach 1.0 for smooth bodies. The parameter appearing to influence the subsonic roll moment most is the fin root chord length, indicating a fin-body juncture effect.

d) Step downs on the afterbody, simulating a fin hinge recess, show additional crossover of the WAF-induced roll moment at supersonic Mach numbers from 1.2 to 3.0.

e) The WAF rolling moment variation with total missile angle of attack is small for absolute angles of attack less than  $2^\circ$ . Above  $2^\circ$  the rolling moment may deviate significantly from the zero angle of attack case depending upon fin geometry and Mach number.

f) Cross derivatives induced by the WAF do not appear to be significant at Mach numbers below 2.5. This may not be the case for Mach numbers above 2.5, for three-fin configurations, WAF configurations where fin opening directions are alternated, or higher angles of attack.

g) Accurate measurement of WAF rolling moment requires sensitive roll moment measurement instrumentation and small tolerance on the individual fin geometric incidence.

h) The WAF moments do not appear to be intolerable, and missile roll rates can be tailored by proper geometric design and fin incidence for many applications.

TABLE 1. FIN CONFIGURATION SUMMARY

Configuration	A (in.)	C <sub>R</sub> (in.)	C <sub>T</sub> /C <sub>R</sub>	Λ (deg)	t (in.)	R <sub>1</sub> (in.)	R <sub>2</sub> (in.)	R <sub>3</sub> (in.)	δ* (deg)	r (in.)	AR	b/2 (in.)
F <sub>1</sub> **	1.900	7.0	1.00	0	0.200	1.900	2.000	1.800	45	0.008	0.75	2.64
F <sub>2</sub>		4.0			0.114		1.957	1.843			1.30	2.60
F <sub>3</sub>		2.0			0.057		1.929	1.871			2.60	2.60
F <sub>4</sub>		7.0			0.200		2.000	1.8000	①		0.76	2.64
F <sub>5</sub>									20		0.76	2.64
F <sub>6</sub>									②		0.76	2.64
F <sub>7</sub>					0.107		1.953	1.847	45		0.76	2.64
F <sub>8</sub>					0.315		2.058	1.743			0.76	2.64
F <sub>9</sub>	2.000				0.200	③					0.75	2.64
F <sub>10</sub> ④	1.900					1.900	2.000	1.800				2.44
F <sub>11</sub>	Fin "F <sub>1</sub> " with tip chord modified						⑤				0.73	2.59
F <sub>12</sub>	1.9	7.0	0.9	14.75	0.200	1.9	2.0	1.8	45		0.79	2.63
F <sub>13</sub>			0.75	33.9							0.86	2.63
F <sub>14</sub>			0.60	46.9							0.94	2.63
F <sub>15</sub>		4.0	1.00	0	0.040	1.880	1.900	1.860			1.28	2.65
F <sub>16</sub>			0.75	20.6	0.114	1.900	2.000	1.800			1.54	2.70
F <sub>17</sub>		7.0	0.36	60.0	0.200						1.11	2.63
F <sub>18</sub>		4.0	0.33	46.9	0.120						1.97	2.61
F <sub>19</sub>			0.00	57.3	0.120						2.55	2.55
F <sub>20</sub>		7.0	1.00	0	0.200						0.61	2.14
F <sub>21</sub>											0.40	1.39

\*Leading edge angle. All trailing edges δ = 45°.

\*\*Standard TTCP WAF.

① Blunt leading edge.

② Unsymmetrical leading edge.

③ Rectangular flat planform, exposed span = 2.658 in.

④ Gap fin.

⑤ Tip chord parallel to root chord.

TABLE 2. SUMMARY OF WAF STATIC TEST

Configuration	Mach No.															
	0.30	0.50	0.80	0.95	1.00	1.05	1.10	1.20	1.30	1.60	1.90	2.36	2.86	2.0	2.5	3.0
B1	●	○	●	●	●	○	●	○	●	○	○	○	○			
B1F1	▲	▲	▲	▲	▲	▲	▲	○	▲	○	○	○	○	○	○	○
B1F2	▲	▲	▲	▲	▲	▲	▲	○	▲	○	○	○	○	○	○	○
B1F3	▲	▲	▲	▲	▲	▲	▲	○	▲	○	○	○	○	○	○	○
B1F4	○	○	○	○	○	○	○	○	○	○	○	○	○	○	○	○
B1F5	○	○	○	○	○	○	○	○	○	○	○	○	○	○	○	○
B1F6	○	○	○	○	○	○	○	○	○	○	○	○	○	○	○	○
B1F7	▲	▲	▲	▲	▲	▲	▲	○	▲	○	○	○	○	○	○	○
B1F8	▲	▲	▲	▲	▲	▲	▲	○	▲	○	○	○	○	○	○	○
B1F9	○	○	○	○	○	○	○	○	○	○	○	○	○	○	○	○
B1F10	○	○	○	○	○	○	○	○	○	○	○	○	○	○	○	○
B1F11	○	○	○	○	○	○	○	○	○	○	○	○	○	○	○	○
B1F12	○	○	○	○	○	○	○	○	○	○	○	○	○	○	○	○
B1F13	○	○	○	○	○	○	○	○	○	○	○	○	○	○	○	○
B1F14	○	○	○	○	○	○	○	○	○	○	○	○	○	○	○	○
B1F15	○	○	○	○	○	○	○	○	○	○	○	○	○	○	○	○
B1F16	○	○	○	○	○	○	○	○	○	○	○	○	○	○	○	○
B2	○	○	○	○	○	○	○	○	○	○	○	○	○	○	○	○
B2F1	○	○	○	○	○	○	○	○	○	○	○	○	○	○	○	○
B2F9	○	○	○	○	○	○	○	○	○	○	○	○	○	○	○	○
B2F10	○	○	○	○	○	○	○	○	○	○	○	○	○	○	○	○
B2F13	○	○	○	○	○	○	○	○	○	○	○	○	○	○	○	○
B3F2	○	○	○	○	○	○	○	○	○	○	○	○	○	○	○	○
B3F16	○	○	○	○	○	○	○	○	○	○	○	○	○	○	○	○
B1F17	○	○	○	○	○	○	○	○	○	○	○	○	○	○	○	○
B1F18	○	○	○	○	○	○	○	○	○	○	○	○	○	○	○	○
B1F19	○	○	○	○	○	○	○	○	○	○	○	○	○	○	○	○
B1F20	○	○	○	○	○	○	○	○	○	○	○	○	○	○	○	○
B1F21	○	○	○	○	○	○	○	○	○	○	○	○	○	○	○	○

Solid symbols: zero roll angle only.

Open symbols: 0, 22.5, and/or 45° roll angle.

TABLE 3. SUMMARY OF WAF OPENING ANGLE TEST

Opening <	Mach No.													
	0.5	0.6	0.8	0.9	0.95	1.00	1.05	1.10	1.20	1.30	1.60	2.00	2.50	3.00
-10.0	▲	▲	●			◻		●	●	●	●	●	●	●
10.0	●		●			●		●	●	●	●	●	●	●
22.5	▲	▲	▲	▲	▲	▲	▲	▲	▲	◻	●	●	●	●
45.0	▲	▲	▲	▲	▲	▲	▲	▲	▲	▲	●	●	●	●
90.0	▲	▲	▲	▲										
112.5	▲	▲	◻	◻	●									

▲ - solid symbols: 0, 22.5, 45, 67.5° roll angle

● - solid symbols: 0, 22.5, 45° roll angle

Open symbols: zero roll angle only

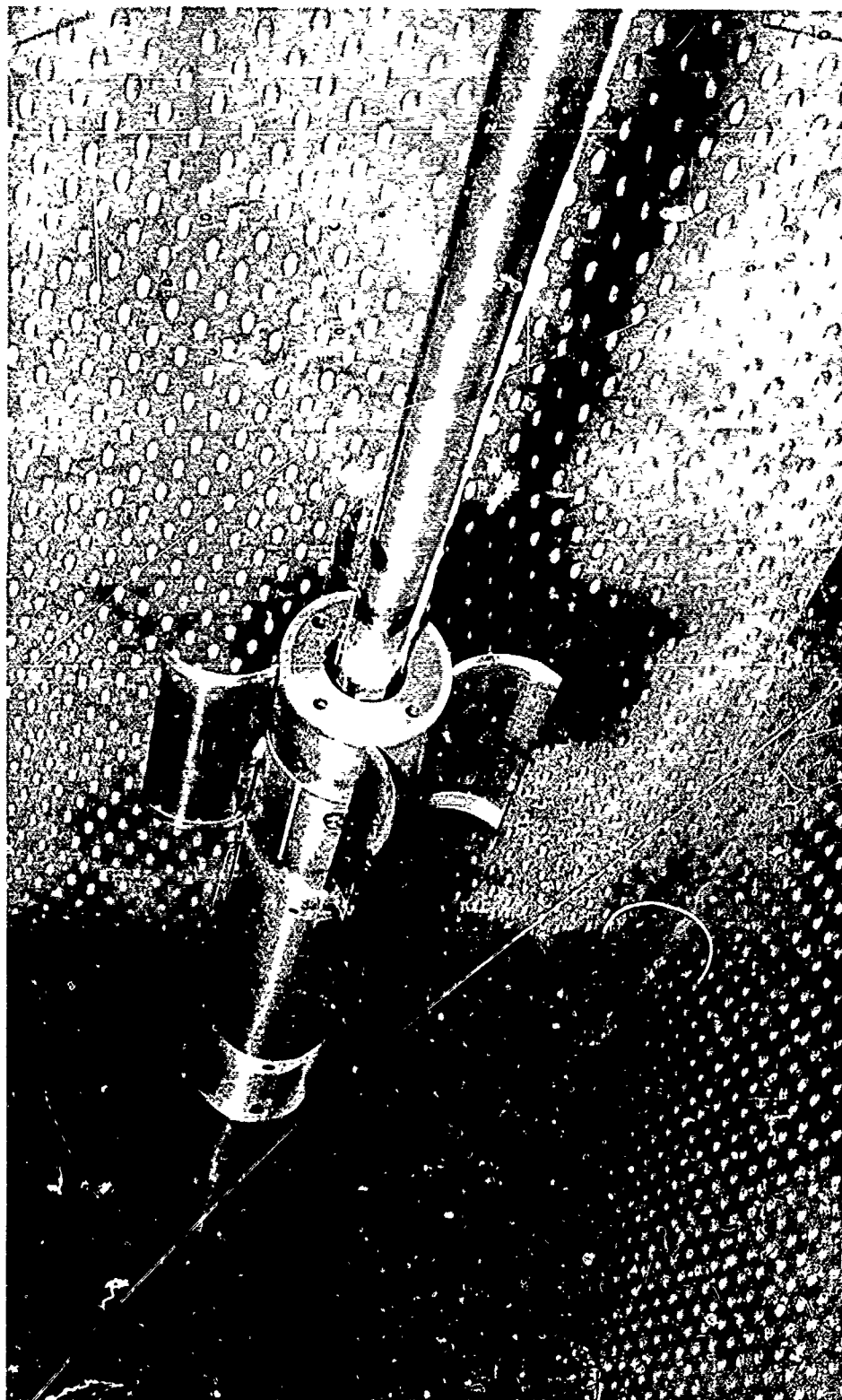


Figure 1. Standard WAF model.



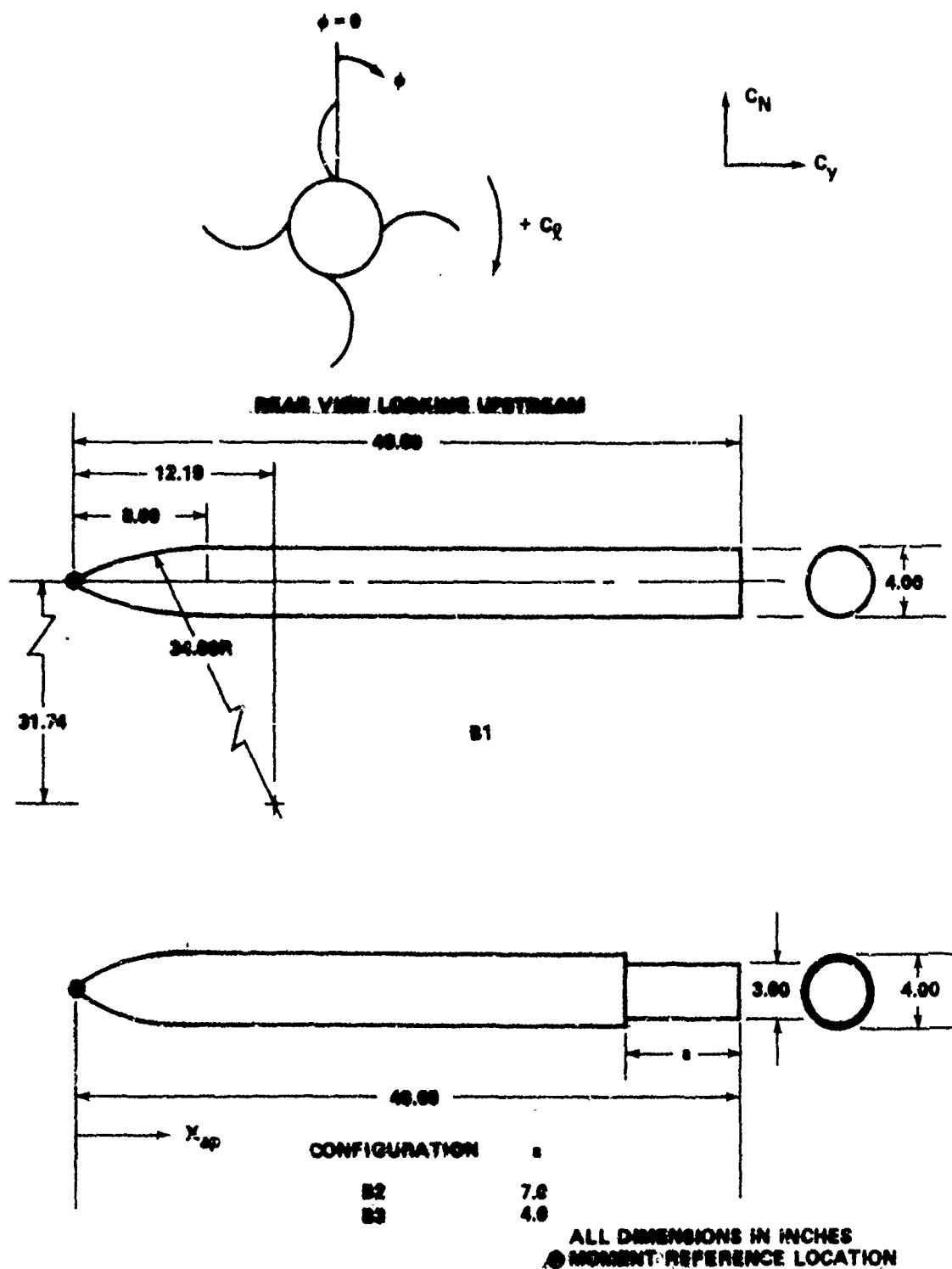


Figure 2. External body geometry.

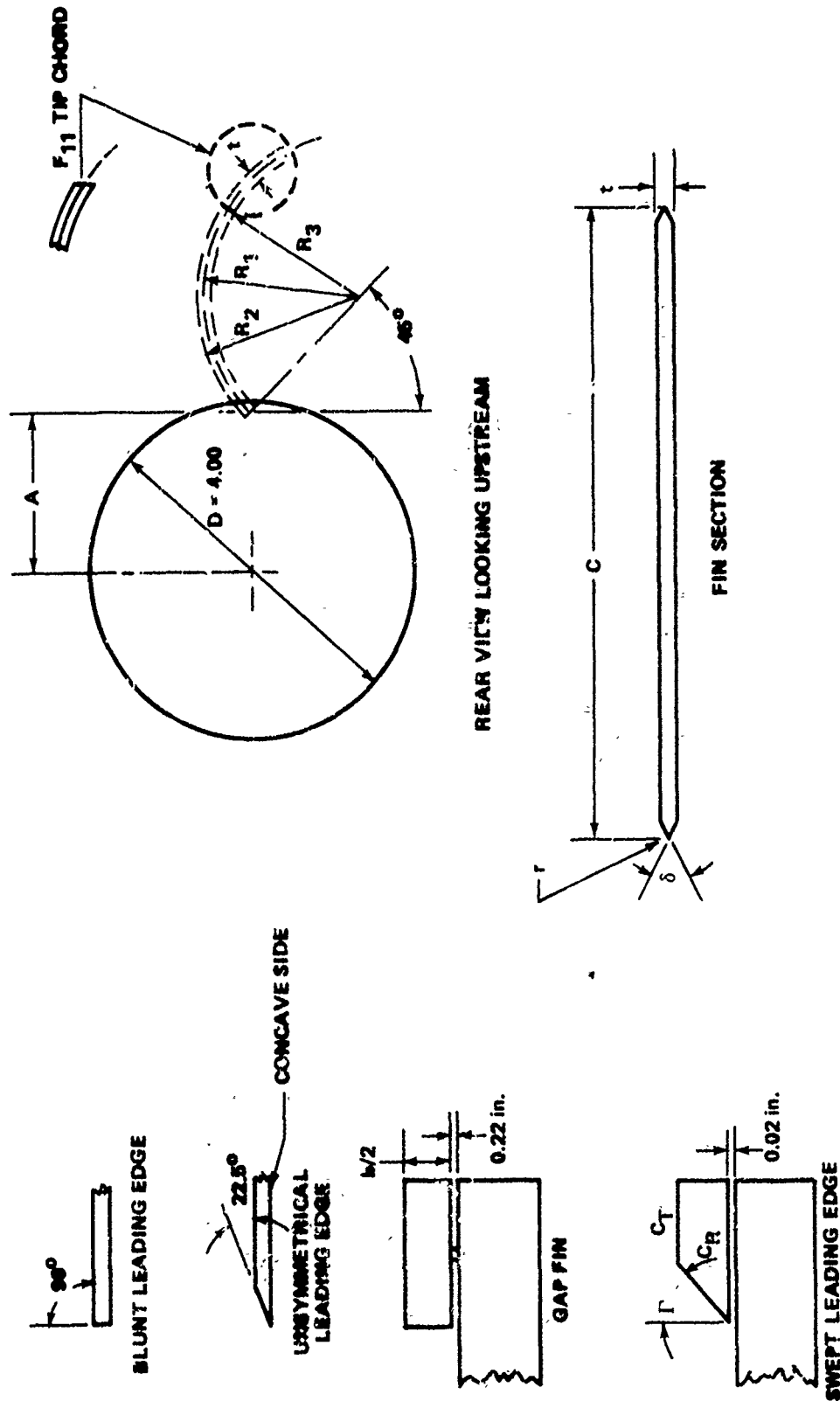


Figure 3. WAF geometry.

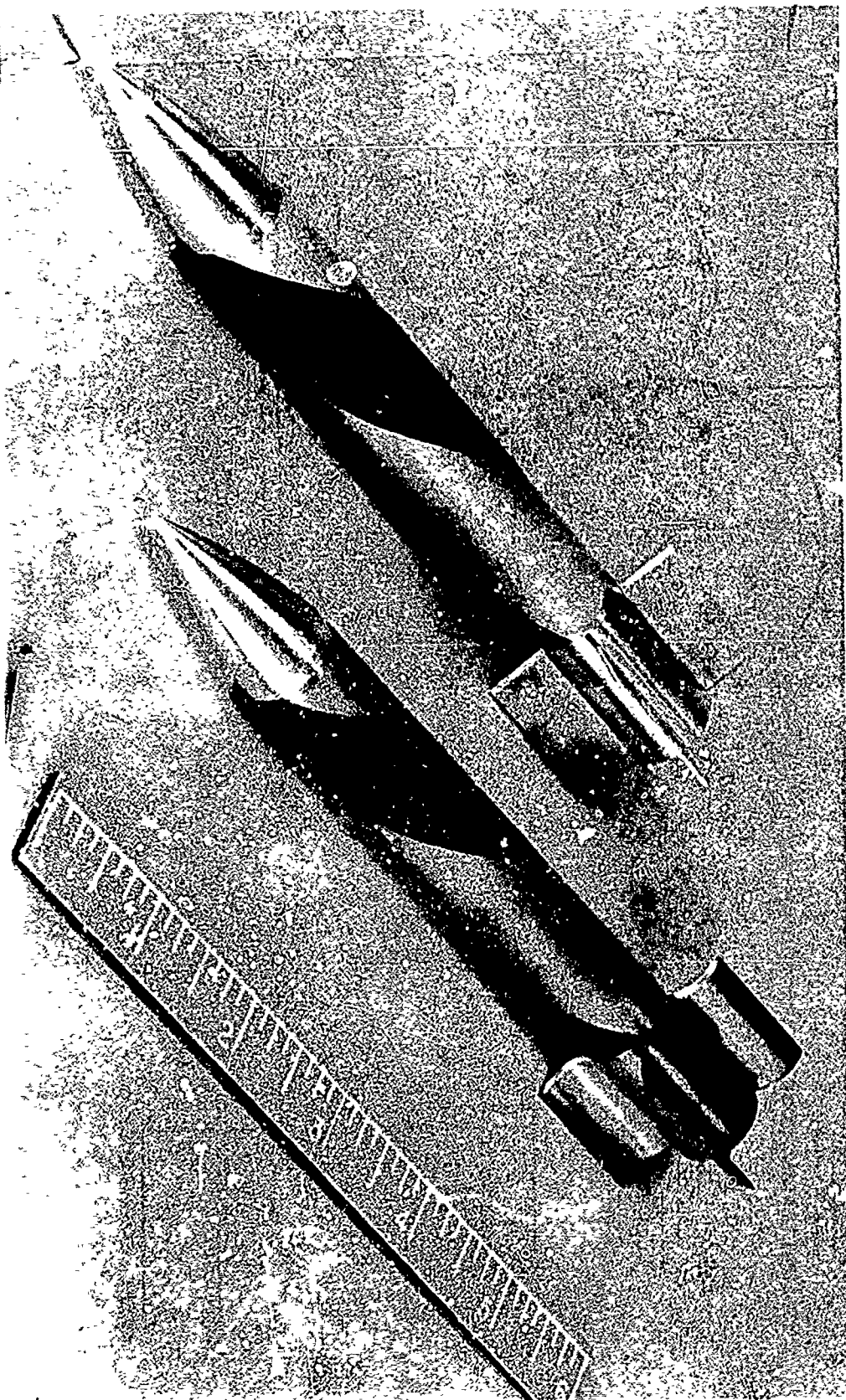


Figure 4. JPL free flight models.

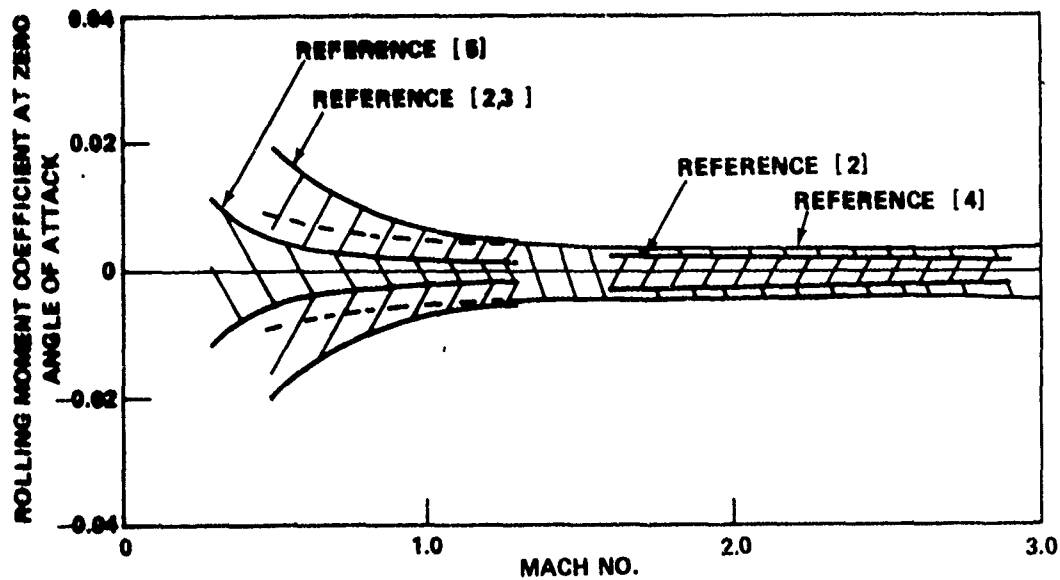
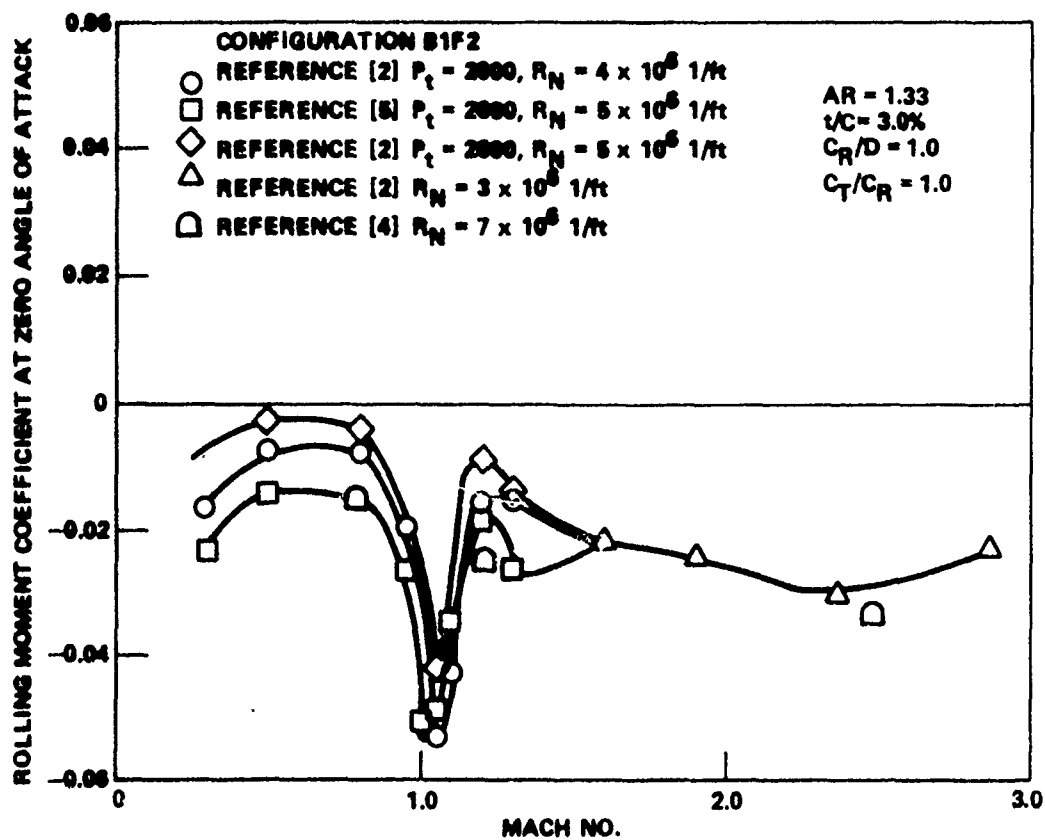


Figure 5. WAF rolling moment data precision.

Figure 6. WAF rolling moment coefficient comparisons from several tests,  $\alpha = 0$ ,  $\phi = 0$ .

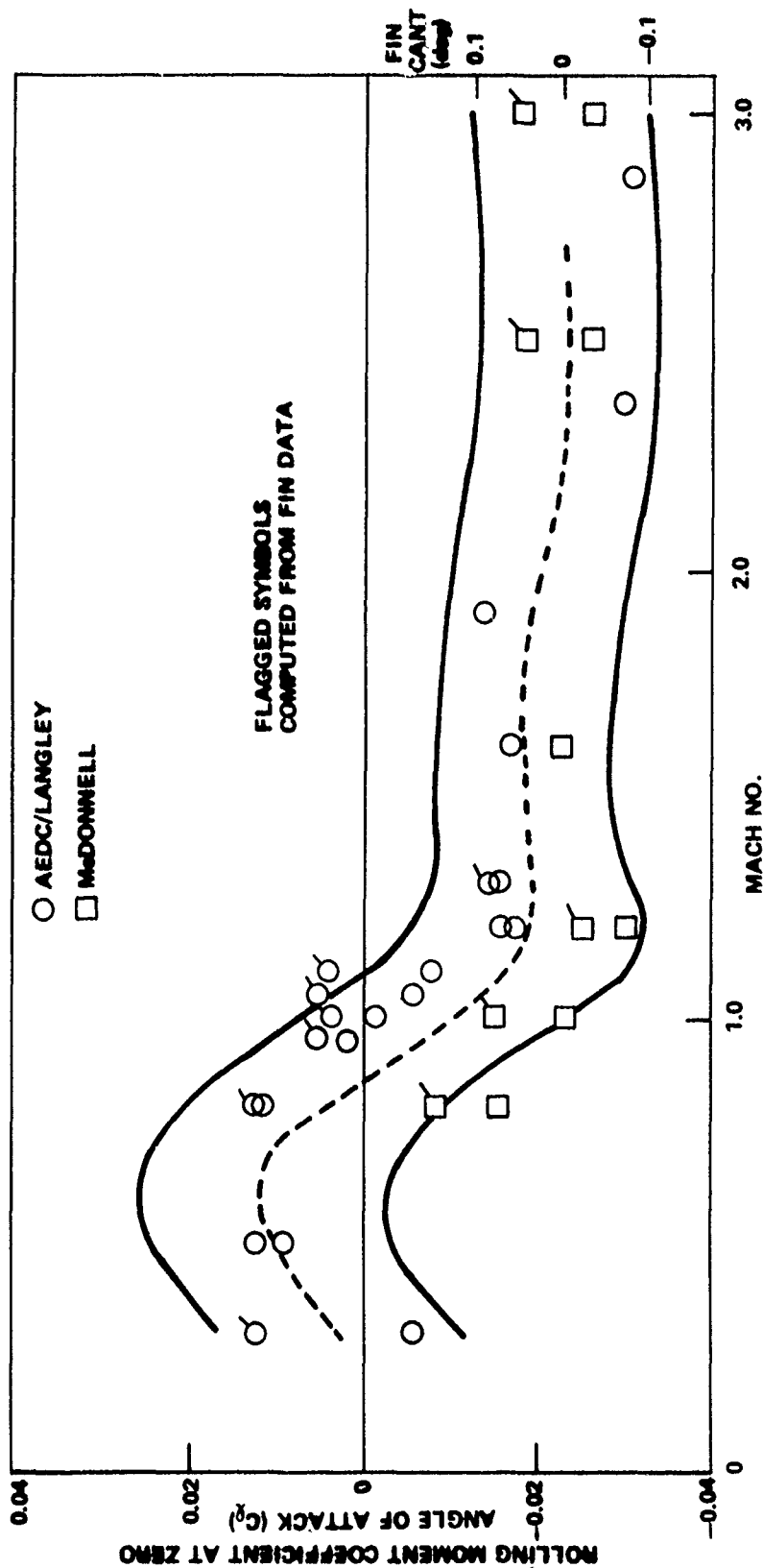


Figure 7. Comparison of data scatter to fin cant tolerance.

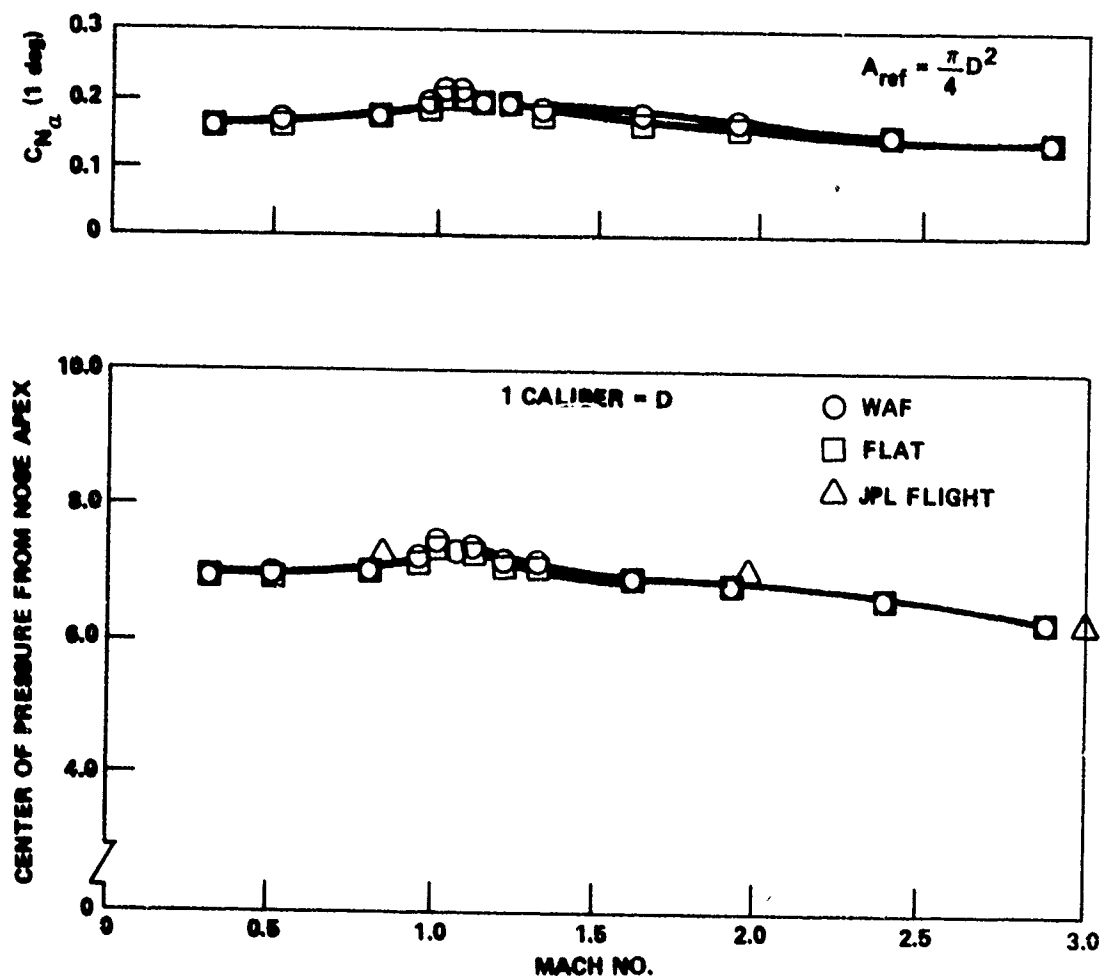


Figure 8. Comparison of flat and WAF static stability derivatives.

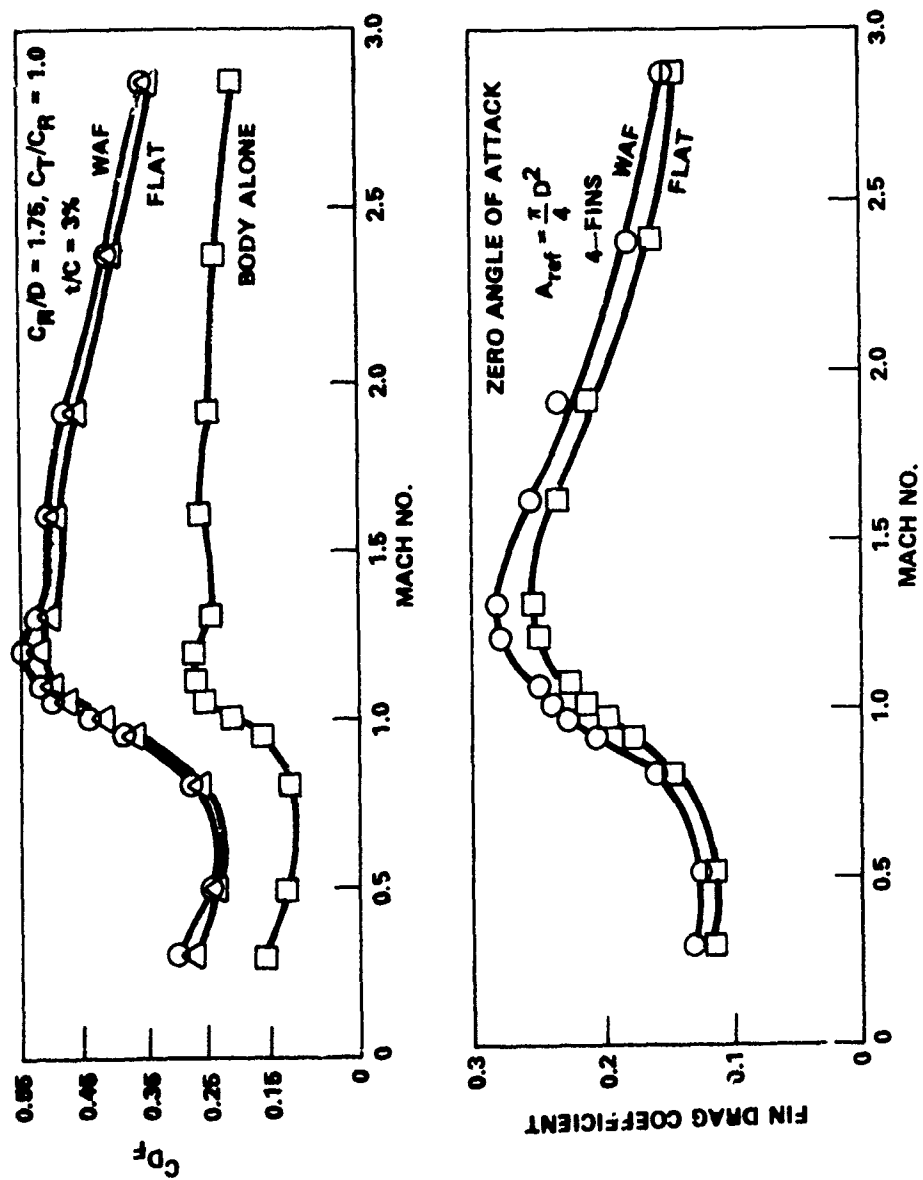


Figure 9. Comparison of flat and WAF drag coefficients.

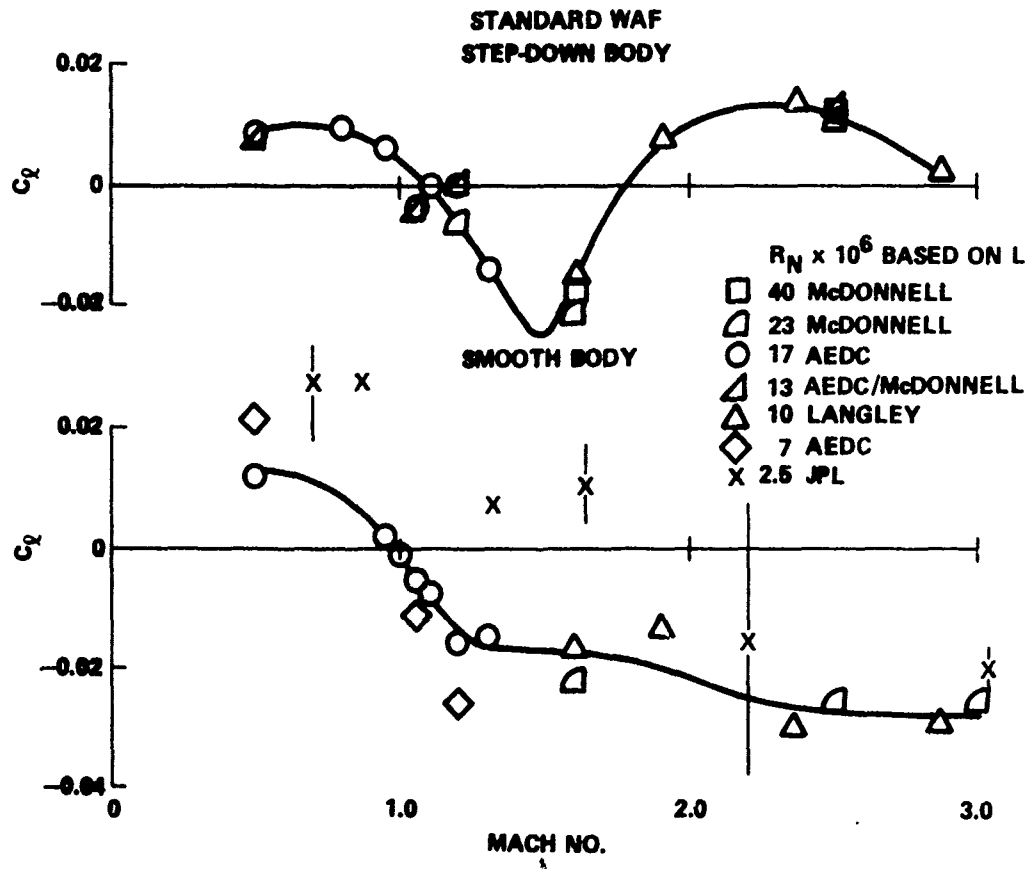


Figure 10. Effect of Reynolds number on zero angle of attack rolling moment coefficient.



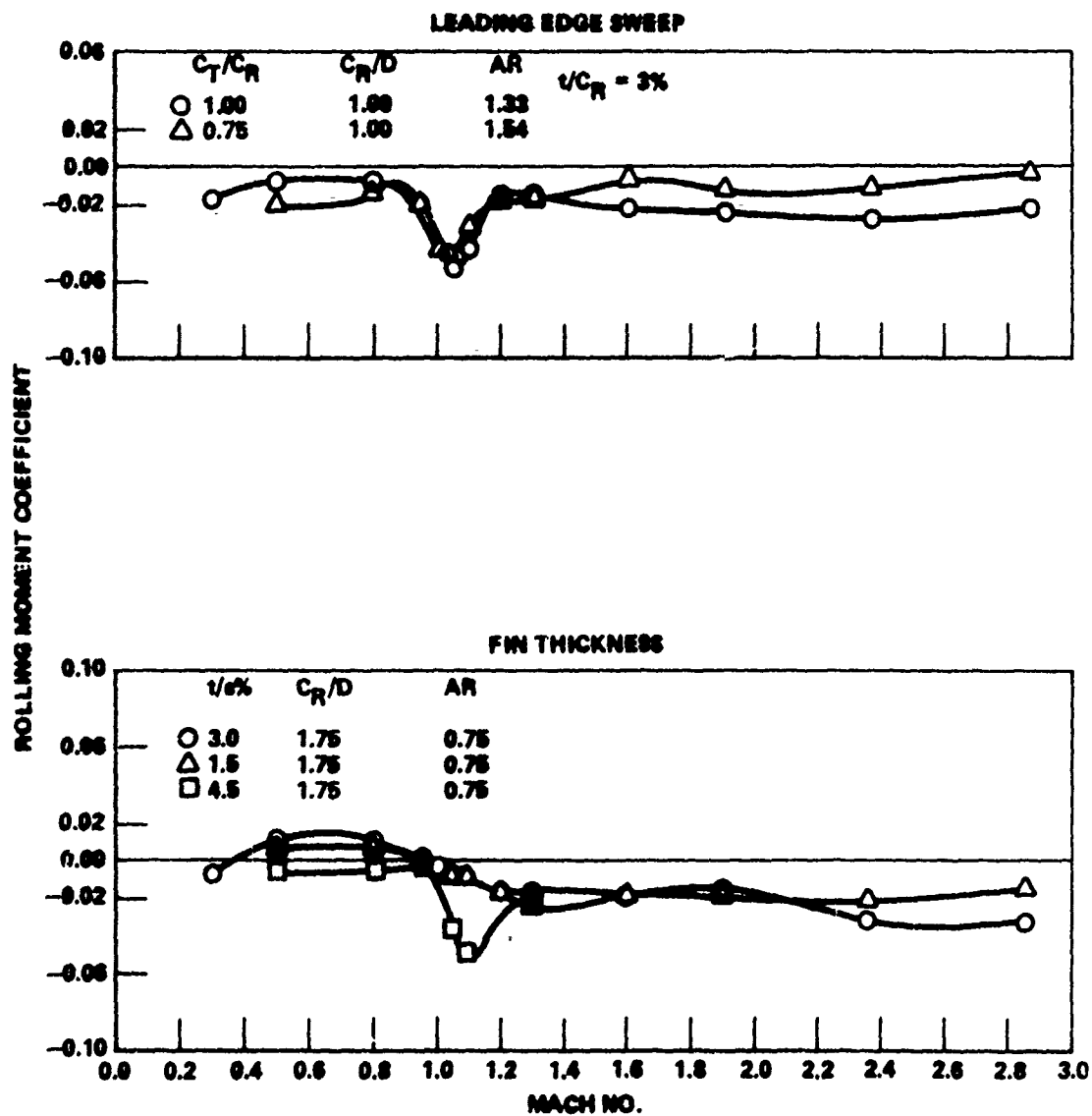


Figure 11. Effect of fin leading edge sweep and fin thickness on WAF rolling moment coefficient,  $\alpha = 0$ .

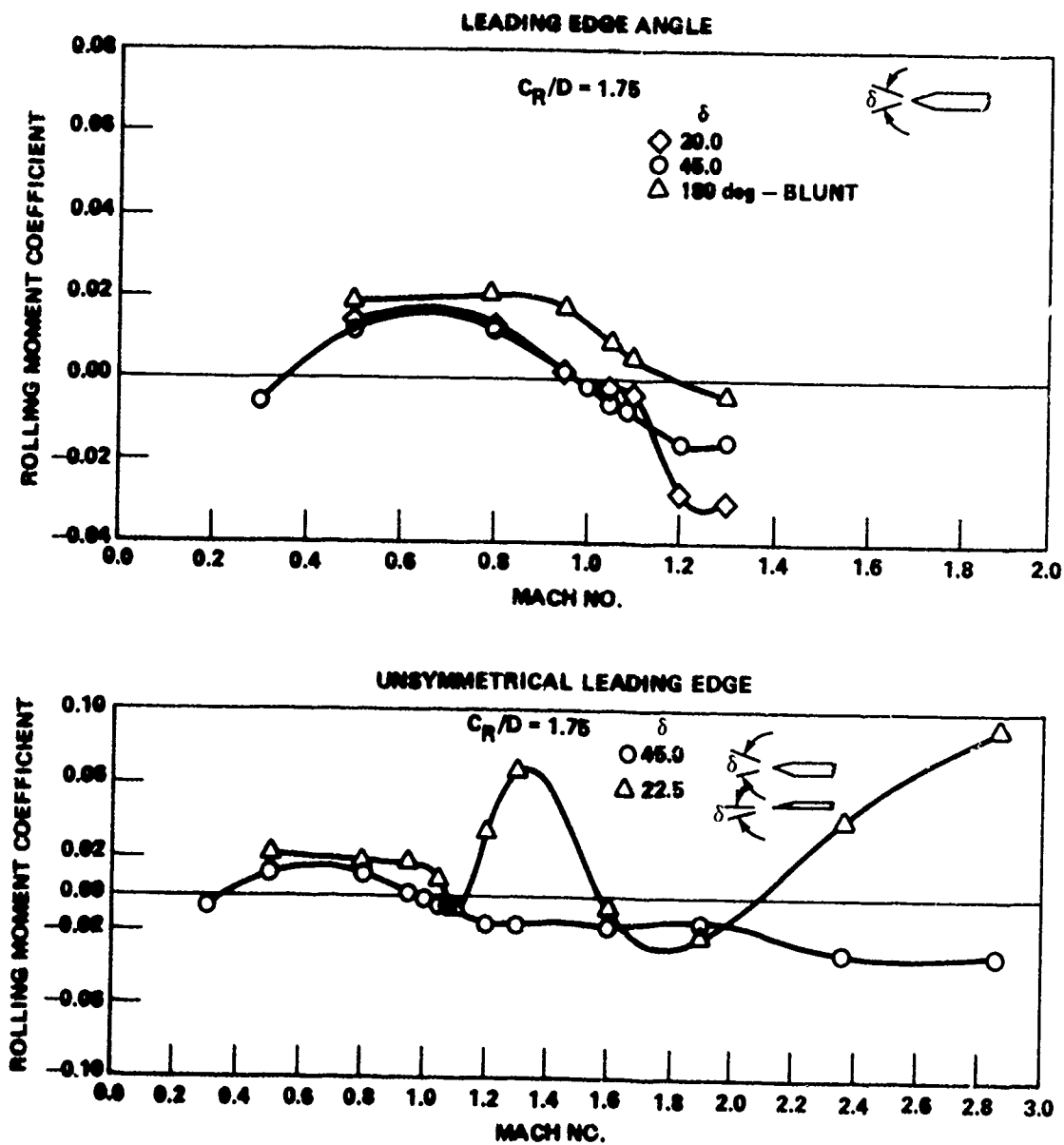


Figure 12. Effect of leading edge shape on WAF rolling moment,  
 $\alpha = 0$ ,  $t/C_R = 3\%$ .

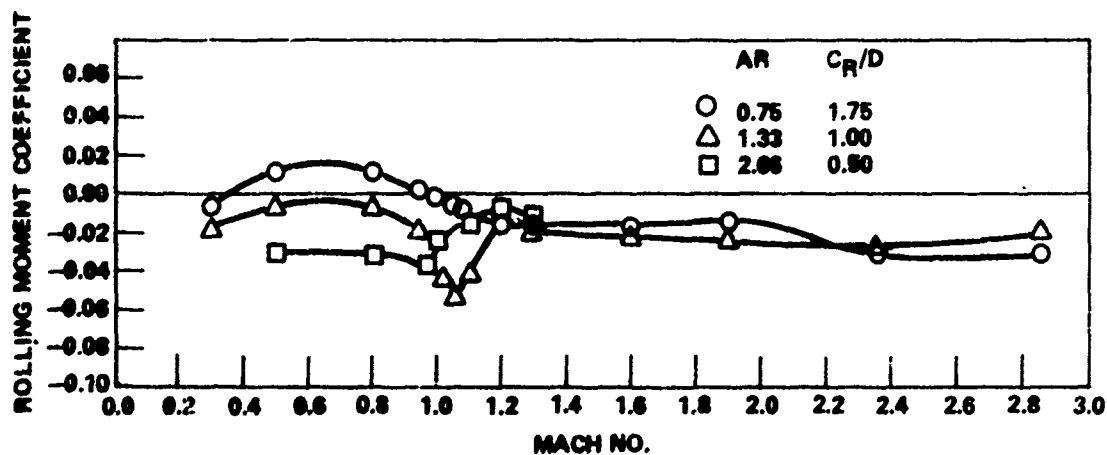


Figure 13. WAF rolling moment coefficient versus Mach No.,  
 $\alpha = 0$ ,  $t/C_R = 3\%$ .

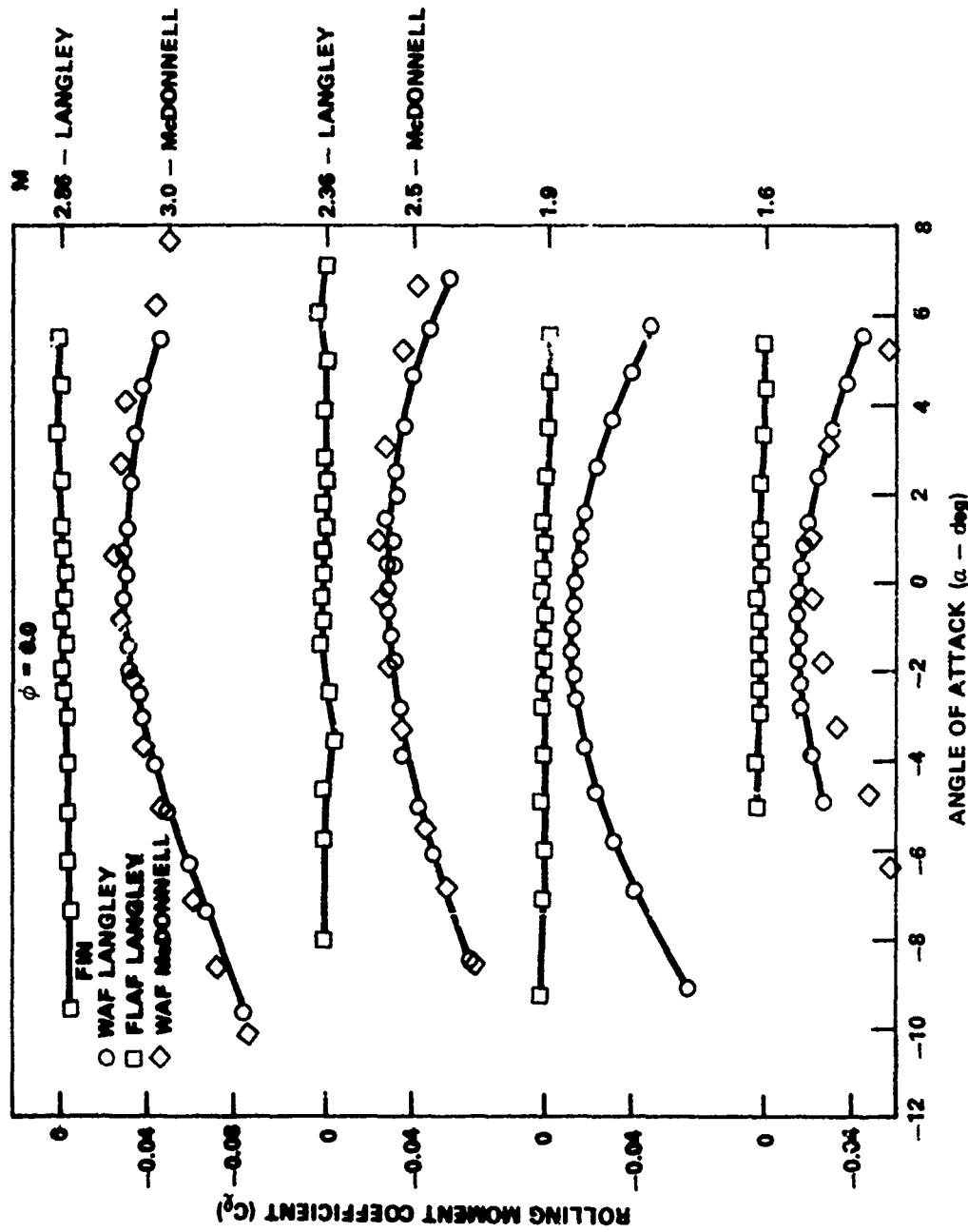


Figure 14. Comparison of flat and WAF rolling moment coefficient versus angle of attack and Mach No.

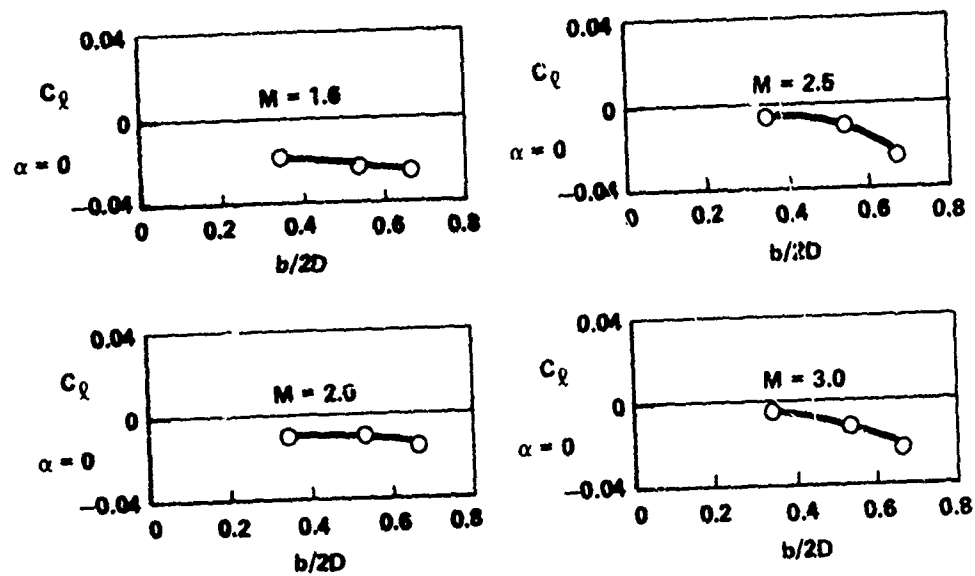


Figure 15. Effects of span on WAF induced rolling moment  
 $C_R/D = 1.75$ .

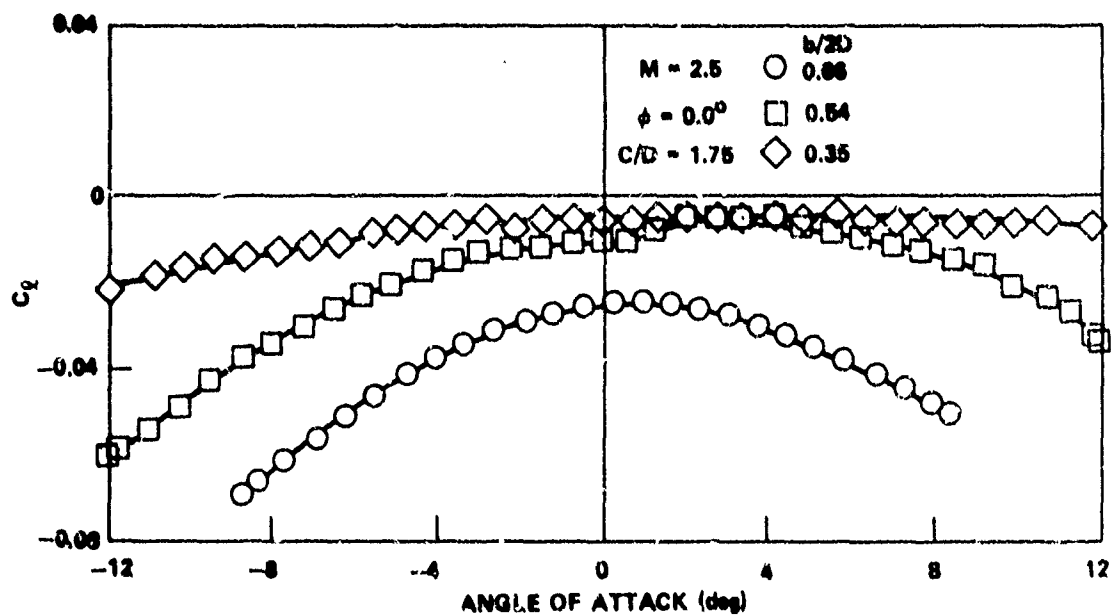


Figure 16. Effect of fin span and angle of attack on WAF rolling moment coefficient.

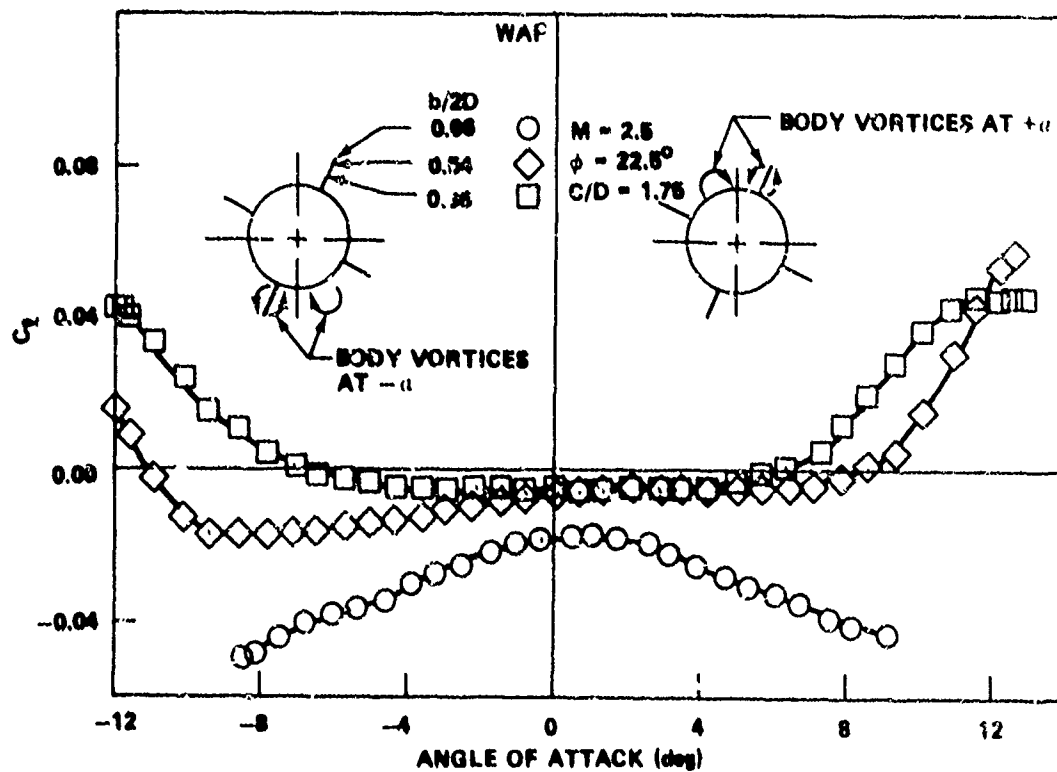


Figure 17. Effect of body vortex at angle of attack on WAF rolling moment.

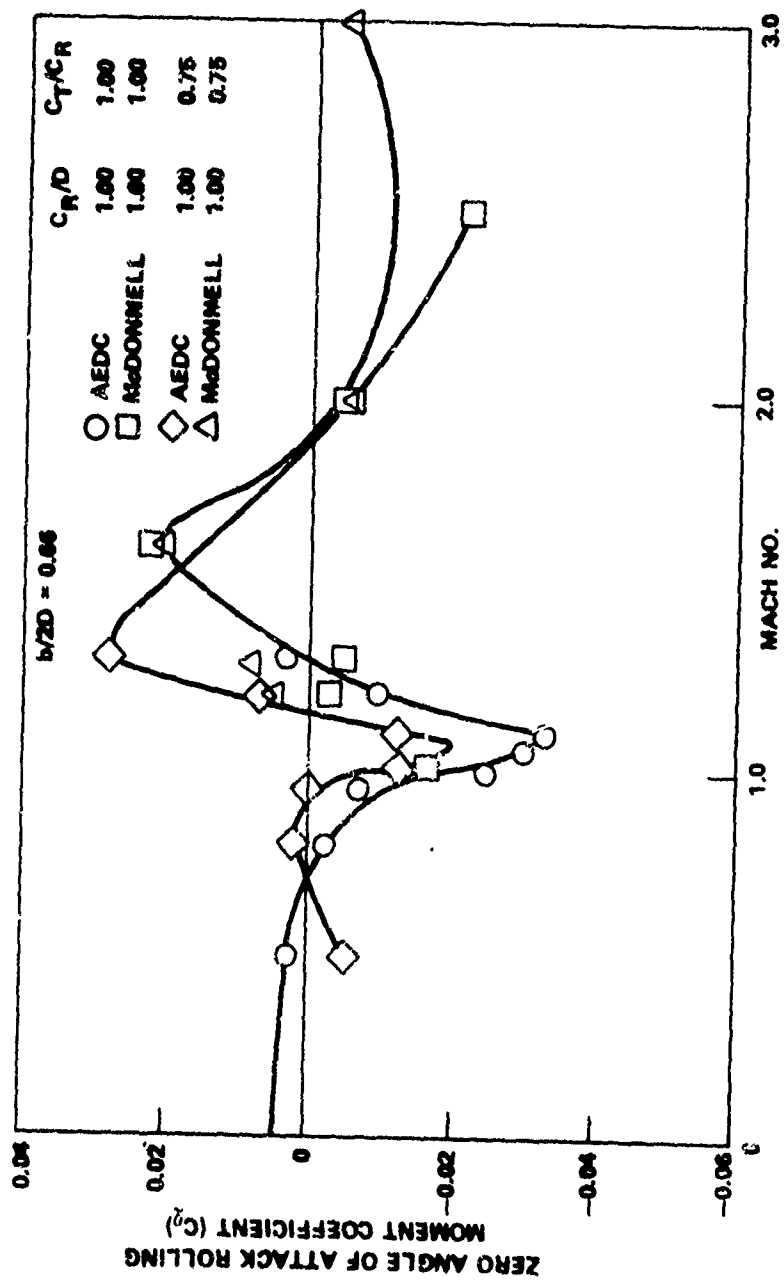


Figure 18. Effect of leading edge sweep and step-down body on roll moment coefficient versus Mach No.

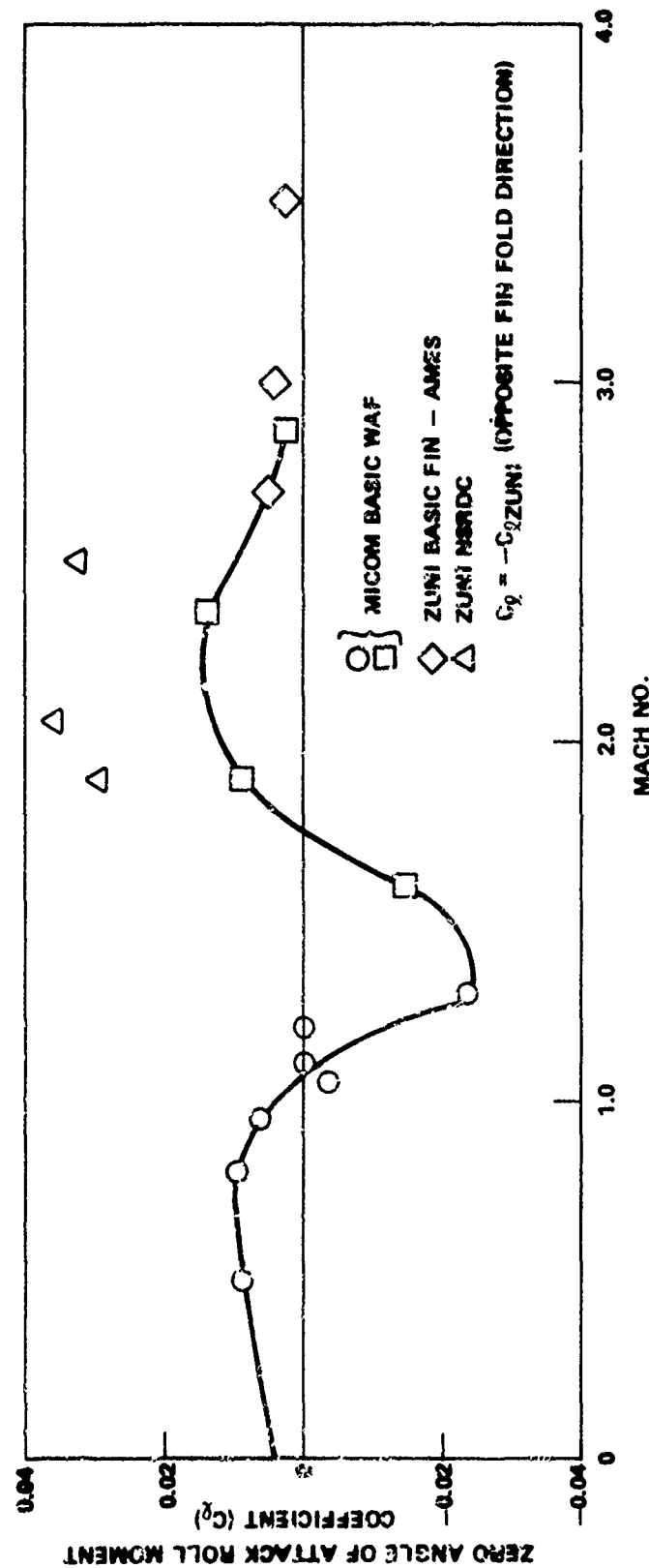


Figure 19. Comparison of step-down body and Zuni roll moment coefficient.



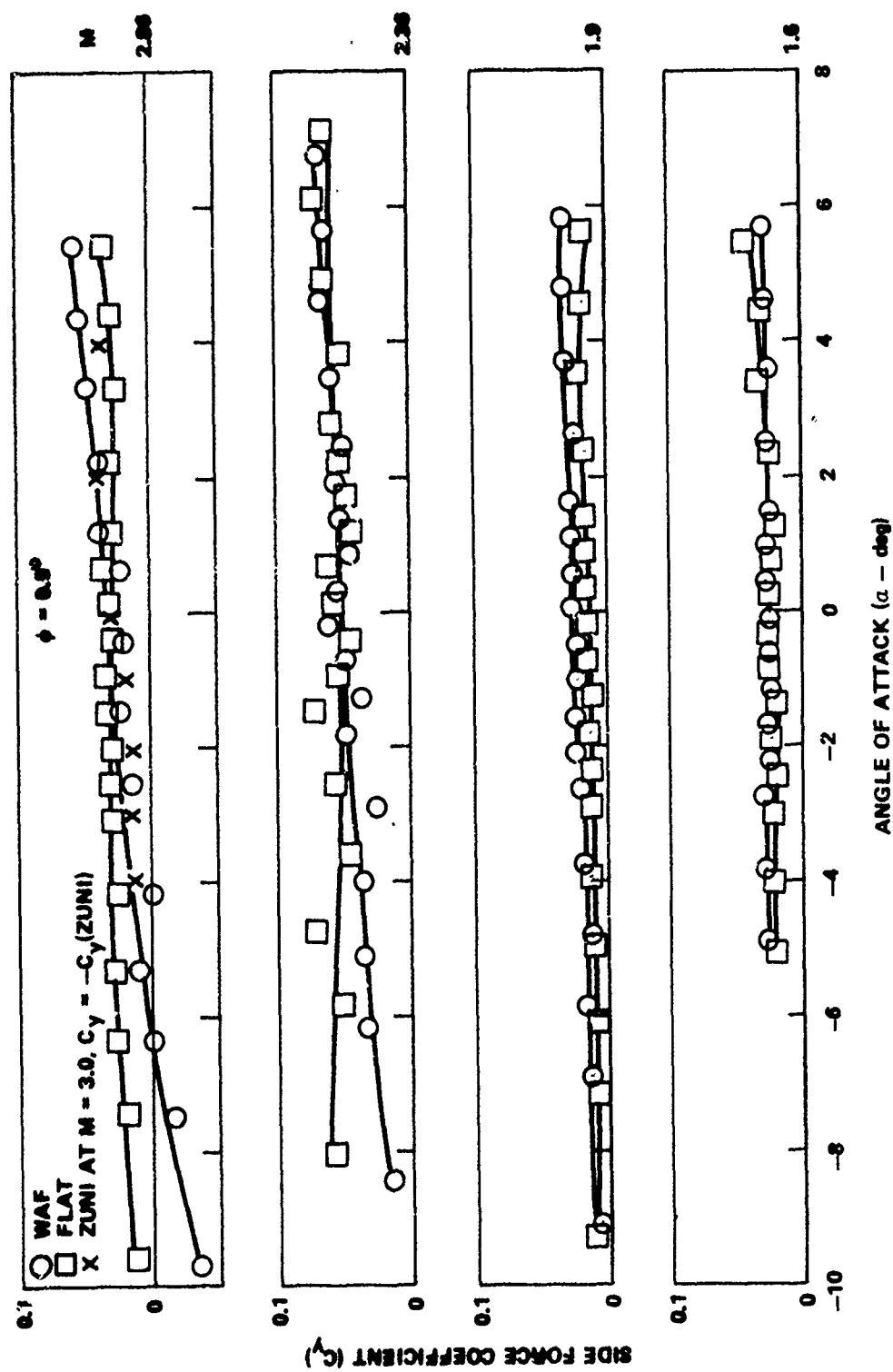


Figure 20. Comparison of WAF and flat fin side force coefficient.

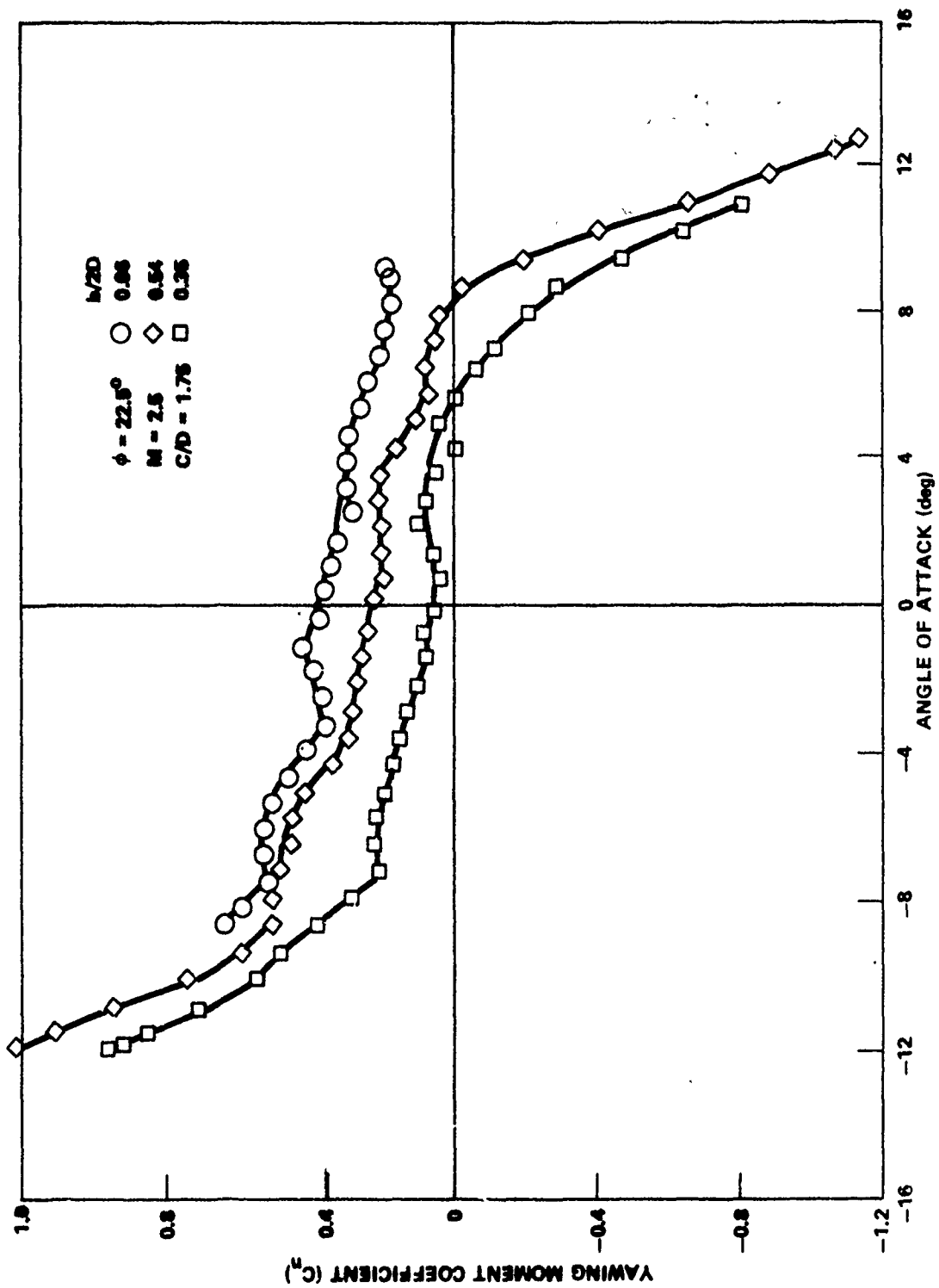


Figure 21. Effect of body on vortex at angle of attack on yawing moment.

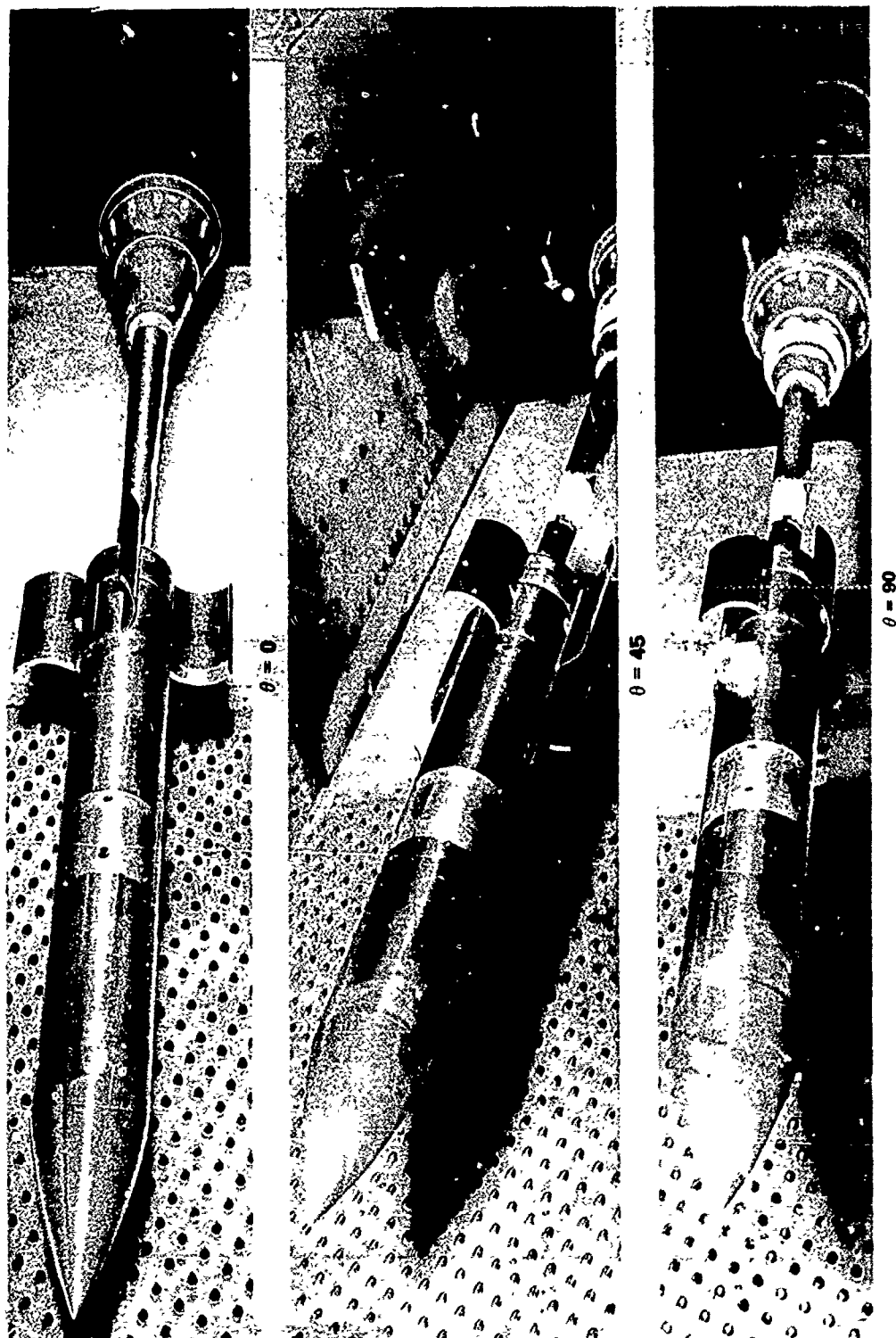


Figure 22. WAF model with opening angle variation.

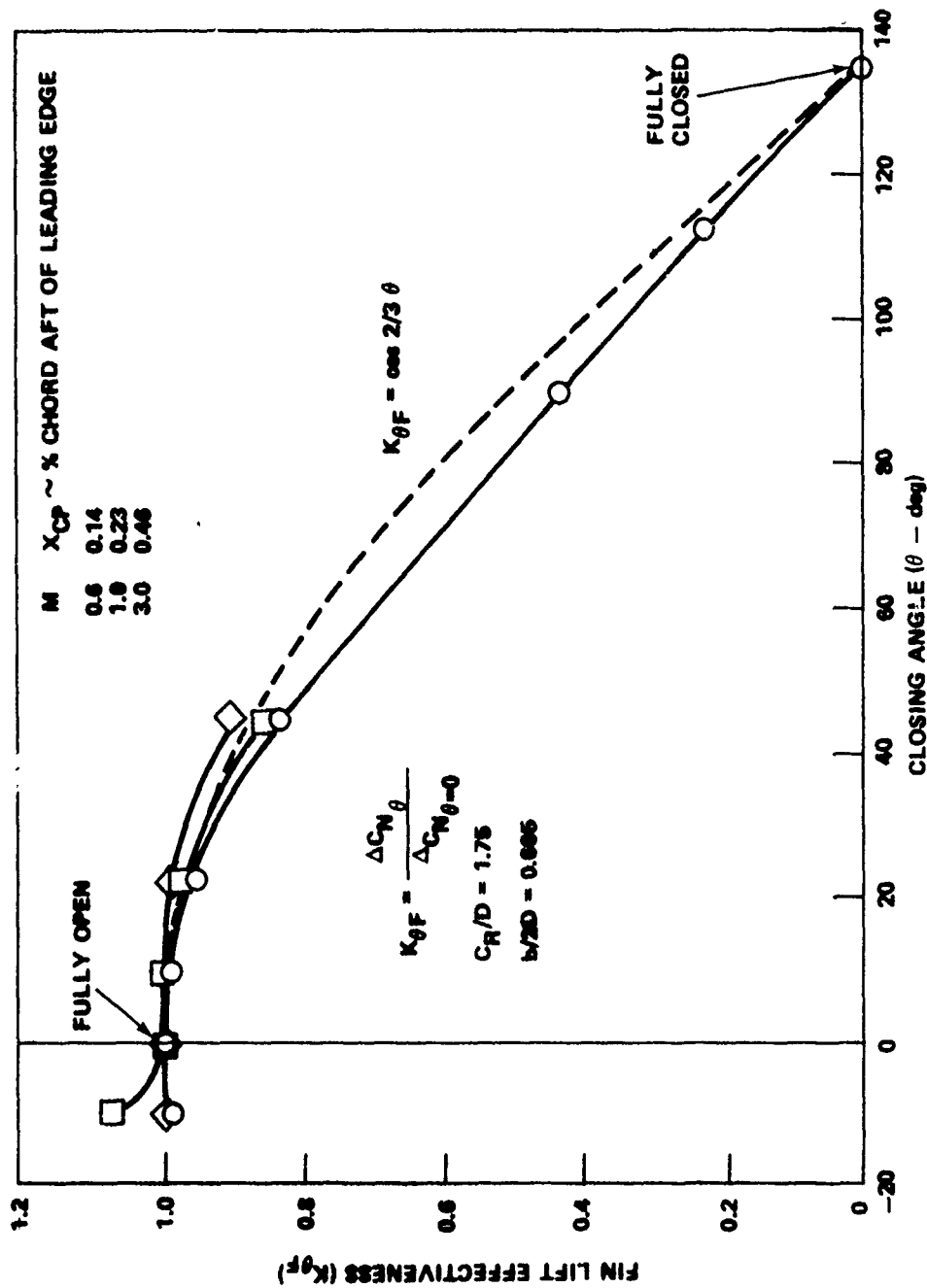


Figure 23. The ratio of fin lift effectiveness at closing angles.

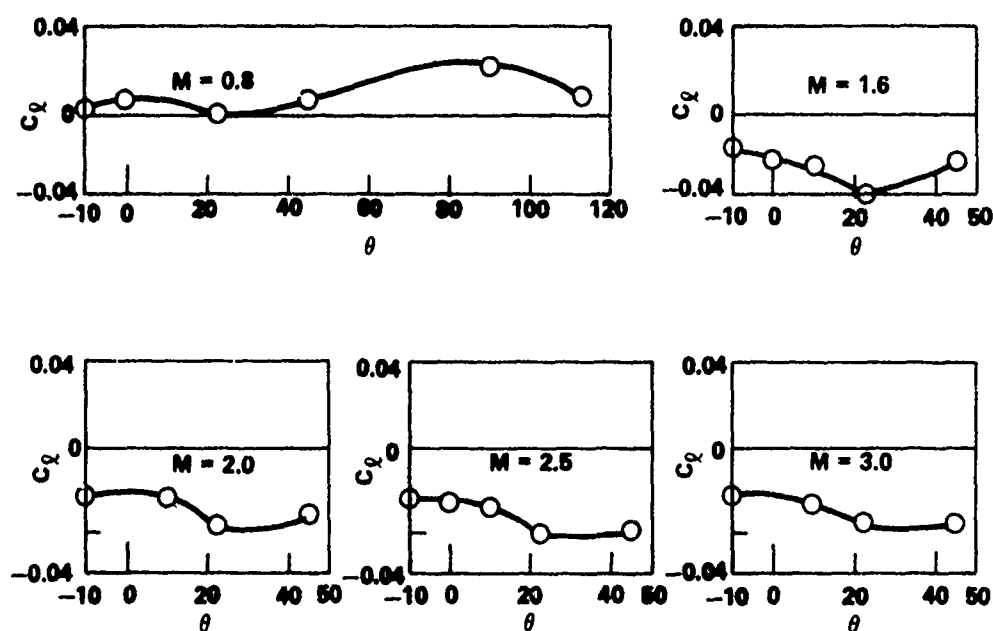


Figure 24. Effects of opening angle on WAF rolling moment  
zero angle of attack  $C_R/D = 1.75$ ,  $b/2D = 0.665$ .

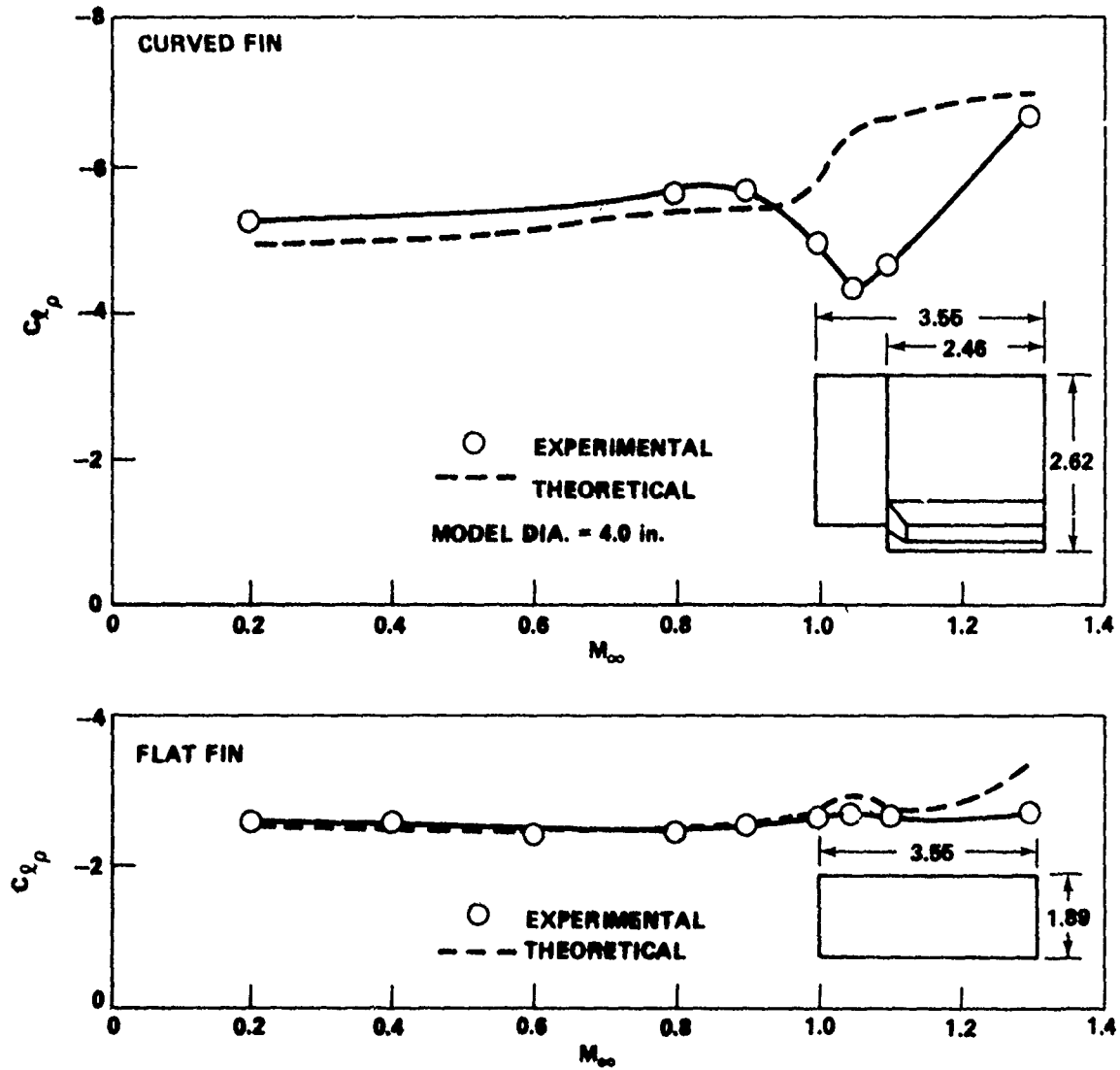


Figure 25. Comparison between theory and experiment.

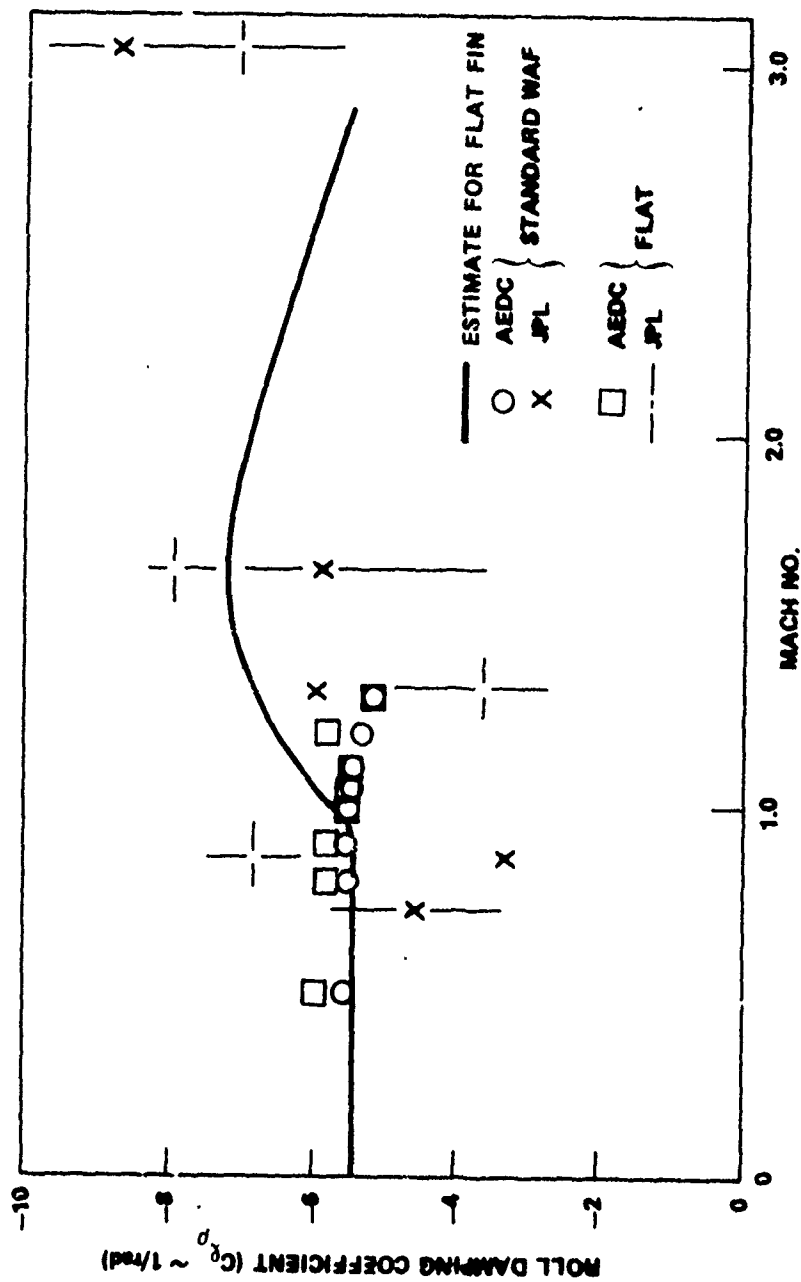


Figure 26. Comparison of roll damping for flat and WAF.

## REFERENCES

1. Holmes, John E., Wrap-Around Fin (WAF) Aerodynamics, Naval Ordnance Laboratory, Silver Spring, Maryland, Paper 9<sup>th</sup> Navy Symposium Aeroballistics.
2. Dahlke, C. Wayne and Craft, J. C., The Effect of Wraparound Fins on Aerodynamic Stability and Rolling Moment Variations, US Army Missile Command, Redstone Arsenal, Alabama, July 1973, Report No. RD-73-17.
3. Dahlke, C. W. and Flowers, L. D., The Aerodynamic Characteristics of Wrap-Around Fins, Including Fold Angle, at Mach Numbers From 0.5 to 1.3, US Army Missile Command, Redstone Arsenal, Alabama, 20 December 1974, Report No. RD-75-19.
4. Dahlke, C. W. and Flowers, L. D., The Aerodynamics Characteristics of Wrap-Around Fins, Including Fold Angle at Mach Numbers From 0.5 to 3.0, US Army Missile Command, Redstone Arsenal, Alabama, 15 November 1974, Report No. RD-75-15.
5. Dunkin, O. L., Influence of Curved-Fin Stabilizers on the Rolling Moment Characteristics of 10-Cal Missiles at Mach Numbers from 0.2 to 1.3, Propulsion Wind Tunnel Facility, Arnold Engineering Development Center, Air Force Systems Command, Arnold Air Force Station, Tennessee, October 1971, Report No. AEDC-TR-71-237.
6. Featherstone, H. A., The Aerodynamic Characteristics of Curved Tail Fin, Convair/Pomona, Convair Division of General Dynamics Corporation, 26 September 1960, Report No. ERR-PO-019.



10th Navy Symposium on Aeroballistics

---

Vol. 1

7. Dahlke, Calvin W., Aerodynamics of Wraparound Fins, A Survey of the Literature, US Army Missile Command, Redstone Arsenal, Alabama, March 1971, Report No. RD-TR-71-7.
8. Stevens, F. L., On, T. J., and Clare, T. A., Wrap-Around vs. Cruciform Fin: Effect on Rocket Flight Performances, Naval Weapons Laboratory, Dahlgren, Virginia, ARAA Paper 74-777 August 1974.
9. Spring, D. J., Static Stability and Roll Damping Characteristics for Several Curved and Planar Fin Configurations at Transonic Speeds, US Army Missile Command, Redstone Arsenal, Alabama, 24 September 1973, Report No. RD-73-32.

PAPER NO. 11

HIGH SUBSONIC AERODYNAMIC LONGITUDINAL STABILITY AND CONTROL  
CHARACTERISTICS OF CONFIGURATIONS INCORPORATING  
WRAP-AROUND SURFACES\*  
(Unclassified)

E. F. Lucero

Applied Physics Laboratory/The Johns Hopkins University  
Silver Spring, Maryland 20910

---

\*This study was supported by NAVSEA-035, Navy Contract N00017-72-C-4401,  
APL/JHU Technical Assignment A31A.

HIGH SUBSONIC AERODYNAMIC LONGITUDINAL STABILITY AND CONTROL  
CHARACTERISTICS OF CONFIGURATIONS INCORPORATING  
WRAP-AROUND SURFACES  
(Unclassified)

E. F. Lucero

Applied Physics Laboratory/The Johns Hopkins University  
Silver Spring, Maryland 20910

ABSTRACT

The feasibility of using wrap-around lifting, stabilizing, and control surfaces on tube-launched, bank-to-turn missile configurations is being investigated at APL/JHU in the subsonic and transonic ranges. Longitudinal and lateral stability and control data have been obtained from wind tunnel tests, mostly at Mach Number 0.8, on configurations having wrap-around monoplane wings, wrap-around horizontal tails, and a planar, all-movable ventral stabilizing and control surface. A description of the configurations tested and some of the significant results obtained in the analysis of the test data are presented in this paper. A comparison with planar surface data and with predictive methods derived for planar surfaces is also shown.

Some of the significant results are:

1. The aerodynamics of curved surfaces can be predicted from theory or empirical methods derived for planar surfaces provided the projected planforms are the same and provided that there is no surface-to-surface interference.
2. When the curved or planar horizontal tails are in the wake of the curved wings, the tail lift efficiency is not predicted well by planar surface methods. An effective tail height parameter has been deduced that, when used with existing downwash formulations, provides a good prediction of tail efficiency for all cases of tail concavity orientation investigated.
3. Pitch and roll control effectiveness of the curved tails is as good or better than that of the planar tails.
4. The pitch control effectiveness is shown to correlate as a single valued function with the effective angle of attack at the tail. This effective angle of attack includes the calculated downwash angle based on the "effective tail height" parameter found in this study.
5. The use of curved surfaces for lift, stability and control of missile configurations appears feasible.

# 10th Navy Symposium on Aeroballistics

Vol. 1

## SYMBOLS AND NOMENCLATURE

$c$	local wing (tail) chord	inches
$C_{\ell}$	rolling moment coefficient = $\frac{\text{rolling moment (in-lbs)}}{qSd}$	
$C_{\ell_{\delta}}$	roll control effectiveness; $C_{\ell_{\delta}} = \frac{C_{\ell}}{\delta}$	
$C_m$	pitching moment coefficient = $\frac{\text{pitching moment (in-lbs)}}{qSd}$	
$C_N$	normal force coefficient = $\frac{\text{normal force (lb)}}{qS}$	
$\Delta C_m$	increment of $C_m$ due to pitch incidence, i.e., $(C_m \text{ at } i_p \neq 0) - (C_m \text{ at } i_p = 0)$	
$d$	reference length = body diameter = 3.0 inches	inches
$h_{t(\text{eff})}$	effective tail height for curved surfaces (see Section I.C)	inches
$i_p$	tail pitch incidence; leading edge up for high wing configuration is positive	degrees
$l_B$	body length	inches
M.A.C.	mean aerodynamic chord $\equiv$ mean geometric chord	inches
$q$	dynamic pressure	lbs/in <sup>2</sup>
$S$	reference area = $\frac{\pi d^2}{4} = 7.07 \text{ in.}^2$	in. <sup>2</sup>
$X_{c.p.}$	longitudinal location of the center of pressure measured from the nose	inches
$X_{c.g.}$	center of gravity location, $X_{c.g.} = 0.55 l_B$	
$C_{X_{\alpha}}$	$\equiv \partial C_x / \partial \alpha$	

SYMBOLS AND NOMENCLATURE (Cont'd)

$\alpha$	angle of attack, angle between velocity vector and the body longitudinal axis $\equiv$ body angle of attack	degrees
$\alpha_{H(\text{eff})}$	effective angle of attack at the 1/4 chord of the M.A.C. of the horizontal tail (see Fig. 16)	degrees
$\delta$	average differential roll control deflection (see Fig. 17)	degrees
$\bar{\epsilon}$	downwash angle at the 1/4 chord of the M.A.C. of the tail	degrees
$\eta_{HV}$	efficiency of the horizontal tail (in the presence of the vertical tail) in producing lift or pitching moment, e.g.	

$$\eta_{HV} \equiv \frac{C_{m_{BWHV}} - C_{m_{BW}}}{C_{m_{BHV}} - C_{m_B}}$$

where B is body

W is wing

H is horizontal tail, and

V is vertical tail

$\theta_W$  wing elevation angle (see Fig. 2)

### INTRODUCTION

Wrap-around finned configurations, WAF, have been considered by some investigators for possible application to tube-launched missiles because of the advantages offered by such a configuration in stowage, handling, and launching (Refs. 1 to 4). Investigations using single fins and configurations with spirally oriented cruciform or triform tails have shown that the curved fins provide about the same normal force and longitudinal stability as a planar fin whose planform is the same as the projected planform of the curved fin (Refs. 4 and 5). These investigations used fins having essentially constant thickness profiles. These fins also obtain a rolling moment at zero angle of attack (due to the difference in pressures on the concave and convex sides) which changes sign as the Mach number is traversed from subsonic to supersonic.

In the present study at the Applied Physics Laboratory/The Johns Hopkins University, wind tunnel investigations were conducted in the subsonic-transonic regime (mostly at Mach number 0.3) with the primary objective to assess the aerodynamic feasibility of bank-to-turn type missile configurations using monoplane wrap-around lifting, stabilizing, and control surfaces. Corollary objectives were (1) to evaluate the relative effectiveness of curved and planar surfaces, and (2) to seek predictive methods for aerodynamics of curved surfaces. The most significant results of the investigations are presented in this paper. Detailed analyses are contained in Refs. 6 and 7.

Related structural studies conducted at APL are presented in Appendix A.

The wrap-around surface project (WASP) configurations consisted of a fineness ratio 10 body upon which were mounted monoplane wings and horizontal tails and a vertical stabilizer (Fig. 1)<sup>\*</sup>. The body had a 2.1 caliber von Karman nose followed by a cylindrical afterbody. Since drag measurement was not a purpose of the test, the body was not contoured nor boattailed. The wings were elevated 30° from the horizontal plane of the cylinder to obtain the maximum wing span when unfolded (Fig. 2) without requiring overlap when folded. The profile of all the surfaces was NACA 64A006. Flexibility was built into the model design to permit configuring several combinations of wing longitudinal position, tail concavity orientation, tail dihedral and anhedral, and to permit component testing. In addition the symmetric profile NASA 64A006 permitted us to obtain information on both high wing and low wing configurations by testing at positive and negative angles-of-attack. Configurations similar to WASP but with planar surfaces (Fig. 3)<sup>\*</sup> were also tested for comparison. These surfaces had the same planform as the projected planform of the curved surfaces. Other geometric parameters are shown in Table I.

The data obtained were normal and side forces and pitching, yawing, and rolling moments. The angle of attack was varied from -12° to 16°. The test Mach number was 0.8; this was the design Mach number for wing and tail planform and profile selection. A limited amount of data were obtained to determine the effects of Reynolds number; the bulk of the data were obtained at a free stream Reynolds number per foot of  $7.7 \times 10^6$ .

\*The vertical stabilizer is shown 180° opposite of its position on the test configuration.



PRESENTATION OF RESULTS

The results of analysis of the WASP experimental data are presented in two sections:

The longitudinal stability ( $C_N$  and  $C_m$ ) characteristics of curved surfaces mounted on a body are presented in Section I. A comparison of the results is made with those obtained with planar surfaces and with selected predictive methods. Some geometric effects on  $C_N$  and  $C_m$  are examined. Finally, the longitudinal stability of a full configuration (body-wing-empennage) is presented and the wing-tail interaction obtained on the curved surfaces is analyzed.

In Section II, the pitch and roll control effectiveness of the curved tails are presented and discussed. A correlation is shown to exist between the increment in pitch control moment and the calculated angle of attack at the tail 1/4 chord of the mean aerodynamic chord.

The reference area for all aerodynamic coefficients is the body cross-sectional area (7.07 square inches); the reference length is the body diameter (3.0 inches); and the reference center-of-gravity is at 55% of the body length.

RESULTSI. Longitudinal Stability CharacteristicsA. Curved Surface Performance, Wing-Body Configurations

Previous investigators have established that at both subsonic and supersonic speeds the longitudinal aerodynamic characteristics of curved wings, whose cross section was essentially constant in thickness, are the same as those of planar wings when their projected planforms are the same (Ref. 5). The test results obtained on the WASP wing (in the presence of the body) show that planar surface data also provide a good estimate of  $C_N$  and  $C_m$  for curved surfaces with subsonic profiles (Figs. 4 and 5). At higher angles of attack the curved and planar surfaces have different values of  $C_N$  and  $C_m$  but these differences are small.

Other observations noted (but not shown herein) are:

1. The center-of-pressure of the wing normal force is about the  $1/4$  chord of the mean aerodynamic chord, M.A.C., and is not very sensitive to angle-of-attack.
2. Stall due to angle of attack is not indicated for the high wing in the range  $0 \leq \alpha \leq 16^\circ$  (Fig. 4).

A limited amount of data obtained at higher angles shows a mild stall at  $\alpha \approx 16.5^\circ$ .

It is concluded from these results that any method for accurately predicting normal force and pitching moment of planar wings can also be used to obtain reasonable estimates of these values

for curved wings provided that the projected planforms are the same for the planar and curved wings. For example, the method of Polhamus (Ref. 8), although not exactly applicable to the wing used in these studies, gives a good prediction of the wing normal force (Fig. 6). Lifting surface theory was found to predict the lift curve slope accurately. Based on the test results from this study, a good estimate for the center-of-pressure location is the wing 1/4 chord of the mean aerodynamic chord.

B. Wing Elevation and Tail Concavity Effects, Body Wing or Body Tail

Several geometric effects on the performance of curved surfaces were investigated in this program. Among these were wing elevation and tail concavity orientation.

The effect of wing elevation on  $C_N$  and  $C_m$  is insignificant for planar wings (Fig. 4) when the elevation is equal and opposite,  $\theta_w = \pm 30^\circ$ , i.e., high and low wing. Test data are not available to permit a direct comparison of this effect for the wrap-around wings; the high and low curved wings tested have opposite concavity. The  $C_N$  and  $C_m$  data for these curved surfaces however show no significant difference up to  $\alpha = 10^\circ$ .

The effects of concavity orientation were investigated using the body tail configuration. This surface has the plane containing its projected planform at midbody and hence elevation effects are eliminated. The results show (Fig. 7) that up to  $\alpha \approx 8^\circ$ ,  $C_N$  (or  $C_m$ ) is the same for

concave side windward and concave side leeward. Above  $\alpha \approx 8^\circ$ , the  $C_m$  data indicate that the tails that have the convex side to the wind are less effective stabilizers than the ones whose concave side is to the wind. Analysis of the body tail minus body data show the onset of tail stall at  $\alpha \approx 10^\circ$ . This stall shows up in the  $C_m$  data of Fig. 7.

It is surmised from the body-planar wing and body-curved wing data of Figs. 4 and 5 and the body-tail data of Fig. 7 that when the wing elevation is equal and opposite for curved surfaces which have the same concavity orientation the  $C_N$  and  $C_m$  would be the same up to  $\alpha = 8^\circ$ .

#### C. Full Configuration (Body-Wing-Empenage) Aerodynamic Performance

For the full configuration, wing-tail interference is present. When the wing is high, the curved and planar surface configurations have the same value of  $C_N$  (or  $C_m$ ) up to  $\alpha \approx 10^\circ$  (Figs. 8 and 9). Above  $\alpha \approx 10^\circ$  there are differences in the aerodynamic characteristics of the two configurations, e.g., at  $\alpha = 16^\circ$  the curved surface configuration has a value of  $|C_m|$  that is about 10% higher than that of the planar surface configuration. When the wing is low,  $C_N$  is different for the planar and curved surface configurations above  $\alpha \approx 8^\circ$ ;  $C_m$  differs considerably above  $\alpha \approx 4^\circ$ . Both low wing configurations have a highly non-linear  $C_m$  and become unstable  $\left( \frac{\partial C_m}{\partial \alpha} > 0 \right)$  at low angles of attack (Fig. 9) because of the interference from the wing vortex to the tail. This wing-tail interference also results in the low wing configuration having a lower value of  $C_N$  than the high wing configuration (Fig. 10).

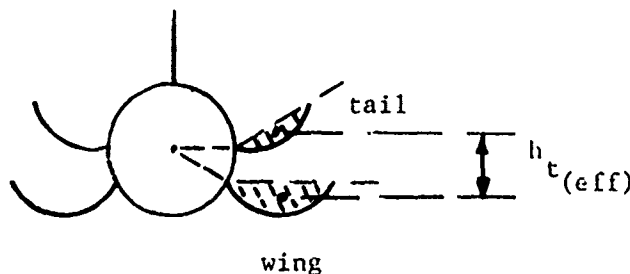
The combination of reduced  $C_N$ , non-linearities in  $C_m$ , and instability at low angles-of-attack of the low wing configuration makes the high wing configuration more desirable from an aerodynamic viewpoint.

The magnitude and persistence of the instability noted above for the low wing configuration was found to be different for the various tail and wing configurations tested (Fig. 11). These geometric variables produce the following six different low wing configurations: curved wings and tails; planar wings and tails; curved wings and planar tails; curved wing- and tail-surfaces with tail concavity reversed; curved wing and tail surfaces with tail anhedral; and curved wing and tail surfaces with the tail having dihedral and its convex side windward. All high wing configurations (with the exception of the last one mentioned above) obtained a  $C_m$  within 10% of each other up to  $\alpha = 16^\circ$  (curve not shown). The low wing configurations however show a significantly different  $C_m$  curve for every configuration (Fig. 11).

Although it has been established from stability considerations that the high wing configurations are preferable to the low wing configurations some maneuvering at small negative angles of attack would be expected for high wing configurations. Thus some understanding of the causes for such varied stability of the low wing configurations (or equivalently high wings at  $\alpha < 0$ ) would be useful. A search into possible geometric and/or aerodynamic causes for the different  $C_m$  trends of the low wing configurations resulted in arriving at a "tail height" parameter,

$h_{t(eff)}^*$  for the curved surface configurations which provides an improved prediction of tail efficiency for curved surface configurations over that obtained by using the usual tail height for planar wings (Figs. 12 and 13). This parameter was used in Decker's downwash formulations (Ref. 9) to calculate the vertical displacement of the vortex core and from this the lag of downwash,  $\partial \bar{e} / \partial \alpha$ , and tail efficiency,  $\eta_{HV}$ . In the region of maximum wing tail interference, where  $C_m$  of the low wing configurations has the most positive value (Fig. 11) and the tail efficiency is lowest (Fig. 13), neither  $\eta_{HV}$  calculated using  $h_{t(eff)}$  nor  $\eta_{HV}$  calculated using the projected planform height provide a good prediction of the test data. Further refinements of the predictions in this region were found possible using correlation parameters involving  $h_{t(eff)}$ ,  $C_m$  and angle of attack. These correlations are detailed in Ref. 6.

\*This parameter  $h_{t(eff)}$  is the vertical distance between the centroids of the shaded segments shown below. These segments are formed by the following two boundaries: a) the wing (or tail) plane containing the root chord and tip chord, and b) the profile centerline.



II. Control CharacteristicsA. Pitch Control

In general the curved surfaces provide pitch control that is equal to or better than that of the planar surfaces (Fig. 14). This is the case both when the tails are in the wing wake (as in the  $-\alpha$  data of Fig. 14) and when there is little or no wing interference ( $+\alpha$  or wing off). When there is no wing present the tails will stall at  $|\alpha + i_p| \approx 10^\circ$  (wing off data, Fig. 14). The wing downwash, however, enhances the control effectiveness of the tail surfaces so that when  $\alpha < 0$  and  $i_p < 0$  (low wing configuration), the load on the tail is reduced and stall does not occur in the range of negative  $\alpha$  tested,  $-10^\circ \leq \alpha \leq 0^\circ$ . The result is that the control moment is fairly constant throughout the angle of attack range tested (Fig. 15). For the configuration selected for the control tests (wing 1/4 chord of M.A.C. at  $0.50 \ell_B$ ), and for the reference center-of-gravity location of 0.55 body length, the trim pitch incidence is less than  $5^\circ$  for  $-10^\circ \leq \alpha \leq 16^\circ$  (the missile is trimmed in pitch when  $C_m = 0$ ). This WASP configuration which has the wing located at  $0.5 \ell_B$  appears to be an aerodynamically feasible configuration based on its longitudinal stability and control characteristics.

B. Pitch Control Effectiveness Correlation

The effective angle of attack at the tail 1/4 chord of the Mean Aerodynamic Chord,  $\alpha_{H(\text{eff})}$ , was calculated by summing the values of the body angle of attack,  $\alpha_B$ , tail incidence,  $i_p$ , and the downwash angle,  $\hat{e}$ , at the 1/4 chord of the M.A.C. The wing downwash angle was calculated using Decker's formulation of Ref. 9 and the aforementioned effective tail height for the curved surfaces,  $h_{t(\text{eff})}$ .

It was found, as could be expected a priori, that when the pitch control effectiveness  $\Delta C_m / i_p$  is plotted against this value of  $\alpha_{H(eff)}$ , the control data for both wing-on and wing-off configurations collapse into essentially one curve (Fig. 16). This correlation of pitch control effectiveness with the effective tail angle of attack (Fig. 16) shows that tail stall occurs at  $\alpha_{H(eff)} \approx 10^\circ$  to  $12^\circ$ . This is in close agreement with the tail stall angle observed from the tail normal force data obtained at zero tail deflection. Since  $\bar{e}$  is linearly dependent on  $h_{t(eff)}$ , the magnitude of  $h_{t(eff)}$  used in the calculation of  $\bar{e}$  is important. The correlation of  $\Delta C_m / i_p$  with  $\alpha_{H(eff)}$  is therefore additional evidence that the formulated value of  $h_{t(eff)}$ , as explained previously, is a workable correlation parameter and thus is useful in estimating longitudinal stability and control characteristics for curved surface configurations.

#### C. Roll Control Effectiveness

The roll control effectiveness,  $C_{l_\delta}$ , of the curved surfaces is equal to or better than that of the planar surfaces (Fig. 17). At  $\alpha > 0$ ,  $C_{l_\delta}$  decreases with increasing  $\alpha$  for the curved surfaces but not as much as it does with planar surfaces. For example, at  $\alpha = 16^\circ$ , the reduction from the  $\alpha = 0^\circ$  value is 77% for the planar tails and 42% for the curved tails. The importance of this reduced value of  $C_{l_\delta}$  at the higher angles of attack on aerodynamic performance depends on potential mission requirements.



CONCLUSIONS

The use of wrap around surfaces for providing lift, stability, and control of span limited missiles is aerodynamically feasible. The aerodynamic characteristics of these curved surfaces can be predicted accurately using methods developed for planar surfaces. For body-wing-tail configurations, where wing-tail interference is present, an effective tail height parameter has been developed in this study for curved surface configurations that can be used to obtain good predictions of tail efficiency.

REFERENCES

1. Featherstone, H. A., The Aerodynamic Characteristics of Curved Tail Fins, General Dynamics/Pomona GDC-ERR-PO-019, September 1960.
2. Wells, R. Franklin, Investigation of the Aerodynamic Characteristics of a Model of a Rocket Missile with Several Arrangements of Folding Fins at Mach Numbers of 1.75, 2.15, 2.48 and 2.87, NASA TM X-234, April 1960.
3. Gauzza, H. J., Static Stability Test of Tangent and Wrap-Around Fin Configurations at Supersonic Speeds, NAVORD Report 3743, 17 January 1955.
4. Regan, F. J., and Schermerhorn, V. L., Supersonic Magnus Measurements of the 10-Caliber Army-Navy Spinner Projectile with Wrap-Around Fins, NOL TR 70-211, 1 October 1970.
5. Proceedings of the Ninth Meeting of the Exterior Ballistics Panel 0-7. The Technical Co-Operation Program, Vol. II, Session I: Weapon Aerodynamics, DREV M-2184/72, September-October 1971.
6. E. F. Lucero, Experimental Results of High Subsonic Aerodynamic Longitudinal Stability Characteristics of Bank-to-Turn Configurations Incorporating Wrap-Around Surfaces with Subsonic Sections, APL/JHU BFD-1-74-009, 12 February 1975.
7. E. F. Lucero, Experimental Study at  $M = 0.8$  of Wrap Around Surface Project (WASP) Missile Configuration Controllability in Pitch, Yaw, and Roll at Zero Angle of Sideslip, APL/JHU BFD-1-75-006, 8 May 1975.
8. Edward C. Polhamus, Predictions of Vortex-Lift Characteristics by a Leading Edge Suction Analogy, Journal of Aircraft, Vol. 8, Number 4, April 1971.
9. Decker, James L., Prediction of Downwash at Various Angles of Attack for Arbitrary Tail Locations, Aeronautical Engineering Review, August 1956.

TABLE I

## GEOMETRIC PARAMETERS OF WING/TAIL SURFACES

<u>Parameter</u> *	<u>Wing</u>	<u>Horizontal Tail</u>	<u>Vertical Tail</u>
Exposed Semi-Span, in.	2.598	1.760	1.760
Root Chord, in.	3.737	2.514	2.514
Tip Chord, in.	1.868	1.257	1.257
Mean Aero. Chord, in.	2.90	1.956	1.956
Lateral Centroid, in.	1.154	0.781	0.781
Projected Surface Area (one surface) in <sup>2</sup>	7.28	3.21	3.21
Taper in Chord	1/2	1/2	1/2
Sweep, deg. (ref.)	35.6°	35.6°	35.6°
Aspect Ratio, one exposed panel	0.925	0.925	0.925
Aspect Ratio, tip to tip	2.30	2.44	--
Elevation angle	30°	0°	--
Section Profile: NACA 64A006 all surfaces			

\*Note: For the curved surface these geometric parameters refer to the projection of the curved surface on the horizontal plane containing both the root and tip chords.

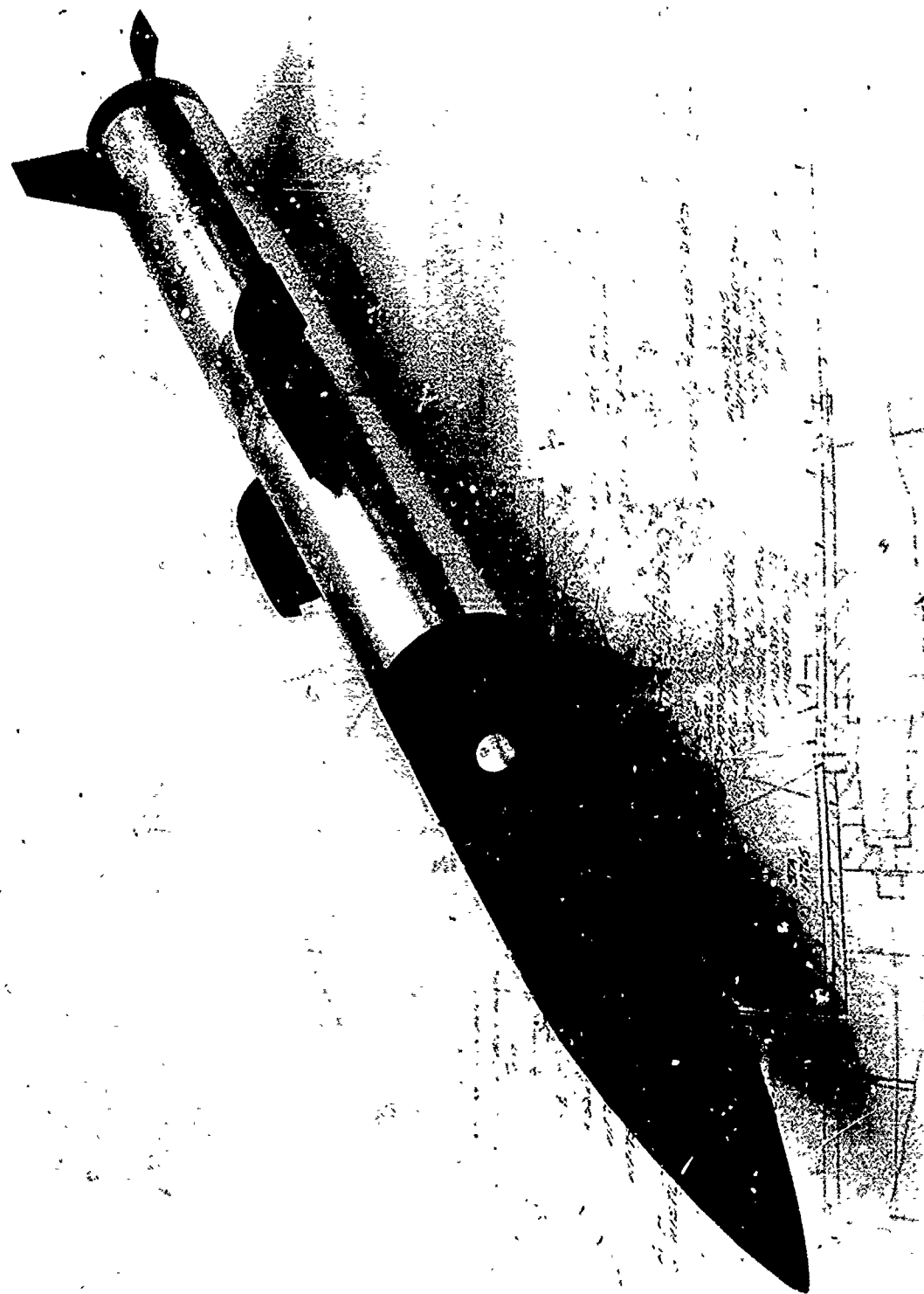


FIG. 1 WRAP-AROUND SURFACE PROJECT (WASP)  
CONFIGURATION

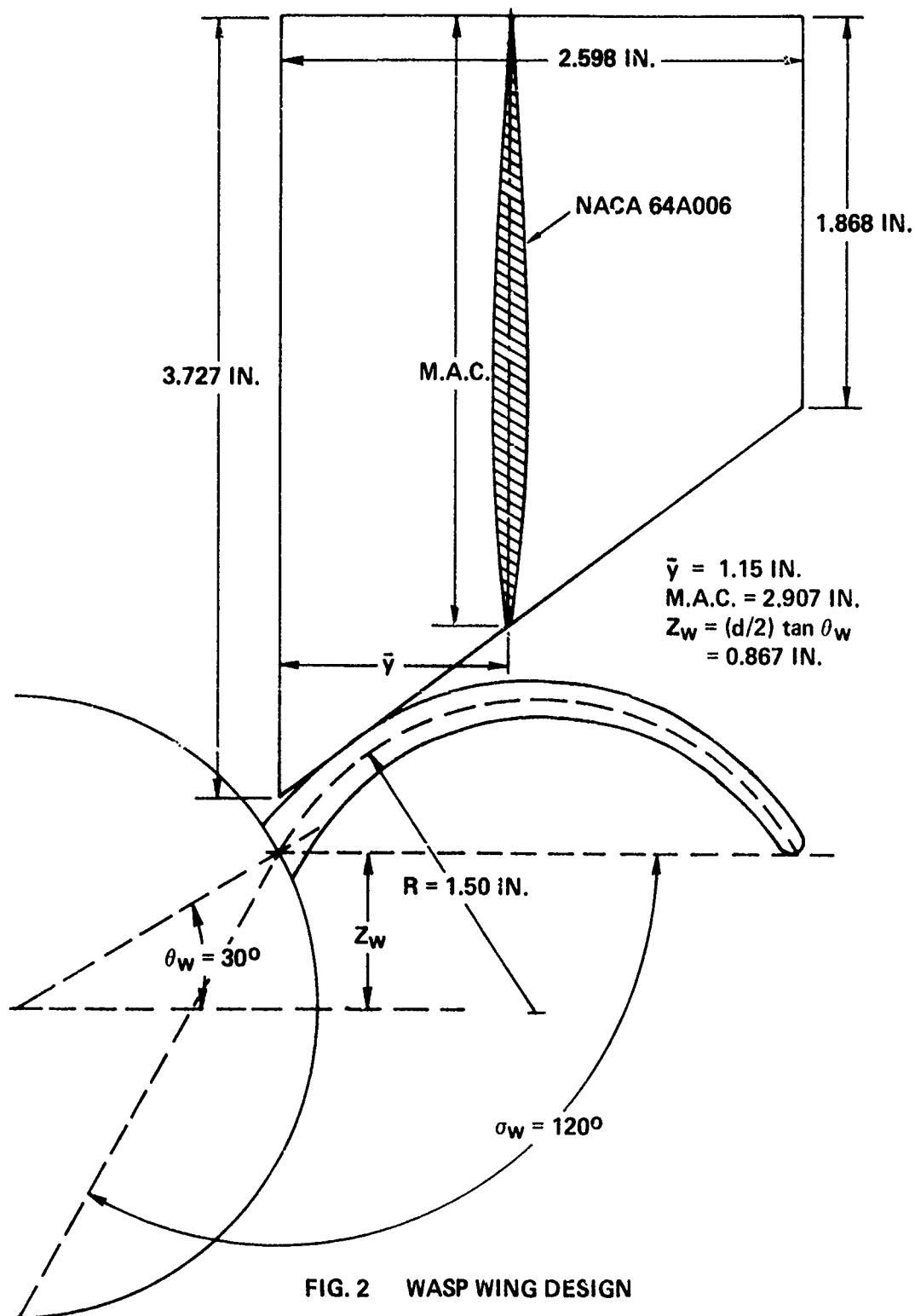


FIG. 2 WASP WING DESIGN



FIG. 3 PLANAR SURFACE CONFIGURATION

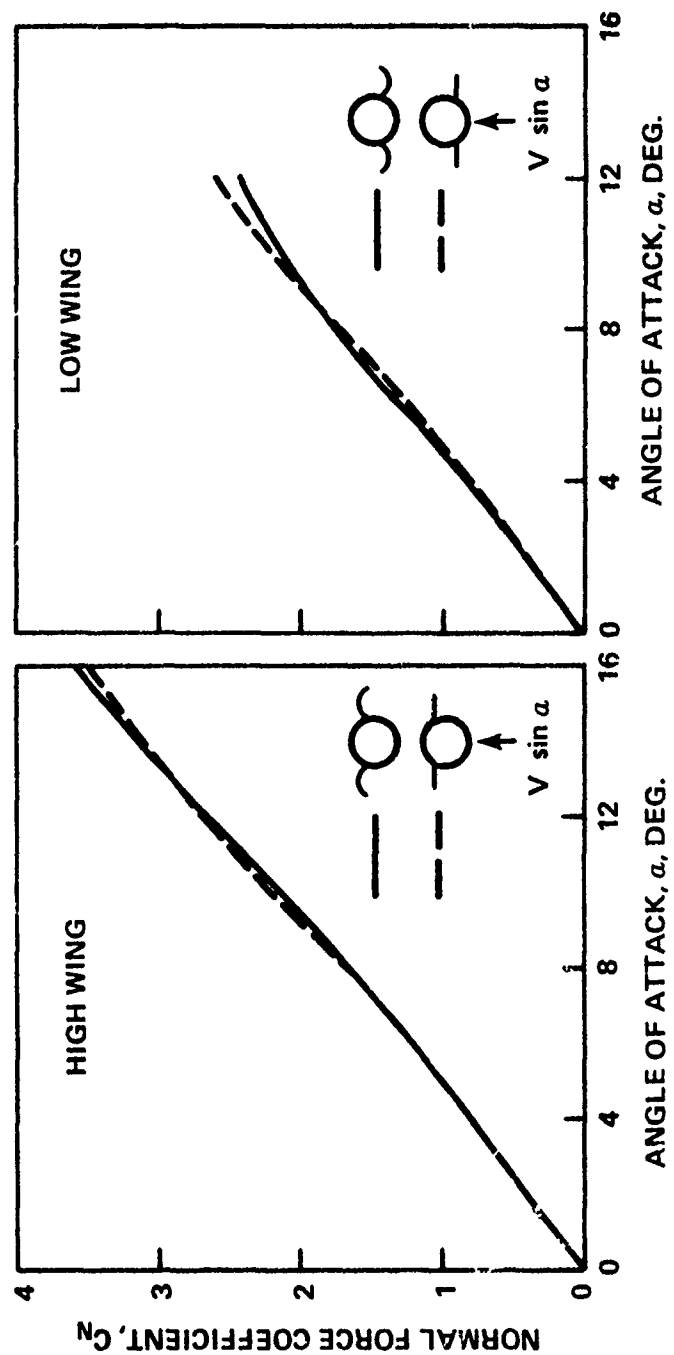


FIG. 4 COMPARISON BETWEEN WRAP-AROUND AND PLANAR WING-BODY NORMAL FORCE COEFFICIENT

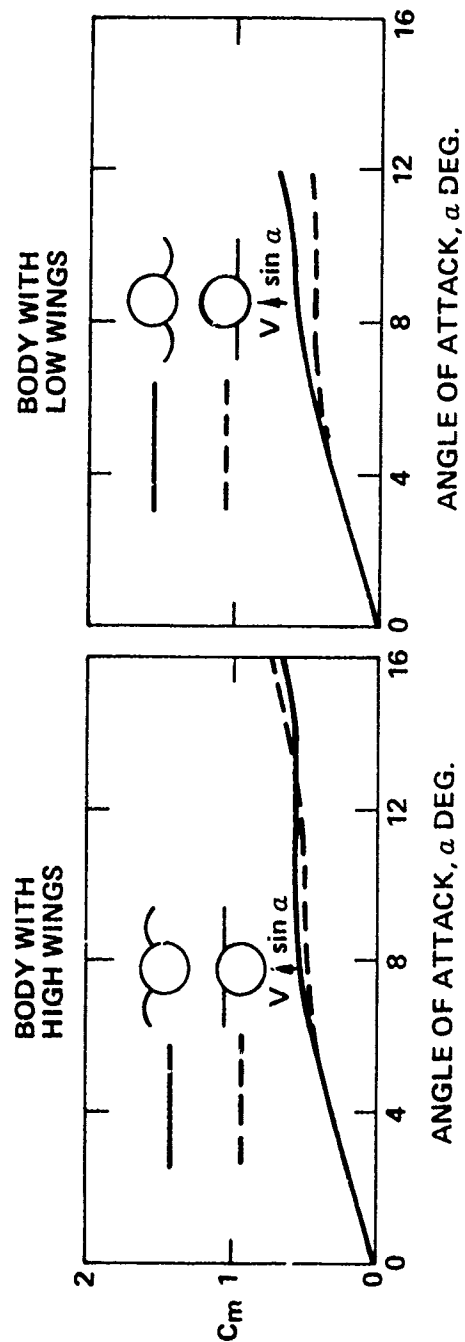


FIG. 5 COMPARISON BETWEEN WRAP-AROUND AND PLANAR WING-BODY PITCHING MOMENT COEFFICIENT  $M = 0.80$



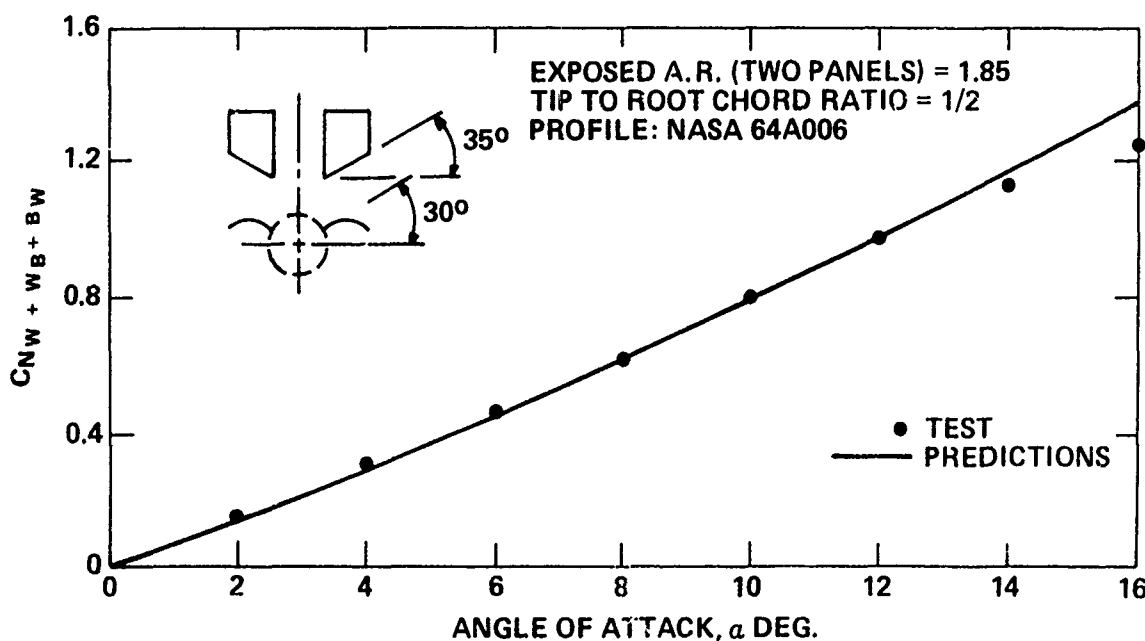
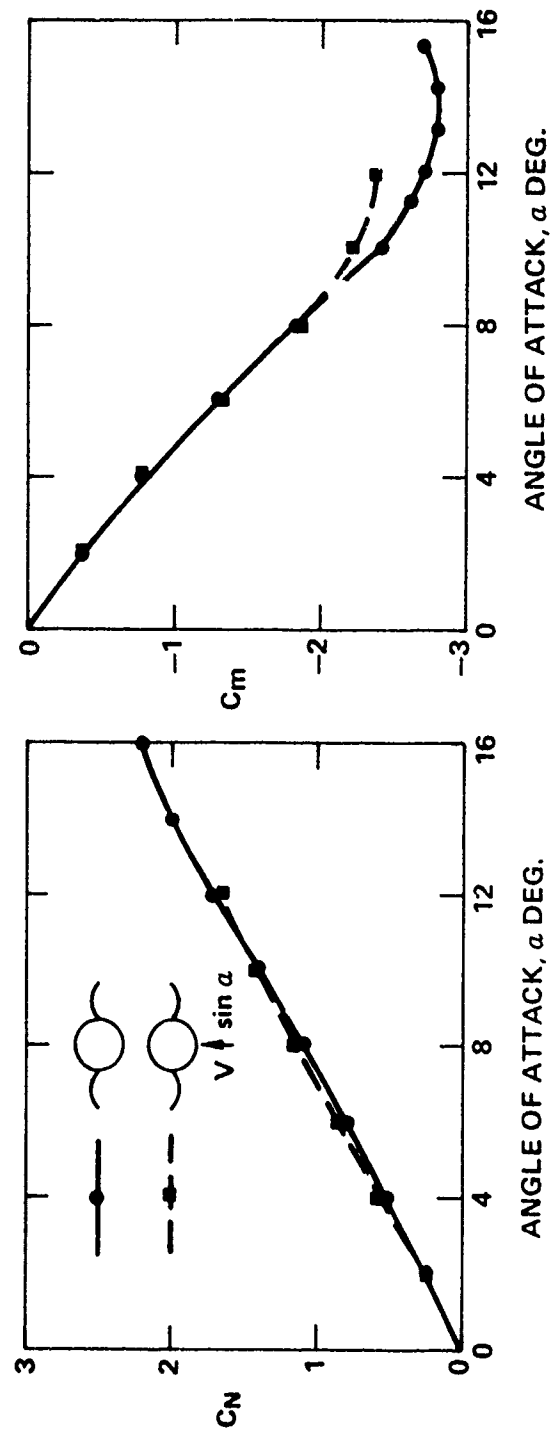


FIG. 6 COMPARISON OF WRAP-AROUND WING NORMAL FORCE (INCLUDING WING-BODY CARRYOVER) WITH PREDICTIONS USING THE LEADING EDGE SUCTION ANALOGY AND SLENDER BODY INTERFERENCE FACTORS  $M = 0.80$  (REFERENCE AREA IS PROJECTED PLANFORM AREA)

Fig. 7 EFFECT OF TAIL CONCAVITY ORIENTATION  $M = 0.8$

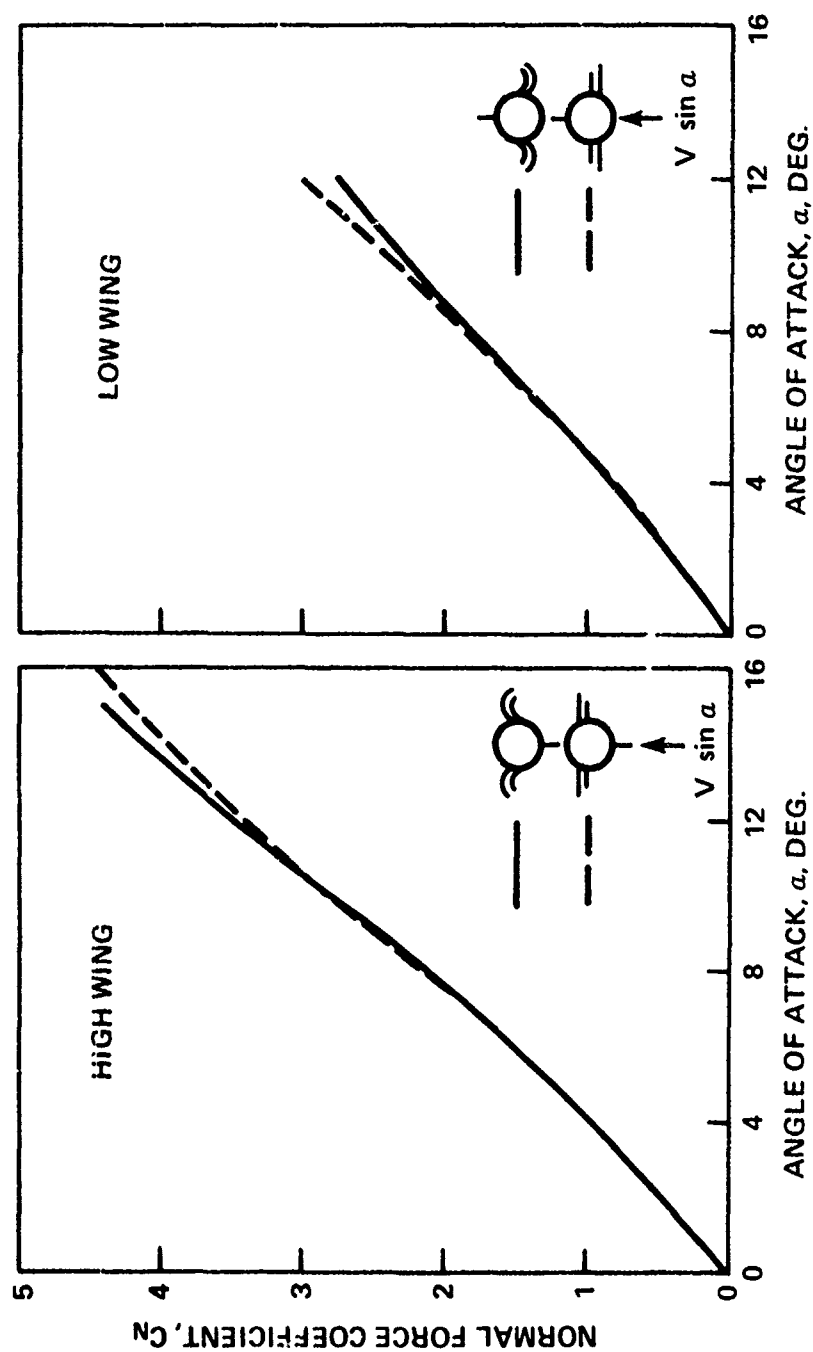


Fig. 8 COMPARISON BETWEEN CURVED SURFACE AND PLANAR SURFACE CONFIGURATIONS NORMAL FORCE COEFFICIENT  
M = 0.80

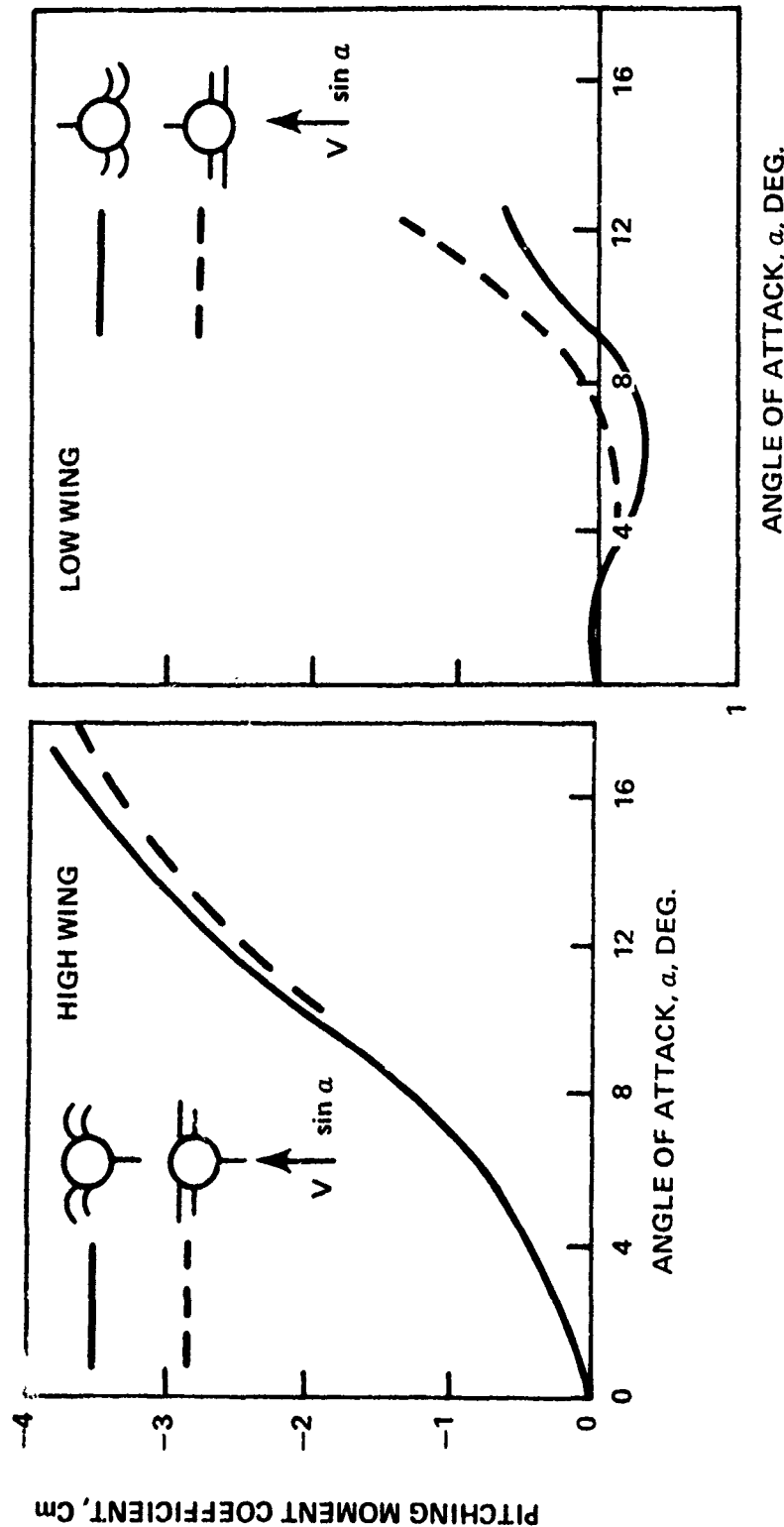


Fig. 9 COMPARISON BETWEEN CURVED SURFACE AND PLANAR SURFACE CONFIGURATIONS PITCHING MOMENT COEFFICIENT  
 $M = 0.80$

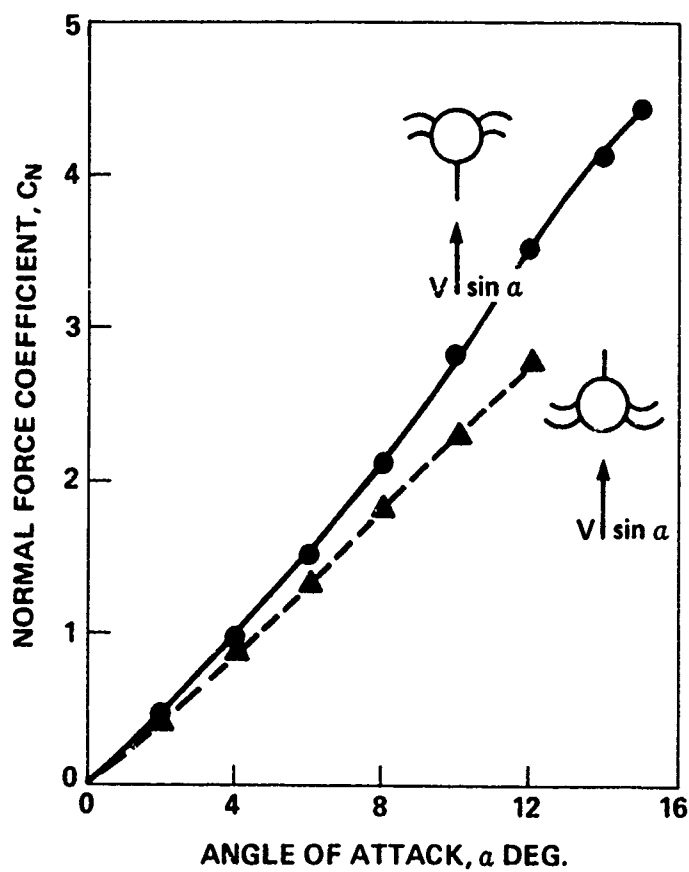


Fig. 10 EFFECT OF CONCAVITY ORIENTATION AND WING ELEVATION ON FULL CONFIGURATION NORMAL FORCE COEFFICIENT  $M = 0.80$

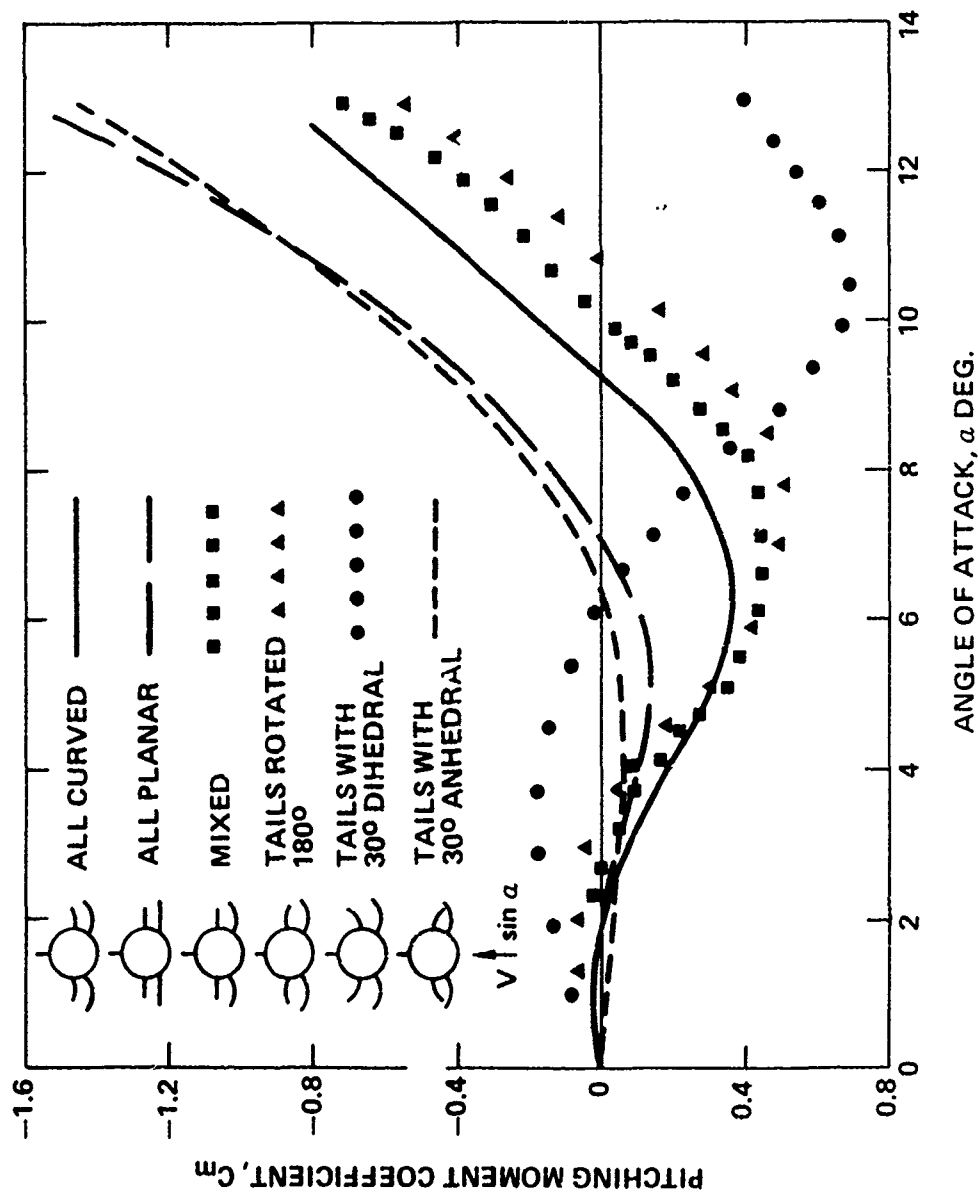


FIG. 11 COMPARISON OF PITCHING MOMENT COEFFICIENT FOR SEVERAL WASP-WING-BODY-TAIL CONFIGURATIONS  $M = 0.8$

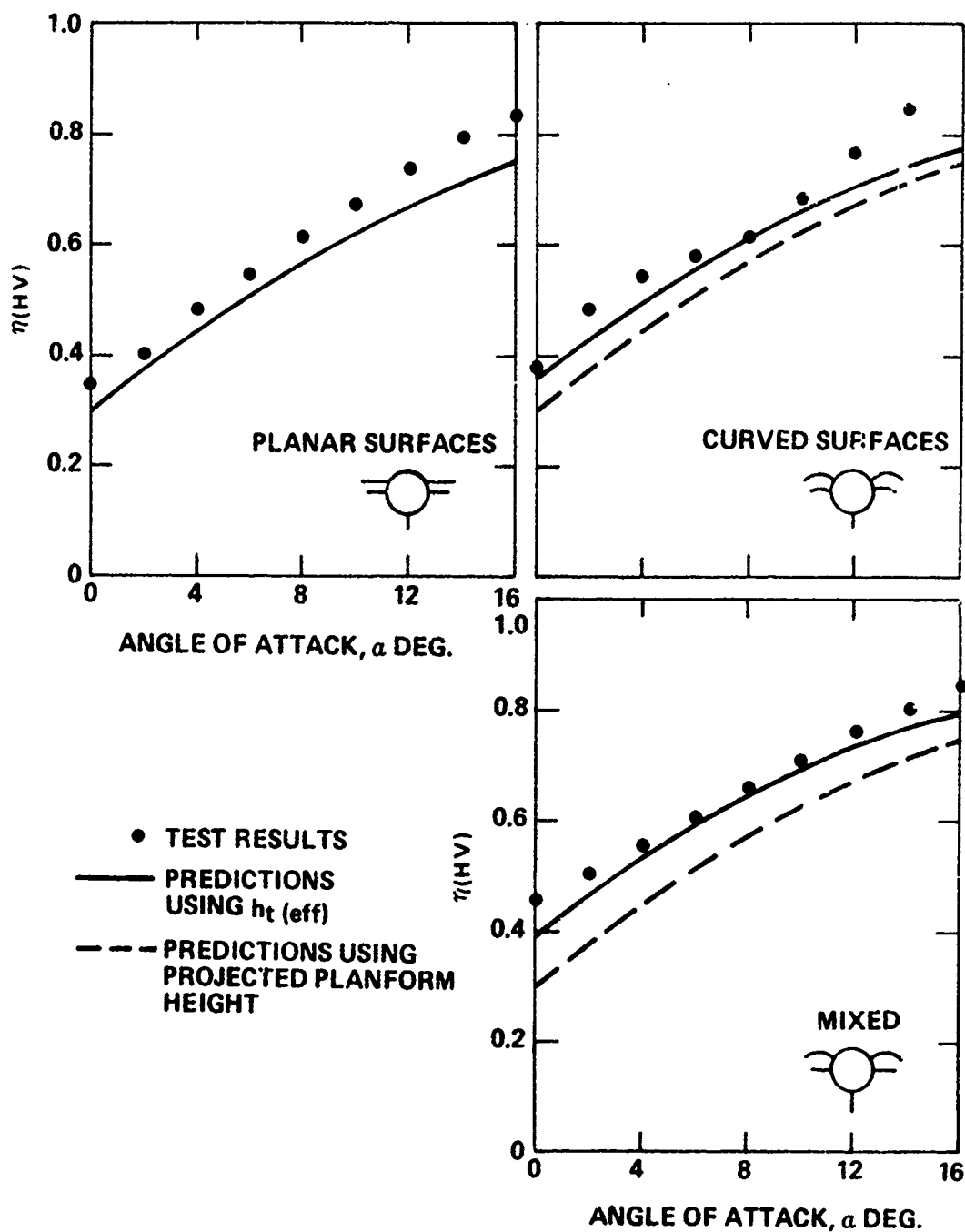


FIG. 12 COMPARISON BETWEEN TEST AND PREDICTED TAIL EFFICIENCY (HIGH WINGS)

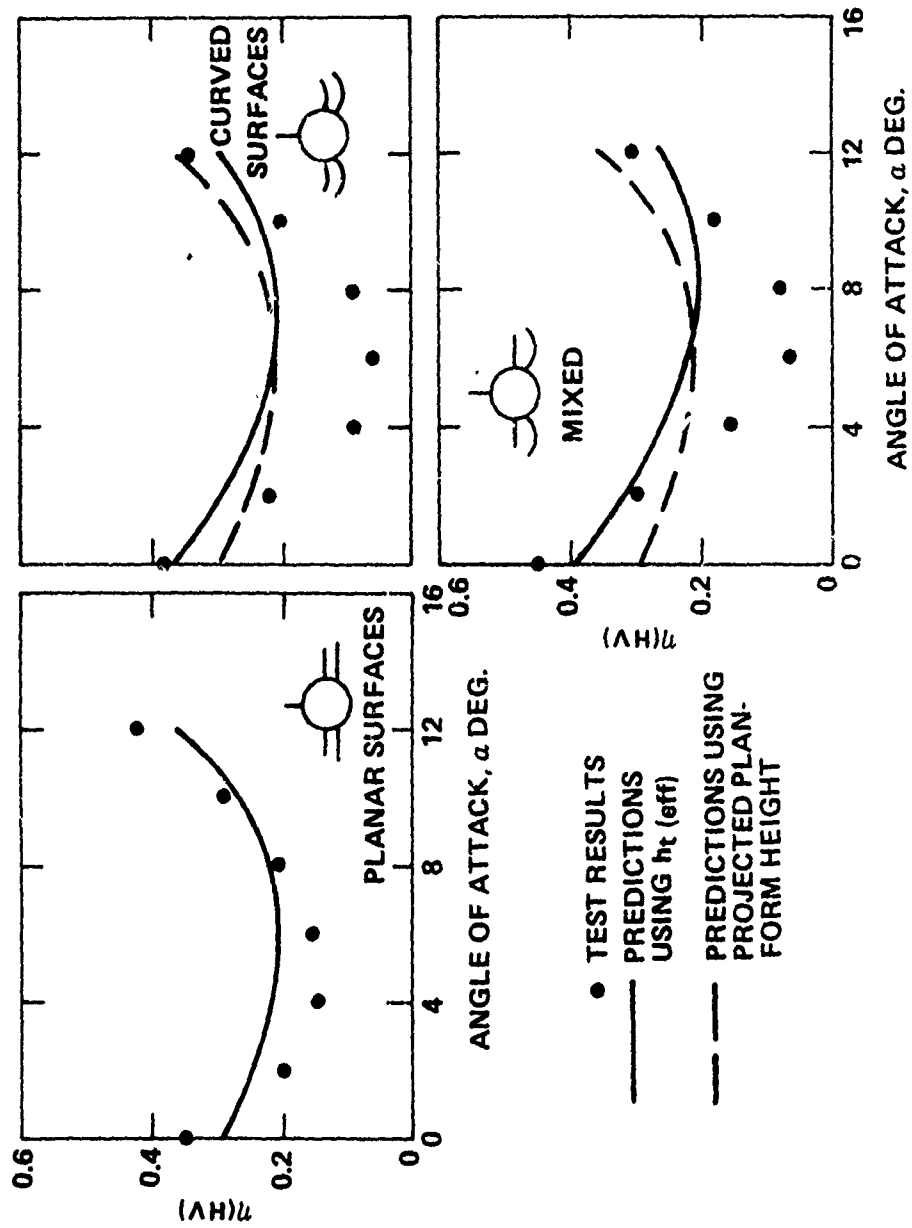


Fig. 13 COMPARISON BETWEEN TEST AND PREDICTED TAIL EFFICIENCY (LOW WINGS)



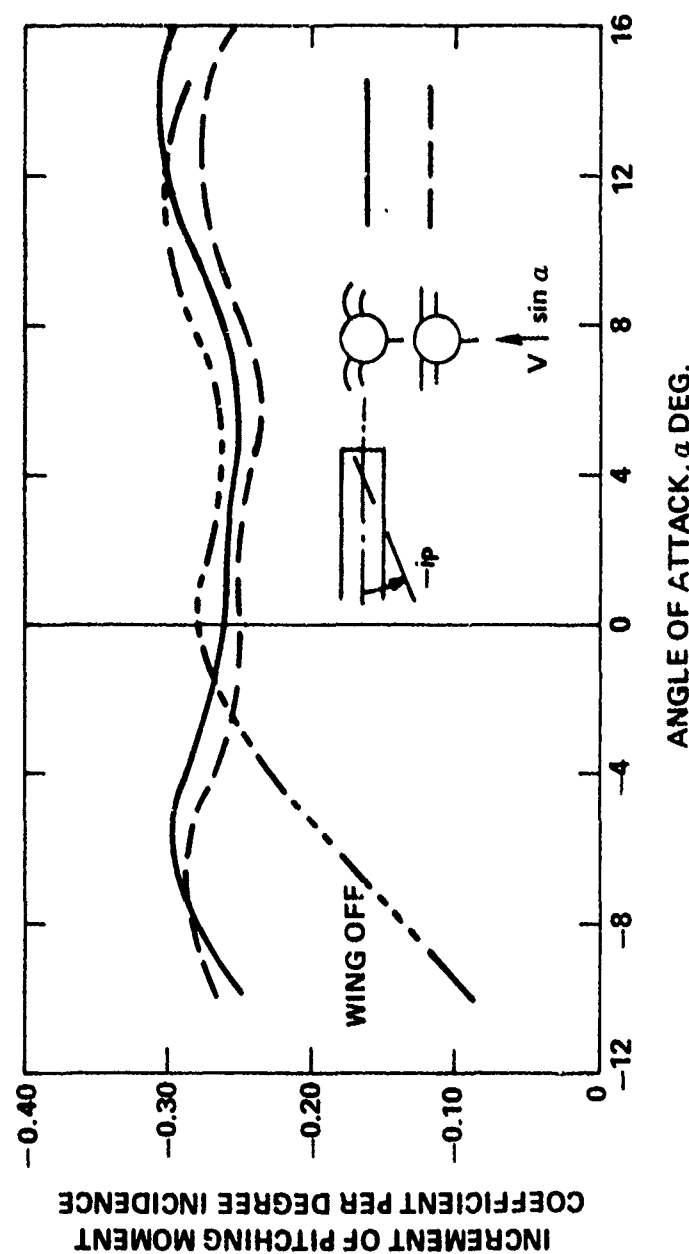


FIG 14 COMPARISON OF PITCH CONTROL CHARACTERISTICS OF WRAP-AROUND AND PLANAR SURFACE CONFIGURATIONS  $M = 0.80$  BASED ON  $ip = -10^\circ$

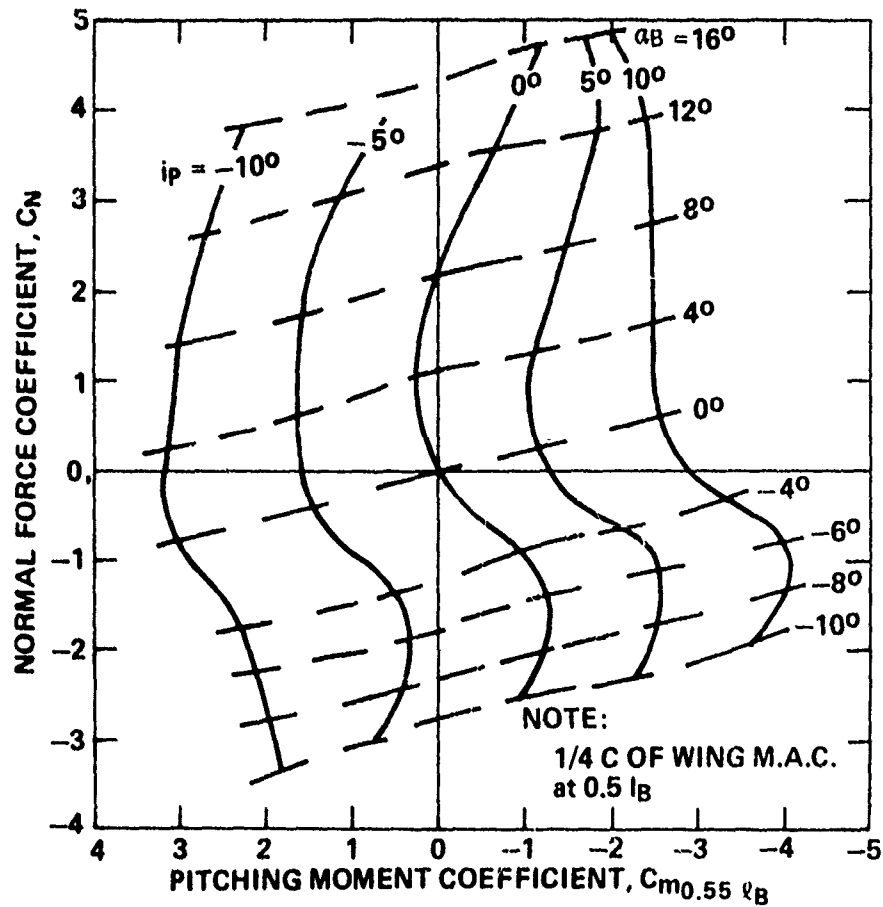


FIG. 15 WASP CONFIGURATION LONGITUDINAL STABILITY AND CONTROL CHARACTERISTICS  $M = 0.80$

SYM	CONFIGURATION	$i_p$	$a_B$
○	BODY-TAIL	$10^\circ$	$> 0$
□	"	$10^\circ$	$< 0$
●	"	$-10^\circ$	$> 0$
■	"	$-10^\circ$	$< 0$
△	BODY-WING-TAIL	$10^\circ$	$> 0$
◇	"	$10^\circ$	$< 0$
▲	"	$-10^\circ$	$> 0$
◆	"	$-10^\circ$	$< 0$

$$a_H(\text{eff}) = |a_B| - i_p - \bar{\epsilon} \quad a < 0$$

$$= |a_B| + i_p - \bar{\epsilon} \quad a > 0$$

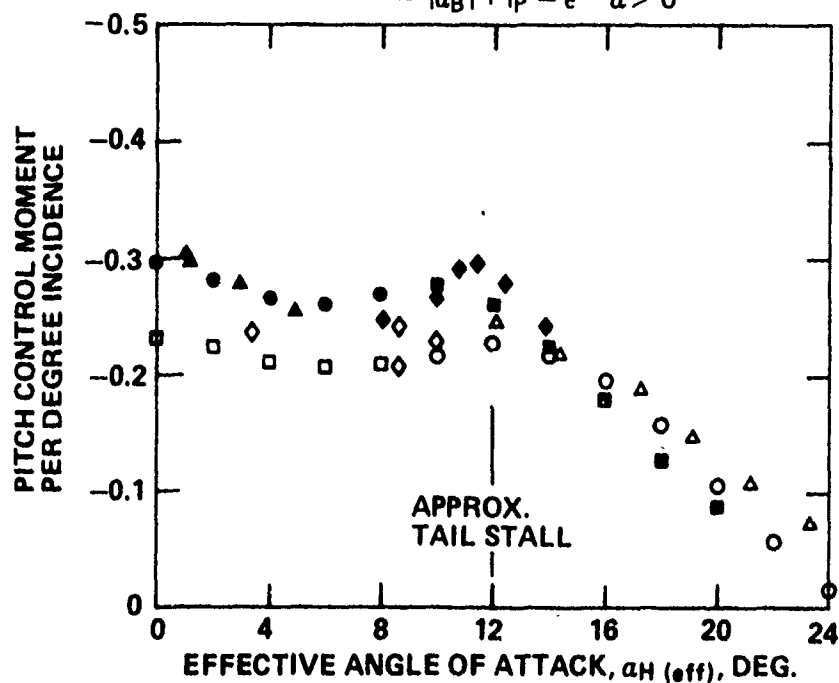


FIG. 16 CORRELATION OF PITCH CONTROL MOMENT WITH EFFECTIVE TAIL ANGLE OF ATTACK  $M = 0.80$

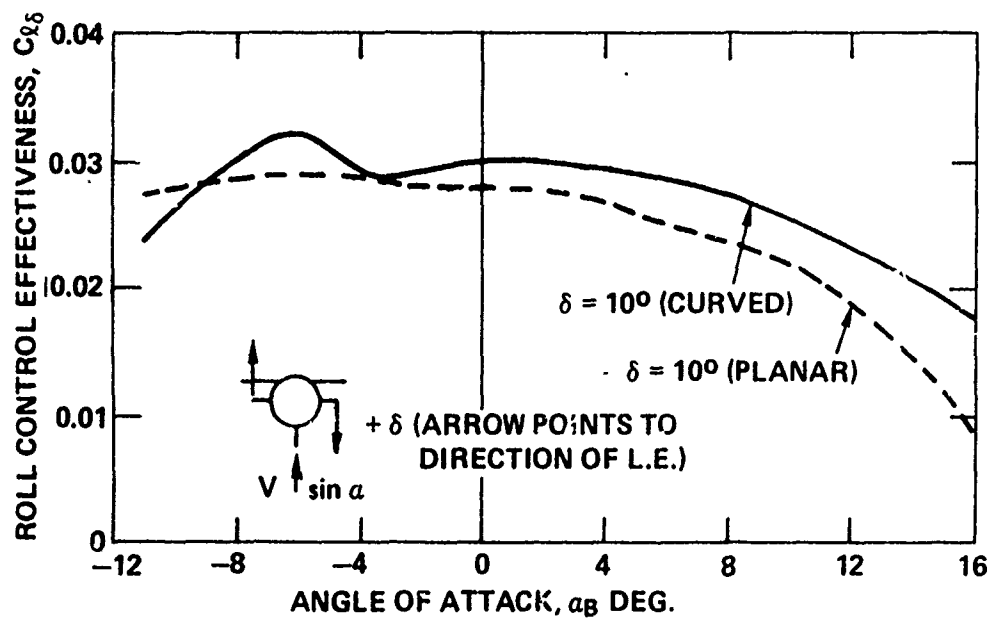


FIG. 17 EFFECT OF ANGLE OF ATTACK AND DIFFERENTIAL DEFLECTION ON ROLL CONTROL EFFECTIVENESS  $M = 0.80$

APPENDIX A

## RELATED STRUCTURAL STUDIES ON CURVED SURFACES

A concurrent structural design study on wrap-around wings suitable for a subsonic cruise missile has been conducted by APL/JHU (Ref. A.1). The study included finite-element stress, deflection, and vibration analyses and a system study on methods for folding the wings to permit stowage in a box or tube launcher. The wings were sized to conform to a selected body diameter and to support a selected panel load. Table AI compares several important design parameters for the wrap-around wing with those for a swept swing wing which retracts into the body. The same panel load and body diameter were used in the design of both wings. It is seen that the total system weight and volume of the wrap-around wings are respectively 53 and 38 percent of those of the swing wing. On the basis of these results and the aerodynamic studies it appears that wrap-around wings warrant further consideration for cruise missiles with folding surfaces.

TABLE AI

COMPARISON OF WRAP-AROUND AND SWING (RETRACTING)  
WING DESIGNS (REF. A.1)

<u>Parameter</u>	<u>Wrap-Around Wing</u>	<u>Swing Wing</u>
Total System Weight, lb	263	499
Total System Volume, in <sup>3</sup>	9,068	23,978
Limit Load Stress, psi	11,800	59,300
Tip Deflection, in	0.94	5.64
First Natural Frequency, cps	172	114

Selected Body Diameter: 34 inches

Selected Panel Load: 8660 pounds

REFERENCE

- A.1 R. M. Rivello, J. S. O'Connor and A. S. Polk, Structural Studies on Wrap-Around Folding Wings, APL/JHU TG-1274, March 1975.

PAPER NO. 12

TRANSONIC FLIGHT DYNAMICS OF LONG SHELL

by

V. Oskay and W. H. Mermagen

U. S. Army Ballistic Research Laboratories

ABSTRACT

Medium caliber projectiles of high fineness ratio, designed to satisfy a need for large payload capacities, have proven dynamically unstable at transonic speeds. Yawsondes were used to measure projectile sensitivity to launch disturbances and obtain yawing data along the flight trajectory. Nonlinear aerodynamics characterize the flight of the shell.

Modifications of the projectile boattail and cylindrical sections improved flight behavior by improving nutational damping. While the unmodified shell became unstable at six degrees initial yaw, the modifications allowed stable flight at up to sixteen degrees yaw. The effect of the design modifications on the projectile's flight behavior are discussed.

## I. BACKGROUND

The U. S. Army has been interested in high L/D shapes as means of delivering large payloads to long impact ranges. Army investigations of these configurations became active at the end of the Second World War and several studies were carried out during late 1940's and early 1950's<sup>1</sup>. As a result of these investigations, several high capacity, low drag shell have been designed during the 1960's for various caliber guns. These shell had L/D ratios of 5-1/2 or larger in order to meet the requirements imposed upon them. The M483 shell, a 155mm "Improved Conventional Munition" round, will be used to demonstrate the development history of a high L/D shell, the testing done to determine its flight behavior, the detection and explanation of poor flight performance, and a solution to the problem.

The M483 shell, shown in Figure 1, is designed to deliver a sub-caliber ammunition payload to target. It is fired from a 1/20-twist 155mm howitzer, either self-propelled or towed. In order to accommodate the maximum amount of payload, the shell has a 2.84-caliber cylindrical section (one caliber is equal to the shell's diameter). A 2.70-caliber long ogive and a 0.51-caliber long boattail were used to increase the impact range of the shell.

During the development of this shell, from 1964 to 1968, several configurations were fired through the Ballistic Research Laboratories' spark range facility (Transonic Range)<sup>2</sup>. The design which appeared to

1. F. E. Grubbs, et al, "A Family of Field Artillery," Ballistic Research Laboratories Report No. 771, September 1951, AD 377101.
2. W. K. Rogers, Jr., "The Transonic Free Flight Range," Ballistic Research Laboratories Report No. 1044, June 1958, AD 200177.

be most acceptable was then subjected to engineering and service tests. Finally, in early 1970's, the shell had gone through proof testing prior to its type classification.

The Transonic Range data indicated that at small yaws, below three degrees, the precessional component of the yawing motion was divergent for Mach numbers less than 0.9. They further indicated a stable, subsonic limit cycle and suggested the possibility of a nutational instability for subsonic Mach numbers at launch yaw levels above  $8^\circ$  to  $10^\circ$ . In contrast, the engineering tests did not give any indication of unacceptable performance. On the other hand, some data possibly indicating flight problems were obtained during the service test of M483 shell in 1968. Unfortunately, the problem occurred during the "Fire for Effect" phase (air burst) of the tests. At the time, it was decided that the problem was caused by fuse malfunction although Picatinny Arsenal (PA) and BRL aeroballisticicians disagreed with this conclusion.

About this time, the BRL was developing an on-board telemetry instrument known as a yawsonde. This instrument had been successfully used during the High Altitude Research Project<sup>3,4</sup>. In 1970, it was decided to use the same device to study the predicted limit cycle behavior of the M483 shell under normal launch conditions. Unfortunately, this round flew to the expected impact range. It gave indications of non-linear Magnus and damping moment coefficients.

3. W. H. Mermagen, "Measurements of the Dynamical Behavior of Projectiles Over Long Flight Paths," Ballistic Research Laboratories Memorandum Report No. 2079, November 1970, AD 717002.
4. W. H. Mermagen, "Projectile High-G Telemetry for Long Range Dynamics Measurements," Ballistic Research Laboratories Memorandum Report No. 2133, October 1971, AD 733305.



In 1970, Chapman and Kirk of NASA had published a paper on a method of analyzing free-flight data<sup>5</sup>. As a result of this paper, it was decided to repeat previous subsonic yawsonde tests of M483 in 1972 with the added intention of determining aerodynamic coefficients at yaw levels higher than the ones observed during Transonic Range firings. In order to achieve the desired yaw levels, a yaw inducer (Figure 2) was designed. The shell fired without induced yaw during this test series confirmed previously observed nonlinear character of the aerodynamic coefficients. On the other hand, the shell fired with induced yaw fell over 1,500 meters short. This was the first time that the M483 was observed misbehaving under controlled test conditions. Another interesting aspect of these test results was that the nutational component of the yawing motion was unstable at these yaw levels as implied by the earlier Transonic Range tests.

In February 1974, a 20-round group of M483 shell was tested at Nicolet, Canada, at transonic launch Mach number and under severe atmospheric conditions (below 10° F and more than 110% of standard ICAO air density)<sup>6</sup>. Thirty-five percent of these shell fell short. This performance under severe but still within military specification conditions indicated the existence of an aeroballistic problem.

---

5. G. T. Chapman and D. B. Kirk, "A Method for Extracting Aerodynamic Coefficients from Free-Flight Data," AIAA Journal, Vol. 8, No. 4, April 1970.

6. R. L. McCoy, J. H. Whiteside, and E. D. Boyer, "155mm Cold Weather Transonic Test (U)," Ballistic Research Laboratories Memorandum Report No. 2397, July 1974, AD 531198L, (CONFIDENTIAL).

Since M483 is a long, spin stabilized shell, it was predicted that the aeroballistic problem was the Magnus characteristics of this projectile. The Magnus moment problems generally can be alleviated by changing the center of mass location, shortening the shell, or reducing the boattail length to improve transonic behavior especially. Relocation of the projectiles center of mass would have required a major redesign effort. Due to logistic problems, PA decided to reduce the boattail length of the projectile to improve its transonic Magnus properties without paying a large drag or payload penalty. A second modification, to be used only as a back-up, was to reduce the cylindrical portion of the shell by 0.3 caliber in addition to the shortened boattail. For both modifications, the removed weight was strategically relocated to improve the projectile's gyroscopic stability. Due to time limitations, only these two modifications have been tested at Yuma Proving Ground (YPG) under the PA auspices and shown to be stable at first maximum yaw levels as high as 13 degrees. The tests at Nicolet under high air density conditions also did not show any flight instabilities.

This paper discusses in detail the test procedures used during the investigation, the aeroballistic data currently available, the characteristic of the flight misbehavior of the M483, the flight improvements obtained by the modified designs, and finally the implications of this investigation for future shell designs.

## II. TEST PROCEDURES

During the development of the 155mm M483 shell, the only available test data were obtained from a 14-round test of the prototype fired in

1964 and a 19-round program of the preproduction shell fired in 1968 at the Transonic Range. Almost all of these rounds were at small yaw with a minimal coverage of the transonic Mach numbers. In 1970 and 1972, these data were supplemented with yawsonde instrumented flights at the Wallops Island Facility of NASA and at YPG.

In 1974, after the first Nicolet tests, several types of data source were used to determine the aeroballistic behavior of the M483 shell and its modifications. These included spark range tests, yawsonde tests, first-maximum-yaw tests, standard time-of-flight and impact-range tests, and wind tunnel tests. The investigative test program of the M483 and its modifications culminated in January-February 1975 with the second Nicolet tests under transonic launch Mach number and high air density conditions.

Wind tunnel tests of the M483 were performed at CALSPAN Corporation in January 1974 and Arnold Engineering and Development Center (AEDC) in September 1974. Tests were performed under PA supervision and the data were analyzed by them. Static moment coefficient from the wind tunnel tests agree within 10% with the spark range data. Although Magnus moment data from both wind tunnels agree with each other, neither the magnitude nor the yaw trends of the wind tunnel data agree with the range data. In particular, the wind tunnel data would not allow a limit cycle behavior. Therefore, the wind tunnel tests will not be included in the discussions because of this unexplained discrepancy.

A. Time-of-Flight and Impact-Range Tests

Most of the time-of-flight and impact-range tests (for the rest of the report the phrase "impact-range tests" will be used as a shorthand) were performed at YPG. The only two exceptions were a group of 35 live

M483 shell fired at Aberdeen Proving Ground (APG)<sup>7</sup> to determine whether the results of the February 1974 tests at Nicole<sup>7</sup> could be repeated and 10-round groups of M483 and XM687 shell fired at Dugway Proving Ground (DPG)<sup>8</sup> to compare their flight performance under similar launch conditions.

All impact-range tests measured muzzle velocity (with GE chronographs), initial shell yawing motion (with orthogonal pairs of smear or Fastax cameras), and impact time and range (with observers). Meteorological data on wind speed and direction as well as air density and temperature were provided as a function of altitude during the test firings.

During the APG firings, two Hawk doppler radars were used to measure shell's velocity history. On the other hand, DPG used a modified M33 tracking radar to determine shell trajectory. Since different tipping rates were induced on both the M483 and its modifications during the YPG tests, yaw cards were used to determine the yaw levels generated. The YPG tests also used a Hawk doppler radar to measure the shell's velocity history.

The APG and DPG programs were designed to obtain specific information and as such a predetermined number of shell were fired. On the other hand, the YPG tests were fired to compare the M483 and its modifications under different launch conditions. Therefore, the test firings

---

7. "Test Program Request, No. SARPA-AD-D-W 1807," Picatinny Arsenal, April 1974.

8. C. C. Sterns and J. Martin, "Engineering Design Test (Inherent Stability) of Projectile, 155mm, GB2, XM687, Data Report," Dugway Proving Ground Document No. DPG-DR-74-320, June 1974.

Vol. 1

were structured around 20-round groups in order to insure statistical significance for the results. The only exception to this procedure was for the case of two or more shots before the end of the 20-round group. Firing was stopped at that point.

B. First-Maximum-Yaw Tests

First- maximum-yaw tests of the M483 were done at YPG and the Transonic Range Facility of BRL at APG. BRL tests<sup>9</sup> consisted of firing a 20-round group of inert M483 shell from the M109A1 howitzer used during the first Nicolet tests approximately at a 15-degree QE in order to have an active recoil system. Since the flight path through the Transonic Range is nearly horizontal, the tube elevation was accomplished by raising the rear of the vehicle. During this test, the shell were temperature conditioned and fired at a Mach number of about 0.93. In addition to the standard Transonic Range instrumentation (see next section), an OPTRON was used. The OPTRON is an optical instrument designed to measure the muzzle movement of a gun during the firing cycle. OPTRON was included in the test program to determine if a correlation could be found between muzzle motion and the first maximum yaw level.

The first-maximum-yaw tests at YPG were part of Picatinny's investigation program. To permit use of yaw cards, an M109A1 self-propelled howitzer was fired at a 17-degree QE. The purpose of the program was to determine the distribution of first maximum yaw for groups of twenty M483 shell fired at transonic Mach numbers from tubes at various stages of their lives (new, 50% worn, and condemned). The

---

9. J. H. Whiteside and V. Oskay, "First Maximum Yaw Tests of 155mm M483 Shell," Ballistic Research Laboratories Memorandum Report in preparation.

primary yaw measurements during these tests were made with three pairs of orthogonal smear cameras. The yaw cards provided a fast indication of the yaw levels and were used during the remainder of YPG impact-range tests. The rest of the instrumentation was similar to those described for the standard time-of-flight and impact-range tests.

#### C. Free Flight Spark Range Tests

The BRL free flight spark range facility (the Transonic Range) is a 360-metre long building with a 7.5 x 7.5-metre cross section. The first 230 metres of Range is instrumented with 25 pairs of orthogonal shadowgraph stations divided into five groups. The five stations within each group are separated by 6 metres and there is a 21-metre interval between each group. The images of the test projectile on the screens of the shadowgraph stations are photographed to obtain a record of position and yawing motion as functions of flight time. The time base is provided by 19 timing stations slaved to the shadowgraph stations. From these data, the aerodynamic coefficients of the projectile are computed. Details of the Transonic Range instrumentation and the method for computing the aerodynamic coefficients are given in Reference 10.

In addition to the shadowgraph data, the Transonic Range can provide a microflash photograph for metal parts integrity and a composite mosaic, which is a full-size direct shadowgraph, for study of flow details.

#### D. Yawsonde Tests

A yawsonde is an on-board instrument capable of measuring the solar aspect angle history of a projectile along its flight path. The solar

---

10. C. H. Murphy, "Free Flight Motion of Symmetric Missiles," Ballistic Research Laboratories Report No. 1216, July 1963, AD 442757.

Vol. 1

aspect angle is defined as the angle between the projectile's axis of symmetry and a sun's ray passing through the shell's center of gravity.

Two silicon solar cells, mounted so that their fields of view form a V, are used to detect the sun as the shell rotates. Each cell sees the sun once during each revolution and at that time produces a voltage pulse which is shaped and amplified by the electronic circuitry of the yawsonde. These signal pulses are transmitted to ground receivers through an FM/FM link and taped for analysis at a later time.

The yawsonde pulses, which are recorded on analog instrumentation tape, are later on reduced by a hybrid computer program to determine spin and solar aspect angle histories of the shell as functions of time of flight. The time interval between yawsonde pulses is measured by the  $10^6$ -bit internal clock of the EAI 680 (the analog portion of the hybrid computer). The spin of the shell is computed from the elapsed time measured between two consecutive pulses generated by the same solar cell. The solar aspect angle history of the shell is obtained from the phase relationships between the yawsonde pulses. For convenience, the complementary solar aspect angle ( $\sigma_n$ ) is determined during the calibration and represents the angle between the solar vector and a vector perpendicular to the missile's axis of symmetry. Complementary solar aspect angle histories will be presented when yawsonde data are discussed in the following sections. Details of yawsonde construction and data analysis are given in Reference 3.

During the instrumented flights of the M483 two types of yawsondes were used. The ogive yawsonde has solar cells mounted on the ogive itself and has been used during the 1970 and 1972 test programs. The fuse-type yawsonde is a unit built to be interchangeable with a standard fuse and

does not require any machining of the ogive. It was developed in late 1972 and has been the main instrumentation used since May 1973. Basic construction and use of the fuse-type yawsonde is similar to the ogive-type and is described in greater detail in Reference 11.

#### E. Nicolet Tests

The Nicolet test program was sponsored by PM-SA and managed by MTD. One of the purposes of the Nicolet test program<sup>12</sup> was to determine the flight behavior of the modified M483 shell under critical Mach number and high density conditions. Standard and modified M483 shell were fired at different Mach numbers, at two quadrant elevations (QE), from two separate howitzers (one self-propelled and the second towed), and on several occasions. In order to make the results statistically significant, all shell were fired in 20-round groups or until two or more shorts were detected. During the test program, several yaw inducers were used to control the launch tip-off rate rather than depending on random disturbances generated by weapon/shell interactions.

Similar to other impact-range tests, the usual meteorological data, muzzle velocimeters, and impact point observers were provided. Due to the requirement of specific meteorological conditions (air temperature below  $-10^{\circ}\text{C}$  and air density above 110 percent of standard ICAO atmosphere), the number of available firing days was very limited. Therefore, redundant instrumentation was used in order to maximize the usage

- 
11. W. H. Mermagen and W. H. Clay, "The Design of a Second Generation Yawsonde," Ballistic Research Laboratories Memorandum Report No. 2368, April 1974, AD 780064.
  12. "Test Program Request, No. SARPA-AD-D-W-1833, Revision 1," Picatinny Arsenal, 5 November 1974.



of the few available days. Three radar chronographs were used to determine muzzle velocity. A Hawk radar was modified so that it could be used in combined doppler/tracker mode. A RCA MPS25 tracking radar was provided as a back-up to the observers.

In addition to standard impact-range testing, some yawsonde instrumented shell were fired to obtain first-maximum-yaw and flight dynamics data. In order to support yawsonde tests, a telemetry receiving station was provided and manned by BRL.

### III. AEROBALLISTIC DATA ON 155MM M483 SHELL

The aeroballistic data available for the 155mm M483 ICM shell can be divided into two groups, before 1973 and after 1974. Test data prior to 1973 consisted of some spark range and yawsonde tests. On the other hand, the data after 1974 included results from spark range firings, yawsonde tests, wind tunnel tests, and large amounts of impact-range test results. In this section, the data available from spark range and yawsonde tests will be discussed. These data are grouped according to their date of demarcation.

#### A. Test Data Prior to 1973

1. Spark Range Tests. Prior to 1973, two spark range programs had been fired in the Transonic Range Facility of BRL for the M483 shell. The test program fired in 1964 used a prototype shell. The prototype XM483 had a fiberglass wrapped boattail in addition to the body wrapping, see Figure 1. Most of the data were at small yaw and several of the data rounds had damaged boattails.

In 1968, a second spark range program was undertaken with the pre-production models of XM483. This model still had the fiberglass wrapping

on the body but the boattail was metal. Again most of the data was at small yaw (under two degrees). A few rounds at higher yaw levels were fired at a gyroscopic stability factor  $s_g \approx 1.0$ . Therefore, some of the spin dependent results, such as Magnus coefficients, were poorly determined.

Figure 3 shows the variation of the static moment coefficient slope ( $C_{M_\alpha}$ ) as a function of Mach number. The lower curve represents the data obtained with the prototype shell. It shows a peak at  $M = 0.85$ . On the other hand, the preproduction model has a higher static moment. The peak of this static moment curve appears to be at  $M = 0.93$ .

An example of the Magnus moment coefficient slope ( $C_{M_{p\alpha}}$ ) as a function of Mach number is given in Figure 4 for the preproduction shell. This curve also has a peak in the transonic region. Although most of the data were at small yaw, there was a slight indication that the Magnus moment may be highly nonlinear function of yaw level.

This combination of high peaks in both the static moment and Magnus moment curves in the transonic Mach number region portends possible trouble at those velocities. Details of the aerodynamic properties, including drag and pitch damping ( $C_{M_q} + C_{M_\alpha}$ ) coefficients, of the prototype and preproduction shell are included as an appendix in Reference 9. The conclusion drawn at that report was that at small yaws the M483 shell is precessionally unstable with a possibility of nutational instability at yaw levels above  $8^\circ$  to  $10^\circ$ .

2. Yawsonde Tests. The 155mm XM483 was one of the first spin-stabilized shell which carried yawsonde instrumentation. Figure 5 shows

an XM483 shell instrumented with a yawsonde installed in its ogive. In 1970 and 1972, three short test programs were fired with instrumented XM483 shell using ogive yawsondes<sup>13</sup>. Two of the three programs were fired at Wallops Island while the third (in February 1972) was fired at YPG.

The first yawsonde program was fired in July 1970 both as a test of yawsonde instrumentation and as a quick look at the limit cycle behavior of the XM483 shell at subsonic Mach numbers. Three rounds were fired with only one of them producing yawsonde data. Figure 6 is a plot of the yawsonde data from this round. The complementary solar aspect angle ( $\sigma_n$ ) is plotted as a function of time of flight. Although the plotted motion is only a one-dimensional representation of the actual motion of the projectile, it gives a good detailed indication of the shell's flight behavior. Figure 6 shows two aspects of the flight characteristics of an XM483 launched at a Mach number of 0.75. First, the shell flies with a yaw level of about three degrees along its entire trajectory. Second, the limit cycle of the XM483 shell contains both fast and slow modes rather than the expected pure mode precessional motion. This limit epicycle behavior is another indication of the non-linear aerodynamics of the XM483 shell at small yaw levels and subsonic Mach numbers. In 1972 it was decided to repeat the 1970 yawsonde tests to obtain yawsonde flight data at higher yaw levels as a supplement to the existing spark range data. About the same time, BRL had developed

---

13. W. H. Mermagen and V. Oskay, "Long Range Dynamics Flight Experiments with the 155mm Projectile, M483," Ballistic Research Laboratories Memorandum Report No. 2396, July 1974, AD 922181L.

a technique for generating intermediate levels of first maximum yaw. The yaw inducer used for this purpose is shown in Figure 2. In early 1972, a 6-round yawsonde program was fired at YPG and partly repeated at Wallops Island in July 1972. All rounds fired during these two programs had induced yaw. Figure 7 shows the flight behavior of a shell fired at Wallops Island (Round E1-6068) with a launch Mach number of 0.80. This shell has several differences in flight behavior when compared to the naturally launched round (Figure 6). With the minimum induced yaw, Round E1-6068 achieved a yaw level of about  $7^\circ$  at two seconds into the flight. Yawsonde data indicate damped precession and nutation until ten seconds into flight. At that point, the yaw amplitude is about  $1^\circ$  with precession as the main component. The rest of the flight, the precessional amplitude grows to about  $3^\circ$  supporting the spark range predictions for small yaw.

When the induced yaw level is increased to about  $12^\circ$ , the result is a flight behavior similar to that shown in Figure 8. This round, Y-1284, was fired at YPG with a launch Mach number of 0.78. It impacted about 1650 metres shorter than the expected impact range. This was the first time an XM483 shell was observed falling short. At one second into the flight, the yawing motion was divided almost equally between nutational and precessional components. By four seconds into the flight, the nutational component has grown to about  $9^\circ$ . The amplitude of the nutational component at eleven seconds is about  $25^\circ$  and the rate of divergence is still increasing.

Other yawsonde data from the 1972 tests indicate that at launch Mach numbers less than 0.80 the XM483 shell will be nutationally unstable if fired with yaw levels above  $10^\circ$ .

Vol. 1

B. Test Data After 1974

Between 1972 and 1974, a false sense of well being prevailed with respect to XM483 flight behavior since no one expected 10° first maximum yaws from normal launches. In 1973, XM483 was type classified. In February 1974, the M483 (the new nomenclature indicates that it was not an experimental shell any longer) projectile was included in a test program designed to determine the flight behavior of a new 155mm shell family under transonic Mach number and high air density conditions<sup>6</sup>. A 20-round group of M483 shell were fired from an M109A1 self-propelled howitzer at an average launch Mach number of 0.93. Seven of these 20 rounds impacted 2,000 - 3,000 metres shorter than the mean impact range of the remaining thirteen rounds. This flight misbehavior led to an immediate flurry of investigative activity. The remainder of this section will discuss some of the preliminary spark range and yawsonde data obtained for the M483 shell during 1974.

1. Spark Range Tests. Two spark range tests were fired as part of the M483 investigative program sponsored by PM-SA. The first program was designed to determine the first maximum yaw distribution of the M483 shell at critical Mach number (0.92 - 0.94) under controlled test conditions using the same weapon as February 1974 tests. The second test was for obtaining more detailed aerodynamic properties of the shell as functions of Mach number and yaw angle.

The first-maximum-yaw tests were fired from a horizontal tube with the rear of the vehicle jacked up to obtain an effective gun elevation of 15°. During the test program, an OPTRON was used in addition to the full complement of Transonic Range instrumentation<sup>2</sup>. At the present time, the analysis of the OPTRON data is still going on and no definite

conclusions can yet be drawn. The aerodynamic data from this program are plotted on Figures 9 and 10. Figure 9 shows a comparison of the static moment coefficients obtained from the 1968 tests of preproduction shell and the inert M483 shell fired in 1974. The 1974 data are within a Mach number region from 0.92 to 0.95. The new data show that the static moment coefficient has a very narrow peak about 7 percent higher than the previous estimate. The width of the peak is about  $\pm .01$  centered around  $M = 0.93$  which was originally considered to be a small data gap. The Magnus moment coefficient, shown in Figure 10, exhibits the same trend as  $C_{M_\alpha}$ . The 1974 data indicate that this coefficient also has a narrow peak centered around  $M = 0.93$ . The new data show a peak four times as high as the 1968 estimate. This would seem to indicate that potential transonic flight problems lie within a very narrow region. Secondly, the increased peak values of static and Magnus moment coefficients determined from these small yaw data would indicate that lower than originally expected values of first maximum yaws would be sufficient to initiate flight problems.

The second spark range program, designed by PA and BRL aeroballisticians, involved 105mm models of M483 shell. Figure 11 is a photograph comparing the full scale M483 with its 105mm model. Analysis of the test data to determine Mach number and yaw trends of the aerodynamic coefficients is continuing. Figure 12 is a mosaic shadowgraph of a 105mm model at a Mach number of 0.917. This round and several others within the transonic region have been analyzed by Whyte of General Electric at Burlington, Vermont, under a PA contract, using Chapman-Kirk technique

Vol. 1

adopted for BRL Transonic Range data<sup>14,15</sup>. Preliminary results of this analysis<sup>16</sup> support the 1974 data shown in Figures 9 and 10. Some of the conclusions from Reference 16 will be used later in this paper to explain the flight behavior of the M483 shell.

2. Yawsonde Tests. As part of the 1974 investigation of M483 behavior and attempts to eliminate its aeroballistic problems, several sizeable yawsonde programs were fired at Wallops Island, YPG, and Nicolet. Standard and modified M483 shell were instrumented with BRL's fuse type yawsondes (see Reference 11 for detailed description). Earlier yawsonde data (obtained in 1970 and 1972) were obtained for launch Mach numbers less than 0.80 which are outside the region of minimum gyroscopic stability according to the latest spark range data on M483. Therefore, a yawsonde test program was instituted at Wallops Island to determine the yaw level beyond which the M483 shell would become unstable at  $M = 0.94$ . It was also attempted to obtain the highest possible yaw level in order to increase the free flight aerodynamic data base. A small group of modified M483 shell were also tested at Wallops Island for comparison. The sole purpose of the yawsonde tests at YPG was to obtain free flight data for the modified M483 shell; therefore, no standard M483s were tested with yawsondes. During the Nicolet

- 
14. R. H. Whyte and A. Jeung, "Aerodynamic Reduction of Free Flight Transonic Range Data Utilizing Numerical Integration," General Electric Report No. 71APB514, April 1971.
  15. R. H. Whyte and W. H. Hathaway, "Aeroballistic Range Data Reduction Technique Utilizing Numerical Integration," General Electric Report No. AFATL-TR-74-71, February 1974.
  16. G. Craver, W. H. Hathaway, and R. H. Whyte, "Analysis of XM483E1 Transonic Range Data Utilizing Numerical Integration," General Electric Report, February 1975.

test in January-February 1975, the standard M483 shell was used as a control. As a result, several M483 shell were instrumented with yawsondes. In the following paragraphs, the Wallops Island and Nicolet test results for the standard M483 shell will be discussed. Yawsonde data for the modified M483 shell will be discussed in Section IV.B.3.

In the past, most of the testing under controlled environment (both spark range and yawsonde) had been done with M483 shell carrying a slug payload designed to simulate the physical properties of the live shell. More recent tests of the shell at Nicolet in February 1974 were done with inert payload. In order to determine if the payload affected the shell's flight behavior, four of the thirteen rounds fired at Wallops Island carried slug payloads. The remainder contained inert payloads. No changes in flight behavior were detected as a result of payload variations. Another feature of this program was that all rounds were fired with yaw inducer 1 (see Figure 2). A summary of the test data is given in Table 1 taken from Reference 17. A study of this table indicates that at Mach numbers outside of the critical region the M483 shell is capable of stable flights. For example, the Round E1-7177 (shown in Figure 13) had over 8 degrees yaw level when launched and still impacted at the expected range. This confirms the result previously obtained from 1970 and 1972 yawsonde tests. Figure 13 shows a strongly damped precession and a very sluggish nutation. In contrast, Figure 14 shows the yawing motion of a round fired at  $M = 0.94$  (E1-7256) with

- 
17. V. Oskay and R. L. Lieske, "Yawsonde Tests of 155mm M483 and XM718 Shell at Wallops Island," Ballistic Research Laboratories Memorandum Report in preparation.



Vol. 1

approximately the same initial yaw level as Round E1-7177,  $7.2^\circ$  versus  $8.2^\circ$ . After the first second of the flight, the yawing motion of the shell is dominated by the nutational component which has an increasing rate of undamping. This contrast holds true for Rounds E1-7160 and E1-7166 whose launch conditions are quite similar. This gives an indication as to the sharp demarcation of launch Mach numbers between a well behaved and an unstable M483 shell. Figure 15 shows the yawing motion of an unstable M483 with the smallest yaw level ( $3.7^\circ$ ) observed. Flight behavior of this shell is quite similar to the other unstable M483.

Yawsonde data from 1975 Nicolet tests are reported in Reference 18. In this paragraph, some of the flight data from those tests will be reviewed. During the Nicolet test program, four different yaw inducers have been used to study the flight behavior of standard and modified M483 shell. A short description of these yaw inducers are given in Table 2. The standard M483 shell instrumented with yawsondes were fired at  $M = 0.92$  with a standard muzzle brake and at the critical Mach number region with yaw inducers 1 and 2. The standard muzzle brake gave yaw levels less than two degrees. Due to this unexpected behavior of the weapon system, most of the remaining Nicolet tests were fired with yaw inducers 1 and 2. Yaw inducers 1 and 2 generated first maximum yaw levels of nine and thirteen degrees, respectively. All yawsonde instrumented M483 shell with induced yaw were unstable and gave a flight behavior similar to that shown in Figure 14.

- 
18. V. Oskay, W. H. Mermagen, W. H. Clay, and J. H. Whiteside, "Flight Behavior of 155mm and 8-Inch Shell at Nicolet, Canada, During the Winter of 1974-1975," Ballistic Research Laboratories Memorandum Report in preparation.

### C. Conclusions

The spark range data obtained from tests of full scale and 105mm models of standard M483 indicate that the static and Magnus moment coefficients of this shell have high but narrow peaks centered at  $M = 0.93$ . Secondly, these aerodynamic coefficients are highly nonlinear with respect to yaw angle. Data from the yawsonde tests support these contentions. After launches with small yaws at subsonic speed, the shell flies with a limit epicycle indicating the nonlinearity of the shell's aerodynamics at small yaws. It has been possible to cause flight instabilities at transonic and subsonic velocities by generating sufficiently high first maximum yaws. The results of 1975 Wallops Island tests indicate that although  $8^\circ - 9^\circ$  yaw levels would be required to get short at  $M = 0.90$ , a  $4^\circ$  first maximum yaw can cause flight misbehavior at  $M = 0.94$ .

### IV. DISCUSSION OF M483 FLIGHT PROBLEMS AND THEIR EXTENT

Since at least  $10^\circ$  of yaw was necessary to produce an M483 short at YPG when tested at a launch Mach number of 0.80 in 1972, it was a surprise to obtain seven shorts from a 20-round group during the Nicolet tests in February 1974. A ten-degree first maximum yaw was not expected from the combination of the M109A1 weapon and the M483 shell and it could not be explained.

In order to determine the effects, expressed as the first maximum yaw level, of the weapon/shell interaction, two programs were launched. The first one was the first maximum yaw test fired at Transonic Range Facility of BRL as explained earlier. This program indicated that, under the test conditions, it was possible to obtain  $3.5^\circ$  to  $4^\circ$  first maximum yaw levels at launch Mach numbers from 0.92 to 0.95.

The second test program to determine weapon/shell interaction was fired at YPG under the auspices of the Project Manager for Selected Ammunition (PM-SA). During this program, smear cameras and yaw cards were used to measure the first maximum yaw distribution of the M483 shell fired from an M109A1 howitzer at critical Mach number and  $17^\circ$  QE. Another aspect of the tests was that tubes of different wear life (new, 50 percent worn, and condemned) were used. The test results indicated that this particular 50-percent-life tube gave an average yaw level almost three degrees higher than the other two tubes. The first maximum yaws measured from the 50-percent worn tube varied from  $2.5^\circ$  to  $6.2^\circ$  with a mean value of  $4.7^\circ$ . Figure 16 gives a plot of range loss as a function of the first maximum yaw level. This graph shows that the onset of flight misbehavior of M483 shell is quite sharp and delineated by a first maximum yaw level of about 5.5 degrees. Results of this test and the 1974 Wallops Island yawsonde tests, discussed in Section III.B.2, indicate that under critical Mach number conditions (from 0.93 to 0.95) the M483 shell does not require first maximum yaw levels as high as  $10^\circ$ . These tests have also shown that yaw levels as low as  $4^\circ$  to  $6^\circ$  can result in unstable flights under appropriate conditions. These yaw levels could easily be attained at Nicolet during February 1974.

The second question raised by the 1974 Nicolet tests was whether even this yaw level would be sufficient to result in a short at the launch Mach numbers, from 0.919 to 0.928. But a closer study of the test conditions indicated that during the M483 firings in February 1974 a 7-knot headwind existed. This head wind increased the effective launch Mach number to within the critical regime (the actual values of launch

Mach number ranged from 0.929 to 0.938). With this launch conditions, four to six degree first maximum yaws would have been sufficient to give the observed shorts.

As was stated above some of the spark range rounds of full scale and 105mm model of M483 have been reduced by the method of Chapman and Kirk<sup>15</sup>. The Magnus moment coefficient,  $C_{M_p}$ , computed during this analysis is presented in Figure 17 at two different Mach numbers, 0.70 and 0.94. Two stability limits,  $S_d < 0.0$  and  $S_d > 2.0$ , shown in the figure are computed for linear aerodynamics and the exact locations of these limits for nonlinear aerodynamics may not be the same. But they are used to explain the trend shown by the yawsonde data. When the M483 shell is fired subsonically (say below  $M = 0.80$ ) with an intermediate yaw level, as shown in Figure 7, the yawing motion is damped to an amplitude less than about three degrees. As can be seen in Figure 17, for  $M = 0.70$ , the yawing motion is damped for a narrow region above the limit cycle angle (angle at which the  $C_{M_p}$  curve crosses the  $S_d \leq 0.0$  boundary). But once the amplitude of the motion is below that boundary, the shell is in a region of precessional instability and its yawing motion grows until a precessional limit cycle is reached (see Figure 10 after 16 seconds into the flight). On the other hand, if the shell is launched near the limit cycle amplitude, as was Round E1-5127 shown in Figure 6, then the limit epicycle behavior of the shell will persist. Finally, if the shell is launched with sufficiently high yaw levels (above the value where  $C_{M_p}$  curve crosses the  $S_d > 2.0$  boundary), then the precessional component of the yawing motion is strongly damped and the nutational mode becomes unstable (see Figure 8).

The analysis of the spark range data and supporting yawsonde rounds show that it is possible to obtain unstable flights of M483 shell at any launch Mach number when sufficiently high first maximum yaw levels are generated. This required yaw level appears to be higher than what could be produced by the weapon/shell interaction at most Mach numbers but a small region, between 0.92 and 0.95, where the required yaw levels are within the capability of the system to produce. Narrowness of this critical Mach number region and the difficulty of producing a required first maximum yaw level by using normal interaction of a gun and shell combination were emphasized during the Nicolet tests performed in January/February 1975<sup>16</sup>. Although seven of the 20-round group had fallen short during the February 1974 tests, a total of 49 M483 shell had to be fired during January 1975 to obtain a short under test conditions similar to February 1974.

From the test results discussed above, it can be concluded that:

- (a) The M483 shell has a very sharp demarcation between stable and unstable flights.
- (b) Although it is possible to obtain unstable flights of M483 at all transonic and subsonic Mach numbers, only at transonic Mach numbers are the required yaw levels for flight misbehavior low enough that they can be induced naturally by the weapon system.
- (c) The Mach number region where the M483 shell is sensitive to launch conditions is very narrow and firing a given number of shell, even at critical Mach number, may not guarantee that an unstable flight will be observed.

- (d) Due to the peculiar aerodynamic characteristics of the M483 shell, the technique of inducing high initial yaws to guarantee unstable flights has been very successful.

#### V. SOLUTION TO THE M483 FLIGHT PROBLEMS

The unstable flights of the M483 shell were due to the influence of the large and highly nonlinear Magnus moment on the dynamic behavior of the shell in the critical Mach number regime where the gyroscopic stability is near or at its minimum. Therefore, the solution to the problem must either increase the gyroscopic stability of the shell or reduce the Magnus moment or, preferably, provide a combination of both. In order to fulfill these requirements, a large number of modifications to the M483 design have been considered. Three of the contenders which have reached testing stage are described in the next section.

##### A. Design Modifications of M483 Shell

Three of the modifications to the M483 shell are described in Table 3. All of these modifications include a shortened boattail in order to reduce the Magnus moment of the shell. In addition to shortened boattail, the M483 Mod I design also has 0.38-caliber shorter cylindrical section to further reduce the Magnus moment coefficient. Reducing the magnitude of the Magnus moment will increase the critical yaw level beyond which the shell will become nutationally unstable (see Figure 17) even if the gyroscopic stability of the projectile remains the same.

M483 Mod I and M483 Mod II designs increase the shell's gyroscopic stability by adding metal to the outside of the shell casing thus increasing the axial moment of inertia. A summary of representative

**Vol. 1**

physical properties of the M483 shell and its modifications is given in Table 4. The values quoted in this table are the averages of the measured physical parameters for the appropriate shell fired during Nicolet tests in January/February 1975. The last column in Table 4,  $(I_a)^2/I_t$ , gives an approximate indication of the gyroscopic stability of the modifications relative to the M483 shell. The value of  $(I_a)^2/I_t$  for the M483 Mod 13B is about the same as the standard shell with its center of mass slightly forward. Therefore, these two projectiles are expected to have similar gyroscopic stability factors. On the other hand, M483 Mod I and M483 Mod II projectiles would have 35% and 11% higher gyroscopic stabilities, respectively. The gyroscopic stability is even further increased by a more forward location of the shell's center of mass.

**B. Test Data on the Modified M483 Shell**

Most of the test data for the modified M483 shell come from the developmental tests at YPG and proof tests at Nicolet. Some jawsonde instrumented shell were also fired during these tests and results will be described later on.

1. Yuma Proving Ground Tests. Developmental tests of the modified M483 shell were done at YPG under the supervision of PA aeroballisticians to determine whether they would survive the highest possible first maximum yaw levels which could be induced. In order to obtain various yaw levels, the yaw inducers described in Table 2 were used. The magnitudes of the first maximum yaws thus generated were measured with yaw cards. A Hawk doppler radar and a GE muzzle velocimeter were used to measure the launch Mach numbers. The impact ranges of the rounds were determined by observers. Since standard M483 shell gave shorts with a standard

muzzle brake at a critical Mach number launch, only the modified M483 shell were fired with yaw inducers 2 and 3. No shorts similar to M483 (several thousand metres) were detected. Table 5 gives a summary of the data from these tests. From this table, a difference between modifications can be detected. Since the M483 Mod I has the largest gyroscopic stability, it attains the lowest first maximum yaw levels for a given tip-off rate. The mean impact range and the maximum range spread for a given group of shell can be strongly correlated to the shell's gyroscopic stability at launch.

2. Nicolet Tests under High Air Density Conditions. During January/February 1975, the M483 and its modifications were fired at Nicolet, Canada, to determine their flight behavior under high air density (above 110% of ICAO standard) and critical launch Mach numbers<sup>18</sup>. Shell were fired with yaw inducers 1 and 2 at a controlled launch tip off rate. In order to increase the statistical significance of the test data, modified M483 shell have been fired at two different occasions with similar launch Mach numbers. A summary of the test data is given in Table 6. Data show that with both yaw inducers the M483 shell gave shorts. On the other hand, under similar launch conditions all of the modified shell had stable flights. When fired at 65° QE, both M483 Mod I and M483 Mod II appear to have similar performance characteristics as indicated by the observed range probable errors (PE). The tendency of the M483 Mod II to fly at higher yaw levels is indicated by shorter mean impact ranges. At the lower QE (30 degrees), all modified shell appear to impact at approximately the same range although a result similar to YPG test is observed, i.e., the projectile with the lower gyroscopic stability has the higher range PE. Test site limitations did not



Vol. 1

permit use of any first-maximum-yaw detection devices such as cameras or yaw cards, therefore, no relative yaw levels could be assigned to the data given in Table 6. At Nicolet, the only first-maximum-yaw data were obtained from yawsondes as explained below.

3. Yawsonde Data from Yuma and Nicolet Tests. Details of the yawsonde tests at Yuma and Nicolet have been covered in References 17 and 18. In this section, some comparative yawsonde data of the modified M483 shell will be discussed. Although the yawsonde data for most of the instrumented rounds exist (some data were lost due to electronic failure and others due to noise in the data train), only the Nicolet test firings included the yaw processor<sup>19</sup> as part of the test instrumentation. The yaw processor is an instrument designed to measure the time interval between solar cell pulses and store this information serially. In conjunction with a desk-top computer, it is possible to obtain preliminary plots of yawing motion, permitting the test engineer to obtain yawing data on site. Table 7 gives a summary of the first-maximum-yaw data from Nicolet computed by the yaw processor for the M483 and its modifications. When these data are compared with those shown in Table 5 (results from YPG tests), several conclusions could be drawn: (a) the yaw inducers (at least 2 and 3) behaved consistently at YPG and Nicolet, (b) the induced yaw levels correlate with the shell's gyroscopic stability leading to the dispersion data summarized in Table 6, (c) it was impossible to obtain yaw levels higher than 12.4 degrees with the M483 Mod I shell, even with yaw inducer 4, because of its high gyroscopic stability, and

---

19. W. H. Clay and W. H. Mermagen, "The Portable Yaw Processor," Ballistic Research Laboratories Memorandum Report in preparation.

(d) the M483 Mod II and M483 Mod 13B shell gave stable flights even at yaw levels above 16 degrees while the standard M483 flew short with 9.4-degree first maximum yaw.

Figures 18 through 23 compare the flight behavior of the modified M483 shell at different launch conditions. Figures 18 and 19 show the effect of the environment on M483 Mod II at two different tip-off rates. Figure 18 shows the shell's flight behavior at Wallops Island and Nicolet after being disturbed by yaw inducer 1. Both flights show the same limit epicycle behavior of about four degrees. But the motion of Round 10C12, fired at Nicolet, has a larger nutational component. Figure 19 shows the yawing motion under the influence of yaw inducer 4. Both at YPG and Nicolet, the induced yaw levels were about 14 degrees almost equally divided between the two modes.

Figures 20 and 21 show the flight behavior of M483 Mod II and M483 Mod I shell, respectively, at Nicolet under the influence of yaw inducers 3 and 4. Unfortunately, when these rounds were fired, all the pre-assessed charges were used and on site charge adjustments were needed. As a result, all four test Mach numbers are higher than 0.96 instead of the desired launch Mach number of 0.93. This will not affect the comparison. The M483 Mod II shell has 15° and 10.3° yaw levels initially under the influence of yaw inducers 4 and 3, respectively. Both motions are equipartioned between precessional and nutational components. At yaw levels above 5° modal amplitude, the precessional mode is strongly damped while the amplitude of the nutational mode has reduced only slightly during the first 5 seconds of flight. The data for M483 Mod I (Figure 21) show a different story. Although the total yaw levels observed for these flights are only 15 to 20 percent lower than those

observed for the M483 Mod II shell under similar conditions, the yawing motion of the M483 Mod I shell is dominated by the precessional component. Both modes of the yawing motion are strongly damped. The round fired under the influence of yaw inducer 3 is already approaching limit epicycle behavior by six seconds into the flight. The other round still has about a two-degree nutational component at six seconds and takes at least another six seconds before it shows a limit cycle behavior<sup>18</sup>.

Figure 22 shows a comparison of the M483 Mod I and M483 Mod II flights fired with yaw inducer 4 at Yuma. The early yaw amplitude of the M483 Mod I shell is smaller than that for the M483 Mod II. Under Yuma environment (i.e., lower air density than Nicolet), both modifications show strongly damped nutational components so that the yawing motion starts to be dominated by the precessional component at 10 seconds into the flight.

A comparison of the flight behavior of the three modifications to the M483 shell is shown in Figure 23. These rounds were fired at Nicolet with yaw inducer 3. The first maximum yaw values were  $5.8^\circ$  for M483 Mod I,  $10.3^\circ$  for M483 Mod II, and  $11.2^\circ$  for M483 Mod 13B. All three rounds start with an initial two-arm motion. The M483 Mod I at the outset shows signs of limit motion behavior while the yawing motions of the other two modifications are strongly dominated by the nutational mode. The nutational mode of the M483 Mod II shell damps sufficiently by twelve seconds into the flight so that its limit cycle behavior begins to emerge<sup>18</sup>. On the other hand, the nutational damping of the M483 Mod 13B is less than that of M483 Mod II; therefore, this shell would require at least 17 seconds of the flight time to approach its limit cycle behavior under the Nicolet test conditions.

### C. Conclusions

Test data for the modifications of the M483 shell, both from YPG and Nicolet tests, indicate that any of these designs should be able to survive the launch and environmental conditions which caused the standard M483 to fall short.

The M483 Mod 13B design involves the least amount of modifications to the original concept and has successfully survived first maximum yaw levels as high as 17 degrees. But this design still has the largest range error when fired under conditions similar to those of the other two modifications. Therefore, this design may be useful only as a quick fix for the existing stockpile.

The M483 Mod II design requires external changes to the shell body although it does not involve any loss of payload. It gives stable flights with first-maximum-yaw levels as high as 16 degrees induced by yaw inducer 4. This design appears to have a higher nutational damping rate than the M483 Mod 13B. As a result, M483 Mod II shell had range probable errors less than 0.8 percent at Nicolet under severe environmental conditions. This shell's improved flight behavior without resulting in any payload penalties makes it a viable candidate as a replacement for the M483.

Best flight behavior was obtained with the M483 Mod I design. It proved impossible to attain yaw levels above 13 degrees with this shell under most severe launch conditions. Since this configuration will result in loss of payload space and require major body modifications, it should be considered only as a back-up for the M483 Mod II design. On the other hand, this design adds valuable information to the data base on long shell.

VI. IMPLICATIONS OF THE MODIFIED M483 SHELL FOR FUTURE DESIGNS

Results of the M483 investigation program strongly indicate that nutational weaknesses of a long shell can be partially eliminated by shortening its boattail at the expense of a slightly increased drag. This minimal modification may not result in a completely satisfactory design as shown by the flight data of the M483 Mod 13B shell. Although this projectile is capable of recovering from yaw levels as high as 17 degrees, it gives large range probable errors under severe launch conditions.

At the other extreme, a shorter shell with reduced boattail length (the M483 Mod I design) gives very good flight performance with range probable errors less than 0.5% of mean range under the severest launch conditions attainable. Unfortunately, this improvement in the flight behavior is obtained only at the expense of 10% reduced payload capacity in addition to increased drag.

A convenient compromise between these two extremes is the M483 Mod II configuration. This design does not sacrifice any payload capacity to obtain acceptable flight behavior. Its increased gyroscopic stability results in smaller range dispersion than the M483 Mod 13B shell. Analysis of the yawsonde flights of this shell highlights the dangers of modifying and testing shell without previous, extensive aerodynamic data.

Several of the yawsonde data for M483 Mod II tests at YPG were analyzed using the Chapman-Kirk technique as modified for yawsondes<sup>20</sup>.

---

20. R. H. Whyte and W. H. Mermagen, "A Method for Obtaining Aerodynamic Coefficients from Yawsonde and Radar Data," Ballistic Research Laboratories Memorandum Report No. 2280, March 1973, AD 759482.

The Magnus moment coefficients obtained from this analysis have larger negative values at small yaw than the M483 coefficients<sup>21</sup>. This indicates that the M483 Mod II should have better large yaw behavior than M483 (as was demonstrated in YPG and Nicolet firings) although it may fly with a larger limit cycle. Static moment coefficients of the M483 Mod II were also computed from YPG yawsonde tests (see Reference 21). These results are compared with the 1974 spark range data and the data for the prototype XM483 shell in Figure 24. The shaded area represents the yawsonde results with  $\pm 5\%$  error limits. The roundness of the static moment peak may be an artifice of the analysis method. In spite of the fact that the only major physical change in the M483 Mod II design was a shortened boattail, the static moment coefficient of the M483 has been strongly affected. First, the magnitude of the coefficient is reduced by more than ten percent. Second, the region of minimum gyroscopic stability is shifted from its original location of  $M = 0.93$  to below  $M = 0.9$ .

This almost unexpected modification of the static moment coefficient as a function of Mach number makes it important to conduct a thorough investigation of the modified shell's aerodynamic behavior, at least in the transonic Mach number regime, whenever configuration changes are introduced into a design.

---

21. General Electric Company Letter Report to Picatinny Arsenal dated 23 April 1975.

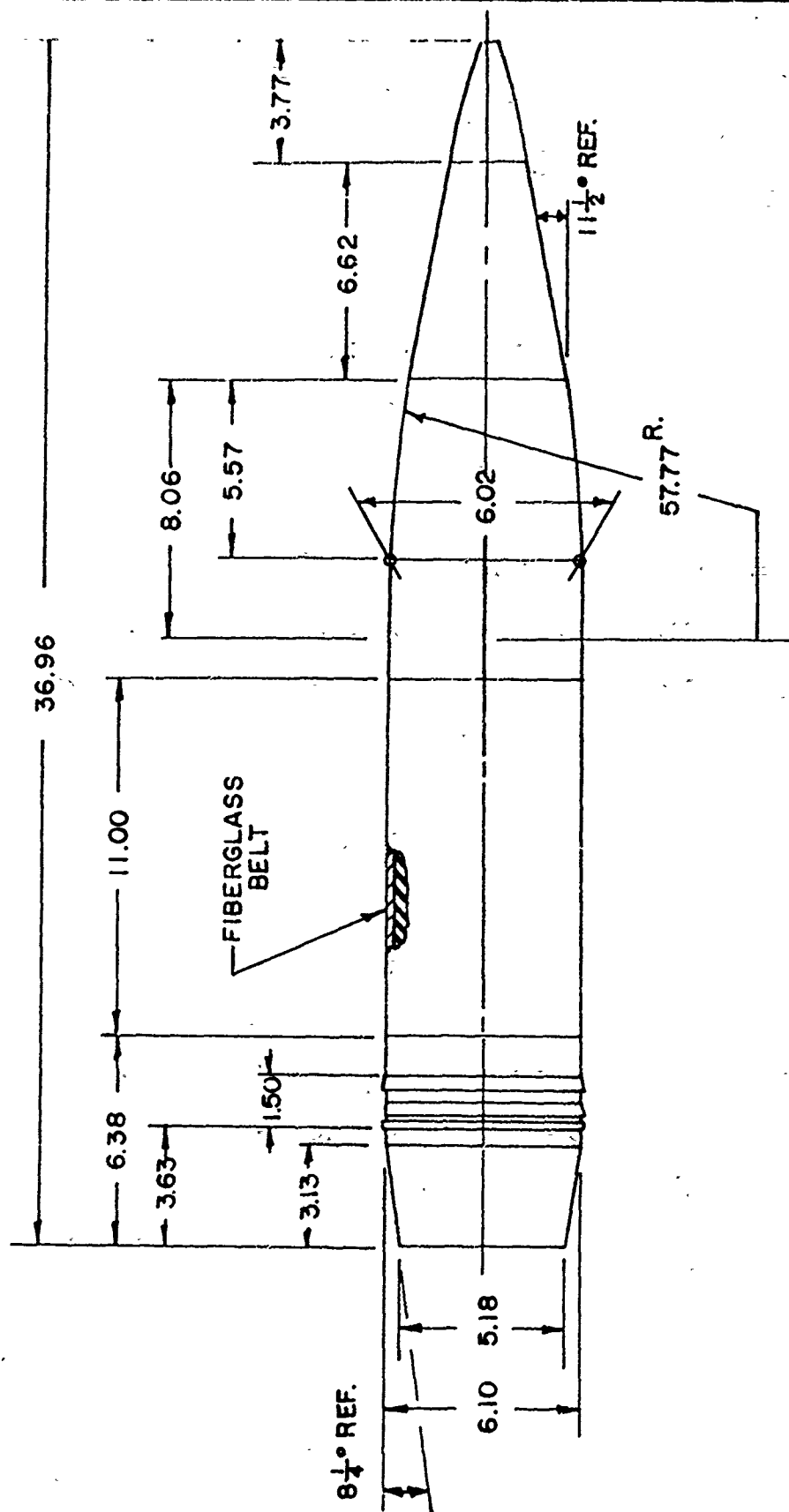


Figure 1. 155mm M483 Shell

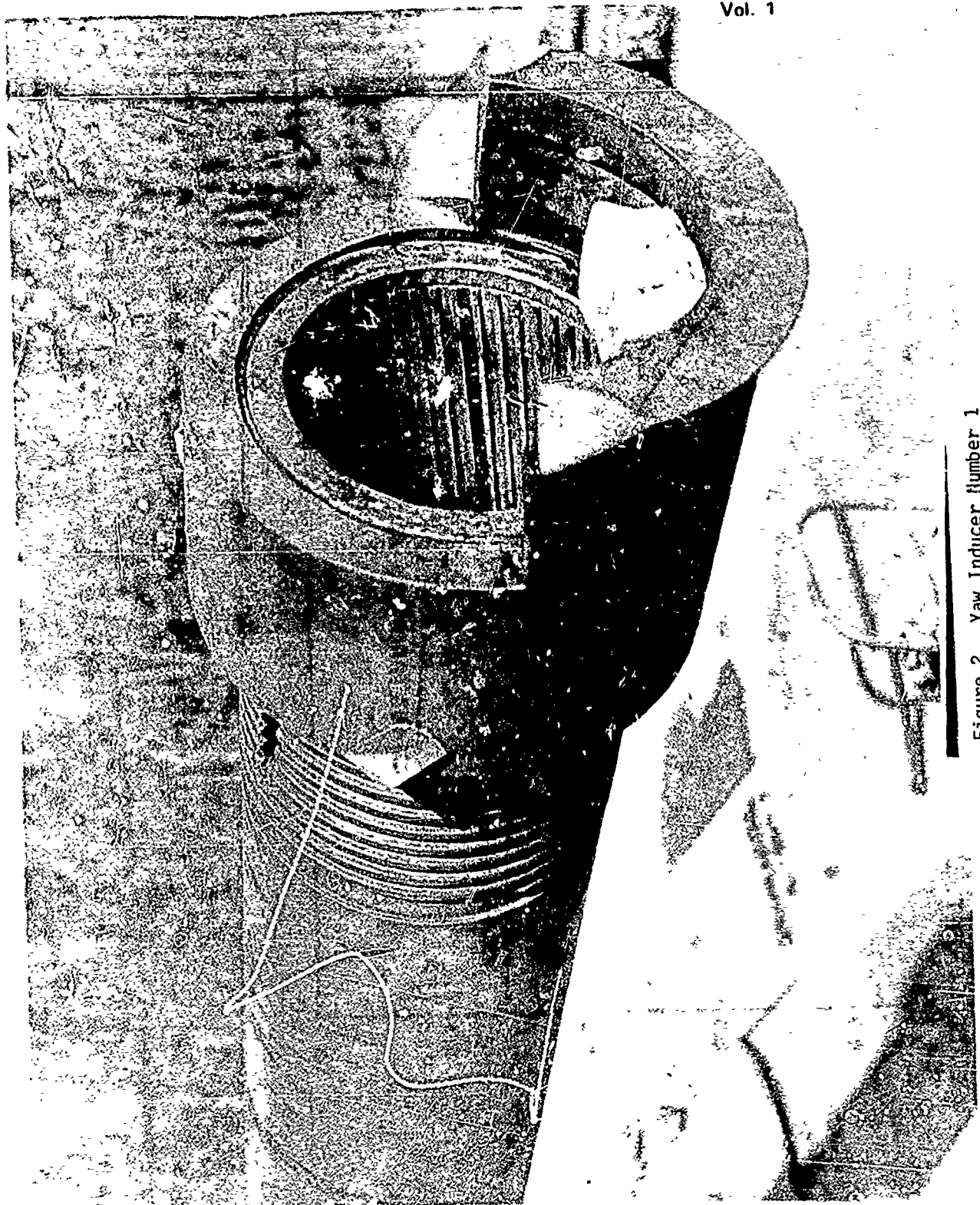


Figure 2. Yaw Inducer Number 1



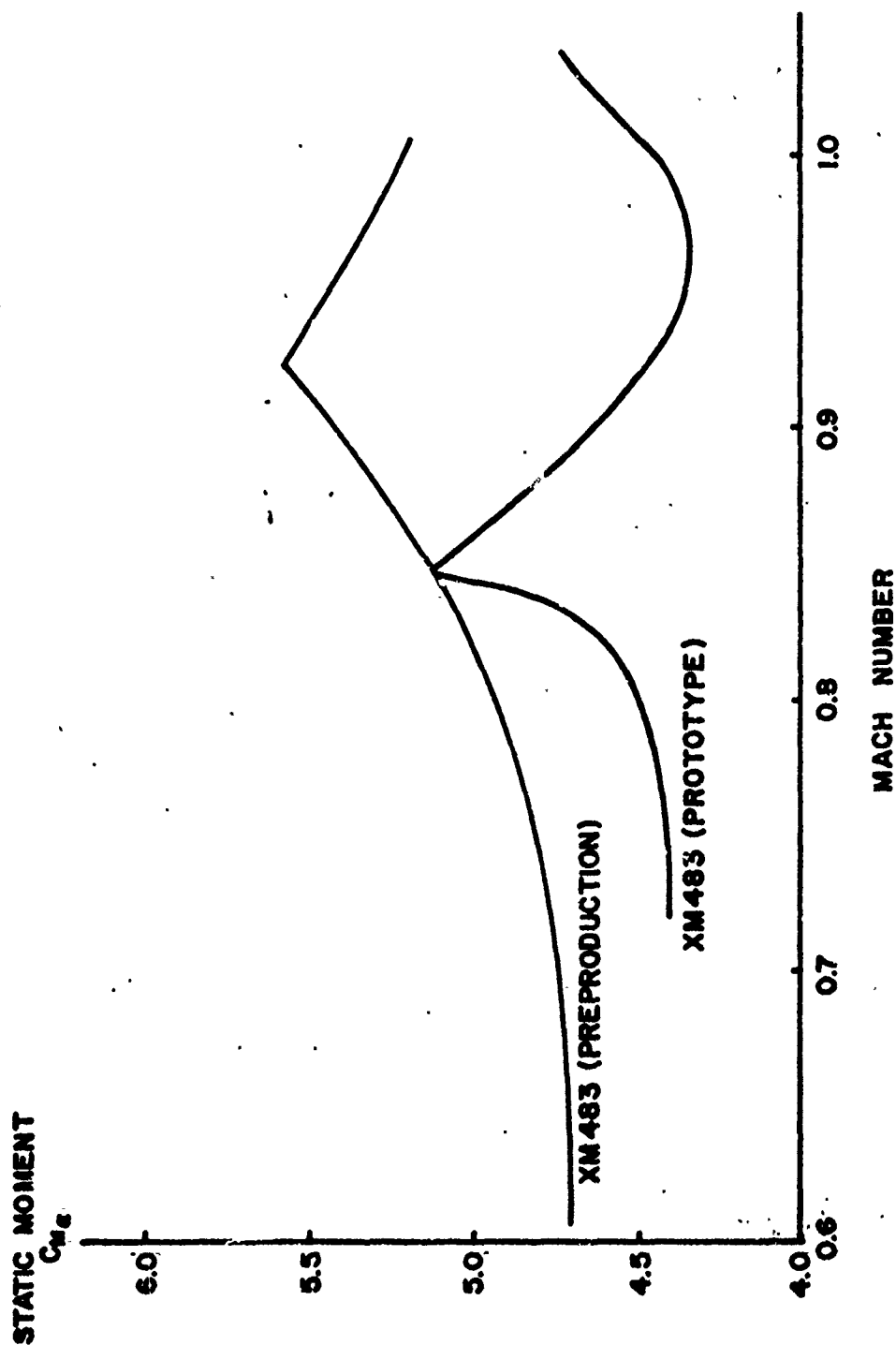


Figure 3. M483 Static Moment Coefficient Slope versus Mach Number

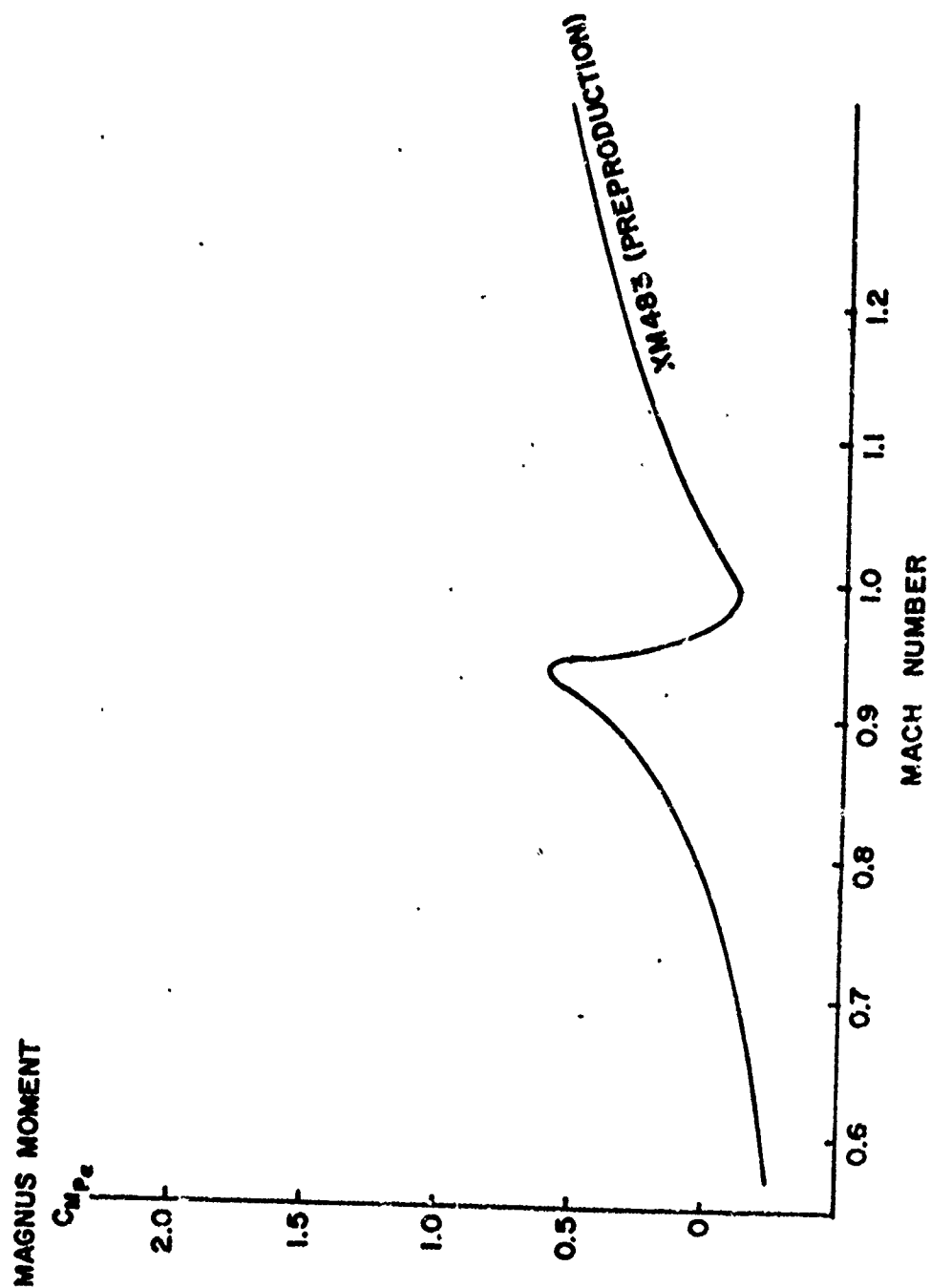


Figure 4. M483 Magnus Moment Coefficient Slope versus Mach Number

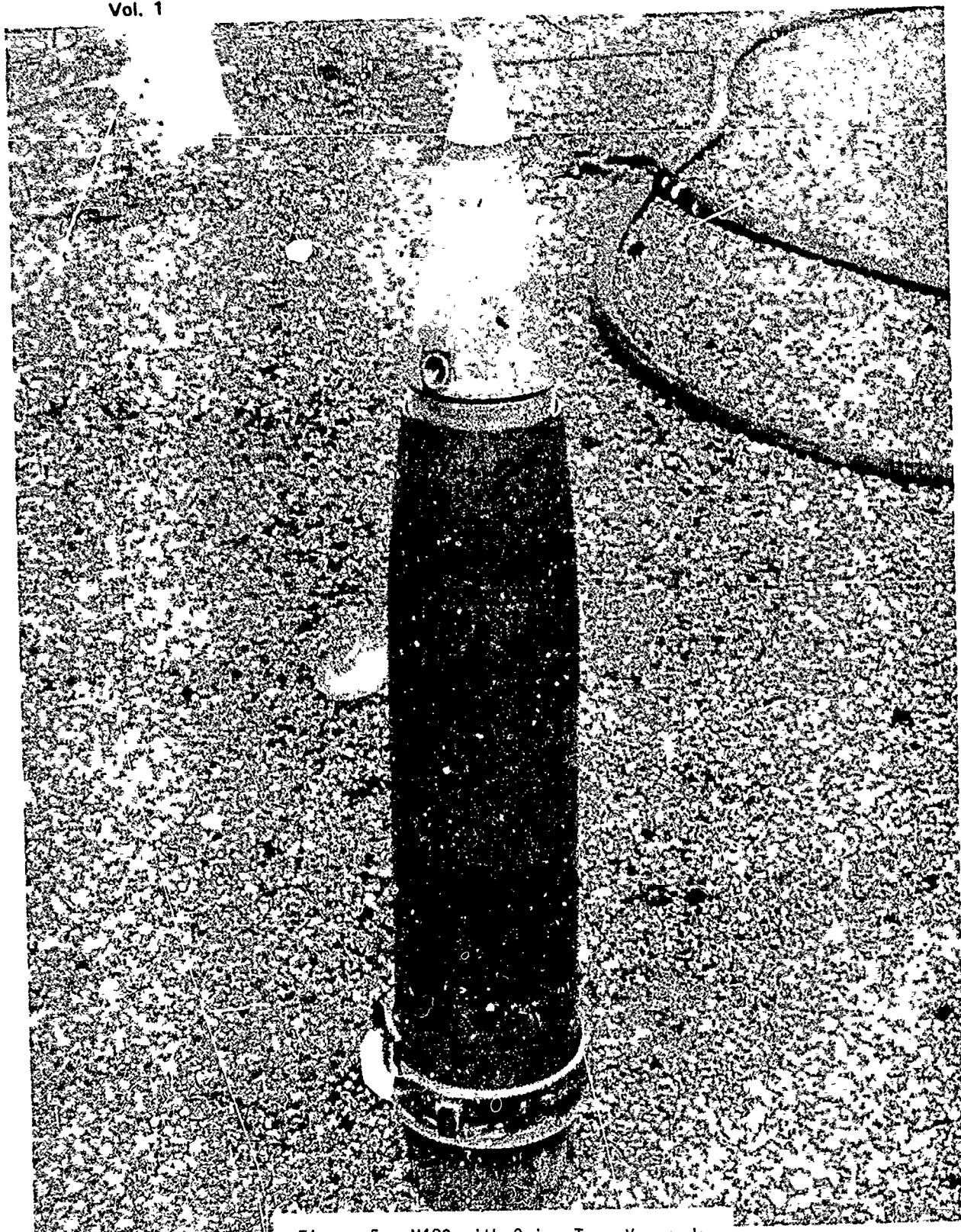


Figure 5. M483 with Ogive Type Yawsonde

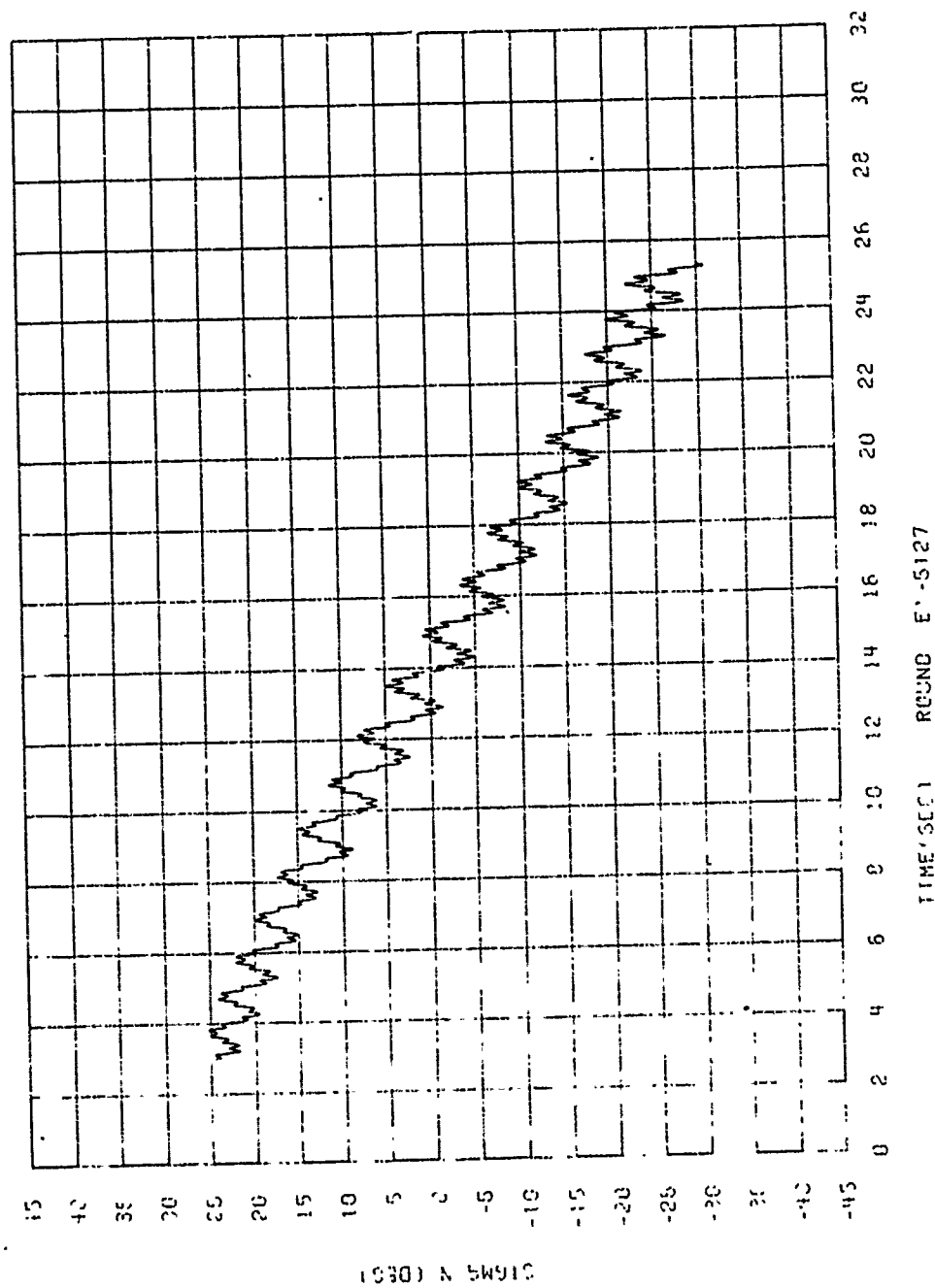


Figure 6. Yawsonde Data for M483 at 253 m/sec, Wallops Island

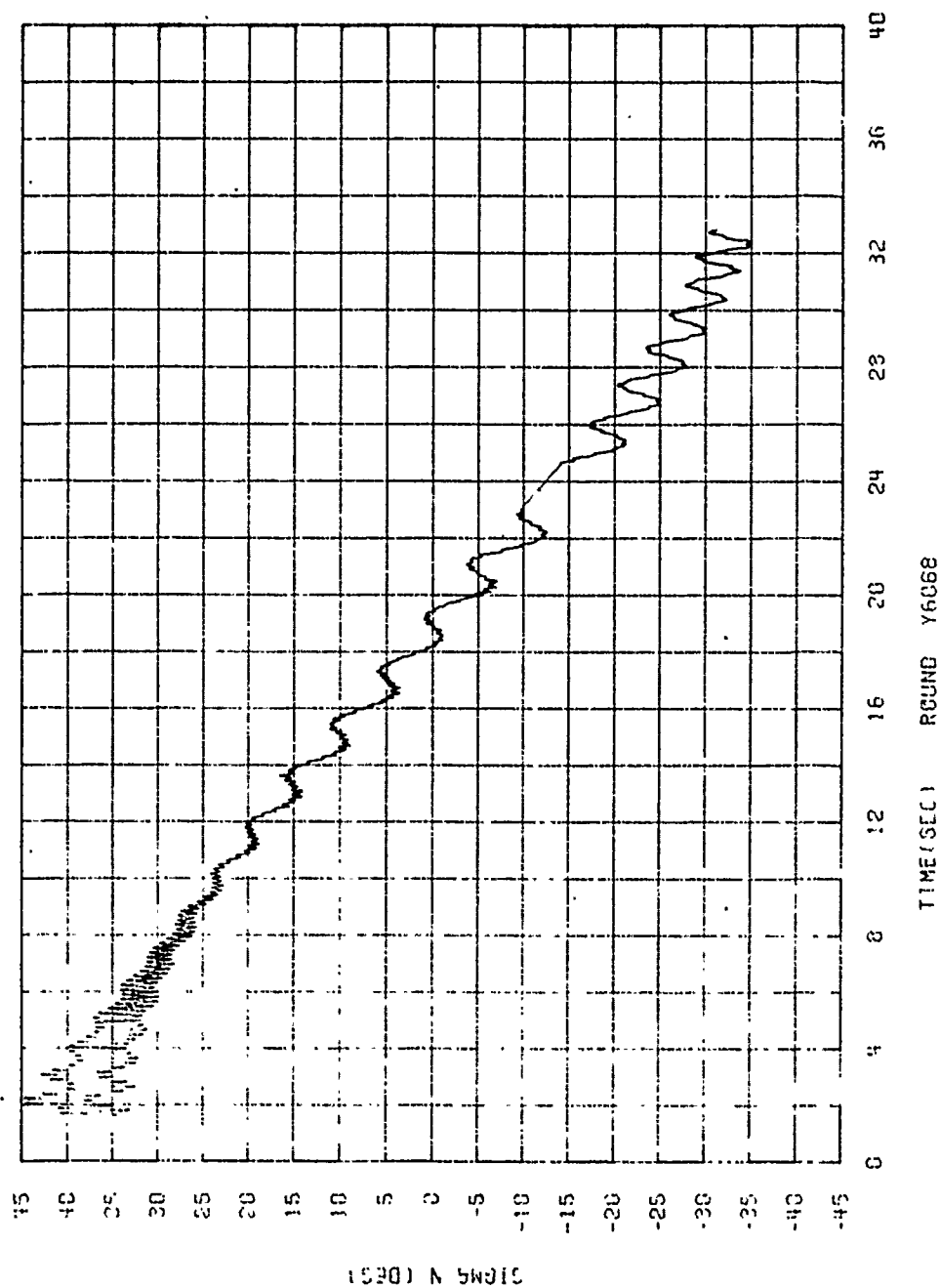


Figure 7. Yawsonde Data for M483 at 274 m/sec, Wallops Island

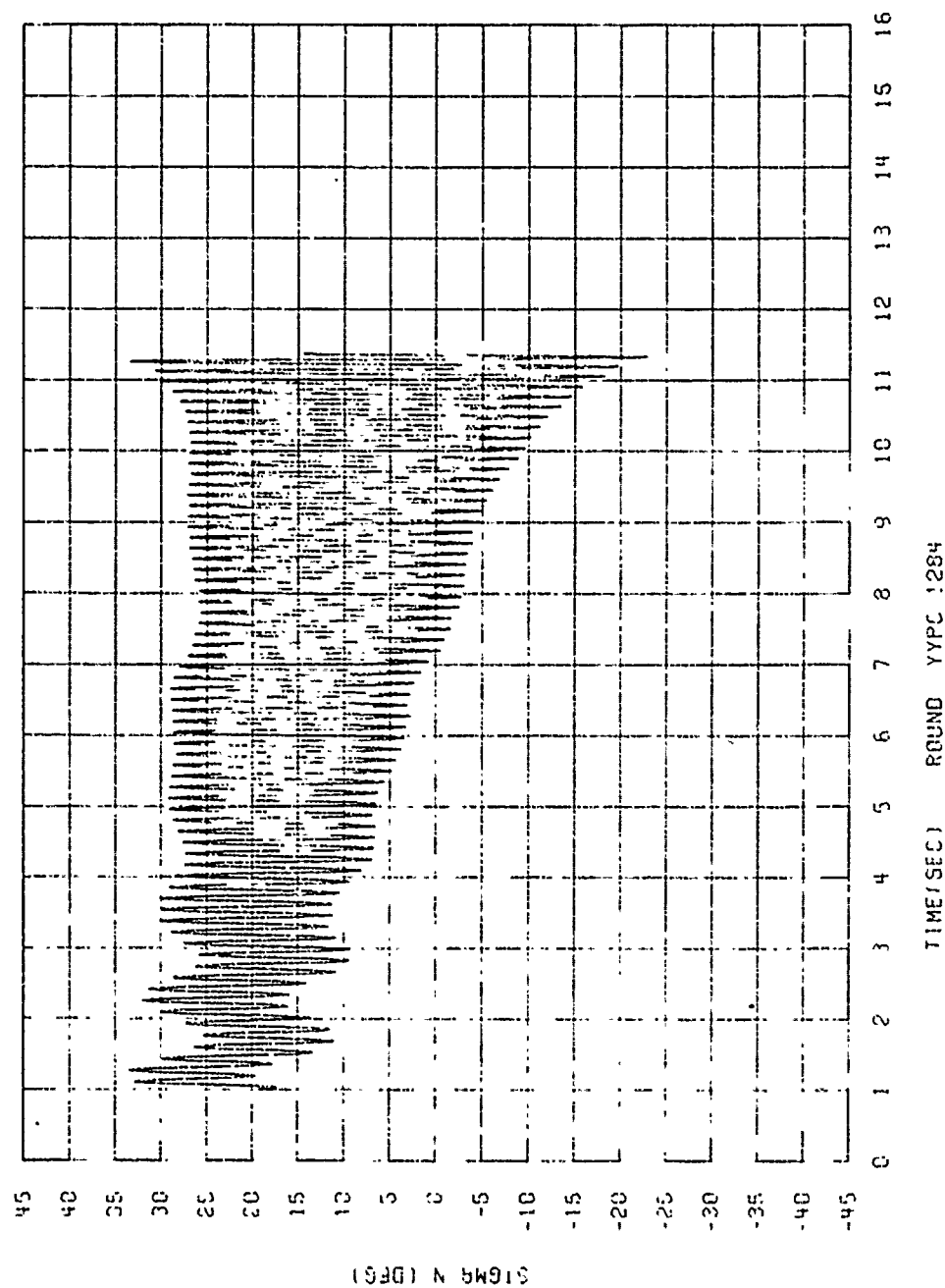


Figure 8. Yawsonde Data for M483 at 267 m/sec, Yuma Proving Ground

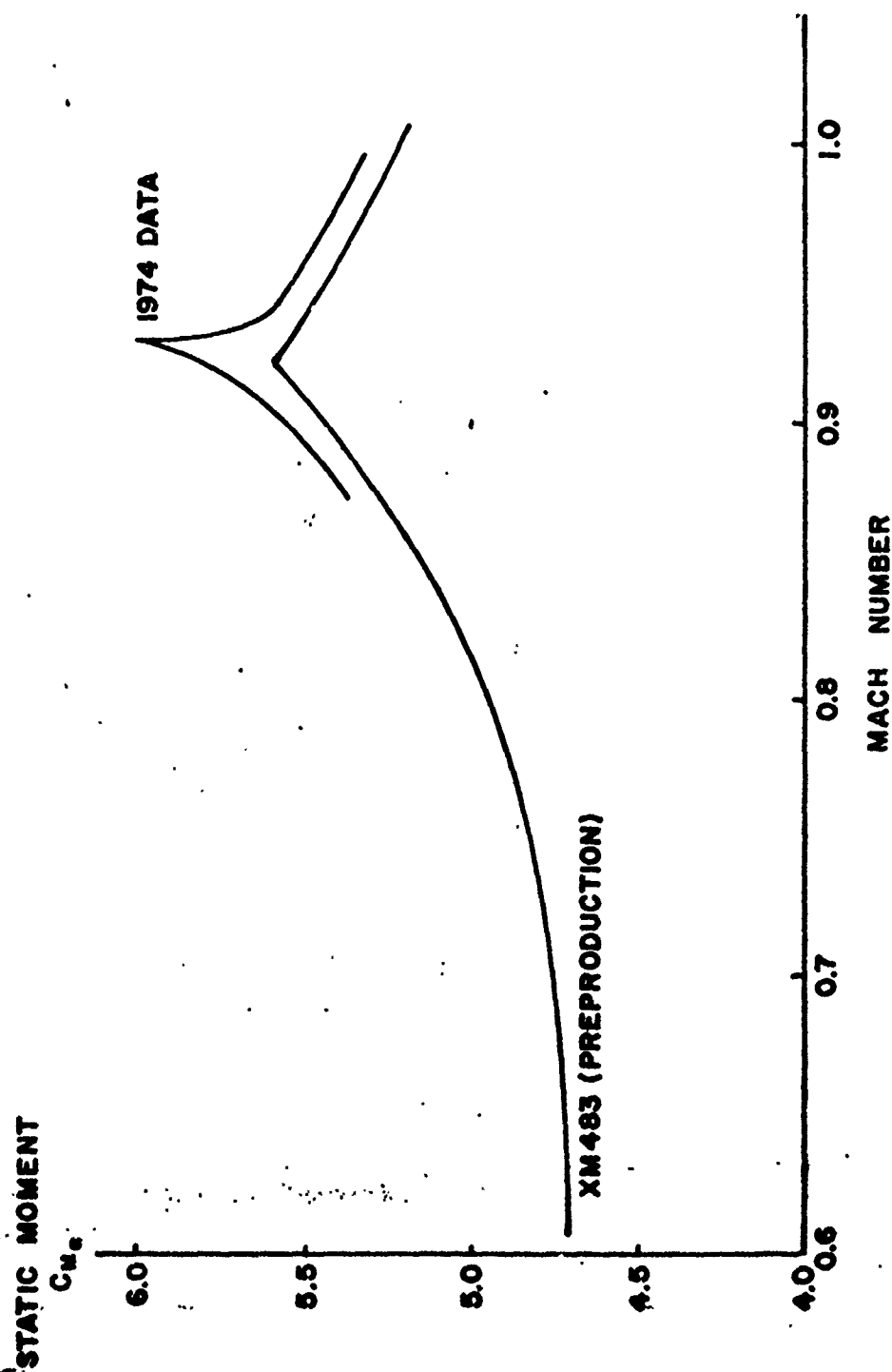


Figure 9. Comparison of Old and New Static Moment Coefficient Slopes

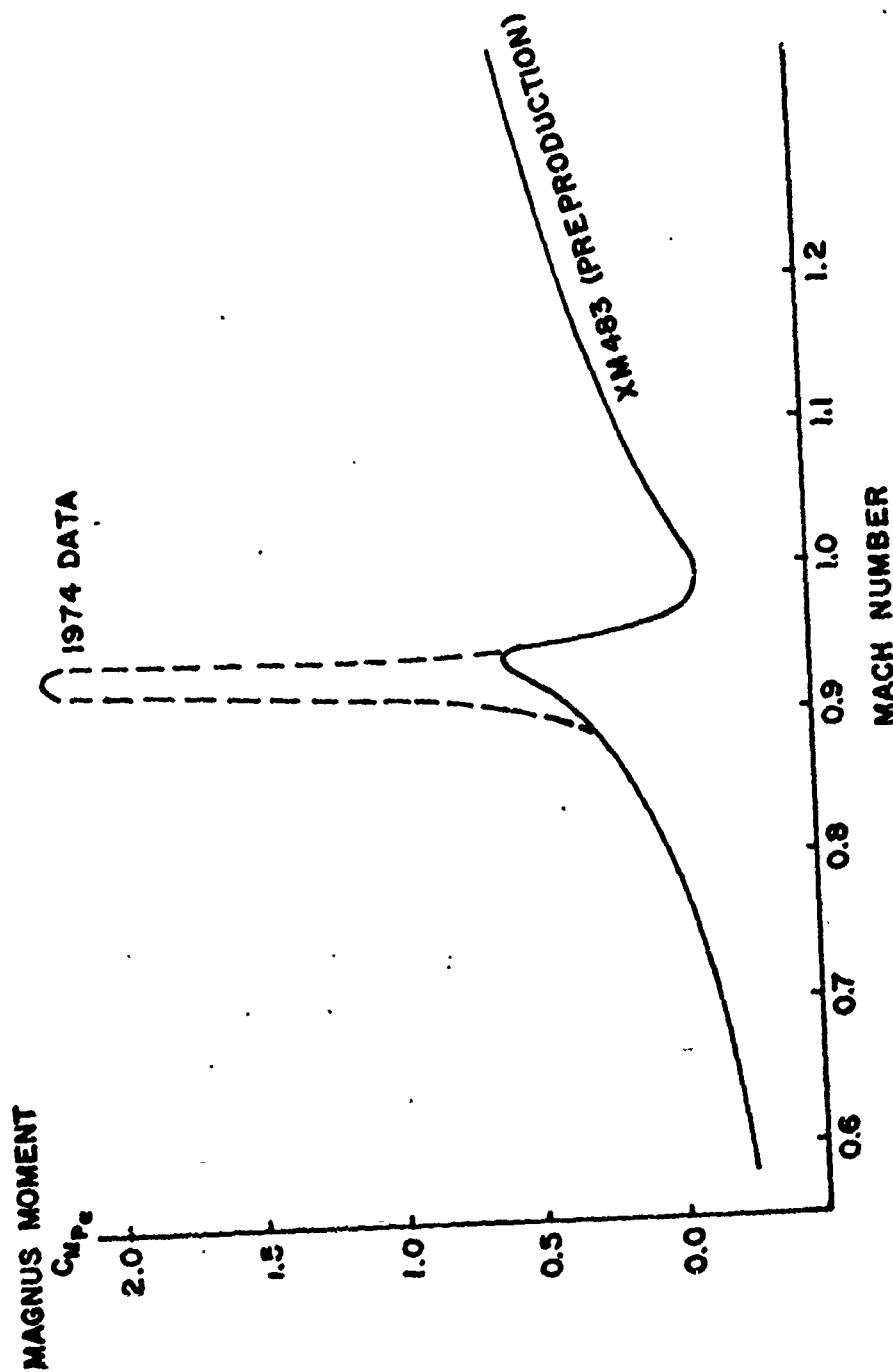


Figure 10. Comparison of Old and New Magnus Moment Coefficient Slopes



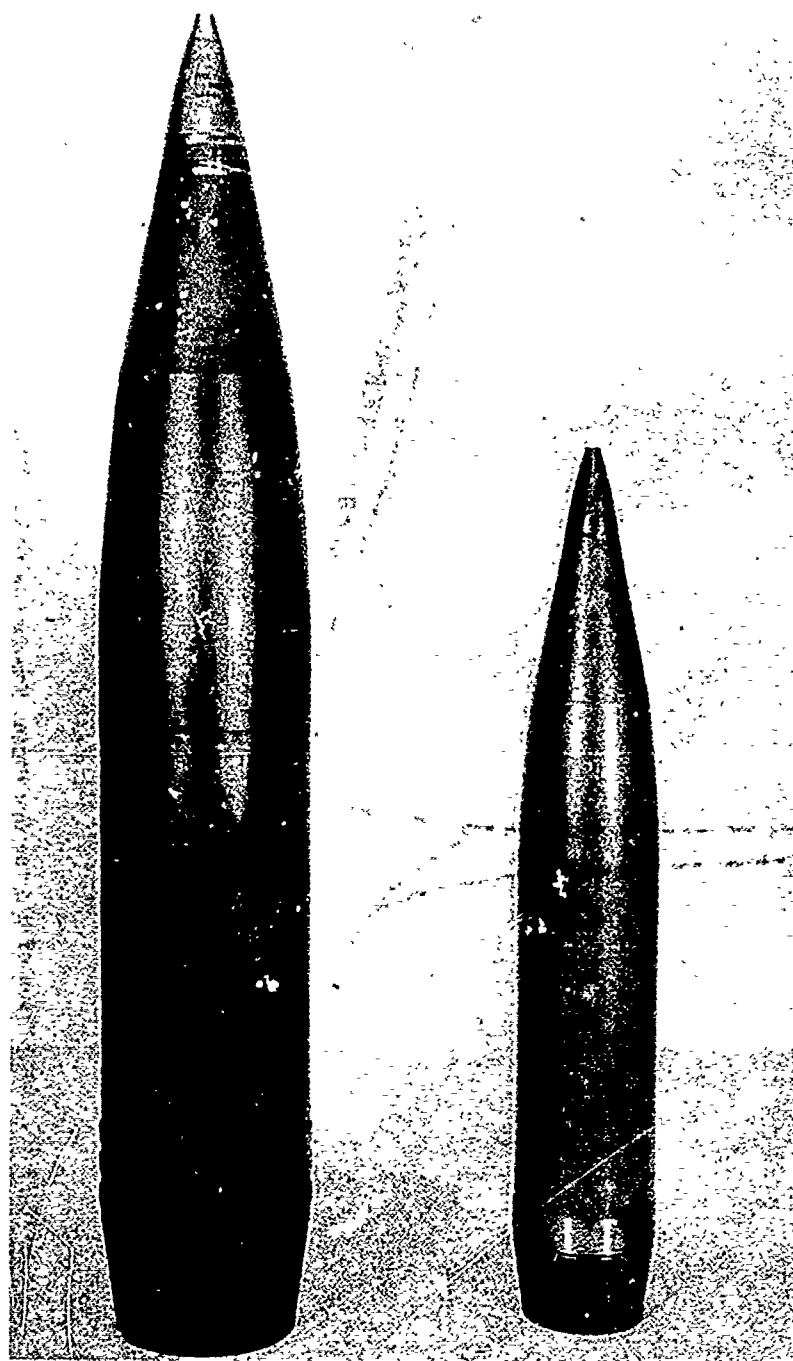


Figure 11. Comparison of M483 and Its 105mm Model

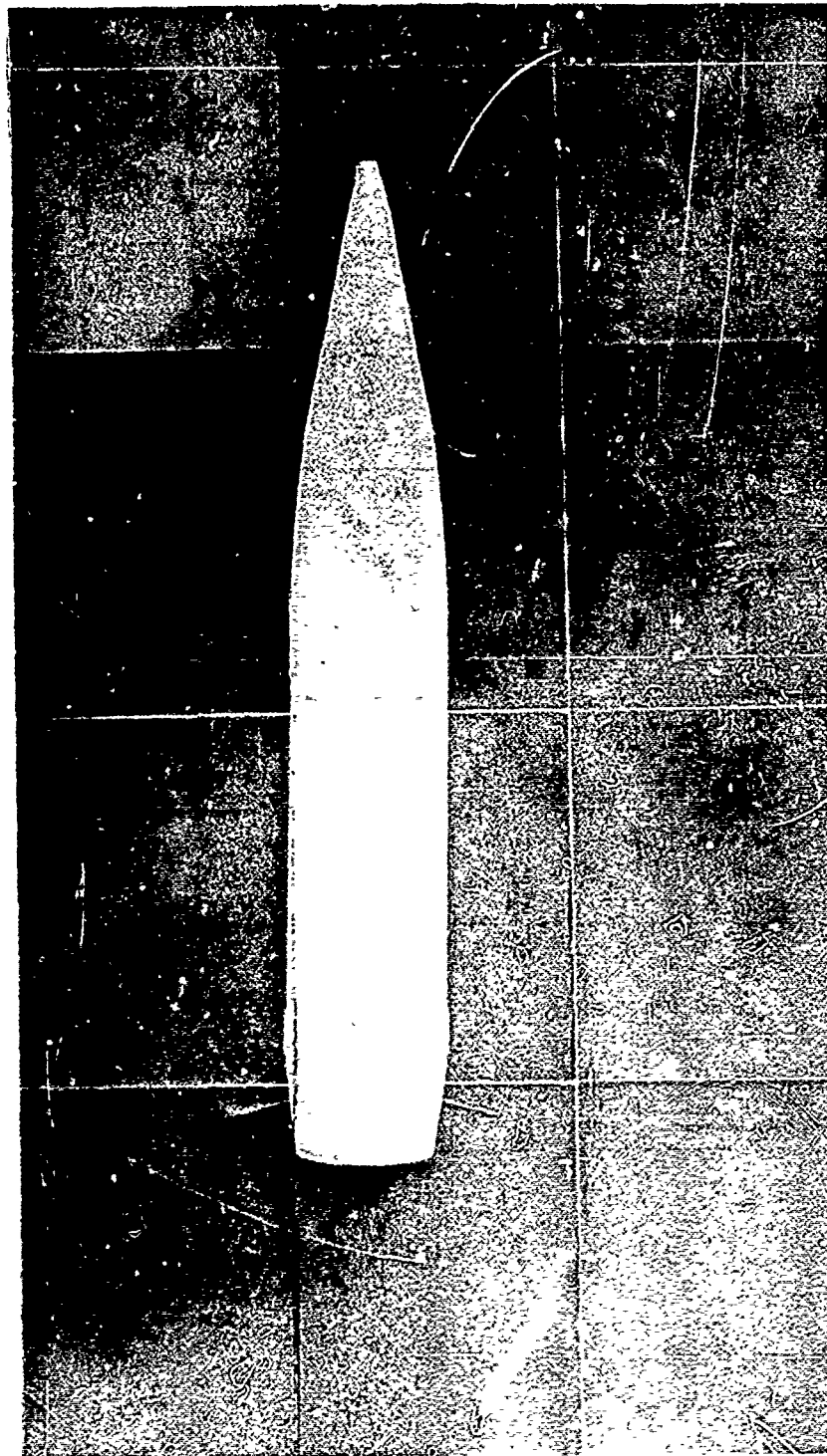


Figure 12. 105mm Model of M483 at 1° Yaw and 0.917 Mach Number

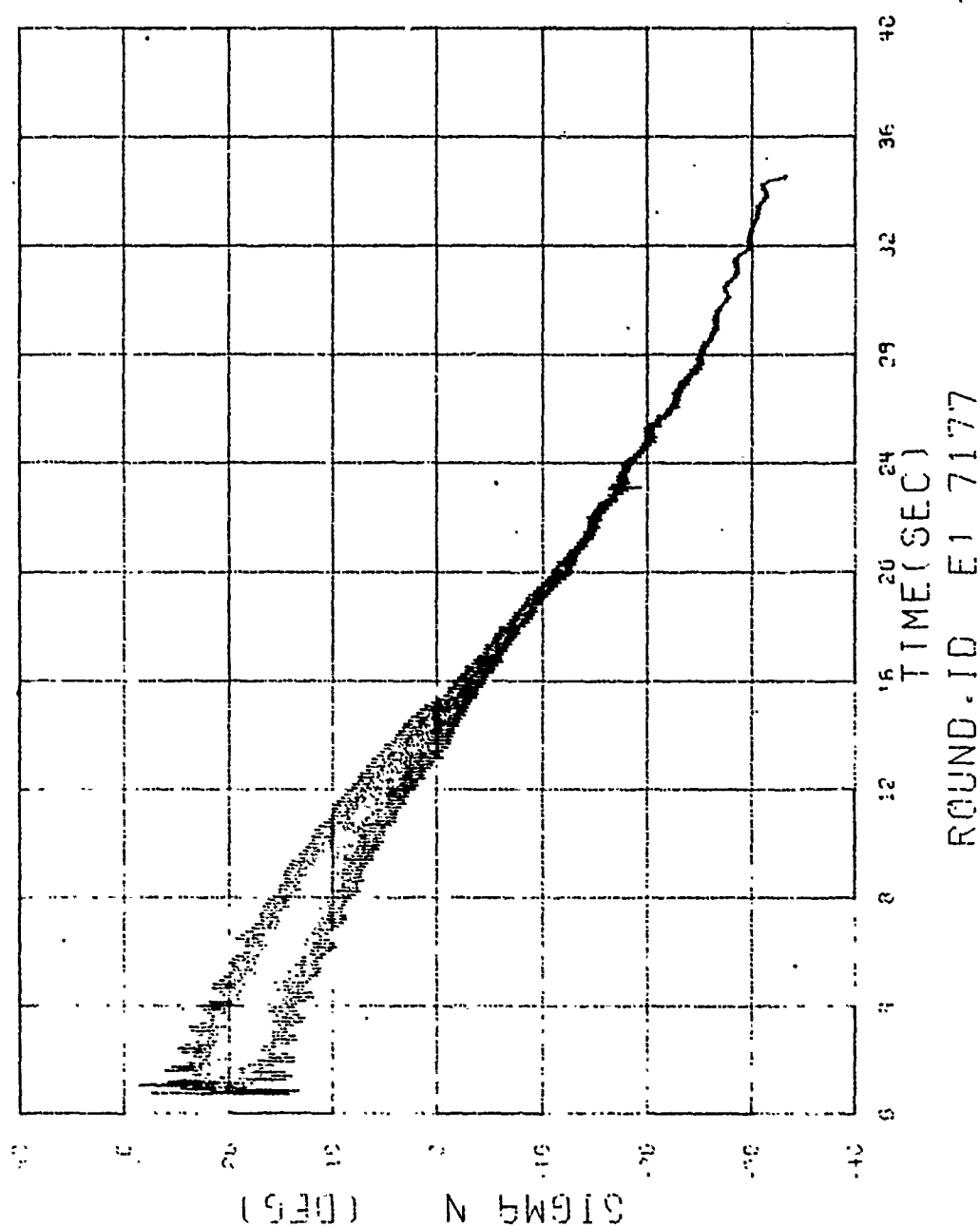


Figure 13. Yawsonde Data for M483 at 329 m/sec, Wallops Island

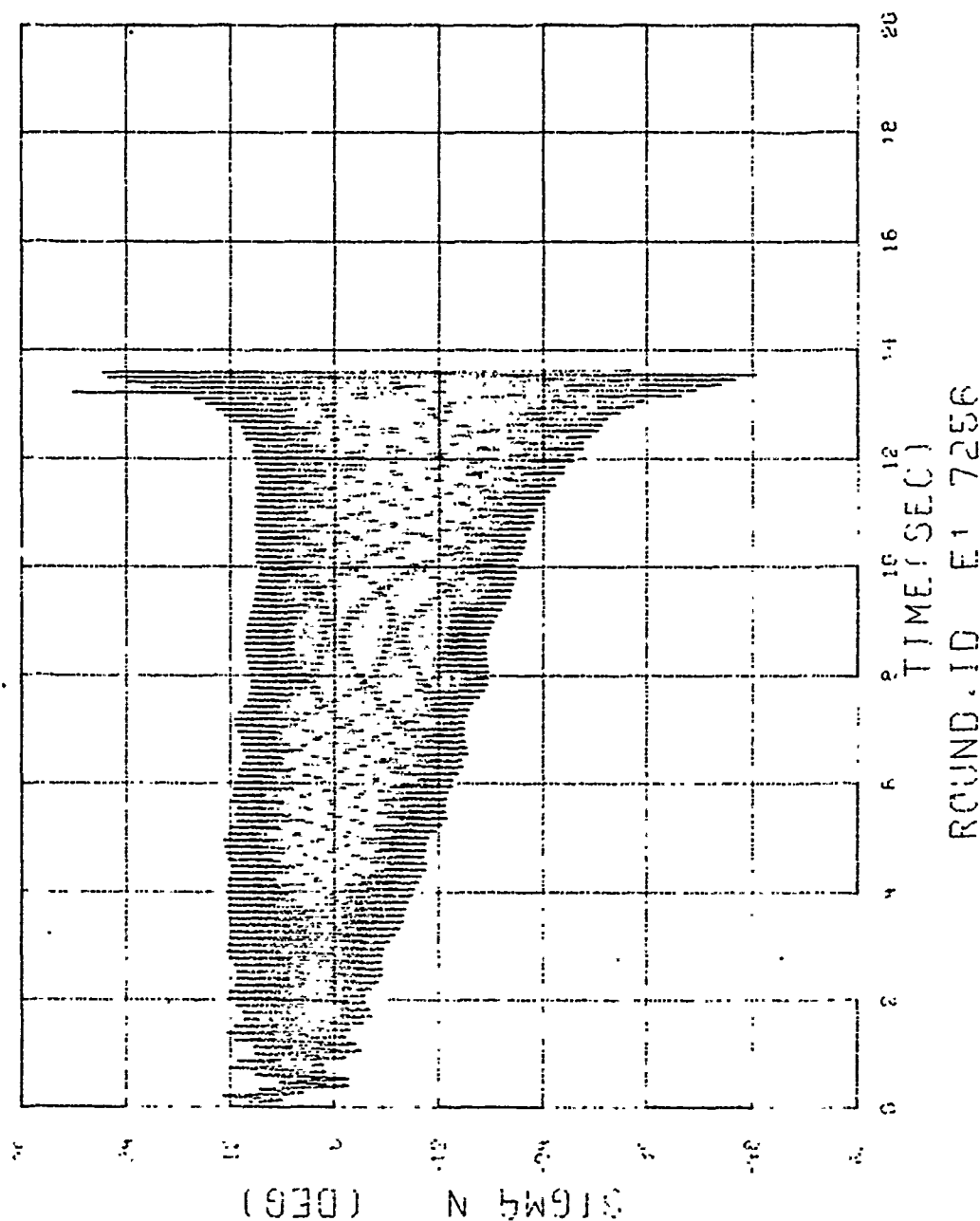


Figure 14. Yawsonde Data for M483 at 334 m/sec, Wallops Island, Induced Yaw

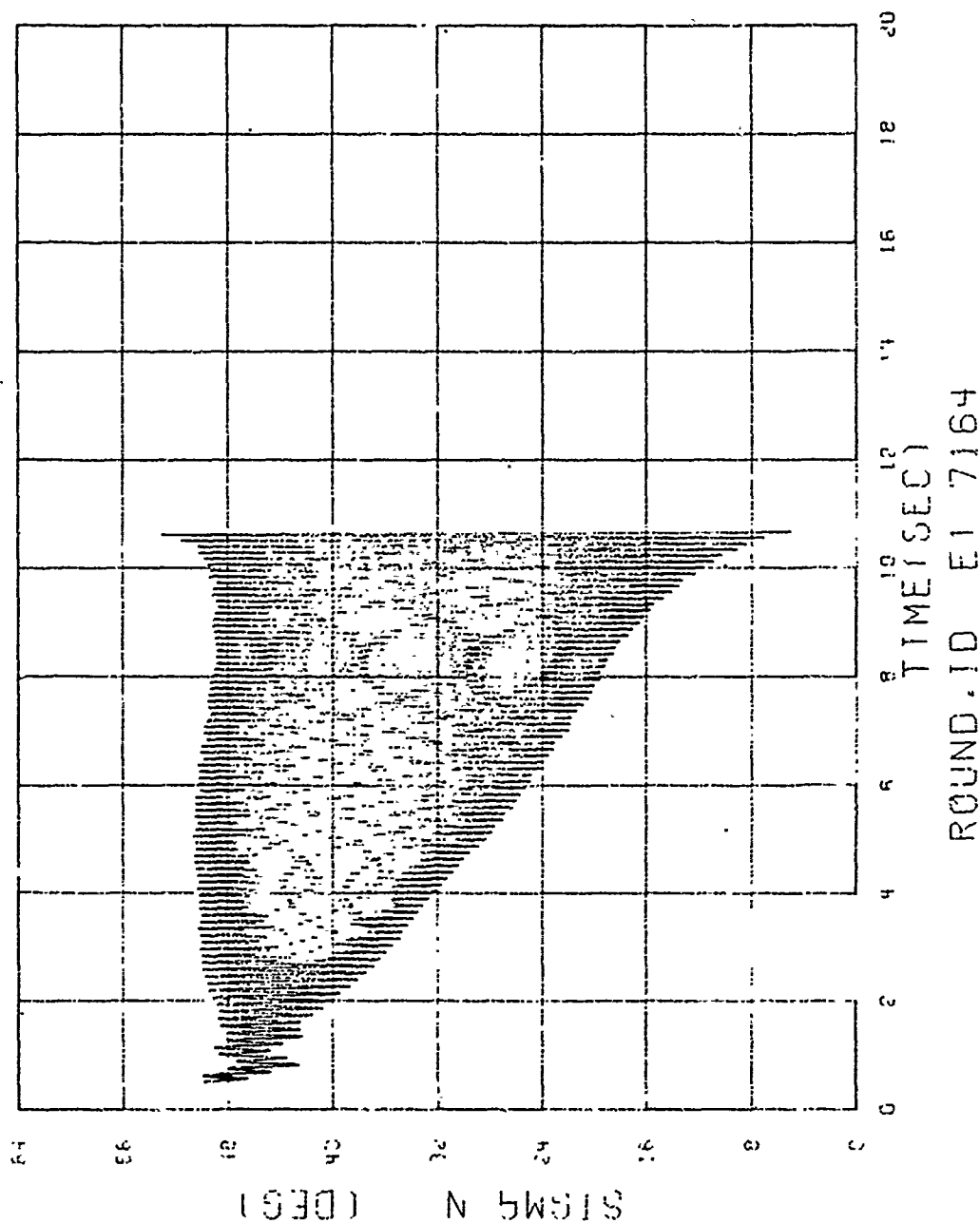


Figure 15. Yawsonde Data for M483 at 320 m/sec, Wallops Island

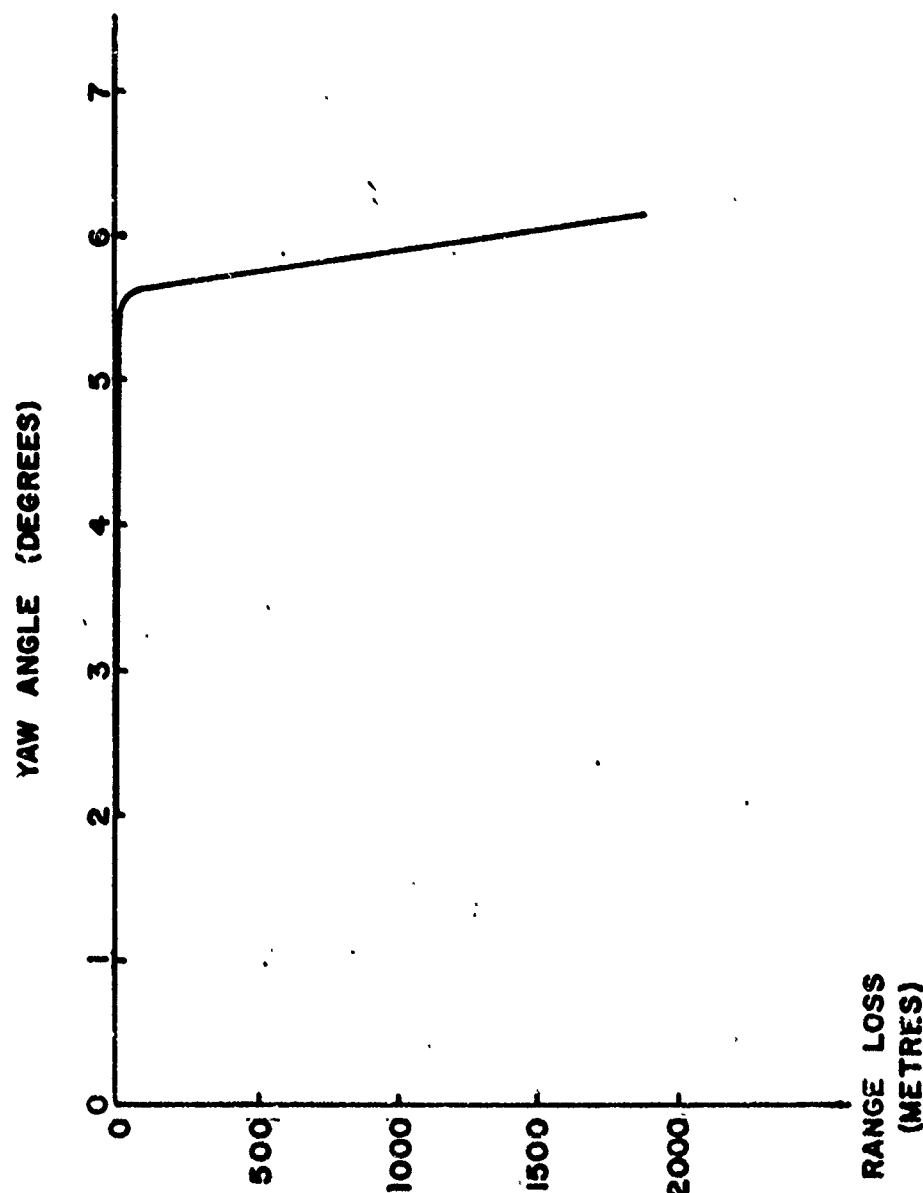


Figure 16. M483 Range Loss versus Launch Yaw Angle

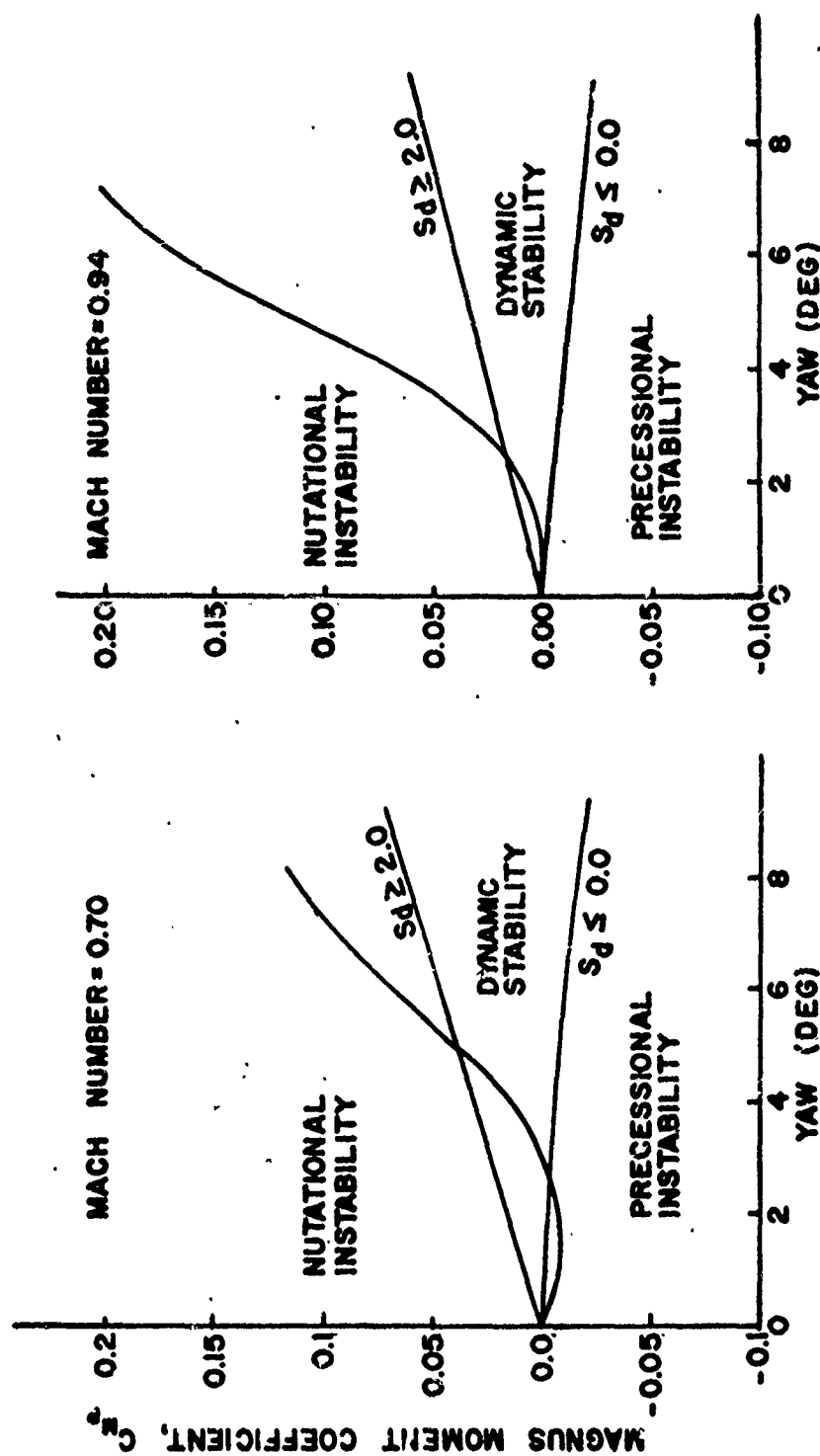


Figure 17. M83 Magnus Moment Coefficient versus Yaw

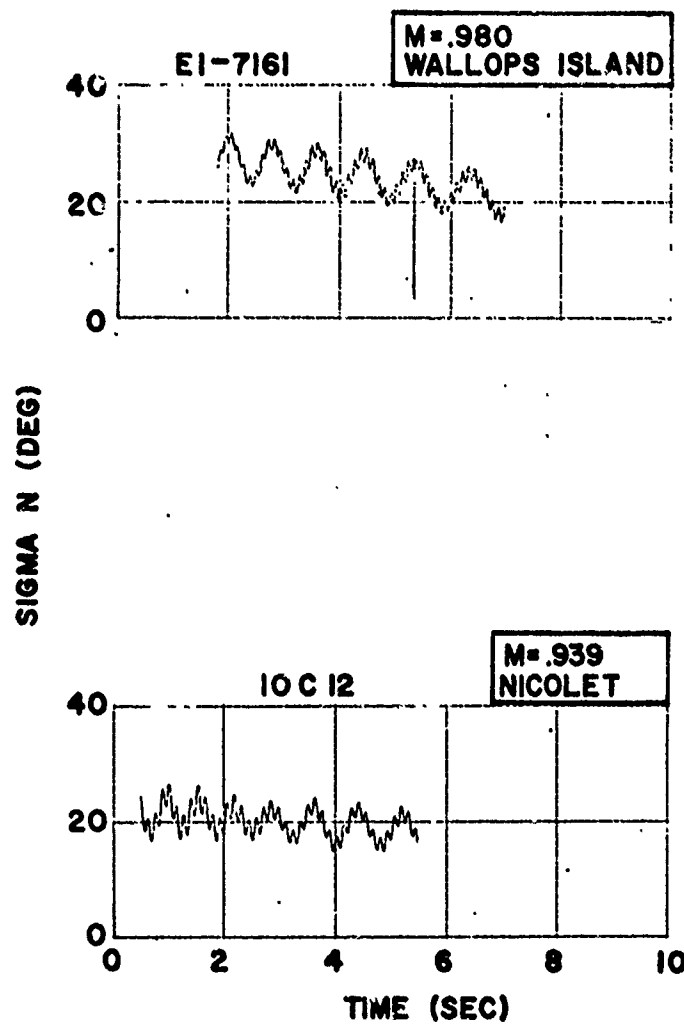


Figure 18. Effect of Environment on M483 Mod II, Yaw Inducer 1



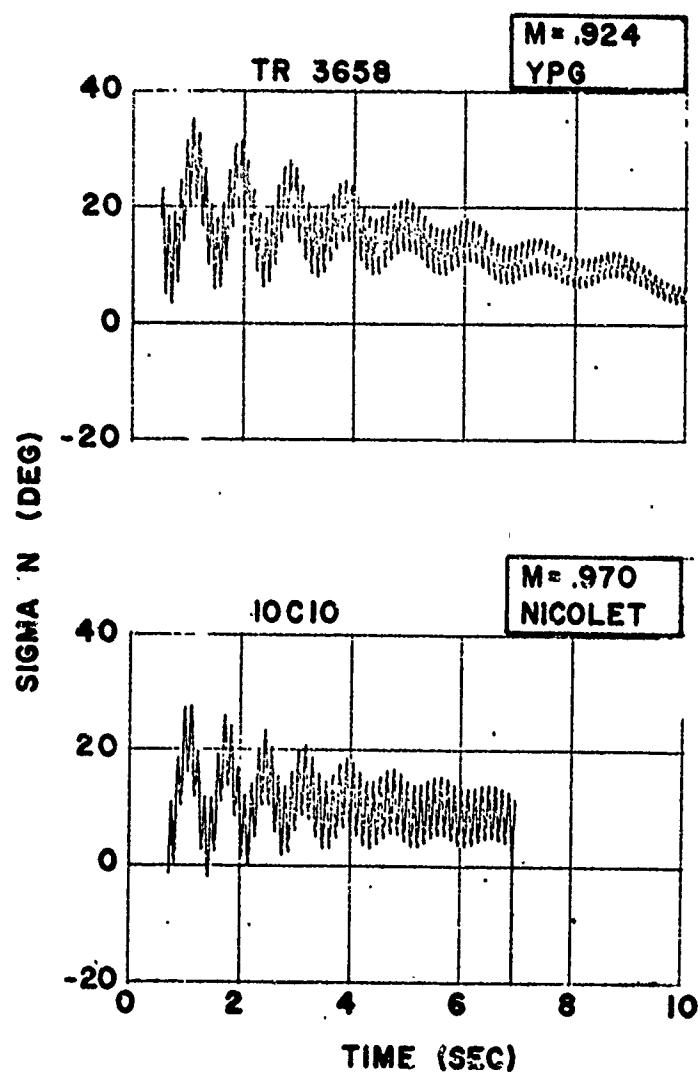


Figure 19. Effect of Environment on M483 Mod II, Yaw Inducer 4

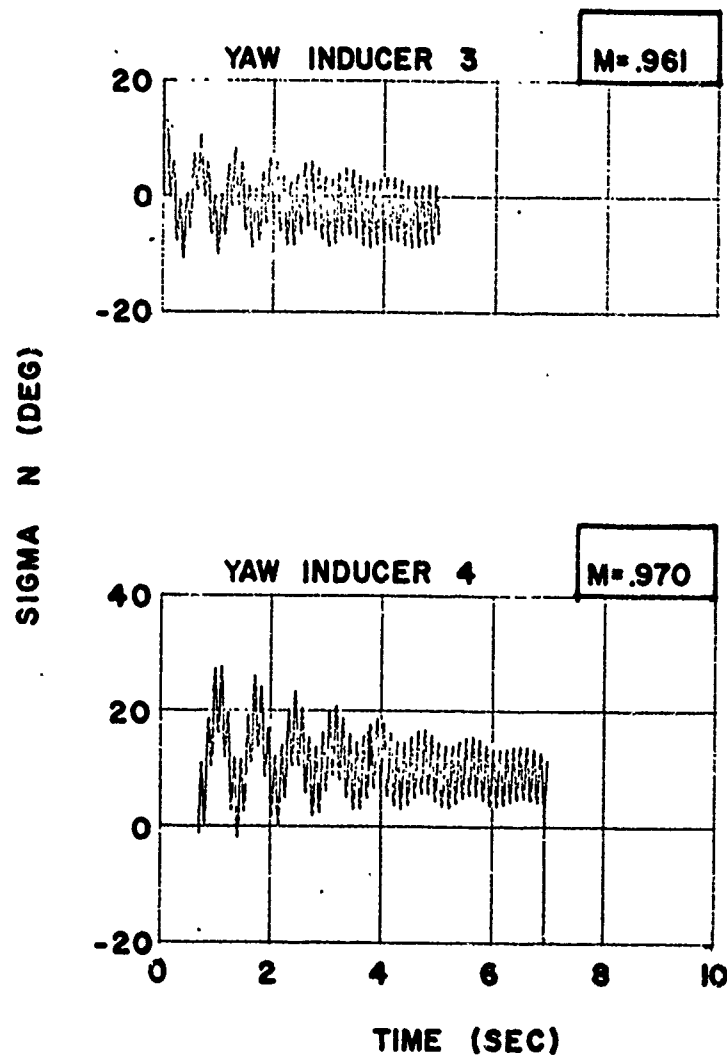


Figure 20. M483 Mod II Flights at Nicolet, Yaw Inducers 3 and 4

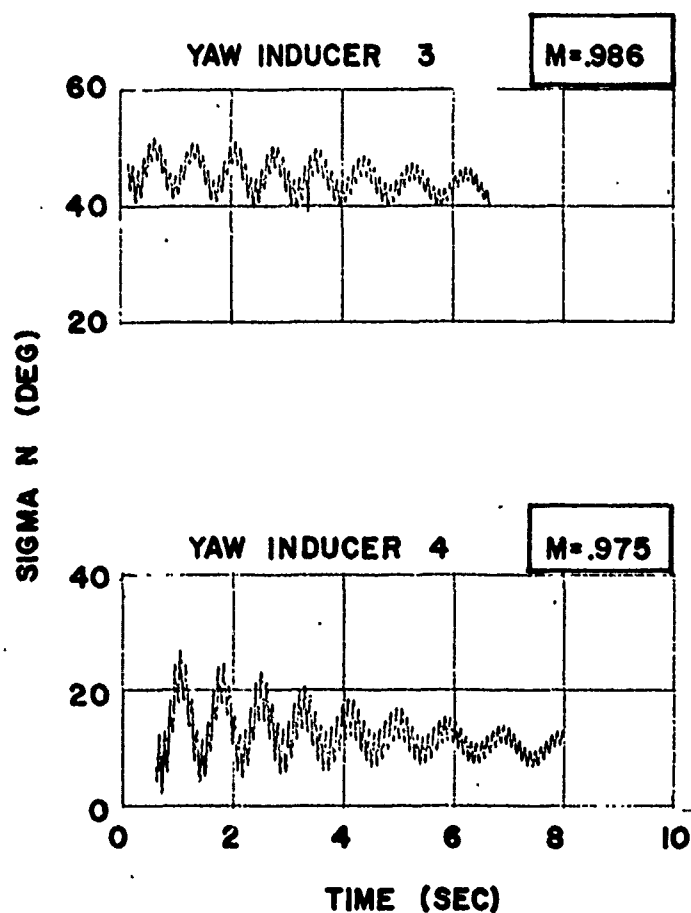


Figure 21. M483 Mod I Flights at Nicolet, Yaw Inducers 3 and 4

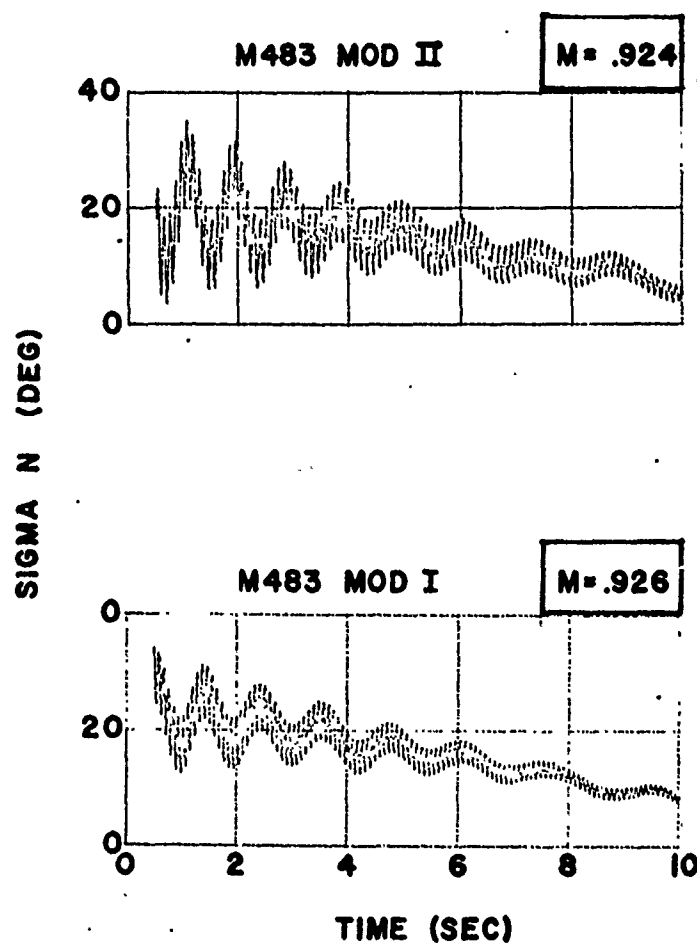


Figure 22. Comparison of M483 Mod I and M483 Mod II Flights at YPG, Yaw Inducer 4

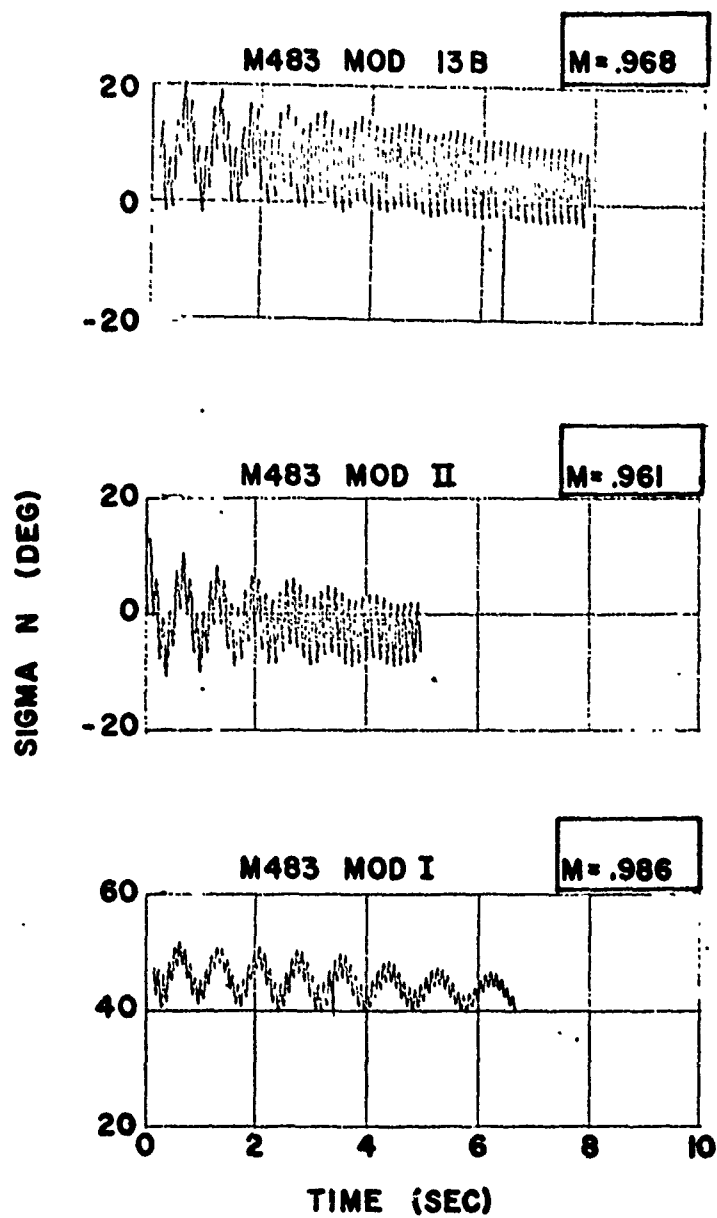


Figure 23. Flight Behavior of Modified M483 Shell at Nicolet, Yaw Inducer 3

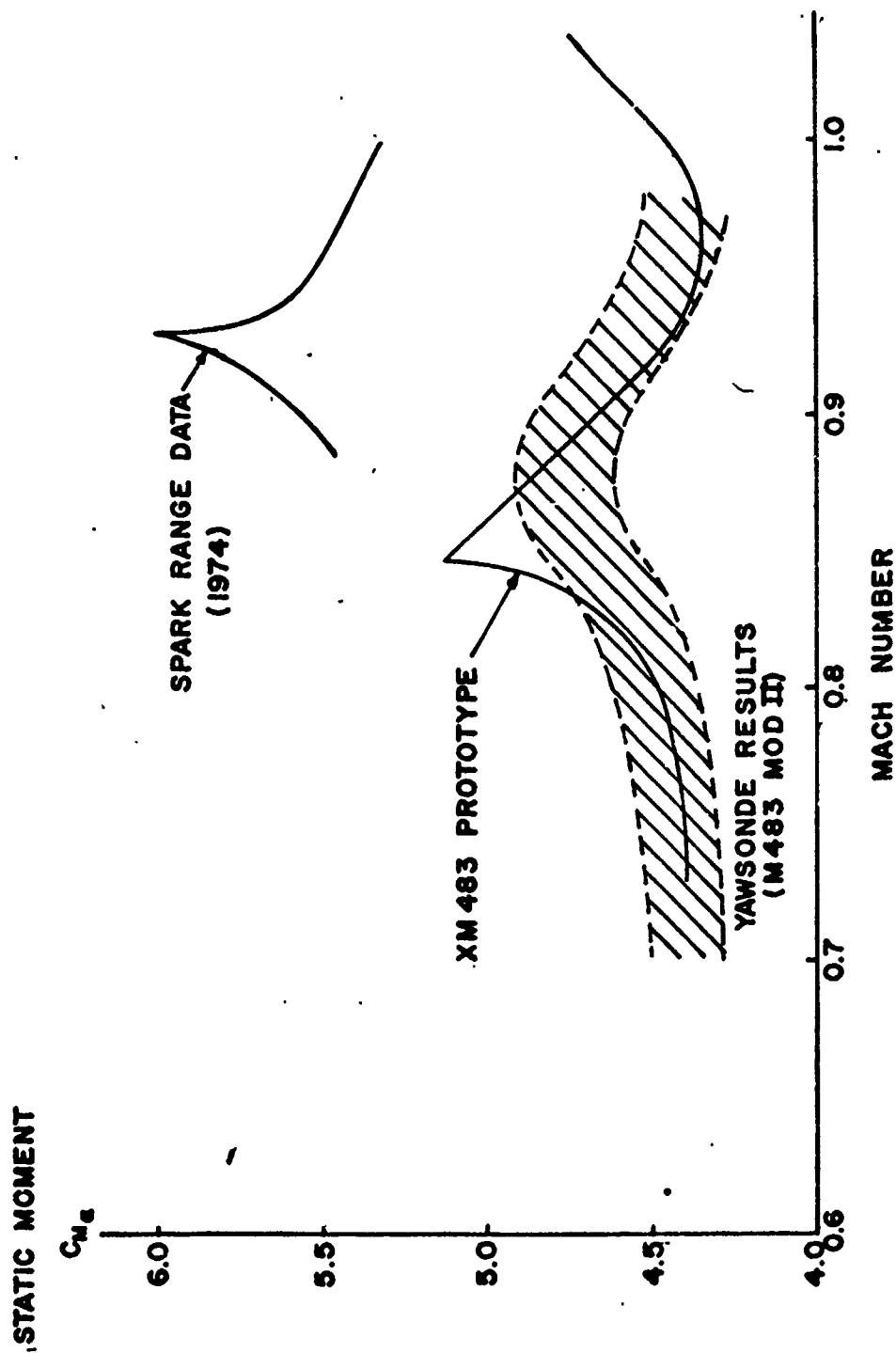


Figure 24. Comparison of M483 and M483 Mod II Static Moment Coefficient Slopes

Table 1. Summary of Yawsonde Tests of M483 at Wallops Island (1974)

Round No.	Launch Mach No.	Impact Range (m)		Measured Yaw	
		Nominal	Observed	Time (sec)	Ampl. (deg)
E1-7158	0.980	8200	8840	0.9	2.3
E1-7160	0.962	8000	8600	0.2	4.8
E1-7162	0.980	8200	8750	0.1	5.6
E1-7164	0.955	7930	5240	0.1	3.7
E1-7165	0.957	7950	4330	---	---
E1-7166	0.955	7930	5270	0.1	5.2
E1-7167	0.930	7600	4850	0.1	6.4
E1-7169	0.955	7930	5240	0.1	6.6
E1-7170	0.958	7950	5550	0.1	4.5
E1-7177	0.910	7800	7770	0.1	8.2
E1-7183*	0.920	7550	8050	0.4	5.2
E1-7252**	0.950	8000	4880	0.1	7.4
E1-7256*	0.940	8000	6000	0.1	7.2

\*Yaw inducer 1 had 1.3-cm plasticine on its lip.

\*\*Yaw inducer 1 had 2.5-cm plasticine on its lip.

Table 2. Yaw Inducers

<u>Type</u>	<u>Yaw Range*</u> <u>(degrees)</u>	<u>Description</u>
1	5 - 9	A short steel lip protruding several inches from underneath the muzzle.
2	6 - 10	A standard muzzle brake cut in half.
3	6 - 12	Type 2 with 2-1/2-inch side plates between the muzzle and the first baffle.
4	12 - 17	Type 2 with 5-inch side plates between the muzzle and the first baffle.

---

\*The expected yaw range depends on the gyroscopic stability of the particular shell.



Table 3. 155mm M483 Shell and Its Modifications

<u>Type</u>	<u>Ogive Length (cal)*</u>	<u>Body Length (cal)</u>	<u>Boattail Length (cal)</u>	<u>Total Length (cal)</u>	<u>Remarks</u>
Standard	2.85	2.62	0.51	5.98	1.80 calibers of cylindrical body wrapped with fiberglass.
Mod 13B	2.85	2.62	0.255	5.72	No changes in body design.
Mod I	2.85	2.24	0.255	5.35	Weight loss due to reduced body and boattail lengths were recovered by replacing some fiberglass with steel.
Mod II	2.85	2.62	0.255	5.72	Weight loss due to reduced boattail length was recovered by reducing length of fiberglass wrapped portion of body to 1.25 calibers

---

\*1 caliber = 0.155 metre

Table 4. Representative Physical Properties of M483 Shell and Its Modifications

Shell Type	Weight (kg)	$X_{cg}$ From Nose (m)	Moments of Inertia ( $\text{kg-m}^2$ )		$(I_a)^2/I_t$
			Axial ( $I_a$ )	Transverse ( $I_t$ )	
M483	46.70	0.571	0.1554	1.8051	0.01338
M483 Mod 13B	46.21	0.565	0.1510	1.7263	0.01321
M483 Mod I	45.78	0.546	0.1600	1.4186	0.01805
M483 Mod II	46.94	0.563	0.1590	1.7015	0.01486

Table 5. Summary of Yuma Firings of Modified M483 Shell

<u>Shell Type</u>	<u>Yaw Inducer</u>	<u>Yaw Level (deg)</u>	<u>Mach Number Range</u>	<u>Average Range (m)</u>	<u>Range Spread (m)</u>
M483 Mod I	2	5.8 - 7.0	.947 - .955	5439	87
M483 Mod II	3	11.3 - 13.8	.942 - .956	5231	146
M483 Mod I	3	8.2 - 9.6	.942 - .956	5299	97
M483 Mod 13B	3	12.2 - 13.0	.946 - .956	5078	164

Table 6. Summary of Nicolet Firings of M483 Shell and Its Modifications

<u>Shell Type</u>	<u>Yaw Inducer</u>	<u>Mach Number Range</u>	<u>Average Range (m)</u>	<u>Range Probable Error (m)</u>	<u>Remarks</u>
M483	2	.931 - .936			3 of 3 shorts
M483 Mod II	2	.928 - .939	6382	20.0	
M483 Mod I	2	.921 - .938	6359	17.1	
M483 Mod 13B	2	.934 - .953	6416	53.4	
M483 Mod II	2	.919 - .933	6350	34.6	
M483 Mod I	2	.925 - .945	5344	17.4	65° QE
M483 Mod II	2	.938 - .948	5166	21.1	65° QE
M483 Mod I	2	.936 - .955	5164	26.8	65° QE
M483 Mod I	2	.931 - .947	6242	19.9	
M483 Mod 13B	2	.951 - .962	6313	21.8	
M483 Mod II	2	.923 - .943	5052	20.9	65° QE
M483	1	.928 - .937			4 of 6 shorts
M483 Mod I	1	.847 - .860	5506	17.4	
M483 Mod II	1	.841 - .865	5447	43.5	

Figure 7. First Maximum Yaw Data from Nicolet Tests of M483 Shell and Its Modifications

<u>Shell Type</u>	<u>Yaw Inducer</u>	<u>Mach Number</u>	<u>First Maximum Yaw (deg)</u>	<u>Remarks</u>
M483	None	.911	1.2	
M483	None	.907	1.8	
M483	1	.928	9.4	3300 m short
M483	1	.944	9.4	3500 m short
M483	2	.931	13.0	3100 m short
M483	2	.930	13.5	3300 m short
M483 Mod 13B	2	.945	10.6	
M483 Mod 13B	2	.945	9.1	
M483 Mod 13B	3	.962	8.4	
M483 Mod 13B	3	.968	11.2	
M483 Mod 13B	4	.941	16.9	
M483 Mod I	1	.951	5.8	
M483 Mod I	2	.946	5.4	
M483 Mod I	2	.946	6.6	
M483 Mod I	2	.950	5.8	
M483 Mod I	3	.981	7.0	
M483 Mod I	3	.986	5.8	
M483 Mod I	3	.936	7.8	
M483 Mod I	3	.926	5.3	
M483 Mod I	4	.975	12.4	

Figure 7. First Maximum Yaw Data from Nicolet Tests of M483 Shell and Its Modifications (continued)

<u>Shell Type</u>	<u>Yaw Inducer</u>	<u>Mach Number</u>	<u>First Maximum Yaw (deg)</u>	<u>Remarks</u>
M483 Mod II	1	.941	6.6	
M483 Mod II	1	.939	5.0	
M483 Mod II	2	.934	8.0	
M483 Mod II	2	.934	7.8	
M483 Mod II	2	.937	7.0	
M483 Mod II	3	.849	10.3	
M483 Mod II	3	.889	7.2	
M483 Mod II	3	.917	9.4	
M483 Mod II	3	.961	7.2	
M483 Mod II	3	.969	7.5	
M483 Mod II	3	.949	10.3	
M483 Mod II	3	.961	10.3	
M483 Mod II	4	.967	16.2	
M483 Mod II	4	.970	15.0	